DEVELOPMENT OF A GENERAL PROCEDURE TO EVALUATE THE PROBABILITY OF BREAKAGE FOR GLASS PLATES IN INSULATING GLASS UNITS DUE TO THERMAL STRESSES INDUCED BY SOLAR IRRADIANCE

A Dissertation

by

MICHAEL SCOTT BRACKIN

Submitted to the Office of Graduate and Professional Studies of
Texas A&M University
in partial fulfillment of the requirements for the degree of

DOCTOR OF PHILOSOPHY

Chair of Committee,	W. Lynn Beason
Committee Members,	C. Eugene Buth
	Harry L. Jones
	Harry A. Hogan
Head of Department,	Robin L. Autenrieth

May 2017

Major Subject: Civil Engineering

ABSTRACT

Over the past several years, there has been a significant increase in the number of glass plate breakages caused by thermally induced stress due to exposure to solar irradiance. Glass plate breakage that is caused by thermal stress has become one of the leading issues that the architectural glass industry faces. The increase in glass plate breakage is coupled with the expanded use of insulating glass (IG) units and the ever increasing demand for more energy-efficient windows. More often than not, the glass plates that break are part of windows that incorporate IG units.

This issue is nothing new to the architectural glass industry and an ASTM International (ASTM) standard practice has been developed to evaluate the probability of breakage (POB) for windows that incorporate monolithic glass plates that are subjected to solar irradiance. However, there is no similar standard practice to evaluate IG units subjected to solar irradiance. A current goal in the architectural glass industry is to develop a similar standard practice for IG units. The primary objective of the research presented herein was to develop procedures that can be used to evaluate the POB of glass plates in IG units that are subjected to solar irradiance. It is anticipated that these newly developed procedures will serve as the basis for the development of a new standard practice.

The research herein shows that the non-linear behavior of the heat exchange process that occurs between the inner and outer glass plates, through the gas space cavity, of an IG unit can be reasonably estimated using a single, linear combined energy exchange coefficient (CEEC). This greatly simplifies the thermal analysis procedure that is required to analyze IG units by removing the need for iteration. A formal test procedure (FTP) was developed herein that can be used to determine the CEEC. The FTP couples straightforward physical experiments with a parameter identification optimization procedure (PIOP) that uses finite element (FE) analyses to determine the optimum CEEC.

The CEEC was then coupled with a formal design procedure (FDP) that was developed to evaluate the POB for a glass plate in a specific IG unit that is subjected to a specific set of environmental conditions. The FDP is the most accurate method to evaluate IG units and requires building a detailed FE model of the insulating glass unit, measuring the CEEC for the gas space cavity, and determining the allowable stress for a given POB using the glass edge strength failure prediction model (ESFPM).

Finally, a simplified design procedure (SDP) was developed that can be used to evaluate the POB for glass plates in generic IG units for a general range of typical environmental conditions. This SDP presents the framework that is needed to develop general procedures that can be incorporated into a design standard, practice, or code and provides a tool for the design of IG units that are subjected to thermal load conditions.

DEDICATION

To Dr. Terry L. Kohutek, in memoriam.

ACKNOWLEDGEMENTS

First and foremost, I would like to thank my committee chair, Dr. W. Lynn Beason, and my committee members, Dr. C. Eugene Buth, Dr. Harry L. Jones, and Dr. Harry A. Hogan for their guidance and support in the preparation of this dissertation. Thank you Dr. Buth for your encouragement to further my education and start working toward a Ph.D.

I would like to thank Mr. A. William Lingnell and Mr. Jeff Haberer for their contributions and technical advice given during the development of this research. Thanks also go to my friends and colleagues at the Texas A&M Transportation Institute. Special thanks go to Dr. Akram Abu-Odeh for his contribution in teaching me finite element analysis and optimization. In addition, thanks go to Mr. James C. Kovar for his assistance in preparing for the physical testing that was performed as part of this research.

Finally, thanks to my wife, Hannah, and children Kase, Katie, and Myles for their patience and love while performing this research and writing this dissertation.

CONTRIBUTORS AND FUNDING SOURCES

Contributors

This work was supervised by a dissertation committee consisting of Professors W. Lynn Beason and Harry L. Jones of the Zachry Department of Civil Engineering, Senior Research Fellow C. Eugene Buth of the Texas A&M Transportation Institute and Professor Harry A. Hogan of the Department of Mechanical Engineering.

All of the work performed as part of the dissertation was completed independently by the student.

Funding Sources

This work was made possible, in part, by the Insulating Glass Manufacturers Alliance (IGMA) and Trulite Glass and Aluminum Solutions.

The contents of this dissertation are solely the responsibility of the author and do not necessarily represent the official views of IGMA or Trulite Glass and Aluminum Solutions.

NOMENCLATURE

α_D	Thermal diffusivity
α_{inner}	Solar absorption of inner glass plate
α_{net}	Net solar absorption
α_{outer}	Solar absorption of outer glass plate
α_{Ratio}	Solar absorption ratio
α_S	Solar absorptance
α_T	Coefficient of thermal expansion
β	Inverse of film temperature
$\boldsymbol{\beta}$	Vector of parameters to be estimated
δ	Deformation, thickness of velocity boundary layer
δ_t	Thickness of temperature boundary layer
$\delta_{Thermal}$	Thermal expansion
$\varepsilon_{1,4}$	Emissivity of surface number 1 or 4 surface
ε_2	Emissivity of surface number 2
$\varepsilon_{2,3}$	Emissivity of surface number 2 or 3 surface
ε_3	Emissivity of surface number 3
ε	Emissivity, strain
$\varepsilon_{effective}$	Effective emissivity
$\varepsilon_{Thermal}$	Thermal strain
λ	Wavelength
μ	Viscosity
v	Poisson's ratio
$\rho_{1,4}$	Solar reflectance of number 1 or 4 surface
$\rho_{2,3}$	Solar reflectance of number 2 or 3 surface
ρ_m	Mass density
ρ_S	Solar reflectance
σ	Stress

σ_{60}	Failure stress for 60-sec load
$\sigma_{allowable}$	Allowable stress
$\sigma_{applied}$	Applied stress
σ_{d}	Failure stress for load duration
σ_{inner}	Maximum thermal stress for the inner glass plate
σ_{max}	Maximum thermal stress
σ_{net}	Net stress
σ_{outer}	Maximum thermal stress for the outer glass plate
$\sigma_{residual}$	Residual stress
σ_{SB}	Steffan-Boltzmann constant
$\sigma_{steady-state}$	Steady-state thermal stress
$\sigma_{thermal}$	Thermal stress
$\sigma_{transient}$	Transient thermal stress
τ	Shear stress
τ_S	Solar transmittance
υ	Kinematic viscosity
A	Area, aspect ratio
A_{COG}	Area of center-of-glass
A_{EOG}	Area of edge-of-glass
AF	Absorption factor
A_{frame}	Area of window frame
A_{window}	Total area of window
a_l	Coefficient l of polynomial equation
B	Risk function
$\boldsymbol{B}$	Vector of coefficients
b	Thermal offset
b_{FEA_1}	Thermal offset for FEA 1
b_{FEA_5}	Thermal offset for FEA 5
b_i	Coefficient i of thermal offset equation

CEEC	Combined energy exchange coefficient
C_p	Specific heat
d_{edge_bite}	Edge bite
E	Modulus of elasticity
$\dot{E}_{generated}$	Rate of energy generated
$\dot{E}_{in}$	Rate of energy in
$\dot{E}_{out}$	Rate of energy out
ESFPM	Edge strength failure prediction model
$\dot{E}_{stored}$	Rate of energy stored
$\boldsymbol{e}$	Vector of errors
FDP	Formal design procedure
FE	Finite element
FT	Fully tempered
FTP	Formal test procedure
GFPM	Glass failure prediction model
Gr	Grashof number
g	Gravitational constant
H	Height
HS	Heat strengthened
h_{cavity_j}	Air space coefficient of layer j
h_{CEEC}	Combined energy exchange coefficient
$h_{convection}$	Convection coefficient
h_{indoor}	Indoor surface film coefficient
$h_{outdoor}$	Outdoor surface film coefficient
$h_{radiation}$	Effective radiation coefficient
h_s	Air space coefficient
h_{total}	Total effective heat transfer coefficient
IG	Insulating glass

I_{inner}	Absorbed solar irradiance of the inner glass plate
I_{outer}	Absorbed solar irradiance of the outer glass plate
I_s	Incident solar irradiance
I_{sc}	Solar constant
k	Thermal conductivity
$k_{effective}$	Effective thermal conductivity
k_{fluid}	Thermal conductivity of bulk fluid
k_j	Thermal conductivity of layer j
k_t	Surface/edge flaw characteristic
L_0	Original length
L	Length
low-E	Low emissivity coating
m	Surface/edge flaw characteristic, thermal slope
m_{FEA_1}	Thermal slope for FEA 1
m_{FEA_5}	Thermal slope for FEA 5
m_i	Coefficient i of thermal slope equation
NPP	Numerical propagation procedure
Nu_1	Nusselt function 1
Nu_2	Nusselt function 2
Nu	Nusselt number
n	Order of polynomial
P_1	First-order polynomial
P_2	Second-order polynomial
P	Load, total error sum of squares
P_b	Probability of failure
$p_{effective}$	Effective perimeter length
PIOP	Parameter identification optimization procedure
P_n	Polynomial of n^{th} degree
POB	Probability of breakage

Pr	Prandtl number
p	Perimeter length
$q_{conduction}$	Conduction heat flow
$q_{convection}$	Convection heat flow
q_{indoor}	Heat flow to indoor environment
q_{net}	Net heat flux per unit area
q_{net_inner}	Net heat flux of inner glass plate control volume
q_{net_outer}	Net heat flux of outer glass plate control volume
$q_{outdoor}$	Heat flow to outdoor environment
$q_{radiation}$	Radiation heat flow
q_{total}	Total heat flow
q_{window}	Steady-state heat flow through window
R^2	Coefficient of multiple determination
Ra	Rayleigh number
Re	Reynolds number
RSS	Sum of the squares of the residuals
SDP	Simplified design procedure
SLF	Solar load factor
SRSM	Sequential response surface method
T_1	Temperature of number 1 surface
T_2	Temperature of number 2 surface
T_3	Temperature of number 3 surface
T_4	Temperature of number 4 surface
T	Fluid temperature
T_{COG}	Temperature of center-of-glass area
T_{COG_i}	Temperature of center-of-glass area at time step i
$T_{environment}$	Temperature of environment
T_{film}	Film temperature
T_{glass}	Temperature of glass surface

T_i	Temperature at time step i
T_{i+1}	Temperature at time step i+1
T_{indoor}	Temperature of indoor environment
T_{inner_i}	Temperature of inner glass plate at time step i
$\hat{T}_{inner_i}$	Estimated temperature of inner glass plate at time step i
T_j	Temperature of surface j
T_k	Temperature of surface k
T_{outer_i}	Temperature of outer glass plate at time step i
$\hat{T}_{outer_i}$	Estimated temperature of outer glass plate at time step i
$T_{outdoor}$	Temperature of outdoor environment
T_{POG}	Temperature of perimeter-of-glass
T_{POG_i}	Temperature of perimeter-of-glass at time step i
T_s	Temperature of surface
TSF	Thermal stress factor
T_∞	Free stream temperature
$\Delta T_{0.25}$	Maximum temperature difference associated with a 25 per-cent net absorption
$\Delta T_{5.7105}$	Maximum temperature difference associated with a solar irradiance of 5.7105 (in.·lb/s)/in.^{2}
ΔT	Change in temperature
$\Delta T_{indoor/outdoor}$	Indoor/outdoor temperature difference
ΔT_{inner}	Maximum center-of-glass/perimeter-of-glass temperature difference for the inner glass plate
ΔT_{max}	Maximum center-of-glass/perimeter-of-glass temperature difference
$\Delta T_{net\_absorption}$	Maximum center-of-glass/perimeter-of-glass temperature difference for a given net absorption

ΔT_{outer}	Maximum center-of-glass/perimeter-of-glass temperature difference for the outer glass plate
$\Delta T_{solar\_irradiance}$	Maximum center-of-glass/perimeter-of-glass temperature difference for a given solar irradiance
Δt	Time step
t_{cavity}	Thickness of gas space cavity
t_{cold}	Thickness of cold glass plate
t_d	Load duration
t_{glass}	Thickness of glass plate
t_{glass_j}	Thickness of layer j
t_{heated}	Thickness of heated glass plate
$t_{overall}$	Overall thickness
U_{COG}	U-Factor for center-of-glass area
U_{EOG}	U-Factor for edge-of-glass area
U_{frame}	U-Factor for frame area
U_{IGU}	U-Value for insulating glass unit
$U_{monolithic}$	U-Value for monolithic glass plate
U_{window}	U-Factor for window assembly
u	Stream velocity
u_∞	Free stream velocity
W	Width
X_i	Input variable i for thermal offset equation
$\mathbf{X}$	Matrix of predictor variables
x	Independent variable, distance in x direction
$\bar{Y}$	Mean of observations
Y_i	Input variable i for thermal slope equation
$\hat{Y}_i$	Predicted response i
$\mathbf{Y}$	Vector of observations

$\widehat{\boldsymbol{Y}}$	Vector of predicted responses
y	Independent variable, distance in y direction
z	Independent variable

TABLE OF CONTENTS

Page

ABSTRACT ii

DEDICATION iv

ACKNOWLEDGEMENTS v

CONTRIBUTORS AND FUNDING SOURCES vi

NOMENCLATURE vii

TABLE OF CONTENTS xv

LIST OF FIGURES xviii

LIST OF TABLES xxxii

CHAPTER I INTRODUCTION 1

CHAPTER II PROBLEM STATEMENT 8

CHAPTER III LITERATURE REVIEW 18

- Glass Plates Subjected to a Uniform Change in Temperature 18
- Glass Plates Subjected to a Differential Change in Temperature 21
  - Thermal Stress in Monolithic Glass Plates 25
  - Thermal Stress in Insulating Glass Units 29
  - Other Considerations for Thermal Stress in Insulating Glass Units 31
- Heat Exchange Between Monolithic Glass Plates and the Surrounding Environment 36
  - Solar Irradiance Applied to Monolithic Glass Plates 39
  - Conduction 45
  - Convection 48
  - Long-Wave Radiation 55
  - Surface Film Coefficients 58
- Heat Exchange Between Insulating Glass Units and the Surrounding Environment 62
  - Solar Irradiance Applied to Insulating Glass Units 64
  - Heat Exchange Across the Gas Space Cavity 66
    - Numerical Propagation Procedure 74
    - ASHRAE Air Space Coefficients 77

Page

Surface Film Coefficients....80
Glass as a Structural Material....81
Annealed Float Glass....82
Heat-Treated Glass....83
Design Philosophy for Glass Plates....88
Glass Failure Prediction Model....88
The Effect of Load Duration on the Strength of Glass Plates....89
Glass Edge Strength Failure Prediction Model....92
ASTM Standard Practice for Monolithic Glass Plates....100
Final Considerations....106
Energy Performance Ratings....106
U-Factor....108
U-Value....109
Energy Performance Software....111
Practical Significance to the Discussion Herein....112

CHAPTER IV FORMAL DESIGN PROCEDURE TO EVALUATE THE PROBABILITY OF BREAKAGE OF GLASS PLATES IN INSULATING GLASS UNITS SUBJECTED TO SOLAR IRRADIANCE....116

Formal Design Procedure....117
Finite Element Analysis....118
Finite Element Modeling Using Half-Model Geometry....119
Steady-State Finite Element Analysis....124
Transient Finite Element Analysis....125
Practical Application....126
Case Study for Applying the Formal Design Procedure....130

CHAPTER V COMBINED ENERGY EXCHANGE COEFFICIENT....139

Proof-of-Concept....140
Parameter Identification Using Optimization....153
Formal Test Procedure....173
Practical Application of the Formal Test Procedure....180
Test Specimen Preparation....182
Insulated Heat Chamber....186
Environmental Test Chamber....190
Data Acquisition....192
Experimental Results....194

CHAPTER VI SIMPLIFIED DESIGN PROCEDURE....209

Thickness....214

Page

Linear Design Variables that Affect the Thermal Behavior of Insulating Glass Units 219
Solar Irradiance 219
Net Absorption 229
Indoor/Outdoor Temperature Difference 231
Proposed Simplified Design Procedure to Evaluate the Probability of Breakage of Insulating Glass Units 241
General Thermal Stress Equation for Insulating Glass Units 242
Case Study to Calculate b and m 248
General Regression Procedure 251
General Polynomial Equation 256
Steady-State Response: Two Independent Variables 257
Transient Response: Three Independent Variables 264
Application of the General Regression Procedure 275
First-Order Polynomial Model 275
Outer Glass Plate with Perfectly Insulated Frame 275
Outer Glass Plate with High-Heat Mass Frame 281
Inner Glass Plate with Perfectly Insulated Frame 287
Inner Glass Plate with High-Heat Mass Frame 292
Second-Order Polynomial Model 298
Outer Glass Plate with Perfectly Insulated Frame 298
Outer Glass Plate with High-Heat Mass Frame 305
Inner Glass Plate with Perfectly Insulated Frame 313
Inner Glass Plate with High-Heat Mass Frame 320
General Summary 327
Practical Application 331

CHAPTER VII CONCLUSIONS 346

Research Summary 346
Major Conclusions 350
Future Research 352

REFERENCES 355

APPENDIX A THERMAL STRESS ANALYSIS OF A MONOLITHIC GLASS PLATE 363

APPENDIX B COMBINED ENERGY EXCHANGE COEFFICIENT PROOF-OF-CONCEPT EXPERIMENT DATASHEET 371

APPENDIX C COMBINED ENERGY EXCHANGE COEFFICIENT EXPERIMENT DATASHEETS 375

LIST OF FIGURES

Page

Fig. 1. Surface Film Coefficients for Use in Monolithic Glass Plate Design 9

Fig. 2. Corner-Cut-Away of a Typical IG Unit 11

Fig. 3. Cross-Section of an IG Unit's Primary Components 15

Fig. 4. Example of Differential Temperature Across a Glass Plate Area 23

Fig. 5. Principle Thermal Areas Considered for Glass Plates 25

Fig. 6. Thermal Stress Block Along the Perimeter of a Glass Plate 27

Fig. 7. Idealized Fracture Pattern of a Monolithic Glass Plate due to Thermal Stress 28

Fig. 8. Glass Plate Breakage due to Thermal Stress 28

Fig. 9. Shadow Pattern Cast on an Exemplar IG Unit 34

Fig. 10. Energy Exchange for a Monolithic Glass Plate with the Surrounding Indoor and Outdoor Environments 38

Fig. 11. Electromagnetic Spectrum (Bergman et al. 2011) 40

Fig. 12. Standard Solar Irradiance Spectrum (ASTM 2014) 41

Fig. 13. Solar Reflectance, Absorptance, and Transmittance of a Monolithic Glass Plate 43

Fig. 14. Residential Window with Different Solar Absorptances 44

Fig. 15. Velocity Boundary Layer Across a Flat Plate (Bergman et al. 2011) 49

Fig. 16. Temperature Boundary Layer Across a Flat Plate (Bergman et al. 2011) 50

Fig. 17. Behavior of Convective Fluid Flow (Bergman et al. 2011) 54

Fig. 18. Idealized Closed System for a Monolithic Glass Plate Using Surface Film Coefficients 61

Page

Fig. 19. Energy Exchange of an IG Unit with the Surrounding Indoor and Outdoor Environments....63

Fig. 20. Ray Tracing Procedure for an IG Unit....65

Fig. 21. IG Unit Center-of-Glass U-Factor vs. Gap Width, Emissivity, and Gas Fill (ASHRAE 2013)....72

Fig. 22. Energy Exchange of an IG Unit with the Surrounding Indoor and Outdoor Environments Using the CEEC Through the Gas Space Cavity....73

Fig. 23. Idealized Residual Stresses in Heat-Treated Glass Plates....84

Fig. 24. Idealized Residual Stresses Near the Edges of Heat-Treated Glass Plates....86

Fig. 25. Normalized Glass Strength vs. Duration of Load....91

Fig. 26. Allowable Stress vs. POB and Glass Plate Perimeter Length....99

Fig. 27. Thermal Stress Factor Chart for the Design of Monolithic Glass Plates (ASTM 2012a)....101

Fig. 28. Idealized Frames Considered for the Design of Monolithic Glass Plates (ASTM 2012a)....103

Fig. 29. POB Chart for the Design of Monolithic Glass Plates (ASTM 2012a)....105

Fig. 30. FE Model of IG Unit....120

Fig. 31. FE Model of Thin, Steel-Channel Spacer....120

Fig. 32. IG Unit Geometry for FE Analyses....121

Fig. 33. Thin, Steel-Channel Spacer Geometry for FE Analyses....121

Fig. 34. Surface Film Coefficients and CEEC....123

Fig. 35. Steady-State Temperatures for FEA 1....131

Fig. 36. Transient Temperatures for FEA 1....133

Fig. 37. Transient Response for the Inner Glass Plate of FEA 1....136

Page

Fig. 38. Transient Response for the Outer Glass Plate of FEA 1 136

Fig. 39. Transient Center/Perimeter Temperature Difference for the Inner Glass Plate of FEA 1 137

Fig. 40. Transient Center/Perimeter Temperature Difference for the Outer Glass Plate of FEA 1 137

Fig. 41. Proof-of-Concept Test Specimen 141

Fig. 42. Proof-of-Concept Test Setup 143

Fig. 43. Proof-of-Concept Center-of-Glass Temperature Data 144

Fig. 44. Difference in Center-of-Glass Temperatures for Proof-of-Concept Test 146

Fig. 45. Proof-of-Concept Detailed FE Model 147

Fig. 46. Cold Glass Plate Temperature Results from NPP 148

Fig. 47. Difference in Center-of-Glass Temperatures from NPP 148

Fig. 48. Cold Glass Plate Center-of-Glass Temperature Data for Proof-of-Concept CEEC FE Cases 150

Fig. 49. Difference in Center-of-Glass Temperatures for Proof-of-Concept CEEC FE Cases 150

Fig. 50. Sum of the Squares of the Residuals vs. CEEC 152

Fig. 51. LS-Opt Graphical User Interface - Optimization Process Flow 156

Fig. 52. Task and Strategy Selection Protocols 156

Fig. 53. Curve Matching Composite and Algorithm Protocols 157

Fig. 54. SRSM Sub Region Reduction Scheme (Stander and Goel 2010) 158

Fig. 55. Metamodel Type and Point Selection Scheme Protocols 159

Fig. 56. Simulation History Curves for Iteration Number 1 160

Fig. 57. Predicted History at Any Point in the Design Space for Iteration Number 1 160

Page

Fig. 58. Simulation History Curves for Iteration Number 2 161

Fig. 59. Predicted History at Any Point in the Design Space for Iteration Number 2 161

Fig. 60. Simulation History Curves for Iteration Number 3 162

Fig. 61. Predicted History at Any Point in the Design Space for Iteration Number 3 162

Fig. 62. Simulation History Curves for Iteration Number 4 163

Fig. 63. Predicted History at Any Point in the Design Space for Iteration Number 4 163

Fig. 64. Simulation History Curves for Iteration Number 5 164

Fig. 65. Predicted History at Any Point in the Design Space for Iteration Number 5 164

Fig. 66. Simulation History Curves for Iteration Number 6 165

Fig. 67. Predicted History at Any Point in the Design Space for Iteration Number 6 165

Fig. 68. Final Iteration of the Metamodel Using LS-Opt to Verify the Best-Fit CEEC Selected 166

Fig. 69. CEEC vs. Iteration Number 167

Fig. 70. Mean Square Error vs. Iteration Number 168

Fig. 71. Comparison of Center-of-Glass Temperature Data Using the PIOP and NPP 169

Fig. 72. Comparison of Difference in Center-of-Glass Temperatures Using the PIOP and NPP 169

Fig. 73. Temperature Distribution Through the IG Unit as a Function of Time 170

Fig. 74. FE Models for Size Requirements 175

Fig. 75. Temperature Results from FE Model at 3600s 176

Fig. 76. Heat Flux Across the Cold Glass Plate 177

Page

Fig. 77. Nusselt Number vs. Reynolds Number and Aspect Ratio Data from Shewen (1986) 178

Fig. 78. Nusselt Number vs. Reynolds Number and Aspect Ratio Data from El Sherbiny et. al (1982) 178

Fig. 79. FTP Specimen 181

Fig. 80. Extraneous Silicone Shown on Test Specimens 182

Fig. 81. Test Specimen Labels 183

Fig. 82. Measurement of Overall Thickness Using Digital Micrometer 184

Fig. 83. Measurement of Glass Plate Thickness Using Digital Caliper 184

Fig. 84. Thermocouples Installed on Test Specimens 186

Fig. 85. Specimen Prepared for Testing 186

Fig. 86. Insulated Heat Chamber for Determining the CEEC 187

Fig. 87. IG Unit Specimen with Thermocouples Installed 188

Fig. 88. Uniformity in Temperature of Special Heating Device 189

Fig. 89. Manometer and Pressure Regulator 190

Fig. 90. Environmental Test Chamber 191

Fig. 91. Specimen Test Rack in the Environmental Test Chamber 192

Fig. 92. Data Acquisition System 193

Fig. 93. Heat Output vs. Voltage for the Special Heating Device 193

Fig. 94. Heat Controller 194

Fig. 95. Temperature Data Measured for Specimens 1 and 2 with Clear Glass Plates 196

Fig. 96. Temperature Data Measured for Specimens 4 and 5 with a Hard-Coat Low-E Coating 196

Page

Fig. 97. Temperature Data Measured for Specimens 7 and 8 with a Soft-Coat Low-E Coating....197

Fig. 98. Summary of Temperature Data Measured for Specimens 1, 4, and 7 198

Fig. 99. Difference in Center-of-Glass Temperature for Specimens 1 Through 6....199

Fig. 100. Center-of-Glass Temperature Data Measured Compared to the CEEC for Specimen 1....200

Fig. 101. Center-of-Glass Temperature Data Measured Compared to the CEEC for Specimen 2....201

Fig. 102. Center-of-Glass Temperature Data Measured Compared to the CEEC for Specimen 4....201

Fig. 103. Center-of-Glass Temperature Data Measured Compared to the CEEC for Specimen 5....202

Fig. 104. Center-of-Glass Temperature Data Measured Compared to the CEEC for Specimen 7....202

Fig. 105. Center-of-Glass Temperature Data Measured Compared to the CEEC for Specimen 8....203

Fig. 106. Glass Plate Temperature Data Measured for Specimens 4 and 4R....205

Fig. 107. Glass Plate Temperature Data Measured for Specimens 7 and 7R....206

Fig. 108. Center-of-Glass Temperature Data Measured Compared to the CEEC for Specimen 4R....207

Fig. 109. Center-of-Glass Temperature Data Measured Compared to the CEEC for Specimen 7R....207

Fig. 110. Thickness Case 1 and 3 - Inner Glass Plate of a Low-E IG Unit at -20 °F Outdoor Temperature....216

Fig. 111. Thickness Case 5 and 7– Inner Glass Plate of a Clear IG Unit at -20 °F Outdoor Temperature....216

Fig. 112. Thickness Case 2 and 4– Outer Glass Plate of a Low-E IG Unit at 120 °F Outdoor Temperature....217

Page

Fig. 113. Thickness Case 6 and 8 - Outer Glass Plate of a Clear IG Unit at 120 °F Outdoor Temperature. 217

Fig. 114. Solar Load Case 1 Through 5 - Outer Glass Plate of a Low-E IG Unit at -20 °F Outdoor Temperature 221

Fig. 115. Solar Load Case 6 Through 10 - Outer Glass Plate of a Clear IG Unit at -20 °F Outdoor Temperature 222

Fig. 116. Solar Load Case 1 Through 5 - Inner Glass Plate of a Low-E IG Unit at -20 °F Outdoor Temperature 222

Fig. 117. Solar Load Case 6 Through 10 - Inner Glass Plate of a Clear IG Unit at -20 °F Outdoor Temperature 223

Fig. 118. Solar Load Case 11 Through 15 - Outer Glass Plate of a Low-E IG Unit at 120 °F Outdoor Temperature 223

Fig. 119. Solar Load Case 16 Through 20 - Outer Glass Plate of a Clear IG Unit at 120 °F Outdoor Temperature 224

Fig. 120. Solar Load Case 11 Through 15 - Inner Glass Plate of a Low-E IG Unit at 120 °F Outdoor Temperature 224

Fig. 121. Solar Load Case 16 Through 20 - Inner Glass Plate of a Clear IG Unit at 120 °F Outdoor Temperature 225

Fig. 122. Solar Load Case 1 Through 5 – Effect of Solar Irradiance on Inner Glass Plate of a Low-E IG Unit at -20 °F Outdoor Temperature 226

Fig. 123. Solar Load Case 6 Through 10 - Effect of Solar Irradiance on Inner Glass Plate of a Clear IG Unit at -20 °F Outdoor Temperature 227

Fig. 124. Solar Load Case 11 Through 15 - Effect of Solar Irradiance on Outer Glass Plate of a Low-E IG Unit at 120 °F Outdoor Temperature 227

Fig. 125. Solar Load Case 16 Through 20 - Effect of Solar Irradiance on Outer Glass Plate of a Clear IG Unit at 120 °F Outdoor Temperature 228

Fig. 126. Temperature Difference Case 1 Through 15 - Effect of Indoor/Outdoor Temperature Difference on the Steady-State Response of a Low-E IG Unit 234

Page

Fig. 127. Temperature Difference Case 16 Through 30 - Effect of Indoor/Outdoor Temperature Difference on the Steady-State Response of a Clear IG Unit 234

Fig. 128. Temperature Difference Case 1 Through 15 - Effect of Indoor/Outdoor Temperature Difference on the Transient Response of the Outer Glass Plate of a Low-E IG Unit 236

Fig. 129. Temperature Difference Case 1 Through 15 - Effect of Indoor/Outdoor Temperature Difference on the Transient Response of the Inner Glass Plate of a Low-E IG Unit 237

Fig. 130. Temperature Difference Case 16 Through 30 - Effect of Indoor/Outdoor Temperature Difference on the Transient Response of the Outer Glass Plate of a Clear IG Unit 237

Fig. 131. Temperature Difference Case 16 Through 30 - Effect of Indoor/Outdoor Temperature Difference on the Transient Response of the Inner Glass Plate of a Clear IG Unit 238

Fig. 132. Temperature Difference Case 1 Through 15 - Effect of Indoor/Outdoor Temperature Difference on the Maximum Center-of-Glass Area/Perimeter-of-Glass Temperature Difference of the Outer Glass Plate of a Low-E IG Unit 238

Fig. 133. Temperature Difference Case 1 Through 15 - Effect of Indoor/Outdoor Temperature Difference on the Maximum Center-of-Glass Area/Perimeter-of-Glass Temperature Difference of the Inner Glass Plate of a Low-E IG Unit 239

Fig. 134. Temperature Difference Case 16 Through 30 - Effect of Indoor/Outdoor Temperature Difference on the Maximum Center-of-Glass Area/Perimeter-of-Glass Temperature Difference of the Outer Glass Plate of a Clear IG Unit 239

Fig. 135. Temperature Difference Case 16 Through 30 - Effect of Indoor/Outdoor Temperature Difference on the Maximum Center-of-Glass Area/Perimeter-of-Glass Temperature Difference of the Inner Glass Plate of a Clear IG Unit 240

Fig. 136. Difference in Temperature Between the Center-of-Glass and Perimeter-of-Glass as a Function of Time for the Inner Glass Plate of FEA 1 249

Page

Fig. 137. Difference in Temperature Between the Center-of-Glass and Perimeter-of-Glass as a Function of Time for the Inner Glass Plate of FEA 5 249

Fig. 138. Steady-State Response for the Outer Glass Plate with a Perfectly Insulated Frame 260

Fig. 139. Steady-State Response for the Outer Glass Plate with a High-Heat Mass Frame 261

Fig. 140. Steady-State Response for the Inner Glass Plate with a Perfectly Insulated Frame 261

Fig. 141. Steady-State Response for the Inner Glass Plate with a High-Heat Mass Frame 262

Fig. 142. Transient Response of the Outer Glass Plate with a Perfectly Insulated Frame 267

Fig. 143. Transient Response of the Outer Glass Plate with a High-Heat Mass Frame 268

Fig. 144. Transient Response of the Inner Glass Plate with a Perfectly Insulated Frame 268

Fig. 145. Transient Response of the Inner Glass Plate with a High-Heat Mass Frame 269

Fig. 146. Absorption Ratio vs. Case Number 272

Fig. 147. Natural Log of Absorption Ratio vs. Case Number 272

Fig. 148. Linear Outer Glass Plate Absorption Over Net Absorption vs. Case Number 273

Fig. 149. Statistics of Steady-State Regression Analysis Using First-Order Polynomial Model for the Outer Glass Plate with Perfectly Insulated Frame 277

Fig. 150. Error in Stress Estimation of Steady-State Regression Analysis Using First-Order Polynomial Model for the Outer Glass Plate with Perfectly Insulated Frame 277

Page

Fig. 151. Statistics of Transient Regression Analysis Using First-Order Polynomial Model for the Outer Glass Plate with Perfectly Insulated Frame 279

Fig. 152. Error in Stress Estimation of Transient Regression Analysis Using First-Order Polynomial Model for the Outer Glass Plate with Perfectly Insulated Frame 279

Fig. 153. Steady-State Regression Analysis Using First-Order Polynomial Model for the Outer Glass Plate with Perfectly Insulated Frame 280

Fig. 154. Transient Regression Analysis Using First-Order Polynomial Model for the Outer Glass Plate with Perfectly Insulated Frame 281

Fig. 155. Statistics of Steady-State Regression Analysis Using First-Order Polynomial Model for the Outer Glass Plate with High-Heat Mass Frame 282

Fig. 156. Error in Stress Estimation of Steady-State Regression Analysis Using First-Order Polynomial Model for the Outer Glass Plate with High-Heat Mass Frame 283

Fig. 157. Statistics of Transient Regression Analysis Using First-Order Polynomial Model for the Outer Glass Plate with High-Heat Mass Frame 284

Fig. 158. Error in Stress Estimation of Transient Regression Analysis Using First-Order Polynomial Model for the Outer Glass Plate with High-Heat Mass Frame 284

Fig. 159. Steady-State Regression Analysis Using First-Order Polynomial Model for the Outer Glass Plate with High-Heat Mass Frame 286

Fig. 160. Transient Regression Analysis Using First-Order Polynomial Model for the Outer Glass Plate with High-Heat Mass Frame 286

Fig. 161. Statistics of Steady-State Regression Analysis Using First-Order Polynomial Model for the Inner Glass Plate with Perfectly Insulated Frame 288

Fig. 162. Error in Stress Estimation of Steady-State Regression Analysis Using First-Order Polynomial Model for the Inner Glass Plate with Perfectly Insulated Frame 288

Page

Fig. 163. Statistics of Transient Regression Analysis Using First-Order Polynomial Model for the Inner Glass Plate with Perfectly Insulated Frame 290

Fig. 164. Error in Stress Estimation of Transient Regression Analysis Using First-Order Polynomial Model for the Inner Glass Plate with Perfectly Insulated Frame 290

Fig. 165. Steady-State Regression Analysis Using First-Order Polynomial Model for the Inner Glass Plate with Perfectly Insulated Frame 291

Fig. 166. Transient Regression Analysis Using First-Order Polynomial Model for the Inner Glass Plate with Perfectly Insulated Frame 292

Fig. 167. Statistics of Steady-State Regression Analysis Using First-Order Polynomial Model for the Inner Glass Plate with High-Heat Mass Frame 293

Fig. 168. Error in Stress Estimation of Steady-State Regression Analysis Using First-Order Polynomial Model for the Inner Glass Plate with High-Heat Mass Frame 294

Fig. 169. Statistics of Transient Regression Analysis Using First-Order Polynomial Model for the Inner Glass Plate with High-Heat Mass Frame 295

Fig. 170. Error in Stress Estimation of Transient Regression Analysis Using First-Order Polynomial Model for the Inner Glass Plate with High-Heat Mass Frame 295

Fig. 171. Steady-State Regression Analysis Using First-Order Polynomial Model for the Inner Glass Plate with High-Heat Mass Frame 297

Fig. 172. Transient Regression Analysis Using First-Order Polynomial Model for the Inner Glass Plate with High-Heat Mass Frame 297

Fig. 173. Statistics of Steady-State Regression Analysis Using Second-Order Polynomial Model for the Outer Glass Plate with Perfectly Insulated Frame 299

Fig. 174. Percent Difference vs. Number of Terms for Steady-State Regression Analysis Using Second-Order Polynomial Model for the Outer Glass Plate with Perfectly Insulated Frame 300

Page

Fig. 175. Error in Stress Estimation of Steady-State Regression Analysis Using Second-Order Polynomial Model for the Outer Glass Plate with Perfectly Insulated Frame 300

Fig. 176. Statistics of Transient Regression Analysis Using Second-Order Polynomial Model for the Outer Glass Plate with Perfectly Insulated Frame 302

Fig. 177. Percent Difference vs. Number of Terms for Transient Regression Analysis Using Second-Order Polynomial Model for the Outer Glass Plate with Perfectly Insulated Frame 302

Fig. 178. Error in Stress Estimation of Transient Regression Analysis Using Second-Order Polynomial Model for the Outer Glass Plate with Perfectly Insulated Frame 303

Fig. 179. Steady-State Regression Analysis Using Second-Order Polynomial Model for the Outer Glass Plate with Perfectly Insulated Frame 304

Fig. 180. Transient Regression Analysis Using Second-Order Polynomial Model for the Outer Glass Plate with Perfectly Insulated Frame 305

Fig. 181. Statistics of Steady-State Regression Analysis Using Second-Order Polynomial Model for the Outer Glass Plate with High-Heat Mass Frame 307

Fig. 182. Percent Difference vs. Number of Terms for Steady-State Regression Analysis Using Second-Order Polynomial Model for the Outer Glass Plate with High-Heat Mass Frame 307

Fig. 183. Error in Stress Estimation of Steady-State Regression Analysis Using Second-Order Polynomial Model for the Outer Glass Plate with High-Heat Mass Frame 307

Fig. 184. Statistics of Transient Regression Analysis Using Second-Order Polynomial Model for the Outer Glass Plate with High-Heat Mass Frame 309

Fig. 185. Percent Difference vs. Number of Terms for Transient Regression Analysis Using Second-Order Polynomial Model for the Outer Glass Plate with High-Heat Mass Frame 310

Page

Fig. 186. Error in Stress Estimation of Transient Regression Analysis Using Second-Order Polynomial Model for the Outer Glass Plate with High-Heat Mass Frame 310

Fig. 187. Steady-State Regression Analysis Using Second-Order Polynomial Model for the Outer Glass Plate with High-Heat Mass Frame 312

Fig. 188. Transient Regression Analysis Using Second-Order Polynomial Model for the Outer Glass Plate with High-Heat Mass Frame 312

Fig. 189. Statistics of Steady-State Regression Analysis Using Second-Order Polynomial Model for the Inner Glass Plate with Perfectly Insulated Frame 314

Fig. 190. Percent Difference vs. Number of Terms for Steady-State Regression Analysis Using Second-Order Polynomial Model for the Inner Glass Plate with Perfectly Insulated Frame 314

Fig. 191. Error in Stress Estimation of Steady-State Regression Analysis Using Second-Order Polynomial Model for the Inner Glass Plate with Perfectly Insulated Frame 315

Fig. 192. Statistics of Transient Regression Analysis Using Second-Order Polynomial Model for the Inner Glass Plate with Perfectly Insulated Frame 317

Fig. 193. Percent Difference vs. Number of Terms for Transient Regression Analysis Using Second-Order Polynomial Model for the Inner Glass Plate with Perfectly Insulated Frame 317

Fig. 194. Error in Stress Estimation of Transient Regression Analysis Using Second-Order Polynomial Model for the Inner Glass Plate with Perfectly Insulated Frame 317

Fig. 195. Steady-State Regression Analysis Using Second-Order Polynomial Model for the Inner Glass Plate with Perfectly Insulated Frame 319

Fig. 196. Transient Regression Analysis Using Second-Order Polynomial Model for the Inner Glass Plate with Perfectly Insulated Frame 319

Fig. 197. Statistics of Steady-State Regression Analysis Using Second-Order Polynomial Model for the Inner Glass Plate with High-Heat Mass Frame 321

Page

Fig. 198. Percent Difference vs. Number of Terms for Steady-State Regression Analysis Using Second-Order Polynomial Model for the Inner Glass Plate with High-Heat Mass Frame 321

Fig. 199. Error in Stress Estimation of Steady-State Regression Analysis Using Second-Order Polynomial Model for the Inner Glass Plate with High-Heat Mass Frame 322

Fig. 200. Statistics of Transient Regression Analysis Using Second-Order Polynomial Model for the Inner Glass Plate with High-Heat Mass Frame 324

Fig. 201. Percent Difference vs. Number of Terms for Transient Regression Analysis Using Second-Order Polynomial Model for the Inner Glass Plate with High-Heat Mass Frame 324

Fig. 202. Error in Stress Estimation of Transient Regression Analysis Using Second-Order Polynomial Model for the Inner Glass Plate with High-Heat Mass Frame 324

Fig. 203. Steady-State Regression Analysis Using Second-Order Polynomial Model for the Inner Glass Plate with High-Heat Mass Frame 326

Fig. 204. Transient Regression Analysis Using Second-Order Polynomial Model for the Inner Glass Plate with High-Heat Mass Frame 326

Fig. 205. Design Worksheet for IG Unit Thermal Stress Evaluation 330

Fig. 206. Allowable Stress for a Glass Plate with a Perimeter Length of 312 in. and a POB of 1 Glass Plate per 10,000 Glass Plates 342

Fig. 207. Allowable Stress for a Glass Plate with a Perimeter Length of 312 in. and a POB of 8 Glass Plates per 1,000 Glass Plates 342

LIST OF TABLES

Page

Table 1. Air Space Coefficient (ASHRAE 2013) 79

Table 2. Material Properties for FE Analyses 122

Table 3. Solar Optical Properties for the Exemplar Glass Plates 127

Table 4. Construction and Frame Type for the Exemplar IG Units 127

Table 5. Thermal Properties for the Exemplar IG Units 128

Table 6. Environmental Conditions Used for Exemplar IG Units 128

Table 7. FE Analysis Cases 128

Table 8. Temperature Results of FE Analyses for Exemplar IG Units 129

Table 9. Stress Results from the FE Analyses for Exemplar IG Units 129

Table 10. CEEC FE Parametric Study 149

Table 11. Results of Least-Squares Regression 151

Table 12. Gas Space Cavity Aspect Ratios for FTP Specimen Dimensions 179

Table 13. IG Units Used for the FTP Practical Application 180

Table 14. Test Specimen Dimensions 185

Table 15. Test Protocol for All Specimens 195

Table 16. CEEC for Each Specimen 200

Table 17. Percentage for Increase in Energy Exchange for Soft-Coat, Hard-Coat, and Clear Glass IG Units 204

Table 18. Specimen Dimensions for Reverse Orientation Tests 205

Table 19. Comparison of CEEC for the Low-E Coating Applied to the Number 2 and 3 Surfaces 206

Table 20. Parameters Used for Each Analysis 215

Page

Table 21. Maximum Temperature Difference Measured for Each Case 218

Table 22. Results from FE Analyses 221

Table 23. Summary of Results for Solar Load Parametric Study 225

Table 24. Absorption Properties for Practical Application 230

Table 25. Indoor/Outdoor Temperature Difference Parametric Study 233

Table 26. Table of Coefficients for Calculating the Thermal Offset, b, of an IG Unit 247

Table 27. Table of Coefficients for Calculating the Thermal Slope, m, of an IG Unit 247

Table 28. Steady-State FE Analyses for a Given Frame, Spacer, and Nominal Glass Plate Thickness 259

Table 29. Matrix of FE Analyses Required per CEEC for a Given Frame, Spacer, and Nominal Glass Plate Thickness.....266

Table 30. Summary of Steady-State Regression Analysis Using First-Order Polynomial Model for the Outer Glass Plate with Perfectly Insulated Frame 276

Table 31. Coefficients for Steady-State Model Using First-Order Polynomial Model for the Outer Glass Plate with Perfectly Insulated Frame.....276

Table 32. Summary of Transient Regression Analysis Using First-Order Polynomial Model for the Outer Glass Plate with Perfectly Insulated Frame 278

Table 33. Coefficients for Transient Model Using First-Order Polynomial Model for the Outer Glass Plate with Perfectly Insulated Frame.....278

Table 34. Overall Summary of Regression Analysis Using First-Order Polynomial Model for the Outer Glass Plate with Perfectly Insulated Frame 280

Table 35. Summary of Steady-State Regression Analysis Using First-Order Polynomial Model for the Outer Glass Plate with High-Heat Mass Frame 282

Page

Table 36. Coefficients for Steady-State Model Using First-Order Polynomial Model for the Outer Glass Plate with High-Heat Mass Frame.....282

Table 37. Summary of Transient Regression Analysis Using First-Order Polynomial Model for the Outer Glass Plate with High-Heat Mass Frame 283

Table 38. Coefficients for Transient Model Using First-Order Polynomial Model for the Outer Glass Plate with High-Heat Mass Frame.....283

Table 39. Overall Summary of Regression Analysis Using First-Order Polynomial Model for the Outer Glass Plate with High-Heat Mass Frame 285

Table 40. Summary of Steady-State Regression Analysis Using First-Order Polynomial Model for the Inner Glass Plate with Perfectly Insulated Frame 287

Table 41. Coefficients for Steady-State Model Using First-Order Polynomial Model for the Inner Glass Plate with Perfectly Insulated Frame.....287

Table 42. Summary of Transient Regression Analysis Using First-Order Polynomial Model for the Inner Glass Plate with Perfectly Insulated Frame 289

Table 43. Coefficients for Transient Model Using First-Order Polynomial Model for the Inner Glass Plate with Perfectly Insulated Frame.....289

Table 44. Overall Summary of Regression Analysis Using First-Order Polynomial Model for the Inner Glass Plate with Perfectly Insulated Frame 291

Table 45. Summary of Steady-State Regression Analysis Using First-Order Polynomial Model for the Inner Glass Plate with High-Heat Mass Frame 293

Table 46. Coefficients for Steady-State Model Using First-Order Polynomial Model for the Inner Glass Plate with High-Heat Mass Frame 293

Table 47. Summary of Transient Regression Analysis Using First-Order Polynomial Model for the Inner Glass Plate with High-Heat Mass Frame 294

Page

Table 48. Coefficients for Transient Model Using First-Order Polynomial Model for the Inner Glass Plate with High-Heat Mass Frame 294

Table 49. Overall Summary of Regression Analysis Using First-Order Polynomial Model for the Inner Glass Plate with High-Heat Mass Frame 296

Table 50. Summary of Steady-State Regression Analysis Using Second-Order Polynomial Model for the Outer Glass Plate with Perfectly Insulated Frame 298

Table 51. Coefficients for Steady-State Model Using Second-Order Polynomial Model for the Outer Glass Plate with Perfectly Insulated Frame 299

Table 52. Summary of Transient Regression Analysis Using Second-Order Polynomial Model for the Outer Glass Plate with Perfectly Insulated Frame 301

Table 53. Coefficients for Transient Model Using Second-Order Polynomial Model for the Outer Glass Plate with Perfectly Insulated Frame 301

Table 54. Overall Summary of Regression Analysis Using Second-Order Polynomial Model for the Outer Glass Plate with Perfectly Insulated Frame 303

Table 55. Summary of Steady-State Regression Analysis Using Second-Order Polynomial Model for the Outer Glass Plate with High-Heat Mass Frame 306

Table 56. Coefficients for Steady-State Model Using Second-Order Polynomial Model for the Outer Glass Plate with High-Heat Mass Frame 306

Table 57. Summary of Transient Regression Analysis Using Second-Order Polynomial Model for the Outer Glass Plate with High-Heat Mass Frame 308

Table 58. Coefficients for Transient Model Using Second-Order Polynomial Model for the Outer Glass Plate with High-Heat Mass Frame 308

Table 59. Overall Summary of Regression Analysis Using Second-Order Polynomial Model for the Outer Glass Plate with High-Heat Mass Frame 311

Page

Table 60. Summary of Steady-State Regression Analysis Using Second-Order Polynomial Model for the Inner Glass Plate with Perfectly Insulated Frame 313

Table 61. Coefficients for Steady-State Model Using Second-Order Polynomial Model for the Inner Glass Plate with Perfectly Insulated Frame 313

Table 62. Summary of Transient Regression Analysis Using Second-Order Polynomial Model for the Inner Glass Plate with Perfectly Insulated Frame 315

Table 63. Coefficients for Transient Model Using Second-Order Polynomial Model for the Inner Glass Plate with Perfectly Insulated Frame 316

Table 64. Overall Summary of Regression Analysis Using Second-Order Polynomial Model for the Inner Glass Plate with Perfectly Insulated Frame 318

Table 65. Summary of Steady-State Regression Analysis Using Second-Order Polynomial Model for the Inner Glass Plate with High-Heat Mass Frame 320

Table 66. Coefficients for Steady-State Model Using Second-Order Polynomial Model for the Inner Glass Plate with High-Heat Mass Frame 320

Table 67. Summary of Transient Regression Analysis Using Second-Order Polynomial Model for the Inner Glass Plate with High-Heat Mass Frame 322

Table 68. Coefficients for Transient Model Using Second-Order Polynomial Model for the Inner Glass Plate with High-Heat Mass Frame 323

Table 69. Overall Summary of Regression Analysis Using Second-Order Polynomial Model for the Inner Glass Plate with High-Heat Mass Frame 325

Table 70. First-Order Coefficient Table of Steady-State Response (m) 327

Table 71. First-Order Coefficient Table of Transient Response (b) 327

Table 72. Second-Order Coefficient Table of Steady-State Response (m) 328

Table 73. Second-Order Coefficient Table of Transient Response (b) 329

Page

Table 74. Practical Application Example Load Cases 331

Table 75. Summary of Temperatures from Regression Analysis Using First-Order Polynomial Model for the Inner Glass Plate 332

Table 76. Summary of Temperatures from Regression Analysis Using Second-Order Polynomial Model for the Inner Glass Plate 332

Table 77. Summary of Temperatures from Regression Analysis Using First-Order Polynomial Model for the Outer Glass Plate 333

Table 78. Summary of Temperatures from Regression Analysis Using Second-Order Polynomial Model for the Outer Glass Plate 333

Table 79. Inputs for SDP 338

Table 80. Summary of Stress from Regression Analysis Using First-Order Polynomial Model for the Inner Glass Plate 339

Table 81. Summary of Stress from Regression Analysis Using Second-Order Polynomial Model for the Inner Glass Plate 339

Table 82. Summary of Stress from Regression Analysis Using First-Order Polynomial Model for the Outer Glass Plate 339

Table 83. Summary of Stress from Regression Analysis Using Second-Order Polynomial Model for the Outer Glass Plate 339

Table 84. Allowable Stress and Risk Function vs. POB 343

Table 85. Summary of Glass ESFPM Applied to the Inner Glass Plate (First-Order Model) 344

Table 86. Summary of Glass ESFPM Applied to the Inner Glass Plate (Second-Order Model) 344

Table 87. Summary of Glass ESFPM Applied to the Outer Glass Plate (First-Order Model) 344

Table 88. Summary of Glass ESFPM Applied to the Outer Glass Plate (Second-Order Model) 344

CHAPTER I
INTRODUCTION

Window glass has been an important building component for several centuries. Over the past several decades however, the use and expectations of window glass have changed dramatically. It has evolved to become a primary structural building component, whereas previously window glass was considered a secondary structural element whose use and design was often ignored by structural engineers (AAMA 1984; McLellan and Shand 1984; Lopez-Anido et al. 2000).

Historically, windows were fabricated using a single plate of glass and were designed based on tradition and empirically generated information (AAMA 1984; Beason and Morgan 1984; Lopez-Anido et al. 2000). The use of a single plate of glass is referred to herein as a monolithic glass plate. The monolithic glass plate was typically clear with no coating, tinting, or film applied. The purpose of the monolithic glass plate was to provide a weather barrier between the indoor and outdoor environments (Turner 1977; Gordon 2001; ASHRAE 2013). The reason for using a transparent medium such as glass was to provide a connection to the outdoor environment and allow for natural light and solar irradiance to enter the indoor environment (Turner 1977; Muneer and Han 1996; Gordon 2001; Carmody et al. 2007). This connection not only helped to improve the health of the human psyche, but the quality of the indoor home and work environments as well (Turner 1977; Muneer et al. 2000).

As the uses and expectations of window glass have increased, a wide variety of factors must now be considered during the window glass design process. Among these factors are energy performance (Turner 1977; Lingnell 1981; Carmody et al. 2007), life-safety concerns, aesthetics, and basic structural adequacy (AAMA 1984; Lopez-Anido et al. 2000). In recent years, the energy performance of windows has become a particularly important factor in window glass design. The requirements promulgated by model

building codes and programs such as the Leadership in Energy and Environmental Design (LEED) have increased the demand for more energy-efficient building concepts and it is likely that this trend will continue in the future.

The primary reasons for such demands are the rising cost of energy that is associated with building operations and the supposed threat of "climate change". Approximately 40 percent of the total energy consumed in the United States (U.S.) is used in the operation of buildings, both residential and commercial (USEIA 2016). The largest contributions to the loss of energy in buildings in the U.S. are the result of inefficiencies of fenestration products including windows (Muneer et al. 1996; Ismail and Hendriquez 2005), doors, and curtain walls. Not only are these products typically less energy-efficient than the adjacent wall system, but today's buildings have larger expanses of glass systems than ever before (Lopez-Anido et al. 2000). It stands to reason that great importance has been placed on improving the energy performance of windows to increase the overall energy-efficiency of the building.

To meet these new demands for more energy-efficient windows, the use of insulating glass (IG) units has become increasingly more common in architectural glazing applications (Turner 1977; Muneer et al. 1996; Carmody et al. 2007). IG units offer several advantages over monolithic glass plates. The two primary advantages are improved sound insulation and improved thermal resistance, which limits the heat that is exchanged between the indoor and outdoor environments of a building.

IG units are fabricated from multiple plates of glass that are coupled together with a gas space cavity between the glass plates. The primary purpose of the gas space cavity is to serve as an insulating medium between the glass plates, while the two glass plates provide vapor barriers between the indoor and outdoor environments. Windows that use IG units of even the most basic construction have proven to be more energy-efficient than

windows with monolithic glass plates (Turner 1977; McLellan and Shand 1984; Lopez-Anido et al. 2000; Gordon 2001; Carmody et al. 2007).

The most common type of IG unit consists of two glass plates of equal thicknesses that are separated by a gas space cavity (Lopez-Anido et al. 2000; Muneer et al. 2000). IG units can be fabricated using various thicknesses of glass plates and can incorporate a number of different coatings, films, and tints for aesthetic and energy performance purposes. Additionally, the gas space cavity can incorporate different fill gases, spacer thicknesses, and spacer types to improve the window's energy performance (Muneer et al. 1997; Lopez-Anido et al. 2000; Carmody et al. 2007; ASHRAE 2013).

With the increase in the demand for windows that incorporate IG units, there has been an increase in glass plate breakage caused by thermal stress when compared to similar windows that incorporate monolithic glass plates. Thermal stress can be induced in glass plates through a number of mechanisms, but solar irradiance is the leading cause of thermal breakage in common applications (Beason and Lingnell 2002; ASHRAE 2013). As such, solar irradiance is the sole focus of this research.

Glass plate breakage due to thermal stress occurs when a large enough temperature difference develops across the area of a glass plate. The most common temperature difference occurs between the center of the glass plate and the perimeter of the glass plate. When the center of the glass plate is warmer than the perimeter, this temperature difference causes tensile thermal stresses to develop along the edge of the glass plate and is maximum at the perimeter of the glass plate (Sasaki 1971; Turner 1977; Wright and Barry 1999; Zhong-wei et al. 1999; Pilkington 2005; PPG 2008). If the tensile stress along the perimeter of the glass plate exceeds the breaking strength of the glass plate, breakage will result.

The first formal efforts to understand thermal breakage of glass plates were narrowly focused on windows that incorporate monolithic glass plates (Beason and Lingnell 2000; Beason and Lingnell 2002). ASTM International (ASTM) standard practice E2431, titled *"Standard Practice for Determining the Resistance of Single Glazed Annealed Architectural Flat Glass to Thermal Loadings",* provides a simplified procedure to evaluate the probability of breakage (POB) of a monolithic glass plate subjected to solar irradiance as a function of the window's frame type and edge bite (ASTM 2012a). While this procedure works well for windows that incorporate monolithic glass plates, it cannot be directly applied to windows that incorporate IG units (Klam 2007; Lingnell and Beason 2013).

A significant amount of research has been performed to understand how thermal stresses develop in IG units that are subjected to solar irradiance. However, these efforts have typically been associated with specific types of IG units under a specific set of environmental conditions. The environmental conditions of interest typically include the indoor and outdoor environments' temperatures, the surface film coefficients that develop on the indoor and outdoor surfaces of the IG unit, and the level of exposure to solar irradiance. Little effort has been expended to develop a technically defensible, analytical design procedure that can be used to evaluate the POB of glass plates in IG units that are subjected to solar irradiance.

The primary focus of this research was to develop such a design procedure. The first part of this effort was focused on developing a formal design procedure (FDP) to evaluate the POB of a glass plate in a specific IG unit subjected to a specific set of environmental conditions. The second part of this effort was focused on developing a simplified design procedure (SDP) to evaluate the POB of glass plates in generic IG units that are subjected to a general range of environmental conditions.

It is assumed for the research presented herein that the surface film coefficients for the indoor and outdoor surfaces that act on an IG unit are identical to those that act on a monolithic glass plate, if both were placed in the same environment. A monolithic glass plate exchanges heat energy with the surrounding indoor and outdoor environments through absorbed solar irradiance, conduction through the glass plate body, convection of the surrounding air, and long-wave radiation from the glass plate surfaces. This heat exchange is identical for IG units however, there is an additional heat exchange that occurs across the gas space cavity (Klam 2007; ASHRAE 2013). Heat is exchanged across the gas space cavity of the IG unit through conduction of the fill gas, natural convection of the fill gas, and long-wave radiation between the adjacent surfaces of the glass plates. Calculating the heat that is transferred through these fundamental mechanisms is complex and requires an iterative procedure. This is the case because the heat transfer mechanisms combine in a non-linear fashion (Wright 1996; Gordon 2001; Muneer et al. 1997).

As part of the FDP, a test method was developed to determine a combined energy exchange coefficient (CEEC) that can be used to linearly approximate the heat transfer through the gas space cavity of an IG unit. Use of the CEEC simplifies the thermal analysis procedure that is required for IG units by removing the need for an iterative solution (Rubin 1982; Muneer and Han 1996; Muneer et al. 2000; Gordon 2001; Klam 2007; Lingnell and Beason 2013). Instead, the use of the linear approximation allows the heat transfer calculation to be determined based on the linear temperature difference between the two glass plates. The CEEC incorporates the effects of heat transfer through conduction, natural convection, and long-wave radiation that occur across the gas space cavity of the IG unit. The CEEC is similar to the surface film coefficients that are provided in ASTM E2431 and the American Society of Heating, Refrigerating, and Air-Conditioning Engineers' (ASHRAE) *"ASHRAE Handbook: fundamentals"* and are used to model the heat that is exchanged between monolithic glass plates and the surrounding indoor

and outdoor environments (Beason and Lingnell 2002; Klam 2007; ASTM 2012a; ASHRAE 2013; Lingnell and Beason 2013).

Once the temperature distribution is defined as a function of time for the inner and outer glass plates of the IG unit, the maximum transient temperature difference between the center of the glass plate and the perimeter can be calculated for either glass plate. Knowing the maximum transient temperature, the maximum thermal stress in the IG unit's glass plates can be calculated using existing techniques that were developed for monolithic glass plates. Finally, POB can be evaluated for the individual glass plates by applying a glass edge strength failure prediction model (ESFPM) (Beason 1989; Beason and Lera 1989; Beason and Lingnell 2002).

The objective of the SDP was to develop a framework for generic procedures that can be incorporated into ASTM and/or Insulating Glass Manufacturers Alliance (IGMA) standards in a convenient form. This was accomplished using a least-squares regression-based technique performed on results generated with a large number of finite element (FE) analyses. The FE models used in this process considered the various factors that affect thermal stresses in IG units that are subjected to solar irradiance.

Ultimately, the results of this research provide a basis for new design codes, standards, and/or practices that provide a tool to evaluate the POB for glass plates in IG units that are subjected to solar irradiance. If the procedures outlined in this research are properly applied, a reasonable thermal evaluation of a common IG unit, subjected to any set of indoor or outdoor temperatures, glass plate absorptions, edge bite, or solar irradiance conditions, can be achieved.

Chapter II presents the problem statement, provides background information on IG units, and discusses the need for the research proposed. Chapter III presents a review of literature that is pertinent to the research presented herein. This includes a discussion on the

heat exchange interaction between windows and the surrounding environment. Chapter IV presents a proposed FDP that can be used to evaluate the POB of a glass plate associated with a specific IG unit subjected to a specific set of environmental conditions. This is done by coupling the CEEC with a detailed FE analysis. Chapter V presents a proposed formal test procedure (FTP) to determine a linear coefficient to approximate the combined energy exchanged across the gas space cavity of IG units. The FTP involves physical testing rather than relying on a theoretical, numerical approach to determine the CEEC. Chapter VI presents the proposed SDP that can be used by design professions to evaluate the POB of a glass plate associated with generic IG units that are subjected to a general range of environmental conditions. Finally, Chapter VII presents a summary of the research, the major conclusions, and the need for future research.

CHAPTER II
PROBLEM STATEMENT

Over the past several years, there has been an increase in the breakage of glass plates caused by thermally induced stress due to exposure to solar irradiance. More often than not, the glass plates that break are part of windows that incorporate insulating glass (IG) units. The increase in glass plate breakage is caused largely by the increasing demand for energy-efficient window systems. In most typical situations, thermal stresses that lead to glass plate breakage are the result of a difference in temperature between the center of the glass plate and the perimeter of the glass plate (Sasaki 1971; Turner 1977; Wright and Barry 1999; Zhong-wei 1999; Pilkington 2005; PPG 2008).

The behavior of monolithic glass plates subjected to thermal loads and the potential for thermal breakage have been studied in detail previously (Beason and Lingnell 2000; Beason and Lingnell 2002; ASTM 2012a). In recent times, the use of monolithic glass plates has been reduced significantly. This is due in large part to the increased use of more energy-efficient windows. Thus, windows incorporate fewer and fewer monolithic glass plates as the solution for meeting the new, more rigorous energy-efficiency requirements for both residential and commercial architectural glazing applications is to employ IG units (Lopez-Anido et al. 2000; Carmody et al. 2007).

The first step to develop a deeper understanding of the effects of thermal load on IG units is to understand the design methodologies that are currently recommended for use in the design of monolithic glass plates and how they relate to the design of IG units. When a monolithic glass plate is subjected to solar irradiance it absorbs a certain percentage of the solar irradiance. The portion of solar irradiance absorbed is then converted to heat energy. In addition, heat transfer occurs between the monolithic glass plate and the surrounding indoor and outdoor environments. The heat that is transferred

between the monolithic glass plate and the surrounding environment occurs via the fundamental heat transfer mechanisms of conduction, convection, and long-wave radiation from the interior and exterior surfaces of the monolithic glass plate.

Surface film coefficients are used to combine the effects of the three heat transfer mechanisms for the design of monolithic glass plates (Beason and Lingnell 2002; ASTM 2012a). The surface film coefficients provide a single, linear coefficient that can be used to describe the heat transfer between the interior and exterior surfaces of a monolithic glass plate and the indoor and outdoor environments, respectively (Beason and Lingnell 2002; ASHRAE 2013). ASTM E2431 provides standardized surface film coefficients for use in monolithic glass design (Beason and Lingnell 2002; ASTM 2012a). Fig. 1 shows a monolithic glass plate and the interaction with the surrounding indoor and outdoor environments through the use of surface film coefficients. The surface film coefficients, as presented in ASTM E2431, represent the design condition to conservatively evaluate the maximum thermal stress in monolithic glass plates (Beason and Lingnell 2002; ASTM 2012a). The indoor surface film coefficient represents a typical indoor heat exchange condition and the outdoor surface film coefficient represents a sheltered outdoor heat exchange condition.

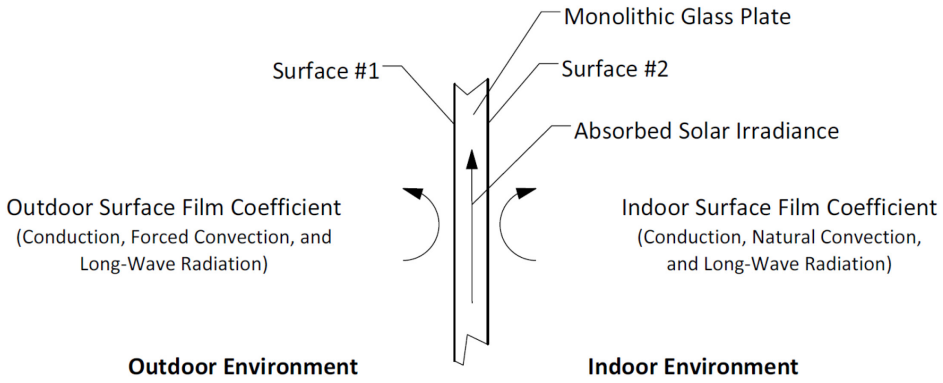

Fig. 1. Surface Film Coefficients for Use in Monolithic Glass Plate Design

The first step to evaluate the probability of breakage (POB) for a monolithic glass plate subjected to solar irradiance is to determine the variation in temperature between the center and the perimeter of the glass plate as a function of time. This is referred to herein as the transient temperature. The maximum stress that is typically associated with thermal breakage occurs along the perimeter of the glass plate and is proportional to the maximum temperature difference between the center of the glass plate and the perimeter of the glass plate (Wright and Barry 1999; Zhong-wei et al. 1999; Pilkington 2005).

ASTM E2431 presents a simplified, standard practice that can be used to evaluate the design thermal stress and POB for a monolithic glass plate subjected to solar irradiance (ASTM 2012a). In addition, ASTM E2431 includes provisions to calculate the design thermal stress and the POB for various types of window frames and edge bite dimensions (ASTM 2012a). While this procedure is concise and user-friendly for monolithic glass plates, the standard practice cannot be directly extended to include applications that employ IG units (Klam 2007; Lingnell and Beason 2013). This is due in large part because of the effect that the heat exchanged through the gas space cavity of the IG unit has on the variation in temperatures across the areas of the glass plates (El Sherbiny et al. 1982b; Wright 1996; Muneer et al. 1997; Klam 2007; Lingnell and Beason 2013).

In the simplest and most common form, IG units are fabricated using two glass plates that are coupled together with a single gas space cavity between the two glass plates (Lopez-Anido et al. 2000; Muneer et al. 2000). While not as common, IG units can be fabricated with more than two glass plates and multiple gas space cavities. IG units with more than two glass plates are typically limited to the northern latitudes that experience extreme cold climates (Lopez-Anido et al. 2000; Carmody et al. 2007). The research discussed herein is focused solely on IG units fabricated using two rectangular glass plates that are separated by a single gas space cavity. The gas fill is typically air, argon, or krypton (PPG 2001; Carmody et al. 2007; ASHRAE 2013; Pilkington 2013b). The

research herein is solely focused on the use of air as the fill gas. Fig. 2 shows a corner-cut-away of a simple IG unit and window assembly.

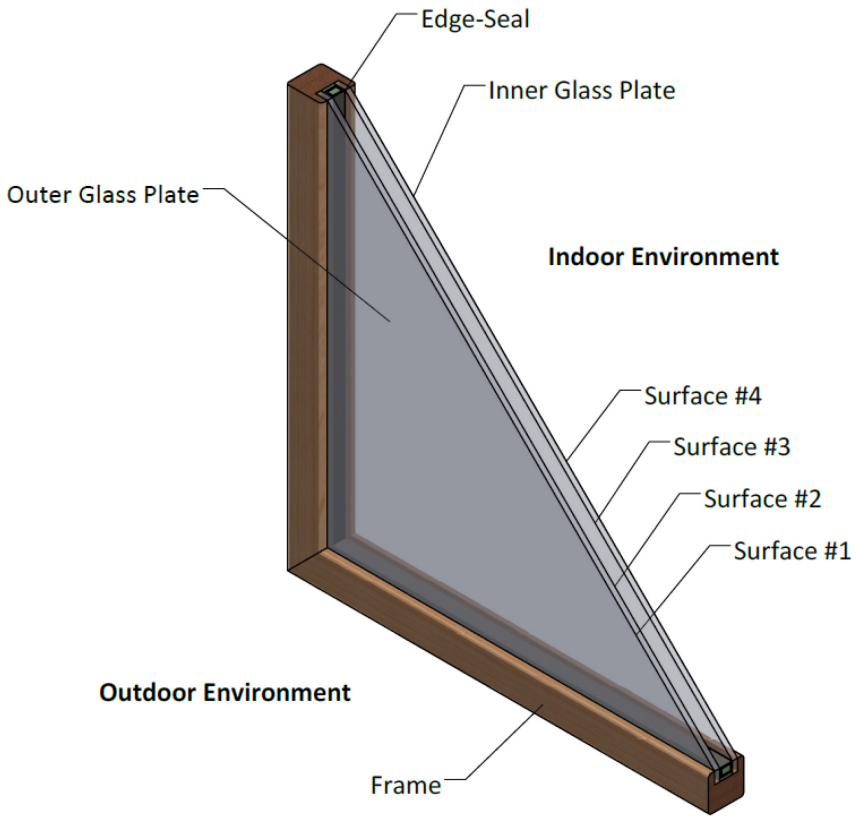

Fig. 2. Corner-Cut-Away of a Typical IG Unit

As shown in Fig. 2, the typical window system is comprised of the IG unit and a frame system around the edges. There are a large number of framing systems that are used in windows to encase the IG unit. These frames are manufactured using various materials and geometries. The most common materials that are used for window frames are wood, polyvinyl chloride (PVC) or vinyl, aluminum, composites, and fiberglass (ASHRAE 2013; Carmody et al. 2007). Additionally, some frames are hybrids that contain a mixture of the aforementioned materials. Frames often represent a large percentage of the

total area of the window assembly. Thus, the energy performance of a window is directly dependent on the energy performance of the window's frame. The heat that is transferred through a window's frame is primarily dependent on the material of the frame.

Perhaps the most common window frame is made from aluminum. Aluminum can be manufactured into any number of complex shapes using an extrusion process. Aluminum is a light, but strong and durable framing system. The primary disadvantage to aluminum frames is that it readily transfers heat. This leads to issues not only with thermal performance, but condensation as well. Some aluminum frames employ a "thermal break" by separating the frame into an interior and exterior region. These regions are connected using a material with improved resistance to heat flow over that of aluminum (ASHRAE 2013).

Historically, the most common window frame material was wood (Carmody et al. 2007). Wood-framed windows are typically viewed as the most aesthetically pleasing and the thermal performance of the wood frame is exceptional compared to aluminum. The primary disadvantage of a wood frame is its low resistance to weathering, moisture penetration, warpage, and organic degradation from insects and mold (ASHRAE 2013).

In recent years, the use of vinyl, fiberglass, composites, and hybrid materials has increased. The primary reasons for the increased use of these materials are improvements in manufacturing capabilities, increased thermal performance to that of aluminum, and reduced costs compared to that of wood frames. Frames that employ these types of materials may or may not contain air cavities or voids within the frame. Frames that do contain air cavities within the frame can be thermally improved by reducing the size of the air cavities to take advantage of reduced heat transfer due to convection. The thermal performance can be further improved by filling these air cavities with an insulating

material such as foam. In general, fiberglass and vinyl-framed windows, whether thermally improved or not, are viewed to provide the best overall thermal performance within the architectural glass industry (Carmody et al. 2007; ASHRAE 2013).

For the IG units considered as part of this research, the outer glass plate was exposed to the outdoor environment and the inner glass plate was exposed to the indoor environment. Surface number 1 (#1) and 4 (#4) would be associated with the outer glass plate's surface directly exposed to the outdoor environment and the inner glass plate's surface directly exposed to the indoor environment, respectively. Surface number 2 (#2) and 3 (#3) would be associated with the outer and inner glass plates' surfaces that are directly exposed to the gas space cavity, respectively. For a monolithic glass plate, the number 1 and 2 surfaces would be directly exposed to the outdoor and indoor environments, respectively.

Almost all of the windows with IG units that are installed in the U.S. have low emissivity (low-E) coatings applied to at least one surface of the IG unit (ASHRAE 2013). Typically, low-E coatings are applied to either the number 2 or 3 surface of an IG unit depending on the geographical region which it is used (Carmody et al. 2007; ASHRAE 2013). Applying the low-E coating to one of the interior surfaces of the IG unit serves to protect the coating from in-service mechanical exposures. For IG units, the low-E coating acts to significantly reduce the heat that is transferred across the gas space cavity due to long-wave radiation. This is often the most significant mechanism of heat transfer for IG units (Gordon 2001; Carmody et al. 2007).

Fig. 3 shows a cross-section detailing the primary components of an IG unit. An IG unit is fabricated with an inner and outer glass plate which are coupled together using an edge-seal. The edge-seal includes a spacer, primary and secondary sealants, and gas space desiccant. The spacer is the structural component that is used to maintain the spatial relationship between the outer and inner glass plates of the IG unit. Therefore, the

gas space thickness is constant across the IG unit and is a function of the width of the spacer. Additionally, the spacer provides an adhesion surface for the primary and secondary seals.

There are a large number of spacers that are used in IG units. These spacers have varying geometries and are made from a number of materials including stainless steel, galvanized steel, tin-plated steel, polymers, foamed silicone, aluminum, etc. The rate of heat transfer around the edge of an IG unit through the edge-seal is primarily dependent on the spacer's geometry and material properties. In recent years, the concept of warm-edge spacers has been introduced to minimize heat transferred through the spacer (Carmody et al. 2007; ASHRAE 2013).

The purpose of the primary seal is to isolate the gas space cavity from the surrounding environment. The secondary seal is located on the backside of the spacer and extends between both the outer and inner glass plates. It serves to protect the primary seal from water and oils. In addition, it serves as the structural bond between the glass plates and the spacer. The seals are typically polyisobutylene (PIB), polysulfide, polyurethane, silicone, or a combination of two. The most common sealant combination is PIB as the primary sealant and silicone as the secondary sealant. Moisture that is trapped in the gas space cavity during the manufacturing process is removed by the gas space desiccant (Beason 1986b; ASHRAE 2013).

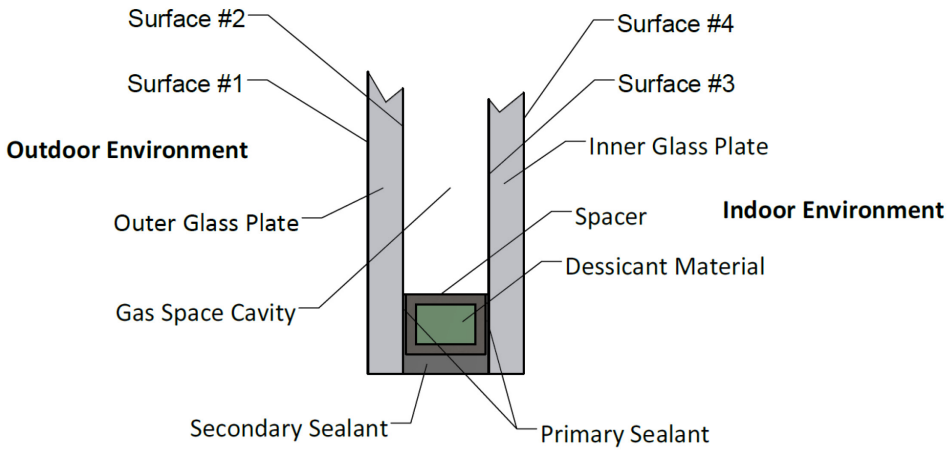

Fig. 3. Cross-Section of an IG Unit's Primary Components

The primary purpose of the research presented herein was to develop a new, simplified procedure that design professionals can use to evaluate the POB for a glass plate in an IG unit that is subjected to solar irradiance. The first part of this effort was focused on developing a formal design procedure (FDP) for evaluating the thermal stress and POB of glass plates in a specific IG unit that is subjected to a specific set of environmental conditions.

As part of the FDP, a test method was developed to experimentally measure a combined energy exchange coefficient (CEEC) that can be used to linearly approximate the heat transfer through the gas space cavity of an IG unit. Using the CEEC simplifies the thermal analysis procedure that is required for IG units by removing the need for an iterative solution (Rubin 1982; Muneer and Han 1996; Muneer et al. 2000; Gordon 2001; Klam 2007; Lingnell and Beason 2013). Using the CEEC, the heat transfer is based on the linear temperature difference between the two glass plates. The CEEC acts to combine the effects of heat transfer through conduction, natural convection, and long-wave radiation across the gas space cavity of the IG unit. The CEEC is similar to that of the surface film coefficients that are provided in ASTM E2431 which describe the heat that is ex-

changed between monolithic glass plates and the surrounding indoor and outdoor environments (Beason and Lingnell 2002; Klam 2007; ASTM 2012a; Lingnell and Beason 2013).

It is reasonable to assume that the surface film coefficients for the number 1 and 4 surfaces of an IG unit and the number 1 and 2 surfaces of a monolithic glass plate that are both exposed to the same indoor and outdoor environmental conditions are the same (Klam 2007). Therefore, the surface film coefficients that are provided in ASTM E2431 and developed for monolithic glass plates can be used for the design of IG units if directly applied to the number 1 and 4 surfaces (ASTM 2012a).

Once the temperature distributions across the areas of the inner and outer glass plates of the IG unit are defined as a function of time, the maximum difference in temperature between the center of the glass plate and the perimeter can be calculated for each glass plate. Knowing this maximum difference in temperature, the maximum thermal stress in the glass plates can be calculated using existing techniques that are used to calculate thermal stresses in monolithic glass plates. Finally, POB can be evaluated for the glass plates by applying a glass edge strength failure prediction model (ESFPM) (Beason 1989; Beason and Lera 1989; Beason and Lingnell 2002).

The second part of this effort was focused on developing a simplified design procedure (SDP) that can be used to evaluate the POB for a glass plate in a generic IG unit that is subjected to a general range of environmental conditions. The objective for developing the SDP was to develop a framework for generic procedures that can be incorporated into ASTM and/or IGMA standards in a convenient equation based form. This was accomplished using a least-squares regression-based technique on the results of a large number of finite element (FE) analyses. The models used in these FE analyses consider the various factors that affect thermal stresses in IG units subjected to solar irradiance.

Ultimately, the results of this research provide a basis for new design procedures that would allow design professionals to evaluate the POB of IG units subjected to solar irradiance. If the procedures outlined as part of this research are properly applied, a reasonable thermal evaluation of a common IG unit, subjected to any set of indoor and outdoor temperatures, glass plate absorptances, edge bite, or solar irradiance conditions, can be achieved.

This dissertation focuses on verifying these procedures for two different types of frames and a thin, steel-channel spacer. The two frames considered were perfectly insulated and high-heat mass. The selection of high-heat mass and perfectly insulated frames provide the upper and lower theoretical boundaries for the maximum and minimum thermal stresses, respectively, that may develop in IG units. If the research performed herein is applied to a commercially available frame it should perform somewhere between the boundaries of a perfectly insulated frame and a high-heat mass frame.

The thin, steel-channel spacer was selected due to its wide commercial availability. In addition, the spacer is commonly used for IG units that are installed in typical architectural glazing applications. Both the geometry and material properties of the spacer used were well described. The research performed herein can be easily applied to another spacer if the material properties and the geometry are known.

Finally, IG units with 0.25 in. thick nominal glass plates were considered. In addition, it was assumed that the thickness of the inner and outer glass plates were equal. The research performed herein can be easily applied to IG units with different nominal glass plate thicknesses if each are assumed to be equal.

CHAPTER III
LITERATURE REVIEW

As a brittle material, special considerations must be taken when glass is used as a structural material. Specifically, it is important to understand the structural behavior of the glass material when exposed to stress. This is particularly important for architectural glazing applications where window systems that employ glass plates will be exposed to situations of extreme temperature differentials that induce thermal stress. The phenomenon that causes thermal stress has long been understood for monolithic glass plates. However, in recent times thermal breakage has become one of the leading causes of window glass failure in buildings that employ insulating glass (IG) units (Beason and Lingnell 2002).

Glass Plates Subjected to a Uniform Change in Temperature

When a glass plate is subjected to a uniform change in temperature it will expand or contract in all directions. When the temperature of the glass plate decreases, it will contract in all directions. When the temperature of the glass plate increases, it will expand in all directions. The overall change in dimension, $\delta_{Thermal}$, in any direction depends on the coefficient of thermal expansion and is proportional to the change in temperature and the original length, as given by Eq. (1) (Gere and Timoshenko 1997; Beer et al. 2012).

$$\delta_{Thermal} = \alpha_T \cdot \Delta T \cdot L_0 \tag{1}$$

Where α_T is the coefficient of thermal expansion of the glass plate, ΔT is the uniform change in temperature with positive being an increase in temperature and negative being a decrease in temperature, and L_0 is the original length before the change in temperature. The coefficient of thermal expansion is a characteristic of the glass plate's material and is taken to be 4.9×10^{-6} (in./in.)/˚F (AAMA 1984).

For a given glass plate the significant expansion given by Eq. (1) is taken to occur in two dimensions. For example, consider a glass plate with original dimensions of 60 in. by 96 in. This is a common size that is used for vision glass in architectural glazing applications. If the temperature of the glass plate increases by 100 °F, it will expand by 0.0294 in. in the direction of the short dimension and 0.0470 in. in the direction of the long dimension. Thus, the dimensions of the expanded glass plate, after heating, are 60.0294 in. by 120.0470 in. While the small increase in length may seem insignificant, it can be of great consequence if the expansion is not accommodated using proper glazing techniques. If the glass plate is supported properly such that the edges are not restrained and are allowed to slip freely in the plane of the glass plate, the glass plate will expand freely and no stresses will develop (Gere and Timoshenko 1997; Pilkington 2005; Beer et al. 2012). This support condition is associated with glass plates that are said to be four side simply (or continuously) supported and represent the typical window application (Beason and Morgan 1984).

The normal strain, ε, along the length of a bar subjected to an axial load can be calculated using Eq. (2).

$$\varepsilon = \frac{\delta}{L_0} \tag{2}$$

Where δ is the deformation of the bar due to the axial load and L_0 is as previously defined.

By substituting Eq. (1) into Eq. (2), the thermal strain, $\varepsilon_{Thermal}$, caused by the change in temperature in an unrestrained glass bar can be calculated, as given by Eq. (3).

$$\varepsilon_{Thermal} = \alpha_T \cdot \Delta T \tag{3}$$

Where all of the variables are as previously defined.

While thermal stresses cannot develop if the glass bar is unrestrained, internal thermal stresses will develop if the ends of the glass bar are restrained. As the temperature of the glass bar increases uniformly, it can no longer expand freely due to the restraints imposed at the ends. Therefore, the overall change in length, $\delta_{Thermal}$, due to the increase in temperature, as given by Eq. (1), must be zero. In addition, the thermal strain, $\varepsilon_{Thermal}$, due to the increase in temperature, as given by Eq. (2), must also be zero. Thus, the glass bar is subjected to a state of stress with zero strain because of the imposed end restrains (Gere and Timoshenko 1997; Beer et al. 2012).

As defined, stress, σ, is the force per unit area that a material experiences when subjected to load, as given by Eq. (4).

$$\sigma = \frac{P}{A} \tag{4}$$

Where P is the applied load and A is the unit area.

The magnitude of the stress caused by the change in temperature in the restrained glass bar can be calculated by solving the statically indeterminate problem using the superposition method. This requires solving the compatibility equation knowing that the total deformation must be zero. The thermal stress, $\sigma_{thermal}$, in the restrained glass bar due to a change in temperature can be calculated using Eq. (5).

$$\sigma_{thermal} = -E \cdot \alpha_T \cdot \Delta T \tag{5}$$

Where E is the modulus of elasticity and all other variables are as previously defined. The modulus of elasticity of plate glass is typically taken to be 10.4×10^6 psi (AAMA 1984; Beason and Lingnell 2002). The significance of the minus sign shows that the thermal stress will be compressive if the temperature increases and tensile if the temperature decreases. As presented, Eq. (5) can be used to calculate the thermal stress for a

uniform change in temperature of prismatic bars (i.e. uniform cross-section) with a constant modulus of elasticity and coefficient of thermal expansion.

Eq. (5) can be extended for use in flat rectangular plates, as given by Eq. (6) (Young and Budynas 2002).

$$\sigma_{thermal} = -\frac{E \cdot \alpha_T \cdot \Delta T}{(1 - v)} \tag{6}$$

Where v is poisson's ratio and all other variables are as previously defined. Poisson's ratio for plate glass is typically taken to be 0.22 (AAMA 1984). Thus, if the edges of the 60 in. by 96 in. glass plate described in the previous example are restrained, the internal compressive stress induced in the glass plate would be 6,533 psi. This level of stress could pose a serious risk of breakage if it were tensile stress.

As shown, the thermal expansion of monolithic glass plates under typical temperature changes is relatively small. So-long-as a glass plate is installed properly with the correct glazing techniques, which allow for in-plane slippage of the glass plate, in-plane thermal stresses do not develop as a result of uniform temperature changes. Therefore, in-service glass plate breakage does not typically occur due to the occurrence of a uniform change in temperature. Rather, glass plate breakage due to thermal stresses is caused by differential temperature changes across the glass plate area (Beason and Lingnell 2002; Pilkington 2005; PPG 2008).

Glass Plates Subjected to a Differential Change in Temperature

Glass plate breakage caused by thermally induced stress is initiated by tensile stresses that exceed the breaking strength of the glass plate. Typically, these tensile stresses occur at the perimeter of the glass plate. The most common cause of such tensile stresses is the result of thermal expansions that occur when the center of the glass plate resides at

a higher temperature than the edge of the glass plate (i.e. differential change in temperature across the area of the glass plate) (Sasaki 1971; Pilette and Taylor 1988).

The classic example that is used to describe the design condition for thermal stress in glass plates is that of a cold winter night. Both the center of the glass plate and the edge of the glass plate areas cool to a steady-state of heat transfer with the outdoor and indoor environments during the night. As the sun slowly rises in the morning, the center of the glass plate is exposed to solar irradiance and begins to absorb solar energy uniformly through the thickness (Pilette and Taylor 1988). The energy that is absorbed is converted into heat (Beason and Lingnell 2002). This heat input raises the temperature of the exposed glass plate area (i.e. any area of glass plate exposure to the sun). As the exposed area is heated it begins to expand in all directions. Meanwhile, a portion of the edge of the glass plate is shielded from the direct solar irradiance by the frame and remains at or near the previous night's temperature.

The heat transfer process is said to be in steady-state when the temperatures across the area and through the thickness of the glass plate do not change as a function of time. This is not the same as the thermal equilibrium state. Thermal equilibrium requires a state of zero heat transfer (Datta 2002). Thus, for thermal equilibrium to occur, the temperature of the glass plate must be equal at all locations. Rather, in the steady-state condition that occurs during the night-time, heat can continue to flow at a constant rate due to the difference in indoor and outdoor temperatures. During steady-state, neither temperature nor heat transfer rate change as a function of time (Datta 2002). Where temperature or heat transfer rates are a function of time, it is an unsteady-state. This is referred to herein as the transient state.

A portion of the edge of the glass plate is typically shielded by the use of a framing system, glazing bead, and/or a fillet of glazing sealant. Thus, the temperature along the edge of the glass plate will rise at a much slower rate than that of the center area of the

glass plate. Therefore, the expansion along the edge of the glass plate will be much slower than the expansion in the center of the glass plate. These differential rates of expansion cause compressive stresses to form in the center of the glass plate and tensile stresses to form along the edge of the glass plate and are maximum along the perimeter of the glass plate (Sasaki 1971; Turner 1977; Pilette and Taylor 1988; Beason and Lera 1989; Wright and Barry 1999; Beason and Lingnell 2002).

Fig. 4 is a photograph of a residential window taken one morning immediately following sunrise, after a warm summer night. The window incorporated an IG unit. While this photograph was not taken on a morning after a cold winter night, it does provide a clear example of the difference in temperature that develops between the center and edge areas of a glass plate. The cold temperature in the center of the glass plate allowed condensation to form, while the warmer edge area prevented any condensation from forming.

Fig. 4. Example of Differential Temperature Across a Glass Plate Area

The fact that thermal breakage is most often observed during winter conditions is most likely due to the solar irradiance being maximized during winter months in the northern hemisphere. Additionally, the sun's angle of elevation in the winter is such that the incident solar irradiance is greater, with respect to vertical glass plates, than during the summer months. While it is generally perceived that the winter months provide a more optimum opportunity for thermal breakage, thermal stresses can become critical during any time given the proper conditions (Beason and Lingnell 2002).

Fig. 5 shows the principle areas of a monolithic glass plate or IG unit that are used to define the typical thermal regions (Carmody et al. 2007). These areas include the center-of-glass, edge-of-glass, and the perimeter-of-glass. The center-of-glass area is the region that is typically heated when exposed to solar irradiance. This area rapidly expands due to the increase in temperature, but is restrained by the cooler edge-of-glass area. This interaction induces compressive stresses in center-of-glass area. While the edge-of-glass area remains cooler in temperature and expands at a slower rate, the faster expansion of the center-of-glass area stretches the perimeter of the glass plate into tension. Thus, the perimeter-of-glass is the extreme edge of the glass plate and is where the maximum tensile stresses develop due to thermal loading. The edge-of-glass area defines the transition region from the perimeter of the glass plate to the center-of-glass area. Currently, the edge-of-glass region is taken to be 2.5 in. from the perimeter of the glass plate (Finlayson et al. 1993; ISO 2003). This area is seemingly meaningless for the purpose of calculating thermal stress. It is typically only used to estimate steady-state heat flow through the window assembly for estimating building energy use.

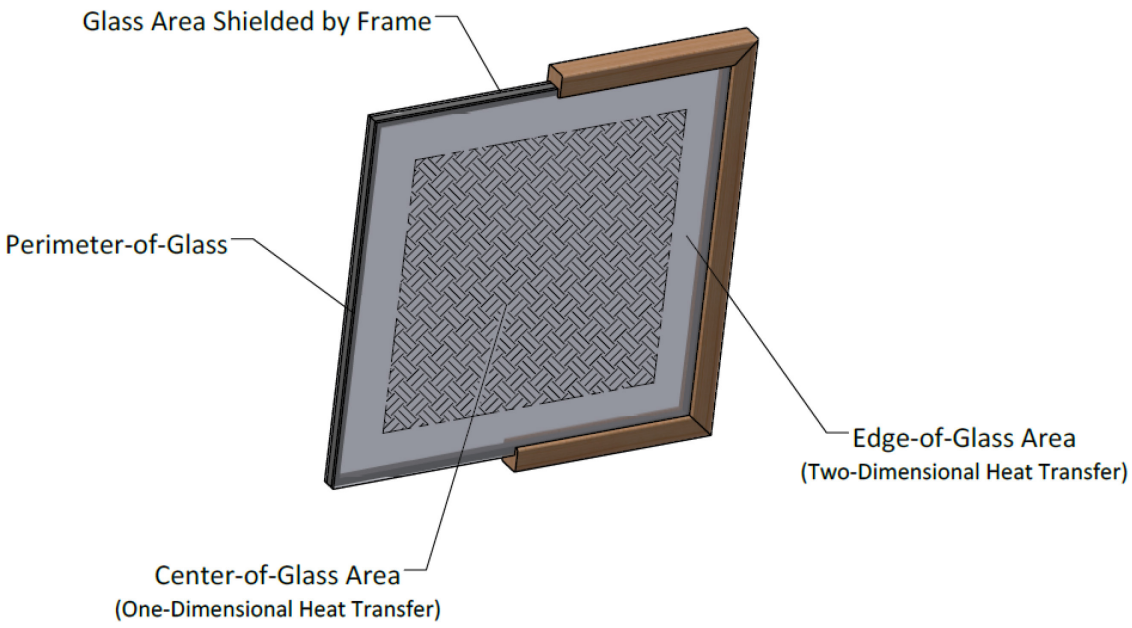

Fig. 5. Principle Thermal Areas Considered for Glass Plates

Thermal Stress in Monolithic Glass Plates

It is commonly accepted that the maximum thermal stress, σ_{max}, that occurs along the perimeter of a monolithic glass plate exposed to solar irradiance can be calculated using Eq. (7) (Turner 1977; Pilette and Taylor 1988; Wright and Barry 1999; Zhong-wei et al. 1999; Pilkington 2005).

$$\sigma_{max} = \alpha_T \cdot E \cdot (T_{COG} - T_{POG}) \tag{7}$$

Where T_{COG} is the center-of-glass temperature, T_{POG} is the perimeter-of-glass temperature, as discussed previously and shown in Fig. 5, and all other variables are as previously defined. Pilkington (2005; 2013c) goes so-far-as to introduce a constant called the "coefficient of thermal stress", which is expressed in units of psi per ºF, that can be multiplied by the difference in temperature between the perimeter of the glass plate and the

center of the glass plate to determine the maximum tensile thermal stress along the perimeter of the glass plate. While this value is slightly lower than multiplying the coefficient of thermal expansion by the modulus of elasticity, it does provide a close approximation.

Thermal stresses that develop due to a temperature differential across the glass plate area (i.e. the center-of-glass and perimeter-of-glass) manifest themselves as in-plane or membrane stresses (Beason 1989; Beason and Lera 1989; Beason and Lingnell 2002). Thus, the stress is constant through the glass plate's thickness and the edge is subjected to either uniform tension or uniform compression (Beason 1989; Beason and Lera 1989; Beason and Lingnell 2002). Further, bending stresses that develop as a result of a temperature differential through the glass plate's thickness have been shown to be negligible compared to the membrane stresses that develop along the perimeter of the glass plate (Pilette and Taylor 1988). An examination of a stress block along the perimeter of a glass plate is shown in Fig. 6. It is clear that the perimeter of the glass plate must be in uniaxial tension or compression due to the fact that all stress components on the free surfaces of the stress block must be zero (Beason 1989; Beason and Lera 1989; Beason and Lingnell 2002).

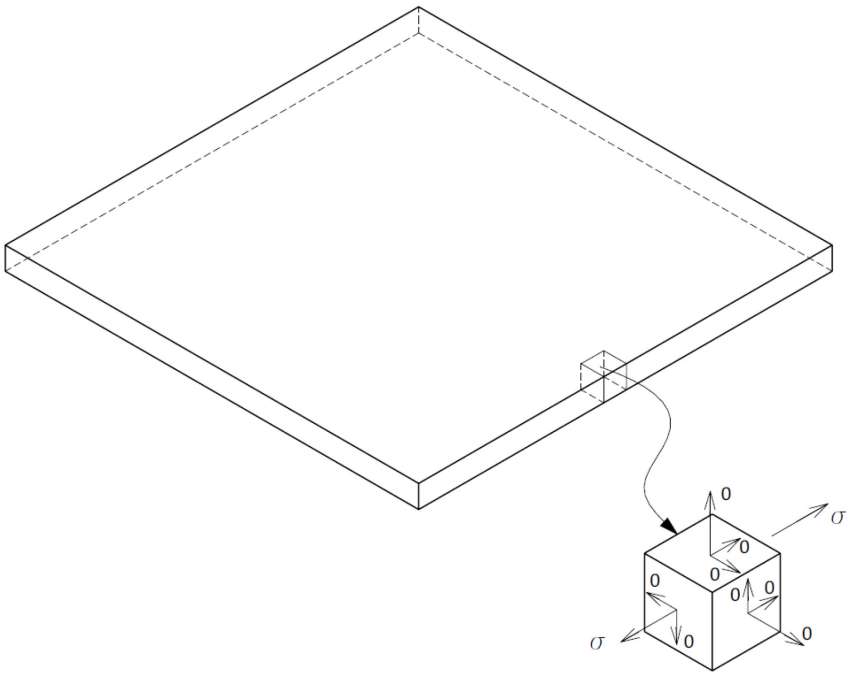

Fig. 6. Thermal Stress Block Along the Perimeter of a Glass Plate

Because thermal stresses manifest themselves as membrane stresses, the stress is constant through the glass plate's thickness and the edge is subjected to either uniform tension or uniform compression (Beason 1989; Beason and Lera 1989; Beason and Lingnell 2002). Thus, glass breakage due to thermal stresses can be identified by a crack normal to both the vertical and horizontal projections of the glass plate's edge (Beason 1989; Beason and Lera 1989; Zhong-wei et al. 1999). This fracture pattern is idealized in Fig. 7.

Upon initiating at the perimeter of the glass plate, the crack propagates inward. As the crack propagates inward it begins to branch. Branching is caused by the more complex stress states that occur in the interior of the glass plate as it fractures. The direction and number of the cracks depend on the local states of stress at the time of branching. Fig. 8 shows an actual thermal breakage of the inner glass plate of an IG unit.

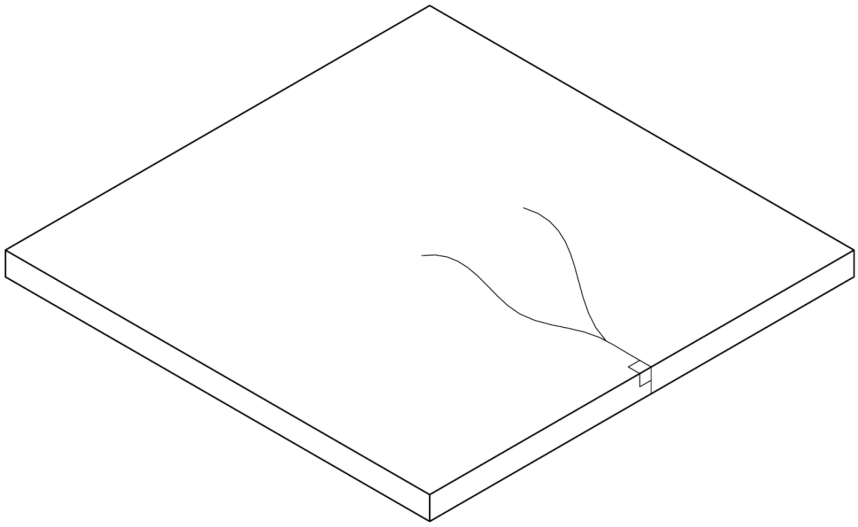

Fig. 7. Idealized Fracture Pattern of a Monolithic Glass Plate due to Thermal Stress

Fig. 8. Glass Plate Breakage due to Thermal Stress

In most instances, glass plates are assumed to have a support system which allows the edges of the glass plate to slip freely in the plane of the glass plate, while the edges are prevented from movement perpendicular to the surface of the glass plate. As mentioned previously, this is consistent with glass plates installed in typical frames that provide for four-sides of continuous lateral support (Beason and Morgan 1984).

As previously discussed, when external restraints are applied such that the edges of the glass plate are prevented from slipping in the plane of the glass plate or rotating about the edge of the glass plate, additional stress states can occur and must be accounted for. Both the magnitude and distribution of thermal stress are influenced by the support conditions of the glass plate (Beason and Lingnell 2002). It is assumed for the research herein that the glass plates are supported in a typical frame that provides four-sides of continuous lateral support. It is also assumed that no external restraints are applied and the edges of the glass plate are allowed to slip freely in the plane of the glass plate and rotate about the edge of the glass plate allowing for normal thermal expansions and contractions.

Clearly, the effects of thermal stress on IG units are more complex than that of monolithic glass plates. Previous research has been performed to determine what effect coupling two monolithic glass plates together has on the IG unit's structural and thermal performance as a whole. This previous research is discussed below.

Thermal Stress in Insulating Glass Units

For monolithic glass plates the initial temperature condition of the glass plate has little effect on the occurrence or severity of thermal stress so-far-as it is in a steady-state of heat transfer prior to being exposed to solar irradiance (Beason and Lingnell 2002; Klam 2007; Lingnell and Beason 2013). The severity of thermal stress in monolithic glass plates is dependent on the solar energy absorbed, the frame support conditions, and the surface film coefficients which describe the heat exchanged between the monolithic glass plate and the surrounding indoor and outdoor environments (Beason and Lingnell 2002).

This is not the case for IG units due to the thermal bridging that occurs across the IG unit's spacer. Thermal bridging increases the heat flow that occurs between the inner

and outer glass plates' edges through the edge-seal. The resistance to heat flow in the center-of-glass area is significantly higher when compared to that of the edge-of-glass (Sasaki 1971). This causes an increase in the temperature difference between the center-of-glass and the perimeter-of-glass compared to that of a monolithic glass plate if placed in the same indoor and outdoor temperature conditions (Pilette and Taylor 1988; Klam 2007; Lingnell and Beason 2013). Therefore, if all of the factors are held constant, the level of maximum thermal stress that a glass plate in an IG unit experiences will be larger than that induced in a monolithic glass plate (Klam 2007; Lingnell and Beason 2013).

Additionally, it seems plausible that the thermal bridging provides the potential for bending stresses to develop along the glass plates' edges. As the heat transfers from one glass plate to the other, it is possible that a temperature gradient could form through the thicknesses of one or both of the glass plates. However, it has been shown that such bending stresses and causal temperature gradients through the thicknesses of each glass plate are negligible (Pilette and Taylor 1988).

In addition to the effects of thermal bridging, the spacer provides the potential to change the flexibility of the support conditions of the IG unit's glass plates from the traditional support system assumed for a monolithic glass plate. Thermal expansion and contraction of the two glass plates will cause shearing stresses to develop in the glazing components (i.e. sealants, gaskets, etc.) as well as the spacer. Consequently, this can have an effect on the stress conditions that develop along the edges of the glass plates. As mentioned previously, both the magnitude and distribution of thermal stresses are influenced by the glass plates' support conditions (Beason and Lingnell 2002). Research has shown however, that these stresses can also be ignored as they are negligible compared to the overall membrane tensile stresses that develop along the perimeter of the glass plate due to thermal stress (Pilette and Taylor 1988). This is due to the flexibility of the spacer and primary and secondary sealants of the IG unit. Further, previous research has shown

that the thermal stresses that develop along the perimeter of the glass plate are independent of the structural properties of the gasket, spacer, or sealants for the ranges of values commonly used in architectural glazing applications (Pilette and Taylor 1988).

Thus, in-plane forces and bending moments due to solar irradiance are not transmitted between the inner and outer glass plates of an IG unit (Pilette and Taylor 1988). Further, the temperature gradients measured through each glass plates' thicknesses were small and produced negligible bending stresses (Pilette and Taylor 1988). Ultimately, it has been shown that the maximum thermal stress for both monolithic glass plates and glass plates employed in IG units is proportional to the temperature difference between the center-of-glass and the perimeter-of-glass and can be calculated using Eq. (7) stated previously (Turner 1977; Pilette and Taylor 1988; Wright and Barry 1999; Zhong-wei et al. 1999; Pilkington 2005). Further, each glass plate employed in an IG unit can be evaluated separately using this same equation.

The thermal stress measured along the perimeter of the glass plate was found to be independent of the physical geometry of the IG unit for aspect ratios and areas common for architectural glazing applications (Pilette and Taylor 1988). Albeit, the overall size will have an effect on the probability of breakage (POB) of the glass plate. This is the case because there is an increased risk of the edge stress along a large glass plate interacting with a critical flaw compared to a small glass plate with the same level of stress (Turner 1977; Beason and Lingnell 2002). This will be discussed in more detail later.

Other Considerations for Thermal Stress in Insulating Glass Units

Often within the glass industry, design professionals mistakenly want to consider the combined effects of a thermal design condition and lateral pressure loads. There are two reasons this approach is in error. First, the thermal design condition requires near still air (i.e. no significant wind speed) to develop the maximum thermal stress. This will be

discussed in more detail later. Secondly, it has been shown that the tensile stresses that develop due to lateral pressure loads, such as wind, occur in the center and corner areas of the glass plate (Pilette and Taylor 1988; Beason and Lera 1989), whereas the maximum tensile stresses from thermal loads occur along the middle-region along the edges of the glass plate and away from the corner areas. For lateral loads, the stresses in this middle-region have been shown to be in compression. Thus, it can be conservatively assumed that the effects of each situation be considered separately (Pilette and Taylor 1988; Beason and Lera 1989).

Note that for the case of IG units, lateral pressure loads can be induced not only by wind, but as the result of atmospheric pressure changes, altitude changes, and/or changes in the temperature of the gas space cavity. Because the gas that is used to fill the gas space cavity behaves as an ideal gas (Beason 1986a), an increase in temperature or decrease in the atmospheric pressure surrounding the IG unit will cause the unit to bulge. Alternatively, a decrease in gas space temperature or increase in the atmospheric pressure surrounding the IG unit will cause the unit to contract. The effects that a change in temperature and/or pressure of the gas fill have on an IG unit is more pronounced with small units that have relatively stiff glass plates (Lopez-Anido et al. 2000).

For the research discussed in this dissertation, it would seem particularly important to consider the effect associated with a change in temperature of the gas space cavity. However, lateral pressures caused by the mechanisms aforementioned behave in the same manner structurally as lateral pressure from wind (Beason 1986a; Beason 1986b; Beason and Lera 1989). While it is important to consider these mechanisms and their effect on the wind load resistance of an IG unit, it is a convenient fact that the effects of these mechanisms can be considered independent of the effects of thermally induced stresses (Beason and Lera 1989).

A second consideration that must be considered when evaluating thermal stress in monolithic glass plates and IG units are shadows and interior reflective devices. Shadows are often caused by deep mullions, building overhangs, shading canopies or awnings, nearby buildings, etc. and have a significant effect on both the magnitude and distribution of thermal stresses that develop in glass plates. Fig. 9 shows an example of an exterior canopy casting a shadow on a window with an IG unit. The thermal fracture shown previously in Fig. 8 was a photograph of the inner glass plate of the same IG unit. The total effect that the shadow has on the magnitude of the thermal stress depends on several factors such as its size, location, and the shadow's shape that is cast on the glass plate. It has been shown that shadows which create a "V" or "L" shape on the glass plate are the most critical for design (Beason and Lingnell 2000). When a shadow is present, the maximum thermal stress typically occurs at the intersection of the shadow line and the edge of the glass plate (Pilette and Taylor 1988). It can be observed from Fig. 9 that shadows tend to be dynamic and move throughout the day with the sun.

Fig. 9. Shadow Pattern Cast on an Exemplar IG Unit

Interior reflective devices are typically used to control solar heat gain in the indoor environment. Common examples of interior reflective devices that are used are Venetian blinds, some types of window treatments such as draperies, and roller shades (Wright and Kotey 2006). These devices alter the overall optical properties of the IG unit and can act to increase the temperature of one or both glass plates by increasing the solar energy that the glass plates are exposed to (Turner 1977; Beason and Lera 1989; Wright and Barry 1999; Wright and Kotey 2006).

The portion of the solar irradiance that is transmitted through the IG unit strikes the interior reflective device and a portion of this energy is reflected back to the IG unit and a portion is absorbed by the interior reflective device. This inter-reflection and absorption

of the energy continues in this manner until all of the reflected solar irradiance is absorbed or transmitted. The increase in the amount of solar energy that is absorbed is a function of several factors including the transmission properties of the IG unit and the reflectivity of the interior reflective device, its orientation, and geometry. In addition, these devices act to reduce the surface film coefficient and hold heat along the inner glass plate's surface (Turner 1977). While this is not an all-inclusive list, interior reflective devices add significant complexity to the design process. This is especially true for IG units where a ray tracing procedure must be employed to determine the amount of solar energy absorbed by each glass plate. This will be discussed in more detail later. While it is possible to have an exterior reflective device these are typically not as common.

Another type of interior reflective device, which also includes a shading component, that is becoming increasingly more common are blinds incorporated in the gas space cavity of the IG unit. Depending on the orientation of the blinds, they can reflect some degree of solar irradiance to the outer glass plate while providing some level of shading to the inner glass plate. In addition to the reflective and shading consideration of blinds located in the gas space cavity, the convection that occurs inside of the gas space cavity is disrupted and/or the long-wave radiation that occurs between the two glass plates is significantly altered. This is a very complex situation to analyze and many variables must be considered.

Situations where shadows and interior reflective devices are used are often non-obvious and require special considerations. It is difficult to capture the effects that shadows and interior reflective devices have on thermal stress in a general design procedure for IG units. As such, the effects of shadows and interior reflective devices were not considered as part of the research herein.

The following section discusses background information on solar irradiance and the fundamental heat transfer mechanisms of conduction, convection, and long-wave radiation as they apply to the heat exchanged between monolithic glass plates and the surrounding environment. Included is a discussion that details the use of surface film coefficients to design monolithic glass plates. This is followed by a discussion of energy exchange between IG units and the surrounding environment.

Heat Exchange Between Monolithic Glass Plates and the Surrounding Environment

When a monolithic glass plate is taken from a state of thermal equilibrium at a room temperature of 70 ºF and is exposed to solar irradiance, the temperature of the glass plate will quickly rise. This change in temperature is due to the interaction of the monolithic glass plate with the surrounding environment. The heat exchange that occurs between the monolithic glass plate and the surrounding environment follows the first law of thermodynamics. The first law of thermodynamics states that for a closed system, energy is conserved. The concept of energy conservation can be applied to a closed system using Eq. (8) (Datta 2002; Bergman et al. 2011).

$$\dot{E_{in}} - \dot{E_{out}} + \dot{E_{generated}} = \dot{E_{stored}} \tag{8}$$

Where $\dot{E_{in}}$ is the rate of energy entering the closed system, $\dot{E_{out}}$ is the rate of energy exiting the closed system, $\dot{E_{generated}}$ is the rate of energy generated by the closed system, and $\dot{E_{storage}}$ is the rate of energy being stored by the closed system.

The closed system in this case is the monolithic glass plate. The monolithic glass plate does not consume or generate energy. Thus, the change in internal energy of the mono-

lithic glass plate can be defined as the difference between the energy that enters the monolithic glass plate and the energy that exits the monolithic glass plate. Thus, Eq. (8) is reduced to Eq. (9).

$$\dot{E_{in}} = \dot{E_{out}} \tag{9}$$

Where all of the variables are as previously defined.

Solar irradiance from the sun inputs energy into the monolithic glass plate. As the energy enters, it generates internal heat and raises the temperature of the monolithic glass plate. Heat is exchanged between the monolithic glass plate and the surrounding indoor and outdoor environments. The heat exchanged with the surrounding indoor and outdoor environments can be quantified using the three fundamental heat transfer mechanisms of conduction, convection, and long-wave radiation (Muneer et al. 2000; Beason and Lingnell 2002; ASHREA 2013).

The conditions of the indoor and outdoor environments have a great effect on the temperatures that develop across the area of the monolithic glass plate as a function of time. The solar irradiance that is absorbed by the monolithic glass plate is converted into heat. This conversion acts to raise the temperature of the monolithic glass plate. Heat is continuously exchanged between the monolithic glass plate and the outdoor environment through conduction, forced convection, and long-wave radiation. Concurrently, heat is continuously exchanged between the monolithic glass plate and the indoor environment through conduction, natural convection, and long-wave radiation. This heat exchange contributes to the transient temperatures experienced by the monolithic glass plate as a function of time when subjected to solar irradiance (Muneer et al. 2000; ASHREA 2013). Fig. 10 illustrates the energy exchange process between a monolithic glass plate and the surrounding indoor and outdoor environments.

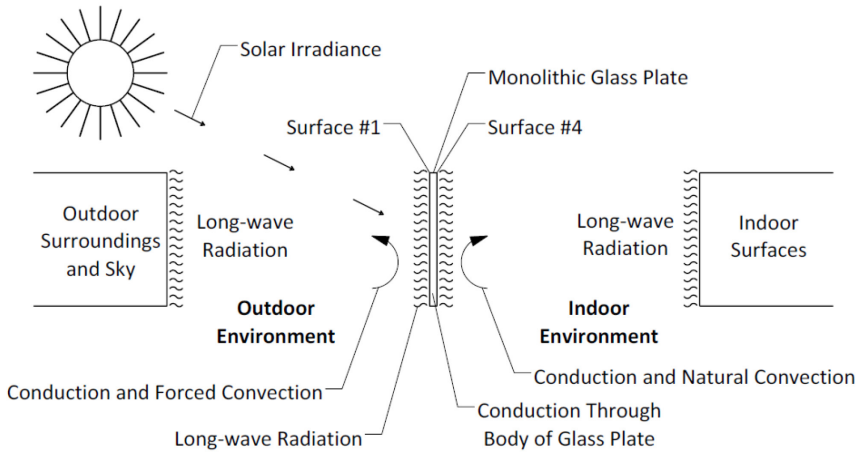

Fig. 10. Energy Exchange for a Monolithic Glass Plate with the Surrounding Indoor and Outdoor Environments

Certain environmental conditions must be defined before a thermal analysis can be performed on a monolithic glass plate that is exposed to indoor and outdoor environments and subjected to solar irradiance. These environmental conditions include the effective indoor and outdoor temperatures and the indoor and outdoor surface film coefficients.

The effective outdoor temperature is defined as the average temperature of the outdoor environment. This includes all objects such as the sky, ground, buildings, greenery, etc. The effective indoor temperature is defined as the average temperature of the indoor environment. This includes the average temperatures of all objects such as the walls, floors, ceilings, furniture, etc. In practice, the effective indoor and effective outdoor temperatures are taken to be the indoor and outdoor ambient air temperatures, respectively (ASHRAE 2013). These are referred to herein simply as the indoor temperature, T_{indoor}, and the outdoor temperature, $T_{outdoor}$.

The indoor surface film coefficient is used to combine the effects of the three heat transfer mechanisms of conduction, natural convection, and long-wave radiation for the indoor environment into a single linear term. This term can then be multiplied by the temperature difference between the effective indoor temperature and the temperature of

the monolithic glass plate to give the heat that is exchanged between the two. The outdoor surface film coefficient is used to combine the effects of the three heat transfer mechanisms of conduction, forced convection, and long-wave radiation for the outdoor environment into a single linear term. This term can then be multiplied by the temperature difference between the effective outdoor temperature and the temperature of the monolithic glass plate to give the energy that is exchanged between the two (ASHRAE 2013).

Solar Irradiance Applied to Monolithic Glass Plates

The sun is the primary source of energy for the Earth (NASA 2008). It follows that the most common mechanism by which thermal load is applied to window glass plates would involve the sun (ASHRAE 2013). While there are a number of mechanisms that can input heat into window glass plates, experience suggests that the breakage of glass plates due to thermal stress is most often the result of heat generated by the sun (Beason and Lingnell 2002). Thus, an accurate thermal analysis of window glass plates, be it monolithic or IG units, must be predicated on a clear understanding of the heat transfer mechanism that the sun imposes on an object near the Earth's surface.

In general, radiation describes the transmission of electromagnetic energy (i.e. travelling waves of electric and magnetic fields) through space at the speed of light (Halliday et al. 2005). This exchange of energy can occur between two objects and/or an object and its environment. Radiation is categorized into bandwidths of wavelengths that form what is known as the electromagnetic spectrum. There are many forms of electromagnetic radiation that exists at wavelengths from long-wave radio to X-rays and Gamma rays (Halliday et al. 2005). Thermal radiation is a specific subset of wavelengths that are loosely defined from 0.1 μm to 100 μm (Bergman et al. 2011). Fig. 11 presents the electromagnetic spectrum. Thermal radiation is further categorized into two wavelength ranges. These ranges are short-wave radiation and long-wave radiation. Long-wave radiation is

typically associated with bodies at temperatures near ordinary ambient temperatures. Ordinary ambient temperatures are those found near the Earth's surface. Long-wave radiation operates at wavelengths greater than 3 µm (Gordon 2001).

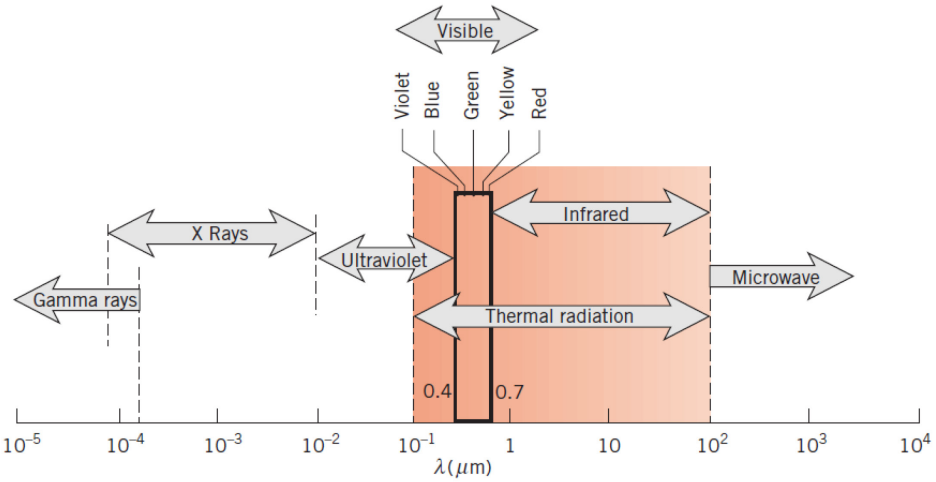

Fig. 11. Electromagnetic Spectrum (Bergman et al. 2011)

Short-wave radiation describes radiation energy that has its origin from the sun. Thus, short-wave radiation is often called solar radiation. Short-wave radiation, at Earth's surface, is described as having wavelengths from approximately 0.3 µm to 3.0 µm (Gordon 2001). The distribution of spectral short-wave radiation outside Earth's atmosphere output by the sun is shown in Fig. 12 as a function of wavelength. These data are shown for the mean Sun-Earth distance and a solar constant of 7.8005 (in.·lb/s)/in.^{2} (ASTM 2014).

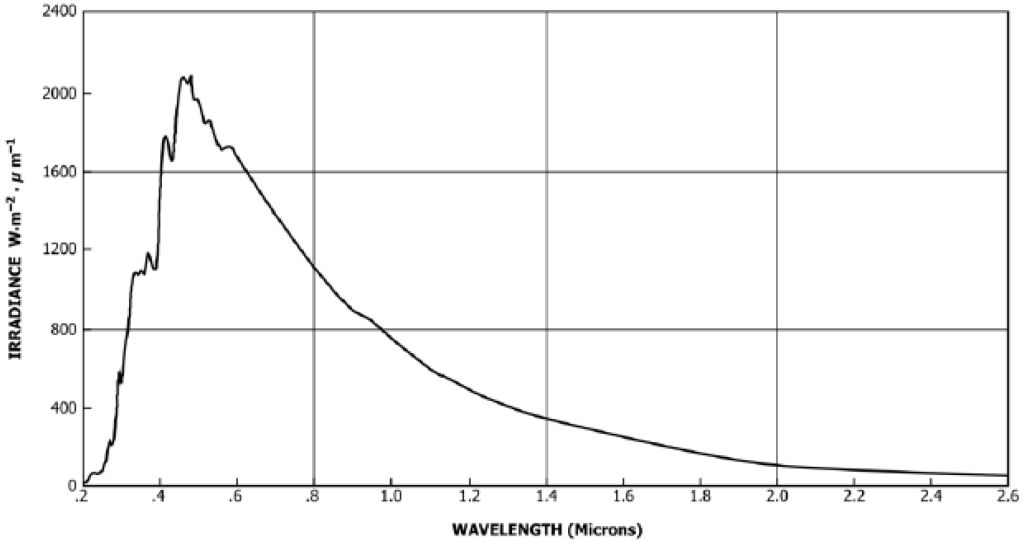

Fig. 12. Standard Solar Irradiance Spectrum (ASTM 2014)

At the outset of Earth's atmosphere, the sun's radiant energy is at a near fixed intensity known as the solar constant, I_{SC}. The current accepted value for the solar constant is 7.8005 (in.·lb/s)/in.^{2} (ASTM 2014) and varies by approximately 3 percent (Duffie and Beckman 1974) over a year timeframe. This value is determined by integrating the sun's radiant energy over the entire range of wavelengths that are shown in Fig. 12. The solar constant represents the flux of electromagnetic radiant energy per unit area received incident (i.e. perpendicular) to a surface located in space at the mean distance between the Earth and Sun (Duffie and Beckman 1974; ASHRAE 2013). The variation in this intensity is associated with the change in distance from Earth's mean distance from the Sun.

Earth's atmosphere plays an important role in attenuating the sun's radiant energy into the usable form we know at Earth's surface (NASA 2008). The radiant energy that arrives at Earth's surface is a function of atmospheric scattering and absorption (Duffie and Beckman 1974). These effects result in an attenuation of the radiation. Thus, Shortwave Radiation arrives at Earth's surface in two forms, beam radiation and diffuse radiation (Duffie and Beckman 1974).

In particular, the sun emits short-wave radiation that can be classified by bandwidths within the visible, ultra-violet, and near-infrared spectrum. Of the sun's energy that reaches Earth's surface, approximately 5 percent is ultra-violet, 40 percent visible light, and 55 percent near-infrared (Gordon 2001). The wave lengths for ultra-violet, visible, and near infrared are $0.3\ \mu m < \lambda < 0.4\ \mu m$, $0.4\ \mu m < \lambda < 0.7\ \mu m$, and $0.7\ \mu m < \lambda < 2.5\ \mu m$, respectively (Gordon 2001).

Solar irradiance, I_s, is taken herein as the sun's radiant energy imposed on a surface of unit area, integrated over all wavelengths and measured at Earth's surface (NASA 2008). In addition, solar irradiance is taken as the sum of the beam and diffuse short-wave radiation on a surface. An approximate maximum solar irradiance that was measured as part of this research at the surface of Earth on a clear day in Texas is 5.7105 $(in.\cdot lb/s)/in.^2$.

Solar irradiance causes solar heat gain in glass plates. Solar heat gain is proportional to the intensity of sunlight (i.e. the level of solar irradiance) and to the amount of energy absorbed by the glass plate (i.e. the glass plate's absorptance coefficient). When a glass plate is subjected to solar irradiance, a portion of the energy is reflected back into the outdoor environment by the glass plate. Another portion of the energy is transmitted through the glass plate and into the indoor environment. The remaining energy is absorbed by the glass plate itself. This process is shown in Fig. 13.

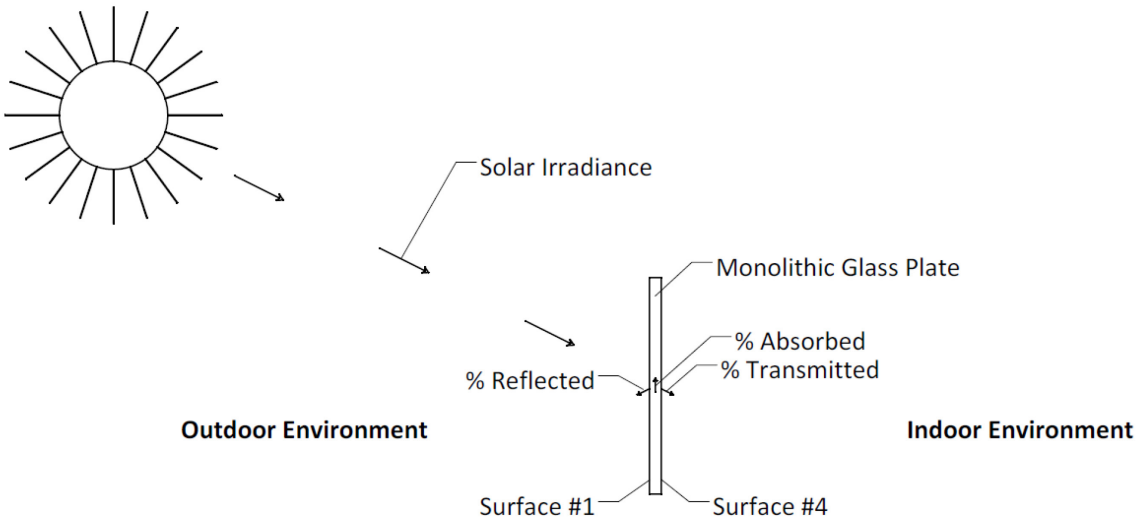

Fig. 13. Solar Reflectance, Absorptance, and Transmittance of a Monolithic Glass Plate

Fig. 14 shows an example of the effect absorption can have on monolithic glass plates when installed in windows. Fig. 14 was taken on a cold winter morning just after sunrise in Texas. The glass plates that were used in the window were true divided, tinted monolithic glass plates, with the exception of the center glass plate which had been previously replaced with a clear glass plate. The tinted glass plates have a higher absorptance coefficient than that of the single clear glass plate. As a result, the levels of solar heat gain in the tinted glass plates were greater than the clear glass plate and the temperatures of the tinted glass plates increased to a level capable of melting the frost that had formed on the window. As shown, the frost remained on the clear glass plate after it had melted from the tinted glass plates.

Fig. 14. Residential Window with Different Solar Absorptances

Once a glass plate has been manufactured, the fabricator can determine the optical properties for the specific type of glass material, plate thickness, and its construction (i.e. applied coatings, tints, films, and etc.). These optical properties are typically published information that is used to quantify the portion of solar irradiance energy that is reflected, absorbed, and transmitted. The three primary optical properties of interest are the solar reflectance, ρ_S, solar transmittance, τ_S, and the solar absorptance, α_S. The relationship between these optical properties is given by Eq. (10), where given any two properties the third may be calculated (Muneer et al. 2000; Gordon 2001; Bergman et al. 2011; ASHRAE 2013).

$$\alpha_S + \rho_S + \tau_S = 1 \tag{10}$$

Interestingly enough glass plates are spectrally selective, meaning that the optical properties are wavelength-dependent and vary across the electromagnetic spectrum. The optical properties also vary with the angle of incidence with the glass plate. The angle of incidence is defined as the angle at which a line-of-action of an optical ray makes with the perpendicular normal of the glass plate's surface at the point of incidence.

Conveniently, it has been shown that the changes in optical properties are of little consequence for incidence angles less than 40 degrees. Since this represents the case of window glass, glass manufacturers typically provide optical properties taken as an average over an entire spectrum of wavelengths when the angle of incidence is zero (i.e. normal to the glass plate's surface). In addition, since the solar spectrum remains relatively constant, the spectrum average is taken over the entire solar spectrum (Gordon 2001; ASHRAE 2013). These measured optical data for most glass manufactured in the U.S. have been conveniently cataloged in the International Glazing Database (IGDB 2016) which is maintained by the Lawrence Berkeley National Laboratory (LBNL).

The temperature of a monolithic glass plate increases when it is exposed to solar irradiance. This change in temperature is caused by the portion of solar irradiance absorbed by the glass plate. Heat is then transferred between the glass plate and the indoor and outdoor environments through the three fundamental heat transfer mechanisms. These mechanisms include heat transfer through conduction, convection, and long-wave radiation and each are discussed below.

Conduction

Conduction is used to quantify the molecule to molecule transfer of heat through a solid, liquid, or gas medium. The molecular energy of an object is proportional to the object's temperature. Therefore, an object's molecular energy increases if its temperature increases. Likewise, an object's molecular energy decreases if its temperature decreases.

The transfer of thermal energy follows the second law of thermodynamics which states that the total entropy of a closed system will never decrease. It can remain constant, if ideal, or increase with time. Simply, this means that energy is transferred from molecules with higher energy states to molecules with lower energy states (Datta 2002; Bergman et al. 2011).

For gases, the mechanism through which heat is transferred is rotational, translational, and/or vibrational energy of the molecules. For solids and liquids, the rotational and translational motion of molecules is restricted, and heat is transferred through vibrational energy of the molecules alone. Because higher temperatures yield a higher molecular level, energy flows from bodies with higher temperatures to bodies with lower temperatures. This phenomenon defines the diffusion or conduction of heat. The rate of conduction is quantified by an object's thermal conductivity, k. Thermal conductivity is the measure of an object's efficiency of heat conduction and can range from a good conductor to an insulator. A good conductor has a high rate of heat transfer and a large value of k. An insulator has a low rate of heat transfer and a small value of k. (Datta 2002; Bergman et al. 2011).

The rate of one-dimensional, steady-state heat transfer by conduction through an object is calculated using Fourier's law of conduction, as shown in Eq. (11) (Datta 2002; Bergman et al. 2011).

$$\frac{q_{conduction}}{A} = \frac{k}{L} \cdot \left(T_j - T_k\right) \tag{11}$$

Where $q_{conduction}$ is the heat transferred by conduction in the transverse direction, A is the cross-sectional area perpendicular to the direction of the heat flow, L is the length of heat flow, T_j and T_k are the temperatures of surfaces j and k when a medium is differentially heated, and k is the thermal conductivity of the medium.

Eq. (11) can be used to describe conduction through a medium if the thermal conductivity remains constant with respect to temperature, the material is isotropic, and the assumption that heat flows in only one-dimension is valid. If any of these properties or assumption are not true, as is the case for two-dimensional steady-state conduction, a finite difference or finite element (FE) method is required to determine the conduction through a medium (Datta 2002; Bergman et al. 2011).

To calculate heat flow through a medium with respect to time, the specific heat, C_p, and density, ρ_m, must be known for the medium. Both the density and specific heat of the medium make up the "thermal mass" of the system. The specific heat defines the amount of energy that is required to raise the temperature of a unit mass one degree. Simply, the thermal conductivity defines the ease of heat flow through a medium, whereas the specific heat describes how resistant the medium is to a change in temperature (Datta 2002; Bergman et al. 2011).

Heat is conducted through both the body of a monolithic glass plate and the air surrounding the glass plate. In the center-of-glass area, as shown in Fig. 5, heat transfer is primarily perpendicular to the plane of the glass plate. For practical purposes, this is considered to be one-dimensional heat flow. Describing the heat flow in the edge-of-glass area is more complex. For practical purposes, this area is considered to be in a state of two-dimensional heat flow (Wright and Sullivan 1989; Finlayson 1993; Wright 1998; Gordon 2001; ASHRAE 2013). As such, heat flow in the center-of-glass area can be calculated using Fourier's law of conduction, as provided in Eq. (11). Heat flow through the edge of the glass plate must be calculated using a finite difference or FE method.

The heat flow that occurs between the interface of the surface of the monolithic glass plate and the surrounding air is typically calculated using a surface film coefficient. The

surface film coefficient combines the effects of conduction and convection into a single linear term (ASHRAE 2013). This is discussed in more detail later.

Convection

Convection describes heat transfer that occurs when a fluid comes in contact with an object's surface that resides at a higher temperature than the surrounding fluid. The fluid can be in the form of either liquid or gas. The two types of convective heat flow are forced convection and natural convection.

Convection is the cumulative heat transferred from a combination of two heat transfer mechanisms. These mechanisms are conduction through random molecular motion and conduction through bulk fluid motion. As such, heat flow due to convection is described by a differential equation that involves both conduction and fluid motion. Modeling heat flow using the explicit form of the convective differential equation is complex and requires the use of powerful computational fluid dynamics (CFD) software (Manz 2003; Gustavsen et al. 2005; Abbey 2014). More often, boundary layer approximations are combined with experimentally developed correlations to simplify and solve the convective heat flow equations. As such, it is often assumed that a velocity boundary layer and a temperature boundary layer form between the surface of the object and the bulk fluid during convection (Datta 2002; Bergman et al. 2011). These boundary layer approximations are discussed in detail below.

As fluid flows across the surface of an object, it is characterized by two distinct regions, the velocity boundary layer and the free stream layer. The velocity boundary layer contains large velocity gradients due to shearing stresses, τ, in the fluid. The free stream layer occurs just outside the velocity boundary layer where the velocity gradients and shearing stresses in the fluid are negligible (Datta 2002; Bergman et al. 2011).

When a fluid flows across a surface during convection it is typically assumed that the fluid velocity, u, decreases asymptotically from the free stream velocity, u_∞, to zero at the surface. The distance over which the fluid velocity has reached 99 percent of the free stream velocity is referred to as the velocity boundary layer thickness, δ, as given by Eq. (12). The velocity boundary layer is illustrated in Fig. 15.

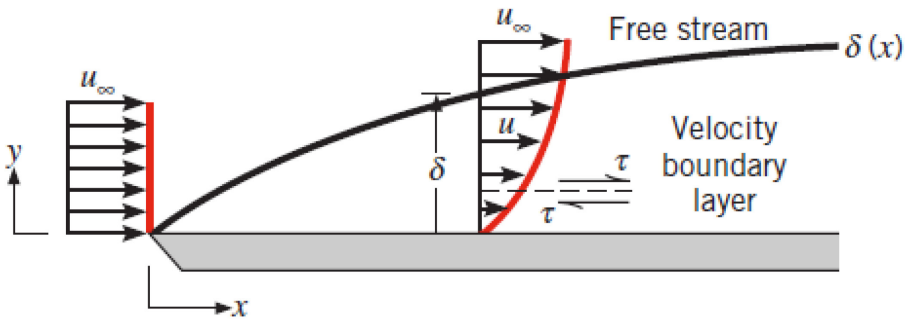

Fig. 15. Velocity Boundary Layer Across a Flat Plate (Bergman et al. 2011)

$$\delta = y|_{u=0.99*u_\infty} \tag{12}$$

The change in fluid velocity occurs due to shear stress between layers of particles. The particles at rest along the surface impede the motion of the adjacent layer of particles. These particles impede the motion of the next layer of particles and so on. At the velocity boundary layer thickness, the effects of these shear stresses become negligible. For most practical applications, including problems involving convection across a glass plate, the significant effects of convection occur within the velocity boundary layer (Datta 2002; Bergman et al. 2011).

When a temperature difference exists between the surface and the bulk fluid, a temperature boundary layer also forms. The temperature boundary layer behaves similar to the

velocity boundary layer. The temperature of the fluid, T, decreases asymptotically from the temperature at the surface, T_s, to the free stream temperature, T_∞. The thickness, δ_t, of the temperature boundary layer is determined using the ratio given in Eq. (13). The temperature boundary layer is illustrated in Fig. 16.

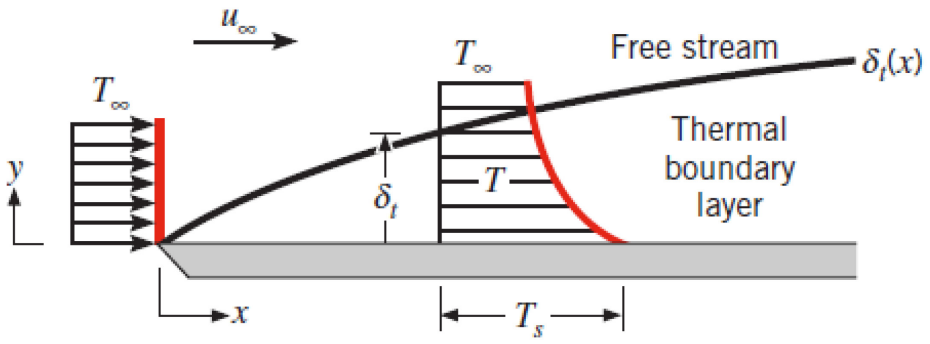

Fig. 16. Temperature Boundary Layer Across a Flat Plate (Bergman et al. 2011)

$$\frac{(T_S - T)}{(T_S - T_\infty)} = 0.99 \tag{13}$$

The variation in temperature across the temperature boundary layer affects the thermal properties of the fluid. The viscosity, density, and thermal conductivity of the fluid vary as a function of temperature. Thus, these properties will vary across the temperature boundary layer and influence the rate of heat transfer. This is treated in a simple way by calculating an average temperature between the bulk fluid and surface temperatures. This average temperature is called the film temperature. The film temperature, T_{film}, is used to describe the thermal properties of the fluid (Datta 2002; Bergman et al. 2011).

For monolithic glass plates, the film temperature is taken to be the average temperature between the surface of the glass plate and the temperature of the environment that it is directly exposed to, as given by Eq. (14).

$$T_{film} = \frac{T_{glass} + T_{environment}}{2} \tag{14}$$

Where T_{glass} is the temperature of the glass plate surface and $T_{environment}$ is the temperature of the surrounding environment.

Using these two simplifying assumptions for the velocity and temperature boundary layers, a convective heat transfer coefficient, $h_{convection}$, can be calculated. The convection coefficient is typically expressed in terms of a dimensionless quantity termed the Nusselt number. The basic equation for the convection coefficient is shown in Eq. (15).

$$h_{convection} = \frac{Nu \cdot k_{fluid}}{L} \tag{15}$$

Where L is the characteristic length of the surface, k_{fluid} is the thermal conductivity of the bulk fluid, and Nu is the Nusselt number that describes a dimensionless temperature gradient at the surface. For the case of monolithic glass plates, the characteristic length would be the distance across the surface of the glass plate that is parallel to the flow of the bulk fluid. Since the convection coefficient, by definition, combines the effects of conduction and convection into a single term, the minimum value for the Nusselt number is taken to be unity which represents the case of heat transfer through pure gaseous conduction across stagnant air (Wright 1996).

Natural convection occurs when a surface is exposed to a bulk fluid that resides at a different temperature. The temperature of the fluid immediately adjacent to the warmer surface begins to rise through conduction. As the fluid is heated, it begins to expand. The expansion of the fluid causes a decrease in density. The buoyant forces caused by the change in density cause the heated fluid to rise along the surface. As the heated fluid rises from its original location, the void is replaced with adjacent fluid and creates a current of fluid flow. This process is repeated as the replacement fluid's temperature begins

to increase and rise. The natural current that develops along the surface of the plate is termed natural convection (Datta 2002; Bergman et al. 2011).

The Nusselt number associated with natural convection for a heated vertical surface is a function of the Rayleigh number, Ra, and Prandtl number, Pr, as given by Eq. (16) (Datta 2002; Bergman et al. 2011).

$$Nu = \left[0.825 + \frac{0.387 \cdot Ra^{\frac{1}{6}}}{\left(1 + \left(\frac{0.492}{Pr}\right)^{\frac{9}{16}}\right)^{\frac{8}{27}}} \right]^2 \tag{16}$$

The Rayleigh number is the product of the Prandtl number and the Grashof number, Gr. This relationship is given in Eq. (17). The Prandtl number is the ratio of the momentum and thermal diffusivities, as given by Eq. (18). The Grashof number is the ratio of buoyancy to viscous forces. This relationship is given by Eq. (19).

$$Ra = Gr \cdot Pr \tag{17}$$

$$Gr = \frac{\beta \cdot g \cdot L^3 \cdot \left(T_{env} - T_{glass}\right)}{\upsilon^2} \tag{18}$$

$$Pr = \frac{\upsilon}{\alpha_D} \tag{19}$$

Where β is the inverse of the film temperature for ideal gases, as given by Eq. (20), g is the local gravitational constant for the surface of Earth, L is the characteristic length, υ is the kinematic viscosity of the fluid, α_D is the thermal diffusivity of the fluid, as given by

Eq. (21), and all other variables are as previously defined (Datta 2002; Bergman et al. 2011).

$$\beta = \frac{1}{T_{film}} \tag{20}$$

$$\alpha_D = \frac{k}{\rho_m \cdot c_p} \tag{21}$$

Where all variables are as previously defined.

Forced convection occurs when a fluid is forcibly exposed to a surface. An example of forced convection would be wind blowing onto the glass façade of a building. The rate of heat transfer associated with forced convection can be significantly higher to that of natural convection. The increase in heat transfer occurs because the fluid is forced across the surface using external forces instead of natural buoyant forces. The rate of heat transfer is described as a function of the Reynolds number, Re, which characterizes the type of fluid motion. The fluid motion ranges from laminar flow to turbulent flow. The equation for Reynolds number is given by Eq. (22).

$$Re = \frac{u_\infty \cdot L \cdot \rho_m}{\mu} \tag{22}$$

Where u_∞ is the free stream velocity as previously defined, L is the characteristic length parallel to the flow of fluid, ρ_m is the density of the fluid, and μ is the viscosity of the fluid (Datta 2002). The Reynolds number is the ratio of inertia force to viscous force of the fluid. A fluid's flow is considered laminar when it occurs in an orderly manner. Laminar flow is typically associated with a Reynolds number less than 2×10^5. A fluid's flow is considered turbulent when it is chaotic and does not occur in an orderly manner. Turbulent flow is typically associated with a Reynolds number greater than

3×10^6. The chaotic behavior of the fluid flow increases the rate of heat transfer. Fluid flow transitions from laminar to turbulent for Reynolds numbers between 2×10^5 and 3×10^6 (Datta 2002). This progression is illustrated in Fig. 17.

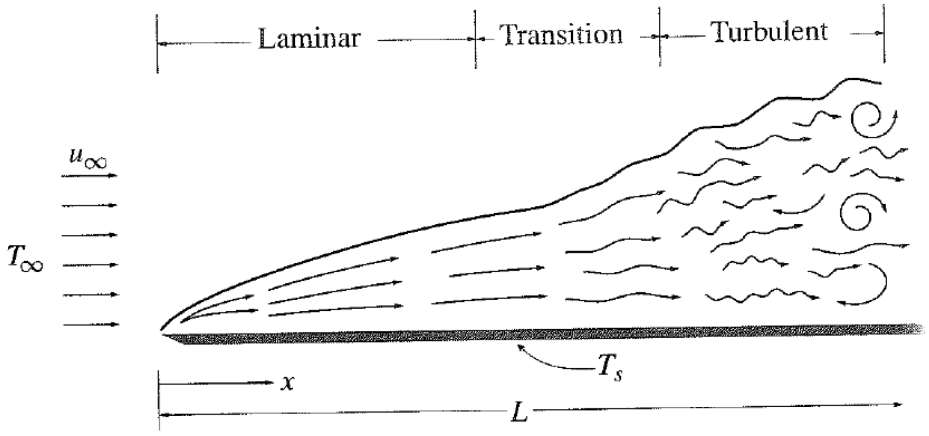

Fig. 17. Behavior of Convective Fluid Flow (Bergman et al. 2011)

The Nusselt number for forced convection with both laminar and turbulent flow across a flat plat is given in Eqs. (23) and (24), respectively (Datta 2002).

$$Nu = 0.664 \cdot Re^{\frac{1}{2}} \cdot Pr^{\frac{1}{3}} \qquad \text{for laminar flow (Re} > 2 \times 10^5\text{)} \qquad (23)$$

$$Nu = 0.0360 \cdot Re^{\frac{4}{5}} \cdot Pr^{\frac{1}{3}} \qquad \text{for turbulent flow (Re} > 3 \times 10^6\text{)} \qquad (24)$$

For monolithic glass plates, heat transferred through convection between the indoor environment and the interior number 2 surface of the glass plate is taken to be natural convection. The heat transferred through convection between the outdoor environment and the exterior number 1 surface of the glass plate is taken to be forced convection. The Nusselt number calculated using Eqs. (16) through (24) can be used to calculate two different convection coefficients for the indoor and outdoor surfaces and the indoor and

outdoor environments, respectively. The convection coefficient is then used to get Newton's law of cooling, as given by Eq. (25). Newton's law of cooling provides the general equation used to calculate the heat transfer due to the combined effects of conduction and convection for a particular situation (i.e. the indoor or outdoor situation for the problem herein).

$$\frac{q_{convection}}{A} = h_{convection} \cdot \left(T_{environment} - T_{glass}\right) \tag{25}$$

Where $q_{convection}$ is the convective heat flow, $h_{convection}$ is the convection coefficient, and all other terms are as previously defined.

Long-Wave Radiation

Electromagnetic energy is emitted by all objects which reside at temperatures above absolute zero (Datta 2002; Halliday et al. 2005; Bergman et al. 2011). Long-wave radiation describes radiation that is associated with objects at temperatures below 2200 °F. This would include virtually all objects near the surface of the earth. Long-wave radiation has wavelengths on the order of approximately 3 μm to 50 μm (Gordon 2001; ASHRAE 2013). The heat flow between two objects due to long-wave radiation is described as a function of the temperature difference between the two, as given by Eq. (26).

$$\frac{q_{radiation}}{A} = \sigma_{SB} \cdot \varepsilon \cdot \left(T_{environment}^4 - T_{glass}^4\right) \tag{26}$$

Where $q_{radiation}$ is the heat flow in the transverse direction due to long-wave radiation, A is the cross-sectional area perpendicular to the transverse direction, σ_{SB} is the Steffan-Boltzmann constant with a value of 3.08451×10^{-11} (in.·lb)/(s·in.^{2}·°F^4), ε is the emissivity of the radiating surface, and both $T_{environment}$ and T_{glass} are as previously defined.

Long-wave radiation is unique from both conduction and convection because it does not require a medium such as a gas, liquid, or solid to transfer heat through. Only a temperature difference is required for heat transfer due to long-wave radiation to occur between two objects (Datta 2002; Bergman et al. 2011).

An object's potential to emit long-wave radiation is quantified by the emissivity of the object's surface. The emissive potential is used to describe the quality and magnitude of the radiation emitted. The maximum possible amount of theoretical radiation that an object can emit is described using a blackbody with an emissivity equal to unity. The emissivity of an object describes the ratio of the objects emissivity power over that of the blackbody at the same temperature. The emissivity of an object typically varies as a function of wavelength. However, it is typically assumed that an average over all wavelengths can be used to accurately describe the emissivity of an object (Gordon 2001; Datta 2002; Bergman et al. 2011; ASHRAE 2013). This assumption is accurate because the sources for thermal radiation are diffusely emitting (Rubin 1982).

In general, radiation heat flow can occur due to long-wave and/or short-wave radiation (i.e. solar irradiance). However, the range of wave-lengths over which each type of radiation occur are different. The temperatures that are associated with long-wave radiation are typically well below 2200 °F. Likewise, the temperatures associated with short-wave radiation are typically well above 2200 °F. For monolithic glass plates that are used in windows, the temperature will be well below 2200 °F. As such, the monolithic glass plate will emit long-wave radiation. Because there is no appreciable overlap between the wavelengths and the temperature ranges associated with long-wave and short-wave radiation, the two phenomenon can be considered independent of one another and analyzed separately (Wright 1998; Gordon 2001; ASHRAE 2013).

The surface emissivity of clear glass is typically taken to be 0.84 however, it is possible to reduce the emissivity of a glass surface by using a low emissivity (low-E) coating.

This has become one of the most significant innovations in energy-efficient windows. As such, there are few glass plates that are used in windows today that do not include some type of low-E coating (Gordon 2001).

The significance of the low-E coating is that it is near transparent to short-wave radiation, while it is capable of reflecting long-wave radiation. The low-E coating is typically applied using one of two methods, pyrolytic or multi-layer sputtered. The pyrolytic coating, often called "hard coat", has an emissivity of approximately 0.15. The multi-layer sputtering method achieves emissivity values that are approximately 0.1 or less (Gordon 2001). Both types of low-E coatings were considered for the research herein.

When a glass plate is exposed to solar irradiance, energy is absorbed. The energy that is absorbed by the glass plate acts to raise its temperature. Heat is then exchanged between the glass plate and the surrounding indoor and outdoor environments through the fundamental heat transfer mechanisms of conduction, convection, and long-wave radiation. For solar irradiance, a portion of the energy input is reflected back into the outdoor environment, a portion of the energy is transmitted into the indoor environment, and the remaining energy is absorbed by the glass plate. This is not the case for long-wave radiation as window glass does not transmit long-wave radiation. Therefore, the long-wave radiation is either reflected or absorbed by the glass plate (Gordon 2001; ASHRAE 2013).

Heat transfer occurs between a monolithic glass plate and the objects of the surrounding indoor and outdoor environments due to long-wave radiation. The air surrounding the monolithic glass plate is permeable to long-wave radiation (ASHRAE 2013). Thus, the air of the surrounding indoor and outdoor environments is considered a non-participating gas and has no effect on the input of solar irradiance or the long-wave radiation (Muneer et al. 1997; Ismail and Henriquez 2005).

Surface Film Coefficients

The heat transfer that occurs between a monolithic glass plate and the surrounding environment through conduction and convection is a linear process. The heat transfer that occurs between a monolithic glass plate and the surrounding environment through long-wave radiation is a non-linear process, which greatly complicates the thermal analysis. In practice, surface film coefficients are used to combine the effects of conduction, convection, and long-wave radiation into a single, linear term that eliminates the need for iteration. In essence, the surface film coefficient is a proportionality constant that simplifies the numerical analysis of the heat transfer that occurs between the monolithic glass plate and the surrounding environment (Gordon 2001; ASHRAE 2013).

The effective convection energy exchange coefficient, $h_{convection}$, is used to describe the portion of heat that is transferred between the monolithic glass plate and the surrounding environment due to conduction and convection combined can be calculated using Eq. (27).

$$h_{convection} = \frac{Nu \cdot k_{fluid}}{L} \tag{27}$$

Where Nu is the Nusselt number and is calculated using Eq. (16) for natural convection and Eq. (23) or (24) for forced convection and all other terms are as previously defined.

If Newton's law of cooling, as given in Eq. (25), is equated with the equation for long-wave radiation energy exchange, as given in Eq. (26), an effective radiation heat exchange coefficient, $h_{radiation}$, can be calculated. This equation is given by Eq. (28) and represents the heat transfer between a monolithic glass plate and the surrounding environment through long-wave radiation (Gordon 2001).

$$h_{radiation} = \sigma_{SB} \cdot \varepsilon \cdot \left(T_{glass} + T_{environment}\right) \cdot \left(T_{glass}^2 + T_{environment}^2\right) \quad (28)$$

Where all of the terms are as previously defined.

The effective radiation heat exchange coefficient, as given by Eq. (28), can be added to the effective convection heat exchange coefficient, as given by Eq. (27), to calculate the total effective heat exchange coefficient, h_{total}. This total effective heat exchange coefficient is known as the surface film coefficient and is given by eq. (29) (Gordon 2001).

$$h_{total} = h_{convection} + h_{radiation} \quad (29)$$

Where all of the terms are as previously defined.

Specific surface film coefficients can now be calculated for the indoor and outdoor environments by equating Eq. (29) with Newton's law of cooling, as given by Eq. (25), and solving for h_{total}. This process is shown in Eq. (30).

$$\frac{q_{total}}{A} = h_{total} \cdot \left(T_{environment} - T_{glass}\right) \quad (30)$$

Where q_{total} is the total heat transferred by conduction, convection, and long-wave radiation in the transverse direction, and all other variables are as previously defined.

The outdoor surface film coefficient, $h_{outdoor}$, represents the heat transfer between the number 1 surface of the monolithic glass plate and the outdoor environment. The outdoor surface film coefficient combines the effects of conduction, forced convection, and long-wave radiation into a single, linear term, as given by Eq. (31) (Gordon 2001; ASHRAE 2013).

$$h_{outdoor} = \frac{q_{outdoor}}{A \cdot \left(T_{outdoor} - T_{glass}\right)} \tag{31}$$

Where $q_{outdoor}$ is the heat exchanged with the outdoor environment, $T_{outdoor}$ is the ambient temperature of the outdoor environment, T_{glass} is the temperature of the monolithic glass plate, and all other variables are as previously defined.

The indoor surface film coefficient, h_{indoor}, represents the heat exchanged between the number 2 surface of the monolithic glass plate and the indoor environment. The indoor surface film coefficient combines the effects of conduction, natural convection, and long-wave radiation into a single, linear term as given by Eq. (32) (Gordon 2001; ASHRAE 2013).

$$h_{indoor} = \frac{q_{indoor}}{A \cdot \left(T_{indoor} - T_{glass}\right)} \tag{32}$$

Where q_{indoor} is the heat exchanged with the indoor environment, T_{indoor} is the ambient temperature of the indoor environment, and all other variables are as previously defined.

The surface film coefficients that are used to describe the heat transfer between a monolithic glass plate and the indoor and outdoor environments can be determined using conservation of energy principles. The monolithic glass plate represents the closed system. Solar irradiance inputs heat energy into the system. Energy leaves the system through the heat exchanged with the indoor and outdoor environments as described by the surface film coefficients (Beason and Lingnell 2002; ASTM 2012a; ASHRAE 2013). This system is illustrated in Fig. 18.

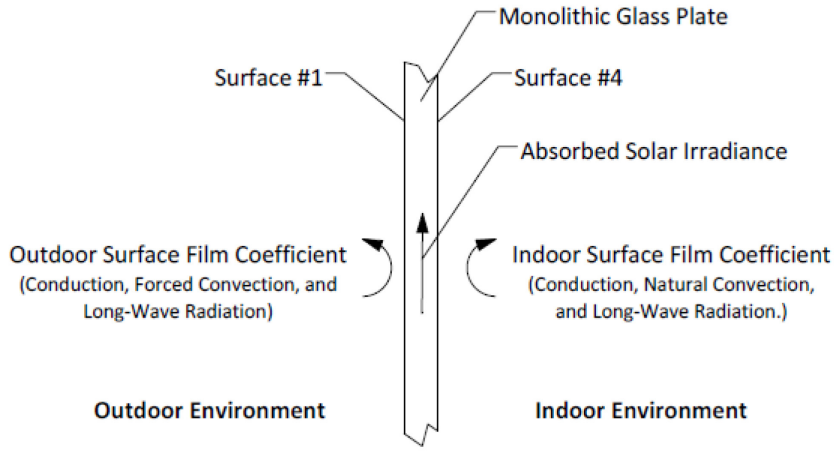

Fig. 18. Idealized Closed System for a Monolithic Glass Plate Using Surface Film Coefficients

Standard surface film coefficients which describe the heat exchange between a monolithic glass plate and the indoor and outdoor environments have been published for the design of monolithic glass plates subjected to solar irradiance. These coefficients assume that the monolithic glass plate exchanges heat with the outdoor and indoor environments at rates of 4.2987×10^{-2} and 2.5507×10^{-2} (in.·lb/s)/(in.^{2}·°F), respectively (Beason and Lingnell 2002; ASTM 2012a).

The indoor surface film coefficient of 2.5507×10^{-2} (in.·lb/s)/(in.^{2}·°F) was originally proposed by Beason and Lingnell (2002). When introduced, this value was within 5 percent of the previously proposed value of 2.6332×10^{-2} (in.·lb/s)/(in.^{2}·°F) recommended by Muneer (and Han 1996; et al. 2000). A 2.5507×10^{-2} (in.·lb/s)/(in.^{2}·°F) indoor surface film coefficient represents the typical indoor heat exchange for monolithic glass plates that do not have indoor heat traps such as Venetian blinds or curtains.

The outdoor surface film coefficient of 4.2987×10^{-2} (in.·lb/s)/(in.^{2}·°F) was also originally proposed by Beason and Lingnell (2002). When introduced, this value was within 10 percent of the previously proposed value of 3.9656×10^{-2} (in.·lb/s)/(in.^{2}·°F) recommended by Muneer (and Han 1996; et al. 2000) for a sheltered condition. A $4.2987 \times$

10^{-2} (in.·lb/s)/(in.^{2}·°F) outdoor surface film coefficient represents a typical sheltered outdoor condition which little heat is exchanged between the monolithic glass plate and the outdoor environment. This would not be the case if the glass plate were exposed to the direct effects of the wind. However, the use of a lower surface film coefficient is desired as this leads to an increase in the glass plate temperature and, consequently, an increase in thermally induced stress.

For the research herein, it is assumed that the indoor and outdoor surface film coefficients are identical for an IG unit and monolithic glass plate under the same set of environmental conditions. While no exhaustive study has been performed to verify that these surface film coefficients provide the optimum design condition for IG units, it is a reasonable assumption. Such a study should be considered in future research, but it is outside the scope of this dissertation. Thus, the research presented herein is based on the use of the surface film coefficients as presented in ASTM E2431 and recommended by Beason and Lingnell (2002) for monolithic glass plates and applied directly to insulated glass units.

Heat Exchange Between Insulating Glass Units and the Surrounding Environment

When an IG unit is taken from a state of thermal equilibrium at a room temperature of 70 °F and exposed to solar irradiance, the temperature of both the inner and outer glass plates will begin to rise. The changes in temperatures are due to the interaction of the IG unit with the surrounding environment. The heat transfer mechanisms of conduction, convection, and long-wave radiation between the IG unit and the surrounding environment can be applied directly, as discussed previously for monolithic glass plates.

Principles of conservation of energy can be applied to IG units, in the same way as monolithic glass plates, to determine the heat that is exchanged with the surrounding environment. For IG units, each glass plate is taken to be a separate and closed system. Solar irradiance inputs a certain amount of energy into each system. The amounts of energy that are input into the inner and outer glass plates are calculated using a well-known ray tracing procedure. This will be discussed in detail later. The solar irradiance that is absorbed by each glass plate is then converted into heat. This conversion acts to raise the temperature of the inner and outer glass plates. Heat is continuously exchanged between the inner and outer glass plates and outdoor environment, across the gas space cavity, and indoor environment through the fundamental heat transfer mechanisms aforementioned. The primary difference between IG units and monolithic glass plates is the heat transfer that occurs across the gas space cavity. Fig. 19 illustrates the heat exchange that occurs between an IG unit and the indoor and outdoor environments.

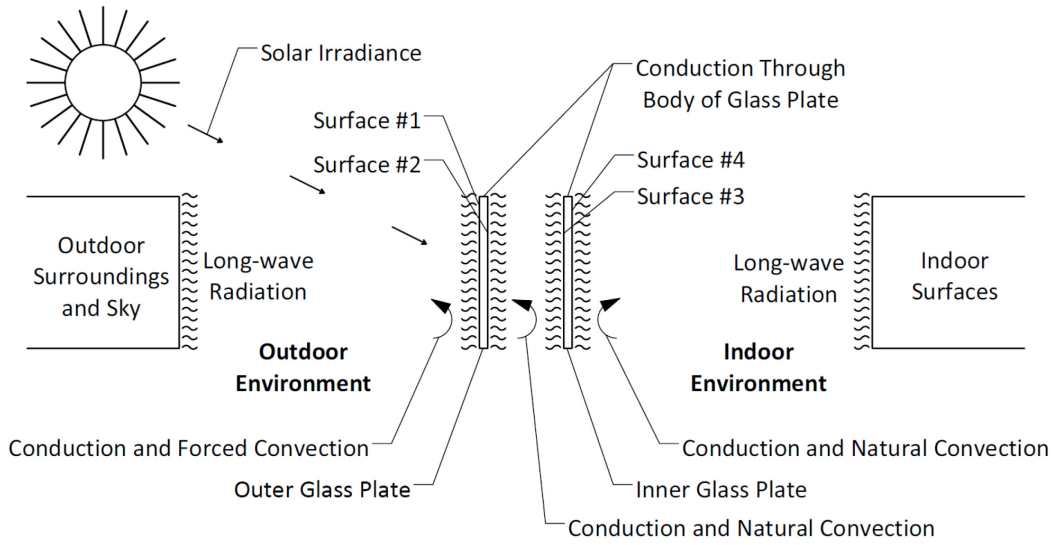

Fig. 19. Energy Exchange of an IG Unit with the Surrounding Indoor and Outdoor Environments

Solar Irradiance Applied to Insulating Glass Units

The process by which solar irradiance heats the inner and outer glass plates of an IG unit is much more involved than that for a monolithic glass plate. In addition to the specular and angular properties of each glass plate, the optical properties of an IG unit are affected by the inner-reflectance between each glass plate layer (ASHRAE 2013). Thus, the energy that is absorbed by each glass plate of the IG unit must be determined using a well-known ray tracing technique. The ray tracing technique is used to process the solar irradiance as it is absorbed, transmitted, and reflected by each glass plate as a function of its position in the IG unit.

When solar irradiance impinges on an IG unit, a portion of the energy is reflected back into the outdoor environment as a function of the outer glass plate's reflectance, a portion of the energy is absorbed as a function of the outer glass plate's absorptance, and the remainder of the energy is transmitted through the outer glass plate. The portion of energy that is transmitted through the outer glass plate then strikes the inner glass plate. A portion of this energy is reflected back to the outer glass plate as a function of the inner glass plate's reflectance, a portion of the energy is absorbed by the inner glass plate, and the remainder of the energy is transmitted through the inner glass plate to the indoor environment. This process begins again using the portion of energy that is reflected back to the outer glass plate. The inner-reflectance between the inner and outer glass plates continues until all of the solar energy is either absorbed or transmitted by the two glass plates. An overview of the ray tracing process is illustrated in Fig. 20 (Wijeysundera 1975; Gordon 2001; ASHRAE 2013).

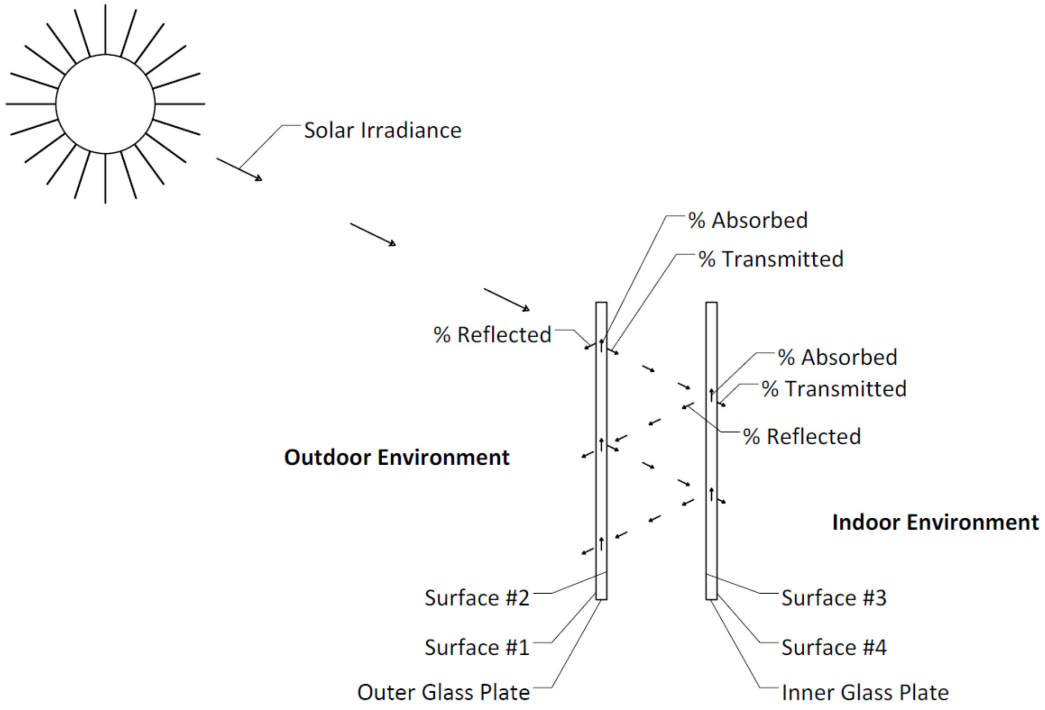

Fig. 20. Ray Tracing Procedure for an IG Unit

The cumulative sum of energy that is absorbed by each glass plate is then converted to heat and raises the temperature of the two glass plates. This defines the heat energy that is input into each glass plate that is taken to be the closed system. Applying the principles of energy conservation, an energy balance equation can be written for each glass plate. The first equation is for the outer glass plate and describes the heat exchanged with the inner glass plate, through the gas space cavity, and the outdoor environment. The second equation is for the inner glass plate and describes the heat exchanged with the outer glass plate, across the gas space cavity, and the indoor environment. The percentage of the total solar irradiance that is absorbed by the inner glass plate is defined herein as the inner glass plate absorption, α_{inner}. Likewise, The percentage of the total solar irradiance that is absorbed by the outer glass plate is defined as the outer glass plate absorption, α_{outer}.

The primary difference between IG units and monolithic glass plates is the heat transfer that occurs through the gas space cavity. The heat transfer between the two glass plates, through the gas space cavity, follows the three fundamental heat transfer mechanisms of conduction, natural convection, and long-wave radiation. These heat transfer mechanisms, as they relate to the gas space cavity, are discussed in the next section.

Heat Exchange Across the Gas Space Cavity

In addition to the heat that is exchanged with the surrounding environment, IG units exchange heat between the two glass plates through the gas space cavity. Heat is transferred using the three fundamental heat transfer mechanisms of conduction, natural convection, and long-wave radiation. The amount of heat that is transferred depends on numerous factors including the properties of the glass plates' surfaces, slope of the gas space cavity, thickness of the gas space cavity, direction of heat flow, mean temperature of the gas space cavity, and the difference in temperature between the two glass plates (ASHRAE 2013).

Extensive research has been performed to understand and mathematically model the transfer of heat across an IG unit's gas space cavity due to conduction and natural convection (DeGraff and Van der Held 1952; Batchelor 1954; Eckert and Carlson 1961; Elder 1965; Hollands et al. 1976; Raithby et al. 1977; Berkovsky and Polevikov 1977; El Sherbiny 1980; El Sherbiny et al. 1982a; El Sherbiny et al. 1982b; Rubin 1982; Korpela et al. 1982; El Sherbiny et al. 1983; Shewen 1986; Muneer and Han 1996; Shewen et al. 1996; Wright 1996; Zhao 1998). The transfer of heat through the center-of-glass area of an IG unit is typically determined using a correlation proposed by Wright (1996). This correlation was developed specifically for IG units that were intended to be used in architectural glazing applications. The correlation was developed based on experiments that were originally performed by El Sherbiny (1980) and Shewen (1986). It is independent of the aspect ratio of the gas space cavity, for the range of typical architectural

glazing applications, and is applicable for gas space cavities that involve high Rayleigh numbers. This correlation is discussed in detail as follows.

Only a temperature difference between the inner and outer glass plates of an IG unit is needed for pure gaseous conduction to occur. However, the effects of conduction are often magnified by convection which can occur in the gas space cavity of an IG unit. The natural convection that can set up in the gas space cavity can range from pure conduction to turbulent convection depending on the temperature difference between the two glass plates and the overall orientation and geometry of the IG unit itself. If an IG unit is oriented vertically and the temperature difference between the two glass plates is small, heat will transfer through pure conduction. As the temperature difference between the two glass plates increases, the heat that is transferred by natural convection increases. The heat flow that is transferred between the two glass plates can be calculated using Eq. (33).

$$\frac{q_{convection}}{A} = h_{convection} \cdot (T_2 - T_3) \tag{33}$$

Where $q_{convection}$ is the heat transferred across the gas space cavity in the transverse direction by conduction and convection combined, $h_{convection}$ is the convection coefficient, T_2 is the temperature of the number 2 surface of the outer glass plate, T_3 is the temperature of the number 3 surface of the inner glass plate, and A is as previously defined. Typically, the number 2 and 3 surface temperatures are taken to be the outer and inner glass plate temperatures, respectively.

The convection coefficient, $h_{convection}$, is determined in terms of the dimensionless Nusselt number, as given by Eq. (34).

$$h_{convection} = \frac{Nu \cdot k_{fluid}}{L} \tag{34}$$

Where Nu is the Nusselt number, k_{fluid} is the thermal conductivity of the gas fill, and L is the vertical height of the gas space cavity. The Nusselt number, Nu, is a function of the Rayleigh number and can be determined using Eqs. (35) through (39).

$$Nu = (Nu_1, Nu_2)_{max} \tag{35}$$

$$Nu_1 = 0.0673838 \cdot Ra^{\frac{1}{3}} \qquad (5 \times 10^4 < Ra) \tag{36}$$

$$Nu_1 = 0.028154 \cdot Ra^{0.4134} \qquad (1 \times 10^4 < Ra \leq 5 \times 10^4) \tag{37}$$

$$Nu_1 = 1 + 1.75967 \times 10^{-10} \cdot Ra^{2.2984755} \qquad (Ra \leq 1 \times 10^4) \tag{38}$$

$$Nu_2 = 0.242 \cdot \left(\frac{Ra}{A}\right)^{0.272} \tag{39}$$

Where Ra is the Rayleigh number and A is the aspect ratio of the gas space cavity.

The correlation proposed by Wright (1996) is the most widely accepted formulation to estimate the heat transfer due to conduction and convection associated with a vertical gas space cavity of an IG unit (ISO 2003). While correlations exist for other orientations of gas space cavities, the research herein only considers vertical glazing applications where the gas space cavity is oriented vertically. In addition, it is generally assumed that the gas space cavity is airtight such that there is no gas leakage or washing along the boundaries (AHSRAE 2013).

Concurrent to the conduction and convection that occurs, heat is transferred across the gas space cavity through long-wave radiation. For the typical vertical glazing application, the IG unit consists of two vertical, parallel glass plates that are separated by a

sealed gas space cavity. The heat that is transferred through long-wave radiation between two vertical, parallel plates with similar surface properties (i.e. surface emissivities) can be calculated using Eq. (40).

$$\frac{q_{radiation}}{A} = \sigma_{SB} \cdot \varepsilon \cdot \left(T_j^4 - T_k^4\right) \tag{40}$$

Where $q_{radiation}$ represents the heat that is transferred due to long-wave radiation between the two parallel plates, T_j is the temperature of the surface of the jth plate, T_k is the temperature of the surface of the kth plate, ε is the emissivity of the i and j surface of the parallel plates, and σ_{SB} is as previously defined.

IG units are not typically fabricated with the same plates of glass and/or the same types of coatings are not typically applied to both the number 2 and 3 surfaces. As such, the emissivities of the number 2 and 3 surfaces do not match. Therefore, Eq. (40) must be modified before it can be applied to IG units with different surfaces emissivities. This is accomplished by calculating an effective emissivity, $\varepsilon_{effective}$, as given by Eq. (41) (Datta 2002; ASHRAE 2013).

$$\varepsilon_{effective} = \frac{1}{\frac{1}{\varepsilon_2} + \frac{1}{\varepsilon_3} - 1} \tag{41}$$

Where ε_2 is the emissivity of the number 2 surface of the outer glass plate and ε_3 is the emissivity of the number 3 surface of the inner glass plate. The effective emissivity can then be combined with Eq. (40) to calculate the heat transferred between two glass plates in an IG unit with different surface properties as given by Eq. (42).

$$\frac{q_{radiation}}{A} = \sigma_{SB} \cdot \varepsilon_{effective} \cdot (T_2^4 - T_3^4) \tag{42}$$

Where $q_{radiation}$ is the heat transferred between the number 2 and 3 surfaces of an IG unit's two glass plates due to long-wave radiation in the transverse direction, across the gas space cavity, $\varepsilon_{effective}$ is the effective emissivities of the number 2 and 3 surfaces, and all other variables are as previously defined.

It follows that the heat transferred between two glass plates of an IG unit can be significantly affected by the type of gas fill used, the emissivities of the number 2 and 3 surfaces, and the spacing of the glass plates (i.e. the thickness of the gas space cavity) (Baker et al. 1989; ASHRAE 2013). Each of these factors affect the fundamental heat transfer mechanisms of conduction, natural convection, and long-wave radiation in different ways. Heat that is transferred through long-wave radiation is primarily affected by the surface emissivities of the glass plates and is independent of the type of gas fill used and the thickness of the gas space cavity. This is the case because the gas fill is a non-participating body in the long-wave radiation process. Once a low-E coating has been applied to an IG unit, convection typically replaces long-wave radiation as the dominant mode for the transfer of heat across the gas space cavity (Gordon 2001).

Heat transferred by both conduction and convection is primarily affected by the type of gas fill and the spacing of the two glass plates. This is the case because the properties of the gas such as thermal conductivity, density, viscosity, etc., all affect the conduction and natural convection processes. While the spacing of the glass plates has a slight affect on conduction, it can have a significant affect on the convection currents that form between the two glass plates (Muneer and Han 1996).

In practice, there is a "sweet spot" for the spacing of the glass plates that minimizes the heat transferred across the gas space cavity for various types of fill gases. In gas space cavities with a small thickness the fluid layers are "squeezed" together. This increases the interlayer shear stresses that develop between the molecules and prevents the driving buoyancy forces from developing. As the thickness of the gas space cavity increases,

the interlayer shear stresses are reduced. At some point, these interlayer shear forces are not large enough to overcome the buoyancy forces that occur between molecules and natural convection currents form (Muneer and Han 1996; Gordon 2001; PPG 2001).

Fig. 21 shows the combined effect each of these factors has on the overall heat transfer that occurs across an IG unit. Note that Fig. 21 includes the effect of conduction through the body of each glass plate in addition to the heat transfer that occurs through the gas space cavity. The overall heat transfer is represented by the U-Factor and is plotted as a function of glass plate spacing (defined as gap width in Fig. 21) for various types of gas fills and surface emissivities. Fig. 21 considers air, argon, and krypton gas types. In addition, clear glass with a surface emissivity of 0.84 and a glass plate with a low-E coating are shown. The surface emissivity of the low-E glass plate was taken to be 0.10. The U-Factor is discussed in more detail later, but in general a lower U-Factor implies that less heat is transferred through the IG unit.

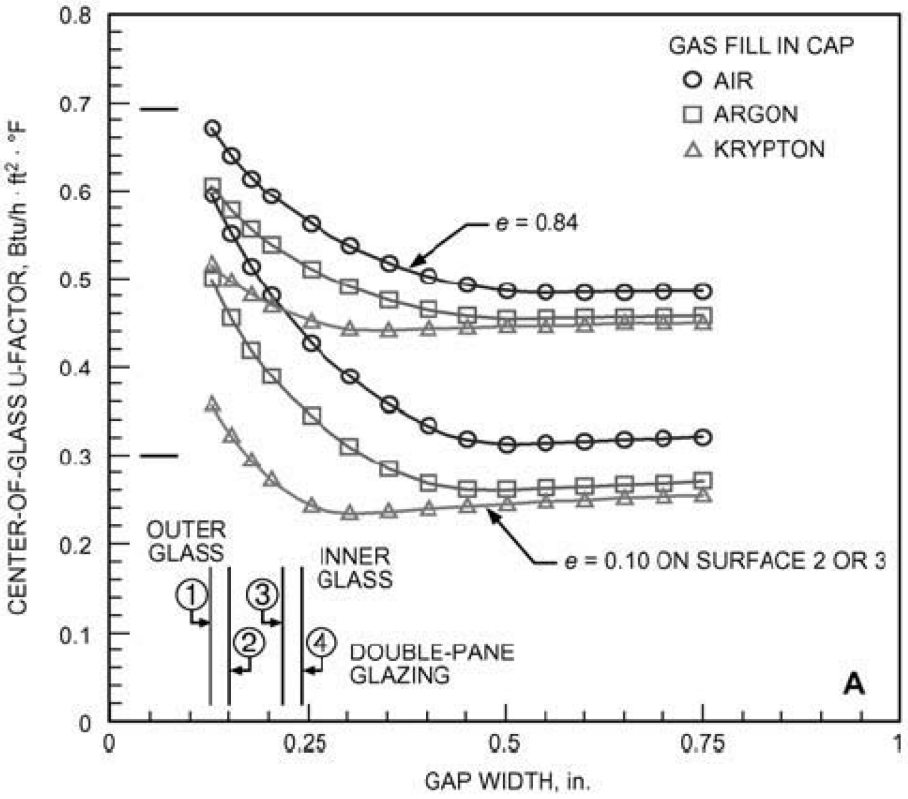

Fig. 21. IG Unit Center-of-Glass U-Factor vs. Gap Width, Emissivity, and Gas Fill (ASHRAE 2013)

As shown in Fig. 21, the optimum gas space cavity thickness for both air and argon is approximately 0.5 in. (Carmody et al. 2007; ASHRAE 2013). The optimum gas space cavity thickness for krypton is approximately 0.25 in. (Carmody et al. 2007; ASHRAE 2013). It is also shown that thicknesses greater than 0.5 in. do not offer a significant increase in resistance to convective heat transfer across the gas space cavity. When combined with a low-E coating, krypton is the most efficient gas fill for reducing heat transfer across the gas space cavity (ASHRAE 2013).

Heat that is transferred due to conduction, natural convection, and long-wave radiation between the inner and outer glass plates of an IG unit can be calculated using Eqs. (33) through (42). These three heat transfer mechanisms combine in a non-linear fashion due to the long-wave radiation. This non-linear behavior greatly complicates the calculation

of the heat flow across the gas space cavity. This is the case because the higher order temperature function used to describe long-wave radiation requires numerical iteration. For the design of IG units, a single linear method was desired to determine the temperature distribution for estimating thermal stresses. This term is called the combined energy exchange coefficient (CEEC) herein. Fig. 22 illustrates the interaction of an IG unit with the surrounding environment using the CEEC concept for the gas space cavity.

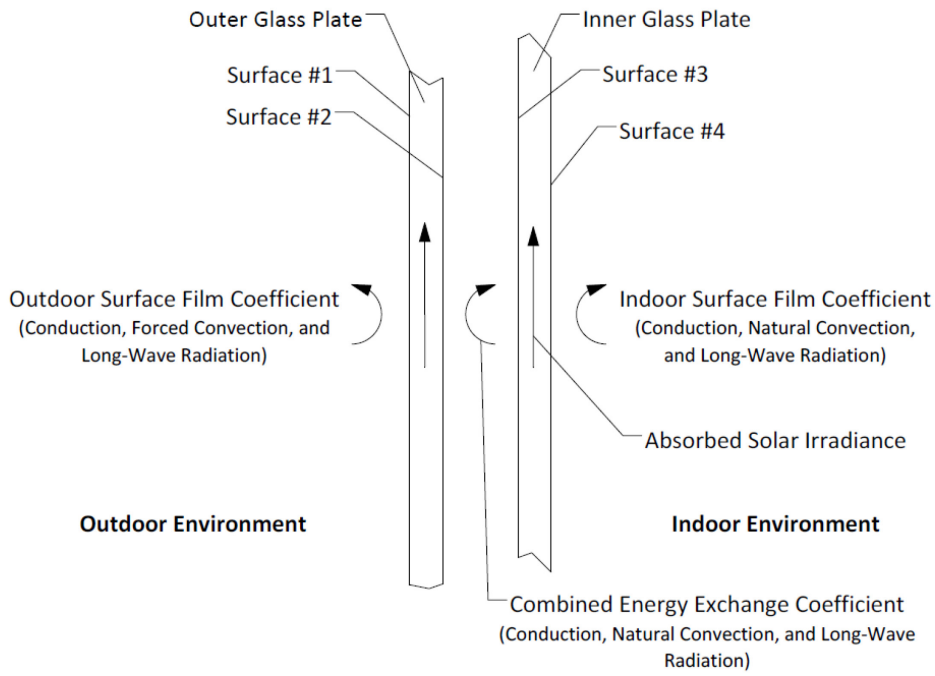

Fig. 22. Energy Exchange of an IG Unit with the Surrounding Indoor and Outdoor Environments Using the CEEC Through the Gas Space Cavity

Theoretical methods have been developed to calculate the CEEC in previous research. These efforts were focused on calculating the CEEC using theoretical approaches that solve the fundamental heat transfer equations using numerical procedures. Two of these theoretical methods are discussed in the next section. To date, no known research has been presented to verify experimentally that these CEEC determined using theoretical

methods are accurate. Chapter V is dedicated to developing a formal test procedure (FTP) that can be used to determine the CEEC experimentally.

Numerical Propagation Procedure

Klam (2007) proposed a theoretical numerical propagation procedure (NPP) specifically developed to determine a CEEC to describe the transfer of heat across the gas space cavity of an IG unit for the purpose of estimating thermal stresses. The method used a combination of a numerical finite difference propagation procedure and a least-squares regression technique to determine a best-fit coefficient which replaced the "gas material" with an effective solid material whose thermal conductivity was selected to model the effects of conduction, natural convection, and long-wave radiation that occur across the gas space cavity. The best-fit coefficient by definition is the CEEC.

This greatly simplifies the thermal analysis by removing the need for iteration. The procedure makes use of conservation of energy to determine the CEEC for a specific set of environmental conditions. It relies on the rate of heat exchanged between the outer glass plate and the outdoor environment and the inner glass plate and the indoor environment and solves for the CEEC.

The first step in the NPP is to model the heat transfer across the gas space cavity explicitly using the fully non-linear equation for long-wave radiation and the linear equation for conduction and convection combined, as given by Eqs. (43) and (44), respectively.

$$q_{convection} = h_{convection} \cdot (T_2 - T_3) \tag{43}$$

$$q_{radiation} = \sigma_{SB} \cdot \varepsilon_{effective} \cdot (T_2^4 - T_3^4) \tag{44}$$

Where $q_{radiation}$ is the heat transferred by long-wave radiation through a unit area of the gas space cavity in the transverse direction, $q_{convection}$ is the heat transferred by conduction and convection through a unit area of the gas space cavity in the transverse direction, T_2 is the temperature of the number 2 surface of the outer glass plate, T_3 is the temperature of the number 3 surface of the inner glass plate, and all other terms are as previously defined.

Next, the net heat fluxes per unit area, q_{net_outer} and q_{net_inner}, which enter and exit the outer and inner glass plates are determined, as given by Eqs. (45) and (46), respectively. Each glass plate is considered to be a separate control volume.

$$q_{net\_outer} = h_{outdoor} \cdot (T_{outdoor} - T_1) + h_{convection} \cdot (T_2 - T_3) + \sigma_{SB} \cdot \varepsilon_{effective} \cdot (T_2^4 - T_3^4) + \alpha_{outer} \cdot I_s \quad (45)$$

$$q_{net\_inner} = h_{indoor} \cdot (T_{indoor} - T_4) + h_{convection} \cdot (T_3 - T_2) + \sigma_{SB} \cdot \varepsilon_{effective} \cdot (T_3^4 - T_2^4) + \alpha_{inner} \cdot I_s \quad (46)$$

Where T_1 is the temperature of the number 1 surface of the outer glass plate, T_4 is the temperature of the number 4 surface of the inner glass plate, $T_{outdoor}$ is the temperature of the outdoor environment, T_{indoor} is the temperature of the indoor environment, $h_{outdoor}$ is the outdoor surface film coefficient, h_{indoor} is the indoor surface film coefficient, I_s is the total incident solar irradiance, α_{outer} is the absorption for the outer glass plate, α_{inner} is the absorption for the inner glass plate, and all other terms are as previously defined.

A positive net heat flux indicates an increase in the temperature of the glass plate, a negative net heat flux indicates a decrease in glass plate temperature. The change in temperature is calculated using Eq. (47).

$$\Delta T = \frac{q_{net} \cdot \Delta t}{1 \cdot \rho_m \cdot t_{glass} \cdot C_P} \tag{47}$$

Where ΔT is the change in temperature of the glass plate for a given time interval, q_{net} is the net heat flux per unit area for a given glass plate, Δt is the given time interval, 1 implies a unit area, ρ_m is the density of glass, t_{glass} is the thickness of the glass plate, and C_P is the specific heat of the glass plate. The new temperature for the next time step, T_{i+1}, can be calculated given Eq. (48).

$$T_{i+1} = T_i + \Delta T \tag{48}$$

The end result of this procedure is the variation of temperature for both the inner and outer glass plates as a function of time.

Now, knowing the variation of temperature given by the fully non-linear NPP, a single linear CEEC can be determined which reasonably represents the heat exchange that occurs across the gas space cavity. This is achieved by rewriting Eqs. (45) and (46) in the form of Eqs. (49) and (50), respectively.

$$q_{net\_outer} = h_{outdoor} \cdot (T_{outdoor} - T_1) + h_{CEEC} \cdot (T_2 - T_3) + \alpha_{outer} \cdot I_s \tag{49}$$

$$q_{net\_inner} = h_{indoor} \cdot (T_{indoor} - T_4) + h_{CEEC} \cdot (T_3 - T_2) + \alpha_{inner} \cdot I_s \tag{50}$$

Where h_{CEEC} is the CEEC and all other terms are as previously defined. The linear conduction and convection heat transfer mechanisms and the non-linear long-wave radiation heat transfer mechanism is replaced with an expression that is described linearly using the CEEC.

The temperature data, calculated using Eqs. (49) and (50), are then compared to those calculated using Eqs. (45) and (46) to select the most representative CEEC given the assumed environmental conditions. The accuracy of the CEEC is determined using a non-linear least-squares regression technique. The temperatures calculated using Eqs. (45) and (46) are taken to be the true temperatures. The temperatures calculated using Eqs (49) and (50) are taken to be the hypothesized temperatures that are based on the estimated value of the CEEC. The total error of the sum of squares, P, for a selected CEEC is given by Eq. (51).

$$P = \sum_{i=1}^{n} \left[\left(T_{outer_i} - \hat{T}_{outer_i} \right)^2 + \left(T_{inner_i} - \hat{T}_{inner_i} \right)^2 \right] \tag{51}$$

Where T_{outer_i} is the true temperature of the outer glass plate at timestep i, $\hat{T}_{outer_i}$ is the hypothesized temperature of the outer glass plate at timestep i, T_{inner_i} is the true temperature of the inner glass plate at timestep i , $\hat{T}_{inner_i}$ is the hypothesized temperature of the inner glass plate at timestep i.

The best-fit value for the CEEC for a particular set of environmental conditions is taken as the value which minimizes the total sum of the squares, P (Kennedy 1976; Klam 2007).

ASHRAE Air Space Coefficients

The second theoretical method that is specifically provided to describe the transfer of heat across the gas space cavity of an IG unit is presented by ASHRAE (2013). Unlike the procedure presented by Klam (2007) which was developed specifically to determine thermal stress in IG units, the procedure in ASHRAE (2013) is presented for the purpose of calculating building energy performance. The specific term used by ASHRAE (2013) to describe the heat exchange across the gas space cavity is the air space coefficient, h_s.

This method simply states that an IG unit constructed using two clear glass plates has an air space coefficient of 23.477×10^{-3} (in.·lb/s)/(in.^{2}·°F) for the assumed environmental conditions used to estimate building energy performance. For glass plates that employ low-E coatings on the number 2 or 3 surfaces of the IG unit, ASHRAE (2013) presents a table of values from which the appropriate air space coefficient can be selected for a range of tabulated environmental conditions.

The procedure presented by ASHRAE (2013) can only be used to describe the transfer of heat across the gas space cavity of an IG unit that has an air gas fill. It does not include provisions for Argon, Krypton, or other types of gas fills. Additionally, the table only provides values for horizontal heat flow in IG units that are oriented vertically. This is not the case for the NPP presented by Klam (2007) as it can be applied to a wide range of conditions. Table 1 shows a selected portion of the air space coefficient table, as presented in ASHRAE (2013), for a gas space cavity thickness of 0.5 in.

The first step in selecting the appropriate air space coefficient is to select the correct row in the table based on the thickness of the gas space cavity, average air space temperature, and the difference in temperature between the indoor and outdoor environments. The air space temperature is taken to be the average of the indoor and outdoor environments. Next, the correct column is selected based on the effective emissivity. The effective emissivity is calculated using Eq. (41), as discussed previously. The air space coefficient is taken to be the intersection of the horizontal row and vertical column.

Table 1. Air Space Coefficient (ASHRAE 2013)

Air Space Thickness (in.)	Air Space Temp. (°F)	Air Temp. Diff. (°F)	Air Space Coefficient, h_s, (10e-3) ((in.·lb/s)/(in.^{2}·°F)) Effective Emissivity					
			0.82	0.72	0.40	0.20	0.10	0.05
0.5	5	10	15.85	14.77	10.81	8.29	7.03	6.30
		25	16.21	14.95	10.99	8.65	7.39	6.66
		55	18.01	16.75	12.79	10.27	9.01	8.47
		70	18.91	17.65	13.69	11.17	9.91	9.19
		90	19.81	18.55	14.59	12.07	10.81	10.27
	32	10	18.01	16.57	11.89	9.01	7.57	6.85
		25	18.19	16.75	12.07	9.19	7.75	7.03
		55	19.45	18.01	13.33	10.27	8.83	8.11
		70	20.17	18.73	14.05	11.17	9.55	8.83
		90	21.08	19.63	14.95	12.07	10.45	9.73
	50	10	19.63	18.01	12.79	9.55	7.93	7.03
		25	19.81	18.19	12.97	9.73	7.93	7.21
		55	20.54	18.91	13.69	10.45	8.83	7.93
		70	21.26	19.63	14.41	11.17	9.55	8.65
		90	22.16	20.54	15.31	12.07	10.27	9.55
	85	10	23.06	20.90	14.59	10.63	8.65	7.57
		25	23.06	21.08	14.59	10.63	8.65	7.75
		55	23.42	21.44	15.13	11.17	9.19	8.11
		70	23.96	21.80	15.49	11.53	9.55	8.47
		90	24.50	22.52	16.21	12.07	10.09	9.19
	120	10	26.66	24.32	16.57	11.89	9.37	8.29
		25	26.84	24.32	16.57	11.89	9.37	8.29
		55	27.02	24.68	16.93	12.07	9.73	8.47
		70	27.20	24.86	17.11	12.25	9.91	8.65
		90	27.56	25.22	17.47	12.61	10.27	9.01

The theoretical calculations that were used to determine the air space coefficients presented in Table 1 are not readily apparent. However, they are most likely determined using current energy performance software packages such as WINDOW and THERM that are often used to determine the thermal performance of windows. The WINDOW and THERM software package provides an "effective thermal conductivity" value for the gas space cavity of an IG unit for use in estimating energy performance ratings.

While the exact procedures for determining the value for the effective thermal conductivity are not known, they are likely similar to the numerical procedure presented by Klam (2007). In both cases these values are determined based on theoretical calculations of the heat transfer mechanisms using numerical methods. These calculations also assume representative optical, thermal, and material properties for the IG units. While the values generated in Table 1 may provide good approximations when the desired analyses are building energy consumption, they were not developed specifically for the purpose of analyzing thermal stress in IG units.

Surface Film Coefficients

It is assumed for the research herein that the heat exchanged between the outer glass plate and the outdoor environment occurs at a rate described by a surface film coefficient with a value of 4.2987×10^{-2} (in.·lb/s)/(in.^{2}·°F), as recommended by Beason and Lingnell (2002) and presented in ASTM E2431. It is assumed that this condition applies directly to the number 1 surface of IG units and represents a sheltered outdoor environment, as discussed previously.

Additionally, it is assumed that the heat exchanged between the inner glass plate and the indoor environment occurs at a rate described by a surface film coefficient with a value of 2.5507×10^{-2} (in.·lb/s)/(in.^{2}·°F), as recommended by Beason and Lingnell (2002) and presented in ASTM E2431. It is assumed that this condition applies directly to the number 4 surface of IG units and represents an open indoor environment without an energy trap such as Venetian blinds or curtains, as discussed previously.

The heat exchange between an IG unit and the environment is much more complex than that of a monolithic glass plate. Thus, the applicability of the surface films that are used in the design of monolithic glass to IG units should ultimately be reviewed. However,

this is outside the scope of the research presented herein. Such research should be performed as part of future research projects to verify that they indeed provide the maximum design condition to evaluate thermal stress in IG units. Ultimately, it is up to the design professional to select the appropriate surface film coefficients for the situation at hand. In general, thermal stresses are maximized for the outdoor glass plate when the outdoor surface film coefficient is low and the outdoor temperatures are high (Pilette and Taylor 1988). Alternatively, thermal stresses are maximized for the inner glass plate when the outdoor surface film coefficient is high and the outdoor temperature is low (Pilette and Taylor 1988).

In addition to an understanding of how thermal stresses develop in IG units, an understanding of how these thermal stresses affect the strength of glass plates is needed. To properly assess the POB of a glass plate due to thermal stress, a clear understanding of the use of glass as a structural material and its behavior under load is necessary. The next section of this paper discusses background information that is pertinent to understanding the use of glass as a structural material. This includes a discussion on the design philosophy that is typically employed for the use of glass as a structural material.

Glass as a Structural Material

The most widely used flat glass product in the U.S. today is annealed float glass (AAMA 1984), referred to herein as annealed glass. Annealed glass is produced using a float glass manufacturing process designed to produce a product with nearly parallel, flat surfaces. In addition, the annealed glass is allowed to cool slowly during the manufacturing process so that the final product has a minimum level of residual stress. When necessary, the strength of annealed glass can be increased using a heat-treatment process. The heat-treatment process locks in a high level of residual compressive stresses along the surfaces and edges of the glass plate (AAMA 1984; GANA 2008). The float glass manufacturing process results in a continuous ribbon of annealed float glass that is cut into

large plates of specified length. These large glass plates are then further cut to convenient sizes depending on the particular application.

Annealed Float Glass

Annealed glass is a brittle material that is perfectly elastic to failure (AAMA 1984; McLellan and Shand 1984; Dalgliesh and Taylor 1990). The strength of annealed glass is controlled by the interaction of stress raising flaws and tensile stresses in the glass plate (Beason 1980; AAMA 1984; Beason and Morgan 1984; McLellan and Shand 1984; Dalgliesh and Taylor 1990; and Beason et al. 1998). The population of these stress raising flaws occur across the surface and throughout the body of the glass plate. The flaws themselves are the inevitable products of a wide variety of mechanical exposures that in-service glass plates experience, as well as mechanical exposures that occur during the manufacturing process (Beason and Morgan 1984). While the manufacturing process inherently results in an initial population of stress raising flaws, the flaws created during the in-service life of the glass plate tend to be more severe and less uniformly distributed (Beason et al. 1998). As such, the strength of annealed glass is at its highest as it exits the manufacturing process.

It has been shown that the strength of annealed glass that has been in-service for a number of years has a significantly lower strength than freshly manufactured glass plates of the same geometry and type (Beason 1980; Abiassi 1981; Norville and Minor 1985). Previous research has also shown that the primary reduction in strength is the result of the cumulative effects of in-service mechanical exposures as well as mechanical exposures during the manufacturing process and not a degradation of the glass material itself (Schrader 1982). Previous research has shown that typical in-service flaws can reduce the strength by 50 percent or more. Simply washing a glass plate can introduce scratches and abrasions that can reduce its strength. As such, the strength of glass plates have historically been based on probabilistic failure prediction approaches.

The failure of a glass plate can almost always be traced back to a single stress concentrating flaw. The flaw at which glass breakage initiates is often termed the "critical flaw" (Beason and Morgan 1984). The location of the critical flaw on the glass plate is often termed the "fracture origin". Whether a particular flaw becomes critical or not depends on its severity, orientation, and level of exposure to tensile stress. Once the level of tensile stress that the critical flaw is exposed to reaches the proper magnitude, glass plate breakage is initiated. Immediately after the initial breakage, two cracks will propagate away from the location of the critical flaw in opposite directions. If the initial breakage occurs along the perimeter of the glass plate, as shown in Figs. 7 and 8, a single crack will propagate away from the location of the critical flaw. These cracks are perpendicular to the direction of the local maximum principle tensile stress. As the cracks propagate away from the critical flaw, they may or may not branch into more cracks. Branching is dependent upon the level of tensile stress in the glass plate. The cracks will continue to propagate through the glass plate until all of the cracks reach an edge of the glass plate or the level of nominal tensile stress reaches a level where further propagation is no longer possible. The number of cracks is a function of the elastic energy that is stored in the glass plate just prior to breakage (Dalgliesh and Taylor 1990).

Heat-Treated Glass

When it becomes necessary, the strength associated with annealed glass can be significantly increased by subjecting the annealed glass to a heat-treatment process. The increase in strength is achieved by locking in a residual stress distribution through the thickness of the glass plate during the heat-treatment process. The process involves heating the annealed glass plate to a temperature just below the softening point of glass and then quickly quenching the surface of the glass plate with air. During the quenching process the surface of the glass plate cools quickly and becomes rigid. Meanwhile, the

interior region of the glass plate remains soft and cools at a slower rate. After the interior of the glass plate cools, a residual stress pattern is locked into the glass plate (AAMA 1984; GANA 2008).

Fig. 23 presents an idealization of the residual stress distribution that is assumed to develop through the thickness of the glass plate due to the heat-treatment process. It is important to note that this distribution is almost certainly different near the edges of the glass plate. This will be discussed in detail later. As shown in Fig. 23, the surfaces of the glass plate are subjected to residual compressive stresses and the interior region of the glass plate is subjected to residual tensile stresses. Conveniently, the heat-treatment process does not alter the elastic properties of the glass material itself (Mencik 1992; Lingnell 1994).

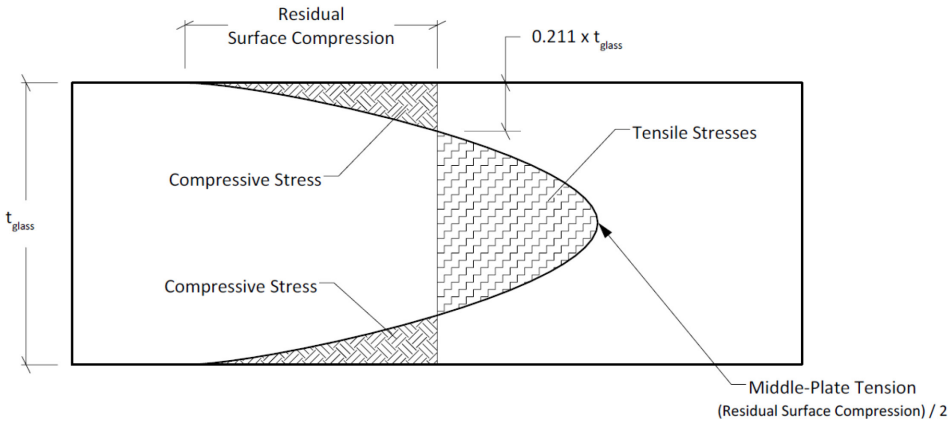

Fig. 23. Idealized Residual Stresses in Heat-Treated Glass Plates

Unlike annealed glass, the strength of heat-treated glass must be analyzed using the net surface tensile stress, σ_{net}, rather than the applied tensile stress, as given by Eq. (52).

$$\sigma_{net} = \sigma_{applied} - \sigma_{residual} \tag{52}$$

Where $\sigma_{applied}$ is the mechanical or thermal stress that the glass plate is subjected to and $\sigma_{residual}$ is the residual surface compressive stress that is locked into the glass plate.

Based on Eq. (52), before the surface of the heat-treated glass plate is subjected to tensile stress, the applied stress must overcome the residual surface compressive stress. Because of this, the strength of a heat-treated glass plate is significantly increased when compared to an annealed glass plate of the same geometry.

As discussed previously, glass plate breakage is the result of the interaction of tensile stresses and stress raising surface flaws. The residual surface compression that is present in heat-treated glass assures that the surface and edge flaws distributed across a glass plate are initially in a state of compression. Thus, there is no risk that glass plate breakage will occur until the net stress acting on the glass plate's surface or edge becomes tensile. This phenomenon greatly increases the strength of heat-treated glass plate when compared to annealed glass plate for most mechanical or thermal loads.

There are two commonly accepted classifications for heat-treated glass. These are heat-strengthened (HS) and fully tempered (FT). For a glass plate to be classified as HS, the residual surface compression must be greater than 3,500 psi and less than 7,500 psi. FT glass has a higher residual surface compressive stress than HS glass. To be classified as FT, the residual surface compressive stress must be greater than 10,000 psi and the residual edge compressive stress must be greater than 9,700 psi. There is no maximum level of residual surface compressive stress or residual edge compressive stress associate with FT glass (ASTM 2012b).

It is commonly assumed that HS glass plates are at least two times greater than the strength of annealed glass plates, of the same size, when exposed to uniform lateral pressure loads such as wind. Likewise, it is commonly assumed that FT glass plates are at least four times greater than the strength of annealed glass plates (Lopez-Anido et al.

2000). Previous research has shown that these factors for HS and FT glass plates are appropriately conservative for designing glass plates to resist a wide range of uniform lateral pressure loads (Oakes 1991; Ditsworth 1992). This is likely the case for thermal load resistance as well.

It is important to note that the residual stress distributions that occur near the edges of a heat-treated glass plate are complex. Fig. 23 presented an idealization of the residual stresses that are assumed to develop through the thickness of a glass plate, away from the edges. The variation of the residual stresses near the edges of the glass plate is not as well defined and is a current topic of debate within the glass industry. However, there is a consensus that the stresses near the edges of the glass plate are most certainly different from those in the center of the glass plate. This is the case because the cooling that occurs near the edges, during the quenching process, is not as uniform as it is away from the edges of the glass plate. Fig. 24 presents an idealization of the assumed distribution of residual stresses that develop through the thickness of the glass plate, near the edges.

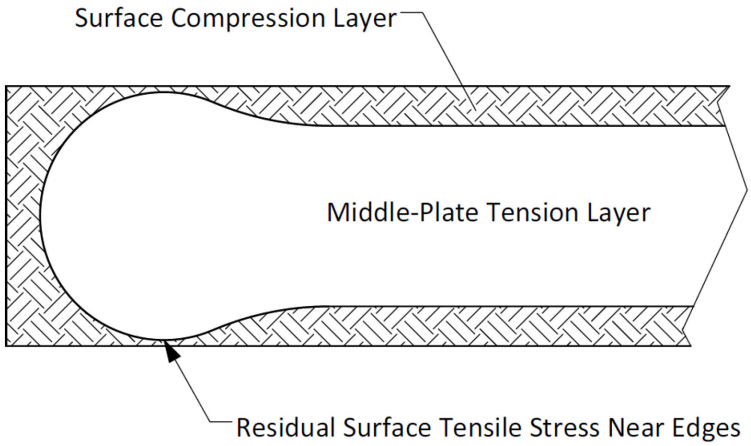

Fig. 24. Idealized Residual Stresses Near the Edges of Heat-Treated Glass Plates

Note that the penetration depth of the residual surface compression shown in Fig. 24 is reduced from that shown previously in Fig. 23, away from the edges. As the thickness of the compression zone reduces the thickness of the residual tension zone expands. In fact, this situation can become so pronounced that the surface of the glass plate is actually exposed to tensile stresses. This has the potential to pose a dangerous situation when thermal stresses exist. The only way to prevent this dangerous expansion of the tension zone near the edges of the glass plate is through proper process supervision along with the use of quality control measures to assure that the glass plate being produced does not have residual tensile stresses that reach the surface of the glass plate (Redner and Hoffman 2001).

If the POB is unacceptably high for a glass plate that is subjected to a thermally induced stress, the POB has historically been lowered through the use of heat-treated glass. Depending on the level of thermal stress that is anticipated, either HS or FT glass plates may be used instead of annealed glass plates. In general, the levels of residual edge and surface compression associated with heat-treated glass plates typically preclude thermal stress breakage problems from occurring at all (Turner 1977; Beason and Lingnell 2002; Pilkington 2005; Pilkington 2013a). The primary advantage of heat-treated glass plates in resisting thermal stress is that the edge of the glass plate is in a state of residual compression as a result of the heat-treatment process. Thus, the thermal stress must exceed the residual edge compressive stress before breakage can occur.

While it is convenient that heat-treated glass plates can withstand most thermal design conditions, its use is not without its disadvantages. For situations where the use of heat-treated glass plates are not a requirement and/or not needed for a particular design condition, annealed glass plates are the preferred products (Dalgleish and Taylor 1990; Lopez-Anido et al. 2000). This is the case for many reasons that are not discussed herein, but well known within the glass industry. There are many considerations that must be taken into account during the design process if the use of heat-treated glass plates is required.

The focus of this research was to determine whether annealed glass plates do or do not meet the expected POB for a particular design condition.

Design Philosophy for Glass Plates

One of the most important aspects to understand about the glass design process, regardless of whether the application is in windows or not, is the premise that "glass breaks" must be accepted. The practical significance of this premise is that glass plates have historically been designed with a focus on reducing the POB to an acceptable level in the event that the glass plate is subjected to the design load condition. Typically, a POB is selected so that it does not exceed a specific number of broken glass plates per 1,000 glass plates when subjected to the design condition. The two most commonly accepted POB are 1 glass plate breakage per 1,000 glass plates and 8 glass plate breakages per 1,000 glass plates. The POB selected typically depends on the life-safety consequences associated with the breakage of the glass plate.

The design philosophy that is used for glass plates is somewhat contrary to the design philosophy typically used by engineers that design conventional structures using predictable building materials such as steel or concrete (AAMA 1984; McLelland and Shand 1984). In the latter case, the possibility of failure is low provided that the structure is designed properly and the materials meet the design specifications. Conversely, selecting the most appropriate glass plate means minimizing the POB for a given design condition. In addition, the design engineer must consider the post-breakage consequences during the design and selection process.

Glass Failure Prediction Model

To predict the strength of a particular glass plate under the application of load, it is first necessary to determine the distribution and magnitude of the tensile stresses that act on

the glass plate. Second, the character and distribution of flaws across the glass plate's surfaces and/or edges must be defined. The most commonly accepted failure prediction model to determine the POB for a glass plate subjected to uniform lateral pressure load is the glass failure prediction model (GFPM) developed by Beason (1980; and Morgan 1984; et al. 1998).

The GFPM is a theoretical formulation that allows for the POB of a glass plate to be calculated as a function of the tensile stresses induced by lateral load and the statistical characteristics of the distribution of surface flaws that occur across the area of the glass plate (Beason and Morgan 1984). The distribution and magnitude of tensile stresses that occur across the surface of the glass plate are typically calculated using a geometrically non-linear plate analysis procedure that was developed by Vallabahn and Wang (1981). After which, the GFPM is used to quantify the affect that various factors such as load duration, plate geometry, and glass surface conditions have on the overall strength of the glass plate. Most glass thickness selection charts that are used in the U.S. are based on the GFPM developed by Beason (1980; and Morgan 1984; et al. 1998; ASTM 2016).

Besides the effect of tensile stresses and distribution of stress raising flaws, there exist many other factors that influence the strength of glass. One of which is that the strength of glass varies with load duration. This is discussed below.

The Effect of Load Duration on the Strength of Glass Plates

It has been well established that the strength of glass plates is affected by the duration of loading in the presence of normal amounts of water vapor that exist in the atmosphere (Beason 1989; Dalgliesh and Taylor 1990; Mencik 1992). As the load duration increases, the strength of the glass plate decreases. It is believed that this effect is caused by the interaction of water vapor with surface flaws in such a way that the stress concentration effects of the surface flaws are magnified as a function of the duration of loading.

Within the glass industry, this phenomenon is frequently referred to as "static fatigue" (Brown 1974; Beason and Morgan 1984). Typically, the term fatigue is applied to situations that involve dynamic loading where the stress would be applied in cycles. Frequently, charts are presented where the strength of a material is described as a function of the number of dynamic cycles to which it will be exposed. As such, the term static fatigue often gives pause to engineers that are unfamiliar with this unique property of glass.

Two elements are necessary for static fatigue to occur in glass plates. These are tensile stresses and exposure to normal amounts of water vapor (i.e. humidity in the air). If either component is missing, there is no static fatigue. Thus, the effects of static fatigue are limited to flaws that are located on the edges or surfaces of the glass plate.

The effect that load duration has on the strength of glass plates subjected to constant stress can be expressed using Eq. (53).

$$\sigma_d = \left(\frac{60}{t_d}\right)^{\frac{1}{16}} \cdot \sigma_{60} \tag{53}$$

Where σ_d is the constant stress associated with a particular load duration, t_d is the load duration of interest, and σ_{60} is the failure stress associated with a 60-s load duration (Beason and Morgan 1984; Beason 1989; Beason and Lera 1989). The selection of a 60-s time duration is somewhat arbitrary, other than to say it was historically used to correctly design glass plates for uniform lateral pressure loads such as wind.

Fig. 25 shows the variation of a normalized failure stress as a function of load duration for an annealed glass plate (Beason and Morgan 1984). The information that is presented in Fig. 25 has been normalized for a load duration of 60 s. Based on the information presented in Fig. 25, a glass plate subjected to a load duration of 1 s would be

approximately 30 percent stronger than if the same glass plate is subjected to a load duration of 1 min. The same glass plate would be approximately 23 percent weaker if it is exposed to a load duration of about 60 min. This would be the case for thermal stresses. Therefore, if tests were performed on a specific set of glass plates and the mean 60-s duration failure stress was 6,000 psi, then the estimated mean failure stress for a 1-h duration would be approximately 4,600 psi for similar glass plates. Experience suggests that the strength of the glass continues to weaken as the duration of the loading increases.

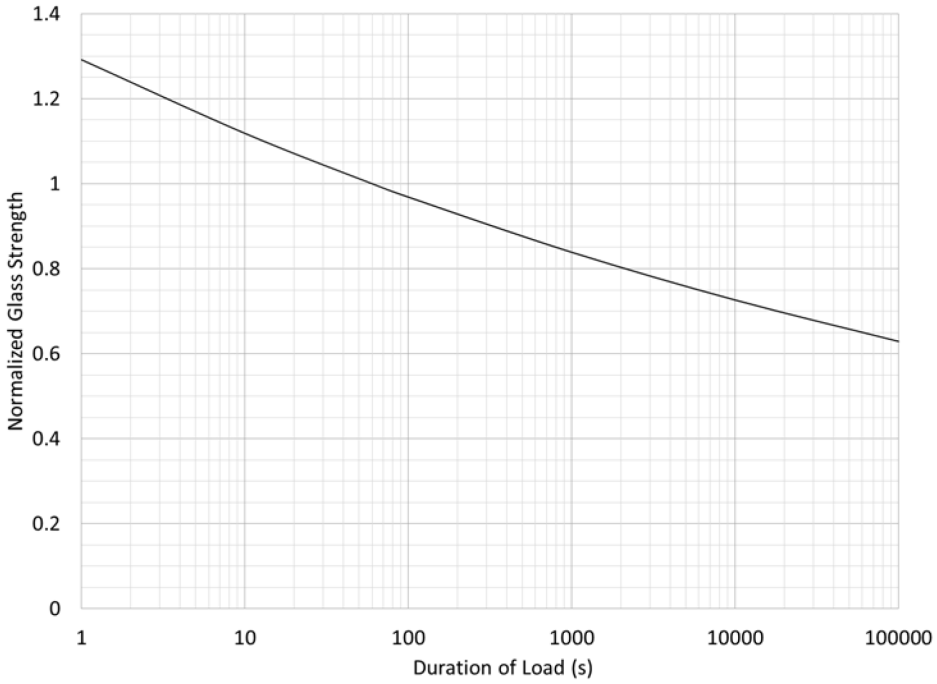

Fig. 25. Normalized Glass Strength vs. Duration of Load

While it is difficult to establish through direct testing, it has generally been accepted that static fatigue ceases to be an issue as the applied tensile stress approaches a level below approximately 1,000 psi (McLellan and Shand 1984). This value is often taken to be the static fatigue limit.

The next section presents background information on the use of a failure prediction model that applies to glass plates that are subjected to thermally induced edge stresses. Ultimately, the glass ESFPM will be used to evaluate the POB of annealed glass plates that are subjected to thermal edge tensile stresses.

Glass Edge Strength Failure Prediction Model

The use of a GFPM has been well established to determine the POB for a glass plate subjected to uniform lateral pressure load. The GFPM allows for the POB of a glass plate to be calculated as a function of the stresses induced by the lateral pressure load and the statistical characteristics of the distribution of surface flaws across the glass plate, as discussed in the previous section. This section presents background information on a similar glass ESFPM that can be used to evaluate the POB for glass plates that are subjected to tensile stresses along the edges of the glass plate (Beason 1989; Beason and Lera 1989; Beason and Lingnell 2002).

For the thermal design condition, the perimeter of the glass plate is almost always subjected to higher tensile stresses than the surfaces of the edge area of the glass plate, away from the perimeter. In addition to the higher stresses along the perimeter of the glass plate, the characteristics of the edge flaws that occur along the perimeter of the glass plate are typically more severe than the characteristics of the surface flaws that occur away from the perimeter (Beason 1989; Zhong-wei 1999; Beason and Lingnell 2002). Thus, the initiation of thermally induced glass plate breakage is typically in close relation to the flaw distributions along the perimeter of the glass plate (Beason 1989; Beason and Lingnell 2002).

While this situation is not common, thermally induced glass plate breakage can originate from severe surface damage or flaws that exist away from the perimeter of the glass

plate (Zhong-wei 1999; Beason and Lingnell 2002). The primary reason that this situation is not a common situation is because the stress concentrating flaws which occur along the perimeter of the glass plate are typically more severe than those that occur across the surface of the glass plate and the thermal stress is maximum along the perimeter of the glass plate (Beason 1989). Other than the discussion below regarding glass plates with a ceramic enamel applied, this situation is not considered as part of this research.

An example of a situation where severe surface damage does typically control the strength of glass plates in resisting thermally induced stress is when a ceramic enamel (i.e. frit) is applied to the surface of the glass plate. There is often a desire to have an IG unit that incorporates an opaque or translucent pattern on one of the glass surfaces. This is most often used in a building façade's spandrel locations. The desired pattern is typically achieved using a ceramic based paint or enamel that is applied to the surface of the glass plate and then fused with the application of heat. This results in a durable, uniform coating that can accomplish various desired visual effects.

In recent years, an increasing number of IG units that employ glass plates with a ceramic enamel coating are breaking due to thermal stresses. It has become increasingly clear within the glass industry that the application of a ceramic enamel to the surface of glass plates can cause a reduction in the strength of the glass plate. While the effects of the ceramic enamel on the strength of the glass plate are outside the scope of this dissertation, it is interesting to note that thermal breakage involving glass plates with a ceramic enamel applied typically occur away from the perimeter of the glass plate and within the glass-ceramic interface. The precise mechanism that causes the reduction in the glass plate's strength is, at the moment, a matter of speculation. However, it is likely that the location of the fracture origin, which consistently occurs a small distance in from the edge, is most likely explained by the possible lack of, or reduction in, residual compression zone that occurs a small distance in from the perimeter of the glass plate, as shown

previously in Fig. 24. Future research is needed to fully understand this issue. However, careful consideration should be used when analyzing glass plates for a thermal design condition when a ceramic enamel is applied. As such, the procedures forwarded in this dissertation may not apply directly to glass plates with a ceramic enamel coating applied.

Glass plate breakage due to thermal stress is typically associated with relatively low levels of tensile stress (Beason and Lingnell 2002). As such, breakage issues that arise from thermal stresses are typically associated with the use of annealed glass plates. This is the case because annealed glass plates have low levels (i.e. near zero) of residual edge and surface compression (GANA 2008). Thus, the potential for glass plate breakage due to thermally induced stress has historically been overcome with the use of heat-treated glass plates, be it HS or FT. The higher levels of residual edge and surface compression that are associated with heat-treated glass plates typically preclude thermal stress breakage problems from occurring (Beason and Lingnell 2002; Pilkington 2013a).

It has long been recognized that glass plates typically fail due to the interaction of surface tensile stresses with a random distribution of stress concentrating surface flaws. For the case of laterally loaded glass plates, the critical flaw can occur at any point across the surface of the glass plate. However, for thermal stresses the maximum tensile stress occurs along the perimeter of the glass plate as do the critical flaws associated with thermal breakage. Thus, it is necessary to employ a failure prediction model specific to the case of thermal stresses.

This failure prediction model is based on the GFPM that was developed for laterally loaded glass plates. However, the glass ESFPM relates the POB to the distribution of edge stresses and the characteristics of edge flaws, whereas the GFPM relates the POB to the distribution of surface stresses and the characteristics of surface flaws.

Both of these failure prediction models are based on the Weibull statistical failure theory for brittle materials (Weibull 1939). According to Weibull's failure theory, the probability of failure, P_b, of a brittle material can be calculated using Eq. (54).

$$P_b = 1 - e^{-B} \tag{54}$$

Where B defines the risk function that is evaluated by integrating the combined effects of flaw severity and tensile stresses experienced by the material. For the case of thermal stresses, the risk function would evaluate the combined effects of edge flaw severity and edge tensile stresses. The development of a reasonable risk function for glass plates subjected to uniform lateral loads have been presented in detail and are not repeated in this dissertation (Beason and Morgan 1984). The development of a reasonable risk function for glass plates subjected to thermal loads is presented below.

Eq. (55) presents the edge strength risk function, B, that is used to evaluate a glass plate's resistance to thermal stress. This equation assumes that the risk of breakage of the glass plate subjected to a thermal load situation is controlled by the length of the perimeter subjected to tensile stresses.

$$B = k_t \cdot \left(\frac{t_d}{60}\right)^{\frac{m}{16}} \cdot \sum_{No.of\ Edges} \left[\int_{Length} [\sigma_{max}(x)]^m dx \right] \tag{55}$$

Where t_d is the time duration of the thermal stress expressed in s, k_t and m are the edge flaw characteristics, and $\sigma_{max}(x)$ is the maximum principal stress along the perimeter of the glass plate. As indicated, the integral is summed along all of the glass plate edges that are subjected to a state of tensile stress. The primary difference between the failure prediction model that is used for glass plates subjected to uniform lateral loads and that used for thermal loads is in the formulation of the risk function (Beason 1989; Beason and Lingnell 2002).

For the case of thermally loaded glass plates, the tensile stresses that develop along the perimeter of the glass plate have a uniform (i.e. constant) magnitude across the middle-region of the four edges of the glass plate (Pilette and Taylor 1988; Zhong-wei et al. 1999; Beason and Lingnell 2002). Further, the tensile stresses that develop along the short dimensions are near identical to those that develop along the long dimension of the glass plate (Pilette and Taylor 1988; Zhong-wei et al. 1999). As such, failure can originate from any of the four edges of the glass plate and from either the edges with short or long dimensions (Zhong-wei et al. 1999).

The stresses near the corner of the glass plate are compressive and increase to the maximum tensile stresses along the middle-regions of the glass plate (Zhong-wei et al. 1999). The transition from the stress at the corner of the glass plate to the maximum tensile stress located along the middle-region occurs over approximately 6 in. (Beason and Lingnell 2002). This allows Eq. (55) to be simplified to include all of the perimeter of the glass plate except the 6 in. transition zones at the corners. Thus, the effective length of the perimeter of the glass plate that is exposed to tensile stress can now be calculated using Eq. (56).

$$p_{effective} = (p - 48) \tag{56}$$

Where $p_{effective}$, is the effective perimeter length and p is the total length of the glass plate's perimeter (Beason and Lingnell 2002). Both of these values are expressed in in.

The effective perimeter of the glass plate is subjected to a near uniform maximum tensile stress, σ_{max}. Thus, Eq. (55) can be rewritten in the form shown in Eq. (57).

$$B = k_t \cdot \left(\frac{t_d}{60}\right)^{\frac{m}{16}} \cdot (p - 48) \cdot (\sigma_{max})^m \tag{57}$$

Where all variables are as previously defined.

For small glass plates with a total perimeter length less than 60 in., it is recommended that the total perimeter length, p, be taken as 60 in. (Beason and Lingnell 2002; ASTM 2012a). This assumption is conservative and provides for a minimum effective perimeter length, $p_{effective}$, of 12 in. Eq. (57) is in the final form that will be used to develop the POB procedure presented in this paper.

To use the glass ESFPM in determining the POB for glass plates that experience thermal stress, representative values for m and k_t must be determined. These factors represent the characteristics of the glass plate's edge condition, as-installed. Beason and Lingnell (2002) recommend the edge flaw parameters, m and k_t, be 7 and 1.68×10^{-28} ($in.^{13}/lb^7$), respectively for glass plate thicknesses up to and including 0.25 in. nominal. The value for m is based on a conservative, expected coefficient of variation associated with glass strength failure data. The value for k_t is based on a large number of controlled glass edge strength experiments (Beason 1989; Beason and Lera 1989; Beason and Lingnell 2002). Both of these values have been accepted as standard for evaluating the POB of glass plates due to thermally induced stress (ASTM 2012a). The application of the glass ESFPM to glass plates thicker than 0.25 in. nominal would require special consideration and is not considered as part of this research.

As discussed previously, it has been well established that the strength of glass is affected by the duration of loading and this includes the thermal design condition (Beason 1989). As the load duration increases, the strength of the glass plate decreases. Thus, it is necessary to correct Eq. (57) to account for a reasonable duration of thermal loadings. It seems reasonable that the duration of loading for wind load situations be relatively short however, thermal stresses usually have a load duration much longer than those of wind loads. Beason and Lingnell (2002) and ASTM E2431 recommend a load duration of

60-min for the design thermal load situation. The 60-min duration equivalent load is defined as the constant duration load that would cause failure of the glass plate if the load had been applied for a period of 60 min. Incorporating this and the values for m and k_t, Eq. (57) can be rewritten in the form given in Eq. (58).

$$B = 1.68 \times 10^{-28} \cdot (p - 48) \cdot (\sigma_{max})^7 \tag{58}$$

Where all of the variables are as previously defined.

Solving for the maximum edge stress, σ_{max}, as a function of the total glass plate perimeter and edge strength risk function, Eq. (58) can be rewritten in the form shown in Eq. (59).

$$\sigma_{max} = \left[1.68 \times 10^{28} \cdot \frac{B}{(p - 48)}\right]^{\frac{1}{7}} \tag{59}$$

Where all of the variables are as previously defined.

Eq. (59) can then be combined with Eq. (54) to develop allowable stress charts that describe the variation of maximum allowable edge tensile stress as a function of POB and the glass plate's total perimeter length. The results of this calculation are shown in Fig. 26 where the allowable stress varies from approximately 700 to 2,500 psi. The POB vary from 0.0001 which corresponds with 1 glass plate breakage per 10,000 glass plates to 0.008 which corresponds with 8 glass plate breakages per 1,000 glass plates.

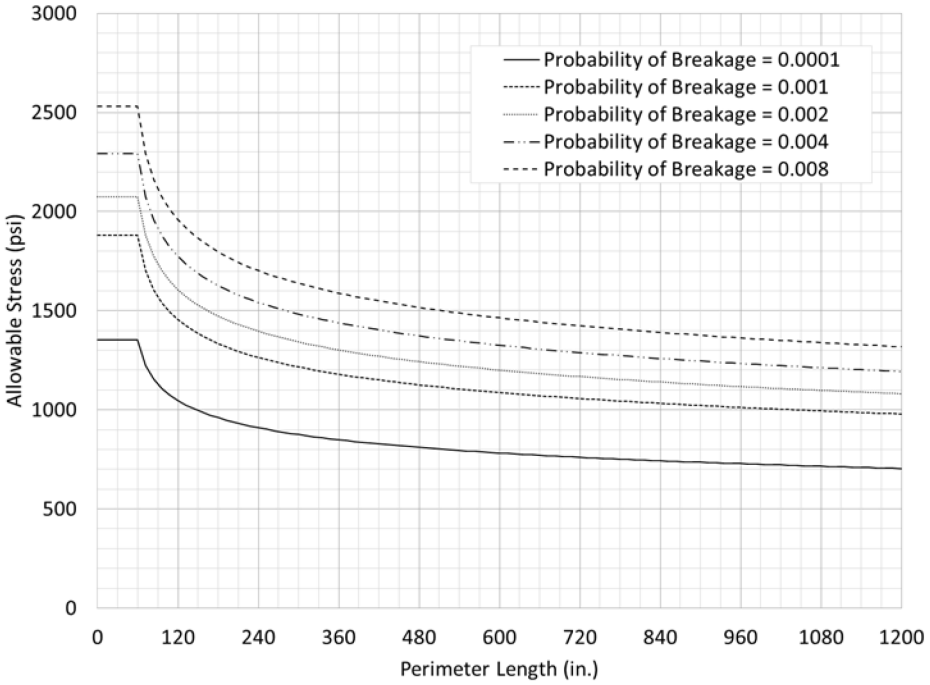

Fig. 26. Allowable Stress vs. POB and Glass Plate Perimeter Length

Fig. 26 can now be used to determine the maximum allowable stress for a glass plate exposed to thermal stress along the perimeter of the glass plate. The maximum allowable stress is calculated by entering the horizontal axis of Fig. 26 at the proper dimension for the glass plate's total perimeter length and project upward to the selected POB and then project leftward to the vertical axis to estimate the allowable edge tensile stress.

While the concept of acceptable POB for glass plates subjected to uniform lateral pressure loads have been well established by the glass industry, no concept of acceptable POB has been established for thermal stress design. The selected POB for a given project depends on a number of factors including the number of glass plates in the building and the consequences that are associated with thermal breakage. For the case of uniform lateral pressure loads, the accepted POB is in the range of 0.001 to 0.008 (Beason and Lingnell 2002).

It is reasonable to assume that the thermal design condition can occur more readily than the design condition for uniform pressure loads due to wind. Thus, the range of POB for the thermal design condition is typically extended beyond the range for uniform lateral pressure loads. In practice, it is reasonable to contemplate the use of a POB as low as 0.0001 for the thermal design condition. Ultimately, the final selection of an acceptable POB is the responsibility of the design engineer (Beason and Lingnell 2002).

It is worth noting that the edge strength of the glass plate is highly dependent on the quality of the cut-edge. It is preferred (i.e. increased thermal stress resistance) that the edge be "clean cut" with a minimum level of serration, hackle, shark teeth, etc. (AAMA 1984; PPG 2002; Pilkington 2013a). Additionally, the glass plate should be fabricated, handled, and installed without damage (Pilkington 2013a). For glass plates that are subjected to uniform lateral pressure loads, the in-service strength typically decreases over time. The reduction in strength is due to continuous in-service mechanical exposures and is often termed "weathering". However, unlike glass surfaces, the edges of glass plates are not perceived to lose in-service strength over time. This is because the edges are typically encapsulated inside of a frame system and/or protected by glazing sealants such that they are not subjected to continuous in-service mechanical exposure that causes the strength reducing flaws (Beason and Lera 1989).

ASTM Standard Practice for Monolithic Glass Plates

Standard design procedures have been published that can be used to evaluate the POB for an annealed monolithic glass plate used in a window that is subjected to solar irradiance (ASTM 2012a). The POB for a monolithic glass plate is influenced by the level of stresses that the perimeter of the glass plate is exposed to, the interaction with stress raising flaws, and the duration of load (Beason and Lingnell 2002; ASTM 2012a). ASTM (2012a) published a standard practice that couples an analysis procedure to determine the level of thermal stress with the glass ESFPM to evaluate the thermal load resistance

of a monolithic glass plate for a specified POB. As a result, a design professional can evaluate the POB for a monolithic glass plate subjected to a particular level of solar irradiance.

The first step in the thermal analysis procedure is to estimate the thermal stress that is induced in the monolithic glass plate when it is subjected to solar irradiation. The thermal stress is a function of the thermal stress factor, TSF, as presented in Fig. 27. Note that the only values provided in ASTM E2431 are metric. The information is presented as information only and nothing was derived using these data.

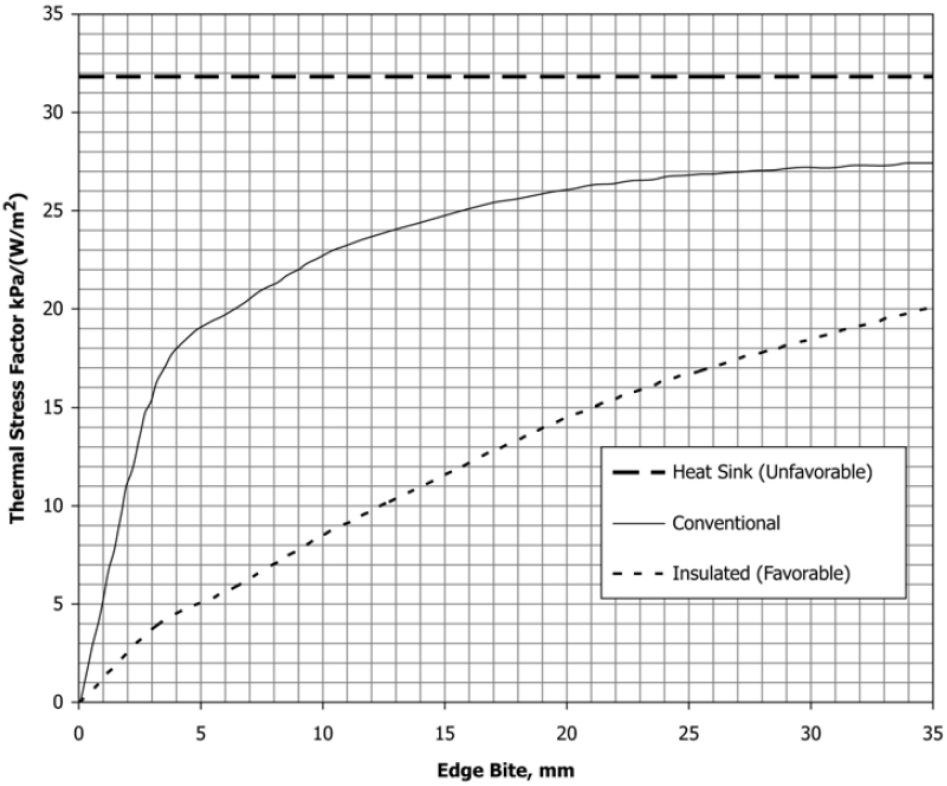

Fig. 27. Thermal Stress Factor Chart for the Design of Monolithic Glass Plates (ASTM 2012a)

Fig. 27 provides the thermal stress factor for a range of edge bite dimensions from 0 to 35 mm. Additionally, the thermal stress factor is defined for three individual frame conditions: insulated, conventional, and high-heat mass. These idealized frame conditions are presented in Fig. 28 below.

The insulated edge is used to represent any situation where zero heat is lost to the frame system. This is considered to be the most favorable edge condition with regard to reduced thermal stress (Beason and Lingnell 2002; ASTM 2012a). The conventional edge condition is based on a generic, commercially available aluminum frame with rubber perimeter gaskets. The high-heat mass edge condition is the most unfavorable edge condition. A high-heat mass edge condition effectively prevents the edge of the glass plate from warming. This is the case because the glass plate is considered to be in intimate thermal contact with the building's structural components.

To determine the thermal stress factor for a particular situation, enter the horizontal axis of Fig. 27 at the edge bite of interest and project upward to the intersection of the curve with the appropriate frame condition and then project leftward to the vertical axis to determine the thermal stress factor. For situations where the intersection of the edge bite and edge condition are not on a discrete value, linear interpolation is used.

The maximum tensile thermal stress, σ_{max}, that is induced in the monolithic glass plate is determined by multiplying the absorbed solar irradiance by the thermal stress factor, as given by Eq.

$$\sigma_{max} = TSF \cdot I_s \cdot \alpha_s \tag{60}$$

Where I_s is the incident solar irradiance expressed in W/m^2, α_s is the solar absorptance coefficient for the monolithic glass plate, and TSF is the thermal stress factor that is determined using Fig. 27.

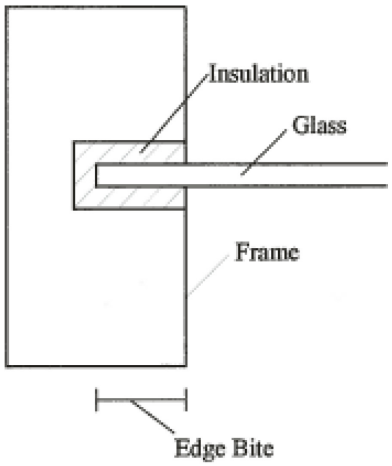

(a) Perfectly Insulated

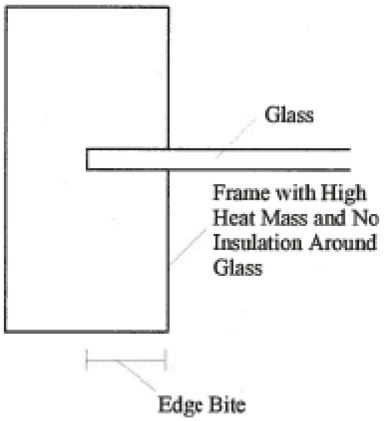

(b) High-Heat Mass

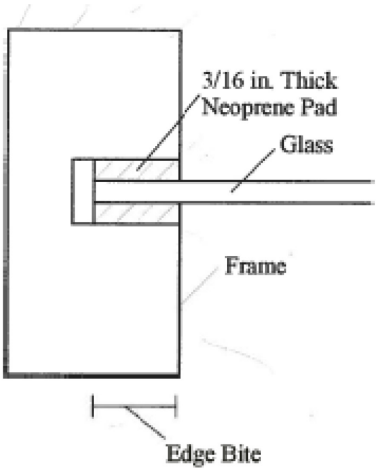

(c) Conventional

Fig. 28. Idealized Frames Considered for the Design of Monolithic Glass Plates (ASTM 2012a)

Now, with the maximum tensile thermal stress known, a decision must be made as to whether the maximum tensile thermal stress meets an acceptable risk level or not. Fig. 29 shows the allowable thermal stress as a function of glass plate perimeter length and POB. A range of total perimeter lengths from 0 to 30 m is shown and a range of POB from 0.0001 that is associated with 1 glass plate breakage per 10,000 glass plates through 0.008 that is associated with 8 glass plate breakages per 1,000 glass plates is shown. After selecting a defensible POB, the maximum allowable thermal stress can be determined.

To determine the maximum allowable thermal stress, enter the horizontal axis of Fig. 29 at the point equal to the total perimeter length of the monolithic glass plate and project upward to the intersection of the selected POB curve and then project leftward to the vertical axis to determine the maximum allowable thermal stress. For situations where the intersection of the POB and/or the total perimeter length do not fall on a discrete value, linear interpolation is used.

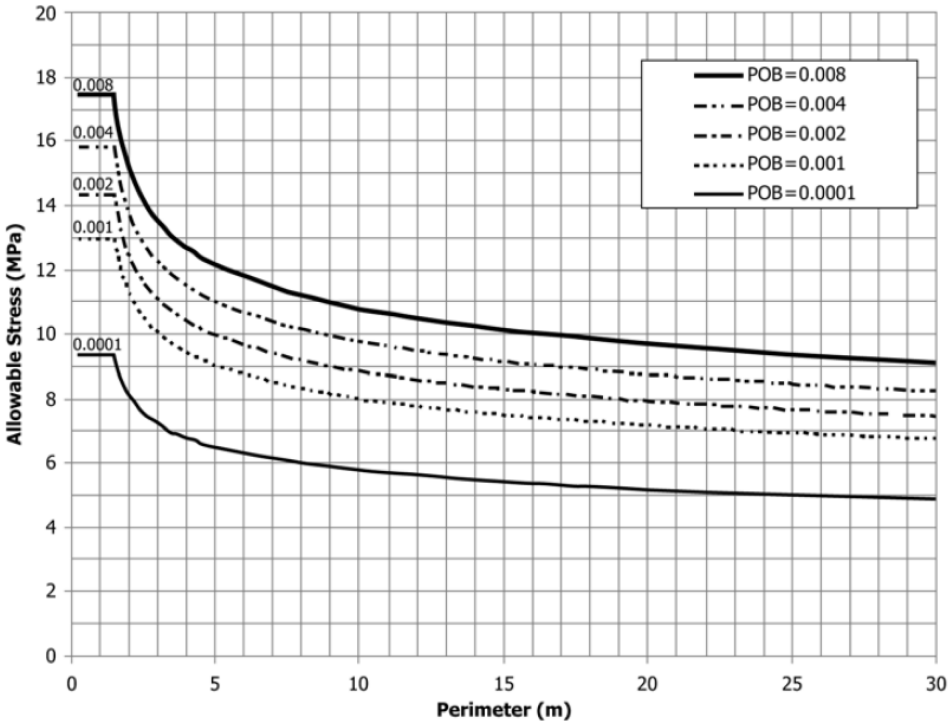

Fig. 29. POB Chart for the Design of Monolithic Glass Plates (ASTM 2012a)

If the maximum thermal stress calculated using Eq. (60) is less than the maximum allowable thermal stress that was determined using Fig. 29, then the risk of glass plate breakage is considered to be acceptable. If the maximum thermal stress is greater than the maximum allowable thermal stress, the risk of glass plate breakage is considered to be unacceptable. ASTM E2431 recommends that a more detailed analysis be performed using FE methods if the risk of glass plate breakage is determined to be unacceptable.

In addition to edge bite and frame conditions, ASTM E2431 has provisions that take into account the effects that shadow patterns and internal reflective devices have on the POB of monolithic glass plates. Shadow patterns and internal reflective devices have a significant effect on how thermal stress develops in monolithic glass plates and should be considered during the design process. However, these situations were not considered herein.

Final Considerations

Windows serve a vital role in the façade of a building and they are an important part of the overall energy performance of the building in which they are installed (Wright 1998; Wright and Kotey 2006). It is unfortunate that windows are one of the largest contributors to building energy loss as more energy is exchanged between the indoor and outdoor environments through windows than any other building assembly (Ismail and Henriquez 2005). As such, the demand for more energy-efficient building products has led to an increase in the number of energy-efficient windows that are available to design professionals. This in-turn has led to the development of analysis tools and approximations that are capable of evaluating the steady-state energy performance of windows.

The use of many of these tools have been extended in an attempt to design for thermal stress in IG units (Wright and Barry 1999; Fisher 2007). Perhaps this is because there is a lack of fundamental understanding in how thermal stresses develop in IG units, or in desperation because there is currently no defined procedures to determine the maximum thermal stress that occurs in IG units. Regardless of the motivation, there exists a distinct difference between evaluating the energy performance of an IG unit and determining the maximum level of thermal stress induced by solar irradiation. This is discussed in detail below. The first part of this discussion provides the reader with some needed background information on the energy performance ratings that are used to select energy-efficient windows and how these ratings are calculated. The last part of this discussion provides a summary on the relevance of these energy performance ratings to the research herein.

Energy Performance Ratings

Perhaps the best method to help explain window energy performance ratings is to start with a practical example. When a consumer is interested in purchasing a new vehicle,

one of the metrics that is often used as a comparator of different vehicles is the estimate of fuel economy, in miles per gallon. As such, most consumers are familiar with the *"EPA/DOT Fuel Economy and Environment Label"* that is part of the vehicle's window sticker. Among other values, this label provides the vehicle's estimated fuel economy that is based on experimental testing.

Because there are many factors that affect a vehicle's fuel efficiency, the tests that are used to measure fuel economy are standardized for all vehicles and performed in a controlled laboratory setting. This ensures reliable, repeatable, and equitable results across the various vehicle models and manufacturers. This allows consumers to make a one-to-one comparison based on fuel economy (EPA 2014).

The fuel economy that is listed on the label represents the best estimate for drivers in the U.S., under average driving conditions. It is considered to be a "real world" estimate because the standardized tests were developed to reflect national-average conditions that include some of the broad range of factors that affect fuel economy. While some drivers may actually achieve a fuel economy that is close to that estimated, it is inevitable that some drivers will experience higher fuel economy and others lower fuel economy.

This process of selecting a vehicle based on fuel economy is somewhat similar to the process that is used to select windows. Instead of measuring fuel economy, a window's energy performance and its effect on building energy use is the metric of measure. These single-value metrics that are used are known as energy performance indices or ratings for windows. Similar to the fuel economy label on cars, most windows manufactured in the U.S. are now labelled with these energy performance ratings.

The U-Factor is one of the most important and widely used energy performance ratings for comparing and selecting windows and evaluating its effect on a building's energy

performance (Turner 1977; Lingnell 1981; Wright 1998; Carmody et al. 2007; Pilkington 2013b; NFRC 2016). In general terms, the U-Factor indicates the air-to-air thermal transmittance or rate of heat flow through a window. It combines the effects of conduction, convection, and long-wave radiation that occur across the window assembly due to a temperature difference between the indoor and outdoor environments. It also includes a component of heat flow that is influenced by the indoor and outdoor surface film coefficients.

U-Factor

The U-Factor is the standard measure of the rate of steady-state heat transfer through a unit area of a window and boundary surface films due to a temperature difference between the indoor and outdoor environments, as given by Eq. (61) (ASHRAE 2013).

$$q_{window} = U_{window} \cdot A_{window} \cdot (T_{outdoor} - T_{indoor}) \tag{61}$$

Where q_{window} is the steady-state heat flow across the window, U_{window} is the U-Factor of the window assembly, A_{window} is the area of the window assembly, $T_{outdoor}$ is the temperature of the outdoor environment, and T_{indoor} is the temperature of the indoor environment.

The U-Factor treats the window as if it were a homogeneous material. In general, a lower U-Factor means the window has a higher insulating value and less heat is lost through it. Thus, the lower the U-Factor the better the window's energy performance rating. The total heat that is transferred through the building's windows is taken as the sum of the heat transferred through all of the individual window assemblies calculated using Eq. (61).

Window assemblies have multiple, parallel paths through which the heat can flow between the indoor and outdoor environments. It is likely that each of these paths have a different thermal transmittance. Thus, an area-weighted average value is used to estimate a U-Factor for the entire window assembly. Typically, the individual heat transfer paths considered for windows include the center-of-glass, edge-of-glass, and frame areas. The area-weighted average U-Factor, U_{window}, for the entire window assembly is calculated using Eq. (62).

$$U_{window} = \frac{U_{frame} \cdot A_{frame} + U_{EOG} \cdot A_{EOG} + U_{COG} \cdot A_{COG}}{A_{window}} \tag{62}$$

Where U_{frame} is the U-Factor of the frame system, A_{frame} is the area of the frame system, U_{EOG} is the U-Factor for the edge-of-glass area, A_{EOG} is the edge-of-glass area, U_{COG} is the center-of-glass area U-Value, A_{COG} is the center-of-glass area, and all other variables are as previously defined.

While the U-Factor considers the window assembly as a whole, the term U-Value is sometimes used to designate the thermal resistance of only the center-of-glass area of the window. This value does not include any transfer of energy through the frame system and/or spacer system. Most often, the center-of-glass U-Value is the best performing component of the window assembly (Carmody et al. 2007; ASHRAE 2013).

U-Value

In the most general case of a single monolithic glass plate, the center-of-glass U-value depends primarily on the indoor and outdoor surface film coefficients. The U-value for a single monolithic glass plate, $U_{monolithic}$, is calculated using Eq. (63).

$$U_{monolithic} = \frac{1}{\frac{1}{h_{outdoor}} + \frac{1}{h_{indoor}} + \frac{t_{glass}}{k}} \tag{63}$$

Where $h_{outdoor}$ is the outdoor surface film coefficient, h_{indoor} is the indoor surface film coefficient, t_{glass} and k are the thickness and thermal conductivity of the monolithic glass plate, respectively.

Calculating the center-of-glass U-Value for IG units, U_{IGU}, is more complex than for monolithic glass plates. The U-value is affected by several factors including the number of glass plates, gas space cavity dimensions and orientation, surface emissivities, and the type of gas fill. In addition to the indoor and outdoor surface film coefficients, the heat flow across the gas space cavity due to conduction, natural convection, and long-wave radiation must be considered (ASHRAE 2013). Thus, Eq. (63) becomes of the form shown in Eq. (64) for IG units.

$$U_{IGU} = \frac{1}{\frac{1}{h_{outdoor}} + \sum_{j=1}^{n} \frac{t_{glass_j}}{k_j} + \sum_{j=1}^{n} \frac{1}{h_{cavity_j}} + \frac{1}{h_{indoor}}} \tag{64}$$

Where t_{glass_j} is the thickness of the jth glass plate, k_j is the thermal conductivity for the jth glass plate, h_{cavity_j} is the heat transfer coefficient for the jth gas space cavity that includes conduction, natural convection, and long-wave radiation, and all other variables are as previously defined.

As shown, the U-Factor (and U-Value) are not only dependent on the thermal properties of the materials from which the window assembly is fabricated, but the specific set of indoor and outdoor environmental conditions as well (ASHRAE 2013). As such, the U-factor is determined for a single set of environmental conditions where the temperature of the indoor and outdoor environments and the surface film coefficients are specifically

defined. Therefore, a different value for a window's U-Factor can be calculated just by changing the environmental conditions.

The American Architectural Manufacturers Association (AAMA) and National Fenestration Ratings Council (NFRC) promulgate the testing protocols for thermal resistance testing in the U.S. AAMA prescribes a testing procedure which involves physical testing to determine the U-Factor for a window assembly (AAMA 2009). NFRC uses a combination of physical testing and thermal modeling with an approved software package to determine the U-Factor for a window assembly (NFRC 2014). NFRC defines the standard method that is currently accepted by the glass industry for use in evaluating the thermal performance of window assemblies, whereas AAMA is a voluntary method for evaluating the thermal performance of window assemblies. To meet the requirements of most international building energy codes, various state building energy codes in the U.S., ASHRAE standards, voluntary or incentive programs such as ENERGY STAR, etc., windows must be rated according to the criteria set forth in NFRC standards. The thermal modeling software packages that are typically used to determine the U-Factor for window assemblies are discussed below.

Energy Performance Software

The thermal performance indices for windows are typically evaluated using the well-known THERM and WINDOW programs. The WINDOW and THERM programs are supported by the Windows and Daylight Group at LBNL. The program is funded by the U.S. Department of Energy (DOE) and is available to the public free-of-charge.

WINDOW and THERM are established, well-supported, and accepted programs for determining thermal performance indices of windows (ASHRAE 2013). Originally developed independently, these two programs have been integrated together and are used to

determine overall window U-Factors, among other things. THERM is a two-dimensional heat transfer analysis program that uses FE methods to solve the governing energy equations. THERM is used to calculate the two-dimensional heat transfer that occurs along the edge of the glass plate area and frame system of a window. WINDOW is a one-dimensional heat transfer analysis program that is based on an iterative numerical solution method. It is used to calculate the one-dimensional center-of-glass heat transfer and optical properties of the IG unit. The algorithms used for these calculations are detailed in the International Organization for Standardization (ISO) Standard 15099 *"Thermal performance of windows, doors and shading devices – Detailed calculations"* (ISO 2003).

Specifically, the U-Factor is determined as given by Eq. (62) previously, which includes any heat-transfer across the center-of-glass area, edge-of-glass area, and the framing system. It is determined based on a set of standardized environmental conditions, product sizes, and testing requirements (NFRC 2014). The standard environmental conditions include the surface film coefficients, which are a function of the wind speed, and the outdoor and indoor air temperatures (Lingnell 1981). By standardizing the test and modeling procedure, designers can compare the energy-efficiency of windows fairly and accurately.

Practical Significance to the Discussion Herein

The practical significance of this discussion to the research herein is two-fold. First, it is possible that the U-Factor may be erroneously assumed as a substitute to the CEEC that is presented as a part of this research. Secondly, while the WINDOW and THERM program package is widely used in practice and is relevant to determine the energy performance ratings of windows for the purpose of estimating steady-state heat transfer, these programs do not provide an accurate substitute for calculating the transient thermal

stress design condition that is caused by solar irradiance. Each of these are discussed in detail below.

It would be tempting to misconstrue the window U-Factor, or perhaps even more so, the center-of-glass U-Value as an alternative to the CEEC that is discussed herein. This can lead to significant errors. The primary reason for this is that both the U-Factor and U-Value are calculated using a specific set of environmental conditions that were not intended to represent the critical thermal stress design condition. Rather, the standard environmental conditions associated with determining the U-Factor were selected for the purpose of estimating building energy use. AAMA (2009) states:

> *The U-Value determined by tests at the standard test conditions can be used in estimating design loads for heating and cooling equipment of most low-rise residential buildings, since the surface coefficients are intended to be the same as those recommended in the ASHRAE method of calculating residential loads. Applicability of the test U-values to other building types should be determined by a competent engineer.*

Further, the U-Factor and U-Value represent the air-to-air heat transfer through the window, whereas the CEEC is specific to the heat transfer that occurs across the gas space cavity of the IG unit. It does not include the conductance through the glass plates or the effects of the indoor and outdoor surface films that develop. In addition, the standard indoor and outdoor temperatures of 32 °F and 68 °F that are used in the U-Factor calculations are not necessarily representative of the temperatures that are reached in the gas space cavity during a thermal design condition. Likewise, the surface film coefficients that are applied are representative of a situation where heat flows more readily from the window to the surrounding indoor and outdoor environments. This is useful when determining building energy use and/or estimating design loads to properly size the building's heating and cooling equipment. However, it does not necessarily represent the thermal

design condition where it is desired to maximize the heat gain in the IG unit's center-of-glass area when exposed to solar irradiance.

Regarding energy-performance software, often times design professionals will use modified NFRC models and the WINDOW and THERM program package, or an equivalent, to estimate the maximum temperature difference that occurs between the center-of-glass and the perimeter-of-glass due to solar irradiance (Wright and Barry 1999; Fisher 2007). More often than not an analysis of this type is simply the product of convenience and/or the lack of an adequate tool to accurately analyze thermal stress in windows that employ IG units. The convenience occurs because NFRC models are created for almost all windows manufactured and sold in the U.S. (Fisher 2007). Prior to the simplified design procedure (SDP) presented herein, advanced FE software packages were required to analyze the transient temperatures that occur in windows with IG units that are subjected to solar irradiance. Even though advanced FE packages are readily available, no formal design procedure (FDP) has been presented to properly analyze thermal stress in IG units prior to the research herein.

The primary reason that the use of energy performance software is ill-advised to estimate thermal stress in IG units is because it typically provides an overly conservative estimate for the maximum temperature difference that develops between the center-of-glass and the perimeter-of-glass. When it is not overly conservative, the estimate is almost never accurate. While this method is convenient, it often leads the design professional to specify heat-treated glass that is not necessarily required.

The reason that the analysis can be overly conservative and is inaccurate is because the transient nature of the temperature data is not calculated. Rather, energy performance software packages employ only a steady-state algorithm to calculate constant temperatures and heat flow that are independent of time. It is shown herein that the maximum thermal stresses develop as a function of time for IG units. This requires the use of a

transient algorithm to accurately calculate the maximum thermal stresses that develop in IG units.

When only a steady-state algorithm is used, two separate analyses are required to estimate the maximum thermal stress that develops in an IG unit. The first analysis calculates the steady-state perimeter-of-glass temperature, during night-time conditions when the IG unit is subjected to an indoor and outdoor temperature difference and zero solar irradiance. The second analysis calculates the steady-state center-of-glass temperature, during daytime conditions when the IG unit is subjected to an indoor and outdoor temperature difference and solar irradiance. The difference in magnitude of the output temperature from each of these analyses is taken as the maximum temperature difference between the center-of-glass and the perimeter-of-glass. It should be clear that under no circumstances is this method an accurate replacement for a proper thermal stress analysis that employs a transient solution.

The next chapter of this paper presents a FDP to evaluate the POB of a glass plate in an IG unit that is subjected to solar irradiance. As part of this effect, detailed FE analyses are used to estimate the thermal stress that develops in the IG unit as a function of time. This is achieved using a transient algorithm to calculate the stress and causal temperatures. The FDP is then used on eight practical applications to show its utility in determining the POB of glass plate in an IG unit that is subjected to solar irradiance.

CHAPTER IV
FORMAL DESIGN PROCEDURE TO EVALUATE THE PROBABILITY OF BREAKAGE OF GLASS PLATES IN INSULATING GLASS UNITS SUBJECTED TO SOLAR IRRADIANCE

There are numerous variables that affect the thermal behavior of insulating glass (IG) units. Thus, calculating the thermal stresses that occur in an IG unit that is exposed to solar irradiance is complex (Klam 2007; Lingnell and Beason 2013). Two of the primary objectives of this research are to further improve the understanding of how thermal stresses develop in IG units and develop a simplified design procedure (SDP) that can be used to evaluate the probability of breakage (POB) for glass plates in generic IG units that are exposed to a set of generic environmental conditions. However, before a SDP can be established, a formal design procedure (FDP) is needed that provides a method to evaluate the POB for glass plates in a specific IG unit that is subjected to a specific set of environmental conditions. Therefore, a FDP was successfully developed as part of this research.

This chapter is dedicated to explaining the steps required to implement the FDP and evaluate the POB for glass plates in a specific IG unit subjected to a specific set of environmental conditions. As part of this effort, it is assumed that the heat transfer through the gas space cavity of the IG unit can be reasonably modeled using the combined energy exchange coefficient (CEEC). This concept will be developed further in Chapter V. The next section of this chapter provides details regarding the steps and developmental process for the FDP. The final section of this chapter presents several examples of practical applications that were analyzed using the FDP.

Formal Design Procedure

The primary purpose of the FDP is to provide specific guidelines that can be used to design glass plates in IG units to withstand thermal stresses that are caused by solar irradiance. The FDP for evaluating a specific IG unit subjected to a specific set of environmental conditions involves the following 10 steps:

1. Define the specific IG unit's geometry including the frame and spacer.
2. Define the specific environmental conditions that the IG unit will be subjected to. This includes the indoor and outdoor temperatures, indoor and outdoor surface film coefficients, and level of solar irradiance.
3. Perform a ray tracing procedure to determine the heat that is generated due to solar irradiance for both the inner and outer glass plates of the IG unit.
4. Measure the CEEC using the formal test procedure (FTP) presented later in Chapter V to estimate the heat transfer through the gas space cavity of the IG unit.
5. Develop a detailed finite element (FE) model that reasonably represents the IG unit, frame, and spacer geometry. In addition, the FE model must reasonably represent the thermal properties of all of the materials used.
6. Perform a steady-state thermal FE analysis using the defined indoor and outdoor temperatures and surface film coefficients that were selected in step 2 with zero solar irradiance applied. This step establishes the initial temperatures for the FE model that will be used for the transient thermal FE analysis in the next step.
7. Perform a transient thermal FE analysis using the initial temperatures that were established in the previous step and applying the solar irradiance that was selected in step 2. The amount of solar irradiance absorbed by the inner and outer glass plates were calculated in step 3. The duration for the load should be 60 min.

8. Using Eq. (66) and the results generated in the previous step, calculate the maximum difference in temperature between the center-of-glass and the perimeter-of-glass for the glass plate of interest (i.e. inner glass plate, outer glass plate, or both)
9. Using Eq. (7) and the temperature(s) from the previous step, calculate the maximum perimeter-of-glass tensile stress for the glass plate(s) of interest.
10. Apply the glass edge strength failure prediction model (ESFPM) and compare the allowable stress to the stress(es) calculated in step 9 for a selected POB.

The FDP presents the steps that are required to properly evaluate the POB of a glass plates when used in a specific IG unit and subjected to a specific set of environmental conditions. Thus, the FDP must be repeated for any changes in the assumed input parameters. As discussed previously, these parameters include the type of frame, type of spacer, types of coatings applied, tints of glass plates, the gas used to fill the gas space cavity, absorptances of each glass plate, indoor and outdoor temperatures, etc.

Finite Element Analysis

Thermal FE analyses are performed in three basic steps as described in steps 5 through 7 above. First, the FE model must be developed, next a steady-state thermal FE analysis must be performed, and finally a transient thermal FE analysis must be performed. The steady-state thermal FE analysis establishes the steady-state temperature conditions that exist just before the IG unit is exposed to solar irradiance. This temperature distribution is the source of an initial stress that develops in the glass plates of the IG unit. The transient thermal FE analysis establishes the critical variation of temperature across the areas if the inner and outer glass plates as a function of time. The center-of-glass and perimeter-of-glass temperatures are then used to determine the maximum perimeter-of-glass

thermal stress for the specific set of environmental conditions of interest. The next section of this paper details the methods that were followed to develop the FE models that were used for the research herein.

Finite Element Modeling Using Half-Model Geometry

The FE analyses performed as part of this research were accomplished using LS-DYNA, an advanced general-purpose FE code developed by Livermore Software Technology Corporation (LSTC) (Hallquist 2006, LSTC 2014a; LSTC 2014b). LS-DYNA is a multi-physics software package that is capable of modeling complex thermal problems (LSTC 1999; Maker 2004; Shapiro 2013). The first step to determine the variation in temperature across the glass plates' areas of an IG unit subjected to a set of environmental conditions as a function of time was to develop a FE model that accurately represents the IG unit of interest. The heat transfer that occurs through the center-of-glass area is one-dimensional, whereas the heat that is transferred through the edge-of-glass area is two-dimensional. Thus, a two-dimensional FE model is required to accurately determine the temperature distribution in the IG unit and window assembly (Wright and Sullivan 1995; Wright 1998; Gordon 2001; Manz 2003; Ismail and Henriquez 2005; ASHRAE 2013).

The geometry of the IG units were modeled using a construct of nodes and elements. Two-dimensional models were constructed using a single row (i.e. width) of 8-noded brick elements for the FE analyses performed as part of this research. A minimum length is needed to fully capture the development of the transition in temperature between the center-of-glass area and the perimeter-of-glass. Unless stated otherwise, a minimum length of at least 12 in. was used for the FE analyses herein. In the longitudinal direction, the nodes were spaced at 0.25 in. In the transverse direction, the nodes were spaced at half of the glass plate's thickness. Based on a simple convergence study,

it was found that this discretization scheme was sufficient to accommodate the temperature distribution in all cases considered. A cross-section of the model used for all of the FE modeling herein is shown in Fig. 30. A close-up view of the spacer and element mesh are shown in Fig. 31.

Fig. 30. FE Model of IG Unit

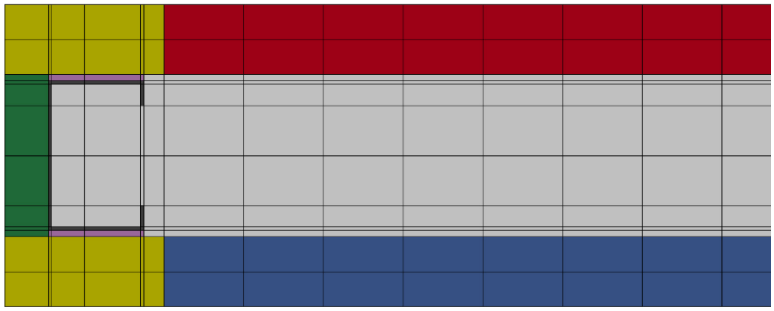

Fig. 31. FE Model of Thin, Steel-Channel Spacer

The FE model shown in Figs. 30 and 31, is a representation of the IG unit shown in Fig. 32. Geometric details of the thin, steel-channel spacer used are shown in Fig. 33. The inner and outer glass plates are shown on top and bottom, respectively.

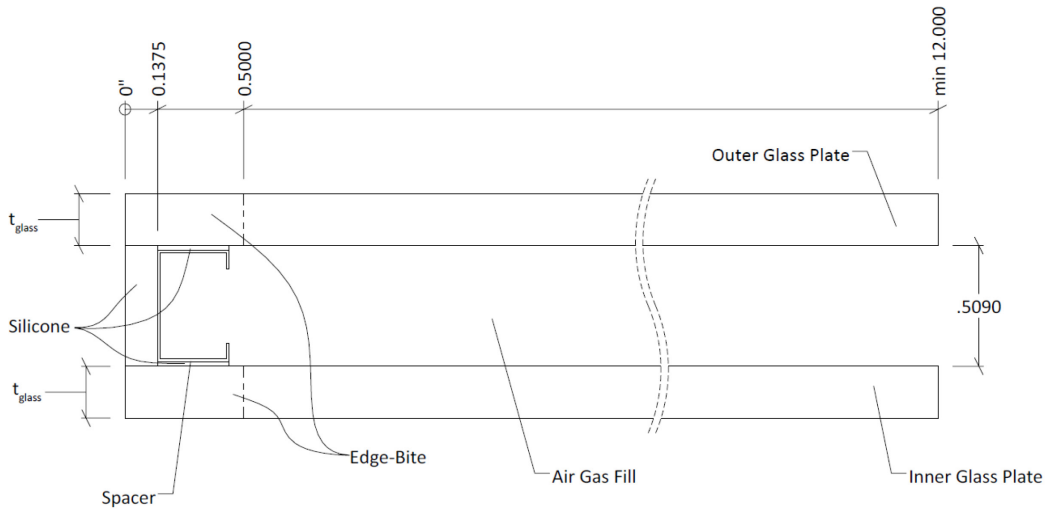

Fig. 32. IG Unit Geometry for FE Analyses

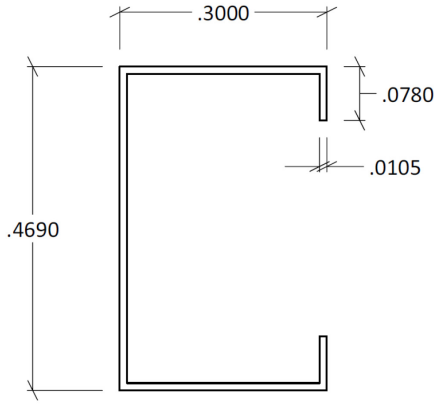

Fig. 33. Thin, Steel-Channel Spacer Geometry for FE Analyses

In addition to defining the geometry of the IG unit, the material properties of each part have to be fully defined. For thermal analyses, the specific heat, thermal conductivity, and density for each material are important. The material properties for glass, steel, silicone, and still air, that were used for this research, are presented in Table 2.

Table 2. Material Properties for FE Analyses

Material	Specific Heat ((in.·lb)/((lb·s^2/in.)·°F))	Thermal Conductivity (in.·lb)/(s·in.·°F)	Density ((lb·s^2/in.)/in.^{3})
Glass	721930	0.1275	0.00023505
Steel	430480	5.8404	0.00073504
Silicone	1.2573	0.038719	0.0000045609
Air	865500	0.003140	0.0000001055

When performing a thermal analysis on an IG unit, it is necessary to determine the distribution of temperatures that occur through the IG unit, across the areas of the glass plates. In addition, the analysis must be capable of determining the distribution of temperatures for a range of solar irradiance exposure levels and environmental conditions. The input parameters to perform a thermal analysis using FE methods include the input solar irradiance, indoor temperature, outdoor temperature, outdoor surface film coefficient, and indoor surface film coefficient. For all cases considered, the outdoor surface film coefficient remained constant at 4.2987×10^{-2} (in.·lb/s)/(in.^{2}·°F), as recommended by Beason and Lingnell (2002) and published in ASTM E2431. In addition, the indoor surface film coefficient remained constant at 2.5507×10^{-2} (in.·lb/s)/(in.^{2}·°F), as recommended by Beason and Lingnell (2002) and published in ASTM E2431. For all cases, it was assumed that the heat gain in each glass plate due to absorbed solar irradiance was uniform through the glass plate's thickness (Wright 1998; Powles et al. 2002).

The heat transferred between the glass plates and the indoor and outdoor environments was modeled using the surface film coefficients. The heat transferred through the gas space cavity of the IG unit was modeled using the CEEC. Once a CEEC has been selected it can be converted into an effective thermal conductivity, $k_{effective}$, for use in the FE model. The effective thermal conductivity was used for the gas space cavity's material model to estimate the heat transfer through the gas space cavity (Gordon 2001; Gustavsen et al. 2005). This is achieved by simply multiplying the CEEC by the thickness of the gas space cavity, as given by Eq. (65).

$$k_{effective} = h_{CEEC} \cdot t_{cavity} \tag{65}$$

Where h_{CEEC} is the CEEC and t_{cavity} is the width or thickness of the gas space cavity.

Fig. 34 shows the indoor and outdoor surface film coefficients that were used for the FE models herein. In addition, Fig. 34 shows the application of the CEEC to the FE model.

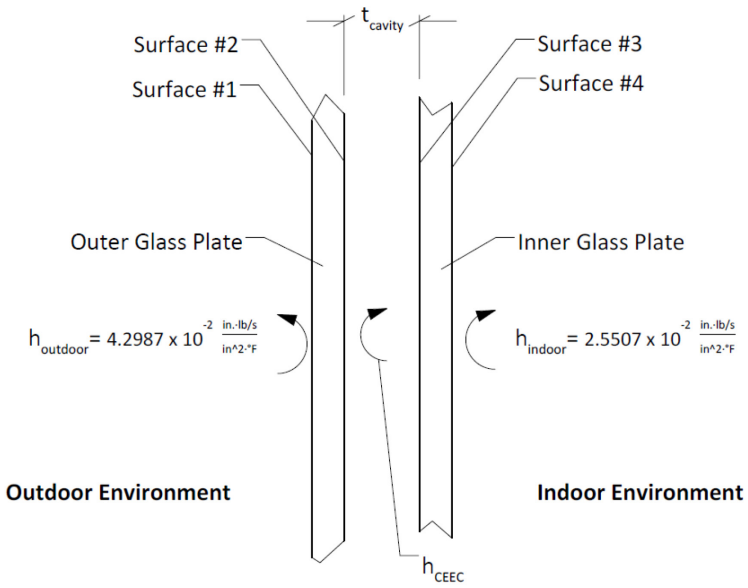

Fig. 34. Surface Film Coefficients and CEEC

Previous research has shown that the heat transfer across the gas space cavity, near the spacer, does experience localized effects (Wright 1996). For the research herein, these localized effects near the spacer were neglected, and a uniform CEEC was used for the entire gas space cavity. Research by Muneer (et al. 1997) has shown that these localized effects for IG units with air as the gas fill were negligible. However, note that these effects may become significant for other gas fills such as Krypton, Argon, etc. (Muneer et al. 1997). The research herein only considered an air filled gas space cavity.

In addition to a constant CEEC, it was also assumed that the temperature distribution across the height of the IG unit remained constant. In fact, the temperature distribution is typically higher at the top of the IG unit than at the bottom. This is the case because of the buoyancy driven effects of convection. In practice, this is often ignored because it requires a much more in depth analysis than is practical. As such, it was not considered herein.

Steady-State Finite Element Analysis

Before the distribution of temperatures, as a function of time, can be determined for an IG unit exposed to solar irradiance, it is necessary to determine the steady-state temperature distribution that develops in the IG unit due to a difference in indoor and outdoor temperatures when no solar irradiance is applied. The results from the steady-state analysis for an IG unit are primarily a function of the indoor temperature, outdoor temperature, indoor surface film coefficient, and outdoor surface film coefficients.

The steady-state thermal FE analysis was used to determine the state of initial stress in the IG unit that is caused by a difference in temperature between the indoor and outdoor environments. This represents the temperatures an IG unit would experience during the night-time conditions with no exposure to solar irradiance. The heat transfer associated with a steady-state thermal analysis remains constant with time. Such an analysis is often incorrectly termed an "equilibrium" analysis. This is incorrect because a thermal equilibrium analysis requires a state of zero heat transfer (Datta 2002). Rather, the steady-state thermal analysis means that the rate of heat transfer is constant and therefore, so are the temperatures that develop throughout the IG unit. The temperatures are not necessarily uniform in magnitude throughout the IG unit.

Transient Finite Element Analysis

Once the distribution of temperatures have been established for the steady-state FE model, the transient distribution of temperatures, as a function of time, due to solar irradiance can be determined. Various time increments were used to determine the minimum time step required for the analyses herein. Ultimately, it was determined that a time step of 15 s was sufficient for all of the situations examined as part of this research. Thus, for all of the FE analyses reported in this dissertation, the time step was taken to be 15 s.

The transient thermal FE analysis provides the perimeter-of-glass and center-of-glass temperatures for the glass plate over a 60-min period. The difference in temperature between the center-of-glass and the perimeter-of-glass can then be calculated for each time step. The maximum temperature difference, ΔT_{max}, corresponds to the maximum perimeter-of-glass thermal stress that the IG unit would experience over 60 min of exposure to solar irradiance. This temperature is calculated using Eq. (66).

$$\Delta T_{max} = \max_{0 \le i \le 3600} \left(T_{COG_i} - T_{POG_i} \right) \tag{66}$$

Where T_{COG_i} is the center-of-glass temperature for time step i and T_{POG_i} is the perimeter-of-glass temperature for time step i. Here, time step i is expressed in s from zero to 3600 s.

The maximum tensile stress that develops in the glass plate is proportional to the maximum difference in temperature between the center of the glass plate and the perimeter of the glass plate. Once the maximum difference in temperature has been established by the transient FE analysis, the maximum thermal stress, σ_{max}, that occurs along the perimeter of the glass plate can be calculated by multiplying by the thermal coefficient of

expansion of the glass, α_t, and the modulus of elasticity, E. This was shown previously in Eq. (7) and is repeated in Eq. (67) for convenience.

$$\sigma_{max} = \alpha_T \cdot E \cdot (T_{COG} - T_{POG}) \tag{67}$$

Where the coefficient of thermal expansion for plate glass is 4.9×10^{-6} (in./in.)/°F (AAMA 1984) and the modulus of elasticity for plate glass is 10.4×10^{6} psi (AAMA 1984; Beason and Lingnell 2002). If the center-of-glass temperature is greater than the perimeter-of-glass temperature, the stress along the perimeter of the glass plate will be tensile and is represented by a positive sign. If the center-of-glass temperature is less than the perimeter-of-glass temperature, the stress along the perimeter of the glass plate will be compressive and is represented by a negative sign.

Practical Application

The FDP discussed previously was used to determine the maximum difference in temperature between the center-of-glass and the perimeter-of-glass and the associated perimeter-of-glass thermal stress for a set of exemplar IG units. The purpose of this practical application was to demonstrate the use of the FDP to calculate the thermal stress using FE analyses of realistic IG units. It was assumed for the following analyses that the surface film coefficients were 2.5507×10^{-2} (in.·lb/s)/(in.^{2}·°F) and 4.2987×10^{-2} (in.·lb/s)/(in.^{2}·°F) for the indoor and outdoor environments, respectively. The FDP was performed on a total of eight cases using various IG unit configurations.

The thickness, solar transmittance, solar absorptances, solar reflectance, and emissivity for two glass plates are presented in Table 3. Where $\rho_{1,4}$ is the solar reflectance of the number 1 or 4 surface of the glass plate. Where $\rho_{2,3}$ is the solar reflectance of the number 2 or 3 surface facing the gas space cavity. Where $\epsilon_{1,4}$ is the surface emissivity of the number 1 or 4 surface of the glass plate. Where $\epsilon_{2,3}$ is the emissivity of the number 2 or

3 surface facing the gas space cavity. Where all other variables are as previously defined.

Table 3. Solar Optical Properties for the Exemplar Glass Plates

Glass Plate	t_{glass} (in.)	τ_S	α_S	$\rho_{1,4}$	$\rho_{2,3}$	$\epsilon_{1,4}$	$\epsilon_{2,3}$
1/4 in. Clear	0.219	0.7855316	0.1436073	0.0708611	0.0708611	0.84	0.84
1/4 in. Low-E, Soft-Coat	0.219	0.3614098	0.3362339	0.3023563	0.4687274	0.84	0.0367495

These two glass plates were used in various combinations with either a perfectly insulated or high-heat mass frame to create four exemplar IG unit configurations. These four configurations are presented in Table 4. The edge bite for all cases was assumed to be 0.5 in. Once the configuration for each IG unit had been defined, the ray tracing procedure was used in combination with the solar optical properties presented in Table 3 to determine the absorption of solar irradiance, α_{inner} and α_{outer}, for the inner and outer glass plates, respectively. These values, along with the assumed CEEC, h_{CEEC}, for each IG unit configuration are presented in Table 5. The CEEC for this exercise was taken from research presented by Klam (2007) and for the purposes of this practical application assumed to be correct.

Table 4. Construction and Frame Type for the Exemplar IG Units

Insulating Glass Unit	Outer Glass Plate	Inner Glass Plate	Frame
IGU 1	1/4 in. Clear	1/4 in. Clear	Perfectly Insulated
IGU 2	1/4 in. Clear	1/4 in. Clear	High-Heat Mass
IGU 3	1/4 in. Low-E, Soft-Coat	1/4 in. Clear	Perfectly Insulated
IGU 4	1/4 in. Low-E, Soft-Coat	1/4 in. Clear	High-Heat Mass

Table 5. Thermal Properties for the Exemplar IG Units

Insulating Glass Unit	α_{outer}	α_{inner}	h_{CEEC} ((in.·lb/s)/(in.·°F))
IGU 1	0.1517	0.1134	0.0202723
IGU 2	0.1517	0.1134	0.0202723
IGU 3	0.3407	0.0537	0.006694
IGU 4	0.3407	0.0537	0.006694

Each of the four configurations of IG units shown in Table 4 were subjected to a set of two environmental conditions. These are shown in Table 6 and the complete set of FE cases that were analyzed is shown in Table 7. Where all of the variables are as previously defined.

Table 6. Environmental Conditions Used for Exemplar IG Units

Environmental Condition	$T_{outdoor}$ (°F)	T_{indoor} (°F)	I_S ((in.·lb/s)/in.^{2})
Env. Condition 1	-10	79	4.9967
Env. Condition 2	105	68	5.9789

Table 7. FE Analysis Cases

Case No.	Outer Glass Plate	Inner Glass Plate	$T_{outdoor}$ (°F)	T_{indoor} (°F)	I_S ((in.·lb/s)/in.^{2})	Frame
FEA 1	1/4 in. Clear	1/4 in. Clear	-10	79	4.9967	Perfectly Insulated
FEA 2	1/4 in. Clear	1/4 in. Clear	-10	79	4.9967	High-Heat Mass
FEA 3	1/4 in. Clear	1/4 in. Clear	105	68	5.9789	Perfectly Insulated
FEA 4	1/4 in. Clear	1/4 in. Clear	105	68	5.9789	High-Heat Mass
FEA 5	1/4 in. Low-E, Soft-Coat	1/4 in. Clear	-10	79	4.9967	Perfectly Insulated
FEA 6	1/4 in. Low-E, Soft-Coat	1/4 in. Clear	-10	79	4.9967	High-Heat Mass
FEA 7	1/4 in. Low-E, Soft-Coat	1/4 in. Clear	105	68	5.9789	Perfectly Insulated
FEA 8	1/4 in. Low-E, Soft-Coat	1/4 in. Clear	105	68	5.9789	High-Heat Mass

Table 8 shows the maximum difference in temperature between the center-of-glass and the perimeter-of-glass for the eight FE cases analyzed using the FDP. Included are the maximum difference in temperature for both the inner, ΔT_{inner}, and outer, ΔT_{outer}, glass

plates. Table 9 shows the perimeter-of-glass thermal stress that is associated with the maximum temperature difference between the center-of-glass and the perimeter-of-glass for the eight FE cases. Included are the maximum thermal stresses for both the inner, σ_{inner}, and outer, σ_{outer}, glass plates. These stress data were calculated by applying Eq. (7) to the temperature data presented in Table 8.

Table 8. Temperature Results of FE Analyses for Exemplar IG Units

Case No.	ΔT_{outer} (°F)	ΔT_{inner} (°F)
FEA 1	-16.06	23.35
FEA 2	1.76	38.52
FEA 3	12.51	-7.72
FEA 4	28.12	15.84
FEA 5	-24.95	30.93
FEA 6	10.65	44.76
FEA 7	27.76	-21.76
FEA 8	53.00	5.07

Table 9. Stress Results from the FE Analyses for Exemplar IG Units

Case No.	σ_{outer} (psi)	σ_{inner} (psi)
FEA 1	-818	1190
FEA 2	90	1963
FEA 3	638	-393
FEA 4	1433	807
FEA 5	-1271	1576
FEA 6	543	2281
FEA 7	1415	-1109
FEA 8	2701	258

In conclusion, the FDP provides an acceptable tool to determine the level of thermal stress that glass plates in a specific IG unit experience when subjected to a specific set of environmental conditions. Ultimately, the final step of the FDP would be to evaluate the

POB for the inner and outer glass plates according to the level of thermal stresses presented in Table 9 using the glass ESFPM. For brevity, this analysis was not performed for these practical application examples, but it is clear that there are several cases that exhibit excessive thermal stress and would likely lead to in-service breakage, even if the edge conditions were acceptable and the glass plates had been installed correctly.

In addition to the excessive edge stresses presented for these FE cases, an important observation is made. The POB associated with the inner glass plate becomes critical when the outdoor temperature is below the indoor temperature. This is exhibited by FEA 1, 2, 5, and 6. In this situation, the thermal stresses in the outer glass plate were either low-level tensile stresses or compressive stresses.

Conversely, the POB associated with the outer glass plate becomes critical when the outdoor temperature is greater than the indoor temperature. This is exhibited by FEA 3, 4, 7, and 8. In this situation, the thermal stresses in the inner glass plate were also either low-level tensile stresses or compressive stresses. These observations are consistent with previous results presented by others (Pilette and Taylor 1988; Wright and Barry 1999; Klam 2007; Lingnell and Beason 2013) and the glass industry's understanding that the inner glass plate is critical in colder climates and the outer glass plate is more critical in warmer climates.

Case Study for Applying the Formal Design Procedure

An example of the application of the FDP is shown in explicit detail for the IG unit considered in FEA 1 previously. The purpose of this example is to develop a deeper understanding of the thermal response of IG units and the use of the FDP. The IG unit considered as part of FEA 1 was constructed with two clear glass plates, the frame was perfectly insulated, and the indoor and outdoor temperatures were -10 and 79 °F, respectively. The IG unit was subjected to 4.9967 $(\text{in.}\cdot\text{lb/s})/\text{in.}^2$ of solar irradiance.

As part of the FDP, a steady-state thermal FE analysis was performed to determine the initial temperature distribution and state of stress that the IG unit experiences during the night-time condition when exposed to an indoor/outdoor temperature difference. This is associated with step 6 of the FDP detailed previously. Fig. 35 shows the temperature results that were determined using the steady-state thermal FE analysis. Note that the temperature scale shown in Fig. 35 is in °R.

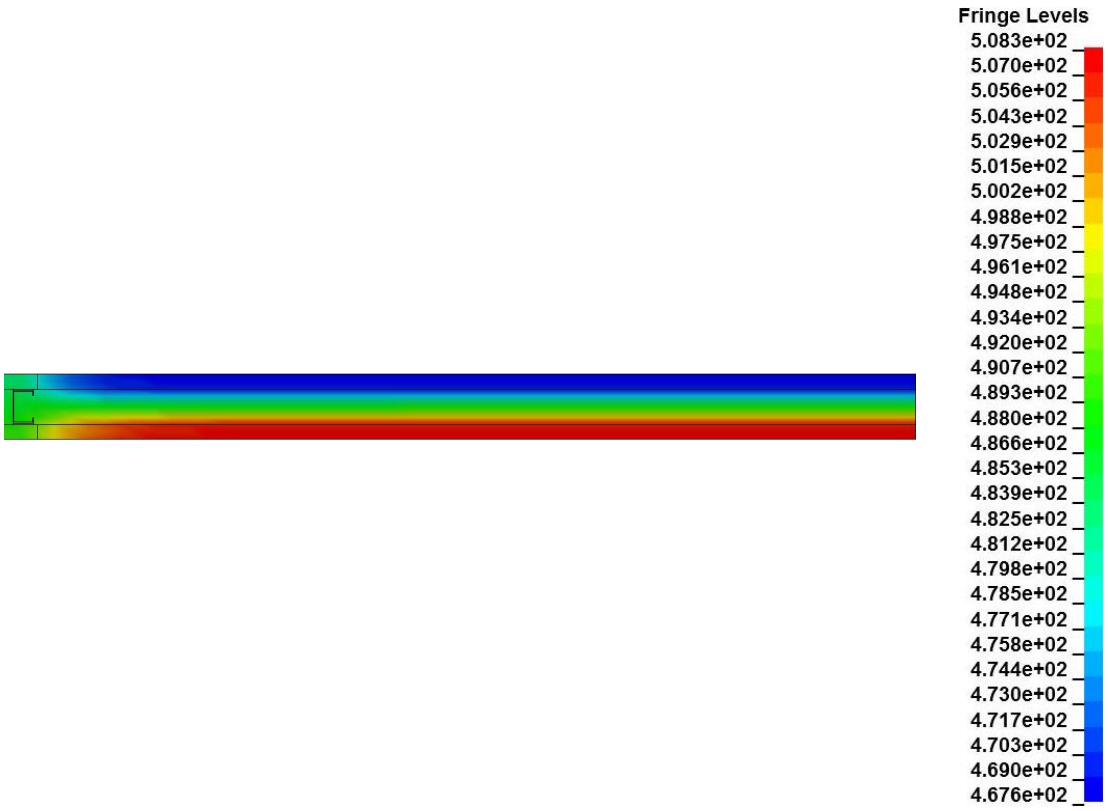

Fig. 35. Steady-State Temperatures for FEA 1

As shown in Fig. 35, the temperatures distributed through the IG unit range from 7.93 °F in the outer glass plate to 48.63 °F in the inner glass plate. The temperature along the edge-of-glass area and edge-seal is approximately 28 °F. The minimum and maximum

temperatures occur in the center-of-glass areas of the outer and inner glass plates, respectively.

Next, the steady-state temperature data are used as the initial temperatures for the transient thermal FE analysis performed as described in step 7 of the FDP. The distribution of temperature through the IG unit, as a function of time, that was calculated using the transient thermal FE analysis is shown in Fig. 36. Note that the temperature scale shown in Fig. 36 is in °R.

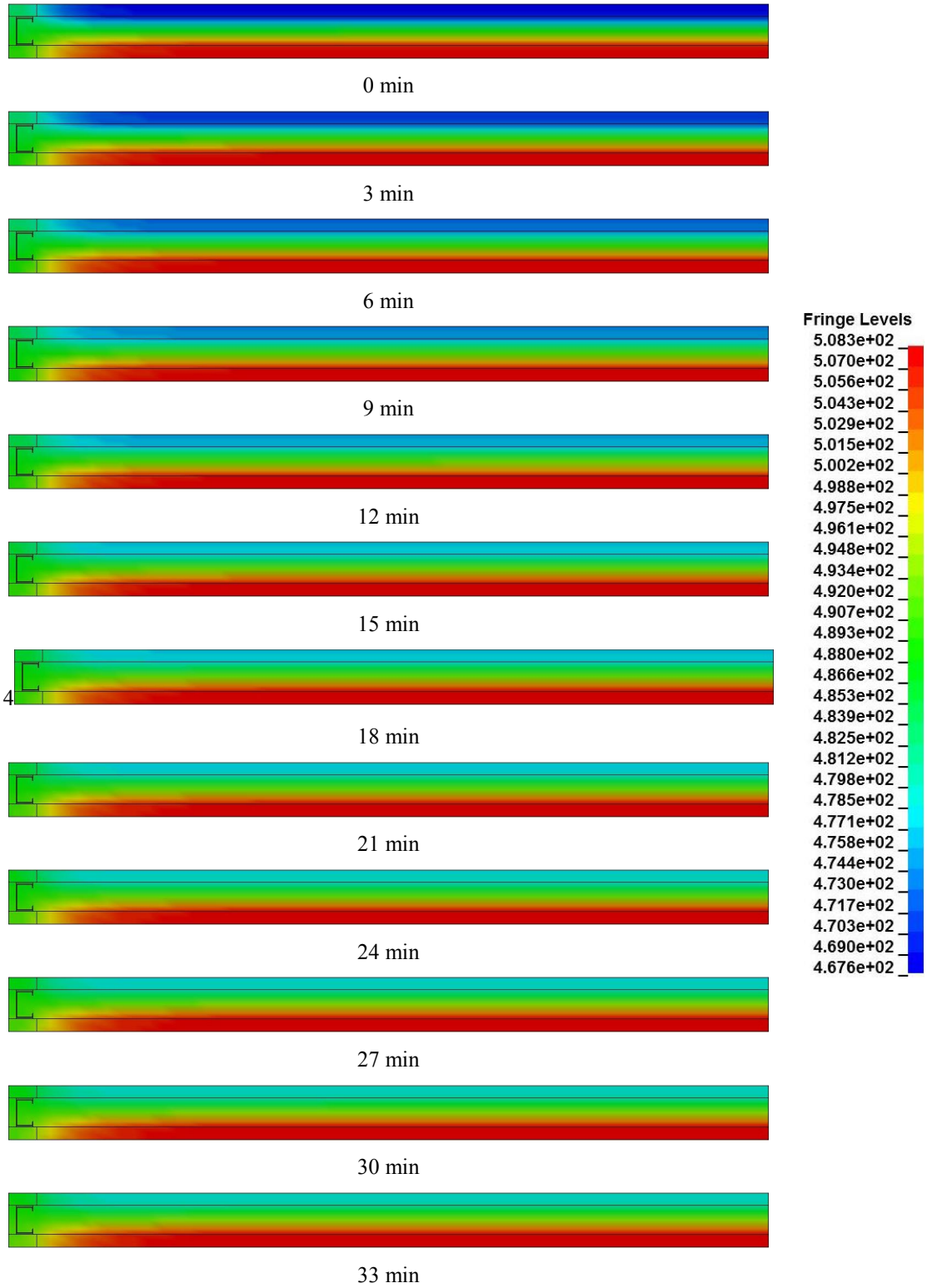

Fig. 36. Transient Temperatures for FEA 1

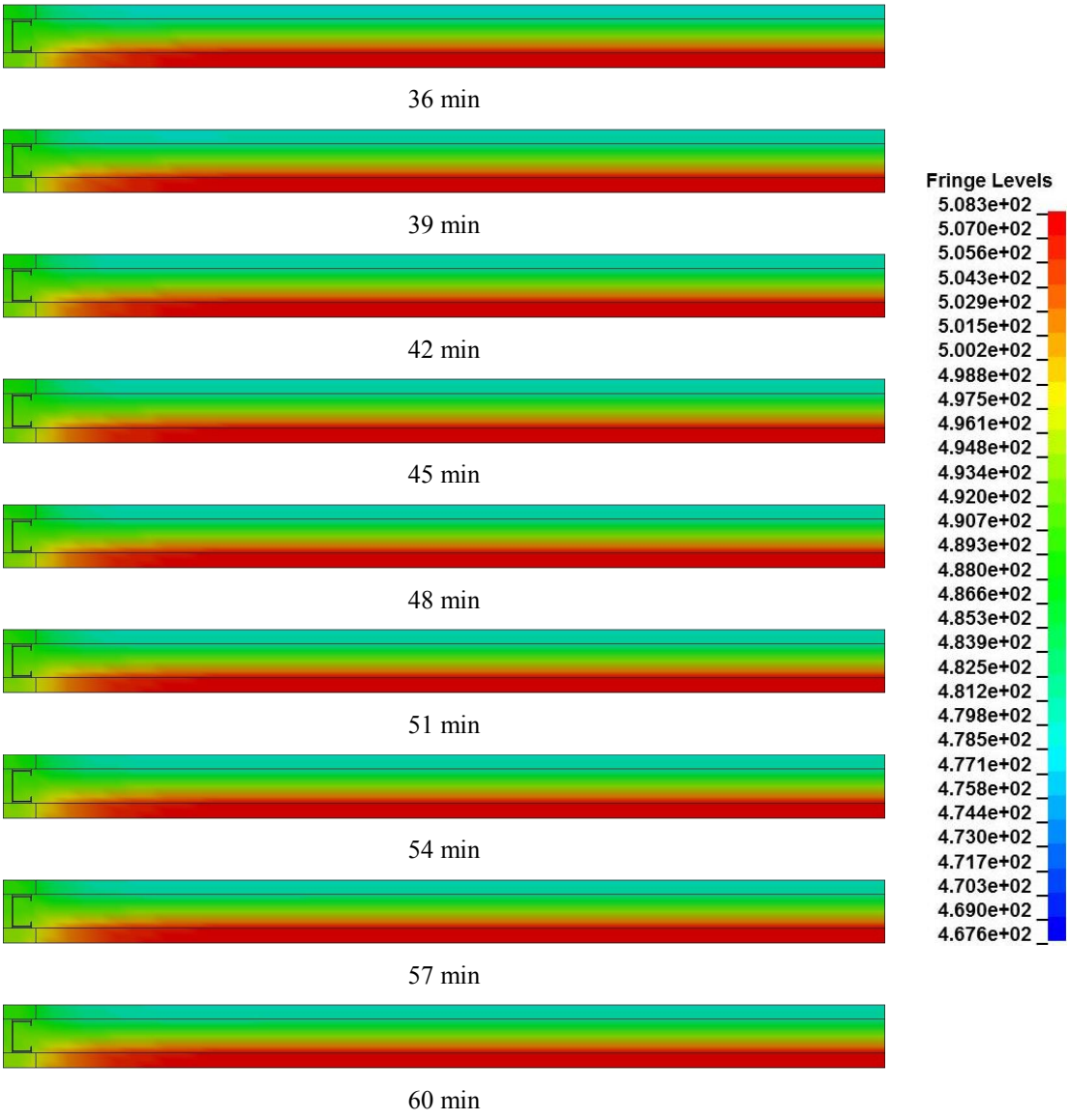

Fig. 36. Continued

As shown in Fig. 36, the temperatures of the center-of-glass areas for both the inner and outer glass plates increase as a function of time when the IG unit is exposed to solar irradiance. After 60-min of exposure to solar irradiance, the IG unit is in a steady-state of heat transfer where the temperature distribution through the IG unit remains constant. It is also shown that the change in temperature along the perimeter-of-glass for each glass

plate occurs at a much slower rate than the center-of-glass areas. As discussed in Chapter III, this differential heating across the area of the glass plate causes thermal stresses to develop. It is also shown in Fig. 36 that the center-of-glass area of the inner glass plate resides at a higher temperature than the perimeter-of-glass temperature. Thus, it is more susceptible to thermal breakage when placed in a cold outdoor environment.

The center-of-glass and perimeter-of-glass temperatures for the inner and outer glass plates are shown in Figs. 37 and 38, respectively. Subtracting these temperature data, the difference in temperature between the center-of-glass and the perimeter-of-glass as a function of time can be calculated. These temperature data, for the outer and inner glass plates, are shown in Figs. 39 and 40, respectively. It is from these temperature data that the maximum difference in temperature between the center-of-glass and the perimeter-of-glass are determined using Eq. (66). This maximum difference in temperature between the center-of-glass and the perimeter-of-glass is used to calculate the maximum thermal stress that occurs along the perimeter of the glass plate using Eq. (67).

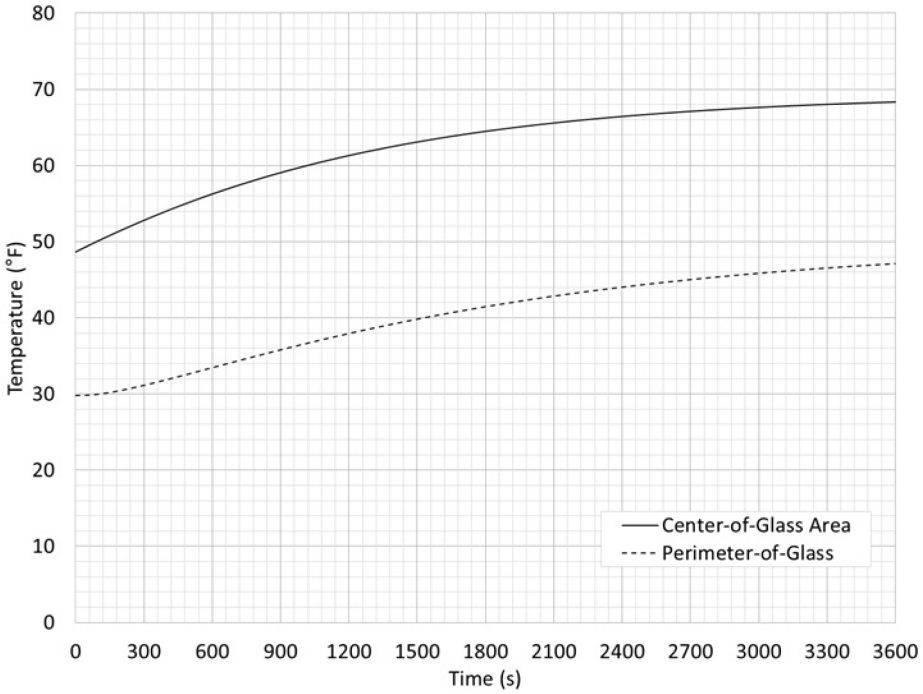

Fig. 37. Transient Response for the Inner Glass Plate of FEA 1

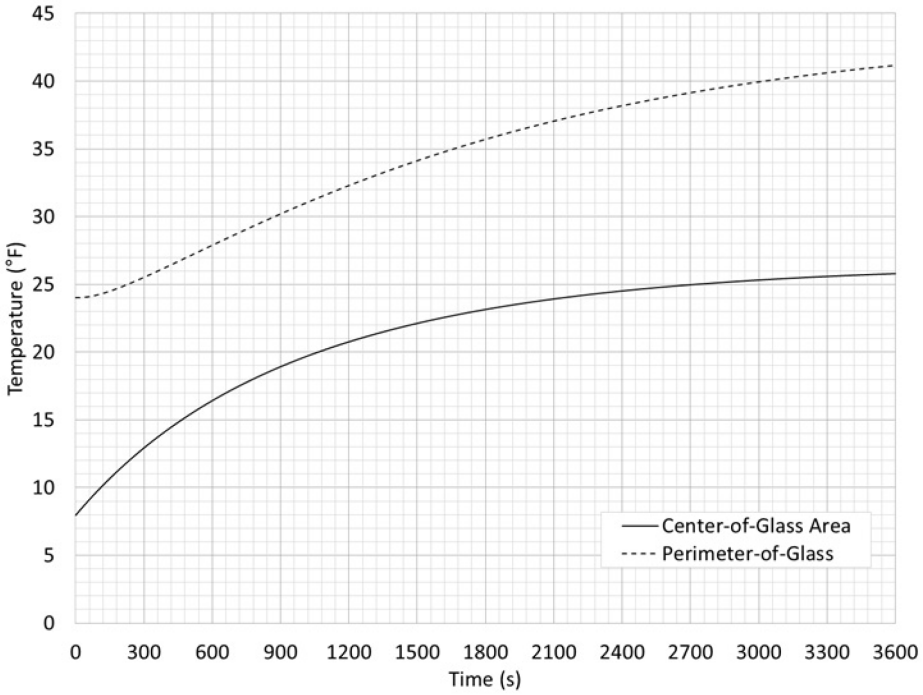

Fig. 38. Transient Response for the Outer Glass Plate of FEA 1

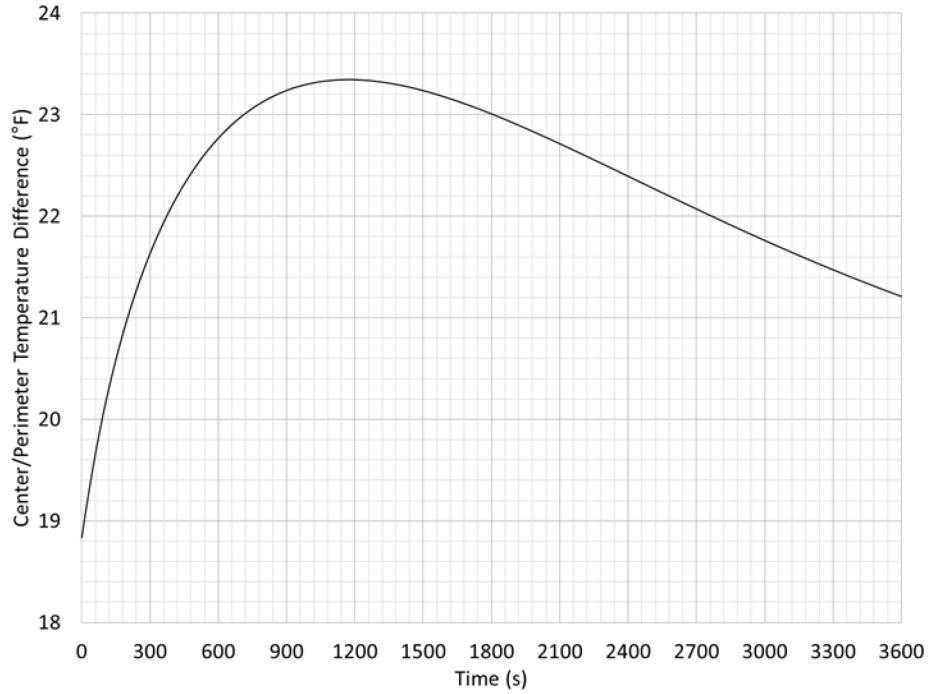

Fig. 39. Transient Center/Perimeter Temperature Difference for the Inner Glass Plate of FEA 1

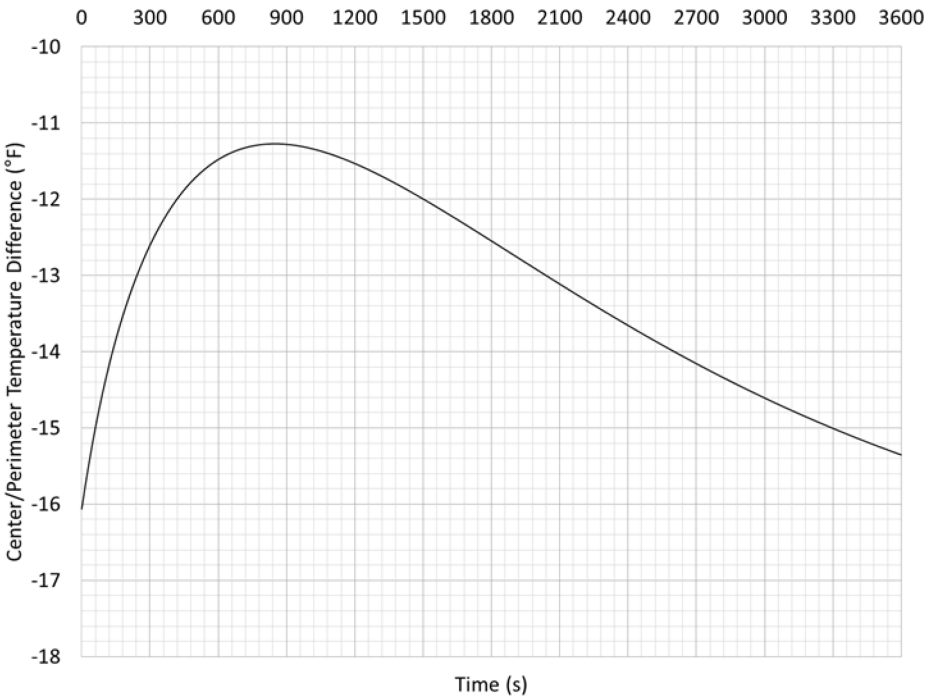

Fig. 40. Transient Center/Perimeter Temperature Difference for the Outer Glass Plate of FEA 1

As shown in Fig. 39, the maximum difference in temperature between the center-of-glass and the perimeter-of-glass for the inner glass plate used in FEA 1 was 23.35 °F which occurred approximately 1170 s after initial exposure to solar irradiance. This value was presented in Table 8 previously for the inner glass plate. As shown in Table 9, this value would be associated with a maximum tensile thermal stress of approximately 1,190 psi along the perimeter of the glass plate.

As shown in Fig. 40, the maximum difference in temperature between the center-of-glass and the perimeter-of-glass for the outer glass plate used in FEA 1 was -16.06 °F which was associated with the initial steady-state temperature prior to exposure to solar irradiance. This value was presented in Table 8 previously for the outer glass plate. As shown in Table 9, this value would be associated with a compressive thermal stress of approximately 818 psi along the perimeter of the glass plate.

The accuracy of the results produced by these FE analyses and the FDP are largely based on a reasonable estimate of the CEEC that was described in step 4. This coefficient offers a convenient way to linearize the thermal analysis and remove the need for iterative calculations. The concept for using the CEEC was originally introduced for the specific purpose of analyzing thermal stress in IG units and was originally determined using a theoretical approximation (Klam 2007).

While using the FDP for a specific situation to calculate the POB is the most desirable and accurate approach, it is not always practical or economically feasible to accomplish this for each individual IG unit and/or situation of interest. Thus, a SDP is needed that can account for generic IG units exposed to generic environmental conditions. Such an analysis would allow for a reasonable estimate of the POB for a large number of IG units subjected to a wide set of environmental conditions without performing the FDP discussed in this chapter. The SDP is discussed in Chapter VI. The CEEC is discussed in detail in the next chapter.

CHAPTER V
COMBINED ENERGY EXCHANGE COEFFICIENT

The primary difference between analyzing a monolithic glass plate and an insulating glass (IG) unit for thermal stress is the heat exchange that occurs between the inner and outer glass plates. Heat is exchanged across the gas space cavity through the fundamental heat transfer mechanisms of conduction, natural convection, and long-wave radiation. These mechanisms combine in a non-linear fashion that requires an iterative numerical analysis to determine the exact development of thermal stresses in the individual glass plates (Wright 1996; Muneer et al. 1997).

Klam (2007) developed a numerical propagation procedure (NPP) that combines the non-linear effects of conduction, natural convection, and long-wave radiation into a single, linear term called the combined energy exchange coefficient (CEEC). His research showed that the use of the CEEC can closely approximate the non-linear behavior of the heat exchanged across the gas space cavity. In addition, its use greatly simplifies the numerical analysis.

The CEEC is used to replace the gas fill of an IG unit with an effective "solid" material whose equivalent thermal conductivity takes into account the combined effects of convection and long-wave radiation which is added to the thermal conductivity of the still gas fill. When the effects of convection and long-wave radiation are combined with conduction, this is known as an effective thermal conductivity.

Until the research herein, no successful attempts have been made to establish an effective thermal conductivity, specifically for the gas space cavity of an IG unit, experimentally. Such an empirical approach provides a "real world" representation of the CEEC rather than a theoretical approximation as Klam (2007) developed.

This chapter is dedicated to the development of a formal test procedure (FTP) to physically measure a coefficient that represents the heat exchange that occurs due to conduction, natural convection, and long-wave radiation between the center-of-glass area of the inner and outer glass plates of an IG unit. The coefficient is referred to herein as the CEEC. The use of the CEEC simplifies the calculations that are required to perform a thermal analysis to predict the temperature distribution in an IG unit that incorporates a gas space cavity. This is done by removing the need for non-linear iterative procedures. This is one of the most important concepts that was used in the development of the simplified design procedure (SDP) to analyze generic IG units subjected to a general range of environmental conditions. In addition, its use was important for applying the formal design procedure (FDP) presented previously in Chapter IV.

The next section of this paper presents proof-of-concept testing that was used to show the feasibility of physically measuring and using the CEEC to describe the transfer of heat across the gas space cavity. This is followed by a section that describes the FTP that can be carried out by a test laboratory to experimentally determine the CEEC for a given IG unit. Finally, the FTP is carried out on a set of practical examples.

Proof-of-Concept

A single experiment was used to determine two things. First, whether the heat exchanged through the gas space cavity of an IG unit could be quantified through physical testing. Second, whether the use of a CEEC could accurately estimate the heat transferred through the gas space cavity of an IG unit subjected to solar irradiance. Previous research has shown that the CEEC can be estimated using fundamental theories (Klam 2007), whereas this initial test served as a feasibility study to determine whether or not the CEEC can be measured experimentally. This section describes this initial experimental effort.

The experiment was performed on an IG unit specimen with 12 in. by 12 in. dimensions. The specimen was fabricated by using two 0.25 in. thick nominal glass plates. A hard-coat low emissivity (low-E) coating was applied to the number 2 surface of the IG unit. The outer glass plate was 0.223 in. thick and the inner plate was 0.220 in. thick. The gas space cavity was 0.55 in. thick and filled with air. These overall dimensions, glass plate thicknesses, coatings, etc. were not selected for any scientific reason. Rather, IG units are commonly available in 12 in. by 12 in. dimensions as sales samples.

For the analyses in this chapter, the outer and inner glass plates are referred to as the heated and cold glass plates, respectively. The finite element (FE) models that are presented for these models are shown with the heated glass plate on top and the cold glass plate on bottom. Fig. 41 shows the specimen prior to the proof-of-concept test.

Fig. 41. Proof-of-Concept Test Specimen

For the experiment, the specimen was enclosed in a foam board insulation "frame" whereby the number 4 surface and the sides of the IG unit were held in intimate contact with the foam board. This prevented any surface films from developing on the number 4 surface or along the edges of the glass plate, which would greatly complicate the thermal

analysis. Only the number 1 surface of the IG unit was exposed to the outdoor environment. The foam board was covered using foil tape to minimize the solar irradiance absorbed by the foam board directly.

The objective of the experiment was to explicitly extract and quantify the heat that is transferred across the gas space cavity of the IG unit. Thus, the goal of the experiment was to apply a heat flux to the number 1 surface of the IG unit and measure the center-of-glass temperatures, as a function of time, on each side of the IG unit. This is an important distinction from the FDP discussed in the previous chapter where the distribution of temperature across the glass plates' areas were important.

The heat flux was applied using actual solar irradiance. The testing was carried out on January 15, 2014 in College Station, Texas. It was a clear, sunny day with an ambient temperature of approximately 50 °F at the time of testing. The solar irradiance on the day of testing was only impeded by intermittent cloud cover.

To maximize the absorption of the heated glass plate, the number 1 surface of the IG unit was painted with flat black spray paint. In addition to maximizing the solar absorption of the heated glass plate, this served to eliminate the need to perform the ray-tracing procedure that was presented in Chapter III. This is because, at least theoretically, no solar irradiance can reach the cold glass plate due to the opaque number 1 surface. In practice, the flat black spray paint most likely does not block 100 percent of the solar irradiance. However, this was considered acceptable for the initial experiment and it was improved upon for the FTP discussed later.

During the experiment the specimen was subjected to incident solar irradiance using a supporting structure. The center-of-glass temperatures of the heated and cold glass plates were measured. Thermocouples were placed on the number 1 and 4 surfaces using small squares of duct tape. Type K thermocouples and thermometers were used to

measure the ambient, number 1 surface, and number 4 surface temperature data. The specimen was exposed to solar irradiance and temperature data were measured for the center-of-glass areas over a 75-min period. After 75 min, a shade was placed in front of the specimen to block the incident solar irradiance and temperature data were measured for another 45 min. The temperature data were measured in 2-min intervals for the first 40 min and 4 to 5-min intervals thereafter. The overall test setup and temperature data measured are shown in Figs. 42 and 43, respectively.

(a) Exposed Specimen (b) Shaded Specimen

Fig. 42. Proof-of-Concept Test Setup

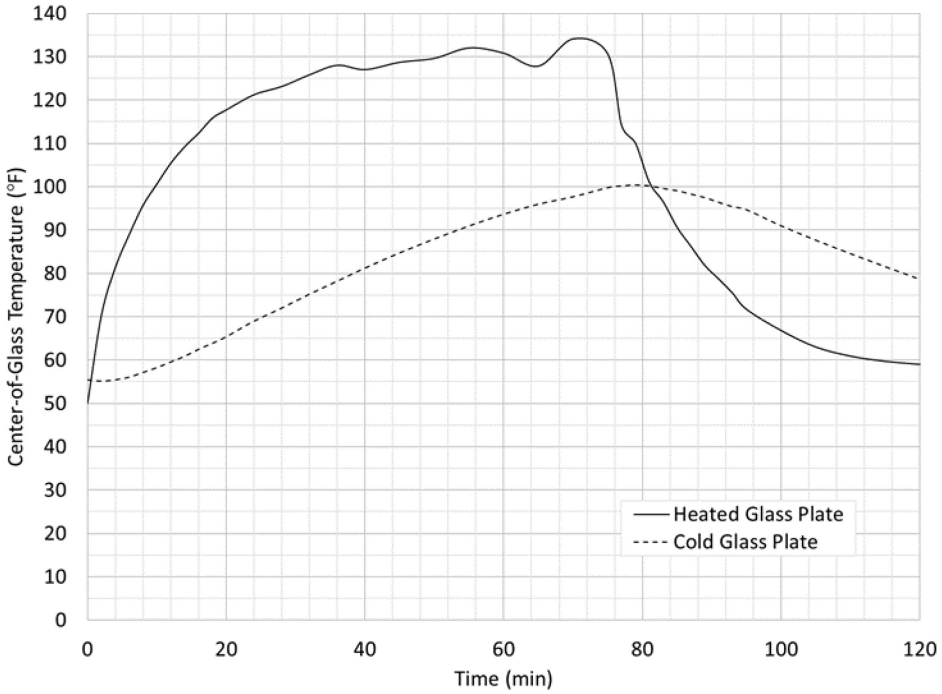

Fig. 43. Proof-of-Concept Center-of-Glass Temperature Data

There are a few interesting observations to be taken from Fig. 43. First, the temperature of the heated glass plate began to stagnate approximately 35 min after initial exposure to solar irradiance. This was the case because the heat transferred to the cold glass plate, combined with the heat lost to the outdoor environment through the surface film coefficient, was equal to the heat flux input by solar irradiance. Secondly, 60 min was not sufficient time for the cold glass plate's temperature to stagnate. The heated glass plate absorbed solar irradiance and increased in temperature rapidly, while the increase in temperature of the cold glass plate occurred at a much slower rate. Note that after the temperature of the heated glass plate began to stagnate, the sudden changes in temperature were due to cloud cover intermittently blocking the solar irradiance and sporadic gusts of wind. The temperature of the heated glass began to immediately reduce when the specimen was shaded from solar irradiance, whereas the cold glass plate continued to increase in temperature for another 8 min before the temperature began to decrease.

Note that there was a 5 °F difference in the initial temperatures between the cold glass plate and the heated glass plate prior to the start of the test. This occurred because the cold glass plate was exposed to solar irradiance during the installation process and sufficient time was not given to allow it to reach thermal equilibrium. For the purposes of this proof-of-concept test this was considered immaterial, but is noted for clarity.

With the number 1 surface painted flat black, the majority of the solar irradiance is either absorbed by the heated glass plate or reflected back into the outdoor environment. Only a small percentage of the solar irradiance is transmitted directly through the heated glass plate to the cold glass plate. With little exposure to solar irradiance, the increase in temperature of the cold glass plate can only be the result of the heat exchange by the fundamental heat transfer mechanisms that occur across the gas space cavity and the thermal bridging that occurs across the edge-seal. Thus, the primary purpose of maximizing and minimizing the absorptions of the heated and cold glass plates, respectively, is apparent. The difference in center-of-glass temperatures between the cold and heated glass plates, measured during the experiment, is shown in Fig. 44.

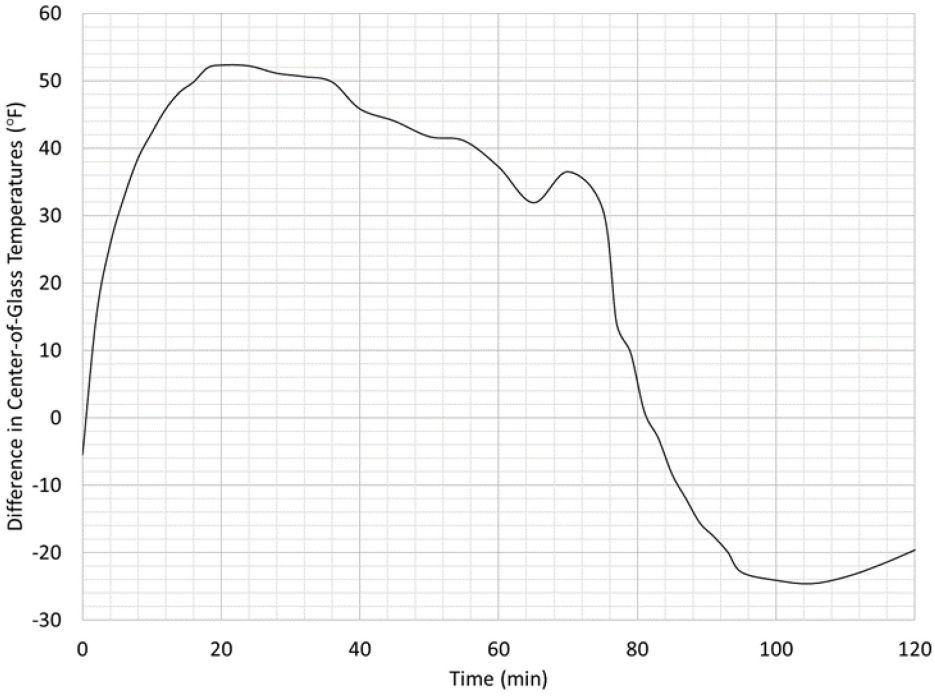

Fig. 44. Difference in Center-of-Glass Temperatures for Proof-of-Concept Test

These data, presented in Fig. 44, show that the maximum difference in the center-of-glass temperatures between the cold and heated glass plates of the IG unit occurred within 60 min of the initial exposure to solar irradiance. Experience within the glass industry has long accepted that thermal loads have durations on the order of 60 min, after which the probability of breakage (POB) is reduced and becomes insignificant in most cases (Beason 1989; Beason and Lera 1989; Beason and Lingnell 2002; ASTM 2012a).

Based on the physical experiment, the center-of-glass temperature distribution as a function of time, when subjected to solar irradiance, for the specimen is known. The next step of the proof-of-concept test was to determine if a "best-fit" coefficient could be identified to estimate the heat transfer across the gas space cavity. This was achieved using a series of parameter identification FE analyses as described below. For these FE analyses, only the first 60 min of the test data were considered.

A detailed FE model of the test specimen was developed using the criteria presented in Chapter IV. A cross-section of the detailed FE model used is presented in Fig. 45. The temperature of the exterior nodes of the heated glass plate (shown on top) was set to follow the temperature data measured during the physical experiment. The cold glass plate's (shown on bottom) temperature was allowed to vary as a function of the CEEC selected to model the gas space cavity.

Fig. 45. Proof-of-Concept Detailed FE Model

The first attempt to determine the CEEC for the test specimen was to employ the NPP presented by Klam (2007). This procedure uses a least-squares regression technique to determine the best-fit coefficient. This procedure was detailed in Chapter III and is not repeated here. In doing so, the NPP led to a best-fit CEEC of 0.01 (in.·lb/s)/(in.·°F) or an effective thermal conductivity of 0.005507 (in.·lb/s)/(in.^{2}·°F) for the 0.55 in. thick gas space cavity.

After the CEEC was determined using the simple NPP, a FE analysis was performed using the value determined for the effective thermal conductivity of the gas space cavity. The results from the FE analysis using this CEEC are shown in Figs. 46 and 47.

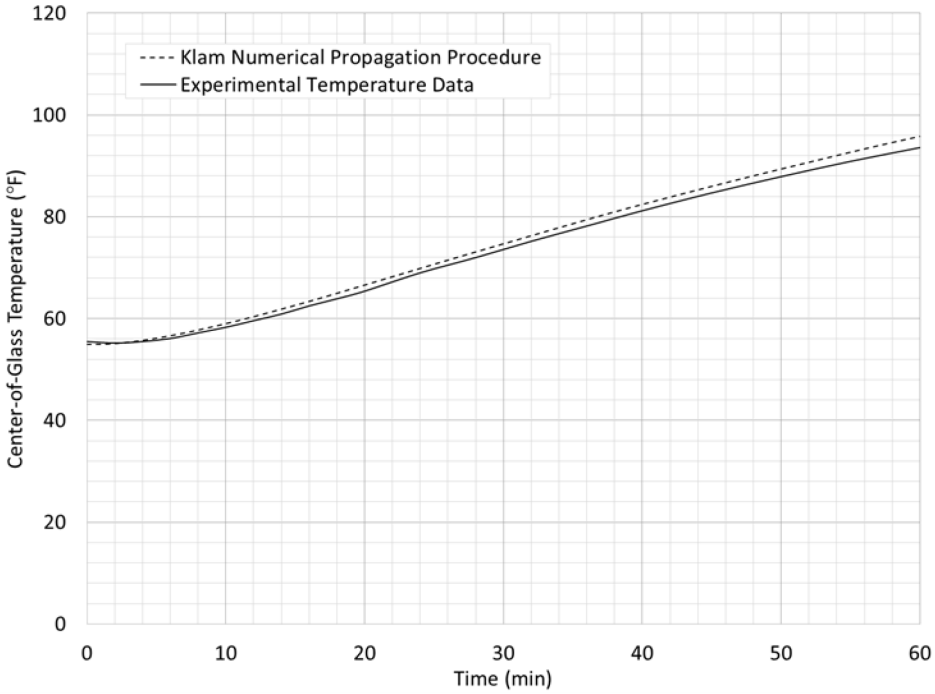

Fig. 46. Cold Glass Plate Temperature Results from NPP

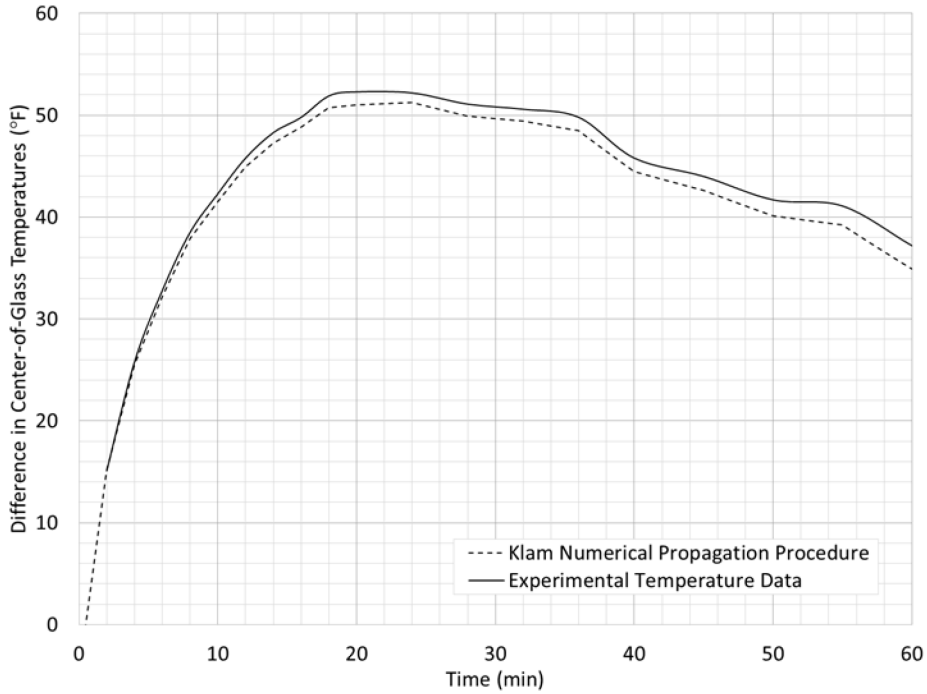

Fig. 47. Difference in Center-of-Glass Temperatures from NPP

As shown, the NPP provides a CEEC that reasonably represents the heat exchange that occurs across the gas space cavity of the test specimen. However, upon visual inspection it appears that this value can be improved upon and a better-fit coefficient be calculated. The maximum error that was associated with using the NPP was 2.26 °F.

In addition to the CEEC selected using the NPP, five additional FE analyses were performed using a range of CEEC from 0.00571 to 0.01091 (in.·lb/s)/(in.^{2}·°F). This parametric study shows the effect selecting an appropriate, or inappropriate, CEEC has on the center-of-glass temperature distribution in an IG unit.

The CEEC was modeled by varying the thermal conductivity of the gas space cavity material model, as discussed previously. Thus, it is reasonable to select a lower bound for the CEEC equal to the thermal conductivity of still air. The thermal conductivity of still air was taken to be 0.00314 (in.·lb/s)/(in.·°F) and corresponds with a CEEC of approximately 0.00571 (in.·lb/s)/(in.^{2}·°F). The remainder of the parametric study started with an effective thermal conductivity of 0.004 (in.·lb/s)/(in.·°F) and was increased by 0.0005 (in.·lb/s)/(in.·°F) for each subsequent FE analysis thereafter. Table 10 shows the values for the effective thermal conductivity and CEEC that were used for each FE analysis. The results of these FE analyses are shown in Figs. 48 and 49.

Table 10. CEEC FE Parametric Study

Case No.	$k_{effective}$ ((in.·lb/s)/(in.^{2}·°F))	h_{CEEC} ((in.·lb/s)/(in.·°F))
CEEC Case 1*	0.003140	0.005709
CEEC Case 2	0.004000	0.007273
CEEC Case 3	0.004500	0.008182
CEEC Case 4	0.005000	0.009091
CEEC Case 5**	0.005507	0.010013
CEEC Case 6	0.006000	0.010909

*Gaseous Conduction of Still Air

**Klam (2007) Numerical Propogation Procedure

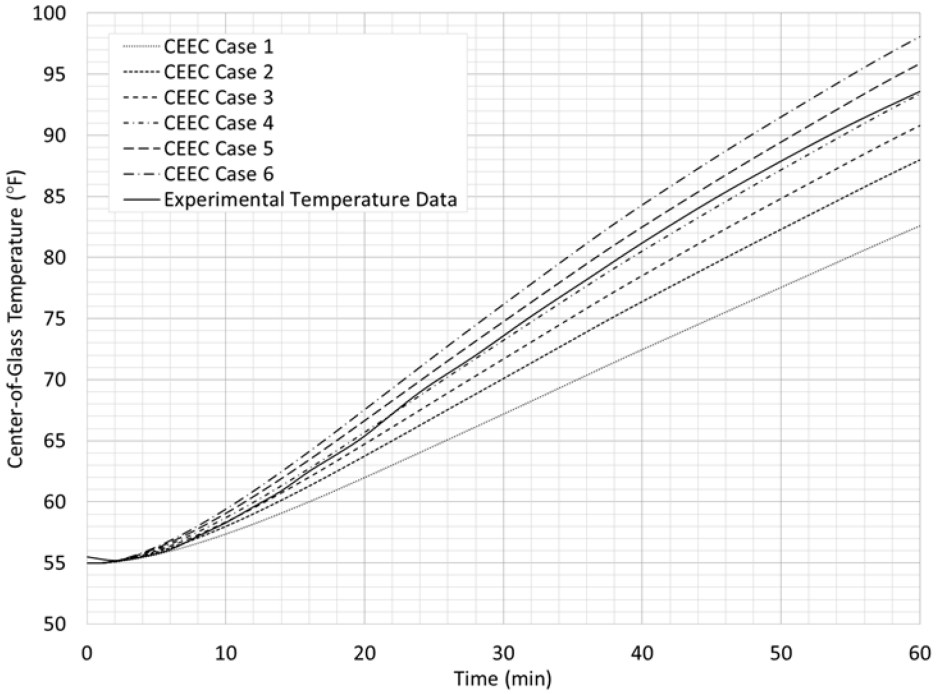

Fig. 48. Cold Glass Plate Center-of-Glass Temperature Data for Proof-of-Concept CEEC FE Cases

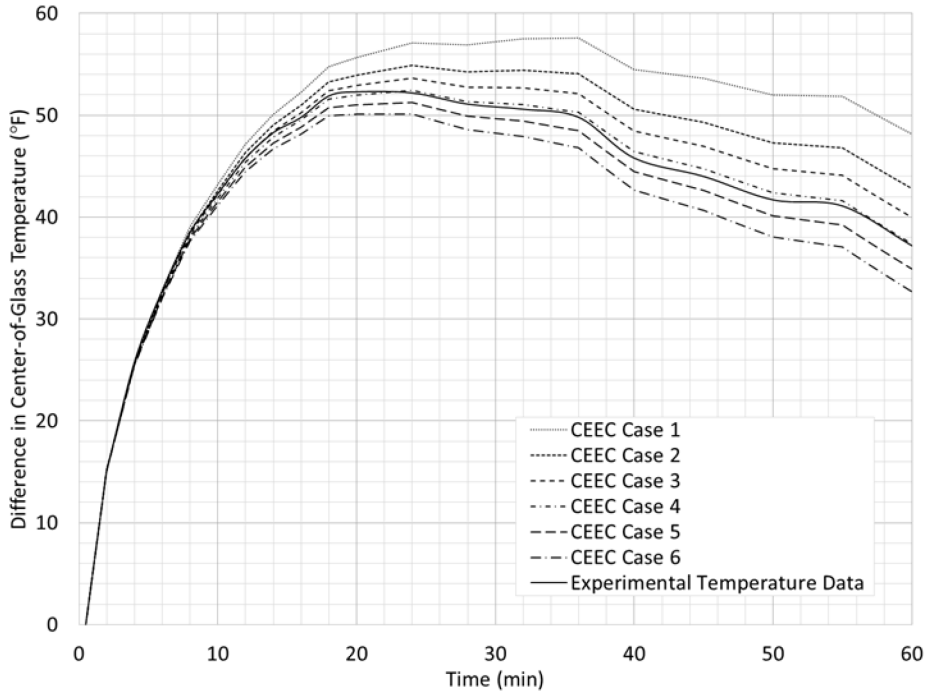

Fig. 49. Difference in Center-of-Glass Temperatures for Proof-of-Concept CEEC FE Cases

A visual inspection would lead to the conclusion that a CEEC of 0.009091 $(in.\cdot lb/s)/(in.^{2}\cdot{}^{\circ}F)$ provides the best-fit for the test specimen. However, a more scientific approach would be to apply a least-squares regression to compare these data against the experimentally measured data. Then, the most appropriate CEEC can be selected without relying on a visual aid. Table 11 shows the results of a least-squares analysis where RSS is the sum of the squares of the residuals. These data are plotted in Fig. 50 as a function of the CEEC. In addition, Table 11 provides the maximum error that is associated with each CEEC selected.

Table 11. Results of Least-Squares Regression

Case No.	h_{CEEC} $((in.\cdot lb/s)/(in.\cdot{}^{o}F))$	RSS	Maximum Error $({}^{o}F)$
CEEC Case 1	0.005709	120.84	10.99
CEEC Case 2	0.007273	32.77	5.72
CEEC Case 3	0.008182	9.53	3.09
CEEC Case 4	0.009091	0.61	0.78
CEEC Case 5	0.010013	5.09	2.26
CEEC Case 6	0.010909	20.07	4.48

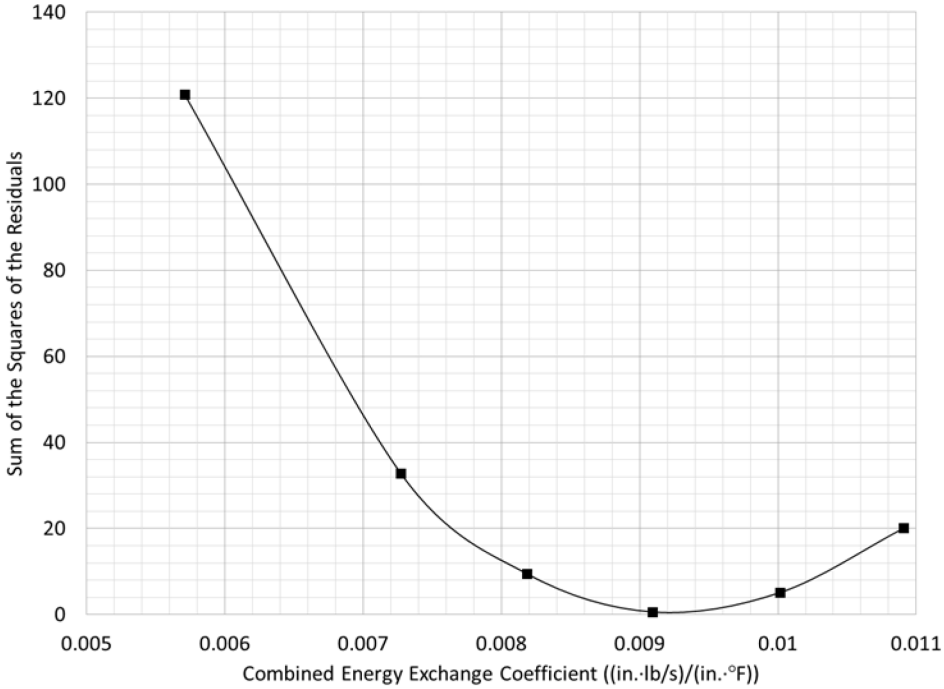

Fig. 50. Sum of the Squares of the Residuals vs. CEEC

From Fig. 50, it is clear that a CEEC of 0.009091 (in.·lb/s)/(in.^{2}·°F), that is associated with CEEC Case 4, provides the best-fit to the experimental temperature data. The CEEC determined using the NPP, that was associated with CEEC Case 5, provided the second best-fit. The maximum error associated with CEEC Case 4 was 0.78 °F. If the CEEC associated with CEEC Case 4 is taken as the "correct" value, then the CEEC determined using the NPP was in error by approximately 10 percent.

While a "shotgun" approach to analyzing a range of CEEC is effective for a small number of problems (one in this case), it is not conducive for a large set of data. In addition, it would be possible to overlook the best-fit coefficient if the interval size selected for the CEEC was too large. Thus, this process can be improved upon by using a parameter identification optimization technique that is incorporated into many FE codes. The next section of this paper discusses the application of a parameter identification optimization procedure (PIOP) to determine the best-fit CEEC for the test specimen. Ultimately, the

PIOP used was coupled with the FTP as a prescribed step to determine the best-fit CEEC.

Parameter Identification Using Optimization

It has been shown that the non-linear behavior of the heat transfer through the gas space cavity of an IG unit can be closely approximated using the CEEC. The benefit to using the CEEC is that its use greatly simplifies the numerical analysis required to determine the temperature distribution in an IG unit. This simplification was critical in developing the proposed simplified design procedure (SDP) for estimating the thermal stresses in generic IG units that will be discussed in Chapter VI. In addition, its use was important for applying the FDP presented previously in Chapter IV.

As shown in Table 11, the accuracy of the linear thermal FE analysis in predicting the center-of-glass temperature distribution of an IG unit, as a function of time, is directly related to the accuracy of the CEEC for the gas space cavity. As such, the accuracy of the proposed SDP in estimating the thermal stresses in generic IG units is directly dependent on an appropriate selection of the CEEC. To achieve the best-fit for the CEEC and thereby improve the accuracy of the linear FE model, a parameter identification procedure using optimization techniques was employed. LS-Opt, in conjunction with the LS-DYNA FE model shown previously, was used as the parameter identification tool whereby the optimum CEEC was selected. LS-Opt is a design optimization and probabilistic analysis package that interfaces directly with LS-DYNA (Stander et. al 2014).

While the theory of the optimization process is well beyond the scope of this research, this section describes the optimization procedures that were used for the FE analyses herein in a general sense. The advantage of using an optimization procedure is apparent

in that it eliminates the need to perform a large sampling of direct simulations. This systematic approach is carried out by performing a simple inverse modeling analysis whereby outcome criteria are specified and the best-fit value for the CEEC is computed.

LS-Opt employs two basic methods for optimization. These are the metamodel-based optimization and direct optimization. The direct optimization method is a sampling algorithm. This method is similar to the example shown previously where a particular number of direct simulations were performed to determine the optimum value for the CEEC. The direct optimization method will converge to an optimum value for a selected objective function however, optimizing a problem using the direct approach typically requires a large number of simulations and is computationally expensive.

The metamodel-based method is a simple and inexpensive approach that limits the number of direct simulations required. This is done by creating and optimizing an approximate mathematical model of the design and then solving for an optimal value, rather than solving for the optimal value through direct simulation. This provides a fast method to determine the best-fit value for the material property or system parameter of interest.

For the research herein, it was desired to select the optimal CEEC for the proof-of-concept experiment. Thus, an inverse modeling analysis was performed whereby the parameter to be optimized was the CEEC. The objective of the optimization analysis was to minimize the mean square error of the difference between the center-of-glass temperatures of the cold glass plate measured during the physical experiment and the results of the FE analysis using the CEEC.

The optimization analysis was performed using the default values and recommended procedures for a single-parameter identification optimization problem defined by LS-

Opt. These default values and procedures were found to be adequate for all of the analyses performed herein. While it may be possible to further refine the optimization problem, this was outside the scope of this research and was not considered herein. The default values and recommended procedures are defined as follows.

To reduce the number of simulations required, a metamodel-based optimization procedure was used to identify the optimal CEEC. The design space for an optimization problem is the region over which the design is limited by the design variables. These design variables are the independent parameters that vary in order to change the design. For the problem at hand, the single design variable is the CEEC. Thus, the design space is limited by the upper and lower boundaries of the CEEC.

The metamodel is the surrogate mathematical model that represents the design space. The metamodel was constructed using the sequential response surface method (SRSM) strategy. The SRSM strategy is the original LS-Opt automation strategy and is ideal for identifying an optimum value for a system parameter (Stander et. al 2014). The SRSM strategy allows for the convergence of a single-objective solution to a prescribed tolerance. As stated previously, the objective function for the problem at hand was to minimize the mean square error in the difference between the center-of-glass temperature of the cold glass plate measured during the physical experiment and the results of the FE analysis using the CEEC. The default tolerance used was 0.01 (Stander et. al 2014). Fig. 51 shows the LS-Opt graphical user interface that was used to setup the optimization process flow. The task and strategy selection protocols and curve matching algorithm protocols are presented in Figs. 52 and 53, respectively.

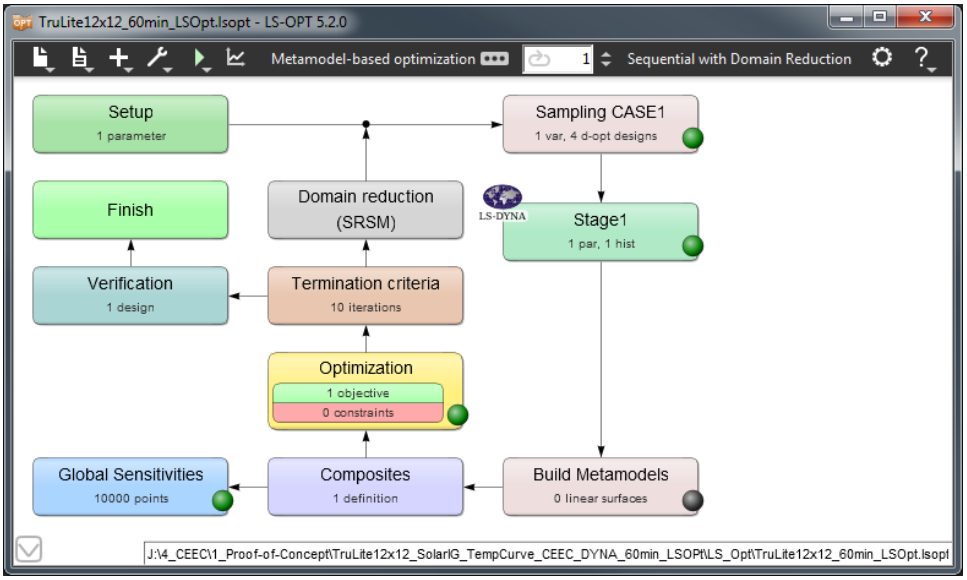

Fig. 51. LS-Opt Graphical User Interface - Optimization Process Flow

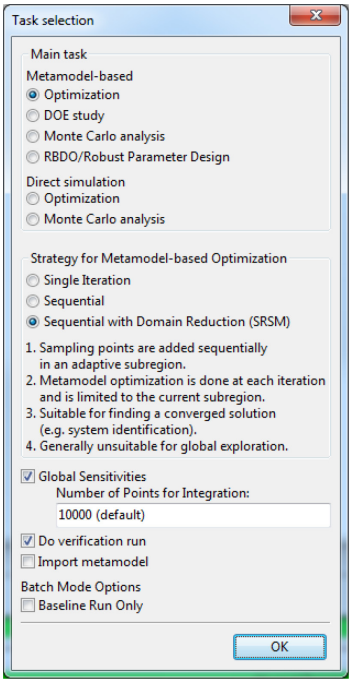

Fig. 52. Task and Strategy Selection Protocols

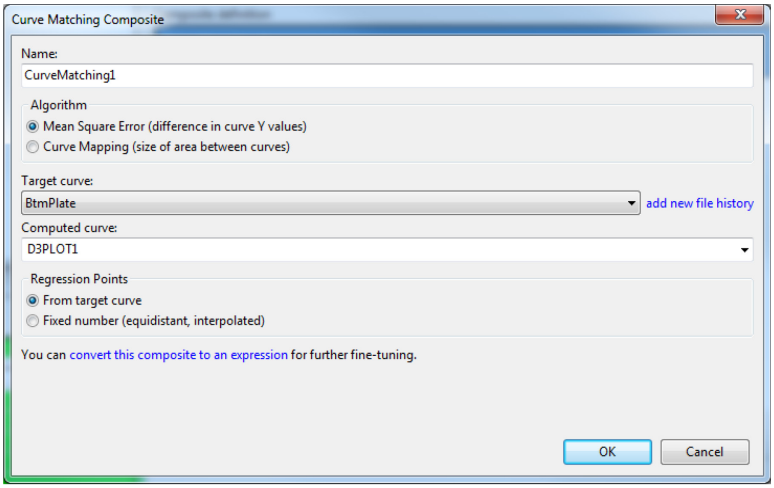

Fig. 53. Curve Matching Composite and Algorithm Protocols

The SRSM strategy uses a region of interest, which is a subspace of the overall design space, to determine the approximate optimal value for the parameter. The range for the initial region of interest for iteration number 1 is defined by the lower and upper boundaries of the CEEC. With each successive iteration, the center of the region of interest is moved (i.e. panned) closer to the optimum value. In addition, the overall size or range of the region is reduced (i.e. zoomed) closer to the optimum value. This concept is shown in Fig. 54 below where the red dot defines the optimum value for the parameter of interest. The boxes shown represent the design space and the iteration number is shown in the corner of each box (Stander and Goel 2010; Stander et. al 2014).

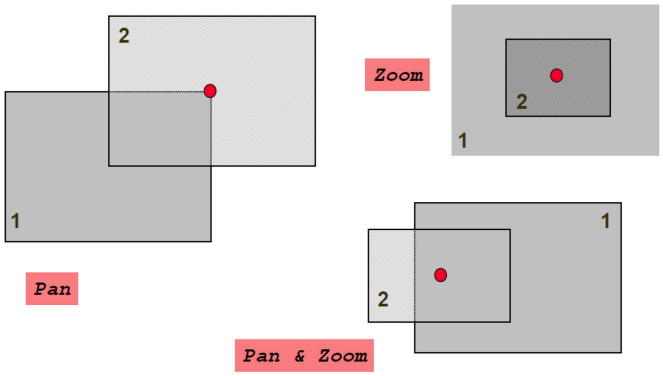

Fig. 54. SRSM Sub Region Reduction Scheme (Stander and Goel 2010)

For each iteration, response values are determined for a set of simulations performed at predetermined design values. The point selection scheme recommended and used to determine the design values for each iteration was D-Optimal (Stander et. al 2014). A total of four experimental points are required per iteration for a single variable, linear approximation (Stander et. al 2014).

Using polynomial-based approximations, a response surface (i.e. metamodel) is fit to these four response values for each iteration. The response curve is a mathematical expression that is used to explain the relationship between the response variables and the design variables. The response surface is fitted to the response values using a least-squares regression analysis. As the optimization progresses, the solution converges on the optimum response surface.

The accuracy of the metamodel in describing the response is limited to the order of the polynomial. The most basic approximation for the basis function is a first-order polynomial. For sequential optimization, it has been shown that the linear SRSM strategy provides excellent results and can be used with confidence (Stander and Goel 2010; Stander et. al 2014). In addition, the temperature response of the cold glass plate that is used in

the objective function has a linear relationship to the CEEC. Thus, a first-order polynomial was used and found to be sufficiently accurate for all of the analyses performed as part of the research herein.

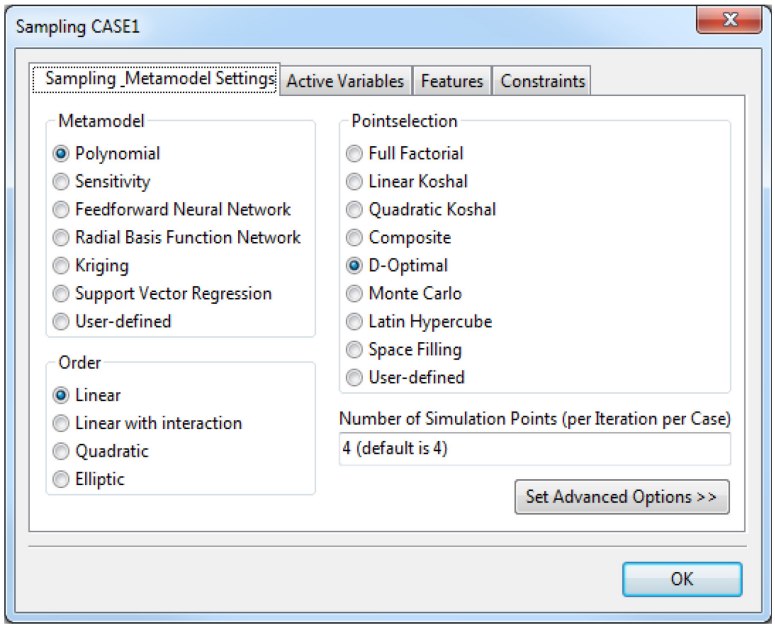

Fig. 55. Metamodel Type and Point Selection Scheme Protocols

The results from the optimization analysis are presented in Figs. 56 through 67. Two graphs are presented for each iteration. The first graph presents the response values for the set of four simulations performed at predetermined design values. The second graph presents the predicted history curve for any point in the design space based on the metamodel. In each graph, "x" denotes the center-of-glass temperature values of the cold glass plate, measured during the physical experiment.

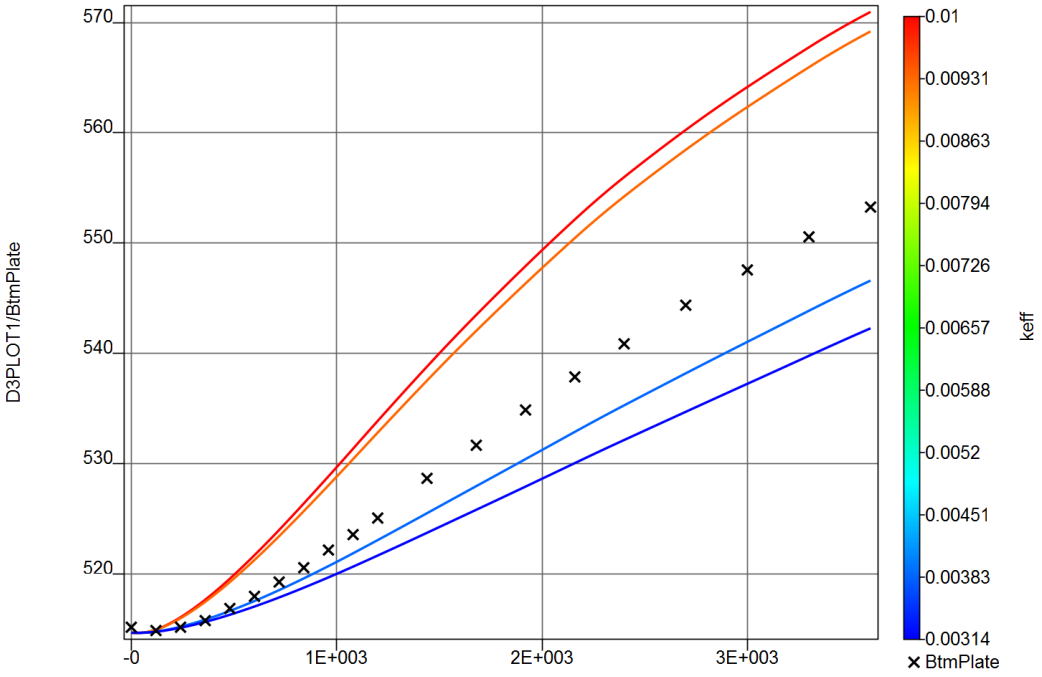

Fig. 56. Simulation History Curves for Iteration Number 1

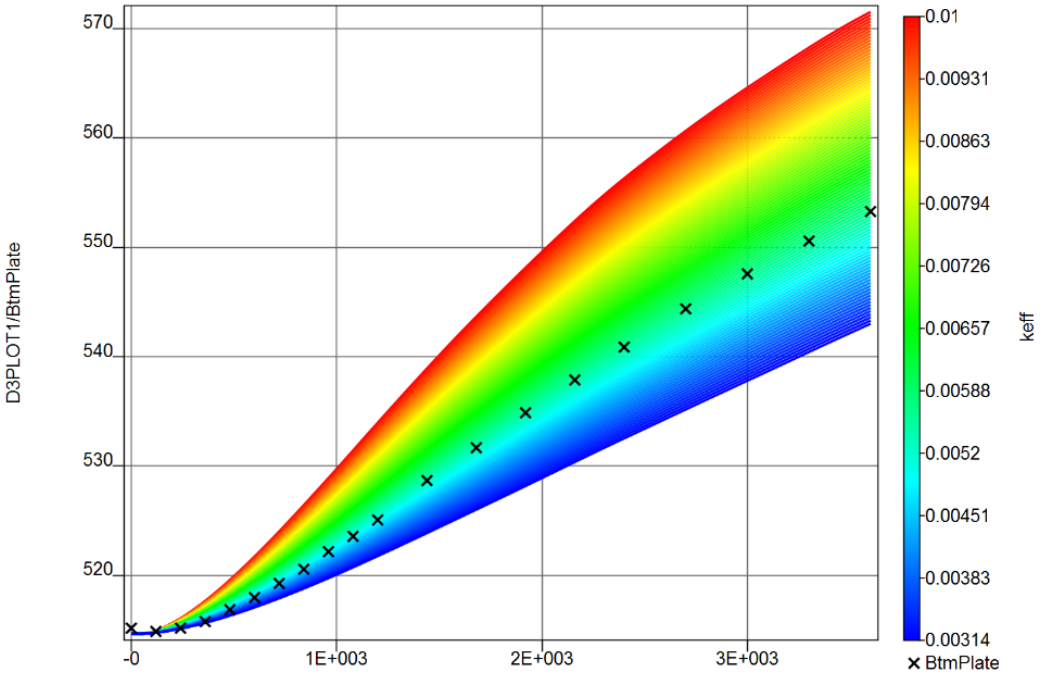

Fig. 57. Predicted History at Any Point in the Design Space for Iteration Number 1

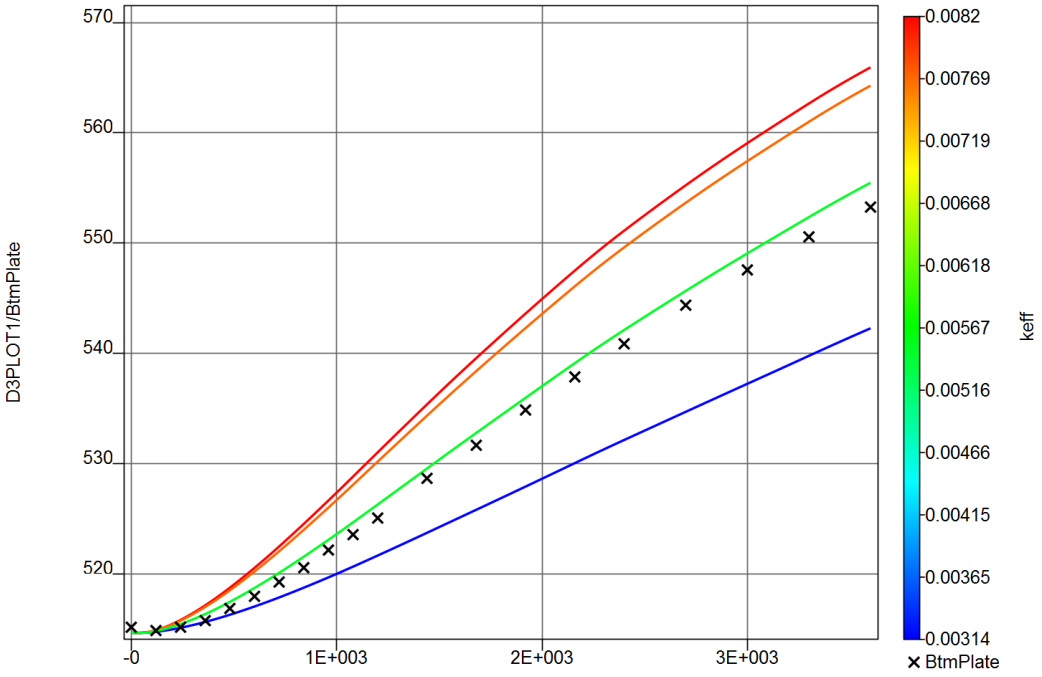

Fig. 58. Simulation History Curves for Iteration Number 2

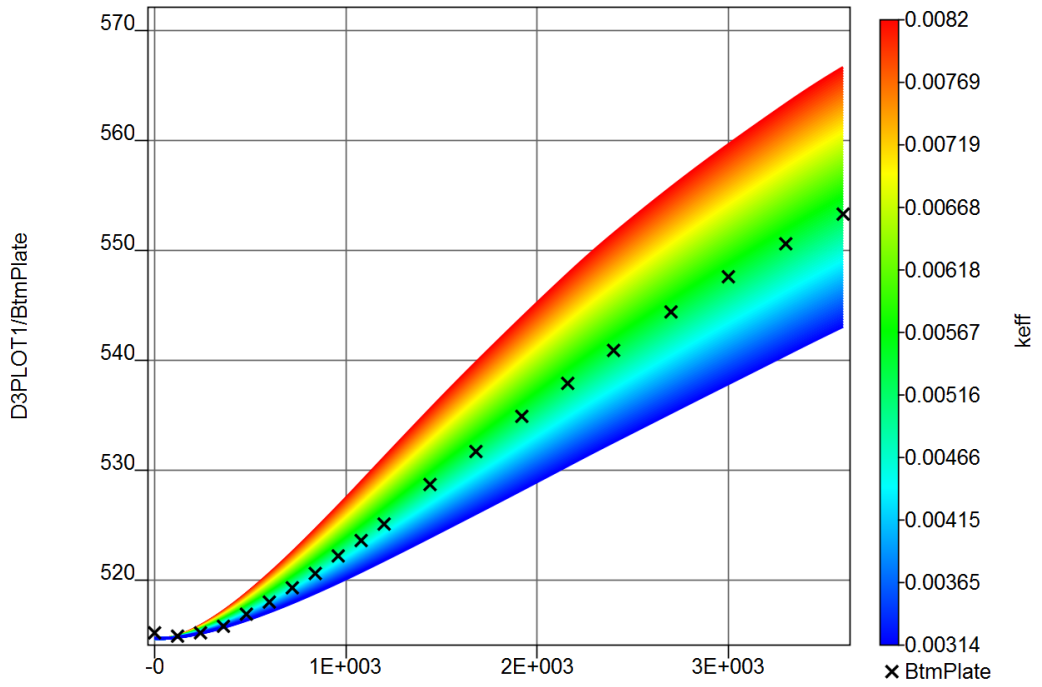

Fig. 59. Predicted History at Any Point in the Design Space for Iteration Number 2

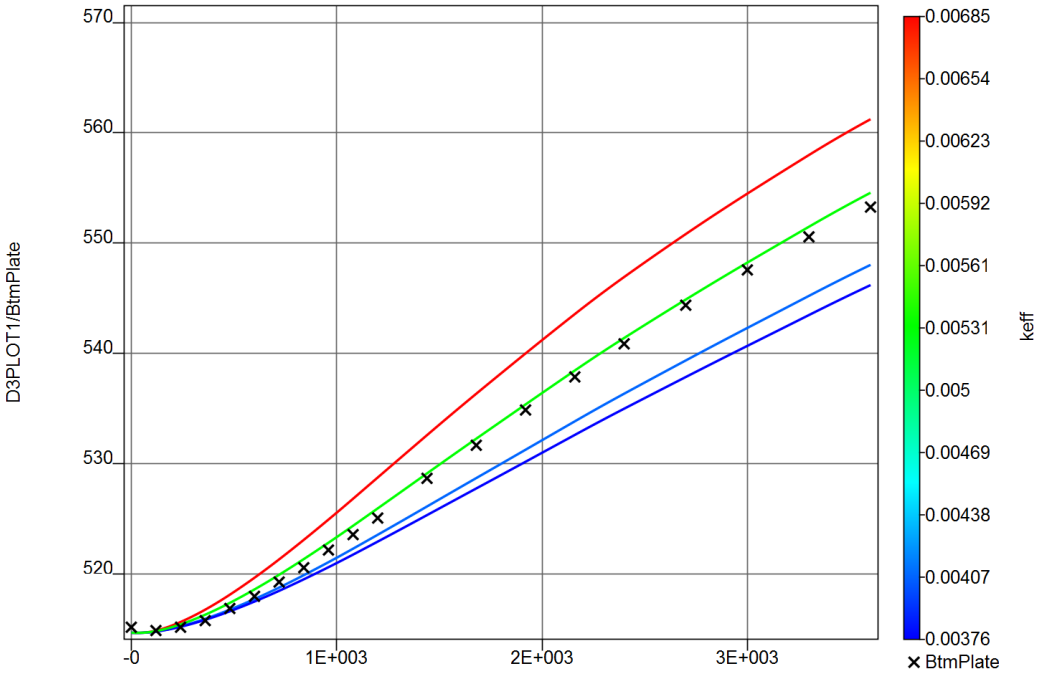

Fig. 60. Simulation History Curves for Iteration Number 3

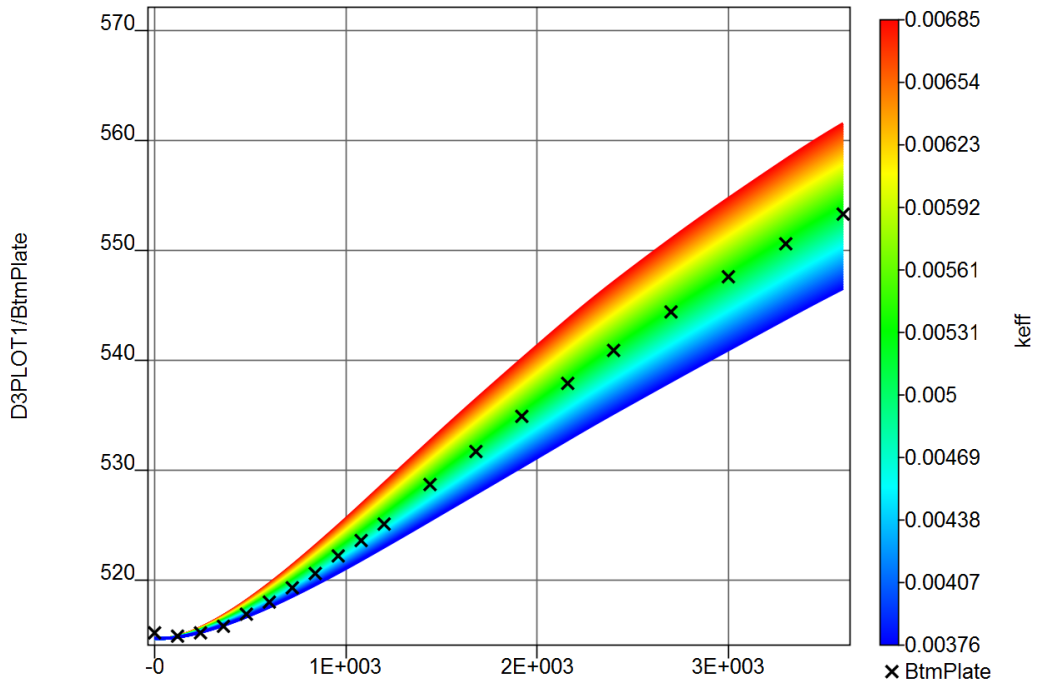

Fig. 61. Predicted History at Any Point in the Design Space for Iteration Number 3

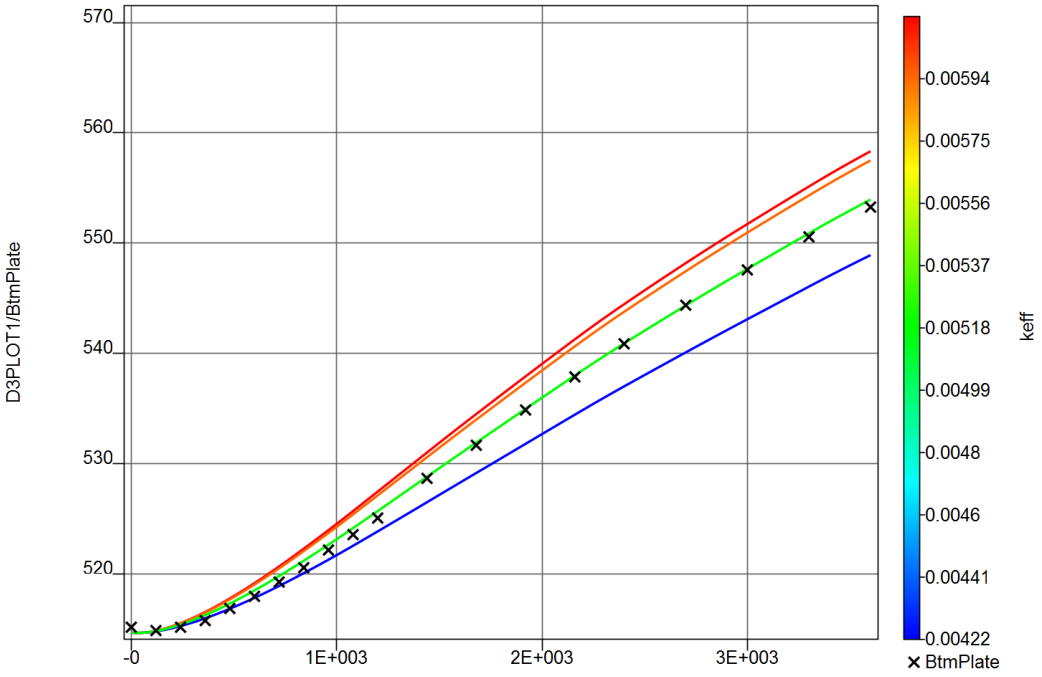

Fig. 62. Simulation History Curves for Iteration Number 4

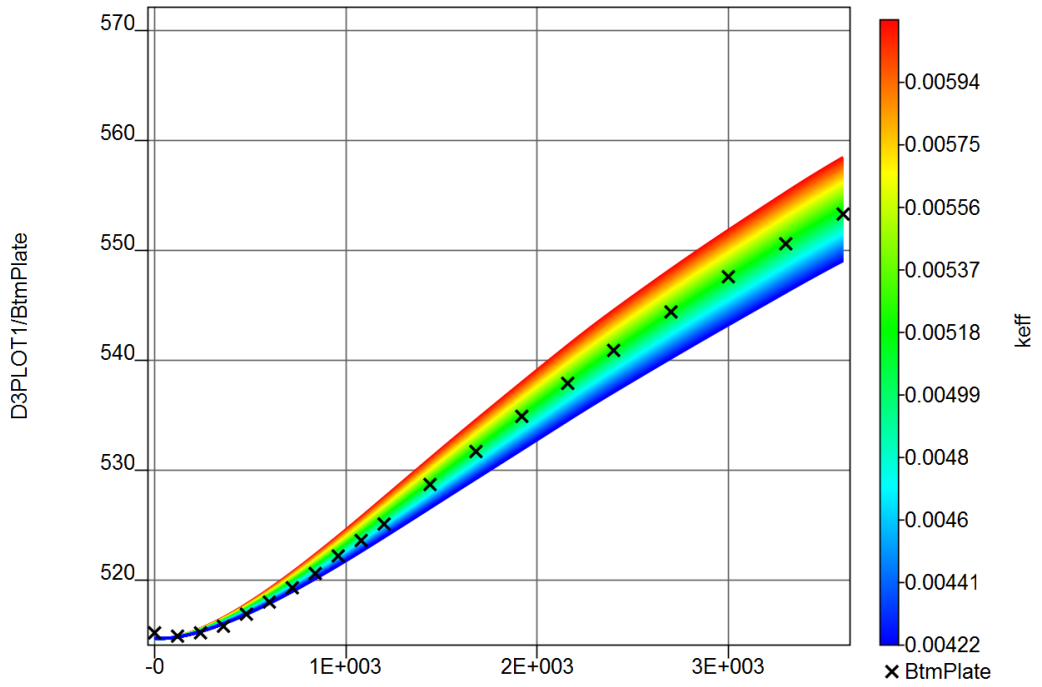

Fig. 63. Predicted History at Any Point in the Design Space for Iteration Number 4

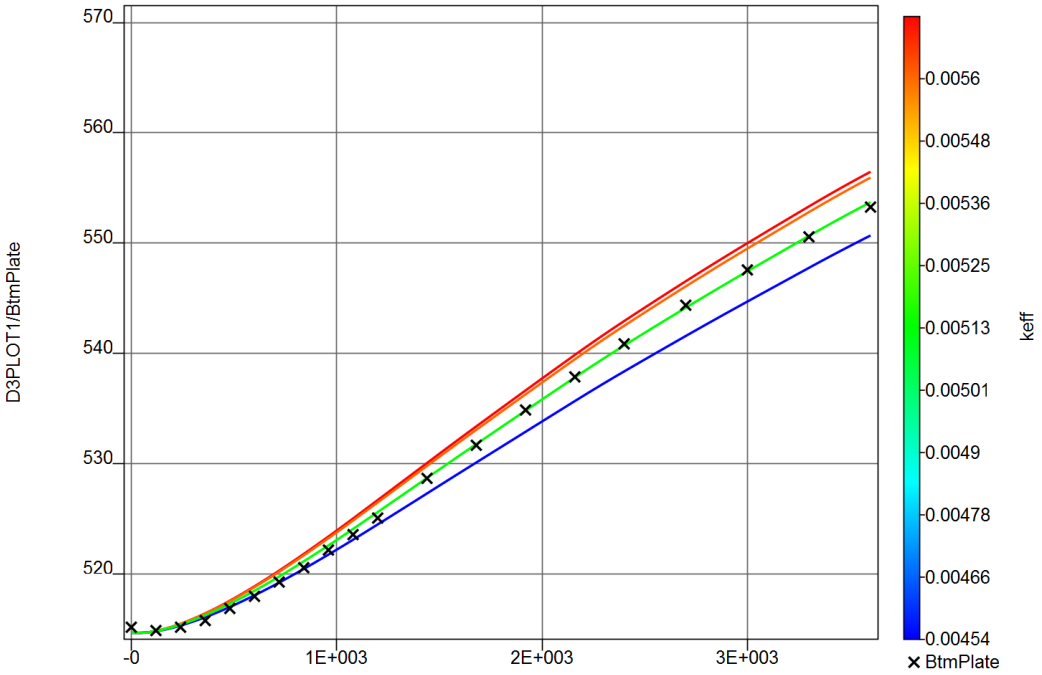

Fig. 64. Simulation History Curves for Iteration Number 5

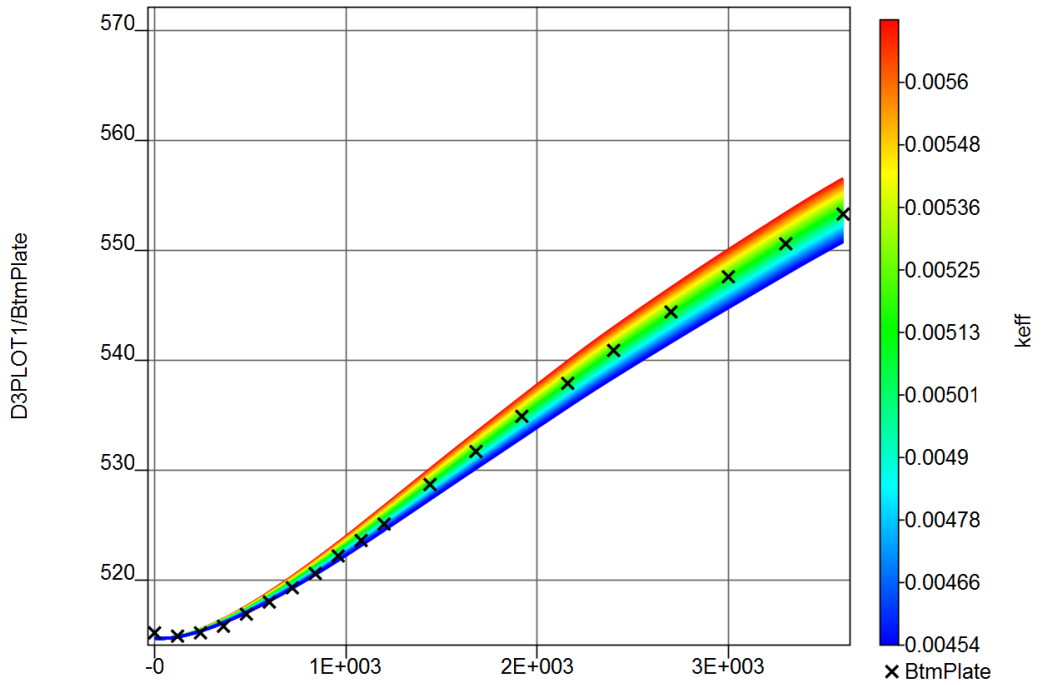

Fig. 65. Predicted History at Any Point in the Design Space for Iteration Number 5

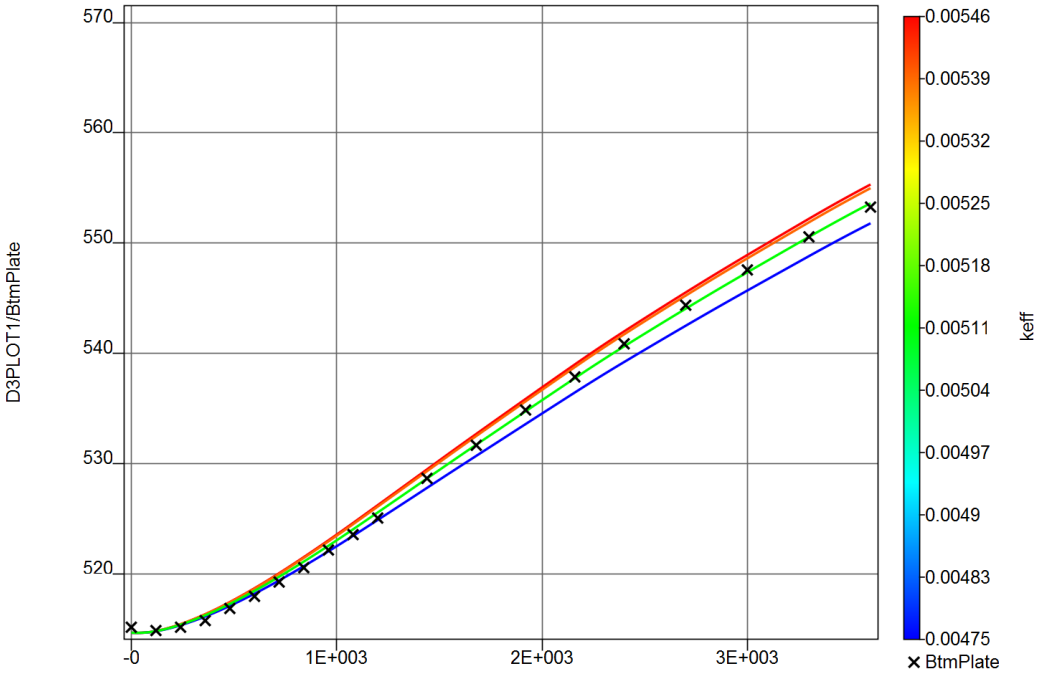

Fig. 66. Simulation History Curves for Iteration Number 6

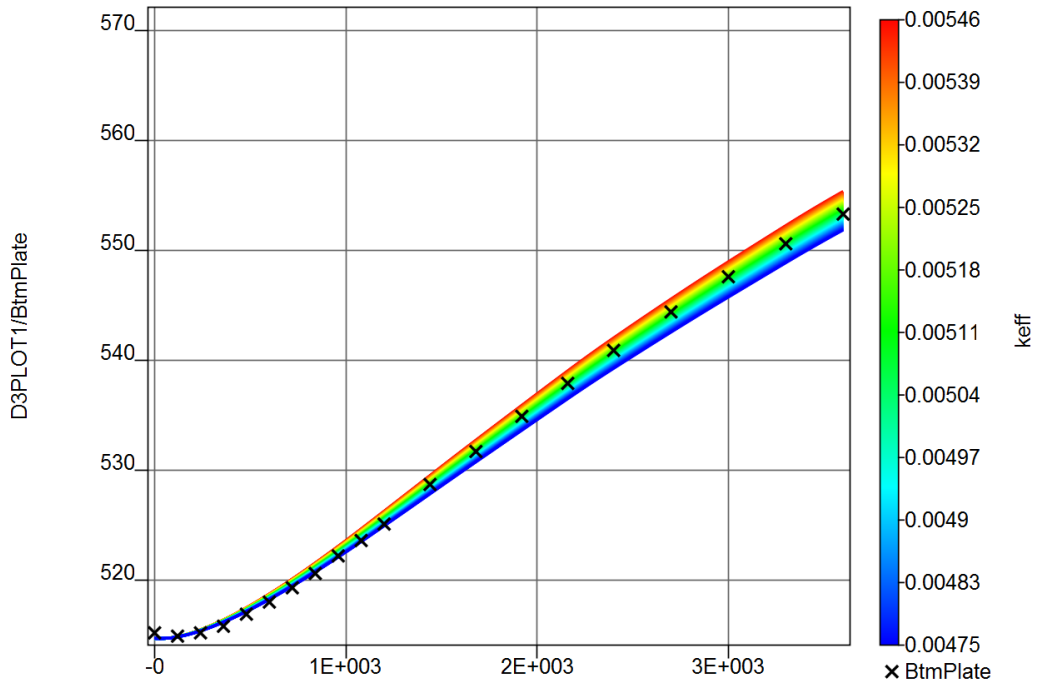

Fig. 67. Predicted History at Any Point in the Design Space for Iteration Number 6

As shown in Figs. 56 through 67, the region of interest is reduced with each successive iteration until the optimal metamodel has been determined. Once the optimal metamodel has been determined, the optimal value for the CEEC is known and a final verification is performed. Fig. 68 shows the results of the final verification simulation.

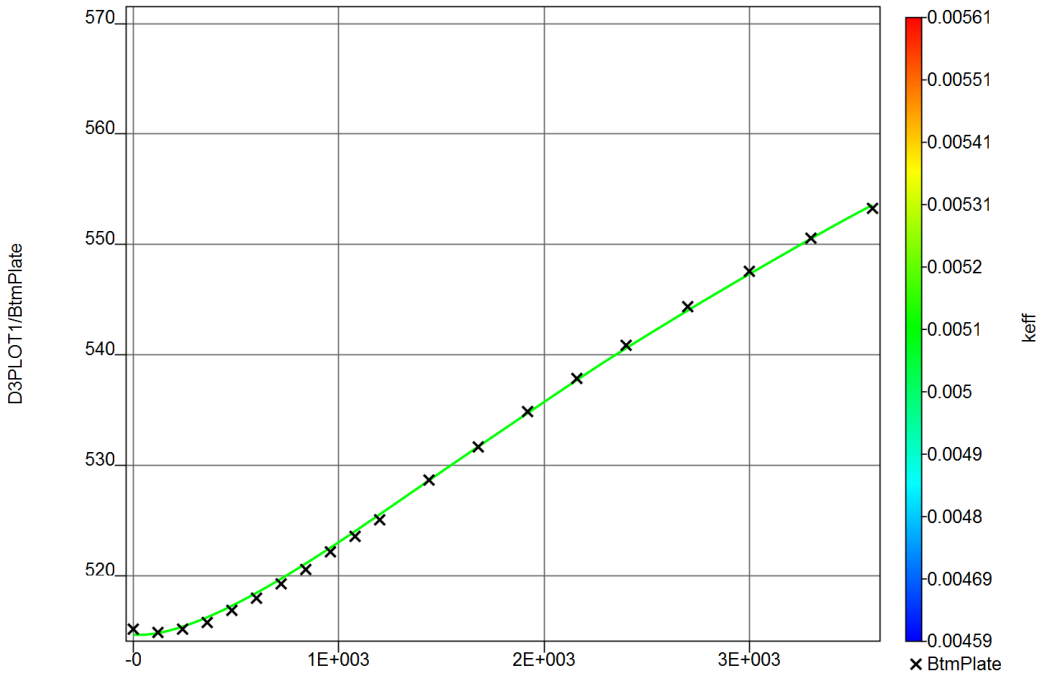

Fig. 68. Final Iteration of the Metamodel Using LS-Opt to Verify the Best-Fit CEEC Selected

The value for the optimal CEEC, determined for each iteration, is shown in Fig. 69. The mean square error of the difference between the center-of-glass temperature data measured during the physical experiment and that calculated using the FE analysis for each iteration is shown in Fig. 70. Included in Fig. 70 is the predicted and calculated mean square error. The mean square error is predicted using the metamodel, where the metamodel is constructed and updated using the set of direct FE analyses at each iteration. The calculated value is based on the first direct FE analysis performed at the beginning

of each iteration. The difference between these values can be taken as the error associated with the lack-of-fit of the metamodel. It is shown in Fig. 70 that as the number of iterations progress this difference is minimized. This implies that the accuracy of the metamodel is improved with each iteration. Both Figs. 69 and 70 show the CEEC converges to an optimal value in six iterations.

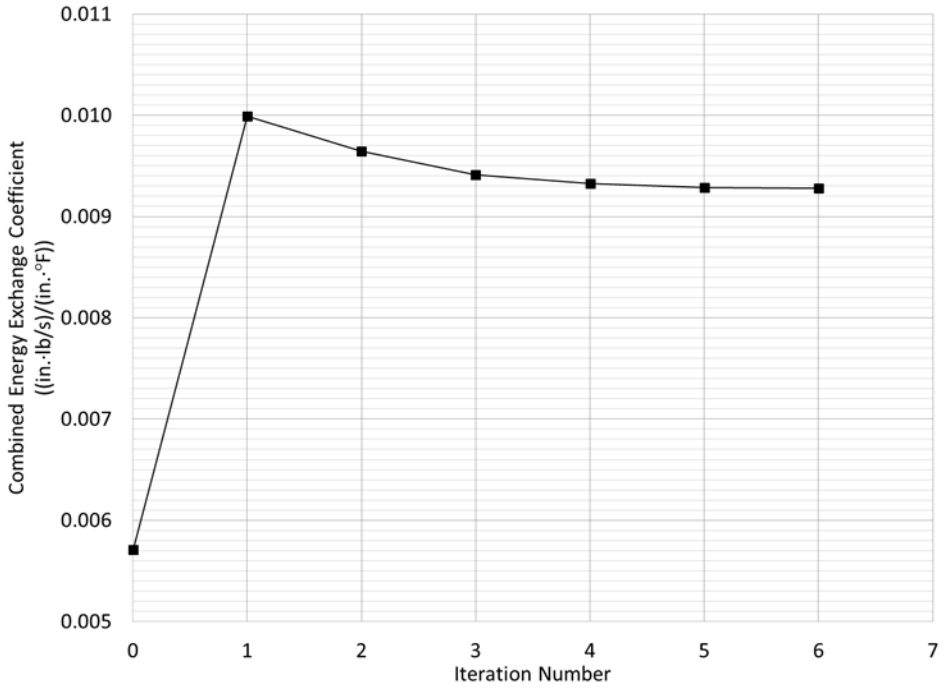

Fig. 69. CEEC vs. Iteration Number

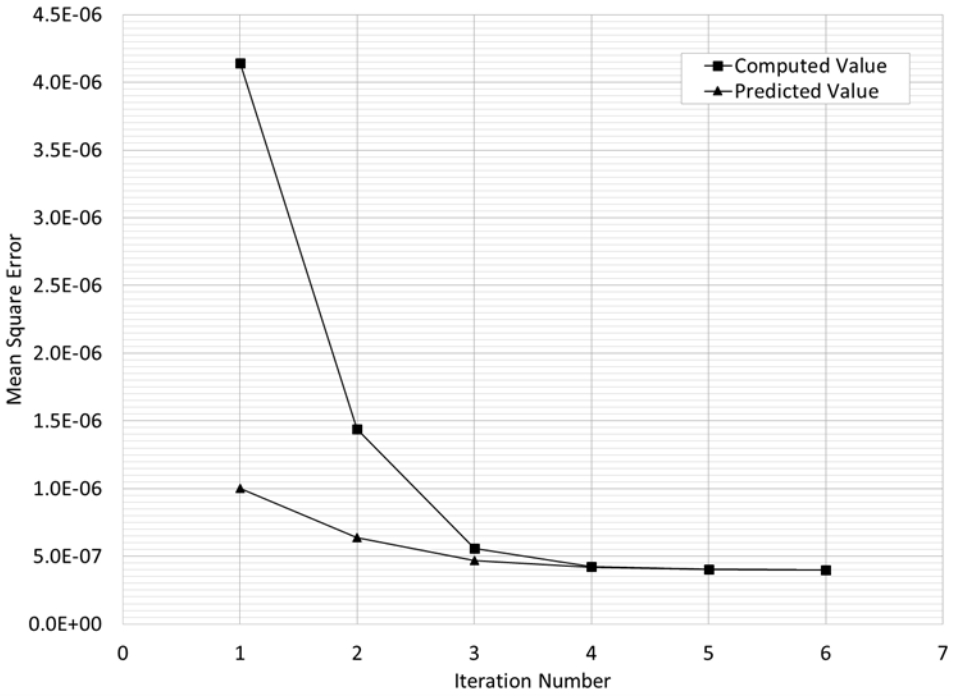

Fig. 70. Mean Square Error vs. Iteration Number

Using the PIOP, the best-fit value for the CEEC was 0.009289 (in.·lb/s)/(in.^{2}·°F). Previously, using the NPP forwarded by Klam (2007), the best-fit CEEC was determined to be 0.010013 (in.·lb/s)/(in.^{2}·°F). If the CEEC determined using the PIOP is now taken as the "correct" value, then the CEEC determined using the NPP is in error by approximately 8 percent.

A comparison of the cold glass plate temperature and the difference in center-of-glass temperature between the cold and heated glass plate for each CEEC are presented in Figs. 71 and 72, respectively. Based on these figures, it is clear that the use of the PIOP provides a systematic approach to selecting the best-fit CEEC. In addition, it provides a more accurate value than the NPP that was developed by Klam (2007).

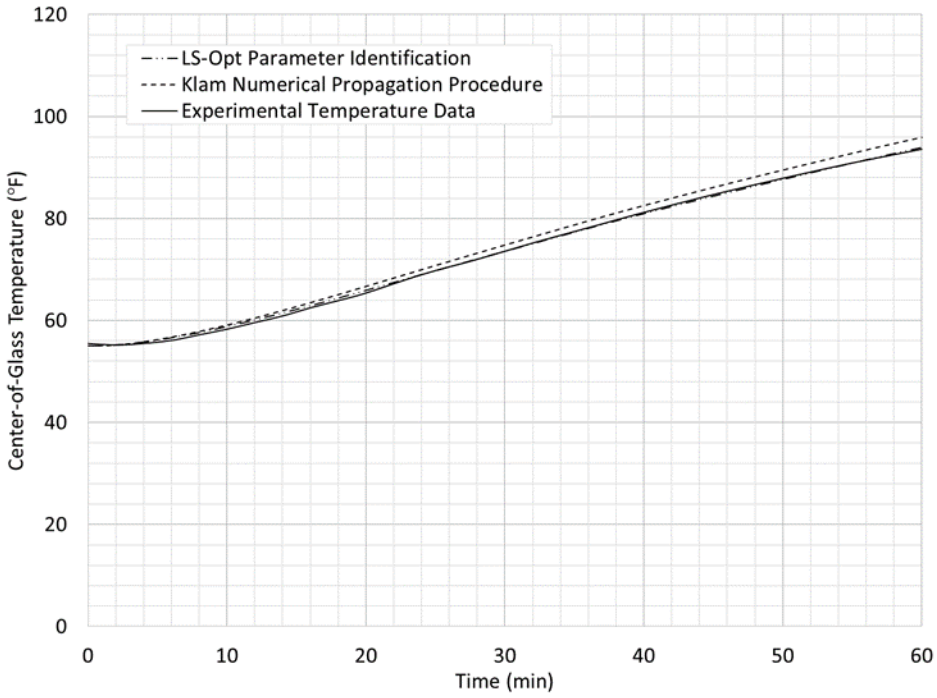

Fig. 71. Comparison of Center-of-Glass Temperature Data Using the PIOP and NPP

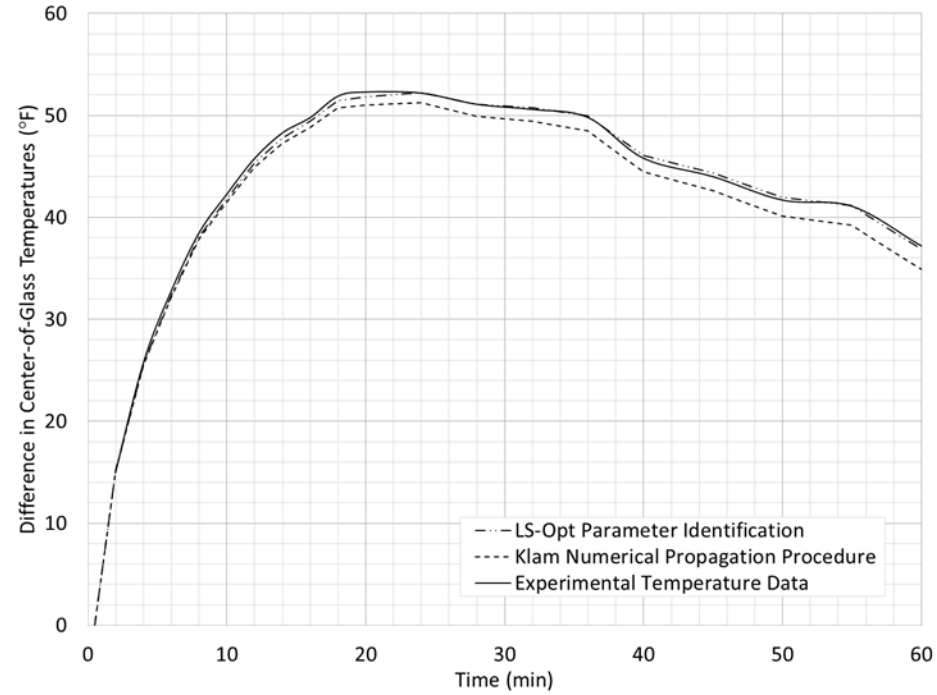

Fig. 72. Comparison of Difference in Center-of-Glass Temperatures Using the PIOP and NPP

Based on the results from the proof-of-concept experiment, it is clear that the use of a CEEC to estimate the heat transfer through the gas space of an IG unit provides reasonable results. Finally, Fig. 73 shows the distribution of temperature, as a function of time, through the IG unit when the optimal CEEC is used to model the heat transferred through the gas space cavity. As shown, heat is transferred through the gas space cavity as well as across the edge-seal of the IG unit. Note that the temperature scale shown in Fig. 73 is in °R. The heat transfer that occurs around the edge-seal will be discussed in more detail in the next section.

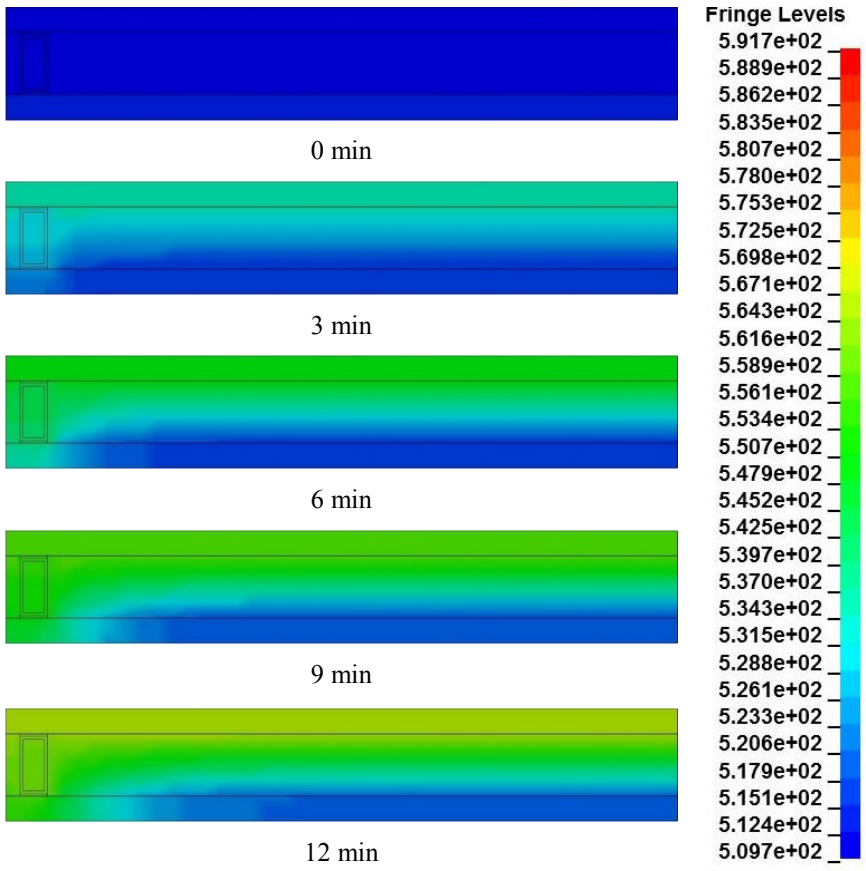

Fig. 73. Temperature Distribution Through the IG Unit as a Function of Time

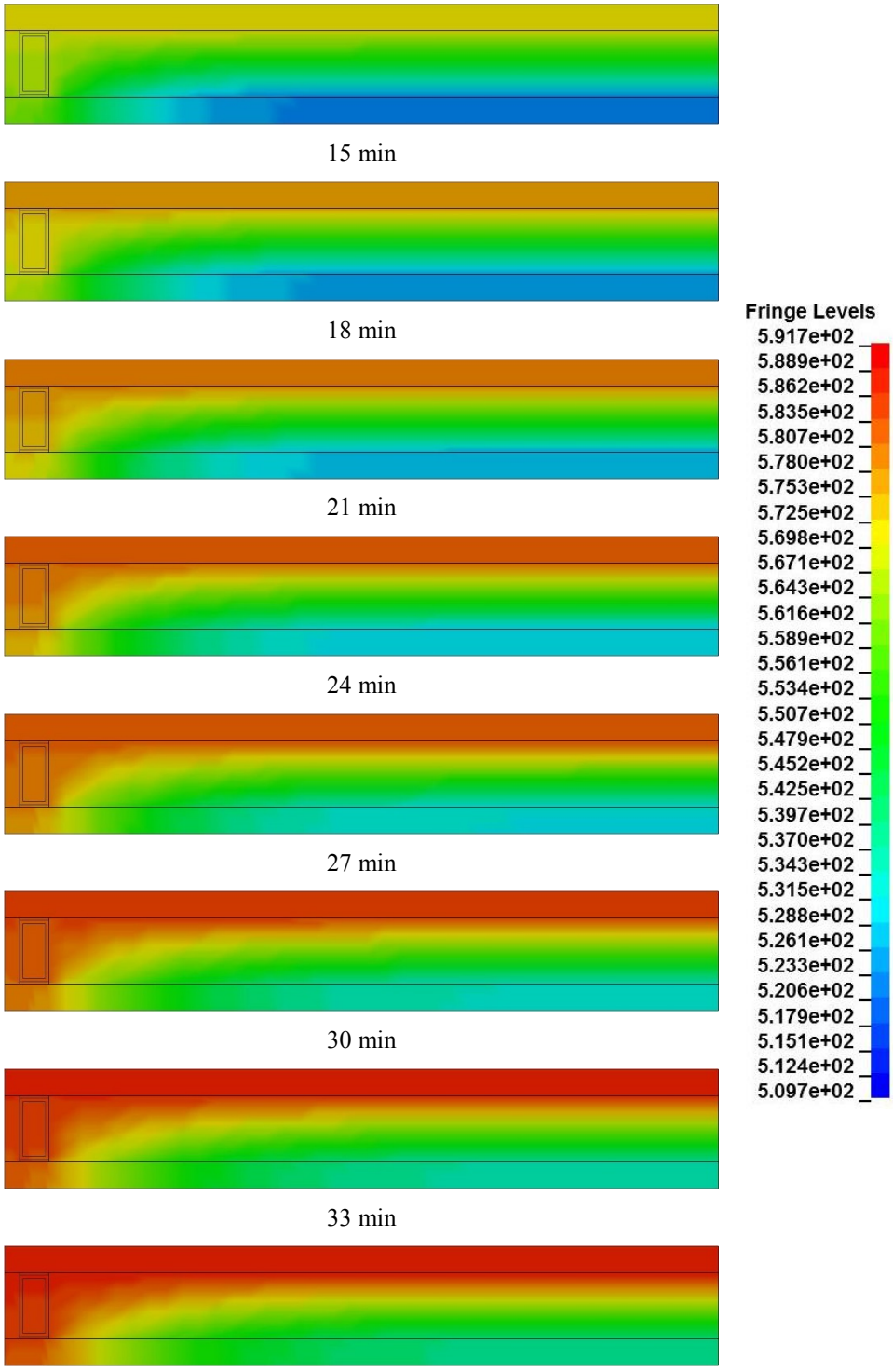

Fig. 73. Continued

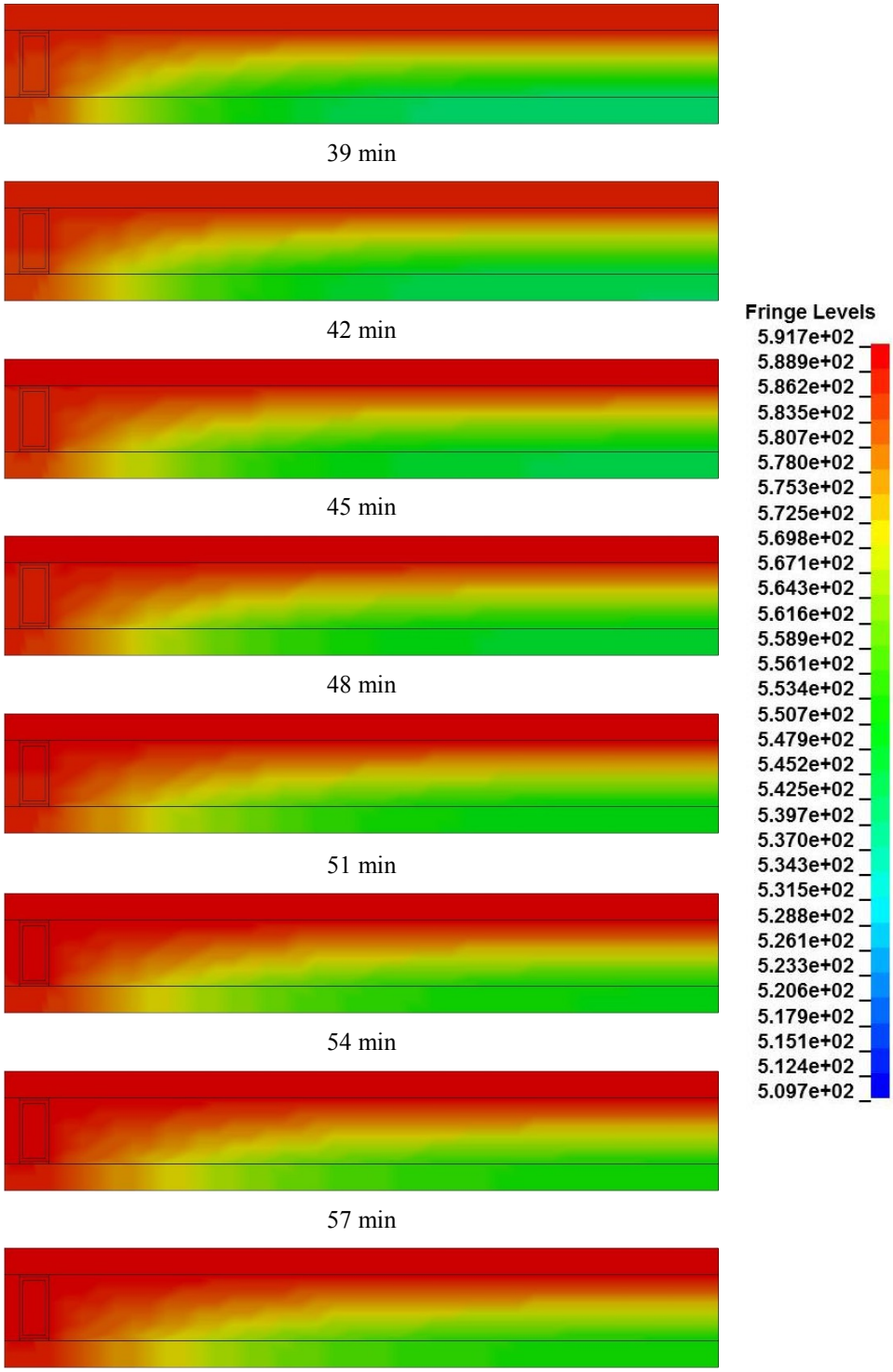

Fig. 73. Continued

The next section of this dissertation discusses a proposed FTP that can be used to estimate the CEEC. This test procedure was developed such that it does not rely on the use of solar irradiance or placing the specimen in a wind-laden environment. This allows the procedure to be performed in a laboratory setting and provide accurate, repeatable results.

Formal Test Procedure

The primary objective of the FTP was to determine an accurate CEEC for a particular IG unit. The CEEC must be determined for each configuration of IG units. This includes the application of various coatings, films, and tints, the construction of the IG unit, the type of gas fill, spacer widths, and the thicknesses of the inner and outer glass plates. Thus, a FTP is required to ensure that the results are accurate and repeatable. This is achieved by removing variabilities associated with the testing procedure. In addition, the FTP incorporates the PIOP discussed previously to determine the optimal CEEC. The FTP involved the development of a unique testing device where 24 in. by 24 in. IG units were completely enclosed and subjected to temperatures ranging from -10 to 200 °F.

The steps to perform the FTP are as follows:

1. The number 1 and 4 surfaces of the IG unit are instrumented with thermocouples.
2. The IG unit is installed in an insulated heat chamber, placed in an environmental test chamber, and allowed to reach a thermal equilibrium temperature of -10 °F.
3. The insulated heat chamber is then pressurized to 14 in. of water and oriented in a plumb, vertical position inside the environmental test chamber.
4. A near uniform heat flux of approximately 5.7105 $(\text{in.}\cdot\text{lb/s})/\text{in.}^2$ is applied to the number 1 surface of the IG unit using a special heating device.
5. Temperature data are measured as a function of time, and the test is considered complete when the temperature of the number 1 surface has reached 200 °F.

6. A FE model is developed, using the procedures detailed in Chapter IV, that reasonably represents the IG unit geometry and materials.
7. A PIOP is performed using the temperature profile measured for the number 1 and 4 surfaces, and the CEEC for the gas space cavity is identified.

This FTP presents the steps that were required to properly estimate the CEEC for each specific IG unit considered as part of this research. Thus, it was repeated for all of the different IG units considered. The FTP can easily be applied to any IG unit.

The termination criteria was selected based largely on experience that is well accepted by design engineers within the glass industry. The maximum temperature for vision glass does not typically exceed 200 °F. Rather, the temperature of the outer glass plate is generally on the order of 50 °F greater than the ambient temperature. In addition, most sealants and spacers that are used in IG units are able to withstand temperatures of 200 °F.

The lower boundary for the outdoor environment was assumed to be -10 °F. By subjecting the heated glass plate to a temperature of 200 °F, the gas space cavity is tested over a range of average temperatures with a lower boundary of -10 °F through an upper boundary of approximately 125 to 165 °F for IG units with low-E coated and clear glass plates, respectively. This provides a CEEC that is suitable for a range of gas space temperatures that covers a broad practical range of geographic regions where IG units are used.

The size of the IG unit was selected for two reasons. First, it was desired to minimize the effect that the edge-seal had on the center-of-glass temperature. Second, the size of the unit was selected so that the most common widths of spacers that are used in IG units provide an aspect ratio of the gas space cavity greater than 40. Each of these are discussed in detail below.

The proof-of-concept experiment was performed on an IG unit that was 12 in. by 12 in. It can be seen from Fig. 73 that significant heat is transferred around the edge-seal of the IG unit, as well as through the gas space cavity. It seems apparent that the center-of-glass temperature would be significantly influenced by the transfer of heat across the edge-seal when the specimen is only 12 in. wide.

To quantify the effect of the specimen's width on the heat that is transferred across the edge-seal to the center-of-glass area, four sizes of IG units were compared using FE analyses. The four sizes considered were 12 in. by 12 in., 14 in. by 20 in., 20 in. by 30 in., and 24 in. by 24 in. Fig. 74 shows a cross-section of the four sizes of FE models. The minimum dimension for each size were analyzed, thus the 12, 14, 20, and 24 in. dimensions were used in the FE model.

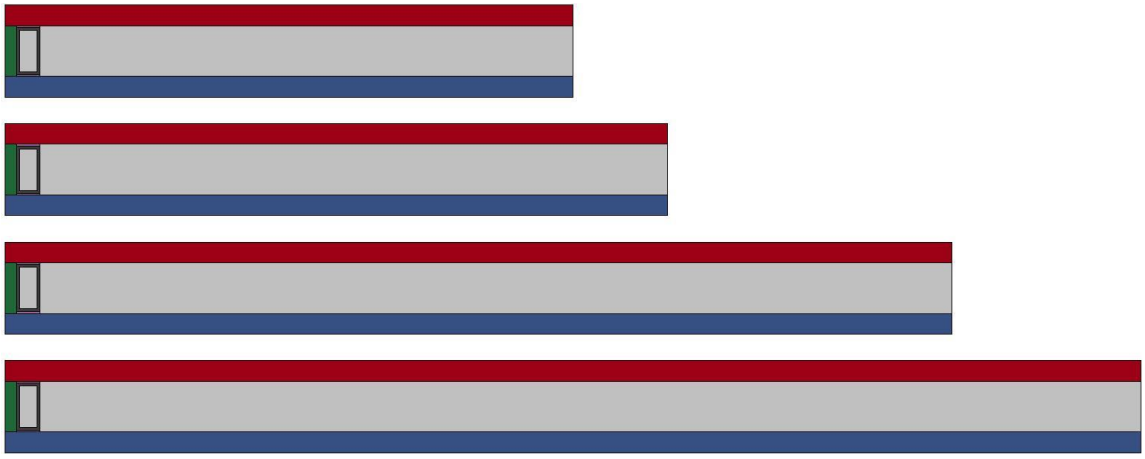

Fig. 74. FE Models for Size Requirements

The heated glass plate of each model was heated uniformly through the thickness by applying a solar irradiance of 5.7105 (in.·lb/s)/in.^{2}. The temperature of the cold glass plate was allowed to vary as a function of the edge-seal and the CEEC. To maximize the ef-

fect of the edge-seal on the center-of-glass temperature, a low value for the CEEC associated with an IG unit with a low-E coating was desired. Thus, the CEEC value of 0.005100 (in.·lb/s)/(in.^{2}·°F) that was determined for the proof-of-concept experiment was used for each case.

Fig. 75 shows the temperature distributions across the IG units after 60 min of exposure to 5.7105 (in.·lb/s)/in.^{2} of solar irradiance. It is clear that the edge-seal's effect on the center-of-glass temperature is reduced as the width of the IG unit is increased. However, it is difficult to quantify the difference graphically due to the limited resolution of the temperature scale shown in Fig. 75. Note that the temperature scale shown is in °R.

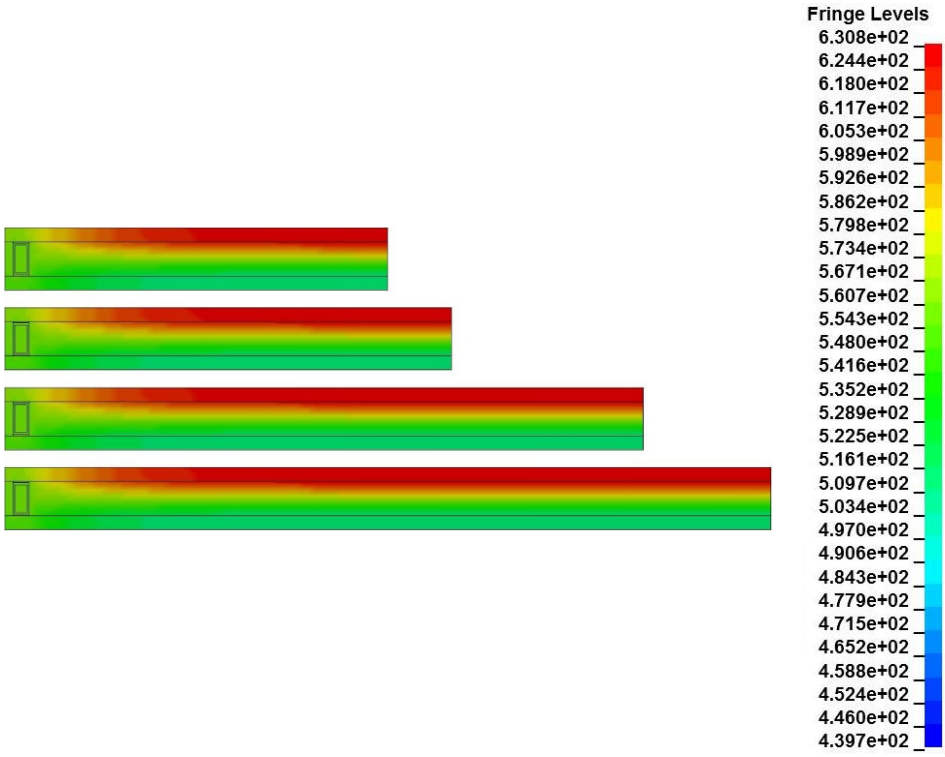

Fig. 75. Temperature Results from FE Model at 3600s

Fig. 76 shows the heat flux measured three in. in from the center of the glass plate, along the direction of the length of the cold glass plate. From Fig. 76, the 12 in. by 12 in. and 14 in. by 20 in. specimens have a maximum heat flux of 0.2856 and 0.0756 (in.·lb/s)/in.^{2} measured at 60 min, respectively. The heat flux for the 20 in. by 30 in. and 24 in. by 24 in. specimens were negligible. Thus, either of these two specimens would be acceptable to minimize the effect that the edge-seal has on the center-of-glass temperature.

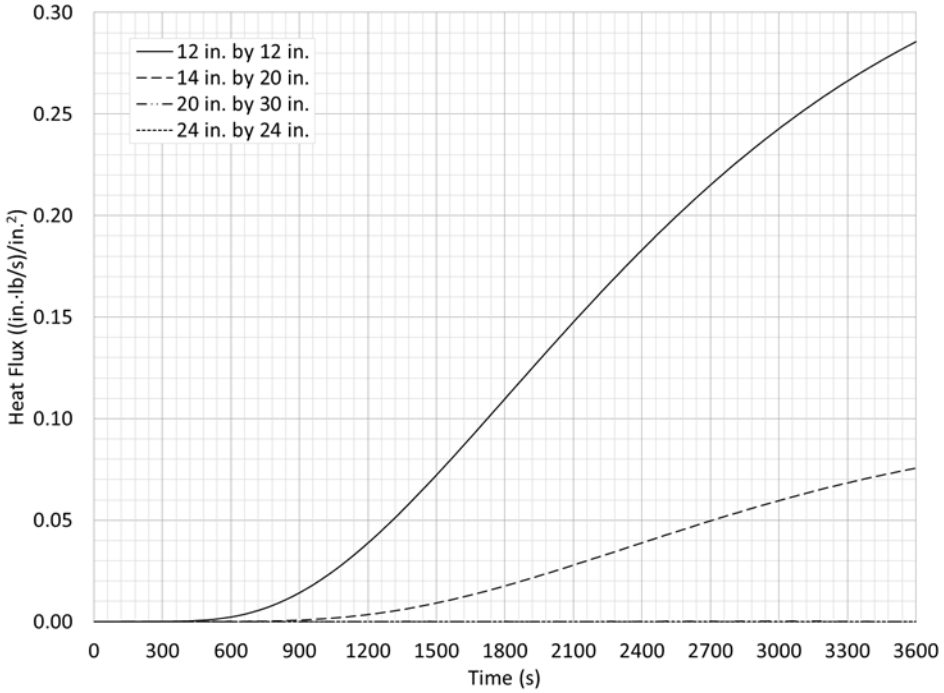

Fig. 76. Heat Flux Across the Cold Glass Plate

In addition to minimizing the effects of the edge-seal on the center-of-glass temperature, another important consideration in selecting an appropriate size for the FTP is the effect that the aspect ratio of the gas space cavity has on the convection currents that develop. Therefore, it was desired to select a size for the IG unit where the aspect ratio of the gas space cavity would exceed 40. This decision was based on the information presented in Figs. 77 and 78, which show the Nusselt number, Nu, Reynolds number, Ra, and aspect

ratio, A, data that were used by Wright (1996) to develop the correlation used to quantify the effects of convection in the gas space cavities of vertical IG units.

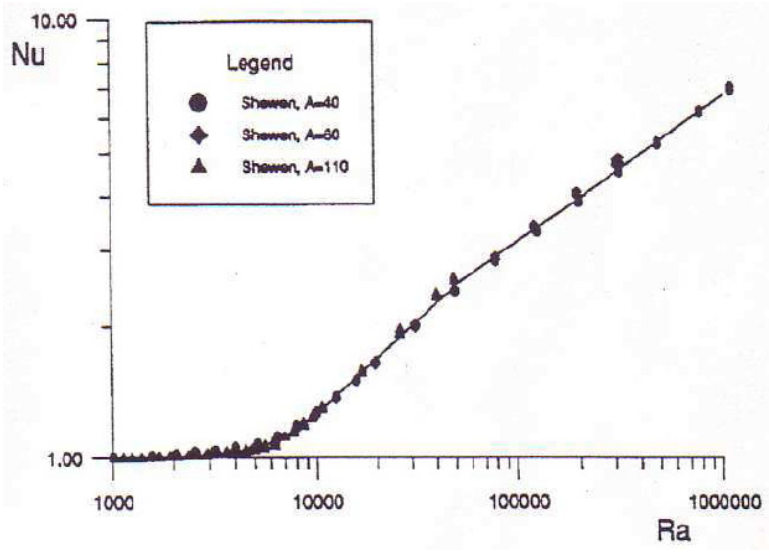

Fig. 77. Nusselt Number vs. Reynolds Number and Aspect Ratio Data from Shewen (1986)

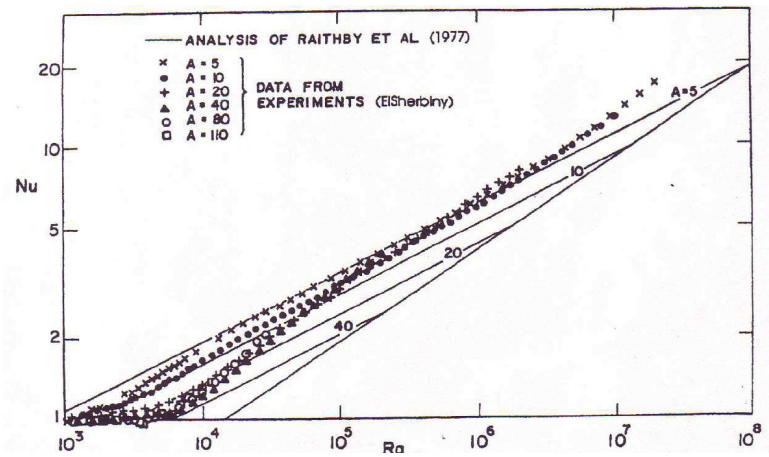

Fig. 78. Nusselt Number vs. Reynolds Number and Aspect Ratio Data from El Sherbiny et. al (1982)

According to El Sherbiny's (et. al 1982) data, the Nusselt number for aspect ratios of 40, 80, and 110 are tightly grouped. The values are within approximately ±3 percent and are on the same order as experimental error. When combined with Shewen's (1986) data,

the overall width of scatter falls within a band of ±4 percent, also on the same order as experimental error. Thus, as the aspect ratio increases for values greater than 40, its effect on the Nusselt number is diminished (Wright and Sullivan 1989; Wright 1996).

The aspect ratio, A, for an IG unit's gas space cavity is calculated by dividing the height of the gas space cavity by the width or thickness, as given by Eq. (68).

$$A = \frac{H}{t_{cavity}} \tag{68}$$

Where H is the overall height of the IG unit, and t_{cavity} is the spacing between the glass plates. In practice, the width of the edge-seals are not taken into account when calculating the height of the gas space cavity.

Table 12 shows the aspect ratio for the four sizes of IG units considered with common spacer widths of 0.25 and 0.5 in. Based on the information in Table 12, the 12 in. by 12 in. and 14 in. by 20 in. sizes are not adequate to meet the aspect ratio criteria selected for the gas space cavity. These specimens do not provide an aspect ratio greater than 40 when a 0.5 in. wide spacer is considered. Both the 20 in. by 30 in. and 24 in. by 24 in. sizes do provide an aspect ratio greater than 40 for both the 0.25 and 0.5 in. wide spacers.

Table 12. Gas Space Cavity Aspect Ratios for FTP Specimen Dimensions

H	t_{cavity} (in.)	
(in.)	0.25	0.5
12	48	24
14	56	28
20	80	40
24	96	48

While the contribution of the edge-seal to the center-of-glass temperature was negligible and the aspect ratio of the gas space cavity was acceptable for the 20 in. by 30 in., the 24 in. by 24 in. specimen was ultimately selected as the most appropriate test size. This was due to the convenient symmetric shape and the fact that a 24 in. by 24 in. specimen was easier to handle compared to a 20 in. by 30 in. specimen.

Practical Application of the Formal Test Procedure

The FTP was carried out on six IG units to verify its accuracy and repeatability in estimating the CEEC. This section is dedicated to outlining the test procedures that were followed and the methods used to determine the CEEC for each IG unit. The six IG units considered are summarized in Table 13 below. Fig. 79 shows an example of one of the specimens that was used for testing.

Table 13. IG Units Used for the FTP Practical Application

Specimen No.	Heated Glass Plate	Gas Space Cavity	Cold Glass Plate
Specimen 1	1/4 in. Clear	1/2 in. Air	1/4 in. Clear
Specimen 2	1/4 in. Clear	1/2 in. Air	1/4 in. Clear
Specimen 3*	1/4 in. Clear	1/2 in. Air	1/4 in. Clear
Specimen 4	1/4 in. Low-E, Hard-Coat	1/2 in. Air	1/4 in. Clear
Specimen 5	1/4 in. Low-E, Hard-Coat	1/2 in. Air	1/4 in. Clear
Specimen 6*	1/4 in. Low-E, Hard-Coat	1/2 in. Air	1/4 in. Clear
Specimen 7	1/4 in. Low-E, Soft-Coat	1/2 in. Air	1/4 in. Clear
Specimen 8	1/4 in. Low-E, Soft-Coat	1/2 in. Air	1/4 in. Clear
Specimen 9*	1/4 in. Low-E, Soft-Coat	1/2 in. Air	1/4 in. Clear

*Spare Specimen

Fig. 79. FTP Specimen

Six practical applications were performed on specimens 1 through 9 using the FTP. Two of each type of IG units were identical in construction. Thus, specimens 2, 5, and 8 were repeat tests of the same type of IG units as specimens 1, 4, and 7 respectively. The use of identical types of IG units provided a level of credibility to the test results obtained. Specimens 3, 6, and 9 were intended to be replacement specimens in the event that either of the first two specimens were damaged before or during testing. The low-E coating that was applied to specimens 4 through 6 was a pyrolytic applied hard-coat. The low-E coating that was applied to specimens 7 through 9 was a sputter applied soft-coat. For the first six tests, the specimens with a low-E coating were oriented such that the glass plate with the low-E coating was heated. This is prescribed by the FTP.

Two additional practical applications were performed using specimens 4 and 7. However, for these tests the specimens were oriented such that the clear glass plate was heated instead of the glass plate with the low-E coating. These two tests were performed to verify that the CEEC was independent of the orientation of the IG unit. Based on the theory for long-wave radiation presented in Chapter III, this must be the case.

Test Specimen Preparation

The specimens were prepared for testing by first removing any extraneous silicone material from the edges. This helped to ensure that the sides of the IG unit would fit tightly against the insulation in the insulated heat chamber. In addition, any extraneous silicone large enough to affect the conformity of the special heating device was removed. In general, smudges or light smearing of silicone were ignored. The silicone pad that was selected for use between the special heating device and the heated glass plate had a low durometer and conformed around these types of small imperfections. In addition, these silicone imperfections did not change the thermal characteristics of the IG unit as a whole. Fig. 80 shows an example of the imperfections that were found prior to testing.

Fig. 80. Extraneous Silicone Shown on Test Specimens

Any dust, debris, etc. on the surfaces of the glass plates were removed using glass cleaner and a rag. A clean, smooth glass surface was important to ensure that the silicone pad and special heating device fit intimately against the glass surface. Note that these specimens are not tested to failure. Unlike glass strength testing, the surfaces and

edges of the glass plates may be handled, cleaned, and even exposed to tools and knives to remove imperfections, if necessary, without compromising the test results.

Next, the specimens were identified and labelled. The label was placed on the upper left hand corner of each specimen. When applicable, the label was located on the glass plate with the low-E coating located on the number 2 surface. In addition, the manufacturer's "LOW-E" sticker was left on the glass specimen. The label included the overall construction of the IG unit, the manufacturer, and the manufacturer's product code. An example label and "LOW-E" sticker are shown in Fig. 81.

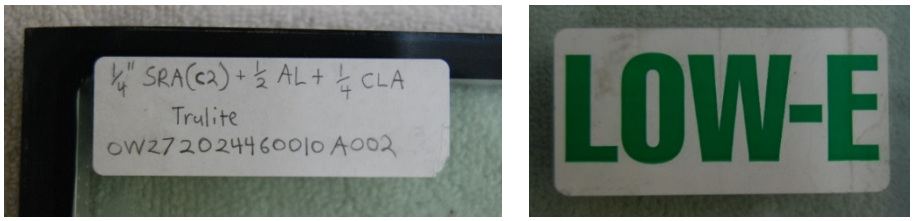

Fig. 81. Test Specimen Labels

Once the specimens were labelled, the overall thickness of the IG unit was measured using a digital micrometer. This process is shown in Fig. 82. The thickness of each glass plate was measured using a digital caliper. This process is shown in Fig. 83.

Fig. 82. Measurement of Overall Thickness Using Digital Micrometer

Fig. 83. Measurement of Glass Plate Thickness Using Digital Caliper

The width or thickness of the gas space cavity, t_{cavity}, was calculated by subtracting the thicknesses of the two glass plates from the overall thickness of the IG unit, as given by Eq. (69). These dimensions were used to construct the detailed FE models for step 6. The measurements for each specimen are shown in Table 14.

$$t_{cavity} = t_{overall} - (t_{heated} + t_{cold}) \tag{69}$$

Where $t_{overall}$ is the overall thickness of the IG unit, t_{heated} is the thickness of the glass plate that is heated inside of the insulated heat chamber, t_{cold} is the thickness of the glass plate that is not heated inside of the insulated heat chamber. The dimensions for each specimen are presented in Table 14.

Table 14. Test Specimen Dimensions

Specimen No.	t_{heated} (in.)	t_{cold} (in.)	$t_{overall}$ (in.)	t_{cavity} (in.)
Specimen 1	0.2200	0.2215	0.95760	0.5161
Specimen 2	0.2210	0.2200	0.95235	0.5114
Specimen 4	0.2250	0.2250	0.95005	0.5001
Specimen 5	0.2230	0.2300	0.95805	0.5051
Specimen 7	0.2190	0.2210	0.95035	0.5104
Specimen 8	0.2195	0.2215	0.94905	0.5081

Finally, each IG unit was instrumented with a thermocouple on the number 1 and 4 surfaces. The center of the glass plate, on the number 1 and 4 surfaces, were marked in both directions. The location of the intersection of these two lines was where the thermocouple was placed for testing. Placing the thermocouples within $\pm$ 0.5 in. of the center of the glass plate did not affect the test results.

Temperature data were performed using type T, special limits of error thermocouples. The limits of error for the thermocouples were taken to be the greater of 0.9 °F or 0.4 percent of full scale. Type T thermocouples were selected for their operating temperature range of -328 to 662 °F and minimal limits of error. The thermocouple wire that was attached to the glass plates was 30 AWG (American Wire Gauge). This size was selected so that the silicone pad used between the special heating device and the heated glass plate would conform around the relatively thin thermocouple wire.

A heat sink compound was applied to the tip of each thermocouple and then the thermocouple was attached to the surface of the glass plate using a 1 in. square piece of duct tape. The heat sink compound was a silicone-based material that was heavily filled with heat conductive metal oxides. This helped to ensure intimate contact with the glass plate's surface and promoted high thermal conductivity between the thermocouple and the glass plate. The duct tape was simply a temporary restraint until the IG unit was

loaded into the insulated heat chamber and pressurized. Fig. 84 shows the top and bottom of the thermocouple applied to a glass plate and ready for testing. Fig. 85 shows a specimen that is ready to be placed in the insulated heat chamber for testing.

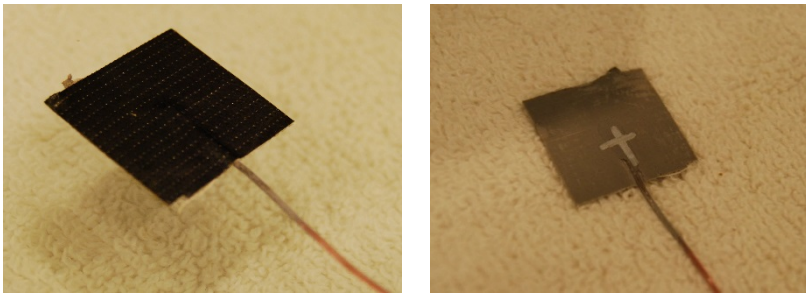

Fig. 84. Thermocouples Installed on Test Specimens

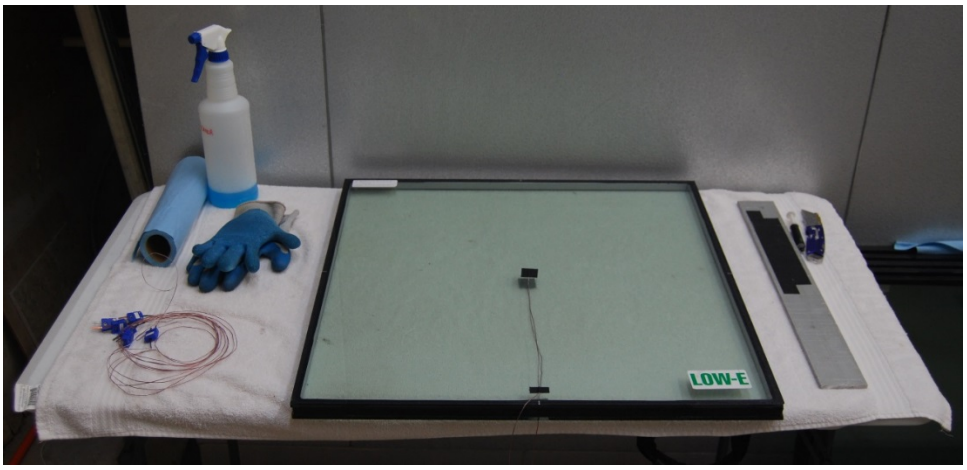

Fig. 85. Specimen Prepared for Testing

Insulated Heat Chamber

Once the specimens were prepared for testing, they were placed into a specially constructed insulated heat chamber to measure the center-of-glass temperature profile, across the IG unit. The insulated heat chamber consisted of a wooden box that completely enclosed the IG unit with insulation. Enclosing the IG unit in insulation served

to remove the possibility of surface films from developing on the glass plates' surfaces and along the edges. It also helped to enforce repeatability and consistency of the test results. The insulated heat chamber is shown in Fig. 86 below.

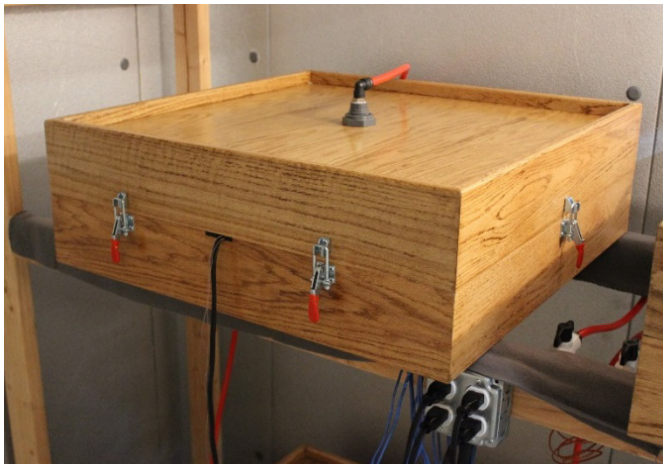

Fig. 86. Insulated Heat Chamber for Determining the CEEC

Heat was applied to the heated glass plate of the IG unit using a special heating device. The special heating device consisted of a wire wound silicone heating pad and layers of silicone pad and aluminum plate. The layers of aluminum plate and silicone pad helped to improve the uniformity of the heat flux that was applied to the heated glass plate. In addition, the low durometer silicone pad was selected so that it would conform around the thin thermocouple wire attached to the surface of the heated glass plate. Fig. 87 shows the glass specimen loaded into the insulated heat chamber before installing the special heating device. In addition, Fig. 87 shows the special heating device installed prior to closing the chamber for testing.

Fig. 87. IG Unit Specimen with Thermocouples Installed

Prior to testing, the uniformity for applying heat flux to the heated glass plate using the special heating device was verified using a matrix of thermocouples. An 8 in. by 8 in. region in the middle of the special heating device maintained a constant temperature within ±0.3 °F. The region between 8 in. and 12 in. maintained a constant temperature within ±2.4 °F and the remaining region between 12 in. and 24 in. maintained a constant temperature within ±4.7 °F. These regions and associated temperature ranges are illustrated in Fig. 88 below.

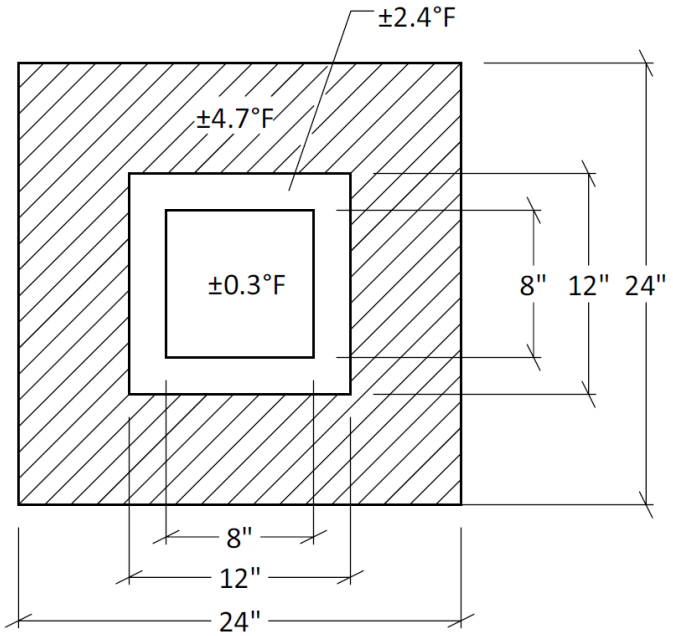

Fig. 88. Uniformity in Temperature of Special Heating Device

Once the instrumented IG unit and special heating device were installed in the insulated heat chamber, a uniform pressure of 14 in. of water (approximately 0.5 psi) was applied. The purpose of this pressure was to ensure a repeatable and uniform contact pressure between the special heating device and the heated glass plate's surface. In addition, the application of a uniform pressure helps ensure an intimate contact between the glass plates' surfaces and the inner and outer thermocouples. The pressure of 14 in. of water was selected so that the layers of silicone pad and aluminum plate would fully conform to the curvature of the IG unit as it contracts and expands during changes in temperature of the gas space cavity. During testing, the pressure was maintained within ±0.25 in. of water using a precision regulator. A 2-ft manometer was used to set and monitor the applied pressure. The regulator and manometer are shown in Fig. 89.

Fig. 89. Manometer and Pressure Regulator

Environmental Test Chamber

Once prepared for testing, the specimens were placed in an environmental test chamber and allowed to reach a thermal equilibrium temperature of -10 °F. During testing, the chamber was maintained at -10 °F ±10. The fluxuation in the ambient temperature had little effect on the results of the CEEC so-long-as the test specimen began at an initial temperature of -10 °F ±2.5 and was completed in approximately 2 hr. This is the case

because the well-insulated heat chamber does not allow the temperature of the IG unit inside to readily change over a short time duration. To help stabilize and maintain the ambient temperature inside of the environmental test chamber, thermal mass was added using a water-filled tank. In addition, the evaporator fans were used to continually circulate air inside the environmental test chamber. Fig. 90 shows the environmental test chamber and the water-filled tank that were used.

Fig. 90. Environmental Test Chamber

The insulated heat chamber was housed inside of the environmental test chamber using the rack shown in Fig. 91. The rack was installed to be earth level so that when the insulated heat chamber was placed on the rack in a vertical position, the IG unit would be plumb. This helped to ensure that the gas space cavity was oriented vertically.

Fig. 91. Specimen Test Rack in the Environmental Test Chamber

Data Acquisition

The temperature data were measured and recorded during each test using an IOtech DaqBook/2020 data acquisition system. This system is shown in Fig. 92. The DaqBook/2020 is a 16-bit, 200-kHz multifunction data acquisition system capable of supporting type T thermocouples directly and has a digital interface that was used to control a heating device. DASYLab Version 13.0 is an icon-based data acquisition software that was used to interface with the DaqBook/2020, log temperature data, and control the experiment.

Fig. 92. Data Acquisition System

A near constant voltage was supplied to the special heating device to ensure that it was delivering approximately 5.7105 (in.·lb/s)/in.^{2} of heat flux to the heated glass plate. The appropriate voltage was selected using the Watt-Voltage calibration curve shown in Fig. 93. As shown, 96.4 VAC was supplied to the special heating device so that its heat flux output was approximately 5.7105 (in.·lb/s)/in.^{2} to the heated glass plate.

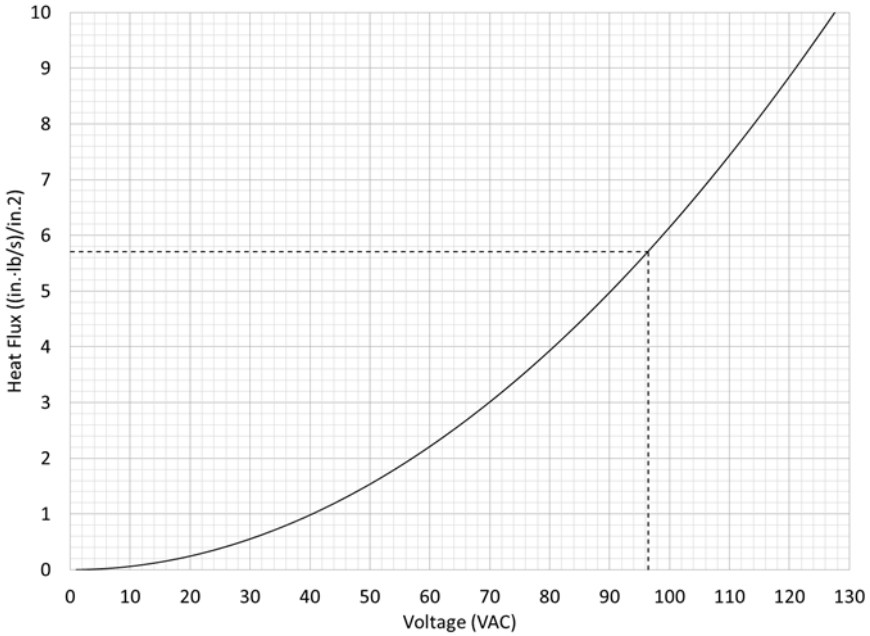

Fig. 93. Heat Output vs. Voltage for the Special Heating Device

An electronic heat controller was used to control the output of the special heating devices. The controller was used to set the initial voltage of each special heating device, prior to testing, and continuously monitor the voltage during testing. A multi-meter attached to the heat controller was used to set and monitor the voltage. In addition to setting the initial supply voltage for each special heating device and monitoring the supply voltage during testing, the electronic heat controller interfaced with the DaqBook/2020. This interface served as a thermostat to turn the special heating devices on and off to prevent the temperature of the heated glass plate from exceeding 200 °F. The electronic heat controller and multi-meter are shown in Fig. 94.

Fig. 94. Heat Controller

Experimental Results

The physical experiments that were performed to measure the specimens' temperature data were conducted over two days. Four insulated heat chambers were used so that four specimens could be tested at once. Table 15 shows the test protocol for all specimens. Table 15 includes the date each test series was performed and the location of each specimen in the environmental test chamber. For the test rack shown in Fig. 91, rack position

1 was associated with the upper-left location, facing the test rack. Each subsequent rack position was located from left-to-right, top-to-bottom. When a low-E coating was applied, it was tested with the coating on the number 2 surface of the heated glass plate of the IG unit.

Table 15. Test Protocol for All Specimens

Test Series	Test Date	Rack Position	Specimen No.
1	10/16/2016	1	4
		2	5
		3	7
		4	8
2	10/17/2016	1	4R
		2	1
		3	7R
		4	2

The temperature data that were measured for the six specimens considered for the practical applications are presented in Figs. 95 through 97. Based on the temperature data presented in Fig. 95, specimens 1 and 2 with clear glass plates had similar responses. Based on the temperature data presented in Fig. 96, specimens 4 and 5 with a hard-coat low-E coating had similar responses. Based on the temperature data presented in Fig. 97, specimens 7 and 8 with a soft-coat low-E coating had similar responses. These similar responses were expected because each of these groups were of identical types of IG units. This provided a level of credibility to the temperature data measured and helped to indicate whether a misnomer had occurred during the testing.

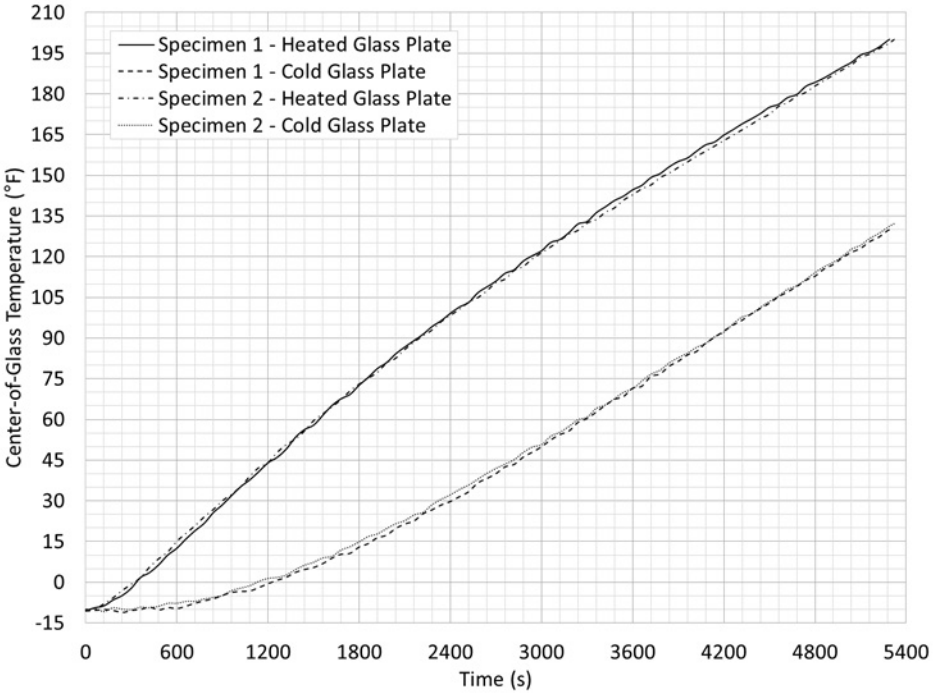

Fig. 95. Temperature Data Measured for Specimens 1 and 2 with Clear Glass Plates

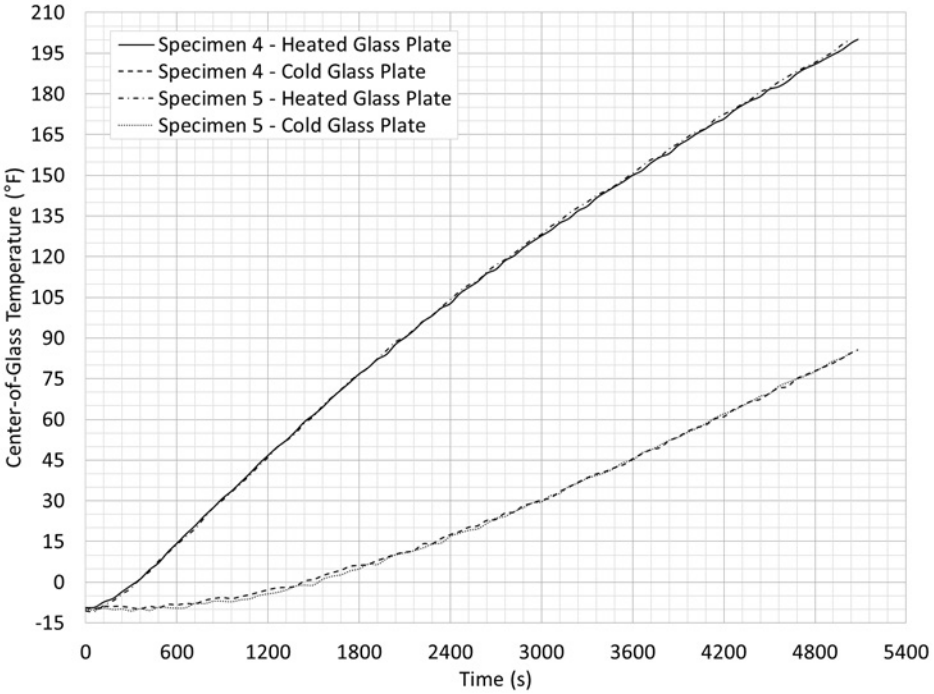

Fig. 96. Temperature Data Measured for Specimens 4 and 5 with a Hard-Coat Low-E Coating

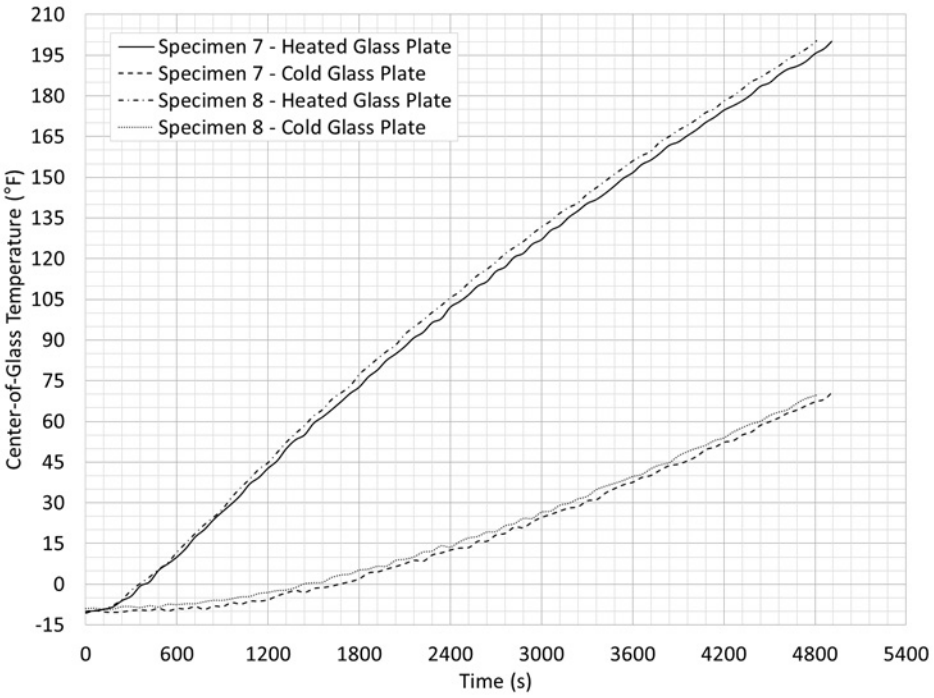

Fig. 97. Temperature Data Measured for Specimens 7 and 8 with a Soft-Coat Low-E Coating

The temperature data measured for specimens 1, 4, and 7 are summarized in Fig. 98. An important observation that can be gathered from these data is that the application of a low-E coating, either hard-coat or soft-coat, acts to increase the center-of-glass temperature of the heated glass plate. In addition, the center-of-glass temperature of the cold glass plate remained cooler than was the case for the specimens with clear glass plates. This is an expected response since the low-E coating acts to reduce the heat that is transferred across the gas space cavity due to long-wave radiation.

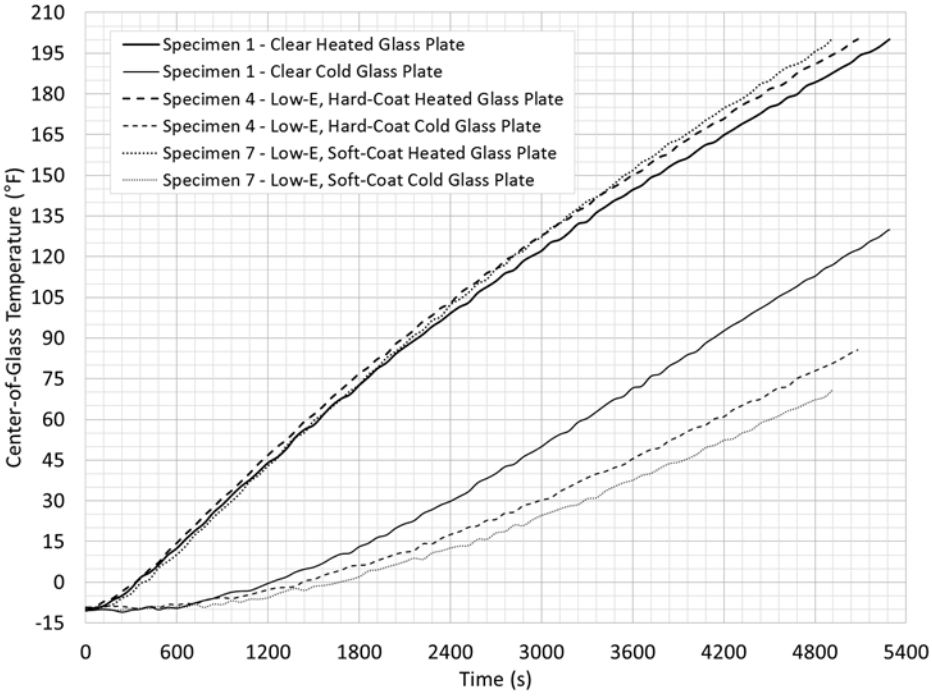

Fig. 98. Summary of Temperature Data Measured for Specimens 1, 4, and 7

Fig. 99 presents the difference in center-of-glass temperatures between the heated and cold glass plates, for each specimen tested. The IG unit is considered more energy-efficient as the difference in center-of-glass temperatures between the cold and heated glass plates increases. This increase in temperature also leads to higher levels of thermal stress along the perimeter of the glass plates. From these data, the IG unit with a soft-coat low-E coating applied provides the most energy-efficient IG unit. The second most energy-efficient IG unit is the hard-coat low-E coating and the clear glass IG unit is the least energy-efficient. The implications of these findings are that the IG unit with the soft-coat low-E coating would experience the highest level of thermal stress. Alternatively, the clear IG unit would be the least likely to experience high levels of thermal stress.

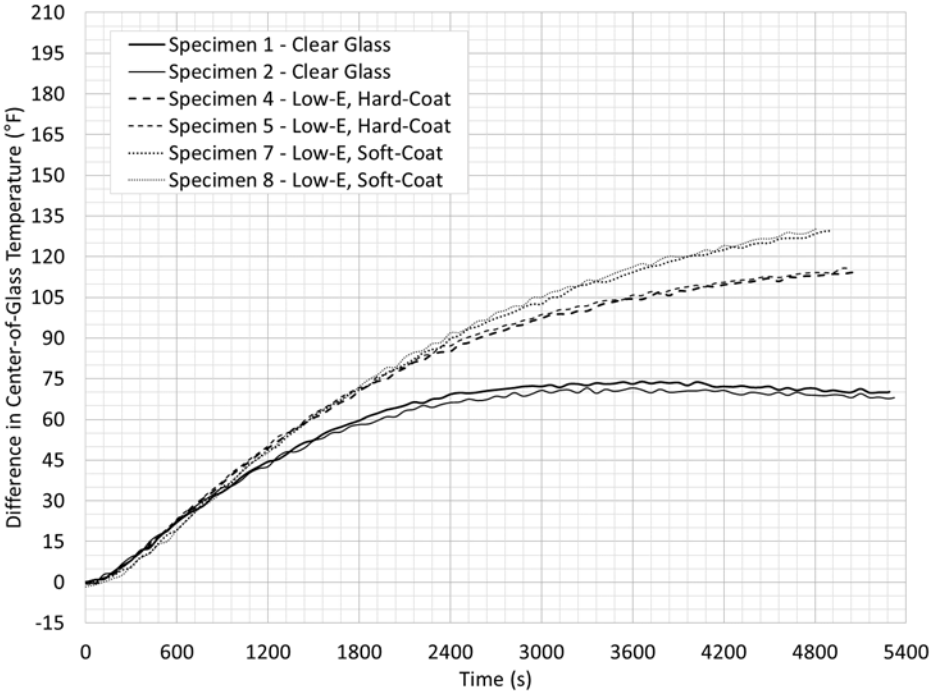

Fig. 99. Difference in Center-of-Glass Temperature for Specimens 1 Through 6

Table 16 presents the best-fit CEEC determined for each specimen. These values were determined by applying the PIOP to the temperature data presented in Figs. 95 through 97. Table 16 also presents the percentage difference in each value for the like specimens tested. It is shown that all like specimens tested were within 3 percent of one another and well within the acceptable range for experimental error. The results from the PIOP are presented in Figs. 100 through 105.

Table 16. CEEC for Each Specimen

Specimen No.	h_{CEEC} ((in.·lb/s)/(in.·°F))	Percent Difference
Specimen 1	0.018557	2.69%
Specimen 2	0.019063	
Specimen 4	0.009754	2.18%
Specimen 5	0.009968	
Specimen 7	0.008007	0.69%
Specimen 8	0.008063	

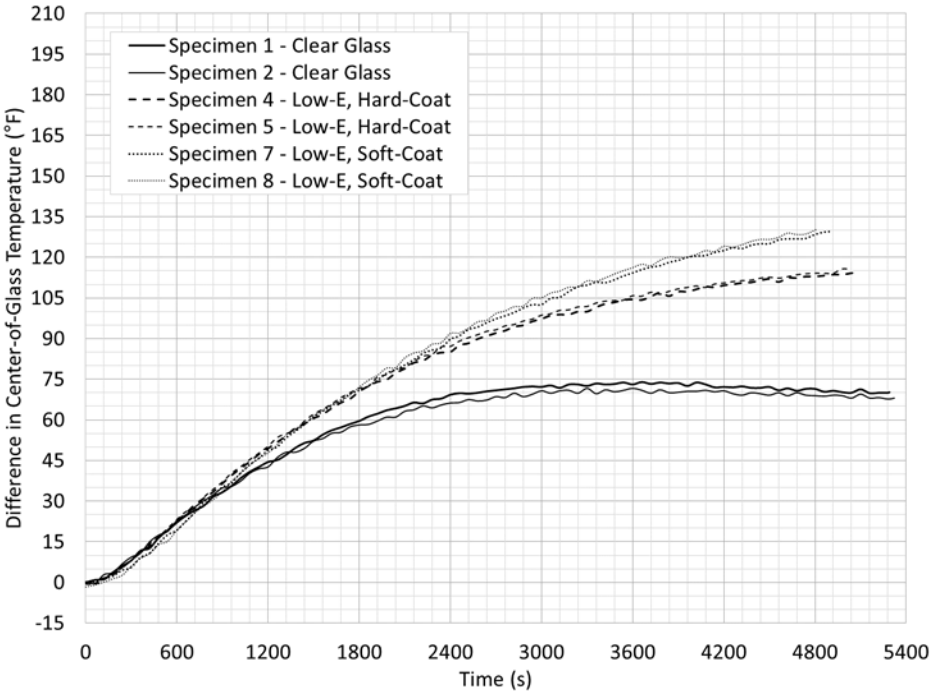

Fig. 100. Center-of-Glass Temperature Data Measured Compared to the CEEC for Specimen 1

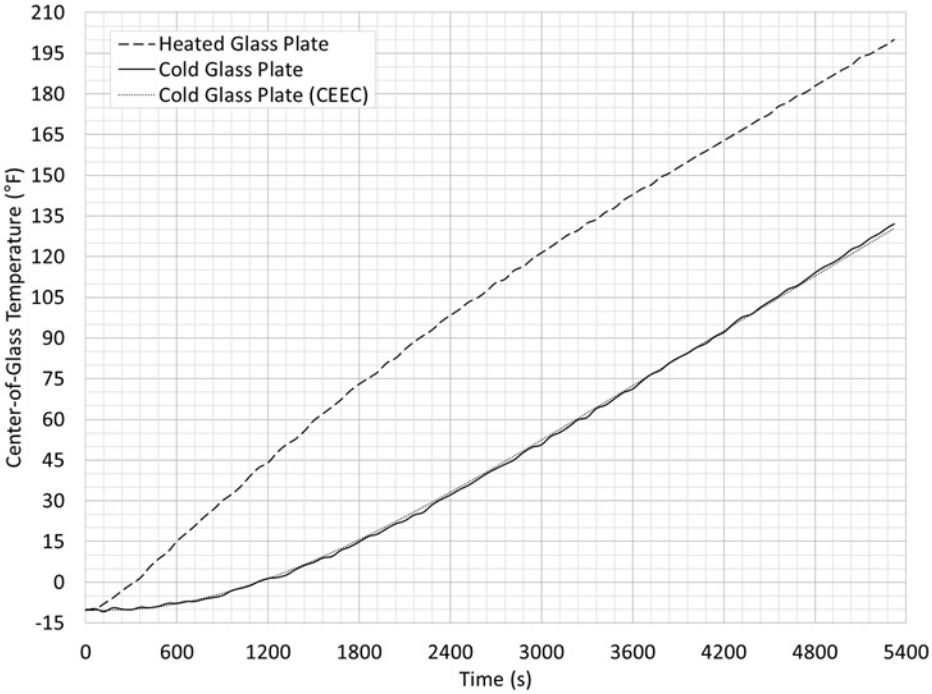

Fig. 101. Center-of-Glass Temperature Data Measured Compared to the CEEC for Specimen 2

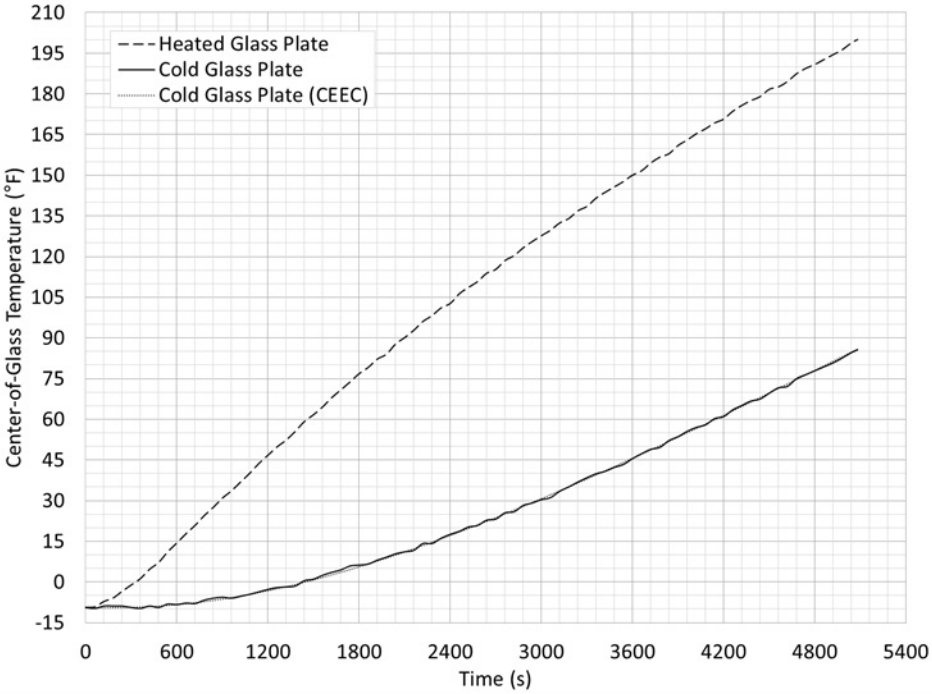

Fig. 102. Center-of-Glass Temperature Data Measured Compared to the CEEC for Specimen 4

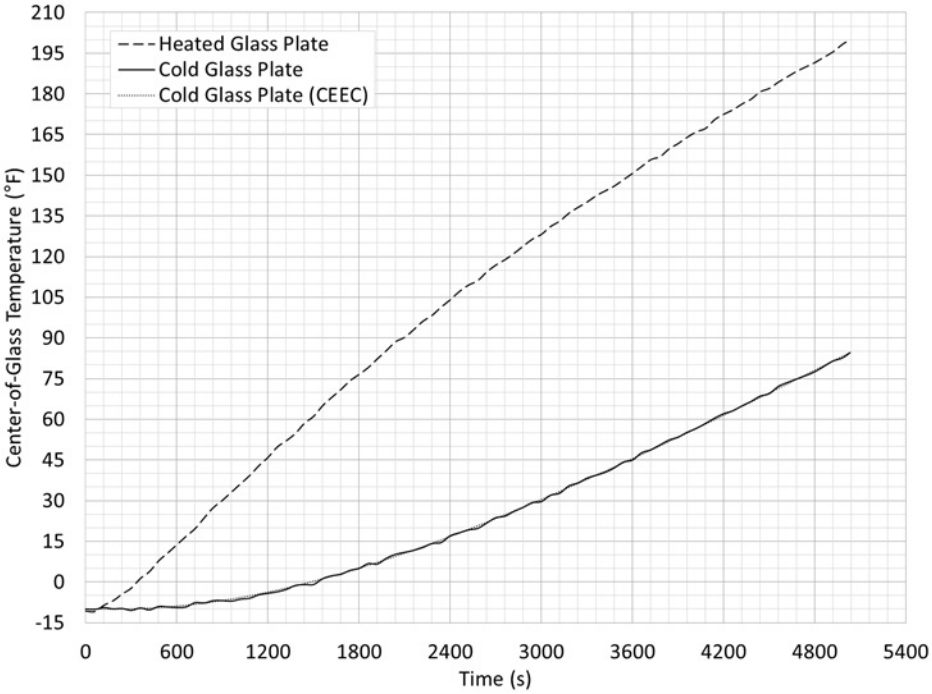

Fig. 103. Center-of-Glass Temperature Data Measured Compared to the CEEC for Specimen 5

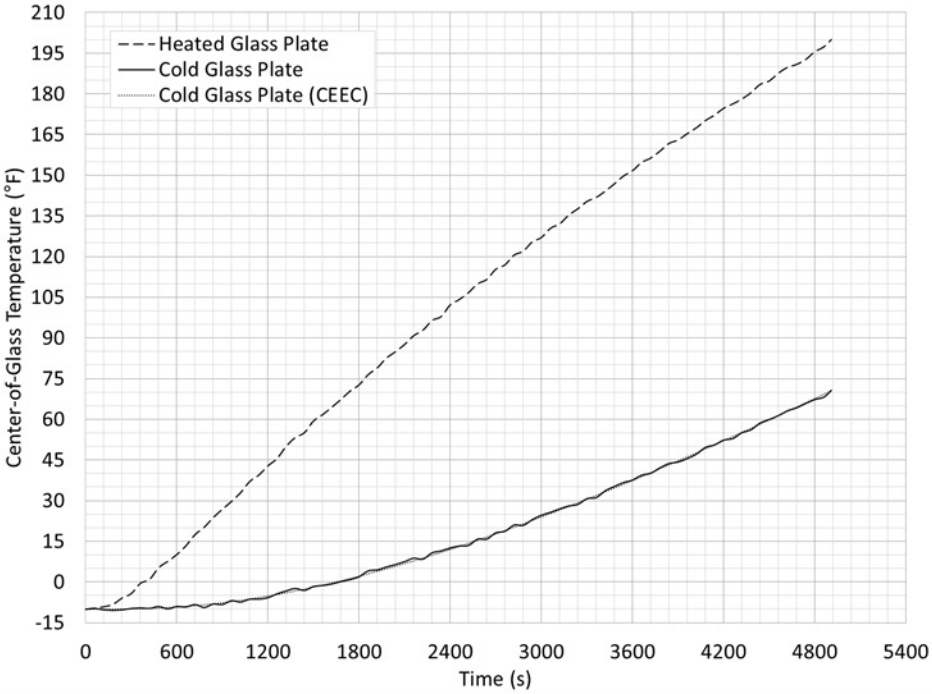

Fig. 104. Center-of-Glass Temperature Data Measured Compared to the CEEC for Specimen 7

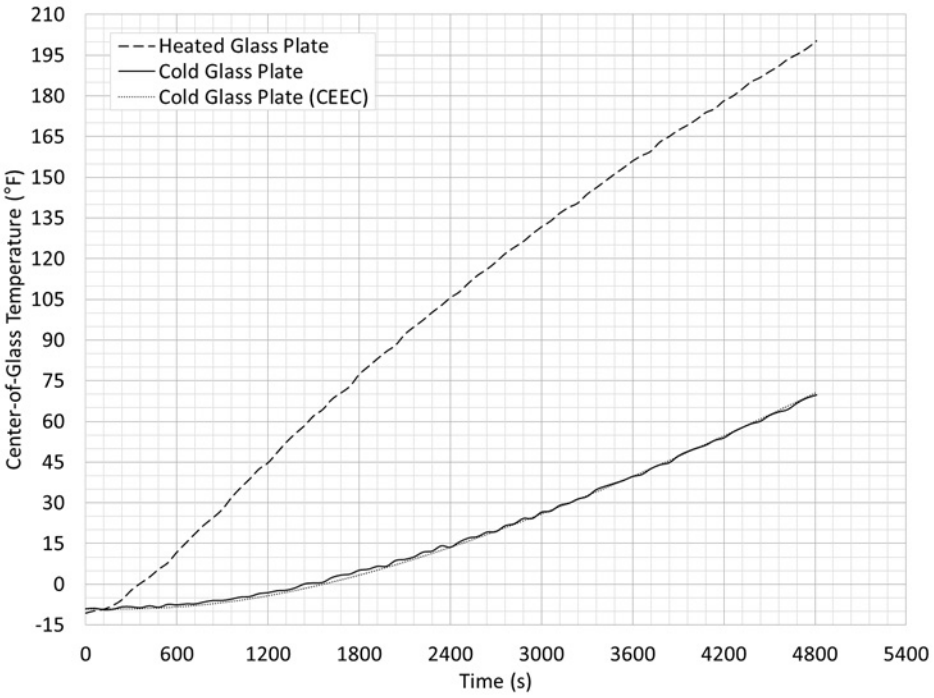

Fig. 105. Center-of-Glass Temperature Data Measured Compared to the CEEC for Specimen 8

From Figs. 100 through 105, it is clear that the CEEC provides the most accurate results for IG units that employ low-E coatings. This is the case because the presence of the low-E coating reduces the heat exchange between the glass plates due to long-wave radiation. This is convenient for two reasons. First, most of the IG units of interest incorporate low-E coatings. Second, the level of thermal stress associated with IG units that incorporate low-E coatings are often much larger than the thermal stresses associated with IG units consisting of clear glass plates (Gordon 2001; Pilkington 2005; Klam 2007; Lingnell and Beason 2013). This means that the CEEC is most accurate for IG units that will experience higher levels of thermal stress because of the use of low-E coatings. This notwithstanding, the experiments performed on IG units with clear glass plates provided acceptable results as well.

Knowing the CEEC for each specimen, as presented in Table 16, the increase in heat exchanged across the gas space cavity for different types of IG units can be quantified. Table 17 presents the percentage increase in the heat exchanged across the gas space cavity for soft-coat, hard-coat, and clear glass IG units. These data were calculated using the CEEC for specimens 1, 4, and 7. Because the IG unit with a soft-coat low-E coating is the most energy-efficient, it was selected as the normal to compare the other types of IG units against.

Table 17. Percentage for Increase in Energy Exchange for Soft-Coat, Hard-Coat, and Clear Glass IG Units

Type of Low-E Coating	h_{CEEC} ((in.·lb/s)/(in.·°F))	Increase in Heat Exchange
Soft-Coat	0.008007	-
Hard-Coat	0.009754	22%
Clear Glass	0.018557	132%

Two final practical applications were performed to confirm that the orientation of the specimens (i.e. whether the low-E coating was applied to the number 2 or 3 surface) does not alter the test results. These two tests were performed using specimens 4 and 7 in the reverse orientation with the low-E coating on the number 3 surface. For clarity, the reverse orientation was denoted with the letter "R" next to the specimen number. The dimensions for each specimen are presented in Table 18. Where all of the variables are as previously defined.

Table 18. Specimen Dimensions for Reverse Orientation Tests

Specimen No.	t_{heated} (in.)	t_{cold} (in.)	$t_{overall}$ (in.)	t_{cavity} (in.)
Specimen 4	0.2250	0.2250	0.95005	0.5001
Specimen 4R	0.2250	0.2250	0.95005	0.5001
Specimen 7	0.2190	0.2210	0.95035	0.5104
Specimen 7R	0.2210	0.2190	0.95035	0.5104

The temperature data measured for specimens 4R and 7R are presented in Figs. 106 and 107, respectively. Included in these figures are temperature data measured for specimens 4 and 7, respectively. As shown, these data seem independent of orientation.

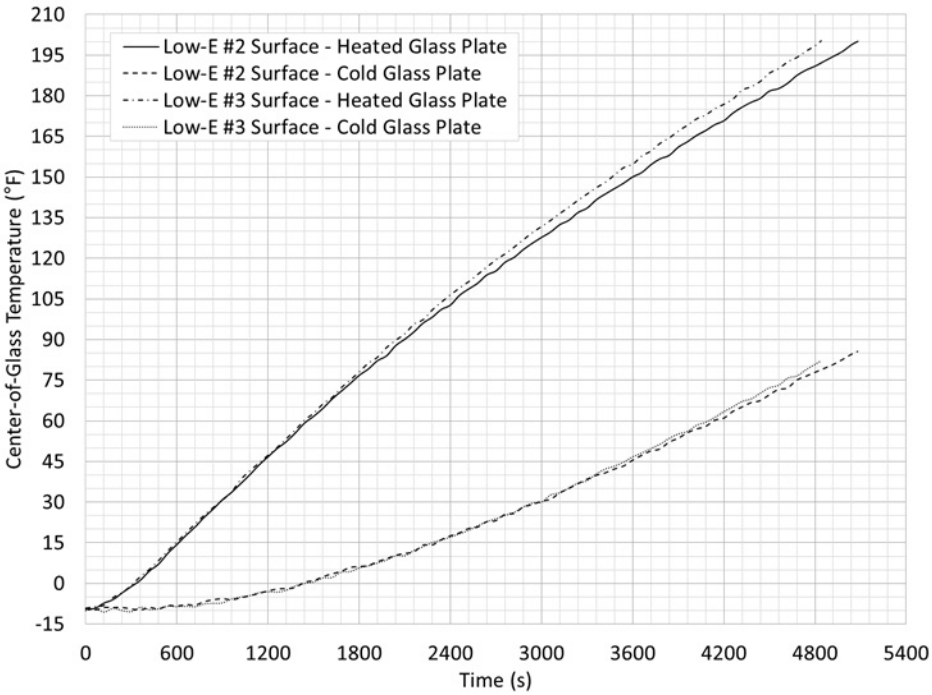

Fig. 106. Glass Plate Temperature Data Measured for Specimens 4 and 4R

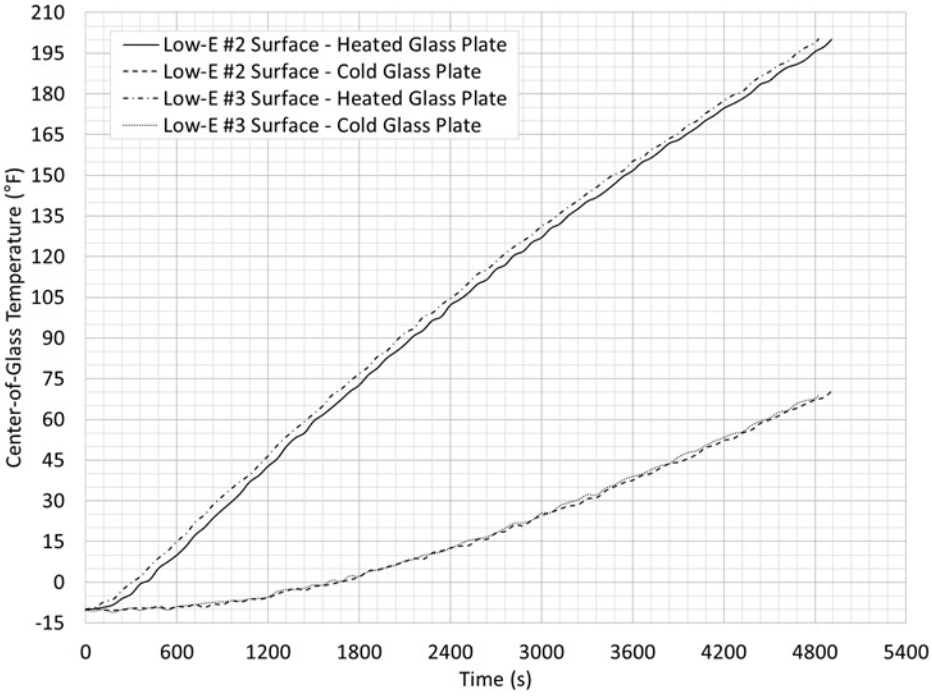

Fig. 107. Glass Plate Temperature Data Measured for Specimens 7 and 7R

Table 19 presents the CEEC for each specimen. These values were determined by applying the PIOP to the temperature data presented in Figs. 106 and 107. Table 19 also presents the percentage difference in each value from specimens 4 and 7. The results from the PIOP are presented in Figs. 108 and 109.

Table 19. Comparison of CEEC for the Low-E Coating Applied to the Number 2 and 3 Surfaces

Specimen No.	Surface No.	h_{CEEC} ((in.·lb/s)/(in.·°F))	Percent Difference
Specimen 4	#2	0.009754	0.01%
Specimen 4R	#3	0.009754	
Specimen 7	#2	0.008007	2.64%
Specimen 7R	#3	0.007799	

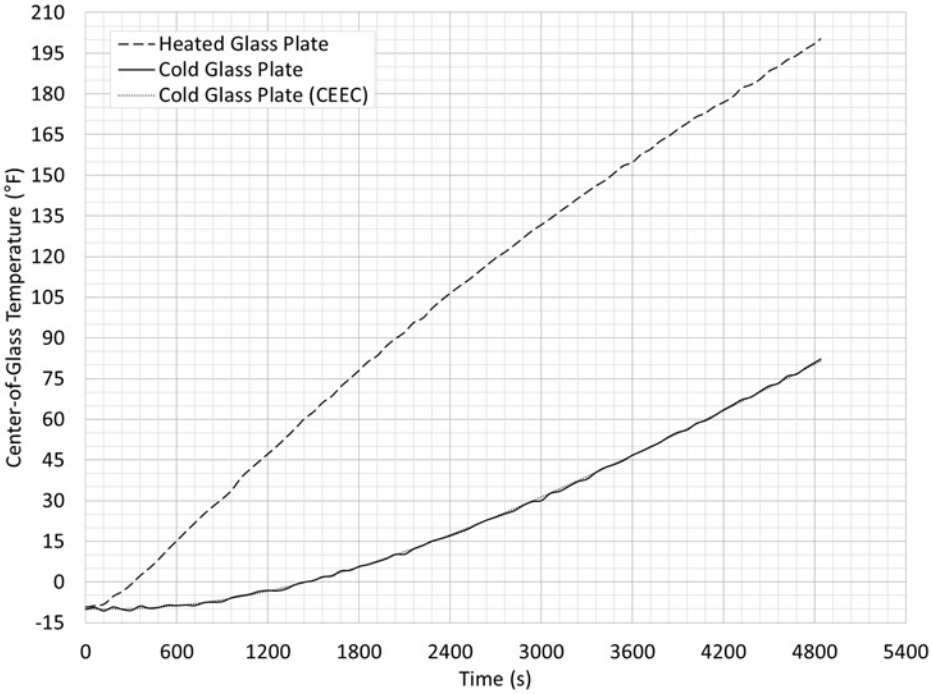

Fig. 108. Center-of-Glass Temperature Data Measured Compared to the CEEC for Specimen 4R

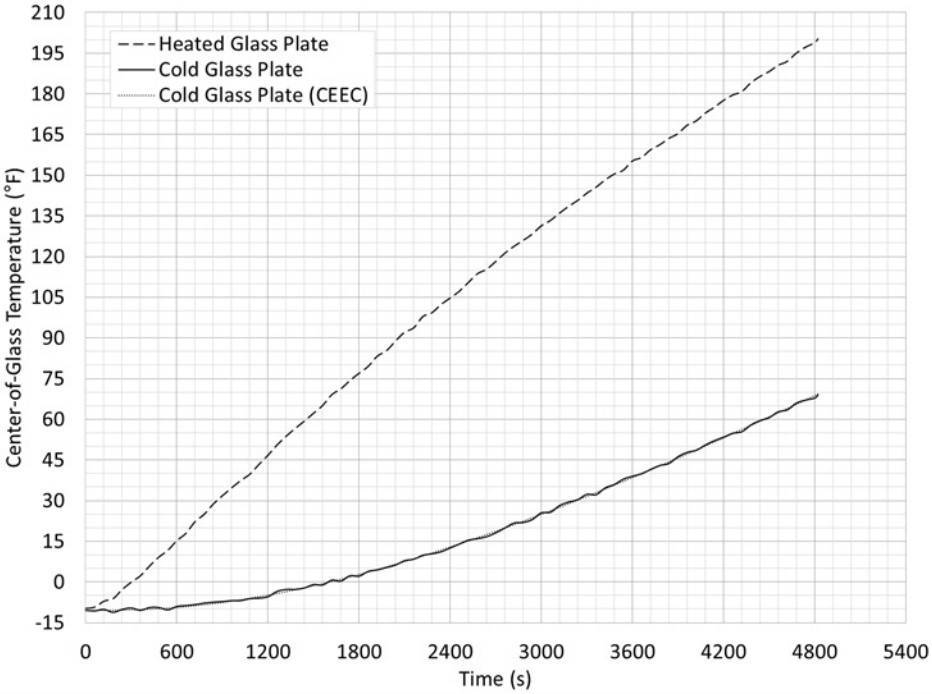

Fig. 109. Center-of-Glass Temperature Data Measured Compared to the CEEC for Specimen 7R

From these data, it is clear that the value determined for the CEEC is independent of the location of the low-E coating (i.e. applied to the number 2 or 3 surface). This was the case for the soft-coat and hard-coat low-E coating. It was shown that the results from these experiments were within 3 percent of each other and well within the acceptable range for experimental error. However, to unify the FTP, the IG unit should be tested with the low-E coating on the number 2 surface of the heated glass plate.

Ultimately, the use of the CEEC was critical in developing the SDP. The SDP combined with the CEEC can be used to evaluate the POB of glass plates in generic IG units subjected to solar irradiance. The next chapter of this paper presents the SDP and its development.

CHAPTER VI
SIMPLIFIED DESIGN PROCEDURE

For monolithic glass plates, it was possible to develop a concise analysis procedure that represents a wide variety of coatings, tints, absorptions, frame systems, and edge bite dimensions (ASTM 2012a). The primary inputs into the analysis procedure for monolithic glass plates are the solar irradiance, solar absorptance of the glass plate, and the frame edge bite dimension. The primary purpose of the research presented herein was to develop a similar procedure that could be used to evaluate the probability of breakage (POB) of glass plates that are used in insulating glass (IG) units subjected to solar irradiance.

With the additional variables that affect the thermal behavior of IG units, calculating the thermal stress that develops is much more complicated than that of monolithic glass plates (Klam 2007; Lingnell and Beason 2013). This chapter is dedicated to developing a simplified design procedure (SDP) to evaluate the POB of glass plates due to thermal stresses that develop in generic IG units that are subjected to a general range of environmental conditions. The SDP was developed by first exercising the formal design procedure (FDP) presented in Chapter IV on these generic IG units under the general range of environment conditions selected. The results from these analyses were then used to develop a SDP that can be applied without using the FDP.

Among the many variables that affect the thermal behavior of IG units are the glass plates' thicknesses, absorptions, surface emissivities, the spacer's properties and geometry, sealant properties, edge bite, the frame's material properties and geometry, and the type of gas fill. Finite element (FE) analyses provide a convenient tool that can be used to analyze the effect each of these variables have on the development of thermal stresses in IG units for a large range of environmental conditions.

For this effort, two assumptions were used to simplify the analysis procedure. These two assumptions were: (1) the maximum tensile stress at the perimeter of the glass plate was calculated using the fundamental equation and (2) the combined energy exchange coefficient (CEEC) was used to linearize the heat transfer across the gas space cavity. The reasons for using these two assumptions are discussed below.

It is convenient to solve complex heat transfer problems using FE methods. Four types of FE analyses exist to solve heat transfer problems: linear steady-state, non-linear steady-state, linear transient, and non-linear transient (Abbey 2014). As discussed previously, anytime long-wave radiation is considered using fundamental theories, a non-linear solution is required. While most FE codes are capable of solving non-linear heat transfer problems, it requires iteration that is typically time consuming. For the analyses herein, the use of the CEEC allows the heat transfer problems to be solved using a linear solution.

In addition, heat transfer analyses are often performed in conjunction with mechanical analyses that calculate the thermal stress that develops. For the analyses herein, coupled thermal-mechanical analyses were not performed. Rather, the FE analyses were used to determine the maximum transient temperature difference between the center-of-glass and the perimeter-of-glass. Then, the fundamental understanding of the effect that differential temperature has on glass plates was applied to determine the maximum level of tensile stress that occurs along the perimeter of the glass plate.

The primary advantages of using the CEEC and performing a thermal only FE analysis were to prevent convergence issues that can arise with non-linear solutions, as-well-as reduce the calculation time required for a fully non-linear, thermal-mechanical FE analysis. These simplifying assumptions provide the ability to solve a large number of problems and consider the many possible combinations of low emissivity (low-E) or solar

control coatings, glass tints, glass plate spacing, substitute gas fills, etc. and are the premise for the SDP.

The SDP was constructed by developing a large database of FE analyses whereby trends could be observed and simplifications made that reduced the effort required to analyze IG units for thermal stress. The SDP is based on the premise that the variables that affect the thermal behavior of IG units can be subdivided into groups. The first group includes the type of frame, spacer system, and the nominal thicknesses of the glass plates that are used. The second group includes the level of solar irradiance, net absorption of both glass plates, and the difference in temperature between the indoor and outdoor environments. The final group includes the CEEC, edge bite, and a term to describe the ratio of solar irradiance that is absorbed between the two glass plates.

The transfer of heat through the edges of an IG unit has a significant effect on how thermal stresses develop. There are many factors that affect the transfer of heat through the edges. This includes the frame design, the thermal resistance of the spacer, thicknesses of sealants, sealant materials, and edge bite (Sasaki 1971). The frame design and glazing method (i.e. pocket glazing vs. structural glazing) have the most significant effect on the thermal stresses that develop (Sasaki 1971). The research herein is solely focused on pocket glazing where a frame is employed. The material and construction of the frame has a significant role on the thermal behavior of an IG unit. If the frame is well insulated from the surrounding building's structure, the perimeter of the glass plate will tend to increase in temperature at a rate closer to that of the center of the glass plate. If the frame is not well insulated and in good thermal contact with the building's structure, the temperature of the perimeter of the glass plate will tend to remain near the steady-state temperature. In this case, the frame is said to provide a high-heat mass. Of the two cases, the perfectly insulated frame is the favorable case as the perimeter-of-glass temperature will rise at a faster rate and reduce the maximum difference in temperature between the center-of-glass area (Beason and Lingnell 2002; ASTM 2012a).

Another factor that plays an important role in influencing the thermal behavior of IG units are the construction details of the unit itself. Glass tints, low-E coatings, films, the type of gas fill, and their locations within the IG unit have an effect on the thermal behavior of the IG unit. The existence and location of tinted glass and coatings primarily affect the absorptions of the inner and outer glass plates.

Typically, the design professional will select the appropriate type of coating and its location to fit the climate for a building's location. This affects both the net absorption and the amount of solar energy proportioned between the inner and outer glass plates. The absorption of solar irradiance and temperature of the inner glass plate will increase when the low-E coating is applied to the number 3 surface of the IG unit. This orientation is typically employed in heating dominated climates as it increases the amount of heat transferred to the indoor environment through passive solar heat gain. This helps to reduce the building's required heating demand. Reversing this orientation and placing the low-E coating on the number 2 surface will cause the outer glass plate to absorb more solar irradiance and increase its temperature. Thus, heat will be transferred more readily to the outdoor environment. This orientation is typically employed in cooling dominated climates (Beason and Lera 1989; Gordon 2001).

It is important to understanding that there are a near infinite number of coatings, tints, absorptions, and construction combinations, in addition to frame edge bite dimensions, that can be applied to IG units. However, with the introduction of the CEEC for the gas space cavity, some simplifying observations can be made. Primarily, the effects of gas fill and low-E coatings are accounted for in the CEEC.

The term used to define the total percentage of solar irradiance that is absorbed by the IG unit is termed the net absorption, α_{net}, herein. The net absorption can be calculated using Eq. (70) below and includes the total percentage of solar irradiance that is absorbed by both the inner and outer glass plates of the IG unit. The absorption ratio, α_{ratio}, is

defined as the absorption of the outer glass plate divided by the absorption of the inner glass plate, as given by Eq. (71). The absorption ratio is used to describe the amount of solar irradiance absorbed by the outer glass plate compared to the inner glass plate.

$$\alpha_{net} = \alpha_{outer} + \alpha_{inner} \tag{70}$$

$$\alpha_{ratio} = \frac{\alpha_{outer}}{\alpha_{inner}} \tag{71}$$

Where α_{outer} is the percentage of the total solar irradiance that is absorbed by the outer glass plate and α_{inner} is the percentage of the total solar irradiance that is absorbed by the inner glass plate.

The values for the outer and inner glass plate absorptions must be determined using the ray tracing procedure presented previously. Note that these values are not the same as the inner and outer glass plate solar absorptance coefficients that are used as inputs into the ray tracing procedure. Taking the CEEC, absorption ratio, and net absorption it is possible to develop a SDP that can represent different combinations of types and locations of coatings, tints, films, etc. that can be incorporated into an IG unit.

The effects of variables in groups 2 and 3 were considered for specific frames, spacers, and a nominal glass plate thickness of 0.25 in. This was the case because no appreciable research had been performed previously that defines the thermal behavior of IG units with various frames, spacers, or nominal glass plate thicknesses. Thus, no simplifying assumptions could be readily made. In addition, there are relatively few frame, spacer, and nominal glass thickness combinations that are possible when compared to the near infinite combinations of environmental conditions, glass plate absorptions, and CEEC. Thus, perfectly insulated and high-heat mass frames with a thin, steel-channel spacer were considered for the analyses herein. In addition, 0.25 in. thick nominal glass plates

were used for all analyses. However, the SDP can easily be extended to any combination of frame, spacer, or nominal glass plate thickness.

Before the effects that the second group of variables have on the thermal behavior of an IG unit can be considered, it is important to determine the appropriate actual glass plate thickness to be used for a thermal analysis. The actual glass plate thickness is dependent on the nominal glass plate thickness being considered. This is explained in detail below.

Thickness

When glass plates are manufactured their thickness is required to fall within a specified range of minimum and maximum thicknesses. For 0.25 in. thick nominal glass plates the specified range of acceptable thicknesses is 0.219 to 0.244 in. (ASTM 2011). When designing a glass plate to resist lateral loads it is clear that the minimum thickness should be used. However, the appropriate thickness that should be used with a thermal design condition is not as apparent. Thus, a parametric study was performed using set of FE analyses to study the effect of glass plate thickness on the development of temperature across the glass plates' areas of IG units.

For each case in the parametric study, the IG unit's frame was assumed to be perfectly insulated with an edge bite of 0.5 in. Two different IG units were considered, each with the minimum and maximum glass thickness. The indoor temperature was held at a constant 70 °F for all cases and the outdoor temperature was analyzed at both -20 and 120 °F. Table 20 below shows the parameters that were used in each analysis. Where all of the variables are as previously defined.

Table 20. Parameters Used for Each Analysis

Case No.	Outer Glass Plate	Inner Glass Plate	t_{glass} (in.)	α_{outer}	α_{inner}	h_{CEEC} ((in.·lb/s)/(in.·°F))	$T_{outdoor}$ (°F)
Thickness Case 1	1/4 in. Low-E, Soft-Coat	1/4 in. Clear	0.219	0.3407	0.0537	0.006694	-20
Thickness Case 2	1/4 in. Low-E, Soft-Coat	1/4 in. Clear	0.219	0.3407	0.0537	0.006694	120
Thickness Case 3	1/4 in. Low-E, Soft-Coat	1/4 in. Clear	0.244	0.3407	0.0537	0.006694	-20
Thickness Case 4	1/4 in. Low-E, Soft-Coat	1/4 in. Clear	0.244	0.3407	0.0537	0.006694	120
Thickness Case 5	1/4 in. Clear	1/4 in. Clear	0.219	0.1517	0.1134	0.0202723	-20
Thickness Case 6	1/4 in. Clear	1/4 in. Clear	0.219	0.1517	0.1134	0.0202723	120
Thickness Case 7	1/4 in. Clear	1/4 in. Clear	0.244	0.1517	0.1134	0.0202723	-20
Thickness Case 8	1/4 in. Clear	1/4 in. Clear	0.244	0.1517	0.1134	0.0202723	120

The FDP that was presented in Chapter IV was used to determine the variation in temperature between the center-of-glass and the perimeter-of-glass, as a function of time, for each case shown. The results from these FE analyses are shown in Figs. 110 through 113. Based on the findings in Chapter IV, the inner glass plate was examined at the -20 °F outdoor temperature, and the outer glass plate was examined at the 120 °F outdoor temperature.

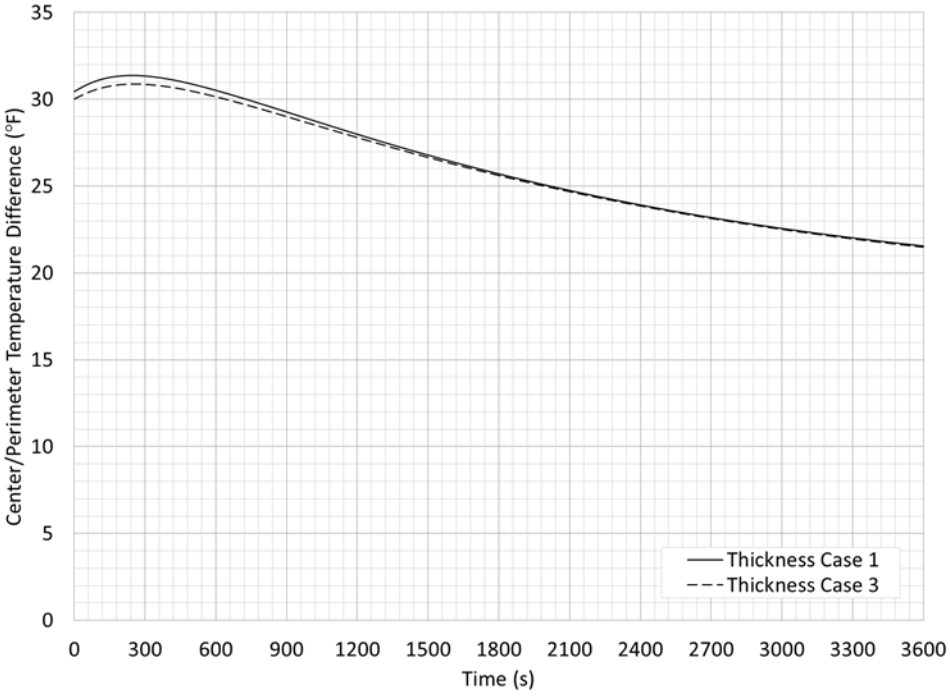

Fig. 110. Thickness Case 1 and 3 - Inner Glass Plate of a Low-E IG Unit at -20 °F Outdoor Temperature

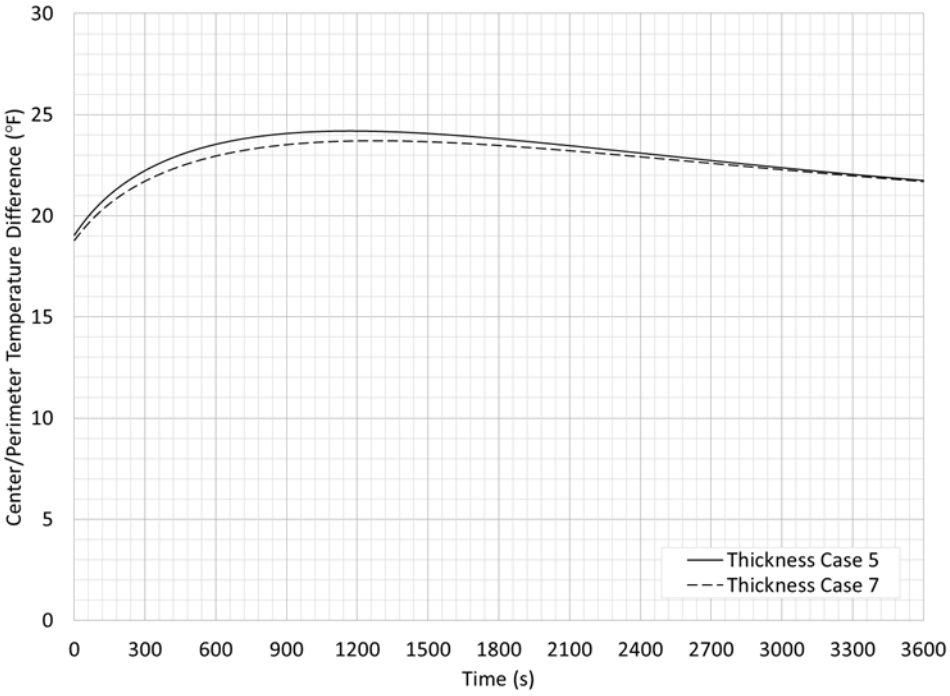

Fig. 111. Thickness Case 5 and 7– Inner Glass Plate of a Clear IG Unit at -20 °F Outdoor Temperature

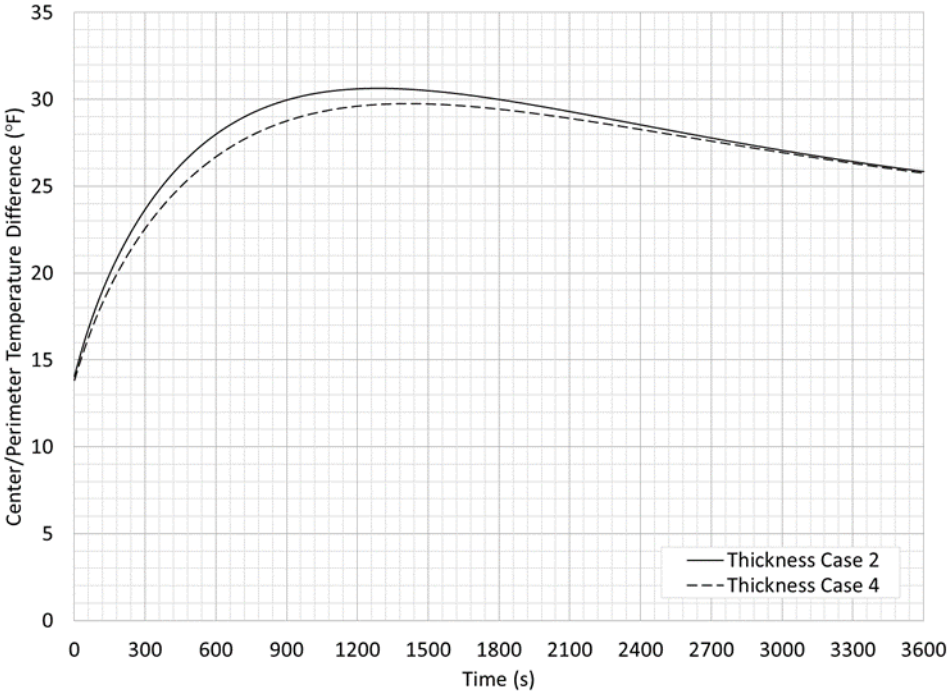

Fig. 112. Thickness Case 2 and 4– Outer Glass Plate of a Low-E IG Unit at 120 °F Outdoor Temperature

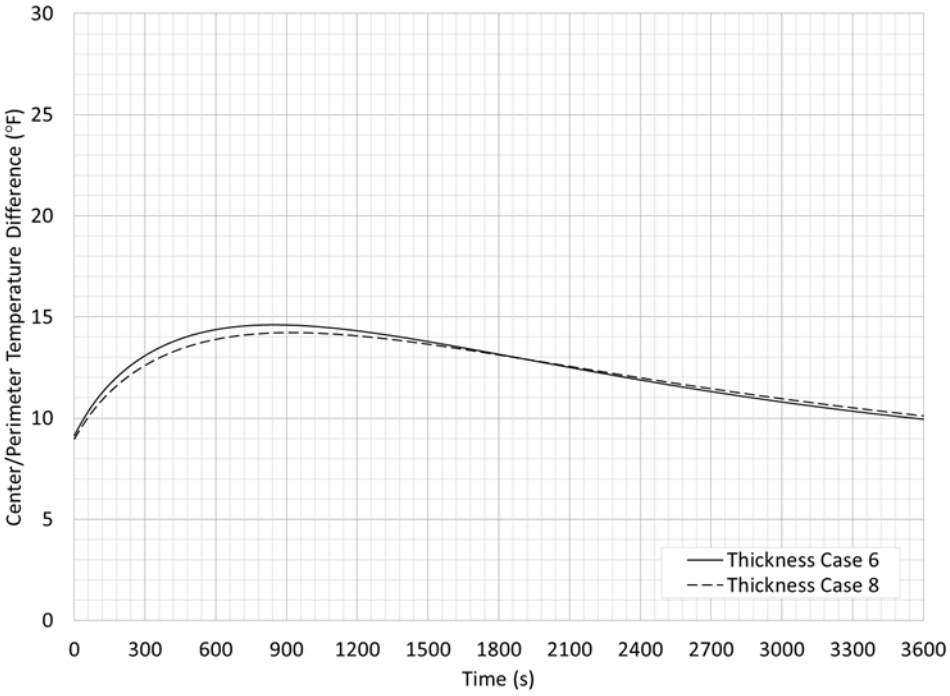

Fig. 113. Thickness Case 6 and 8 - Outer Glass Plate of a Clear IG Unit at 120 °F Outdoor Temperature.

It is clear from Figs. 110 through 113, that in all cases the thinner, 0.219 in. thick glass plate maintained a slightly greater difference in the center-of-glass and perimeter-of-glass temperature difference than the thicker, 0.244 in. thick glass plate. It is also shown that the thinner glass plate reached its maximum difference in temperature at a faster rate than the thicker glass plate. Likewise, the thinner glass plate begins to cool at a faster rate than the thicker glass plate. This is due to the increase in thermal mass of the thicker glass plate compared to the thinner glass plate. It takes more heat energy to change the temperature of the thicker glass plate than it does the thinner glass plate. Thus, this phenomenon shifts the temperature-time curve slightly, as would be expected. The maximum temperature difference, ΔT_{max}, between the center-of-glass and the perimeter-of-glass measured for each case is summarized in Table 21 below. Where all other variables are as previously defined.

Table 21. Maximum Temperature Difference Measured for Each Case

Case No.	Outer Glass Plate	Inner Glass Plate	t_{glass} (in.)	$T_{outdoor}$ (°F)	ΔT_{max} (°F)	Glass Plate
Thickness Case 1	1/4 in. Low-E, Soft-Coat	1/4 in. Clear	0.219	-20	31.38	Inner
Thickness Case 2	1/4 in. Low-E, Soft-Coat	1/4 in. Clear	0.219	120	30.64	Outer
Thickness Case 3	1/4 in. Low-E, Soft-Coat	1/4 in. Clear	0.244	-20	30.89	Inner
Thickness Case 4	1/4 in. Low-E, Soft-Coat	1/4 in. Clear	0.244	120	29.74	Outer
Thickness Case 5	1/4 in. Clear	1/4 in. Clear	0.219	-20	24.19	Inner
Thickness Case 6	1/4 in. Clear	1/4 in. Clear	0.219	120	14.61	Outer
Thickness Case 7	1/4 in. Clear	1/4 in. Clear	0.244	-20	23.70	Inner
Thickness Case 8	1/4 in. Clear	1/4 in. Clear	0.244	120	14.24	Outer

When considering the inner glass plate, the 0.219 in. thick glass plate had a maximum temperature difference 0.49 °F greater than the 0.244 in. thick glass plate for both the low-E IG unit (Thickness Cases 1 and 3) and the clear IG unit (Thickness cases 5 and 7). When considering the outer glass plate, the 0.219 in. thick glass plate had a maximum temperature difference of 0.89 and 0.38 °F greater than the 0.244 in. thick glass plate for the low-E IG unit (Thickness Cases 2 and 4) and the clear IG unit (Thickness Cases 6

and 8), respectively. Based on these findings, all further analyses were performed using the minimum specified glass thickness of 0.219 in. In practice, these difference are most likely negligible. However, it is clearly conservative to use the minimum thickness for the nominal glass plate thickness being considered.

Now the effects that the second group of variables have on the thermal behavior of an IG unit with perfectly insulated and high-heat mass frames with a thin, steel-channel spacer can be determined. These variables include the solar irradiance, net absorption, and the indoor/outdoor temperature difference. This is discussed in detail in the next section of this chapter.

Linear Design Variables that Affect the Thermal Behavior of Insulating Glass Units

A series of parametric studies were performed to understand the effects that the level of solar irradiance, net absorption of the IG unit, and the difference in temperature between the indoor and outdoor environments have on the thermal behavior of IG units. Each of these factors are discussed in detail below. From these parametric studies, a SDP was developed that incorporates a model to estimate the thermal design stress of an IG unit subjected to solar irradiance that includes these factors as input variables.

Solar Irradiance

A second parametric study was performed to understand the effect of solar irradiance on the temperatures that develop in IG units. There are many factors that affect the amount of solar irradiance that is converted to heat within a glass plate. However, this amount of heat can be calculated based on the glass plates absorption and the amount of solar irradiance that it is exposed to.

The total amount of solar irradiance that a window is subjected to depends on several factors. The primary factors include cloud cover, the altitude and latitude of the building's location, the time of the day, and the month of the year (Turner 1977, Lingnell 1981). These factors not only influence the intensity of the sun, but the angle of incidence at which the sun impinges on the glass plates within a window. Solar irradiance that is absorbed by a window is maximum when the sun's rays are perpendicular to the surface of the window (Lingnell 1981). As the angle of incidence decreases, the solar irradiance intercepted by the window will also decrease.

Additionally, the building's orientation will play a significant role in the amount of solar irradiance that a window will receive during certain hours of the day and months of the year (Turner 1977, Lingnell 1981). Thus, in most cases it is necessary to plot the monthly or yearly path of the sun and measure its intensity to properly determine the design solar irradiance for a particular building location and window (Lingnell 1981). As such, a SDP is needed that can be used for a wide range of solar irradiances.

For the analyses herein, solar irradiance ranging from 2.8553 to 5.7105 (in.·lb/s)/in.^{2} were considered. FE analyses were performed using solar irradiance levels in increments of 0.7138 (in.·lb/s)/in.^{2}, for a total of 5 data points per case. For each case the IG unit's frame was assumed to be perfectly insulated with an edge bite of 0.5 in. Two different IG units were analyzed, one with a low-E coating and another with clear glass plates. The indoor temperature was held at a constant 70 °F for all cases, and the outdoor temperature was analyzed at both -20 and 120 °F. Table 22 shows the parameters that were used in each analysis. Where all of the variables are as previously defined. The results from each analysis are shown in Figs. 114 through 121.

Table 22. Results from FE Analyses

Case No.	Outer Glass Plate	Inner Glass Plate	α_{outer}	α_{inner}	h_{CEEC} ((in.·lb/s)/(in.·°F))	I_S ((in.·lb/s)/in.^{2})	$T_{outdoor}$ (°F)
Solar Load Case 1	1/4 in. Low-E, Soft-Coat	1/4 in. Clear	0.3407	0.0537	0.0066940	2.8553	-20
Solar Load Case 2	1/4 in. Low-E, Soft-Coat	1/4 in. Clear	0.3407	0.0537	0.0066940	3.5691	-20
Solar Load Case 3	1/4 in. Low-E, Soft-Coat	1/4 in. Clear	0.3407	0.0537	0.0066940	4.2829	-20
Solar Load Case 4	1/4 in. Low-E, Soft-Coat	1/4 in. Clear	0.3407	0.0537	0.0066940	4.9967	-20
Solar Load Case 5	1/4 in. Low-E, Soft-Coat	1/4 in. Clear	0.3407	0.0537	0.0066940	5.7105	-20
Solar Load Case 6	1/4 in. Clear	1/4 in. Clear	0.1517	0.1134	0.0202723	2.8553	-20
Solar Load Case 7	1/4 in. Clear	1/4 in. Clear	0.1517	0.1134	0.0202723	3.5691	-20
Solar Load Case 8	1/4 in. Clear	1/4 in. Clear	0.1517	0.1134	0.0202723	4.2829	-20
Solar Load Case 9	1/4 in. Clear	1/4 in. Clear	0.1517	0.1134	0.0202723	4.9967	-20
Solar Load Case 10	1/4 in. Clear	1/4 in. Clear	0.1517	0.1134	0.0202723	5.7105	-20
Solar Load Case 11	1/4 in. Low-E, Soft-Coat	1/4 in. Clear	0.3407	0.0537	0.0066940	2.8553	120
Solar Load Case 12	1/4 in. Low-E, Soft-Coat	1/4 in. Clear	0.3407	0.0537	0.0066940	3.5691	120
Solar Load Case 13	1/4 in. Low-E, Soft-Coat	1/4 in. Clear	0.3407	0.0537	0.0066940	4.2829	120
Solar Load Case 14	1/4 in. Low-E, Soft-Coat	1/4 in. Clear	0.3407	0.0537	0.0066940	4.9967	120
Solar Load Case 15	1/4 in. Low-E, Soft-Coat	1/4 in. Clear	0.3407	0.0537	0.0066940	5.7105	120
Solar Load Case 16	1/4 in. Clear	1/4 in. Clear	0.1517	0.1134	0.0202723	2.8553	120
Solar Load Case 17	1/4 in. Clear	1/4 in. Clear	0.1517	0.1134	0.0202723	3.5691	120
Solar Load Case 18	1/4 in. Clear	1/4 in. Clear	0.1517	0.1134	0.0202723	4.2829	120
Solar Load Case 19	1/4 in. Clear	1/4 in. Clear	0.1517	0.1134	0.0202723	4.9967	120
Solar Load Case 20	1/4 in. Clear	1/4 in. Clear	0.1517	0.1134	0.0202723	5.7105	120

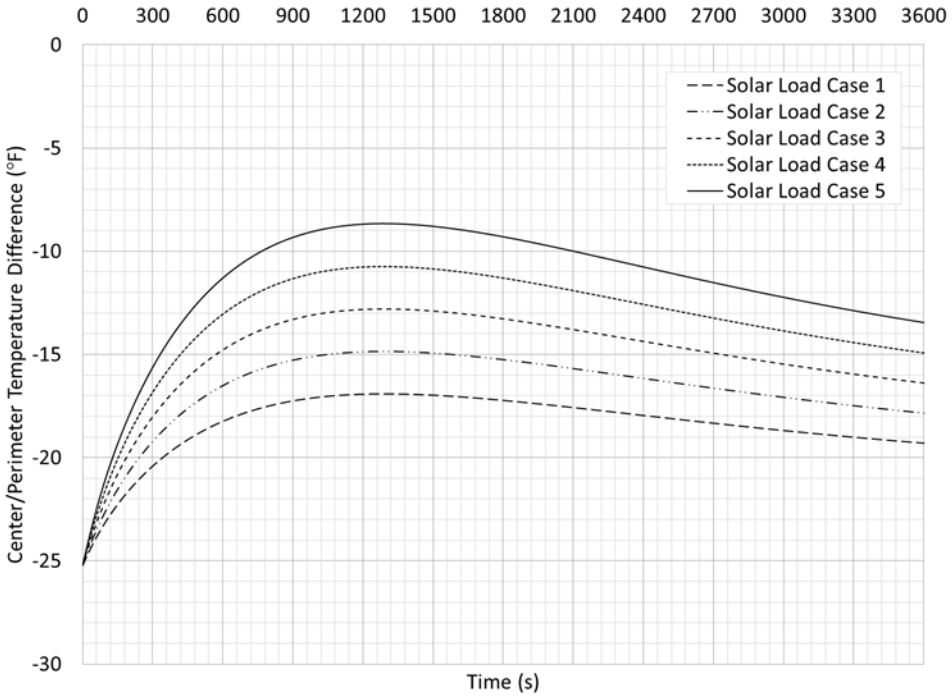

Fig. 114. Solar Load Case 1 Through 5 - Outer Glass Plate of a Low-E IG Unit at -20 °F Outdoor Temperature

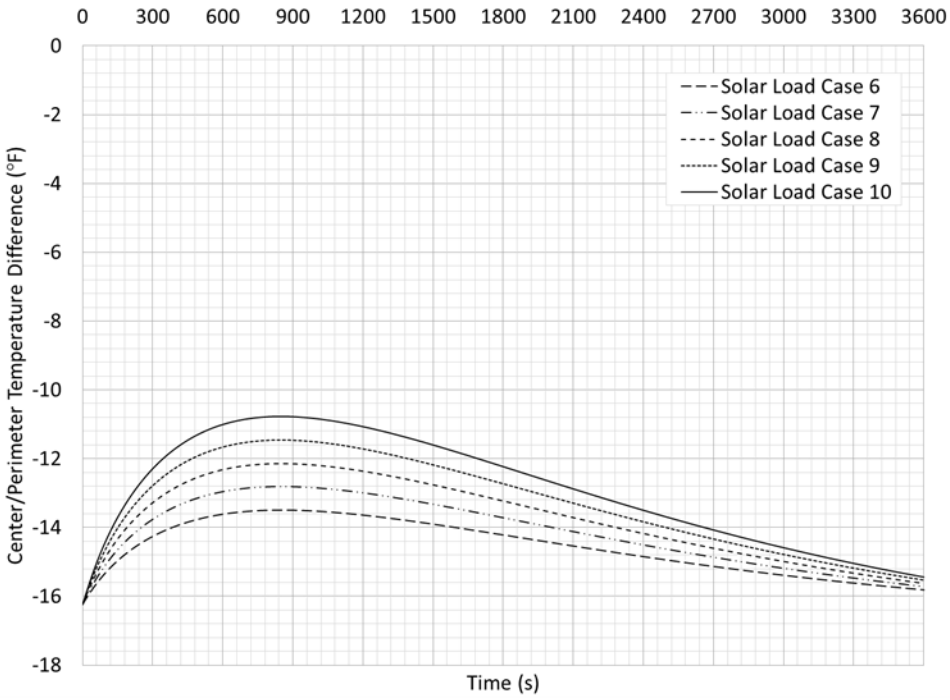

Fig. 115. Solar Load Case 6 Through 10 - Outer Glass Plate of a Clear IG Unit at -20 °F Outdoor Temperature

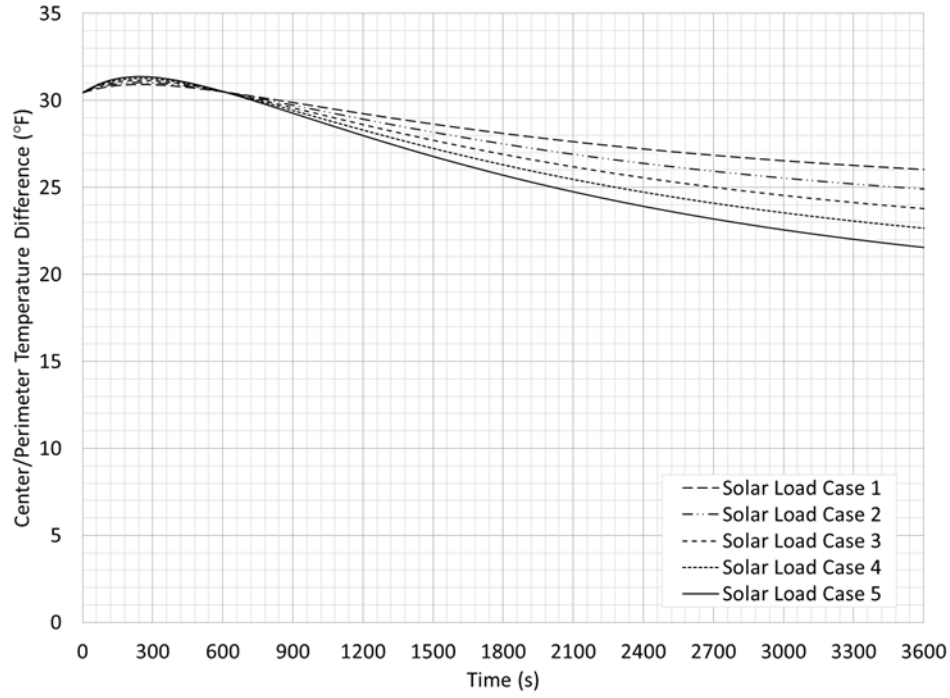

Fig. 116. Solar Load Case 1 Through 5 - Inner Glass Plate of a Low-E IG Unit at -20 °F Outdoor Temperature

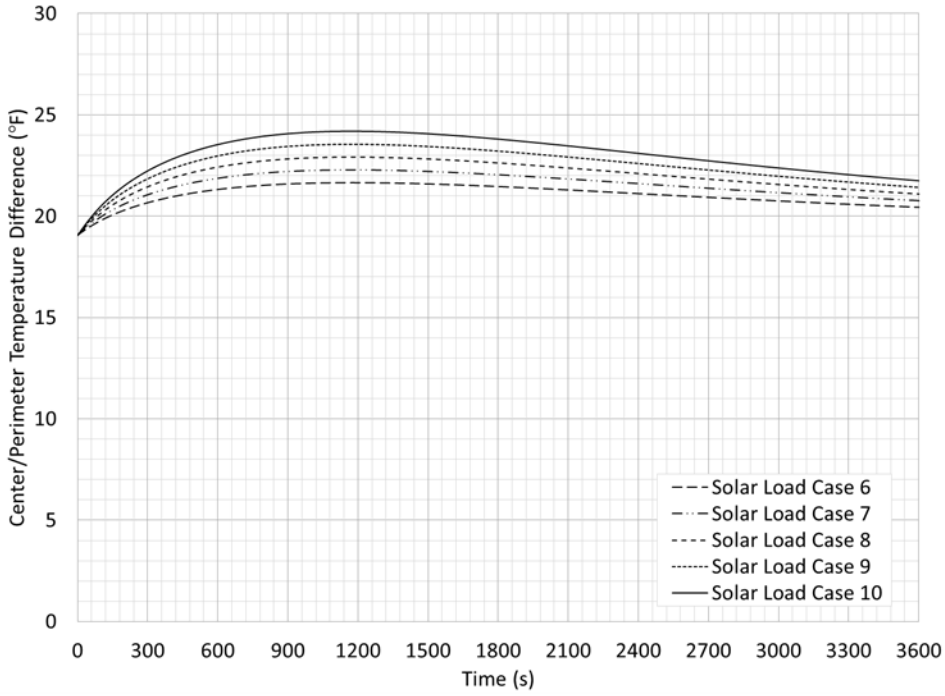

Fig. 117. Solar Load Case 6 Through 10 - Inner Glass Plate of a Clear IG Unit at -20 °F Outdoor Temperature

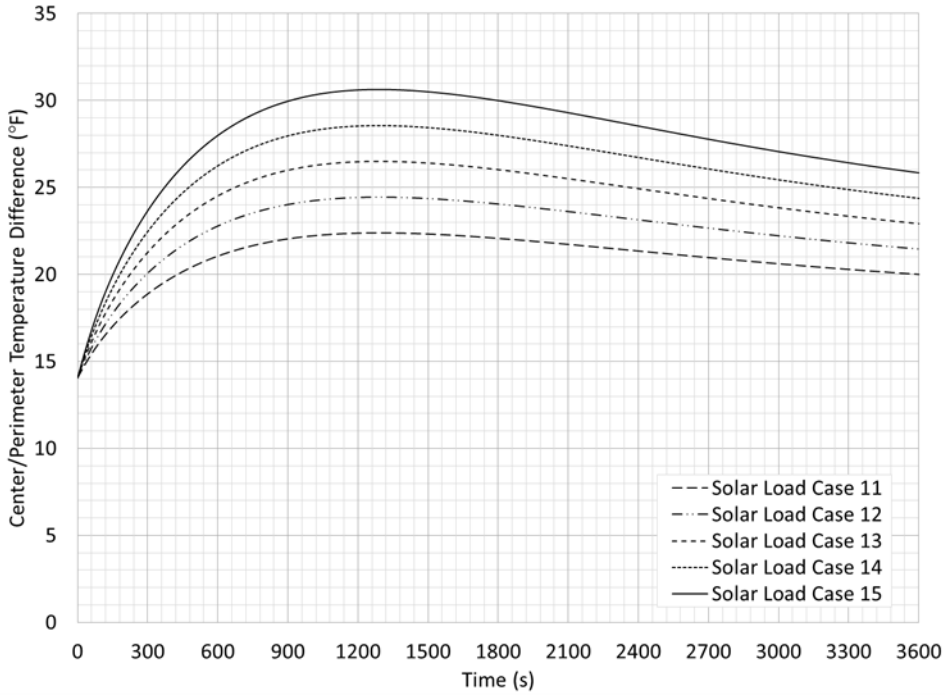

Fig. 118. Solar Load Case 11 Through 15 - Outer Glass Plate of a Low-E IG Unit at 120 °F Outdoor Temperature

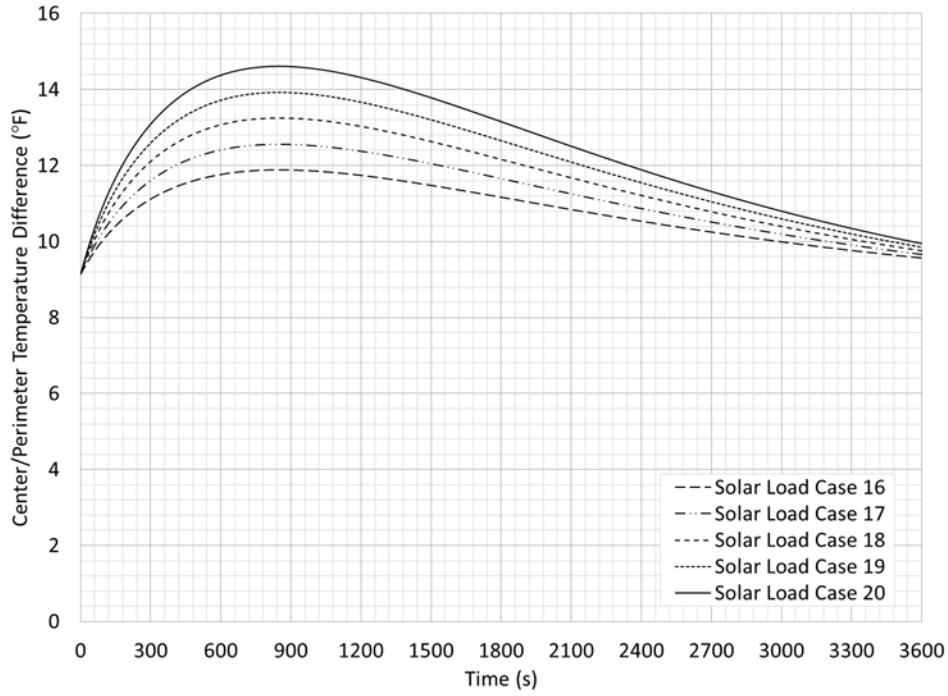

Fig. 119. Solar Load Case 16 Through 20 - Outer Glass Plate of a Clear IG Unit at 120 °F Outdoor Temperature

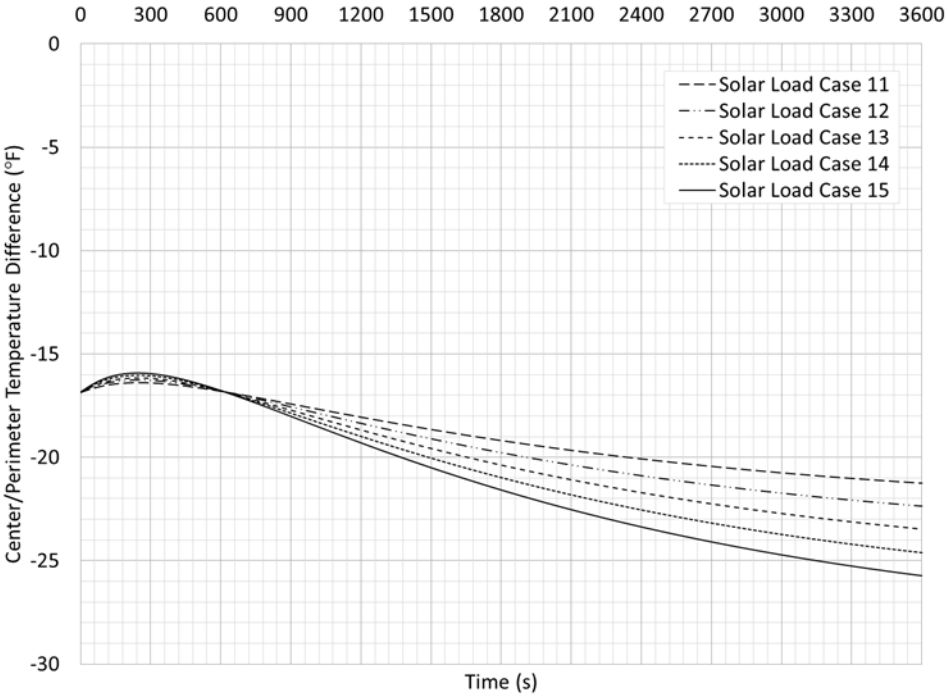

Fig. 120. Solar Load Case 11 Through 15 - Inner Glass Plate of a Low-E IG Unit at 120 °F Outdoor Temperature

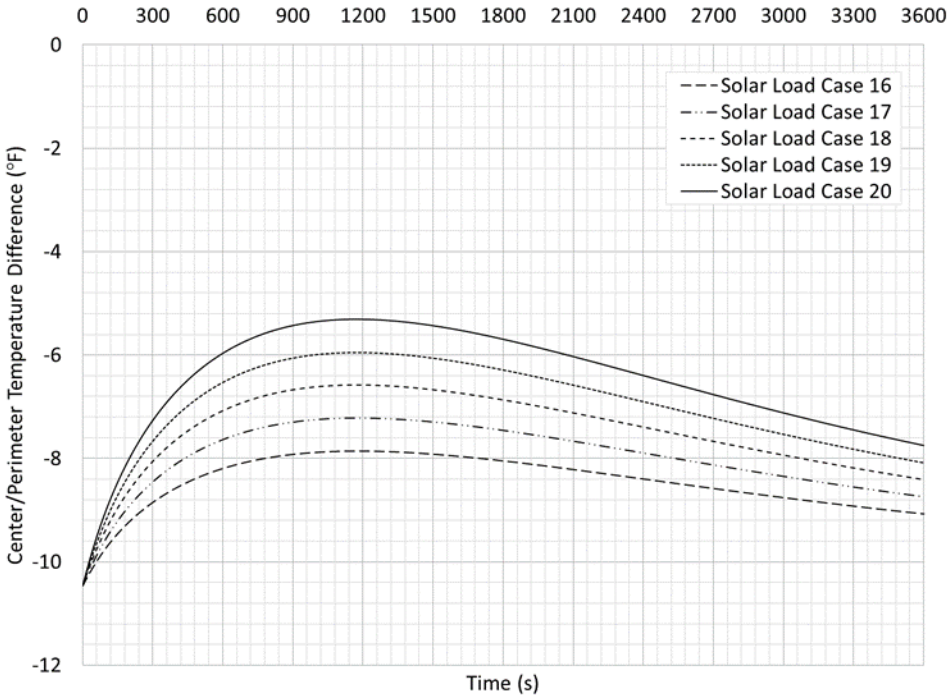

Fig. 121. Solar Load Case 16 Through 20 - Inner Glass Plate of a Clear IG Unit at 120 °F Outdoor Temperature

From Figs. 114 through 121, it is again clear that the inner glass plate is critical for outdoor temperatures that are below the indoor temperature and the outer glass plate becomes critical for outdoor temperatures that are above the indoor temperature. Therefore, taking the maximum temperature difference between the center-of-glass and the perimeter-of-glass, for the inner and outer glass plates, for an outdoor temperature of -20 and 120 °F, respectively, gives the temperature data summarized in Table 23.

Table 23. Summary of Results for Solar Load Parametric Study

Case No.	Outer Glass Plate	Inner Glass Plate	I_S ((in.·lb/s)/in.2)					Glass Plate
			2.85525	3.5690625	4.282875	4.9966875	5.7105	
Solar Load Case 1 - 5	1/4 in. Low-E, Soft-Coat	1/4 in. Clear	30.92	31.04	31.15	31.26	31.38	Inner
Solar Load Case 6 - 10	1/4 in. Clear	1/4 in. Clear	21.64	22.28	22.92	23.55	24.19	Inner
Solar Load Case 11 - 15	1/4 in. Low-E, Soft-Coat	1/4 in. Clear	22.38	24.44	26.51	28.57	30.64	Outer
Solar Load Case 16 - 20	1/4 in. Clear	1/4 in. Clear	11.89	12.57	13.25	13.93	14.61	Outer

Based on the data shown in Table 23, Figs. 122 through 125 show the maximum temperature difference between center-of-glass and the perimeter-of-glass as a function of solar irradiance for each case analyzed. By fitting a line through these data points, it is clear that the effect that solar irradiance has on the maximum temperature difference between center-of-glass and the perimeter-of-glass for a given glass plate in an IG unit is linear. This is in complete agreement with previous research performed by Klam (2007) and Lingnell and Beason (2013).

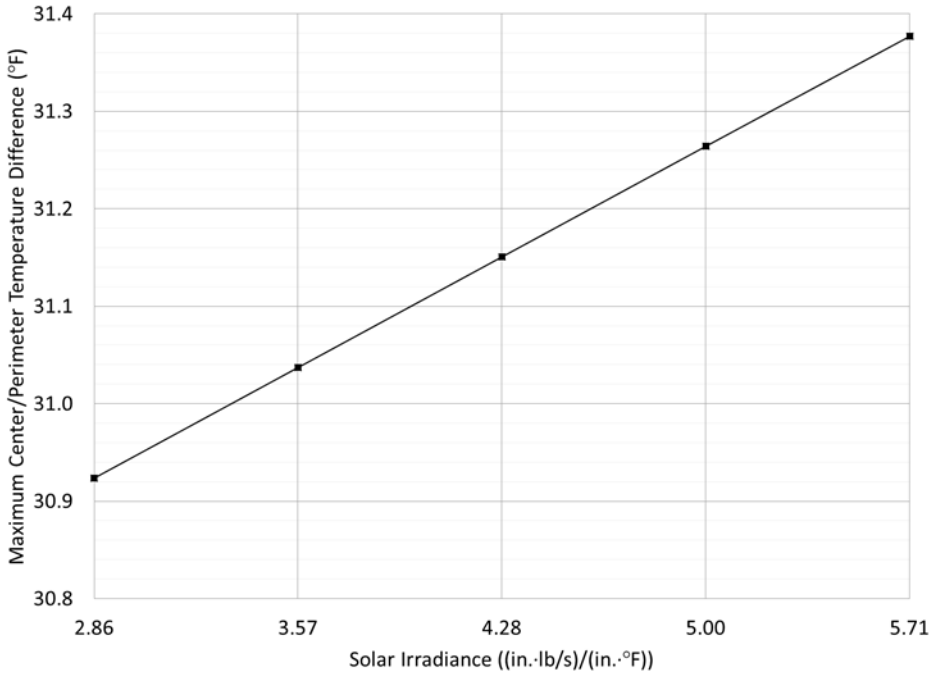

Fig. 122. Solar Load Case 1 Through 5 – Effect of Solar Irradiance on Inner Glass Plate of a Low-E IG Unit at -20 °F Outdoor Temperature

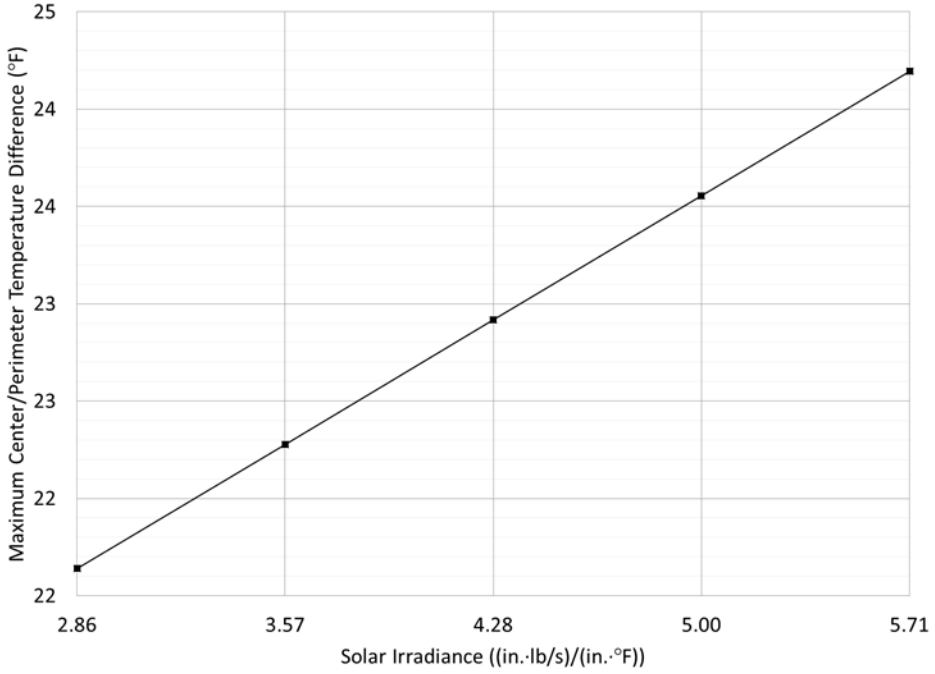

Fig. 123. Solar Load Case 6 Through 10 - Effect of Solar Irradiance on Inner Glass Plate of a Clear IG Unit at -20 °F Outdoor Temperature

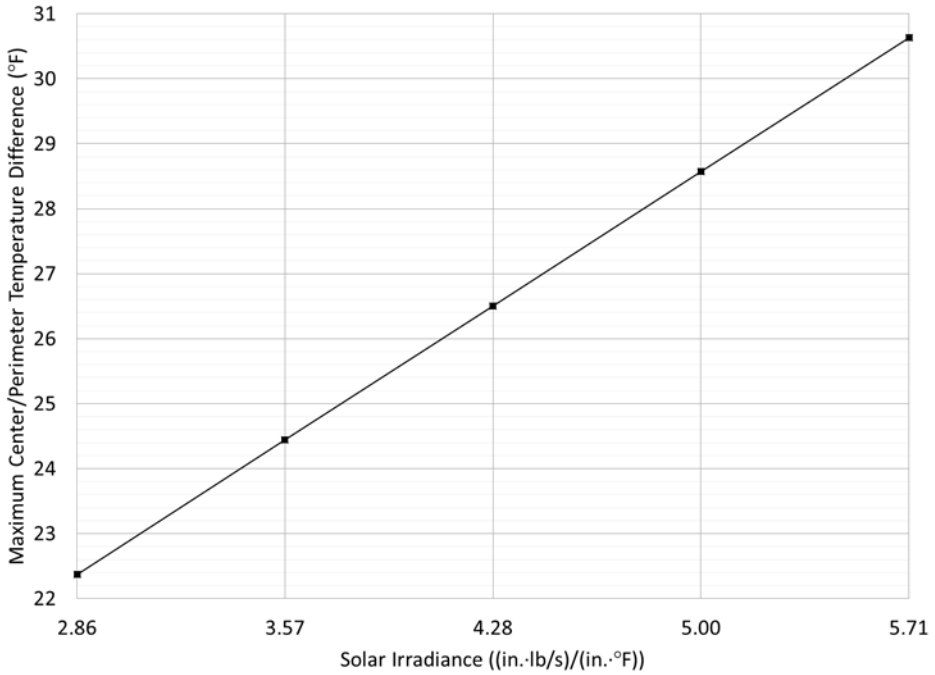

Fig. 124. Solar Load Case 11 Through 15 - Effect of Solar Irradiance on Outer Glass Plate of a Low-E IG Unit at 120 °F Outdoor Temperature

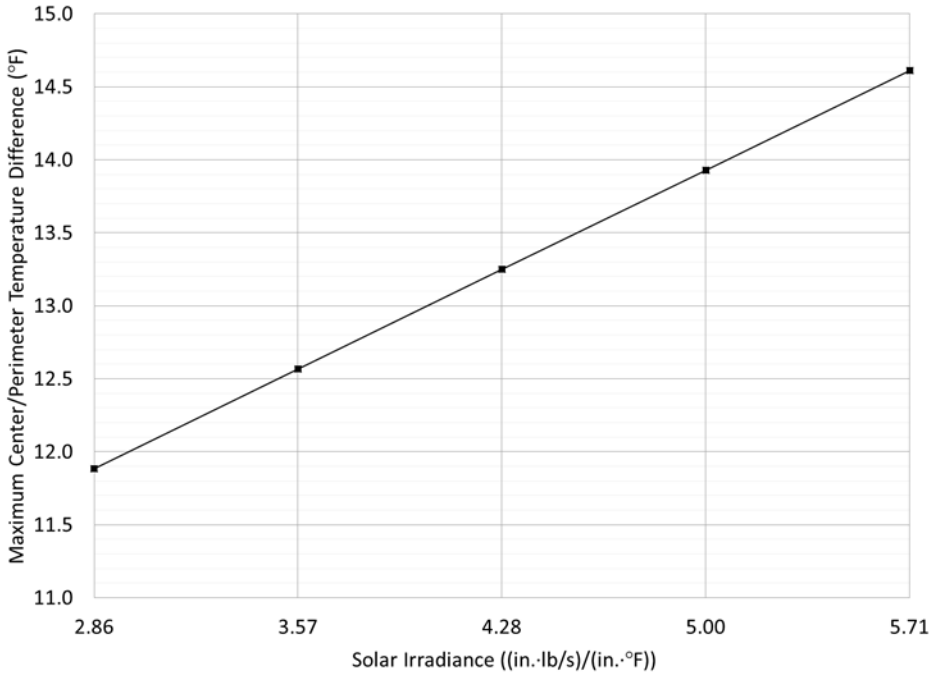

Fig. 125. Solar Load Case 16 Through 20 - Effect of Solar Irradiance on Outer Glass Plate of a Clear IG Unit at 120 °F Outdoor Temperature

Based on the findings presented in Figs. 122 through 125, the maximum difference in temperature between the center-of-glass and the perimeter-of-glass can be calculated for a particular level of solar irradiance based on the percentage of the solar irradiance that was used in the original FE analysis. Thus, all further analyses were performed using a solar irradiance of 5.7105 (in.·lb/s)/in.^{2} and the maximum center-of-glass to perimeter-of-glass temperature difference, $\Delta T_{solar\_irradiance}$, for a particular level of solar irradiance can be calculated using Eq. (72).

$$\Delta T_{solar\_irradiance} = \frac{I_s}{5.7105} \cdot \Delta T_{5.7105} \tag{72}$$

Where I_s is the solar irradiance of interest, expressed in (in.·lb/s)/in.^{2} and $\Delta T_{5.7105}$ is the maximum difference in temperature between the center-of-glass and the perimeter-of-glass when subjected to a solar irradiance of 5.7105 (in.·lb/s)/in.^{2}. A solar irradiance of

5.7105 (in.·lb/s)/in.^{2} was selected because it is representative of the sun on a clear day in Texas.

Net Absorption

In addition to the intensity of the solar irradiance, the net amount of solar irradiance that is absorbed by the IG unit's glass plates and converted to heat must be considered. As stated previously, the net absorption is the percentage of the total solar irradiance that is absorbed by both glass plates and converted to heat in an IG unit. It is calculated by simply adding the absorptions of the inner and outer glass plates together, as given by Eq. (70) previously.

As shown in the previous section, the maximum difference in temperature that develops between the center-of-glass and the perimeter-of-glass is a linear function of the applied solar irradiance. The amount of solar irradiance that is absorbed and converted to heat within each glass plate is directly proportional to the net absorption of the IG unit. Thus, the effect of net absorption on the maximum temperature difference between the center-of-glass and the perimeter-of-glass must also be linear and can be treated using a similar method to that used for solar irradiance. Increasing the net absorption of an IG unit would be exactly equivalent to increasing the solar irradiance that is applied to the IG unit if the net absorption were held constant.

The net absorption of the IG unit is a function of the solar optical properties of each glass plate and the overall construction of the IG unit. There are three generations of glass that must be considered with any thermal analysis. The first generation of glass was clear. Clear glass allows for a high level of light and solar transmission. The second generation of glass is what is known as heat-absorbing glass. Heat-absorbing glass helps control glare, brightness, and solar heat gain by increasing the absorption of the glass through the use of tinting and films. The third generation of glass came with the

advent of coatings such as low-E coatings. These coatings help to reflect and/or absorb solar radiation and are available in highly reflective to subdued and transparent coatings (Lingnell 1981).

Glass is also manufactured in a wide variety of tints and colors. In addition, there are a variety of films available that can be applied to different surfaces of the IG units. Thus, the net absorption of the IG unit is dependent on the generation, tint, and color of each glass plate, as well as the type and location of various coatings and films that may be applied. Because there are many variables that can alter the net absorption of an IG unit, it is convenient that the relationship between net absorption and the maximum center-of-glass to perimeter-of-glass temperature difference that occurs is linear. Thus, a simple percentage factor similar to that used for the solar irradiance can be used for net absorption.

Consider the practical examples from Chapter IV. Table 24 shows the absorptions for the inner and outer glass plates and the net absorption of the two IG units considered. Where all of the variables are as previously defined.

Table 24. Absorption Properties for Practical Application

Insulating Glass Unit	Outer Glass Plate	Inner Glass Plate	α_{outer}	α_{inner}	α_{net}
IGU 1	1/4 in. Clear	1/4 in. Clear	0.1517	0.1134	0.2651
IGU 2	1/4 in. Clear	1/4 in. Clear	0.1517	0.1134	0.2651
IGU 3	1/4 in. Low-E, Soft-Coat	1/4 in. Clear	0.3407	0.0537	0.3944
IGU 4	1/4 in. Low-E, Soft-Coat	1/4 in. Clear	0.3407	0.0537	0.3944

For the case of a clear IG unit, the net absorption is approximately 26.5 percent. Thus, for all of the analyses performed as part of this research for generic IG units, a baseline

net absorption of 25 percent was selected. Then, the maximum center-of-glass to perimeter-of-glass temperature difference, $\Delta T_{net\_absorption}$, for a particular glass plate and net absorption can be calculated using Eq. (73) below.

$$\Delta T_{net\_absorption} = \frac{\alpha_{net}}{0.25} \cdot \Delta T_{0.25} \tag{73}$$

Where α_{net} is the net absorption for the IG unit and $\Delta T_{0.25}$ is the maximum difference in temperature between the center-of-glass and the perimeter-of-glass when the net absorption is 25 percent.

Therefore, the maximum center-of-glass to perimeter-of-glass temperature difference for the clear IG unit, with a net absorption of 26.5 percent, would be 6 percent greater than the maximum center-of-glass to perimeter-of-glass temperature difference associated with a 25 percent net absorption. The maximum center-of-glass to perimeter-of-glass temperature difference for the Low-E IG unit, with a net absorption of 39.4 percent, would be approximately 57.8 percent greater than the maximum center-of-glass to perimeter-of-glass temperature difference associated with a 25 percent net absorption.

Note that the net absorption does not account for the distribution of solar irradiance that is absorbed between the inner and outer glass plates. Not only does the construction of the IG unit (i.e. the location of coatings, tints, films, etc.) have an effect on the net absorption, it alters the distribution of absorption for both the inner and outer glass plates. This was taken into account using the absorption ratio introduced previously.

Indoor/Outdoor Temperature Difference

A third parametric study was performed to understand the effect an indoor/outdoor temperature difference has on the thermal stresses that develop in IG units. It has been

shown that pre-stresses develop in the glass plates when an IG unit is subjected to a difference in temperature between the indoor and outdoor environment. In addition, these pre-stresses do not require the presence of solar irradiance to develop.

The range of indoor environment temperatures is relatively small compared to range of possible outdoor environment temperatures. When combined, there is an infinite number of combinations. For most thermal analyses, the temperature of the indoor environment is held constant at 70 °F. This is the case because the temperature of the indoor environment depends primarily on human comfort factors, whereas the temperature of the outdoor environment primarily depends on the geographical location of the building (Lingnell 1981).

For each case considered as part of this study, the IG unit's frame was assumed to be perfectly insulated with an edge bite of 0.5 in. Two IG units were analyzed, one with a low-E coating and another with clear glass plates. The indoor temperature was held at a constant 70 °F for all cases and a range of outdoor temperatures from -20 to 120 °F were considered. The FE analyses were performed in increments of 10 °F for a total of 15 data points for each IG unit. Table 25 below shows the parameters that were used in each analysis. The difference between the indoor and outdoor temperatures, $\Delta T_{indoor/outdoor}$, was calculated using Eq. (74). The results from each FE analysis are shown in Figs. 126 and 127.

$$\Delta T_{indoor/outdoor} = T_{outdoor} - T_{indoor} \tag{74}$$

Where all of the variables are as previously defined.

Table 25. Indoor/Outdoor Temperature Difference Parametric Study

Case No.	Outer Glass Plate	Inner Glass Plate	T_{indoor} (°F)	$T_{outdoor}$ (°F)	$\Delta T_{indoor/outdoor}$ (°F)
Temp. Diff. Case 1	1/4 in. Low-E, Soft-Coat	1/4 in. Clear	70	-20	-90
Temp. Diff. Case 2	1/4 in. Low-E, Soft-Coat	1/4 in. Clear	70	-10	-80
Temp. Diff. Case 3	1/4 in. Low-E, Soft-Coat	1/4 in. Clear	70	0	-70
Temp. Diff. Case 4	1/4 in. Low-E, Soft-Coat	1/4 in. Clear	70	10	-60
Temp. Diff. Case 5	1/4 in. Low-E, Soft-Coat	1/4 in. Clear	70	20	-50
Temp. Diff. Case 6	1/4 in. Low-E, Soft-Coat	1/4 in. Clear	70	30	-40
Temp. Diff. Case 7	1/4 in. Low-E, Soft-Coat	1/4 in. Clear	70	40	-30
Temp. Diff. Case 8	1/4 in. Low-E, Soft-Coat	1/4 in. Clear	70	50	-20
Temp. Diff. Case 9	1/4 in. Low-E, Soft-Coat	1/4 in. Clear	70	60	-10
Temp. Diff. Case 10	1/4 in. Low-E, Soft-Coat	1/4 in. Clear	70	70	0
Temp. Diff. Case 11	1/4 in. Low-E, Soft-Coat	1/4 in. Clear	70	80	10
Temp. Diff. Case 12	1/4 in. Low-E, Soft-Coat	1/4 in. Clear	70	90	20
Temp. Diff. Case 13	1/4 in. Low-E, Soft-Coat	1/4 in. Clear	70	100	30
Temp. Diff. Case 14	1/4 in. Low-E, Soft-Coat	1/4 in. Clear	70	110	40
Temp. Diff. Case 15	1/4 in. Low-E, Soft-Coat	1/4 in. Clear	70	120	50
Temp. Diff. Case 16	1/4 in. Clear	1/4 in. Clear	70	-20	-90
Temp. Diff. Case 17	1/4 in. Clear	1/4 in. Clear	70	-10	-80
Temp. Diff. Case 18	1/4 in. Clear	1/4 in. Clear	70	0	-70
Temp. Diff. Case 19	1/4 in. Clear	1/4 in. Clear	70	10	-60
Temp. Diff. Case 20	1/4 in. Clear	1/4 in. Clear	70	20	-50
Temp. Diff. Case 21	1/4 in. Clear	1/4 in. Clear	70	30	-40
Temp. Diff. Case 22	1/4 in. Clear	1/4 in. Clear	70	40	-30
Temp. Diff. Case 23	1/4 in. Clear	1/4 in. Clear	70	50	-20
Temp. Diff. Case 24	1/4 in. Clear	1/4 in. Clear	70	60	-10
Temp. Diff. Case 25	1/4 in. Clear	1/4 in. Clear	70	70	0
Temp. Diff. Case 26	1/4 in. Clear	1/4 in. Clear	70	80	10
Temp. Diff. Case 27	1/4 in. Clear	1/4 in. Clear	70	90	20
Temp. Diff. Case 28	1/4 in. Clear	1/4 in. Clear	70	100	30
Temp. Diff. Case 29	1/4 in. Clear	1/4 in. Clear	70	110	40
Temp. Diff. Case 30	1/4 in. Clear	1/4 in. Clear	70	120	50

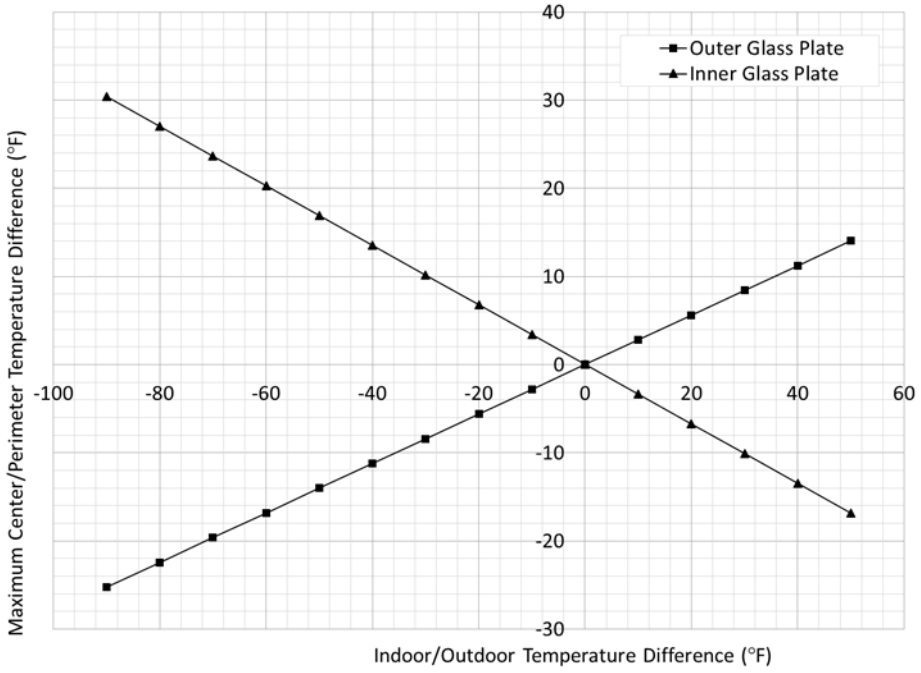

Fig. 126. Temperature Difference Case 1 Through 15 - Effect of Indoor/Outdoor Temperature Difference on the Steady-State Response of a Low-E IG Unit

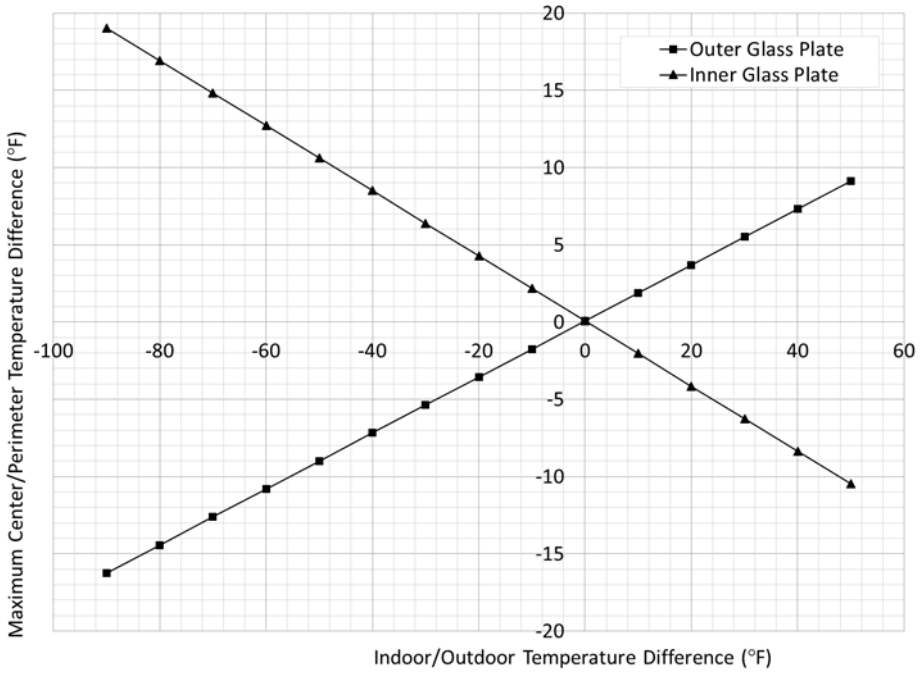

Fig. 127. Temperature Difference Case 16 Through 30 - Effect of Indoor/Outdoor Temperature Difference on the Steady-State Response of a Clear IG Unit

Figs. 126 and 127 show the maximum difference in temperature between the center-of-glass and the perimeter-of-glass as a function of the difference between the outdoor temperature and the indoor temperature for a low-E and clear IG unit, respectively. Included in each figure is the response of the inner and outer glass plate.

There are two major observations that can be obtained from Figs. 126 and 127. First, the maximum difference in temperature between the center-of-glass and the perimeter-of-glass has a linear relationship to the indoor/outdoor temperature difference. Second, the negative slope that is associated with the inner glass plate in Figs. 126 and 127 shows that its POB becomes critical when the outdoor temperature is below the indoor temperature. Conversely, the positive slope that is associated with the outer glass plate shows that its POB becomes critical when the outdoor temperature is above the indoor temperature. Both of these observations are in complete agreement with the glass industry's understanding of thermal stresses in IG units, previous research performed by Klam (2007), Lingnell and Beason (2013), and results presented previously herein.

The maximum difference in temperature between the center-of-glass and the perimeter-of-glass that is shown in Figs. 126 and 127, develops solely due to the thermal bridging that occurs across the edge-seal of the IG unit. This is called the pre-stress, as described in Chapter IV, and occurs in the presence of a temperature difference between the indoor and outdoor environments. It is important to note that all four of the curves plotted in Figs. 126 and 127 pass through the origin. This must be the case because if the outdoor and indoor temperatures are equal, the IG unit is in a state of thermal equilibrium and there is no heat transferred between the two glass plates. Therefore, a pre-stress condition cannot develop.

The steady-state response or pre-stress is determined when zero solar irradiance is applied. As such, these data are only dependent on the CEEC, the frame of the IG unit including the edge bite, and the indoor/outdoor temperature difference. Figs. 128 through

131 show the transient response of each case when a solar irradiance of 5.7105 (in.·lb/s)/in.^{2} is applied for 60 min. Figs. 132 through 135 show the maximum difference in temperature between the center-of-glass and the perimeter-of-glass determined from Figs 128 through 131.

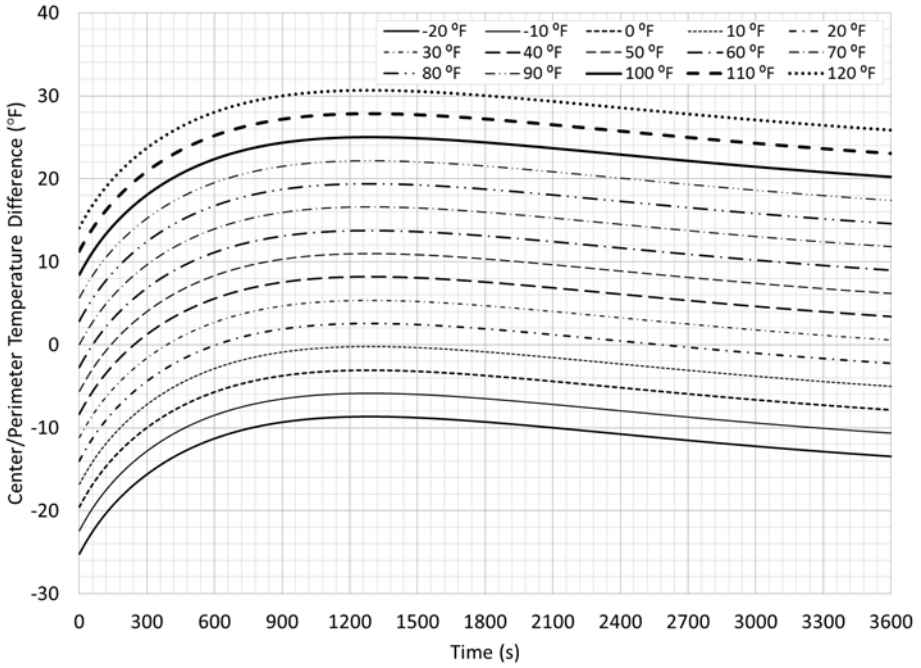

Fig. 128. Temperature Difference Case 1 Through 15 - Effect of Indoor/Outdoor Temperature Difference on the Transient Response of the Outer Glass Plate of a Low-E IG Unit

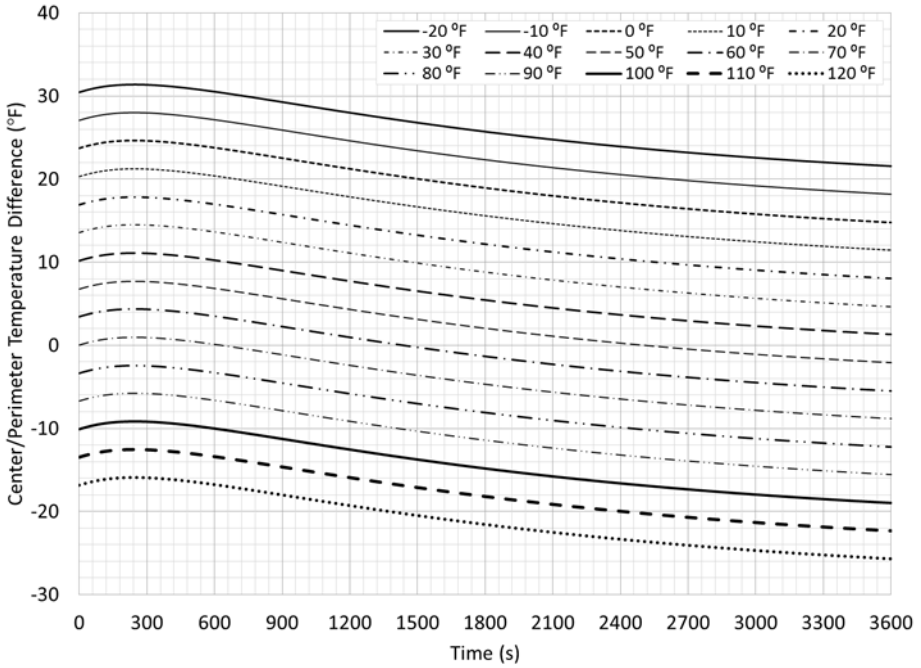

Fig. 129. Temperature Difference Case 1 Through 15 - Effect of Indoor/Outdoor Temperature Difference on the Transient Response of the Inner Glass Plate of a Low-E IG Unit

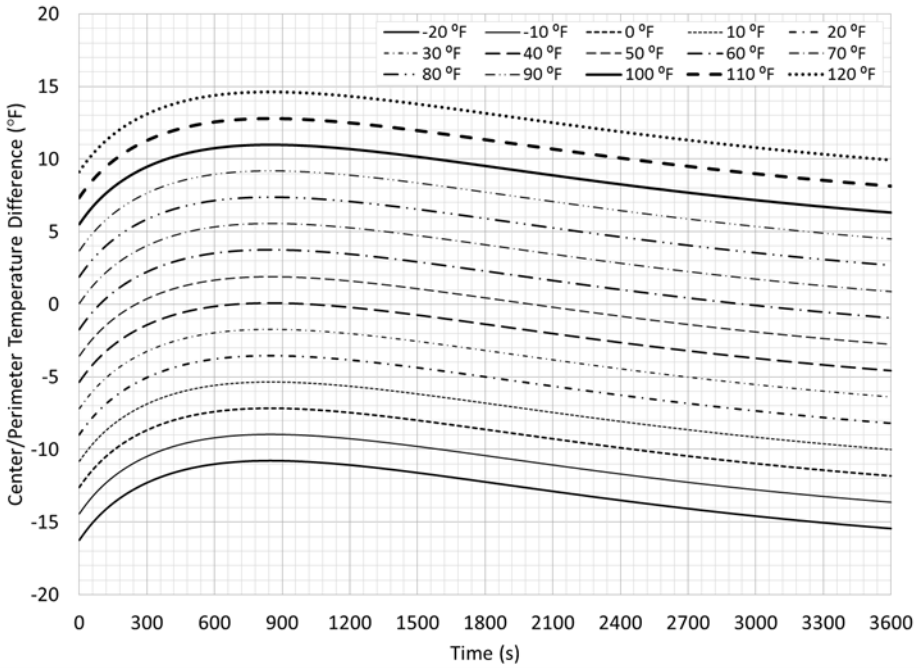

Fig. 130. Temperature Difference Case 16 Through 30 - Effect of Indoor/Outdoor Temperature Difference on the Transient Response of the Outer Glass Plate of a Clear IG Unit

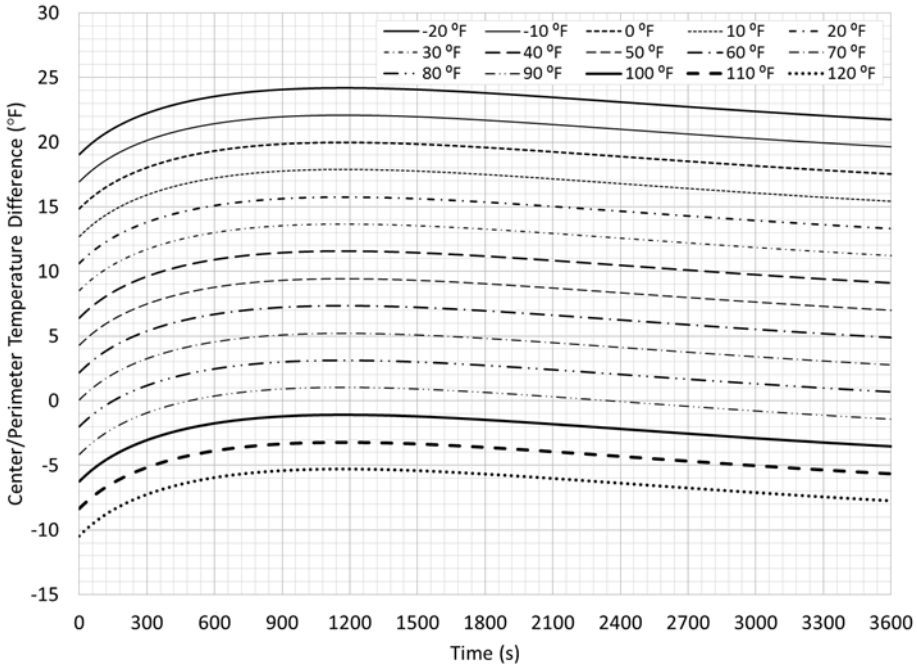

Fig. 131. Temperature Difference Case 16 Through 30 - Effect of Indoor/Outdoor Temperature Difference on the Transient Response of the Inner Glass Plate of a Clear IG Unit

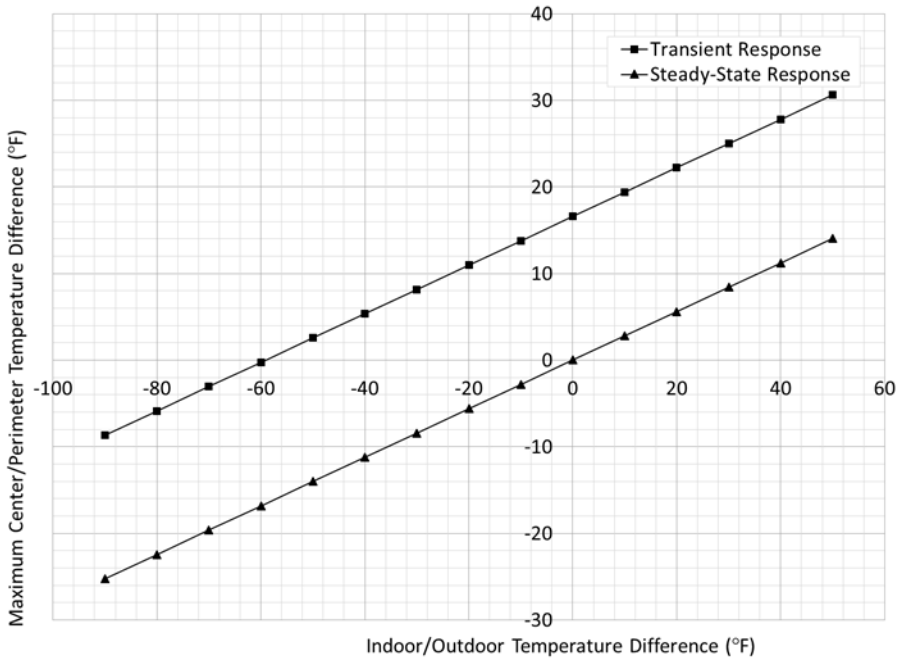

Fig. 132. Temperature Difference Case 1 Through 15 - Effect of Indoor/Outdoor Temperature Difference on the Maximum Center-of-Glass Area/Perimeter-of-Glass Temperature Difference of the Outer Glass Plate of a Low-E IG Unit

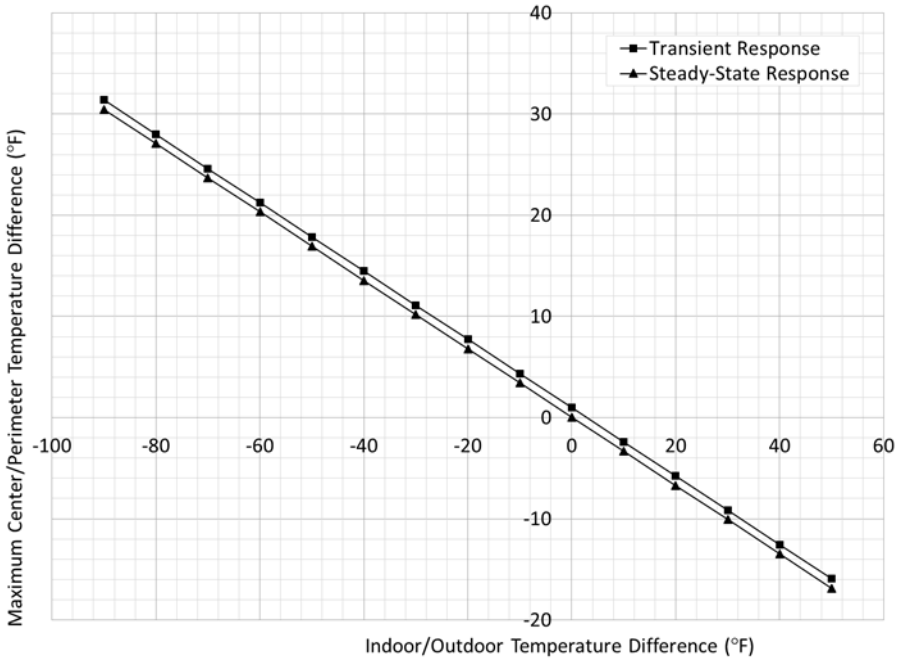

Fig. 133. Temperature Difference Case 1 Through 15 - Effect of Indoor/Outdoor Temperature Difference on the Maximum Center-of-Glass Area/Perimeter-of-Glass Temperature Difference of the Inner Glass Plate of a Low-E IG Unit

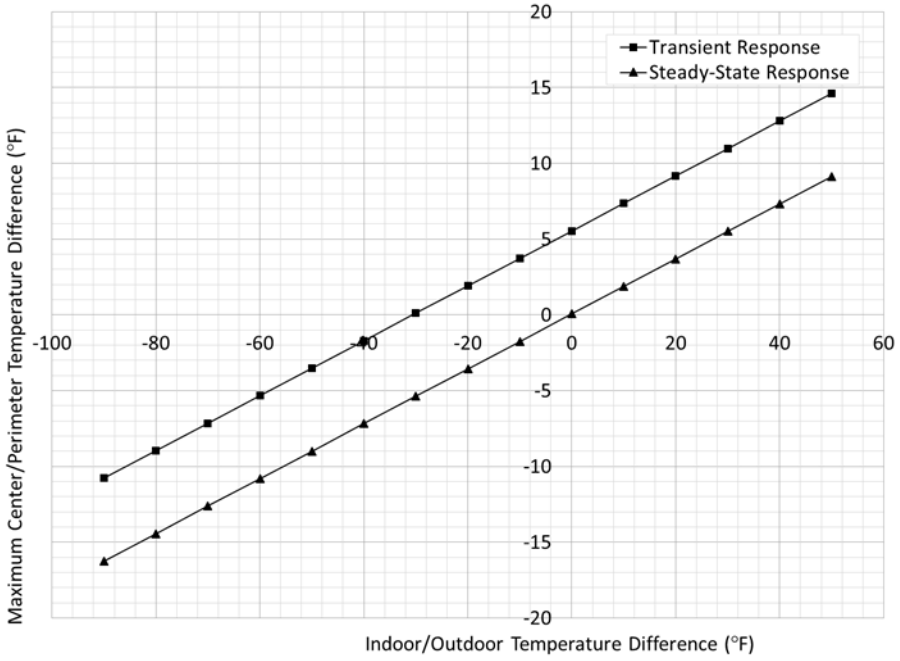

Fig. 134. Temperature Difference Case 16 Through 30 - Effect of Indoor/Outdoor Temperature Difference on the Maximum Center-of-Glass Area/Perimeter-of-Glass Temperature Difference of the Outer Glass Plate of a Clear IG Unit

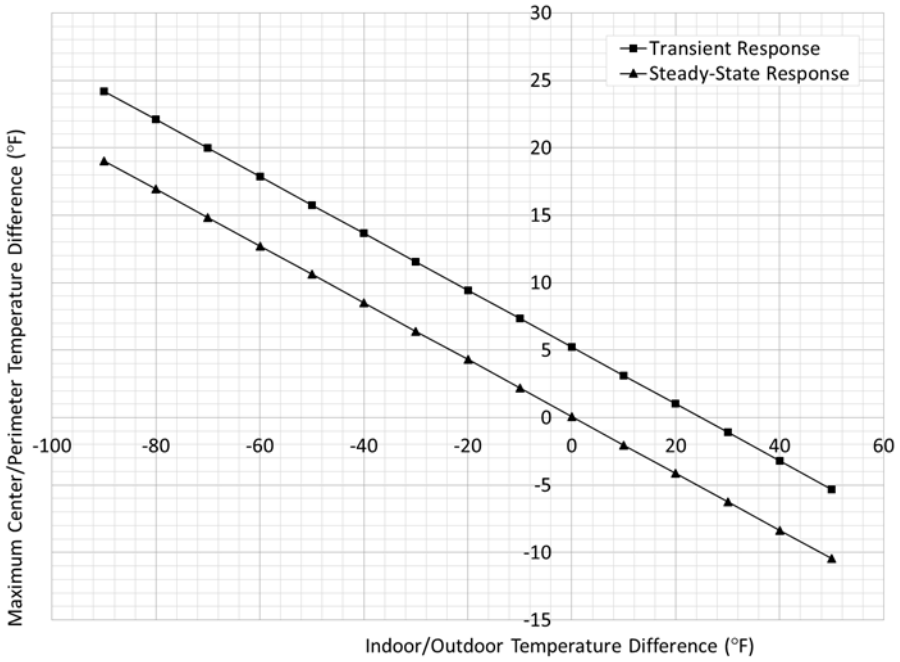

Fig. 135. Temperature Difference Case 16 Through 30 - Effect of Indoor/Outdoor Temperature Difference on the Maximum Center-of-Glass Area/Perimeter-of-Glass Temperature Difference of the Inner Glass Plate of a Clear IG Unit

From Figs. 132 through 135, it is clear that the transient response remains linear as a function of the difference in temperature between the indoor and outdoor environments. When an IG unit is subjected to a difference in temperature between the indoor and outdoor environments, an initial thermal stress develops. When an IG unit is subjected to solar irradiance, a transient thermal stress develops and is additive to the thermal pre-stress caused by the indoor/outdoor temperature difference.

This is convenient because the analysis to determine the thermal stress associated with an IG unit can be analyzed using an independent steady-state analysis and a transient analysis. Then the method of superposition can be applied to combine the effects for an overall thermal stress. This is discussed in more detail later.

Finally, the third group of variables must be considered to develop a SDP. The effects that the CEEC, edge bite, and the absorption ratio have on the thermal behavior of IG units are not well defined or well behaved. These factors are more difficult to simplify using a straight-forward linear method as was the case for solar irradiance, net absorption, and the indoor/outdoor temperature difference. Ultimately, this third group of variables were dealt with using a least-squares regression-based technique on the results of a large number of FE analyses. The models used in these FE analyses consider the effects that the CEEC, edge bite, and the absorption ratio have on the thermal behavior of IG units subjected to solar irradiance. Then, a simple model can be used that incorporates all of the design variables from the three groups. This model is discussed next.

Proposed Simplified Design Procedure to Evaluate the Probability of Breakage of Insulating Glass Units

Based on the observations that were presented in the previous section, a simplified equation or model can be developed to determine the maximum thermal stress that is induced in an IG unit subjected to solar irradiance. In the most general case, the maximum thermal stress, σ_{max}, in a monolithic glass plate is calculated using Eq. (75).

$$\sigma_{max} = \alpha_T \cdot E \cdot (T_{COG} - T_{POG}) \tag{75}$$

Where α_T is the coefficient of thermal expansion for plate glass, E is the modulus of elasticity of plate glass, T_{COG} is the center-of-glass temperature, and T_{POG} is the perimeter-of-glass temperature. When a glass plate is subjected to solar irradiance, the temperature of the glass plate begins to heat. The level of heat gain in the glass plate is a linear function of the solar absorptance coefficient and level of solar irradiance it is exposed to.

A simple extension of Eq. (75) can be developed for IG units that incorporates the observations presented previously. These primary observations are as follows: (1) the maximum thermal stress generated for both the outer and inner glass plates are fully linear with respect to the difference in temperature between the indoor and outdoor environments and (2) the maximum thermal stress is proportional to the solar irradiance that it is subjected to and the net absorption of the IG unit. These observations are true regardless of the IG unit properties.

General Thermal Stress Equation for Insulating Glass Units

When IG units are subjected to solar irradiance, the temperature of each glass plate begins to rise. The level of heat gain in each glass plate is a function of the solar transmittance, solar reflectance, and solar absorptance of each glass plate. The ray tracing procedure must be employed to determine the overall level of solar irradiance absorbed by the IG unit. The maximum thermal stress, $\sigma_{transient}$, that occurs along the perimeter of a particular glass plate in an IG unit that is subjected to solar irradiance can be calculated using Eq. (76).

$$\sigma_{transient} = \alpha_T \cdot E \cdot b \tag{76}$$

Where α_T and E are as previously defined and b is a thermal offset that defines the transient thermal behavior of the IG unit. The value for b represents the maximum difference in temperature between the center-of-glass and the perimeter-of-glass for an IG unit due to exposure to solar irradiance when the indoor and outdoor temperatures are equal.

In the absence of solar irradiance, any IG unit that is subjected to an indoor/outdoor temperature differential will develop a pre-stress condition along the edge of each glass plate. This is the result of heat that is exchanged across the edge-seal of the IG unit. This relationship is linear as a function of the indoor/outdoor temperature difference.

Thus, the pre-stress, $\sigma_{steady-state}$, that occurs along the perimeter of a particular glass plate in an IG unit can be determined using Eq. (77).

$$\sigma_{steady-state} = \alpha_T \cdot E \cdot m \cdot (T_{outdoor} - T_{indoor}) \tag{77}$$

Where α_T and E are as previously defined, $T_{outdoor}$ is the ambient air temperature for the outdoor environment, T_{indoor} is the ambient air temperature for the indoor environment, and m is a thermal slope that defines the steady-state thermal behavior of the IG unit. The value for m represents the slope of the linear function that describes the relationship between the pre-stress and the indoor/outdoor temperature differential.

The parametric studies performed previously showed that the effects of solar irradiance and the pre-stress that develops due to an indoor/outdoor temperature difference are additive. Thus, Eqs. (76) and (77) can be combined using the superposition method for the most common situation where an indoor/outdoor temperature difference and solar irradiance exist simultaneously. For this case, the overall thermal behavior can be calculated using Eq. (78).

$$\sigma_{max} = \sigma_{steady-state} + \sigma_{transient} \tag{78}$$

Substituting Eqs. (76) and (77) into Eq. (78), the maximum thermal stress, σ_{max}, that occurs along the perimeter of a particular glass plate in an IG unit can be determined. This is shown in Eq. (79).

$$\sigma_{max} = \alpha_T \cdot E \cdot [b \pm m \cdot (T_{outdoor} - T_{indoor})] \tag{79}$$

Where all terms are as previously defined. The significance of the ±m is whether or not the value is taken for the outer or inner glass plate. If the outer glass plate is considered,

m is a negative value. If the inner glass plate is considered, m is a positive value. This can be seen from Figs. 126 and 127.

The maximum thermal stress associated with a particular level of solar irradiance can be used to determine the maximum thermal stress for a different level of solar irradiance based on a simple percentage difference between the two. This was shown in Eq. (72) previously. In addition, the maximum thermal stress associated with a particular net absorption can be used to determine the maximum thermal stress for a different net absorption based on a simple percentage difference between the two. This was shown in Eq. (73) previously.

As such, the thermal offset of an IG unit that is associated with the transient response has a linear relationship with the level of solar irradiance that the IG unit is exposed to. Likewise, the thermal offset of an IG unit has a linear relationship with the net absorption of the IG unit. Therefore, if the thermal offset is determined for an IG unit with a specific solar irradiance and net absorption and the IG unit is subjected to a different set of solar irradiance and/or net absorption, then the thermal offset must be adjusted.

The adjustment for a different level of solar irradiance is made using the solar load factor, SLF, herein. The adjustment for a different net absorption of an IG unit is made using the absorption factor, AF, herein. The solar load factor and absorption factor represent the linear relationships between solar irradiance and net absorption, respectively, on the maximum thermal stress that develops in an IG unit.

Conveniently, solar irradiance and net absorption do not alter the steady-state response of an IG unit that is associated with the thermal slope. Therefore, the solar load factor and absorption factor must be used in combination with Eq. (79) such that the thermal offset is adjusted and the thermal slope remains unchanged. Therefore, the maximum

thermal stress, σ_{max}, in an IG unit for different levels of solar irradiance and net absorptions can be determined using Eq. (80).

$$\sigma_{max} = \alpha_T \cdot E \cdot [SLF \cdot AF \cdot b \pm m \cdot (T_{outdoor} - T_{indoor})] \tag{80}$$

Where all of the terms are as previously defined.

For the analyses performed as part of this research that involve generic IG units, a decision was made to use a baseline net absorption of 25 percent and a baseline solar irradiance of 5.7105 (in.·lb/s)/in.^{2}. The justifications for using these baseline values were discussed in detail previously. As such, the solar load factor and absorption factor can be calculated using Eqs. (81) and (82), respectively.

$$\text{SLF} = \frac{I_S}{5.7105} \tag{81}$$

$$\text{AF} = \frac{\alpha_{net}}{0.25} \tag{82}$$

Where the equation for the SLF is a simple adaptation of Eq. (72) that is based on a solar irradiance of 5.7105 (in.·lb/s)/in.^{2}, the equation for the AF is a simple adaptation of Eq. (73) that is based on a net absorption of 25 percent, and all other variables are as previously defined.

Now, consider that a set of equations can be used to solve for the values of b and m using the variables that affect the thermal behavior of the IG unit as inputs. Assuming that the transient thermal behavior of an IG unit subjected to solar irradiance can be modeled using a polynomial, the equation for b would be of the form given by Eq. (83).

$$b = b_0 + b_1 \cdot X_1 + b_2 \cdot X_2 + \cdots + b_{n-1} \cdot X_{n-1} + b_n \cdot X_n \tag{83}$$

Where b_i are linear coefficients and X_i are the input variables. To calculate b the input variables include the CEEC, absorption ratio, and the frame edge bite dimension.

Assuming the steady-state thermal behavior of an IG unit subjected to an indoor/outdoor temperature differential can also be modeled using a polynomial, the equation for m would be of the form given by Eq. (84).

$$m = m_0 + m_1 \cdot Y_1 + m_2 \cdot Y_2 + \cdots + m_{n-1} \cdot Y_{n-1} + m_n \cdot Y_n \qquad (84)$$

Where m_i are linear coefficients and Y_i are the input variables. To calculate m the input variables would include the CEEC and the frame edge bite dimension.

The coefficients, b_i and m_i, for Eqs. (83) and (84) can then be selected from a table to estimate the thermal offset, b, and thermal slope, m, for a specific IG unit. The tables would have the form shown in Tables 26 and 27, respectively, and must be developed for each set of frame, spacer, and nominal glass plate thickness. Tables 26 and 27 show the layout for exemplar perfectly insulated and high-heat mass frames with three spacer variants that includes a steel, aluminum, and foam spacer. In addition, a set of exemplar coefficients are shown for both the inner and outer glass plates.

Table 26. Table of Coefficients for Calculating the Thermal Offset, b, of an IG Unit

Coefficients:		b_0	b_1	b_2	...	b_{n-1}	b_n	
Perfectly Insulated Frame	Steel Spacer	--	--	--		--	--	Inner Glass Plate
		--	--	--		--	--	Outer Glass Plate
	Foam Spacer	--	--	--		--	--	Inner Glass Plate
		--	--	--		--	--	Outer Glass Plate
	Aluminum Spacer	--	--	--		--	--	Inner Glass Plate
		--	--	--		--	--	Outer Glass Plate
High-Heat Mass Frame	Steel Spacer	--	--	--		--	--	Inner Glass Plate
		--	--	--		--	--	Outer Glass Plate
	Foam Spacer	--	--	--		--	--	Inner Glass Plate
		--	--	--		--	--	Outer Glass Plate
	Aluminum Spacer	--	--	--		--	--	Inner Glass Plate
		--	--	--		--	--	Outer Glass Plate

Table 27. Table of Coefficients for Calculating the Thermal Slope, m, of an IG Unit

Coefficients:		m_0	m_1	m_2	...	m_{n-1}	m_n	
Perfectly Insulated Frame	Steel Spacer	--	--	--		--	--	Inner Glass Plate
		--	--	--		--	--	Outer Glass Plate
	Foam Spacer	--	--	--		--	--	Inner Glass Plate
		--	--	--		--	--	Outer Glass Plate
	Aluminum Spacer	--	--	--		--	--	Inner Glass Plate
		--	--	--		--	--	Outer Glass Plate
High-Heat Mass Frame	Steel Spacer	--	--	--		--	--	Inner Glass Plate
		--	--	--		--	--	Outer Glass Plate
	Foam Spacer	--	--	--		--	--	Inner Glass Plate
		--	--	--		--	--	Outer Glass Plate
	Aluminum Spacer	--	--	--		--	--	Inner Glass Plate
		--	--	--		--	--	Outer Glass Plate

Using the SDP to both determine the thermal stress induced in IG units caused by exposure to solar irradiance and an indoor/outdoor temperature difference and to evaluate the POB would involve the following steps:

1. Establish the edge bite dimension of the frame in the range of 0.5 to 1.5 in. This should include the glazing bead if applicable.
2. Determine the CEEC using the FTP presented in Chapter IV.
3. Determine the absorption ratio between the inner and outer glass plate and the total net absorption using the ray tracing technique.

4. Calculate the absorption factor using Eq. (82).
5. Select the proper coefficients from tables of the form shown in Tables 26 and 27 for the particular combination of frame, spacer, nominal glass plate thickness, and glass plate (i.e. inner or outer) of interest.
6. Calculate the values for b and m using Eqs. (83) and (84), respectively.
7. Define the critical value for the indoor/outdoor temperature difference.
8. Define the maximum level of solar irradiance that the IG unit will be exposed to and calculate the solar load factor using Eq. (81).
9. Calculate the maximum thermal stress using Eq. (80).
10. Finally, apply the glass ESFPM and compare the allowable stress to the stress calculated in step 9 for a given POB.

Case Study to Calculate b and m

As an example, discrete values for b and m were determined explicitly for two of the practical application examples that were presented in Chapter IV. The two cases considered were FEA 1 and 5. FEA 1 involved an IG unit with two clear glass plates. FEA 5 involved an IG unit with a clear inner glass plate and an outer glass plate with a low-E coating that was applied to the number 2 surface. The frame that was used for both cases was assumed to be perfectly insulated with a 0.5 in. edge bite. More details for each analysis were provided previously in Chapter IV and are not repeated here.

The IG units were exposed to 4.9967 $(\text{in.}\cdot\text{lb/s})/\text{in.}^2$ of solar irradiance. The temperature of the indoor and outdoor environments were -10 and 79 °F, respectively. Figs. 136 and 137 show the difference in temperature between the center-of-glass and the perimeter-of-glass as a function of time for FEA 1 and 5, respectively. Included in these figures are data labels with the initial steady-state and maximum transient differences in temperature. These data were determined using the FDP that was presented in Chapter IV.

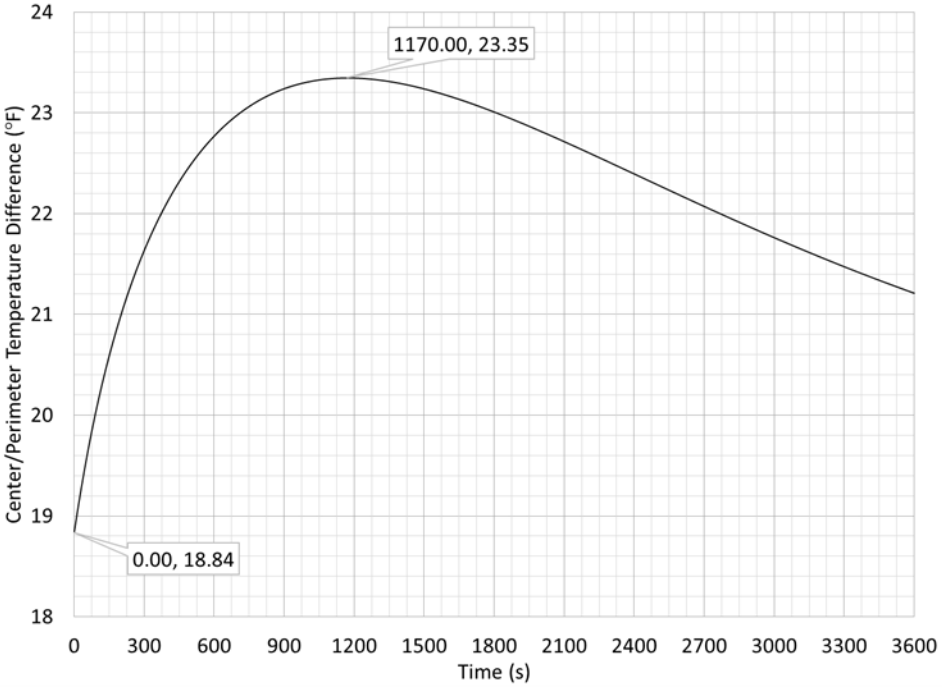

Fig. 136. Difference in Temperature Between the Center-of-Glass and Perimeter-of-Glass as a Function of Time for the Inner Glass Plate of FEA 1

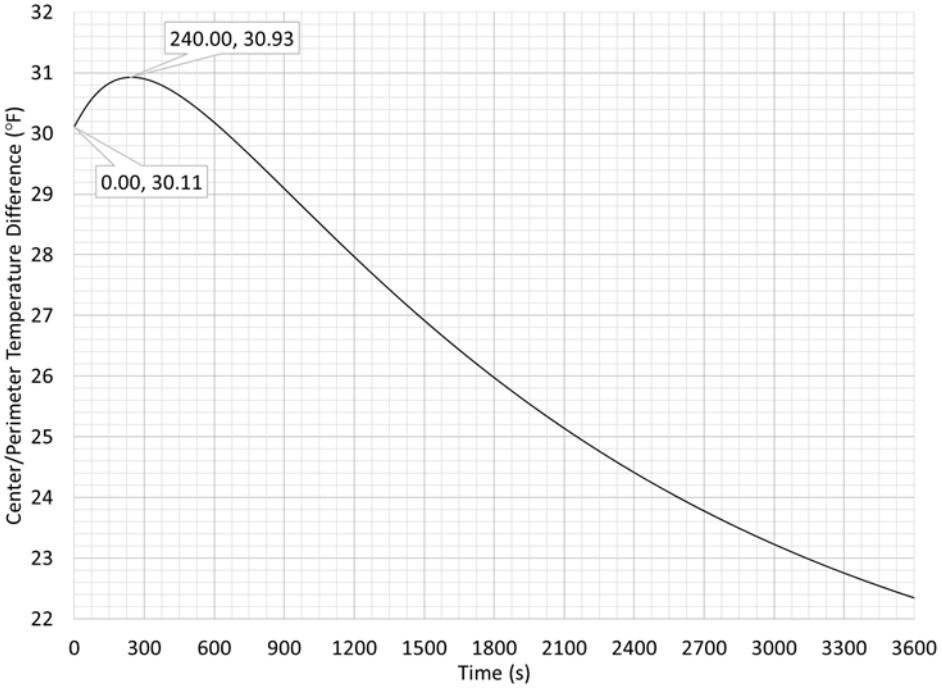

Fig. 137. Difference in Temperature Between the Center-of-Glass and Perimeter-of-Glass as a Function of Time for the Inner Glass Plate of FEA 5

The initial difference in temperature at time zero is shown in Figs. 136 and 137. This initial temperature is due to the difference in temperature between the indoor and outdoor environments. For FEA 1 and 5, the initial temperatures are 18.84 and 30.11 °F, respectively. In addition, the maximum differences in temperatures that occur when the IG units are exposed to solar irradiance are shown. For FEA 1 and 5, the maximum difference in temperature between the center-of-glass and the perimeter-of-glass are 23.35 and 30.93 °F, respectively.

The values for the thermal offset, b, and the thermal slope, m, can be determined from these data for each IG unit. It was shown previously that the linear equation that describes the relationship between the initial temperature and the difference in temperature between the indoor and outdoor environments must pass through the origin. Thus, the thermal slope, m, can be calculated by dividing the initial temperatures shown in Figs. 136 and 137 by the difference in the outdoor environment and the indoor environment shown previously in Eq. (74). Therefore, the thermal slope, m, associated with the inner glass plate for FEA 1 and 5 are -0.2117 and -0.3383, respectively. These calculations are shown in Eqs. (85) and (86).

$$m_{FEA\_1} = \frac{18.84\ °\text{F}}{\left((-10)\ °\text{F} - 79\ °\text{F}\right)} = \frac{18.84\ °\text{F}}{-89\ °\text{F}} = -0.2117\ \frac{°\text{F}}{°\text{F}} \tag{85}$$

$$m_{FEA\_5} = \frac{30.11\ °\text{F}}{\left((-10)\ °\text{F} - 79\ °\text{F}\right)} = \frac{30.11\ °\text{F}}{-89\ °\text{F}} = -0.3383\,\frac{°\text{F}}{°\text{F}} \tag{86}$$

It was shown previously that the thermal offset and thermal slope can be determined independently and added together using the method of superposition. Therefore, the thermal offset, b, can be determined from Figs. 136 and 137 by simply subtracting the maximum difference in temperature from the initial temperature at time zero. Thus, the thermal offset associated with the inner glass plate for FEA 1 and 5 are 4.51 and 0.82 °F, respectively. These calculations are shown in Eqs. (87) and (88).

$$b_{FEA\_1} = (23.35\ °\text{F} - 18.84\ °\text{F}) = 4.51\ °\text{F} \quad (87)$$

$$b_{FEA\_5} = (30.93\ °\text{F} - 30.11\ °\text{F}) = 0.82\ °\text{F} \quad (88)$$

These two examples show the procedure that can be used to determine the thermal offset, b, and thermal slope, m, for specific cases. While there are many variables that affect the thermal behavior of IG units, the values for b and m can be described in a general sense for a given frame, spacer, and nominal glass plate thickness using three variables. These three variables include the CEEC, the absorption ratio, and an edge bite dimension. Thus, a set of equations are needed to solve for b and m using the CEEC, absorption ratio, and edge bite as input parameters.

The next section of this chapter discusses the methodology that was used to determine these equations and to populate the values for Tables 26 and 27 presented previously. The coefficients for each equation were determined using regression techniques that are applied to a large set of data gathered using FE analyses. These FE analyses incorporate the various ranges of values for the CEEC, absorption ratios, and frame edge bite dimensions to determine the contribution of each to the thermal behavior of an IG unit with a particular frame, spacer, and nominal glass plate thickness. In addition, the effects of each of these variables on b and m are presented.

General Regression Procedure

While a functional relationship between variables typically exists for natural processes, they are often too complex to describe in a simple manner (Draper and Smith 1998). However, such relationships can often be approximated using mathematical functions that describe the relationship. For instance, a polynomial function may be selected to represent a more complex problem over short ranges of variables of interest. Regression

analyses are often used to mathematically model such relationships between measureable variables (Weisberg 1980; Draper and Smith 1998).

Regression analyses involve two types of variables, predictor variables or independent variables and response variables or dependent variables. The predictor variables are values that can be observed and are seen to have a correlation with the response variables. Typically, the purpose of a regression analysis is to optimize the correlation between the predictor and response variables (Draper and Smith 1998).

For the research herein, data were collected using FE analyses for a wide range of predictor variables. These predictor variables included the CEEC, edge bite, and absorption ratio. Regression analyses were then used to describe the relationship among these variables and predict values for the steady-state and transient response of an IG unit with a particular frame, spacer, and nominal glass plate thickness.

A general regression analysis, in matrix form, of a model selected for consideration is shown in Eq. (89) (Weisberg 1980; Draper and Smith 1998). Matrices provide a convenient method for solving multivariate regression analyses where more than one independent variable is present. The **boldface** type is used to denote a single letter as representing a matrix of numbers.

$$\boldsymbol{Y} = \boldsymbol{X\beta} + \boldsymbol{e} \tag{89}$$

Where **Y** is the vector of observations or response variables and has the form given by Eq. (90).

$$\boldsymbol{Y} = \begin{bmatrix} y_0 \\ y_1 \\ \vdots \\ y_n \end{bmatrix} \tag{90}$$

X is the matrix of predictor variables and has the form given by Eq. (91).

$$\boldsymbol{X} = \begin{bmatrix} 1 & x_{01} & x_{02} & \dots & x_{0p} \\ 1 & x_{11} & x_{12} & \dots & x_{1p} \\ \vdots & \vdots & & \vdots & \\ 1 & x_{n1} & x_{n2} & \dots & x_{np} \end{bmatrix} \tag{91}$$

$\boldsymbol{\beta}$ is the vector of parameters or coefficients to be estimated and has the form given by Eq. (92).

$$\boldsymbol{\beta} = \begin{bmatrix} \beta_0 \\ \beta_1 \\ \vdots \\ \beta_n \end{bmatrix} \tag{92}$$

and $\boldsymbol{e}$ is the vector of errors or residuals as given by Eq. (93).

$$\boldsymbol{e} = \begin{bmatrix} e_0 \\ e_1 \\ \vdots \\ e_n \end{bmatrix} \tag{93}$$

An estimate for the parameters in the $\boldsymbol{\beta}$ vector that minimize the sum of the squares of the error vector (i.e. least-squares estimate for $\boldsymbol{\beta}$) is the vector **B** and can be calculated using Eq. (94) (Draper and Smith 1998).

$$\boldsymbol{B} = (\boldsymbol{X}'\boldsymbol{X})^{-1}\boldsymbol{X}'\boldsymbol{Y} \tag{94}$$

The fitted values that estimate the Y values can be obtained using Eq. (95).

$$\widehat{\boldsymbol{Y}} = \boldsymbol{X}\boldsymbol{B} \tag{95}$$

The vector of errors or residuals can be obtained using Eq. (96).

$$\boldsymbol{e} = \boldsymbol{Y} - \widehat{\boldsymbol{Y}} \tag{96}$$

Because FE analyses are used for the observed data that defines the relationship between the predictor and response variables, there is no random or statistical error introduced. Rather, the response data are generated using FE analyses, and their values will not change regardless of the number of times the FE analyses are performed. However, fixed error due to the model's lack of fit to the data does exist. This error is the difference between the correct value and the predicted value determined using FE analysis.

The best-fit of the predicted responses, $\widehat{\boldsymbol{Y}}$, to the actual responses, $\boldsymbol{Y}$, is typically determined by minimizing the sum of the squares of the residuals. However, the sum of the squares of residuals has scaling issues associated with each particular application. Thus, frequently goodness of fit is evaluated using the coefficient of multiple determination, which overcomes this scaling issue. While both the sum of the squares of the residuals and the coefficient of multiple determination are appropriate measures of the goodness of fit of the regression model, the coefficient of multiple determination was primarily used herein.

The coefficient of multiple determination, R^2, is given by Eq. (97) (Draper and Smith 1998).

$$R^2 = \frac{\sum_{i=1}^{n}\left(\hat{Y}_i - \overline{Y}\right)^2}{\sum_{i=1}^{n}\left(Y_i - \overline{Y}\right)^2} \qquad (0 \le R^2 \le 1) \tag{97}$$

Where $\hat{Y}_i$ is the estimated value at i, Y_i is the observation at i, and $\overline{Y}$ is the mean of the observations, **Y**. A perfect model for the data where $\widehat{\boldsymbol{Y}}$ exactly equals **Y** would yield a coefficient of multiple determination equal to unity.

The sum of the squares of the residuals, RSS, is given by Eq. (98) (Draper and Smith 1998).

$$RSS = \sum_{i=1}^{n} \left(Y_i - \hat{Y}_i\right)^2 \tag{98}$$

Where all of the variables are as previously defined.

Once a mathematical model of interest was selected for the regression analysis, the "best subset" of predictor variables was selected using a computer algorithm. The MATLAB platform was selected to execute the computer algorithm as it provides a powerful matrix-based language for performing computational mathematics.

The goal for selecting the best subset of predictor variables was to minimize the number of predictor terms needed to reasonably represent the response variable. A subset of predictor variables was considered acceptable when the coefficient of multiple determination, R^2, was maximized or exhibited diminishing returns as more terms were added to the model.

As stated previously, three predictor variables were considered in this analysis. These included the CEEC, absorption ratio, and edge bite dimension for a particular frame, spacer, and nominal glass plate thickness. In addition, both linear and quadratic cross terms and quadratic terms were considered in the list of potential predictor variables. This is discussed in detail later.

Once a complete model was selected, a set of linear regression procedures were performed to determine the single most correlated predictor variable with regard to the coefficient of multiple determination. Next, a second set of linear regression procedures

were performed that include the previously identified, best correlated, term in combination with each of the remaining predictor variables. The best second term is selected and added to the regression model. This procedure was continued until all of the predictor variables were placed into the model in rank order of highest coefficient of determination to lowest. Once the predictor variables were placed into the model in rank order, graphs of the coefficient of multiple determination and the sum of the squares of the residuals were examined to identify the most efficient number of terms that should be included in the final regression model. Note that each model always included a constant term.

General Polynomial Equation

To establish an appropriate model to be used in the regression analysis, it is useful to first observe the nature of the steady-state and transient response data collected using the FE analyses. These data are shown in Figs. 138 through 145 later. Upon inspection, it becomes clear that polynomial equations may provide accurate models for these data. Thus, it was desired to fit a set of n^{th} order polynomials to the steady-state and transient data presented.

Ultimately, two orders of polynomials were considered for the research herein, first-order and second-order. The first-order polynomial was selected for its simplicity as it provides the least number of terms to be evaluated and no higher power terms. It can also be observed from the data presented in Figs. 138 through 145 that a second-order polynomial will likely fit the data more accurately than a first-order, but will still provide for an acceptable number of maximum terms to be evaluated. It is the opinion of the writer that a third-order equation would not provide substantial benefit and the terms would be too numerous for practical purposes. Thus, a third-order polynomial was not considered herein. That is not to say that it would not be possible.

A final parametric study was performed to understand the effects of the predictor variables, including the CEEC, absorption ratio, and edge bite dimension, on the thermal response or behavior of an IG unit. Two frame types were considered for this study, perfectly insulated and high-heat mass. The thin, steel-channel spacer was used for all cases and the glass plates were 0.25 in. nominal thickness. A total of five edge bites were considered ranging from 0.5 to 1.5 in. A total of eight absorption ratios were considered with a range from 0.25 to 9.

The absorption ratio of 0.25 meant that the outer glass plate absorbed 20 percent of the net absorption and the inner glass plate absorbed 80 percent. The absorption ratio of 9 meant that the outer glass plate absorbed 90 percent of the net absorption and the inner glass plate absorbed 10 percent. The percent of solar irradiance absorbed by the outer glass plate was increased and the inner glass plate decreased in increments of 10 percent with each absorption ratio considered.

A total of 10 CEEC were considered with a range of 0.0059 to 0.0236 (in.·lb/s)/(in.^{2}·°F). A CEEC of 0.0059 (in.·lb/s)/(in.^{2}·°F) is associated with pure gaseous conduction across the gas space cavity and the 0.0236 (in.·lb/s)/(in.^{2}·°F) is an upper limit greater than a CEEC associated with an IG unit with clear glass plates. The effect of each of these variables on the steady-state and transient responses are discussed in detail below.

Steady-State Response: Two Independent Variables

The thermal slope that is associated with the steady-state response of an IG unit is calculated when zero solar irradiance is applied. Because the analysis is performed with zero solar irradiance, the absorption ratio is not included as a predictor variable in the regression model. The only two variables that affect the steady-state response of the IG unit are the CEEC and the edge bite for a given frame, spacer, and nominal glass plate thickness. Because the relationship between the indoor\outdoor temperature difference and

pre-stress (i.e. steady-state response) is linear and it is known that the line must pass through the origin at zero, a single FE analysis is needed for each CEEC and edge bite to establish the slope, m, of this line (i.e. the thermal slope).

Thus, for each spacer, frame, and nominal glass plate thickness a total of 50 FE analyses are needed. Each FE analysis was performed with an indoor temperature of 70 °F, outdoor temperature of -20 °F, and zero solar irradiance. Table 28 shows the CEEC, edge bite, and indoor and outdoor temperatures that are needed for each FE analyses and required for each frame, spacer, and nominal glass plate thickness.

Table 28. Steady-State FE Analyses for a Given Frame, Spacer, and Nominal Glass Plate Thickness

Case No.	h_{CEEC} ((in.·lb/s)/(in.·°F))	d_{edge_bite} (in.)	T_{indoor} (°F)	$T_{outdoor}$ (°F)
Case 1	0.005894	0.50	70	-20
Case 2	0.005894	0.75	70	-20
Case 3	0.005894	1.00	70	-20
Case 4	0.005894	1.25	70	-20
Case 5	0.005894	1.50	70	-20
Case 6	0.007859	0.50	70	-20
Case 7	0.007859	0.75	70	-20
Case 8	0.007859	1.00	70	-20
Case 9	0.007859	1.25	70	-20
Case 10	0.007859	1.50	70	-20
Case 11	0.009823	0.50	70	-20
Case 12	0.009823	0.75	70	-20
Case 13	0.009823	1.00	70	-20
Case 14	0.009823	1.25	70	-20
Case 15	0.009823	1.50	70	-20
Case 16	0.011788	0.50	70	-20
Case 17	0.011788	0.75	70	-20
Case 18	0.011788	1.00	70	-20
Case 19	0.011788	1.25	70	-20
Case 20	0.011788	1.50	70	-20
Case 21	0.013752	0.50	70	-20
Case 22	0.013752	0.75	70	-20
Case 23	0.013752	1.00	70	-20
Case 24	0.013752	1.25	70	-20
Case 25	0.013752	1.50	70	-20
Case 26	0.015717	0.50	70	-20
Case 27	0.015717	0.75	70	-20
Case 28	0.015717	1.00	70	-20
Case 29	0.015717	1.25	70	-20
Case 30	0.015717	1.50	70	-20
Case 31	0.017682	0.50	70	-20
Case 32	0.017682	0.75	70	-20
Case 33	0.017682	1.00	70	-20
Case 34	0.017682	1.25	70	-20
Case 35	0.017682	1.50	70	-20
Case 36	0.019646	0.50	70	-20
Case 37	0.019646	0.75	70	-20
Case 38	0.019646	1.00	70	-20
Case 39	0.019646	1.25	70	-20
Case 40	0.019646	1.50	70	-20
Case 41	0.021611	0.50	70	-20
Case 42	0.021611	0.75	70	-20
Case 43	0.021611	1.00	70	-20
Case 44	0.021611	1.25	70	-20
Case 45	0.021611	1.50	70	-20
Case 46	0.023576	0.50	70	-20
Case 47	0.023576	0.75	70	-20
Case 48	0.023576	1.00	70	-20
Case 49	0.023576	1.25	70	-20
Case 50	0.023576	1.50	70	-20

Once these FE analyses have been performed, the thermal slope, m, associated with the steady-state response can be calculated using Eq. (99).

$$m = \frac{(T_{COG} - T_{POG})}{(T_{outdoor} - T_{indoor})} = \frac{(T_{COG} - T_{POG})}{-90\ °\text{F}} \tag{99}$$

Figs. 138 and 139 show the steady-state response of the outer glass plate as a function of edge bite and CEEC for perfectly insulated and high-heat mass frames, respectively. Figs. 140 and 141 show the same data for the inner glass plate. An interesting observation to note is that there appears to be little to no difference in the steady-state response between an IG unit with a high-heat mass frame to that with a perfectly insulated frame. This is true for both the inner and outer glass plates as well. It seems reasonable that the steady-state response would be the same for both high-heat mass and perfectly insulated frames.

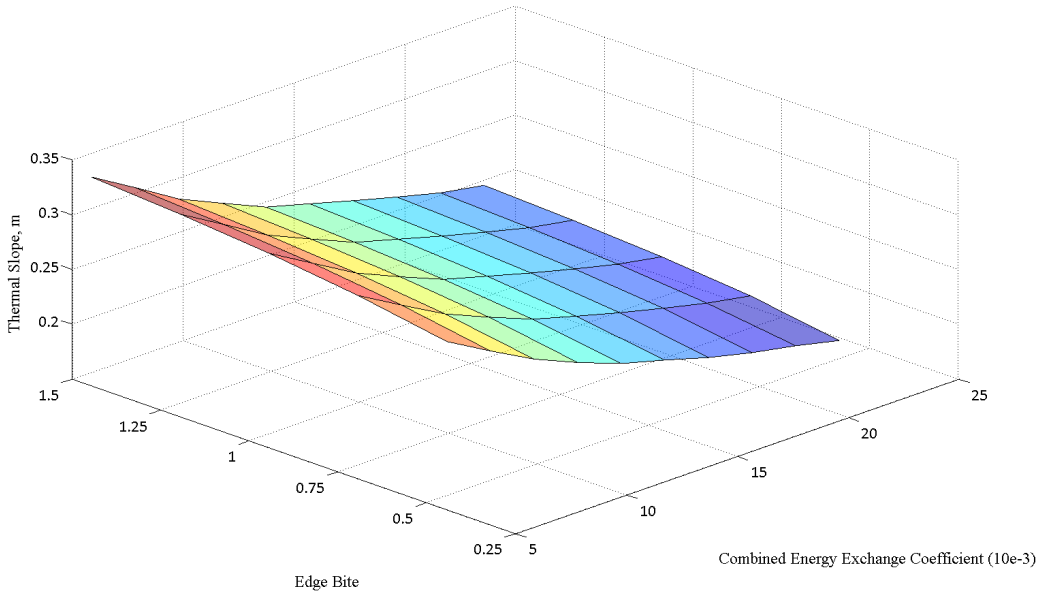

Fig. 138. Steady-State Response for the Outer Glass Plate with a Perfectly Insulated Frame

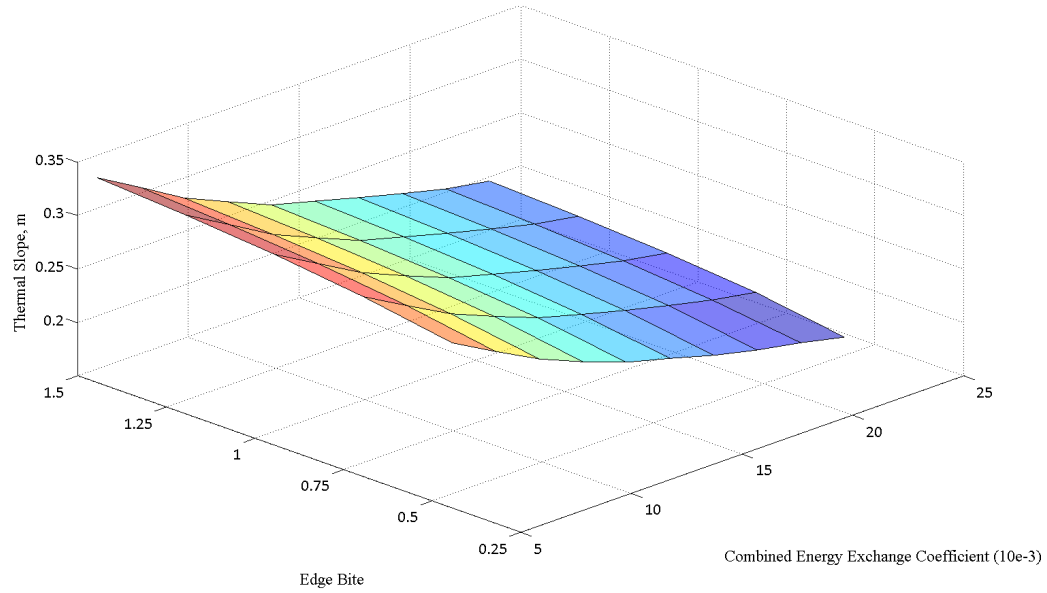

Fig. 139. Steady-State Response for the Outer Glass Plate with a High-Heat Mass Frame

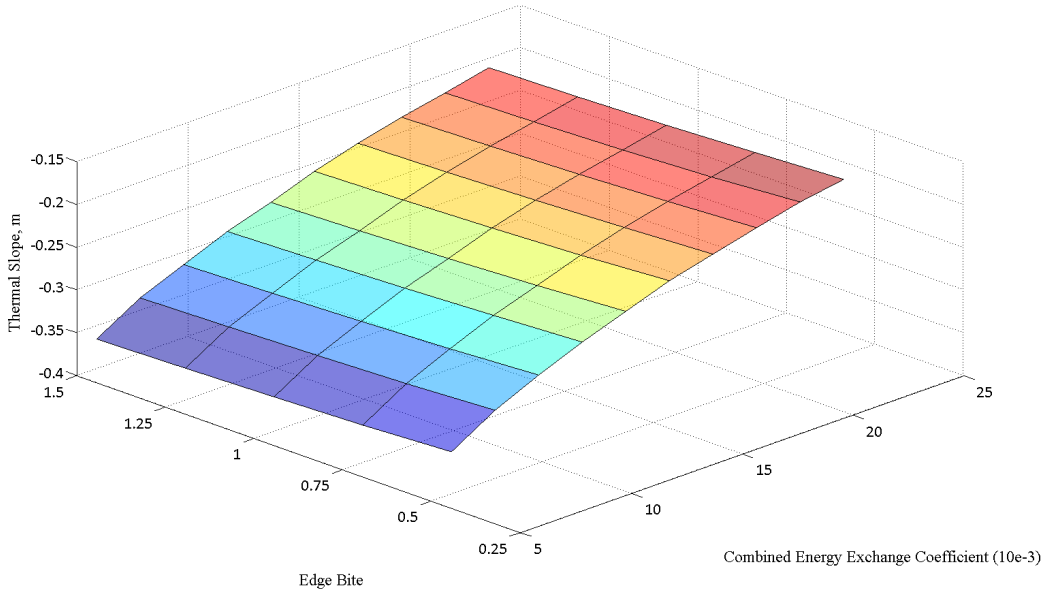

Fig. 140. Steady-State Response for the Inner Glass Plate with a Perfectly Insulated Frame

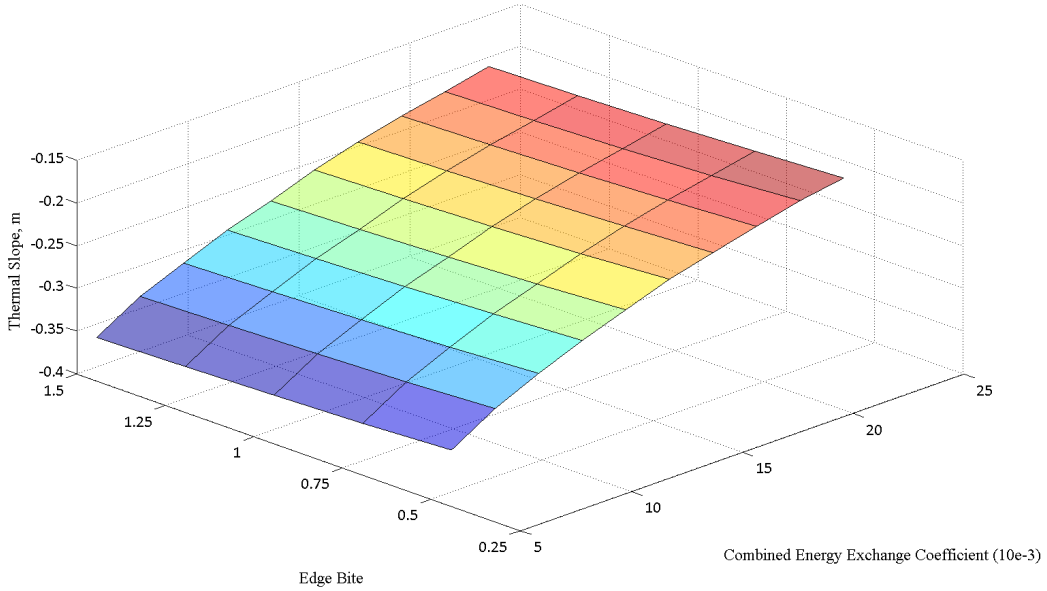

Fig. 141. Steady-State Response for the Inner Glass Plate with a High-Heat Mass Frame

Consider a polynomial regression model for the steady-state response. An important observation is that the steady-state response of an IG unit is a function of the edge bite and the CEEC. Thus, a general polynomial with two independent variables must be used to describe the steady-state behavior of each glass plate. The complete n^{th} degree polynomial, P_n, is given by Eq. (100) (Kaliakin 2016).

$$P_n(x,y) = \sum_{l=0}^{n} a_l \cdot x^i \cdot y^j \qquad (i+j \le l) \qquad (100)$$

Where x and y are the independent variables, a_l are the equation coefficients, and n is the degree of order. The total number of terms that are possible for a polynomial with two independent variables is given by Eq. (101) (Kaliakin 2016).

$$No.of\ terms = \frac{(n+1)\cdot(n+2)}{2} \tag{101}$$

The polynomial equation, P_1, for a first-order, linear plane with n equal to one is shown in Eq. (102).

$$P_1(x,y) = a_0 + a_1 \cdot x + a_2 \cdot y \tag{102}$$

Where all of the variables are as previously defined.

The polynomial equation, P_2, for a second-order, quadratic surface with n equal to two is shown in Eq. (103).

$$P_2(x,y) = a_0 + a_1 \cdot x + a_2 \cdot y + a_3 \cdot x^2 + a_4 \cdot x \cdot y + a_5 \cdot y^2 \tag{103}$$

Where all of the variables are as previously defined. As such, the first-order polynomial with two independent variables has a total of three terms and the second-order polynomial has a total of six terms.

If the x independent variable is taken as the CEEC and the y independent variable as the edge bite dimension, Eqs. (102) and (103) for the steady-state response become Eqs. (104) and (105) for linear and quadratic surfaces, respectively.

$$P_1\left(h_{CEEC}, d_{edge\_bite}\right) = a_0 + a_1 \cdot h_{CEEC} + a_2 \cdot d_{edge\_bite} \tag{104}$$

$$\begin{aligned} P_2\left(h_{CEEC}, d_{edge\_bite}\right) & \\ &= a_0 + a_1 \cdot h_{CEEC} + a_2 \cdot d_{edge\_bite} + a_3 \cdot {h_{CEEC}}^2 + a_4 \\ &\cdot h_{CEEC} \cdot d_{edge\_bite} + a_5 \cdot {d_{edge\_bite}}^2 \end{aligned} \tag{105}$$

Where P_1 is the first-order polynomial used to model the steady-state response, P_2 is the second-order polynomial used to model the steady-state response, h_{CEEC} is the CEEC, d_{edge_bite} is the edge bite dimension, and all other variables are as previously defined.

Transient Response: Three Independent Variables

The transient response of an IG unit is calculated when solar irradiance is applied. Unlike the steady-state response, the absorption ratio does have an effect on the transient response. Therefore, the transient response must be represented using a four-dimensional data presentation, as it is affected by three independent variables. These variables are the IG unit's CEEC, absorption ratio, and edge bite dimension for a given frame, spacer, and nominal glass plate thickness. This defines the thermal offset, b, for an IG unit.

For each spacer, frame, and nominal glass plate thickness, a total of 400 FE analyses are needed. As shown previously, the steady-state and transient responses can be decoupled and solved individually. The results of each analysis can then be coupled together using the method of superposition for the overall thermal stress. This allows the FE analyses to be performed with an indoor temperature equal to the outdoor temperature to get the transient offset temperature directly, rather than having to perform analyses for various outdoor temperatures. Thus, a temperature of 70 °F was used for each analysis.

Each FE analysis was performed with a solar irradiance of 5.7105 (in.·lb/s)/in.^{2} and a net absorption of 25 percent, as discussed previously. As such, the total solar irradiance absorbed, I_{outer} and I_{inner}, by the outer and inner glass plates are calculated using Eqs. (106) and (107), respectively.

$$I_{outer} = I_s \cdot \alpha_{net} \cdot \frac{\alpha_{ratio}}{(\alpha_{ratio} + 1)} \tag{106}$$

$$I_{inner} = I_s \cdot \alpha_{net} \cdot \frac{1}{(\alpha_{ratio} + 1)} \tag{107}$$

Where all terms are as previously defined.

Table 29 shows the 40 FE analyses required for the first CEEC considered. Values for the edge bite, absorption ratio, absorption of the inner and outer glass plates, net absorption, and the solar irradiance absorbed by the inner and outer glass plates for each FE analysis are shown. Where all of the variables are as previously defined. This matrix of FE analyses is then repeated for the nine other CEEC and each frame, spacer, and nominal glass plate thickness.

Table 29. Matrix of FE Analyses Required per CEEC for a Given Frame, Spacer, and Nominal Glass Plate Thickness

Case No.	h_{CEEC} ((in.·lb/s)/(in.·°F))	d_{edge_bite} (in.)	α_{ratio}	α_{outer}	α_{inner}	α_{net}	I_{outer} ((in.·lb/s)/in.^{2})	I_{inner} ((in.·lb/s)/in.^{2})
Case 1	0.005894	0.50	0.250	0.20	0.80	0.25	0.2855	1.1421
Case 2	0.005894	0.50	0.429	0.30	0.70	0.25	0.4283	0.9993
Case 3	0.005894	0.50	0.667	0.40	0.60	0.25	0.5711	0.8566
Case 4	0.005894	0.50	1.000	0.50	0.50	0.25	0.7138	0.7138
Case 5	0.005894	0.50	1.500	0.60	0.40	0.25	0.8566	0.5711
Case 6	0.005894	0.50	2.333	0.70	0.30	0.25	0.9993	0.4283
Case 7	0.005894	0.50	4.000	0.80	0.20	0.25	1.1421	0.2855
Case 8	0.005894	0.50	9.000	0.90	0.10	0.25	1.2849	0.1428
Case 9	0.005894	0.75	0.250	0.20	0.80	0.25	0.2855	1.1421
Case 10	0.005894	0.75	0.429	0.30	0.70	0.25	0.4283	0.9993
Case 11	0.005894	0.75	0.667	0.40	0.60	0.25	0.5711	0.8566
Case 12	0.005894	0.75	1.000	0.50	0.50	0.25	0.7138	0.7138
Case 13	0.005894	0.75	1.500	0.60	0.40	0.25	0.8566	0.5711
Case 14	0.005894	0.75	2.333	0.70	0.30	0.25	0.9993	0.4283
Case 15	0.005894	0.75	4.000	0.80	0.20	0.25	1.1421	0.2855
Case 16	0.005894	0.75	9.000	0.90	0.10	0.25	1.2849	0.1428
Case 17	0.005894	1.00	0.250	0.20	0.80	0.25	0.2855	1.1421
Case 18	0.005894	1.00	0.429	0.30	0.70	0.25	0.4283	0.9993
Case 19	0.005894	1.00	0.667	0.40	0.60	0.25	0.5711	0.8566
Case 20	0.005894	1.00	1.000	0.50	0.50	0.25	0.7138	0.7138
Case 21	0.005894	1.00	1.500	0.60	0.40	0.25	0.8566	0.5711
Case 22	0.005894	1.00	2.333	0.70	0.30	0.25	0.9993	0.4283
Case 23	0.005894	1.00	4.000	0.80	0.20	0.25	1.1421	0.2855
Case 24	0.005894	1.00	9.000	0.90	0.10	0.25	1.2849	0.1428
Case 25	0.005894	1.25	0.250	0.20	0.80	0.25	0.2855	1.1421
Case 26	0.005894	1.25	0.429	0.30	0.70	0.25	0.4283	0.9993
Case 27	0.005894	1.25	0.667	0.40	0.60	0.25	0.5711	0.8566
Case 28	0.005894	1.25	1.000	0.50	0.50	0.25	0.7138	0.7138
Case 29	0.005894	1.25	1.500	0.60	0.40	0.25	0.8566	0.5711
Case 30	0.005894	1.25	2.333	0.70	0.30	0.25	0.9993	0.4283
Case 31	0.005894	1.25	4.000	0.80	0.20	0.25	1.1421	0.2855
Case 32	0.005894	1.25	9.000	0.90	0.10	0.25	1.2849	0.1428
Case 33	0.005894	1.50	0.250	0.20	0.80	0.25	0.2855	1.1421
Case 34	0.005894	1.50	0.429	0.30	0.70	0.25	0.4283	0.9993
Case 35	0.005894	1.50	0.667	0.40	0.60	0.25	0.5711	0.8566
Case 36	0.005894	1.50	1.000	0.50	0.50	0.25	0.7138	0.7138
Case 37	0.005894	1.50	1.500	0.60	0.40	0.25	0.8566	0.5711
Case 38	0.005894	1.50	2.333	0.70	0.30	0.25	0.9993	0.4283
Case 39	0.005894	1.50	4.000	0.80	0.20	0.25	1.1421	0.2855
Case 40	0.005894	1.50	9.000	0.90	0.10	0.25	1.2849	0.1428

Once these FE analyses have been performed, the thermal offset, b, of the transient response can be calculated using Eq. (108).

$$b = \max_{0 \le i \le 3600} \left(T_{COG_i} - T_{POG_i} \right) \tag{108}$$

Where all of the variables are as previously defined and the timestep i is expressed in s from zero to 3600 s.

Figs. 142 and 143 show the transient response of the outer glass plate as a function of the CEEC and the percent absorption of the outer glass plate over the net absorption for perfectly insulated and high-heat mass frames, respectively. The reason for using the absorption of the outer glass plate over the net absorption, instead of the absorption ratio, will be discussed in detail later. There are five surfaces shown in each figure. These surfaces represents the five edge bite dimensions. The lower surface represents the thermal offset for the 0.5 in. edge bite and each subsequent surface is associated with the next largest edge bite thereafter. Figs. 144 and 145 show the same data for the inner glass plate. An interesting observation is that the transient response seems independent of edge bite when a high-heat mass frame is used. This observation is reasonable.

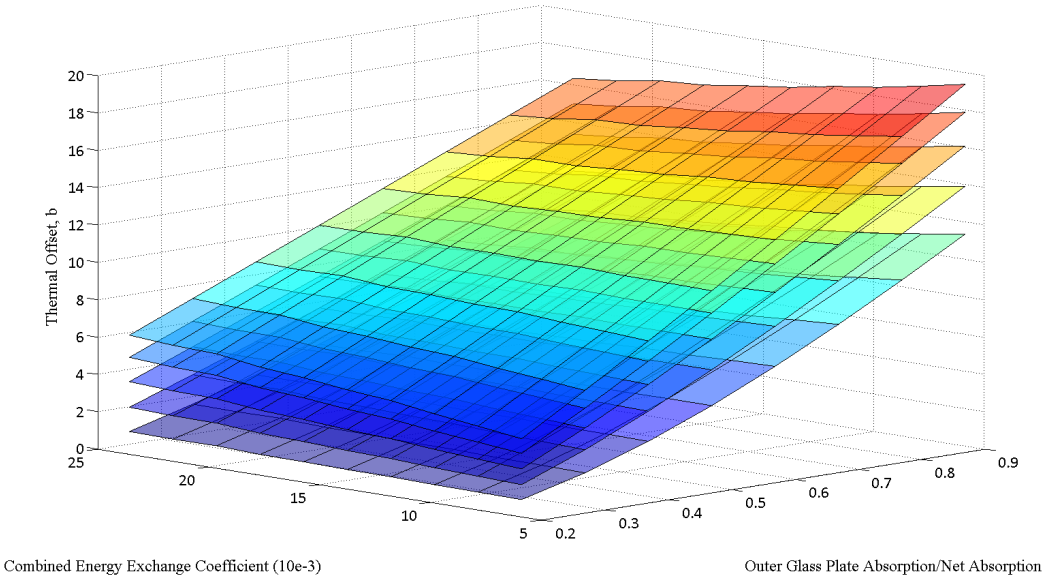

Fig. 142. Transient Response of the Outer Glass Plate with a Perfectly Insulated Frame

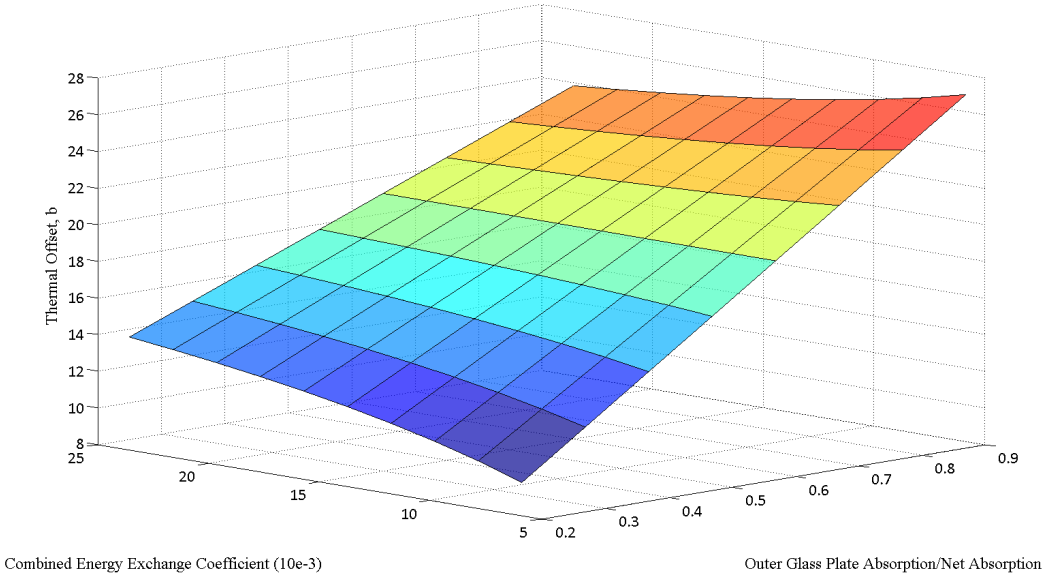

Fig. 143. Transient Response of the Outer Glass Plate with a High-Heat Mass Frame

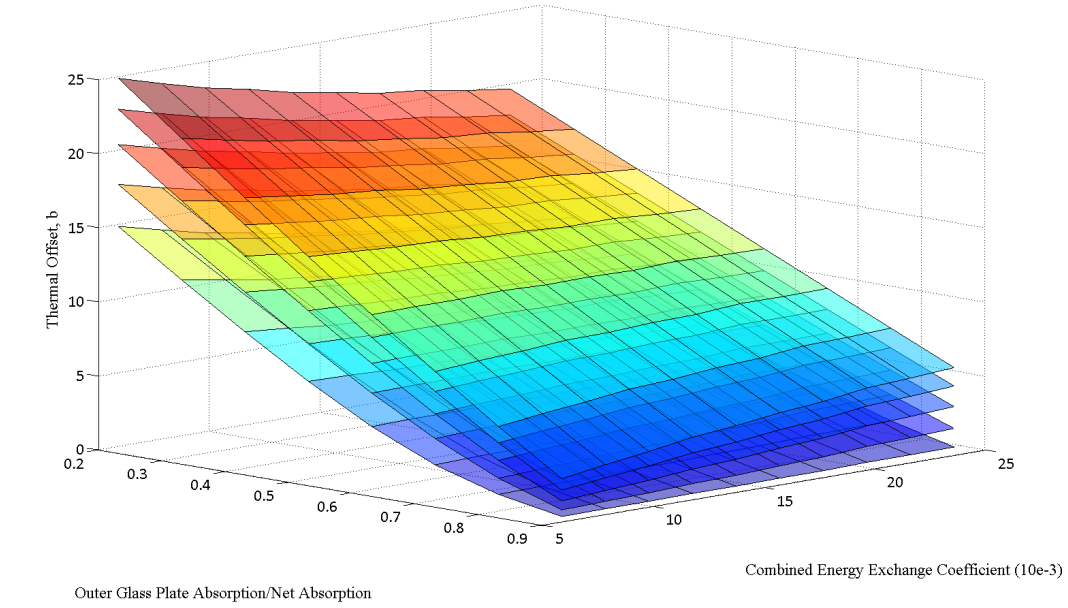

Fig. 144. Transient Response of the Inner Glass Plate with a Perfectly Insulated Frame

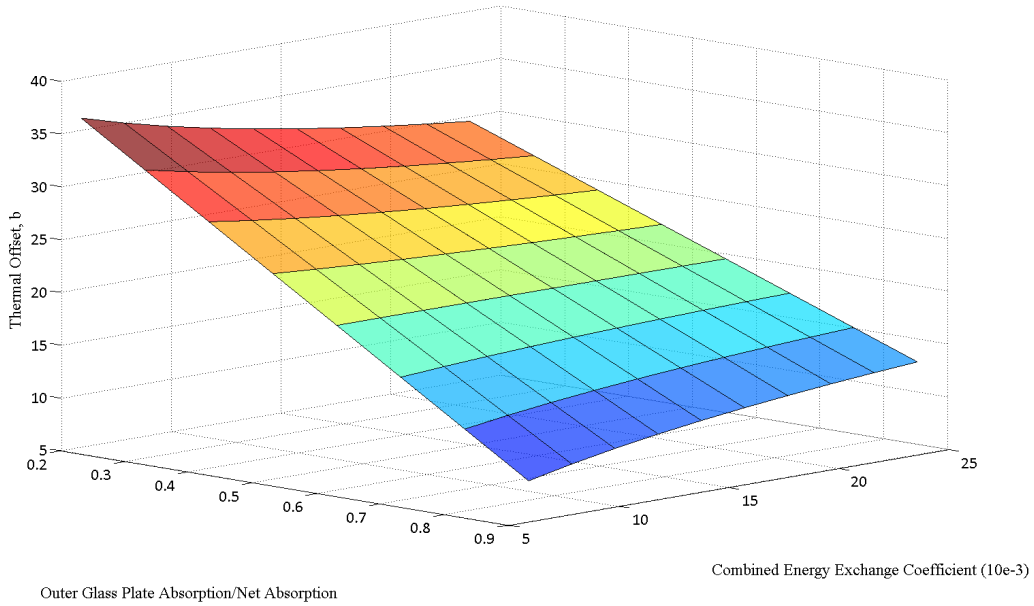

Fig. 145. Transient Response of the Inner Glass Plate with a High-Heat Mass Frame

While it would be convenient to determine the thermal response of an IG unit when subjected to solar irradiance using a set of two-dimensional charts for each case of interest, it is apparent from Figs. 138 through 145 that the nature of these response data is not conducive to a two-dimensional graphical representation. This is true for both the steady-state and transient responses. Since a simplification scheme could not be found, a two-dimensional graphical representation would require a large number of charts for each case of interest. In addition, the error that would be associated with using this type of graphical representation would be significant. Thus, a more accurate presentation format for representing the response data was needed. Ultimately, this led to the regression-based equation technique that is presented herein. The use of the regression model helped to reduce the presentation format into something that was more manageable than a large set of two-dimensional graphical charts.

The transient response of an IG unit is a function of the edge bite, CEEC, and absorption ratio. Therefore, a general polynomial with three independent variables must be used to

describe the transient behavior of each glass plate. The complete n^{th} degree polynomial, P_n, is given by Eq. (109) (Kaliakin 2016).

$$P_n(x,y,z) = \sum_{l=0}^{n} a_l \cdot x^i \cdot y^j \cdot z^k \qquad (i+j+k \leq l) \tag{109}$$

Where x, y, and z are the independent variables, a_l are the equation coefficients, and n is the degree of order. The total number of terms that are possible for a polynomial with three independent variables is given by Eq. (110) (Kaliakin 2016).

$$No.of\ terms = \frac{(n+1)\cdot(n+2)\cdot(n+3)}{2} \tag{110}$$

The polynomial equation, P_1, for a first-order polynomial with n equal to one is shown in Eq. (111).

$$P_1(x,y,z) = a_0 + a_1 \cdot x + a_2 \cdot y + a_3 \cdot z \tag{111}$$

Where all of the variables are as previously defined.

The polynomial equation, P_2, for a second-order polynomial with n equal to two is shown in Eq. (112).

$$\begin{aligned} P_2(x,y,z) = a_0 + a_1 \cdot x + a_2 \cdot y + a_3 \cdot z + a_4 \cdot x \cdot y + a_5 \cdot x \cdot z + a_6 \\ \cdot y \cdot z + a_7 \cdot x^2 + a_8 \cdot y^2 + a_9 \cdot z^2 \end{aligned} \tag{112}$$

Where all of the variables are as previously defined. As such, the first-order polynomial with three independent variables has a total of four terms and the second-order polynomial has a total of ten terms.

Thus, if the x independent variable is taken as the CEEC, the y independent variable as the edge bite dimension, and z as the absorption ratio as given by Eq. (71), Eqs. (111) and (112) for the transient response become Eqs. (113) and (114) for first-order and second-order polynomials, respectively.

$$P_1\left(h_{CEEC}, d_{edge\_bite}, \alpha_{ratio}\right) = a_0 + a_1 \cdot h_{CEEC} + a_2 \cdot d_{edge\_bite} + a_3 \cdot \alpha_{ratio} \tag{113}$$

$$\begin{aligned} P_2\left(h_{CEEC}, d_{edge}, \alpha_{ratio}\right) &= a_0 + a_1 \cdot h_{CEEC} + a_2 \cdot d_{edge\_bite} + a_3 \cdot \alpha_{ratio} + a_4 \\ &\cdot h_{CEEC} \cdot d_{edge\_bite} + a_5 \cdot h_{CEEC} \cdot \alpha_{ratio} + a_6 \\ &\cdot d_{edge\_bite} \cdot \alpha_{ratio} + a_7 \cdot {h_{CEEC}}^2 + a_8 \cdot {d_{edge\_bite}}^2 \\ &+ a_9 \cdot {\alpha_{ratio}}^2 \end{aligned} \tag{114}$$

Where P_1 is the first-order polynomial used to model the transient response, P_2 is the second-order polynomial used to model the transient response, h_{CEEC} is the CEEC, d_{edge_bite} is the edge bite dimension, α_{ratio} is the absorption ratio, and all other variables are as previously defined.

Note that the absorption ratio, as defined, is not a linear term. However, non-linear variables that are used in a regression analysis can often be linearized using mathematic techniques. Fig. 146 presents the absorption ratio for the range of FE analyses that were performed as part of this regression analyses. As shown, these data exhibit an exponential response, thus it would be more convenient to linearize these data.

One common method that is used to make exponential data more linear is to take the natural log. The natural log of the data shown in Fig. 146 are shown in Fig. 147. While manipulating the data using the natural log does provide a near linear response, it does

not appear to provide the most effective linear fit to the data. The coefficient of multiple determination for a straight line fit through these data was 0.9889, as shown in Fig. 147.

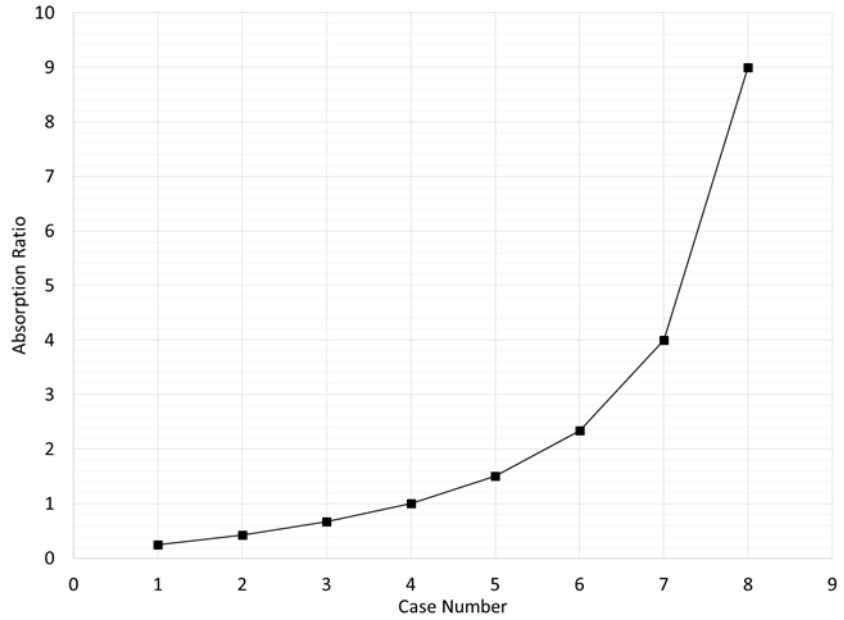

Fig. 146. Absorption Ratio vs. Case Number

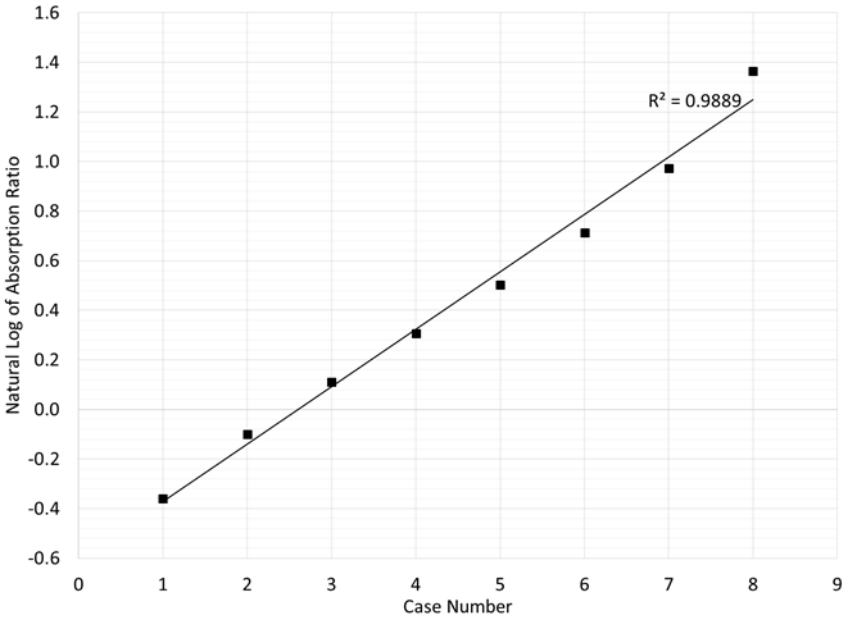

Fig. 147. Natural Log of Absorption Ratio vs. Case Number

A better approach to linearize the absorption ratio is to base the regression equation on the percentage of solar irradiance that would be absorbed by the outer glass plate compared to the net absorption. The relationship between this ratio and the absorption ratio is shown in Eq. (115). These data are shown in Fig. 119, and it is clear that the ratio of outer glass plate absorptance over the net absorptance is a linear relationship. Thus, it was used for all further regression analyses performed herein.

$$\frac{\alpha_{ratio}}{(1+\alpha_{ratio})} = \frac{\alpha_{outer}}{\alpha_{outer}+\alpha_{inner}} = \frac{\alpha_{outer}}{\alpha_{net}} \tag{115}$$

Where all of the variables are as previously defined.

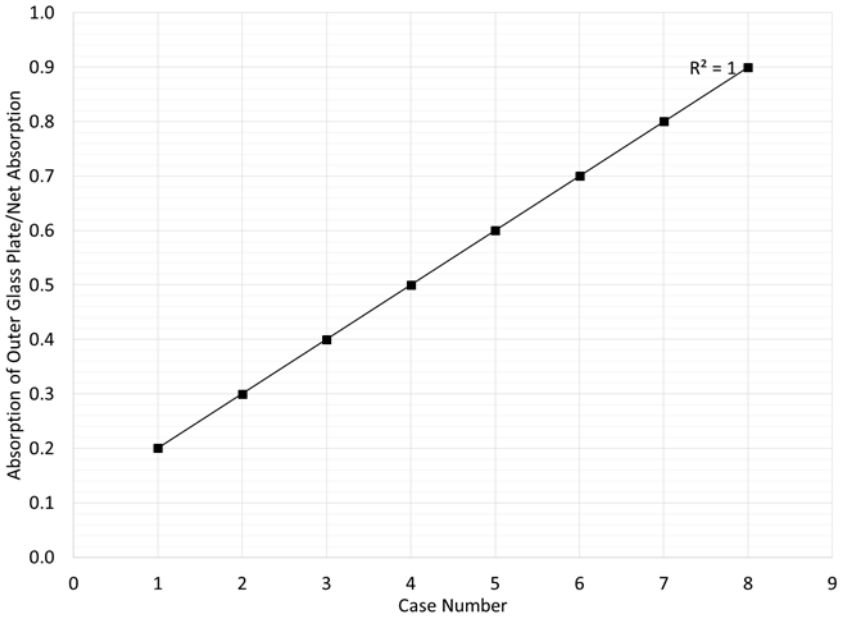

Fig. 148. Linear Outer Glass Plate Absorption Over Net Absorption vs. Case Number

Thus, if the x independent variable is taken as the CEEC, the y independent variable as the edge bite dimension, and z as the ratio of outer glass plate absorption to net absorption as given by Eq. (115), Eqs. (111) and (112) for the transient response become Eqs. (116) and (117) for linear and second-order polynomials.

$$P_1\left(h_{CEEC}, d_{edge\_bite}, \left(\frac{\alpha_{outer}}{\alpha_{net}}\right)\right) = a_0 + a_1 + a_2 \cdot d_{edge\_bite} + a_3 \cdot \left(\frac{\alpha_{outer}}{\alpha_{net}}\right) \tag{116}$$

$$\begin{aligned} P_2\left(h_{CEEC}, d_{edge\_bite}, \left(\frac{\alpha_{outer}}{\alpha_{net}}\right)\right) &= a_0 + a_1 \cdot h_{CEEC} + a_2 \cdot d_{edge_{bite}} + a_3 \cdot \left(\frac{\alpha_{outer}}{\alpha_{net}}\right) + a_4 \\ &\cdot h_{CEEC} \cdot d_{edge_{bite}} + a_5 \cdot h_{CEEC} \cdot \left(\frac{\alpha_{outer}}{\alpha_{net}}\right) + a_6 \\ &\cdot d_{edge_{bite}} \cdot \left(\frac{\alpha_{outer}}{\alpha_{net}}\right) + a_7 \cdot {h_{CEEC}}^2 + a_8 \cdot {d_{edge\_bite}}^2 \\ &+ a_9 \cdot \left(\frac{\alpha_{outer}}{\alpha_{net}}\right)^2 \end{aligned} \tag{117}$$

Where all of the variables are as previously defined.

The first-order hypothesized models for the steady-state and transient response of an IG unit that are given by Eqs. (104) and (116) were used to represent the relationship between the dependent and independent variables. In addition, the second-order hypothesized models for the steady-state and transient response of an IG unit that are given by Eqs. (105) and (117) were also used to represent the relationship between the dependent and independent variables. The next section is dedicated to explaining the application of a multivariate regression model to mathematically represent the thermal response of the data presented in Figs. 138 through 145 using the models discussed above.

Application of the General Regression Procedure

First-Order Polynomial Model

This section presents the results of the regression analyses discussed previously applied to the steady-state and transient data shown in Figs. 138 through 145 using the first-order polynomial models. The two hypothesized polynomial models used for the steady-state and transient responses were given by Eqs. (104) and (116), respectively.

For each of these analyses, a maximum over estimation stress was calculated and represents the maximum amount in which the model over estimates the actual thermal stress that would be calculated using the FDP. This stress is of little significance with regard to a safe design as it will provide a value larger than the actual stress that the glass plate experiences. Likewise, a maximum under estimation stress was calculated and represents the maximum amount in which the model under predicts the actual thermal stress that would be calculated using the FDP. This stress has significance in that it helps to define the level of conservatism of the model. These maximum stresses were evaluated at the extent of what is considered the applicable range for the outdoor temperature. An indoor/outdoor temperature difference of 50 °F was used for the outer glass plate and -90 °F was used for the inner glass plate. These values correspond with outdoor temperatures of 120 and -20 °F when considering the outer glass plate and inner glass plate, respectively, and a constant indoor temperature of 70 °F.

Outer Glass Plate with Perfectly Insulated Frame

Table 30 presents a summary of results from the steady-state regression analysis using the first-order polynomial model for the outer glass plate with a perfectly insulated frame. Included are the coefficient of multiple determination and sum of the squares of the residuals for the regression analysis in order of the terms added. In addition, the

maximum under and over estimation stress are included. The fifth column of Table 30 defines the rank order in which the terms were added to the model. The coefficients that are associated with each model are presented in Table 31.

Table 30. Summary of Steady-State Regression Analysis Using First-Order Polynomial Model for the Outer Glass Plate with Perfectly Insulated Frame

No. of Terms	R^2	Percent Difference	RSS	Term Added	Maximum Stress (psi)	
					Under Estimation	Over Estimation
1	-	-	-	Constant	-	-
2	89.653	-	0.073	h_{CEEC}	70.36	75.51
3	96.325	7.44%	0.026	d_{edge_bite}	33.55	42.22

Table 31. Coefficients for Steady-State Model Using First-Order Polynomial Model for the Outer Glass Plate with Perfectly Insulated Frame

No. of Terms	Coefficients, m_i		
2	0.3402	-7.0653	0
3	0.3094	-7.0653	0.0308

Fig. 149 shows the coefficient of multiple determination and sum of the squares of the residuals as a function of the number of terms added to the model. In general, the coefficient of multiple determination increases and the sum of the squares of the residuals decreases as the number of terms in the model increase. Fig. 150 shows the maximum under and over estimation stresses as a function of the number of terms added to the model. In general, both the maximum under and over estimation stresses decrease as the number of terms added to the model increase.

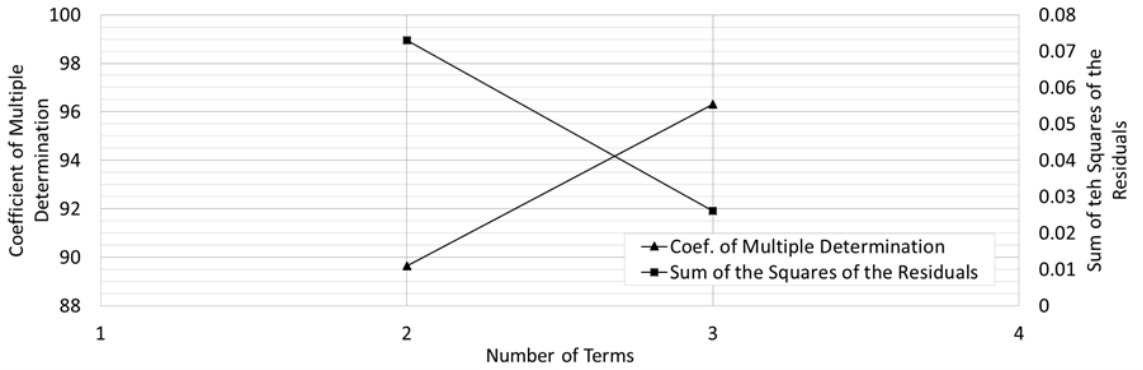

Fig. 149. Statistics of Steady-State Regression Analysis Using First-Order Polynomial Model for the Outer Glass Plate with Perfectly Insulated Frame

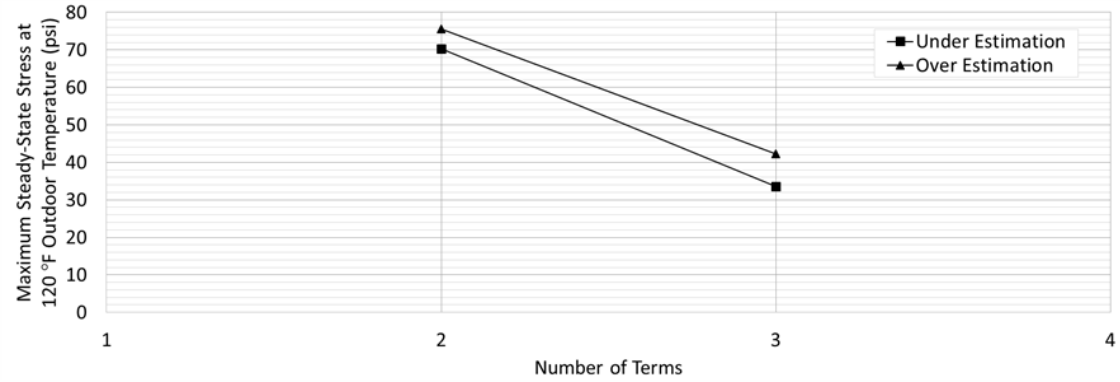

Fig. 150. Error in Stress Estimation of Steady-State Regression Analysis Using First-Order Polynomial Model for the Outer Glass Plate with Perfectly Insulated Frame

Table 32 presents a summary of results from the transient regression analysis using the first-order polynomial model for the outer glass plate with a perfectly insulated frame. Included are the coefficient of multiple determination and sum of the squares of the residuals for the regression analysis in rank order of the terms added and the maximum under and over estimation. The fifth column of the table defines the order in which each term was added to the model. The coefficients that are associated with each model are presented in Table 33.

Table 32. Summary of Transient Regression Analysis Using First-Order Polynomial Model for the Outer Glass Plate with Perfectly Insulated Frame

No. of Terms	R^2	Percent Difference	RSS	Term Added	Maximum Stress (psi)	
					Under Estimation	Over Estimation
1	-	-	-	Constant	-	-
2	70.909	-	2131.028	$(\alpha_{outer}/\alpha_{net})$	268.49	259.65
3	97.801	37.92%	161.051	d_{edge_bite}	112.10	103.91
4	97.901	0.10%	153.795	h_{CEEC}	101.35	114.66

Table 33. Coefficients for Transient Model Using First-Order Polynomial Model for the Outer Glass Plate with Perfectly Insulated Frame

No. of Terms	Coefficients, b_i			
2	-0.0615	15.7274	0	0
3	-6.3384	15.7274	6.2769	0
4	-5.9867	15.7274	6.2769	-23.8679

Fig. 151 shows the coefficient of multiple determination and sum of the squares of the residuals as a function of the number of terms added to the model. In general, the coefficient of multiple determination increases and the sum of the squares of the residuals decreases as the number of terms in the model increases. Fig. 152 shows the maximum under and over estimation stresses as a function of the number of terms added to the model. In general, both the maximum under and over estimation stresses decrease as the number of terms added to the model increases. Once the number of terms exceeds three, there is little increase in the fit of the polynomial model to the response data.

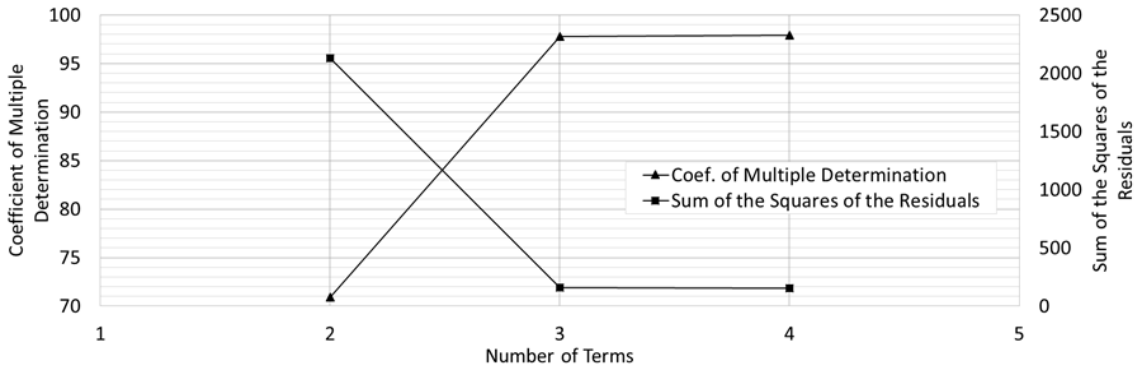

Fig. 151. Statistics of Transient Regression Analysis Using First-Order Polynomial Model for the Outer Glass Plate with Perfectly Insulated Frame

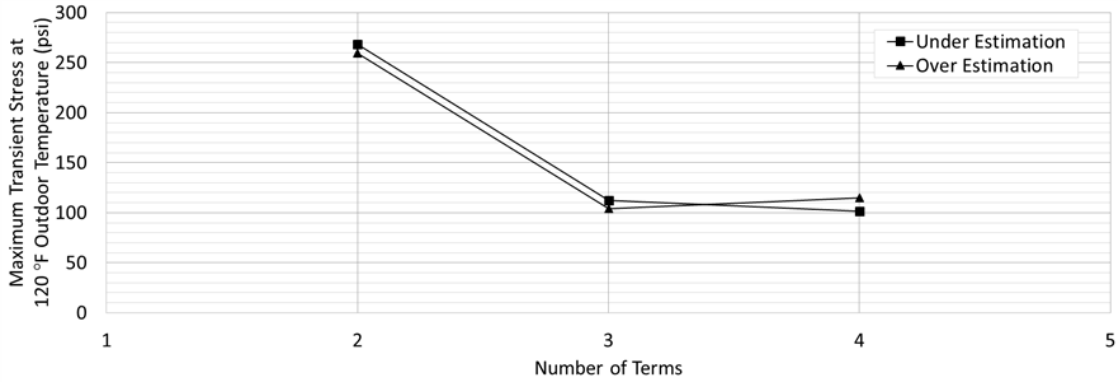

Fig. 152. Error in Stress Estimation of Transient Regression Analysis Using First-Order Polynomial Model for the Outer Glass Plate with Perfectly Insulated Frame

Table 34 summarizes the combined steady-state and transient results from the regression analysis for the number of terms selected. From the regression analyses, the model for the steady-state response is given in Eq. (118) below. Likewise, the transient response is given in Eq. (119) below. These equations and their fit to the actual response data are shown in Figs. 153 and 154.

Table 34. Overall Summary of Regression Analysis Using First-Order Polynomial Model for the Outer Glass Plate with Perfectly Insulated Frame

	No. of Terms	R^2	Maximum Stress (psi)	
			Under Estimation	Over Estimation
Steady-State	3	96.325	33.55	42.22
Transient	3	97.801	112.10	103.91
Total	6		145.65	146.13

$$m = 0.3094 - 7.0653 \cdot h_{CEEC} + 0.0308 \cdot d_{edge\_bite} \tag{118}$$

$$b = -6.3384 + 15.7274 \cdot \left(\frac{\alpha_{outer}}{\alpha_{net}}\right) + 6.2769 \cdot d_{edge\_bite} \tag{119}$$

Where all of the variables are as previously defined.

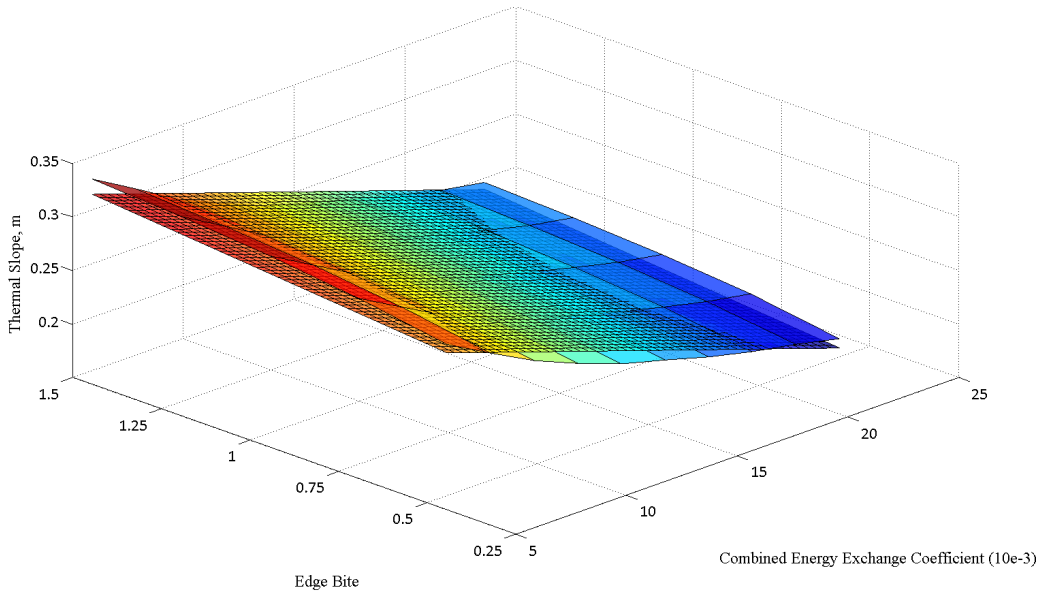

Fig. 153. Steady-State Regression Analysis Using First-Order Polynomial Model for the Outer Glass Plate with Perfectly Insulated Frame

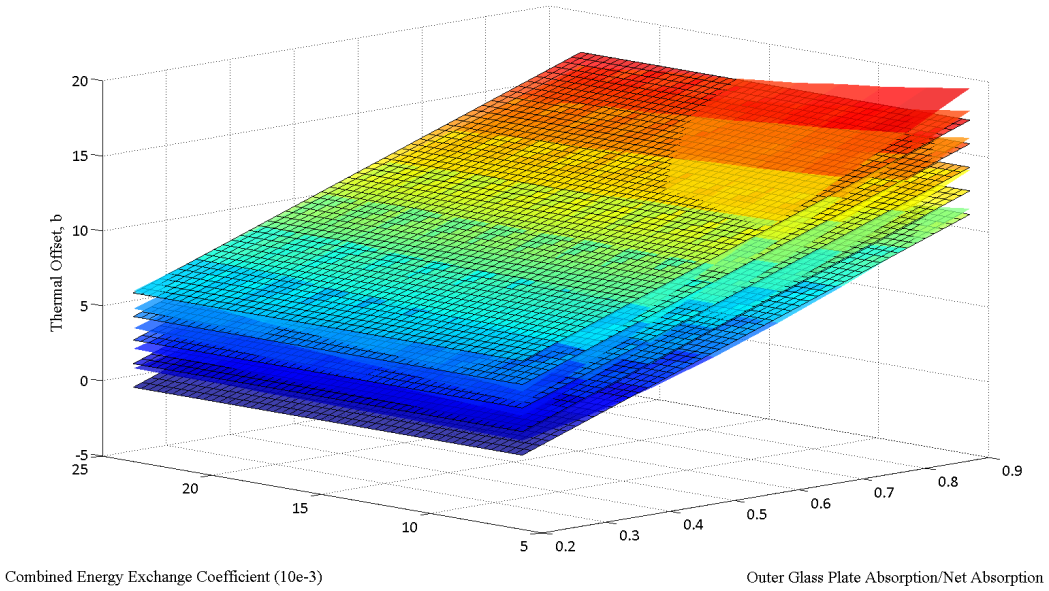

Fig. 154. Transient Regression Analysis Using First-Order Polynomial Model for the Outer Glass Plate with Perfectly Insulated Frame

Outer Glass Plate with High-Heat Mass Frame

Table 35 presents a summary of results from the steady-state regression analysis using the first-order polynomial model for the outer glass plate with a high-heat mass insulating frame. Included are the coefficient of multiple determination and sum of the squares of the residuals for the regression analysis in order of the terms added. In addition, the maximum under and over estimation stress are included. The fifth column of the table defines the rank order in which the terms were added to the model. The coefficients that are associated with each model are presented in Table 36.

Table 35. Summary of Steady-State Regression Analysis Using First-Order Polynomial Model for the Outer Glass Plate with High-Heat Mass Frame

No. of Terms	R^2	Percent Difference	RSS	Term Added	Maximum Stress (psi)	
					Under Estimation	Over Estimation
1	-	-	-	Constant	-	-
2	89.653	-	0.073	h_{CEEC}	70.36	75.51
3	96.325	7.44%	0.026	d_{edge_bite}	33.55	42.22

Table 36. Coefficients for Steady-State Model Using First-Order Polynomial Model for the Outer Glass Plate with High-Heat Mass Frame

No. of Terms	Coefficients, m_i		
2	0.3402	-7.0653	0
3	0.3094	-7.0653	0.0308

Fig. 155 shows the coefficient of multiple determination and sum of the squares of the residuals as a function of the number of terms added to the model. In general, the coefficient of multiple determination increases and the sum of the squares of the residuals decreases as the number of terms in the model increase. Fig. 156 shows the maximum under and over estimation stresses as a function of the number of terms added to the model. In general, both the maximum under and over estimation stresses decrease as the number of terms added to the model increase.

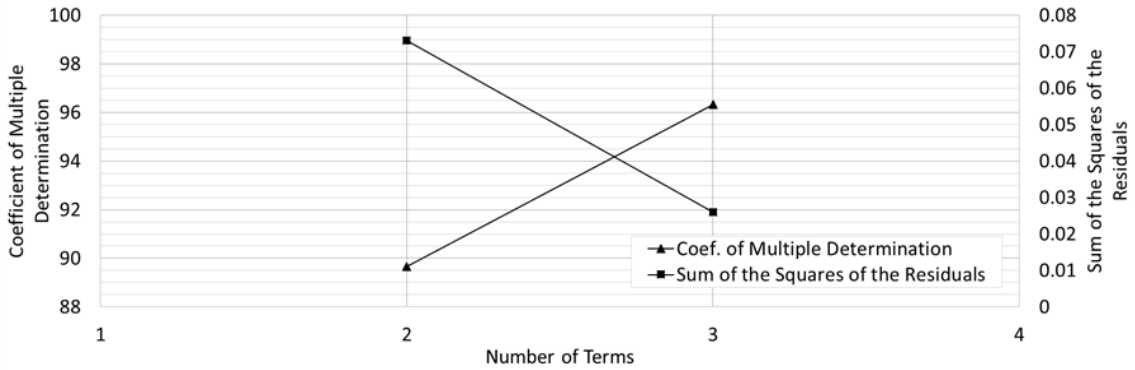

Fig. 155. Statistics of Steady-State Regression Analysis Using First-Order Polynomial Model for the Outer Glass Plate with High-Heat Mass Frame

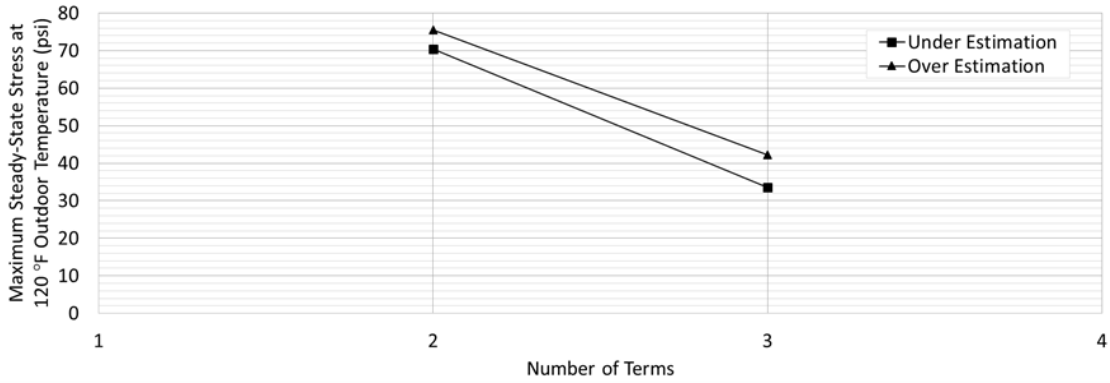

Fig. 156. Error in Stress Estimation of Steady-State Regression Analysis Using First-Order Polynomial Model for the Outer Glass Plate with High-Heat Mass Frame

Table 37 presents a summary of results from the transient regression analysis using the first-order polynomial model for the outer glass plate with a high-heat mass insulating frame. Included are the coefficient of multiple determination and sum of the squares of the residuals for the regression analysis in rank order of the terms added and the maximum under and over estimation. The fifth column of the table defines the order in which each term was added to the model. The coefficients that are associated with each model are presented in Table 38.

Table 37. Summary of Transient Regression Analysis Using First-Order Polynomial Model for the Outer Glass Plate with High-Heat Mass Frame

No. of Terms	R^2	Percent Difference	RSS	Term Added	Maximum Stress (psi)	
					Under Estimation	Over Estimation
1	-	-	-	Constant	-	-
2	96.479	-	253.957	$(\alpha_{outer}/\alpha_{net})$	93.01	129.08
3	96.691	0.22%	238.653	h_{CEEC}	108.62	113.47
4	96.691	0.00%	238.653	d_{edge_bite}	108.62	113.47

Table 38. Coefficients for Transient Model Using First-Order Polynomial Model for the Outer Glass Plate with High-Heat Mass Frame

No. of Terms	Coefficients, b_i			
2	8.7098	18.2034	0	0
3	8.1990	18.2034	34.6634	0
4	8.1990	18.2034	34.6634	0.0000

Fig. 157 shows the coefficient of multiple determination and sum of the squares of the residuals as a function of the number of terms added to the model. In general, the coefficient of multiple determination increases and the sum of the squares of the residuals decreases with the number of terms in the model increases. Fig. 158 shows the maximum under and over estimation stresses as a function of the number of terms added to the model. In general, both the maximum under and over estimation stresses decrease as the number of terms added to the model increases. Once the number of terms exceeds three, there is little increase in the fit of the polynomial model to the response data.

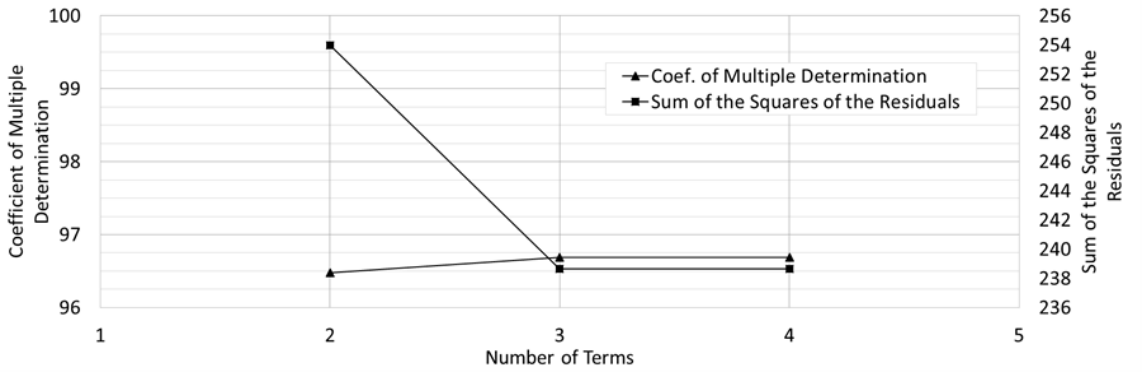

Fig. 157. Statistics of Transient Regression Analysis Using First-Order Polynomial Model for the Outer Glass Plate with High-Heat Mass Frame

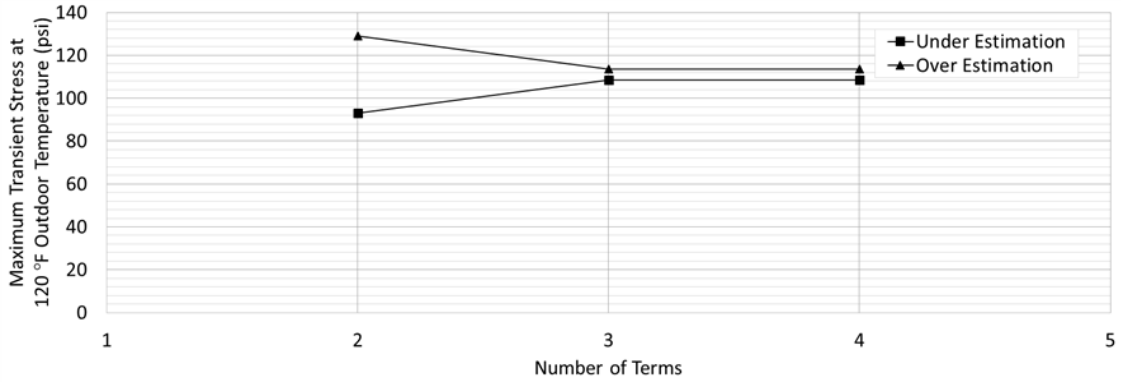

Fig. 158. Error in Stress Estimation of Transient Regression Analysis Using First-Order Polynomial Model for the Outer Glass Plate with High-Heat Mass Frame

Table 39 summarizes the combined steady-state and transient results from the regression analysis for the number of terms selected. From the regression analysis, the model for the steady-state response is given by Eq. (120) and the transient response is given by Eq. (121) below. These equations and their fit to the response data are shown in Figs. 159 and 160.

Table 39. Overall Summary of Regression Analysis Using First-Order Polynomial Model for the Outer Glass Plate with High-Heat Mass Frame

	No. of Terms	R^2	Maximum Stress (psi)	
			Under Estimation	Over Estimation
Steady-State	3	96.325	33.55	42.22
Transient	3	96.691	108.62	113.47
Total	6		142.17	155.68

$$m = 0.3094 - 7.0653 \cdot h_{CEEC} + 0.0308 \cdot d_{edge\_bite} \tag{120}$$

$$b = 8.1990 + 18.2034 \cdot \left(\frac{\alpha_{outer}}{\alpha_{net}}\right) + 34.6635 \cdot h_{CEEC} \tag{121}$$

Where all of the variables are as previously defined.

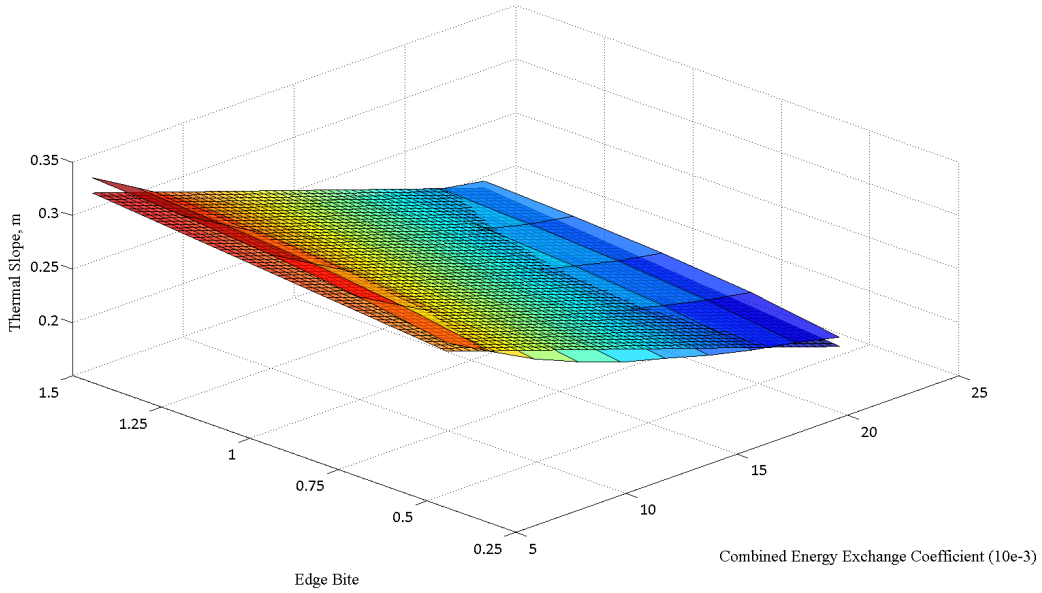

Fig. 159. Steady-State Regression Analysis Using First-Order Polynomial Model for the Outer Glass Plate with High-Heat Mass Frame

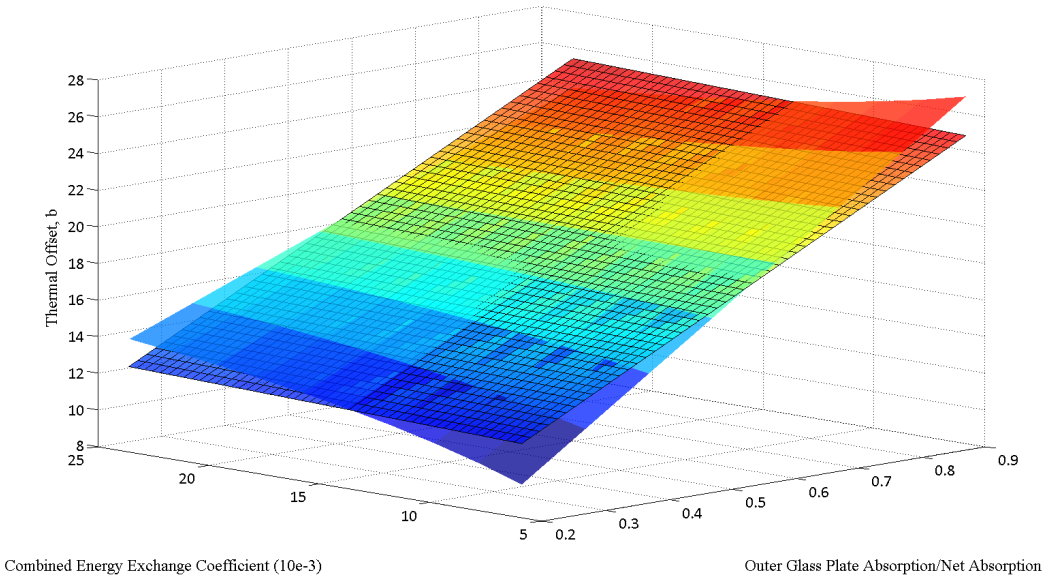

Fig. 160. Transient Regression Analysis Using First-Order Polynomial Model for the Outer Glass Plate with High-Heat Mass Frame

Inner Glass Plate with Perfectly Insulated Frame

Table 40 presents a summary of results from the steady-state regression analysis using the first-order polynomial model for the inner glass plate with a perfectly insulating frame. Included are the coefficient of multiple determination and sum of the squares of the residuals for the regression analysis in order of the terms added. In addition, the maximum under and over estimation stress are included. The fifth column of the table defines the rank order in which the terms were added to the model. The coefficients that are associated with each model are presented in Table 41.

Table 40. Summary of Steady-State Regression Analysis Using First-Order Polynomial Model for the Inner Glass Plate with Perfectly Insulated Frame

No. of Terms	R^2	Percent Difference	RSS	Term Added	Maximum Stress (psi)	
					Under Estimation	Over Estimation
1	-	-	-	Constant	-	-
2	95.946	-	0.039	h_{CEEC}	100.20	86.30
3	97.491	1.61%	0.024	d_{edge_bite}	76.32	46.61

Table 41. Coefficients for Steady-State Model Using First-Order Polynomial Model for the Inner Glass Plate with Perfectly Insulated Frame

No. of Terms	Coefficients, m_i		
2	-0.3939	8.5453	0
3	-0.3766	8.5453	-0.0173

Fig. 161 shows the coefficient of multiple determination and sum of the squares of the residuals as a function of the number of terms added to the model. In general, the coefficient of multiple determination increases and the sum of the squares of the residuals decreases as the number of terms in the model increase. Fig. 162 shows the maximum under and over estimation stresses as a function of the number of terms added to the model. In general, both the maximum under and over estimation stresses decrease as the number of terms added to the model increase.

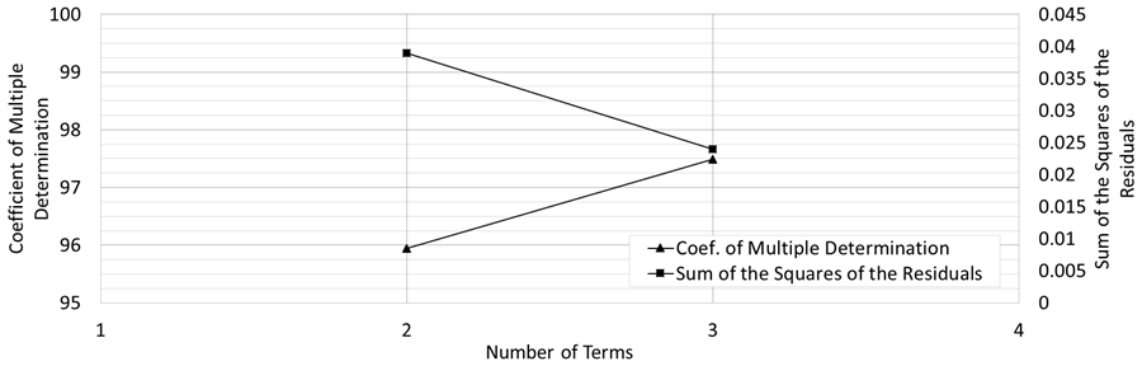

Fig. 161. Statistics of Steady-State Regression Analysis Using First-Order Polynomial Model for the Inner Glass Plate with Perfectly Insulated Frame

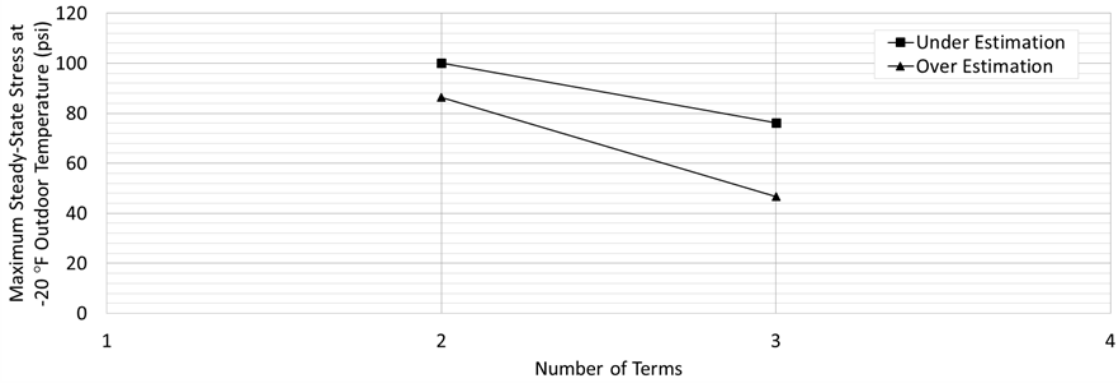

Fig. 162. Error in Stress Estimation of Steady-State Regression Analysis Using First-Order Polynomial Model for the Inner Glass Plate with Perfectly Insulated Frame

Table 42 presents a summary of results from the transient regression analysis using the first-order polynomial model for the inner glass plate with a perfectly insulating frame. Included are the coefficient of multiple determination and sum of the squares of the residuals for the regression analysis in rank order of the terms added and the maximum under and over estimation. The fifth column of the table defines the order in which each term was added to the model. The coefficients that are associated with each model are presented in Table 43.

Table 42. Summary of Transient Regression Analysis Using First-Order Polynomial Model for the Inner Glass Plate with Perfectly Insulated Frame

No. of Terms	R^2	Percent Difference	RSS	Term Added	Maximum Stress (psi)	
					Under Estimation	Over Estimation
1	-	-	-	Constant	-	-
2	75.787	-	3144.333	$(\alpha_{outer}/\alpha_{net})$	387.84	335.68
3	95.881	26.51%	404.984	d_{edge_bite}	199.24	147.08
4	97.095	1.27%	377.296	h_{CEEC}	178.24	167.20

Table 43. Coefficients for Transient Model Using First-Order Polynomial Model for the Inner Glass Plate with Perfectly Insulated Frame

No. of Terms	Coefficients, b_i			
2	21.5723	-21.6485	0	0
3	14.1705	-21.6485	7.4018	0
4	14.8575	-21.6485	7.4018	-46.6239

Fig. 163 shows the coefficient of multiple determination and sum of the squares of the residuals as a function of the number of terms added to the model. In general, the coefficient of multiple determination increases and the sum of the squares of the residuals decreases with the number of terms in the model increases. Fig. 164 shows the maximum under and over estimation stresses as a function of the number of terms added to the model. In general, both the maximum under and over estimation stresses decrease as the number of terms added to the model increases.

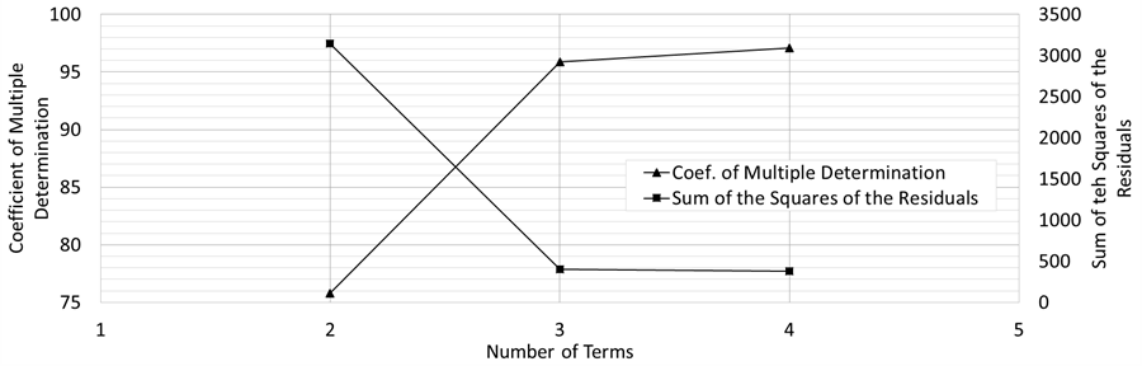

Fig. 163. Statistics of Transient Regression Analysis Using First-Order Polynomial Model for the Inner Glass Plate with Perfectly Insulated Frame

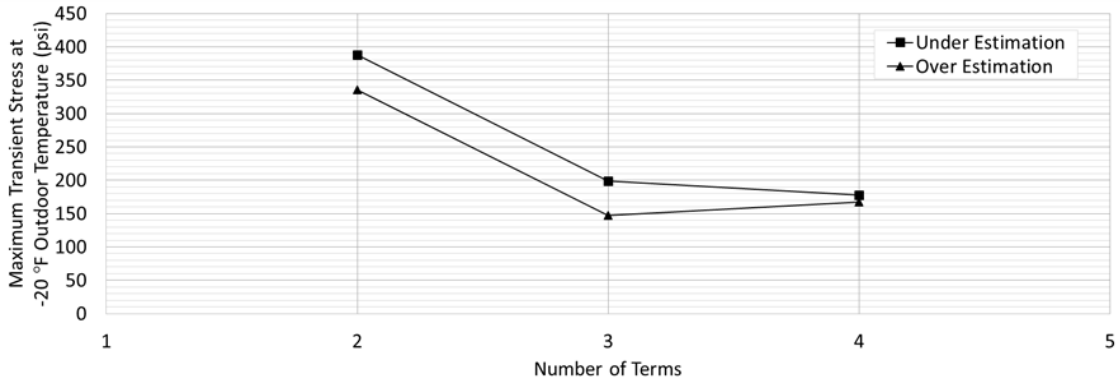

Fig. 164. Error in Stress Estimation of Transient Regression Analysis Using First-Order Polynomial Model for the Inner Glass Plate with Perfectly Insulated Frame

Table 44 summarizes the combined steady-state and transient results from the regression analysis for the number of terms selected. From the regression analysis, the model for the steady-state response is given by Eq. (122) and the transient response is given by Eq. (123) below. These equations and their fit to the response data are shown in Figs. 165 and 166.

Table 44. Overall Summary of Regression Analysis Using First-Order Polynomial Model for the Inner Glass Plate with Perfectly Insulated Frame

	No. of Terms	R^2	Maximum Stress (psi)	
			Under Estimation	Over Estimation
Steady-State	3	97.491	76.32	46.61
Transient	4	97.095	178.24	167.20
Total	7		254.55	213.81

$$m = -0.3766 + 8.5453 \cdot h_{CEEC} - 0.0173 \cdot d_{edge\_bite} \tag{122}$$

$$b = 14.8575 - 21.6485 \cdot \left(\frac{\alpha_{outer}}{\alpha_{net}}\right) + 7.4018 \cdot d_{edge\_bite} - 46.6239 \cdot h_{CEEC} \tag{123}$$

Where all of the variables are as previously defined.

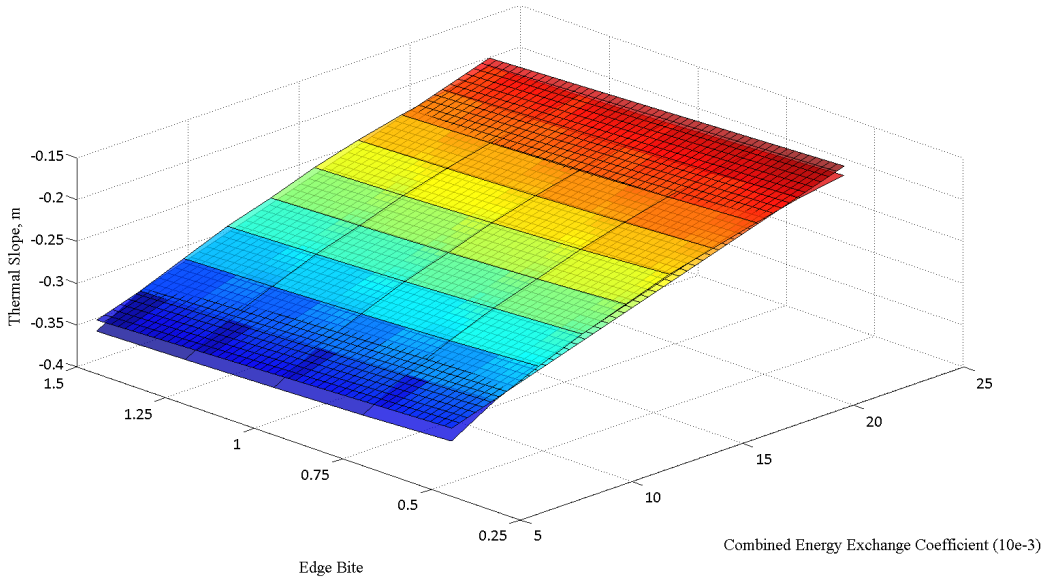

Fig. 165. Steady-State Regression Analysis Using First-Order Polynomial Model for the Inner Glass Plate with Perfectly Insulated Frame

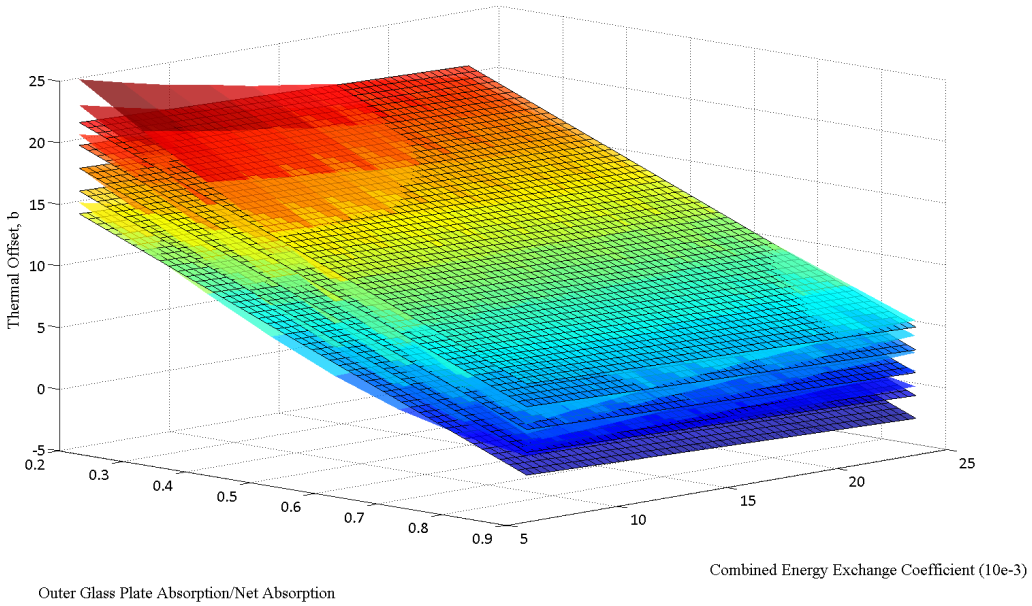

Fig. 166. Transient Regression Analysis Using First-Order Polynomial Model for the Inner Glass Plate with Perfectly Insulated Frame

Inner Glass Plate with High-Heat Mass Frame

Table 45 presents a summary of results from the steady-state regression analysis using the first-order polynomial model for the inner glass plate with a high-heat mass frame. Included are the coefficient of multiple determination and sum of the squares of the residuals for the regression analysis in order of the terms added. In addition, the maximum under and over estimation stress are included. The fifth column of the table defines the rank order in which the terms were added to the model. The coefficients that are associated with each model are presented in Table 46.

Table 45. Summary of Steady-State Regression Analysis Using First-Order Polynomial Model for the Inner Glass Plate with High-Heat Mass Frame

No. of Terms	R^2	Percent Difference	RSS	Term Added	Maximum Stress (psi)	
					Under Estimation	Over Estimation
1	-	-	-	Constant	-	-
2	95.946	-	0.039	h_{CEEC}	100.20	86.30
3	97.491	1.61%	0.024	d_{edge_bite}	76.32	46.61

Table 46. Coefficients for Steady-State Model Using First-Order Polynomial Model for the Inner Glass Plate with High-Heat Mass Frame

No. of Terms	Coefficients, m_i		
2	-0.3939	8.5453	0
3	-0.3766	8.5453	-0.0173

Fig. 167 shows the coefficient of multiple determination and sum of the squares of the residuals as a function of the number of terms added to the model. In general, the coefficient of multiple determination increases and the sum of the squares of the residuals decreases as the number of terms in the model increase. Fig. 168 shows the maximum under and over estimation stresses as a function of the number of terms added to the model. In general, both the maximum under and over estimation stresses decrease as the number of terms added to the model increases.

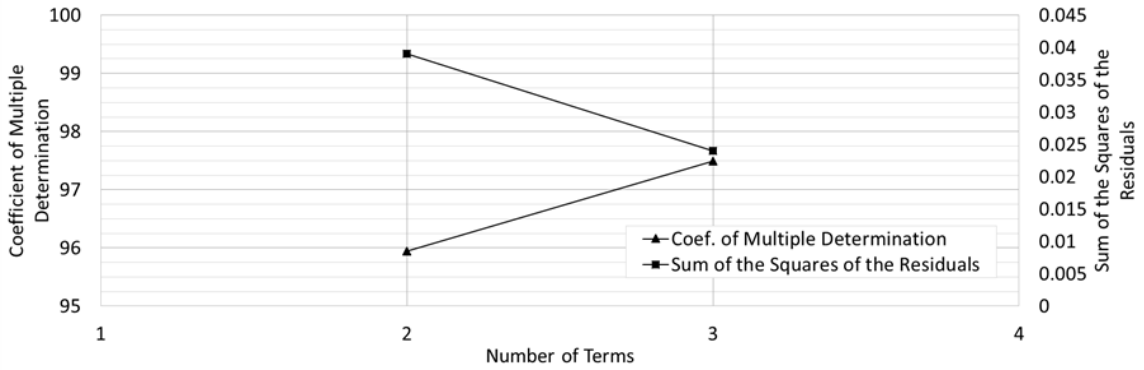

Fig. 167. Statistics of Steady-State Regression Analysis Using First-Order Polynomial Model for the Inner Glass Plate with High-Heat Mass Frame

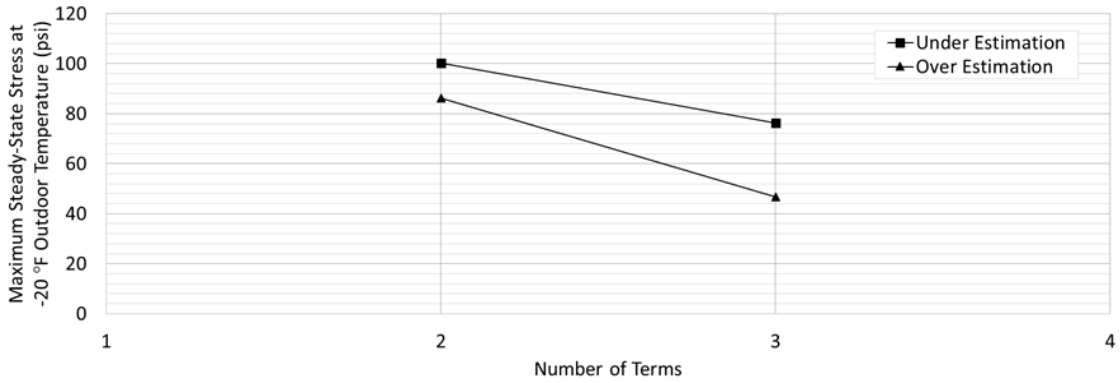

Fig. 168. Error in Stress Estimation of Steady-State Regression Analysis Using First-Order Polynomial Model for the Inner Glass Plate with High-Heat Mass Frame

Table 47 presents a summary of results from the transient regression analysis using the first-order polynomial model for the inner glass plate with a high-heat mass frame. Included are the coefficient of multiple determination and sum of the squares of the residuals for the regression analysis in rank order of the terms added and the maximum under and over estimation. The fifth column of the table defines the order in which each term was added to the model. The coefficients that are associated with each model are presented in Table 48.

Table 47. Summary of Transient Regression Analysis Using First-Order Polynomial Model for the Inner Glass Plate with High-Heat Mass Frame

No. of Terms	R^2	Percent Difference	RSS	Term Added	Maximum Stress (psi)	
					Under Estimation	Over Estimation
1	-	-	-	Constant	-	-
2	96.777	-	602.738	$(\alpha_{outer}/\alpha_{net})$	195.63	146.51
3	96.932	0.16%	573.89	h_{CEEC}	174.18	167.96
4	96.932	0.00%	573.89	d_{edge_bite}	174.18	167.96

Table 48. Coefficients for Transient Model Using First-Order Polynomial Model for the Inner Glass Plate with High-Heat Mass Frame

No. of Terms	Coefficients, b_i			
2	38.1978	-29.3585	0	0
3	38.8991	-29.3585	-47.5907	0
4	38.8991	-29.3585	-47.5907	0.0000

Fig. 169 shows the coefficient of multiple determination and sum of the squares of the residuals as a function of the number of terms added to the model. In general, the coefficient of multiple determination increases and the sum of the squares of the residuals decreases with the number of terms in the model increases. Fig. 170 shows the maximum under and over estimation stresses as a function of the number of terms added to the model. In general, both the maximum under and over estimation stresses decrease as the number of terms added to the model increases. Once the number of terms exceeds three, there is little increase in the fit of the polynomial model to the response data.

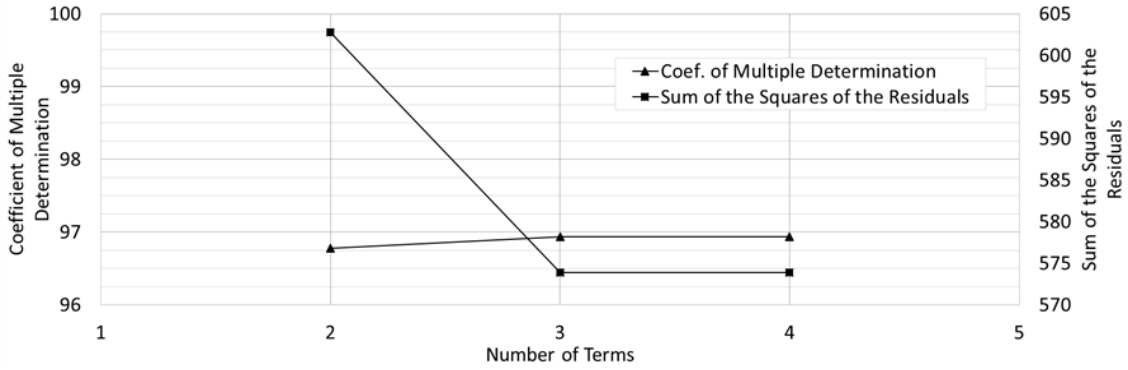

Fig. 169. Statistics of Transient Regression Analysis Using First-Order Polynomial Model for the Inner Glass Plate with High-Heat Mass Frame

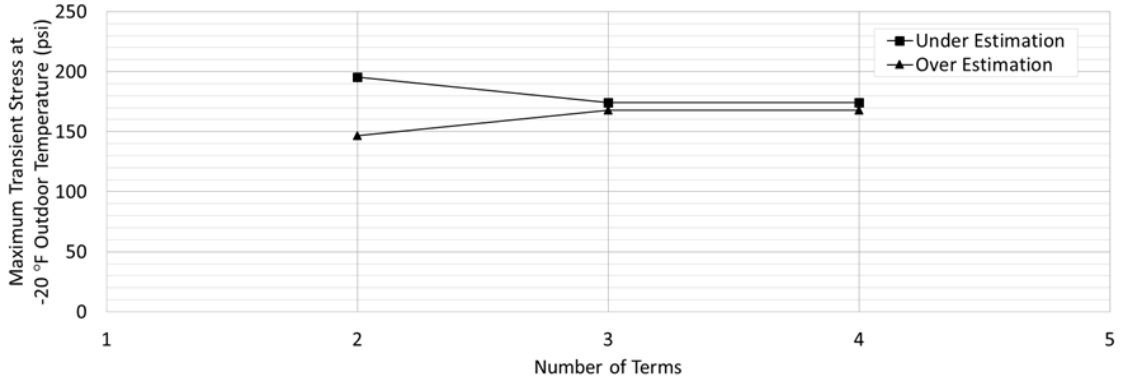

Fig. 170. Error in Stress Estimation of Transient Regression Analysis Using First-Order Polynomial Model for the Inner Glass Plate with High-Heat Mass Frame

Table 49 summarizes the combined steady-state and transient results from the regression analysis for the number of terms selected. From the regression analysis, the model for the steady-state response is given by Eq. (124) and the transient response is given by Eq. (125) below. These equations and their fit to the response data are shown in Figs. 171 and 172.

Table 49. Overall Summary of Regression Analysis Using First-Order Polynomial Model for the Inner Glass Plate with High-Heat Mass Frame

	No. of Terms	R^2	Maximum Stress (psi)	
			Under Estimation	Over Estimation
Steady-State	3	97.491	76.32	46.61
Transient	3	96.932	174.18	167.96
Total	6		250.50	214.56

$$m = -0.3766 + 8.5453 * h_{CEEC} - 0.0173 * d_{edge\_bite} \quad (124)$$

$$b = 38.8991 - 29.3585 * \left(\frac{\alpha_{outer}}{\alpha_{net}}\right) - 47.5907 * h_{CEEC} \quad (125)$$

Where all of the variables are as previously defined.

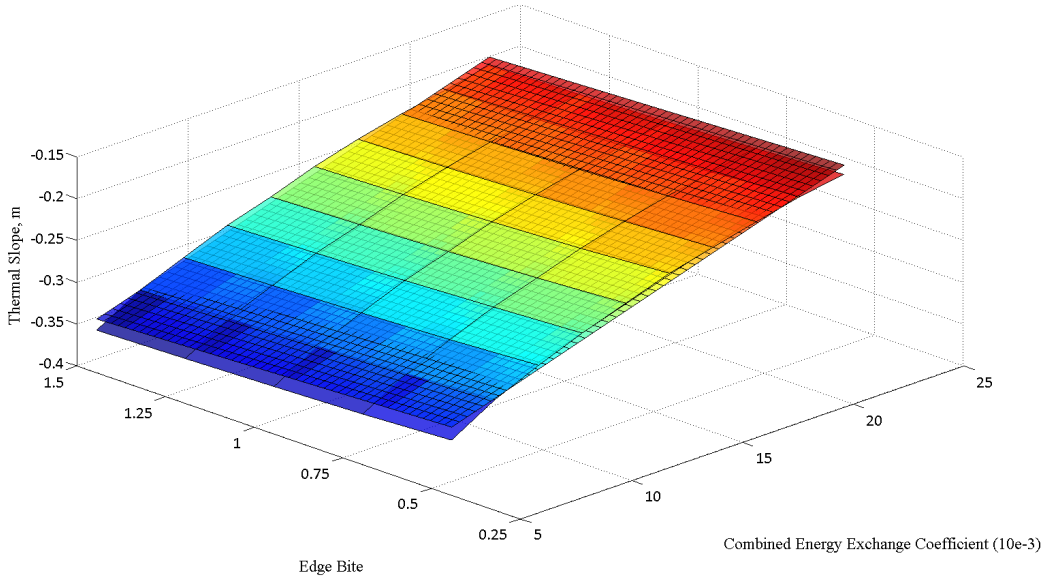

Fig. 171. Steady-State Regression Analysis Using First-Order Polynomial Model for the Inner Glass Plate with High-Heat Mass Frame

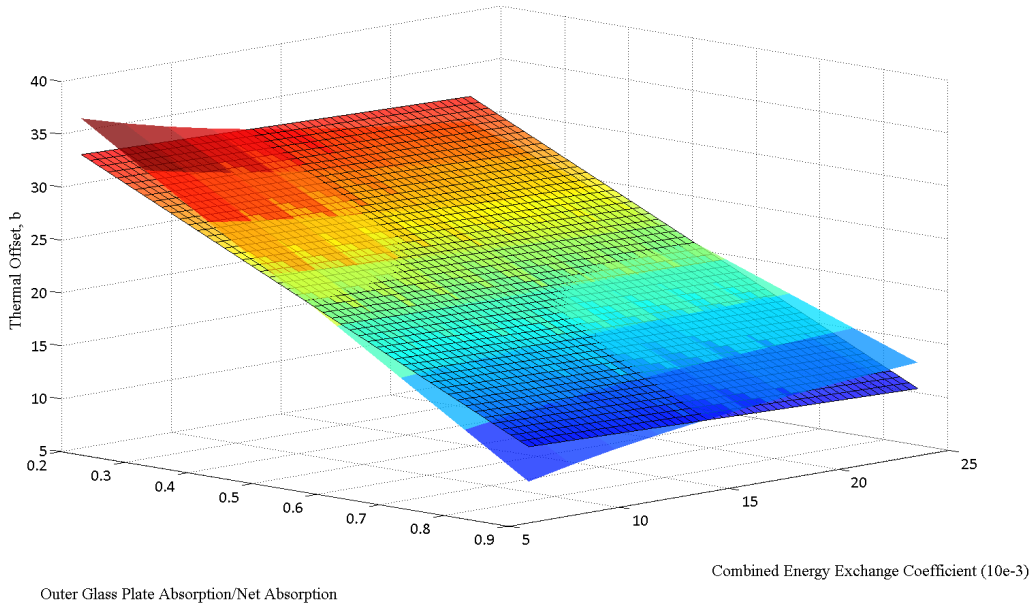

Fig. 172. Transient Regression Analysis Using First-Order Polynomial Model for the Inner Glass Plate with High-Heat Mass Frame

Second-Order Polynomial Model

This section presents the results of the regression analyses discussed previously to the steady-state and transient data using the second-order polynomial models. The hypothesized polynomial models used for the steady-state and transient responses were given by Eqs. (105) and (117), respectively. Again, the maximum stresses were evaluated at an indoor/outdoor temperature difference of 50°F for the outer glass plate and -90°F for the inner glass plate.

Outer Glass Plate with Perfectly Insulated Frame

Table 50 presents a summary of results from the steady-state regression analysis using the second-order polynomial model for the outer glass plate with a perfectly insulated frame. Included are the coefficient of multiple determination and sum of the squares of the residuals for the regression analysis in order of the terms added. In addition, the maximum under and over estimation stress are included. The fifth column of the table defines the rank order in which the terms were added to the model. The coefficients that are associated with each model are presented in Table 51.

Table 50. Summary of Steady-State Regression Analysis Using Second-Order Polynomial Model for the Outer Glass Plate with Perfectly Insulated Frame

No. of Terms	R^2	Percent Difference	RSS	Term Added	Maximum Stress (psi)	
					Under Estimation	Over Estimation
1	-	-	-	Constant	-	-
2	89.653	-	0.073	h_{CEEC}	70.36	75.51
3	96.325	7.44%	0.026	d_{edge_bite}	33.55	42.22
4	99.492	3.29%	0.004	h_{CEEC}^2	15.49	12.09
5	99.785	0.29%	0.002	$d_{edge\_bite}^2$	8.55	11.73
6	99.85	0.07%	0.001	$h_{CEEC} \cdot d_{edge\_bite}$	8.41	6.76

Table 51. Coefficients for Steady-State Model Using Second-Order Polynomial Model for the Outer Glass Plate with Perfectly Insulated Frame

No. of Terms	Coefficients, m_i					
2	0.3402	-7.0653	0	0	0	0
3	0.3094	-7.0653	0.0308	0	0	0
4	0.3589	-14.9387	0.0308	267.1727	0	0
5	0.3398	-14.9387	0.0744	267.1727	-0.0218	0
6	0.3319	-14.4008	0.0823	267.1727	-0.0218	-0.5379

Fig. 173 shows the coefficient of multiple determination and sum of the squares of the residuals as a function of the number of terms added to the model. In general, the coefficient of multiple determination increases and the sum of the squares of the residuals decreases as the number of terms in the model increase. Fig. 174 shows the percent change in the coefficient of determination as terms are added to the model. Fig. 175 shows the maximum under and over estimation stresses as a function of the number of terms added to the model. In general, both the maximum under and over estimation stresses decrease as the number of terms added to the model increase.

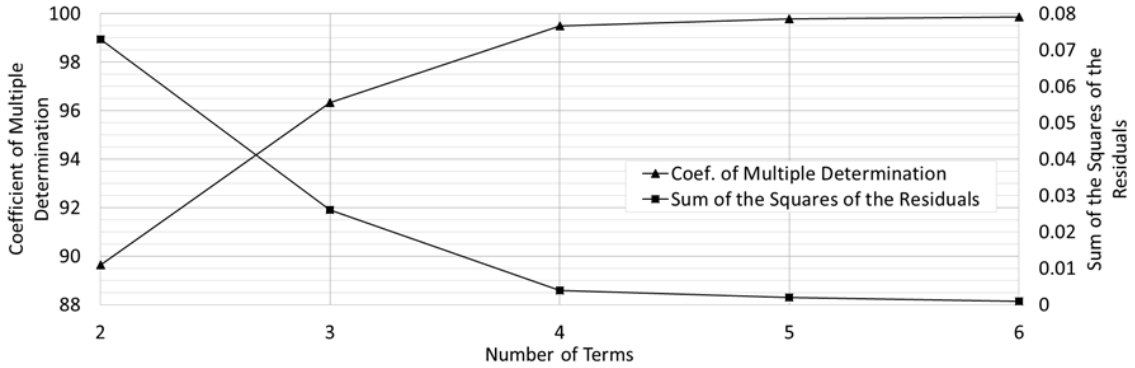

Fig. 173. Statistics of Steady-State Regression Analysis Using Second-Order Polynomial Model for the Outer Glass Plate with Perfectly Insulated Frame

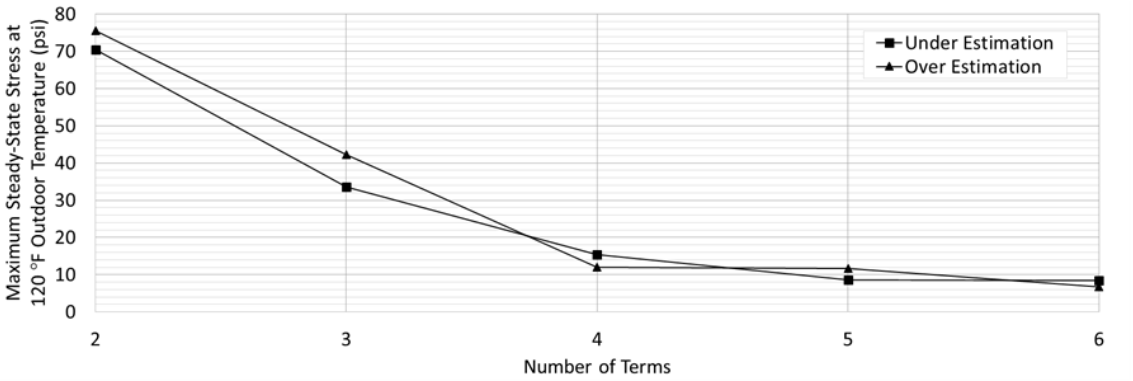

Fig. 174. Percent Difference vs. Number of Terms for Steady-State Regression Analysis Using Second-Order Polynomial Model for the Outer Glass Plate with Perfectly Insulated Frame

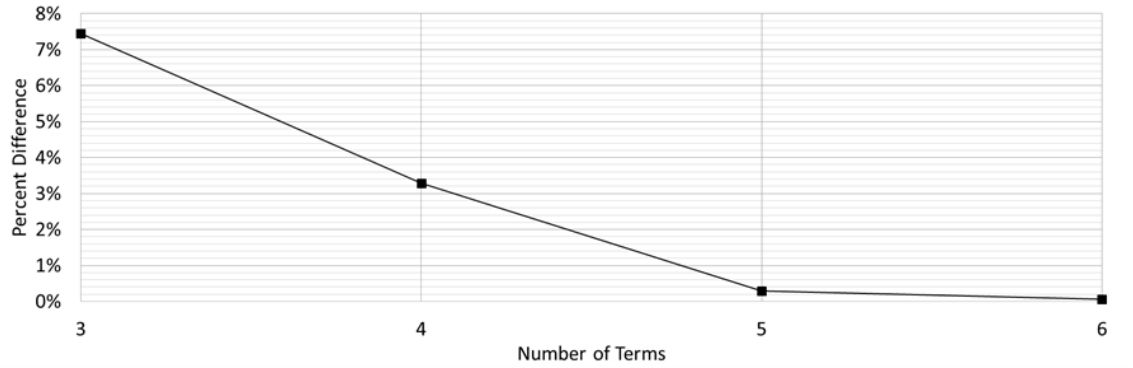

Fig. 175. Error in Stress Estimation of Steady-State Regression Analysis Using Second-Order Polynomial Model for the Outer Glass Plate with Perfectly Insulated Frame

Table 52 presents a summary of results from the transient regression analysis using the second-order polynomial model for the outer glass plate with a perfectly insulating frame. Included are the coefficient of multiple determination and sum of the squares of the residuals for the regression analysis in rank order of the terms added and the maximum under and over estimation. The fifth column of the table defines the order in which each term was added to the model. The coefficients that are associated with each model are presented in Table 53.

Table 52. Summary of Transient Regression Analysis Using Second-Order Polynomial Model for the Outer Glass Plate with Perfectly Insulated Frame

No. of Terms	R^2	Percent Difference	RSS	Term Added	Maximum Stress (psi)	
					Under Estimation	Over Estimation
1	-	-	-	Constant	-	-
2	93.368	-	485.803	$d_{edge\_bite} \cdot (\alpha_{outer}/\alpha_{net})$	208.24	147.23
3	97.1	4.00%	212.446	$(\alpha_{outer}/\alpha_{net})$	114.79	124.53
4	98.541	1.48%	106.881	d_{edge_bite}	100.52	86.57
5	98.986	0.45%	74.261	$h_{CEEC} \cdot (\alpha_{outer}/\alpha_{net})$	66.08	71.05
6	99.6	0.62%	29.305	h_{CEEC}	50.00	29.86
7	99.788	0.19%	15.5	$d_{edge\_bite}^2$	61.32	18.54
8	99.836	0.05%	12.001	$(\alpha_{outer}/\alpha_{net})^2$	54.04	23.15
9	99.842	0.01%	11.556	$h_{CEEC} \cdot d_{edge\_bite}$	50.27	24.67
10	99.843	0.00%	11.53	h_{CEEC}^2	49.59	25.09

Table 53. Coefficients for Transient Model Using Second-Order Polynomial Model for the Outer Glass Plate with Perfectly Insulated Frame

No. of Terms	Coefficients, b_i									
2	1.2815	13.2855	0	0	0	0	0	0	0	0
3	-0.0615	10.3966	5.3308	0	0	0	0	0	0	0
4	-3.8399	4.5427	11.1847	3.7784	0	0	0	0	0	0
5	-3.8399	4.5427	12.4362	3.7784	-84.9355	0	0	0	0	0
6	-6.1162	4.5427	15.9629	3.7784	-324.2811	154.4867	0	0	0	0
7	-7.6705	4.5427	15.9629	7.3310	-324.2811	154.4867	-1.7763	0	0	0
8	-7.1603	4.5427	13.7178	7.3310	-324.2811	154.4867	-1.7763	2.0410	0	0
9	-6.9139	4.5427	13.7178	7.0847	-324.2811	137.7658	-1.7763	2.0410	16.7209	0
10	-6.8603	4.5427	13.7178	7.0847	-324.2811	129.2407	-1.7763	2.0410	16.7209	289.2860

Fig. 176 shows the coefficient of multiple determination and sum of the squares of the residuals as a function of the number of terms added to the model. In general, the coefficient of multiple determination increases and the sum of the squares of the residuals decreases with the number of terms in the model increases. Fig. 177 shows the percent change in the coefficient of determination as terms are added to the model. Fig. 178 shows the maximum under and over estimation stresses as a function of the number of terms added to the model. In general, both the maximum under and over estimation stresses decrease as the number of terms added to the model increases. Once the number

of terms exceeds six, there is little increase in the fit of the polynomial model to the response data.

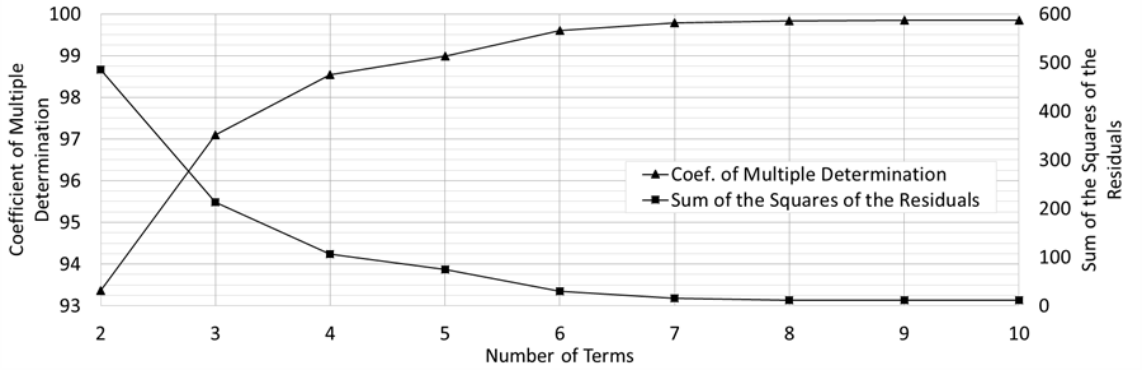

Fig. 176. Statistics of Transient Regression Analysis Using Second-Order Polynomial Model for the Outer Glass Plate with Perfectly Insulated Frame

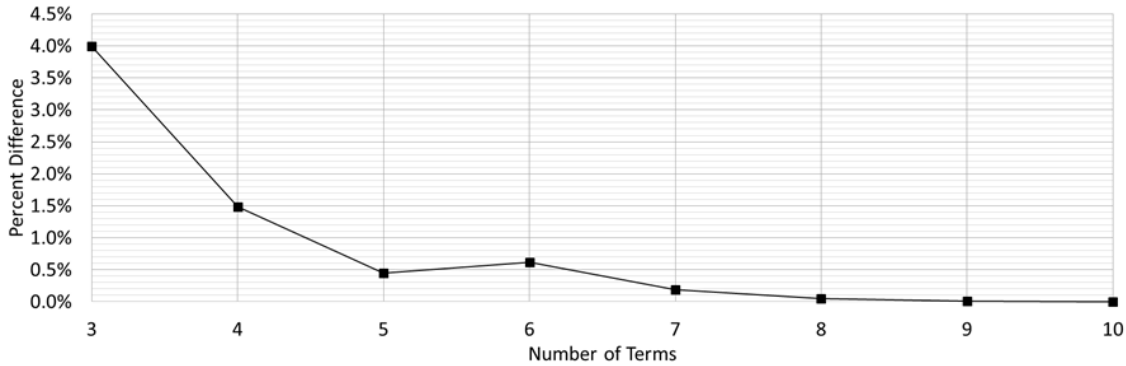

Fig. 177. Percent Difference vs. Number of Terms for Transient Regression Analysis Using Second-Order Polynomial Model for the Outer Glass Plate with Perfectly Insulated Frame

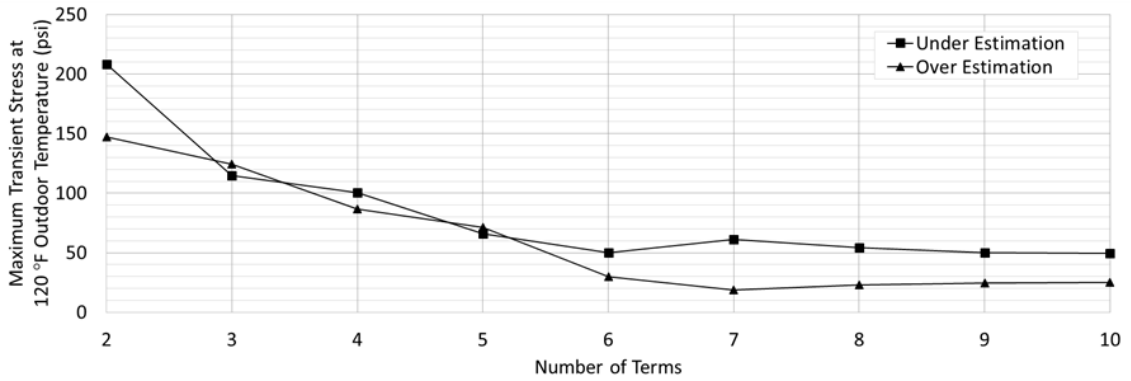

Fig. 178. Error in Stress Estimation of Transient Regression Analysis Using Second-Order Polynomial Model for the Outer Glass Plate with Perfectly Insulated Frame

Table 54 summarizes the combined steady-state and transient results from the regression analysis for the number of terms selected. From the regression analysis, the model for the steady-state response is given by Eq. (126), and the transient response is given by Eq. (127) below. These equations and their fit to the response data are shown in Figs. 179 and 180.

Table 54. Overall Summary of Regression Analysis Using Second-Order Polynomial Model for the Outer Glass Plate with Perfectly Insulated Frame

	No. of Terms	R^2	Maximum Stress (psi)	
			Under Estimation	Over Estimation
Steady-State	5	99.785	8.55	11.73
Transient	6	99.6	50.00	29.86
Total	11		58.55	41.59

$$m = 0.3398 - 14.9387 * h_{CEEC} + 0.0744 * d_{edge\_bite} + 267.1727 * {h_{CEEC}}^2 - 0.0218 * {d_{edge\_bite}}^2 \quad (126)$$

$$b = -6.1162 + 4.5427 * d_{edge\_bite} * \left(\frac{\alpha_{outer}}{\alpha_{net}}\right) + 15.9629 * \left(\frac{\alpha_{outer}}{\alpha_{net}}\right) + 3.7784 * d_{edge\_bite} - 324.2811 * h_{CEEC} * \left(\frac{\alpha_{outer}}{\alpha_{net}}\right) + 154.4867 * h_{CEEC} \quad (127)$$

Where all of the variables are as previously defined.

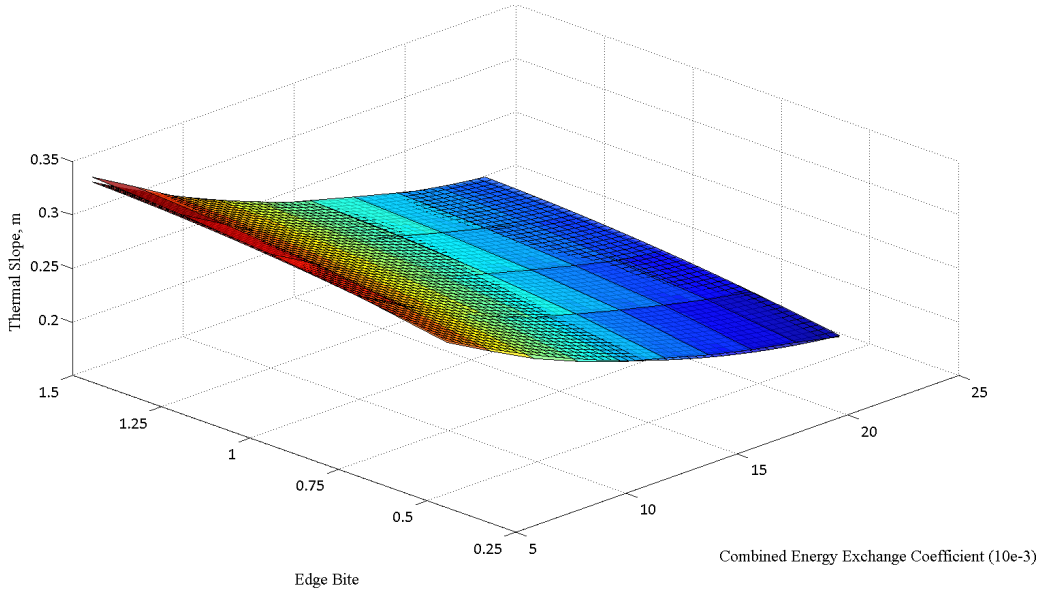

Fig. 179. Steady-State Regression Analysis Using Second-Order Polynomial Model for the Outer Glass Plate with Perfectly Insulated Frame

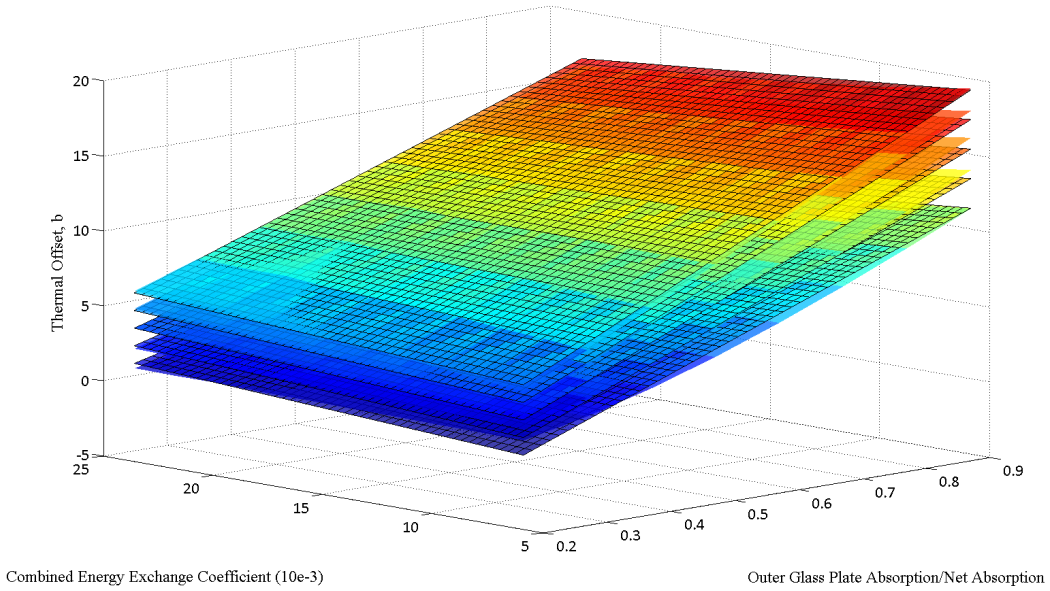

Fig. 180. Transient Regression Analysis Using Second-Order Polynomial Model for the Outer Glass Plate with Perfectly Insulated Frame

Outer Glass Plate with High-Heat Mass Frame

Table 55 presents a summary of results from the steady-state regression analysis using the second-order polynomial model for the outer glass plate with a high-heat mass frame. Included are the coefficient of multiple determination and sum of the squares of the residuals for the regression analysis in order of the terms added. In addition, the maximum under and over estimation stresses are included. The fifth column of the table defines the rank order in which the terms were added to the model. The coefficients that are associated with each model are presented in Table 56.

Table 55. Summary of Steady-State Regression Analysis Using Second-Order Polynomial Model for the Outer Glass Plate with High-Heat Mass Frame

No. of Terms	R^2	Percent Difference	RSS	Term Added	Maximum Stress (psi)	
					Under Estimation	Over Estimation
1	-	-	-	Constant	-	-
2	89.653	-	0.073	h_{CEEC}	70.36	75.51
3	96.325	7.44%	0.026	d_{edge_bite}	33.55	42.22
4	99.492	3.29%	0.004	h_{CEEC}^2	15.49	12.09
5	99.785	0.29%	0.002	$d_{edge\_bite}^2$	8.55	11.73
6	99.85	0.07%	0.001	$h_{CEEC} \cdot d_{edge\_bite}$	8.41	6.76

Table 56. Coefficients for Steady-State Model Using Second-Order Polynomial Model for the Outer Glass Plate with High-Heat Mass Frame

No. of Terms	Coefficients, m_i					
2	0.3402	-7.0653	0	0	0	0
3	0.3094	-7.0653	0.0308	0	0	0
4	0.3589	-14.9387	0.0308	267.1727	0	0
5	0.3398	-14.9387	0.0744	267.1727	-0.0218	0
6	0.3319	-14.4008	0.0823	267.1727	-0.0218	-0.5379

Fig. 181 shows the coefficient of multiple determination and sum of the squares of the residuals as a function of the number of terms added to the model. In general, the coefficient of multiple determination increases and the sum of the squares of the residuals decreases as the number of terms in the model increase. Fig. 182 shows the percent change in the coefficient of determination as terms are added to the model. Fig. 183 shows the maximum under and over estimation stresses as a function of the number of terms added to the model. In general, both the maximum under and over estimation stresses decrease as the number of terms added to the model increases.

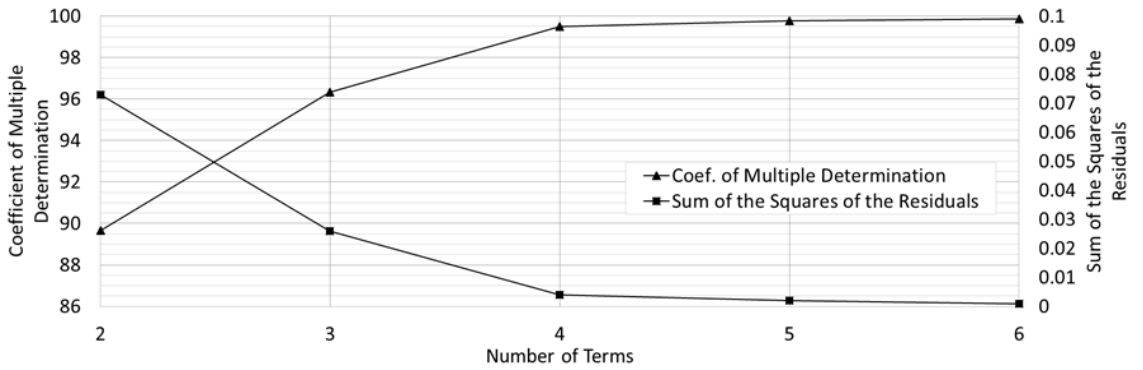

Fig. 181. Statistics of Steady-State Regression Analysis Using Second-Order Polynomial Model for the Outer Glass Plate with High-Heat Mass Frame

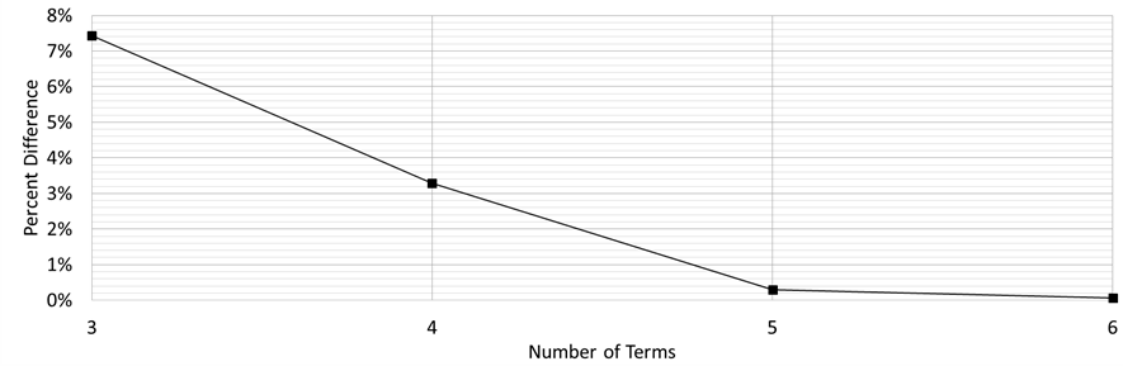

Fig. 182. Percent Difference vs. Number of Terms for Steady-State Regression Analysis Using Second-Order Polynomial Model for the Outer Glass Plate with High-Heat Mass Frame

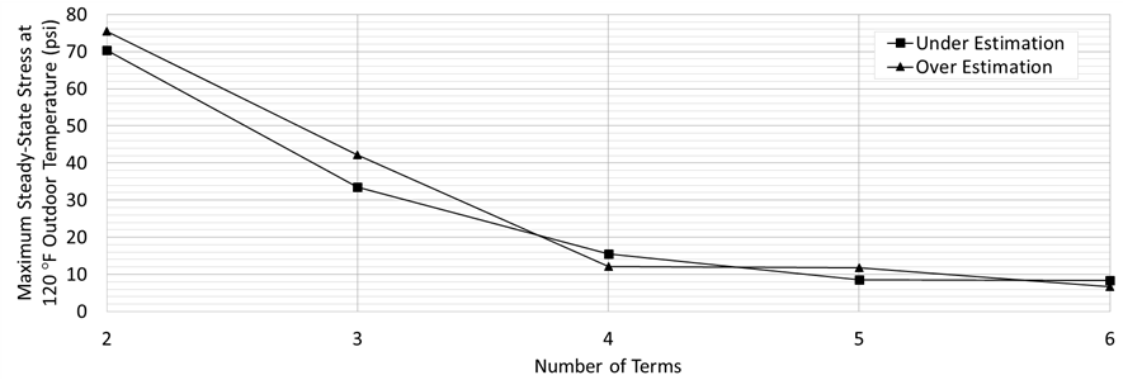

Fig. 183. Error in Stress Estimation of Steady-State Regression Analysis Using Second-Order Polynomial Model for the Outer Glass Plate with High-Heat Mass Frame

Table 57 presents a summary of results from the transient regression analysis using the second-order polynomial model for the outer glass plate with a high-heat mass frame. Included are the coefficient of multiple determination and sum of the squares of the residuals for the regression analysis in rank order of the terms added and the maximum under and over estimation. The fifth column of the table defines the order in which each term was added to the model. The coefficients that are associated with each model are presented in Table 58.

Table 57. Summary of Transient Regression Analysis Using Second-Order Polynomial Model for the Outer Glass Plate with High-Heat Mass Frame

No. of Terms	R^2	Percent Difference	RSS	Term Added	Maximum Stress (psi)	
					Under Estimation	Over Estimation
1	-	-	-	Constant	-	-
2	96.479	-	253.957	$(\alpha_{outer}/\alpha_{net})$	93.01	129.08
3	96.691	0.22%	238.653	h_{CEEC}	108.62	113.47
4	99.91	3.33%	6.511	$h_{CEEC}\cdot(\alpha_{outer}/\alpha_{net})$	15.72	20.56
5	99.914	0.00%	6.235	h_{CEEC}^2	17.93	18.35
6	99.914	0.00%	6.235	$(\alpha_{outer}/\alpha_{net})^2$	17.91	18.37
7	99.914	0.00%	6.235	$d_{edge\_bite}^2$	17.91	18.37
8	99.914	0.00%	6.235	d_{edge_bite}	17.91	18.37
9	99.914	0.00%	6.235	$h_{CEEC}\cdot d_{edge\_bite}$	17.91	18.37
10	99.914	0.00%	6.235	$h_{CEEC}\cdot(\alpha_{outer}/\alpha_{net})$	17.91	18.37

Table 58. Coefficients for Transient Model Using Second-Order Polynomial Model for the Outer Glass Plate with High-Heat Mass Frame

No. of Terms	Coefficients, b_i									
2	8.7098	18.2034	0	0	0	0	0	0	0	0
3	8.1990	18.2034	34.6634	0	0	0	0	0	0	0
4	3.4241	26.8851	358.7196	-589.1930	0	0	0	0	0	0
5	3.2504	26.8851	386.3467	-589.1930	-937.4817	0	0	0	0	0
6	3.2520	26.8779	386.3467	-589.1930	-937.4817	0.0065	0	0	0	0
7	3.2520	26.8779	386.3467	-589.1930	-937.4817	0.0065	0.0000	0	0	0
8	3.2521	26.8779	386.3467	-589.1930	-937.4817	0.0065	0.0000	-0.0001	0	0
9	3.2521	26.8779	386.3461	-589.1930	-937.4817	0.0065	0.0000	-0.0001	0.0007	0
10	3.2521	26.8779	386.3461	-589.1930	-937.4817	0.0065	0.0000	-0.0001	0.0007	0.0000

Fig. 184 shows the coefficient of multiple determination and sum of the squares of the residuals as a function of the number of terms added to the model. In general, the coefficient of multiple determination increases and the sum of the squares of the residuals decreases with the number of terms in the model increases. Fig. 185 shows the percent change in the coefficient of determination as terms are added to the model. Fig. 186 shows the maximum under and over estimation stresses as a function of the number of terms added to the model. In general, both the maximum under and over estimation stresses decrease as the number of terms added to the model increases. Once the number of terms exceeds four, there is little increase in the fit of the polynomial model to the response data.

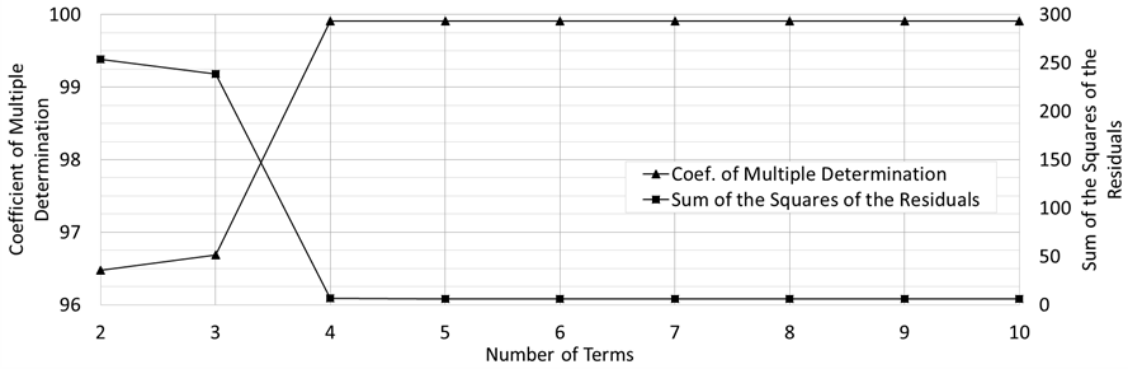

Fig. 184. Statistics of Transient Regression Analysis Using Second-Order Polynomial Model for the Outer Glass Plate with High-Heat Mass Frame

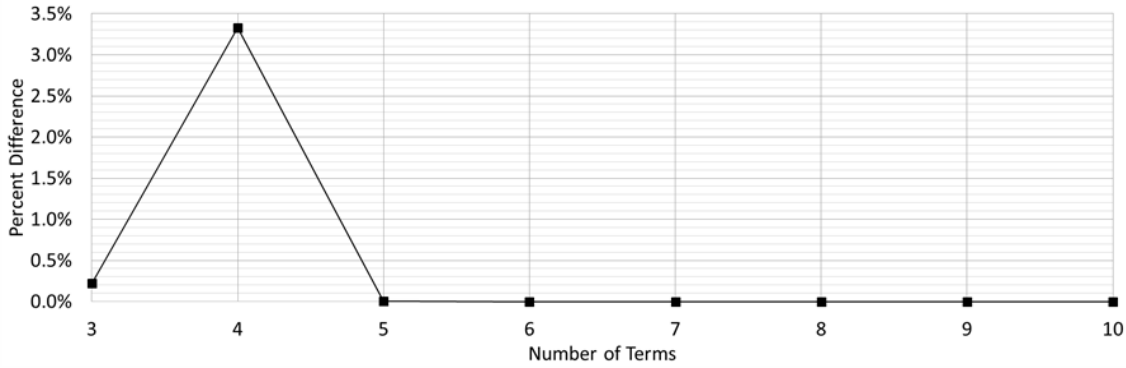

Fig. 185. Percent Difference vs. Number of Terms for Transient Regression Analysis Using Second-Order Polynomial Model for the Outer Glass Plate with High-Heat Mass Frame

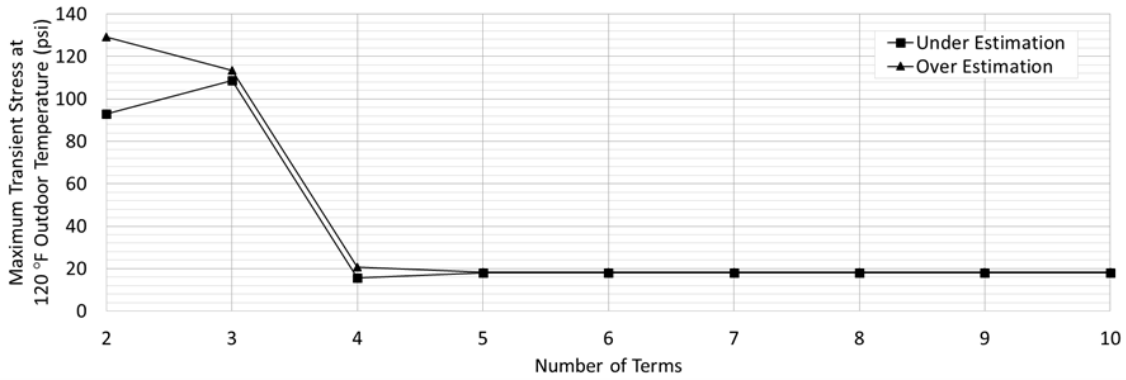

Fig. 186. Error in Stress Estimation of Transient Regression Analysis Using Second-Order Polynomial Model for the Outer Glass Plate with High-Heat Mass Frame

Table 59 summarizes the combined steady-state and transient results from the regression analysis for the number of terms selected. From the regression analysis, the model for the steady-state response is given by Eq. (128) and the transient response is given by Eq. (129) below. These equations and their fit to the response data are shown in Figs. 187 and 188.

Table 59. Overall Summary of Regression Analysis Using Second-Order Polynomial Model for the Outer Glass Plate with High-Heat Mass Frame

	No. of Terms	R^2	Maximum Stress (psi)	
			Under Estimation	Over Estimation
Steady-State	3	96.325	33.55	42.22
Transient	4	99.91	15.72	20.56
Total	7		49.27	62.77

$$m = 0.3094 - 7.0653 * h_{CEEC} + 0.0308 * d_{edge\_bite} \quad (128)$$

$$b = 3.4241 + 26.8851 * \left(\frac{\alpha_{outer}}{\alpha_{net}}\right) + 358.7196 * h_{CEEC} - 589.1930 * h_{CEEC} * \left(\frac{\alpha_{outer}}{\alpha_{net}}\right) \quad (129)$$

Where all of the variables are as previously defined.

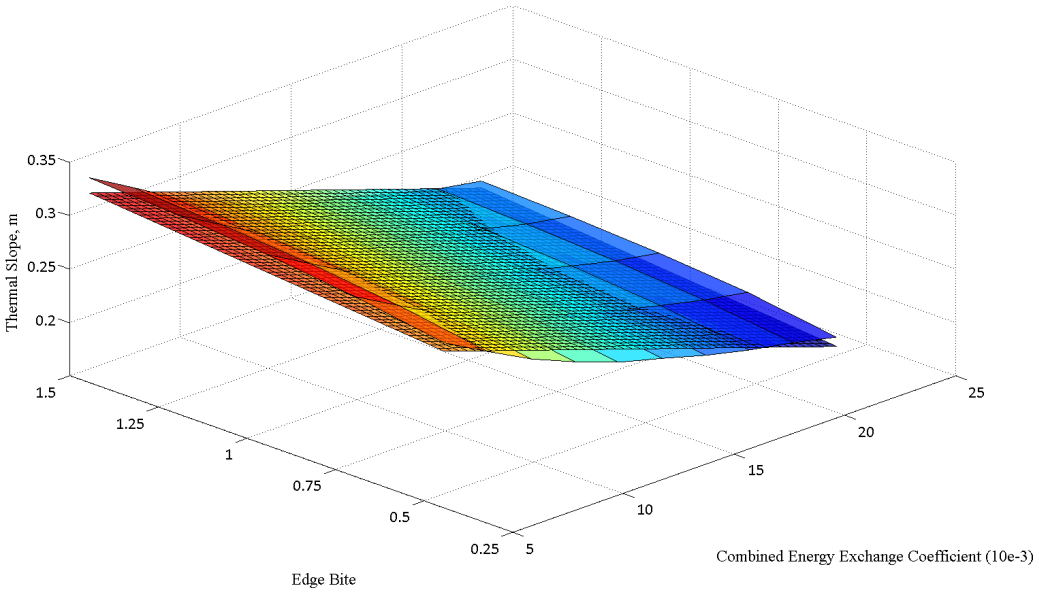

Fig. 187. Steady-State Regression Analysis Using Second-Order Polynomial Model for the Outer Glass Plate with High-Heat Mass Frame

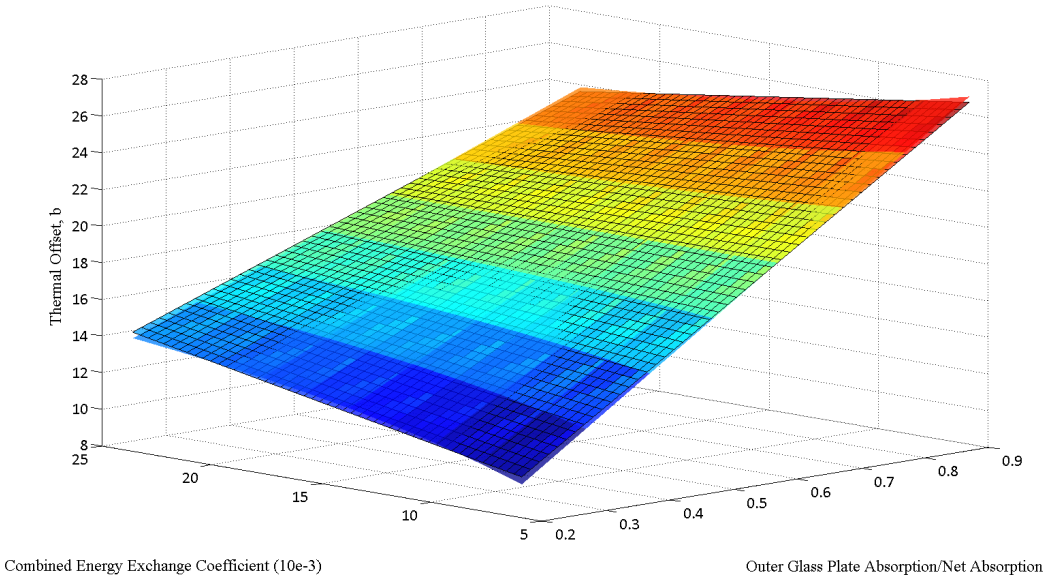

Fig. 188. Transient Regression Analysis Using Second-Order Polynomial Model for the Outer Glass Plate with High-Heat Mass Frame

Inner Glass Plate with Perfectly Insulated Frame

Table 60 presents a summary of results from the steady-state regression analysis using the second-order polynomial model for the inner glass plate with a perfectly insulating frame. Included are the coefficient of multiple determination and sum of the squares of the residuals for the regression analysis in order of the terms added. In addition, the maximum under and over estimation stresses are included. The fifth column of the table defines the rank order in which the terms were added to the model. The coefficients that are associated with each model are presented in Table 61.

Table 60. Summary of Steady-State Regression Analysis Using Second-Order Polynomial Model for the Inner Glass Plate with Perfectly Insulated Frame

No. of Terms	R^2	Percent Difference	RSS	Term Added	Maximum Stress (psi)	
					Under Estimation	Over Estimation
1	-	-	-	Constant	-	-
2	95.946	-	0.039	h_{CEEC}	100.20	86.30
3	98.327	2.48%	0.016	h_{CEEC}^2	45.59	50.77
4	99.872	1.57%	0.001	d_{edge_bite}	18.78	19.52
5	99.9	0.03%	0.001	$d_{edge\_bite}^2$	17.95	15.00
6	99.903	0.00%	0.001	$h_{CEEC} \cdot d_{edge\_bite}$	15.57	13.70

Table 61. Coefficients for Steady-State Model Using Second-Order Polynomial Model for the Inner Glass Plate with Perfectly Insulated Frame

No. of Terms	Coefficients, m_i					
2	-0.3939	8.5453	0	0	0	0
3	-0.4441	16.5269	-270.8000	0	0	0
4	-0.4268	16.5269	-270.8000	-0.0173	0	0
5	-0.4199	16.5269	-270.8000	-0.0331	0.0079	0
6	-0.4216	16.6444	-270.8000	-0.0313	0.0079	-0.1175

Fig. 189 shows the coefficient of multiple determination and sum of the squares of the residuals as a function of the number of terms added to the model. In general, the coefficient of multiple determination increases and the sum of the squares of the residuals decreases as the number of terms in the model increase. Fig. 190 shows the percent change in the coefficient of determination as terms are added to the model. Fig. 191 shows the maximum under and over estimation stresses as a function of the number of terms added to the model. In general, both the maximum under and over estimation stresses decrease as the number of terms added to the model increases.

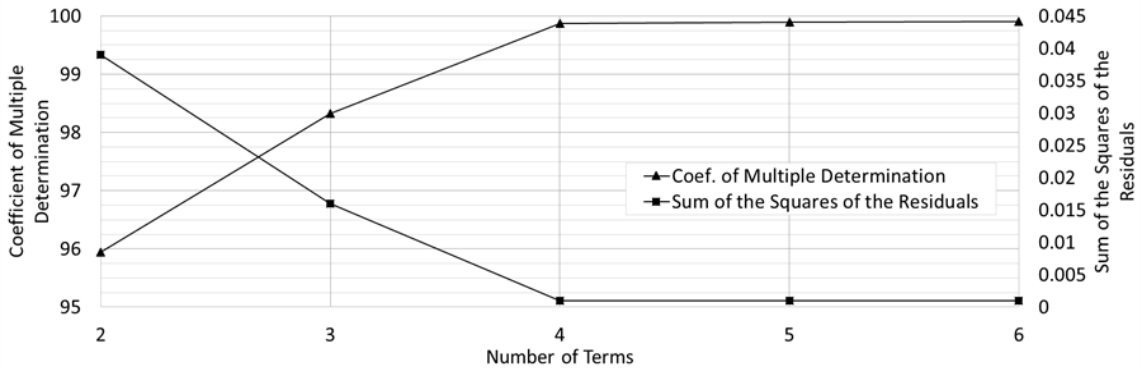

Fig. 189. Statistics of Steady-State Regression Analysis Using Second-Order Polynomial Model for the Inner Glass Plate with Perfectly Insulated Frame

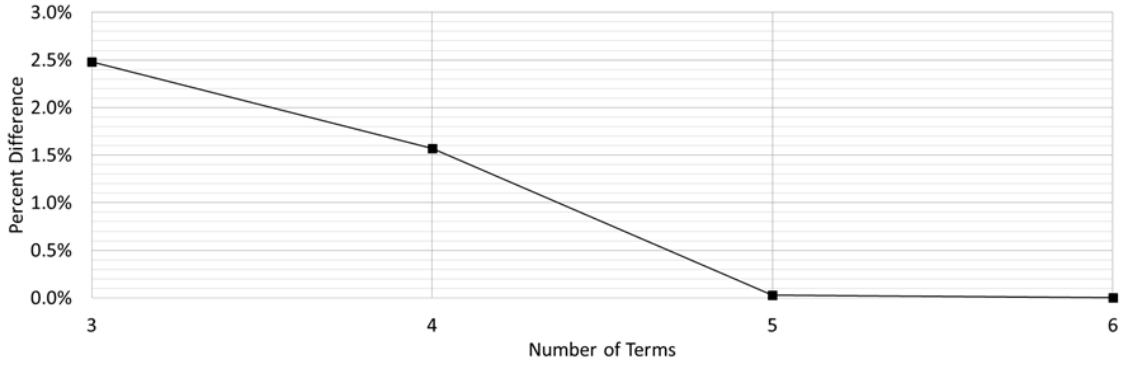

Fig. 190. Percent Difference vs. Number of Terms for Steady-State Regression Analysis Using Second-Order Polynomial Model for the Inner Glass Plate with Perfectly Insulated Frame

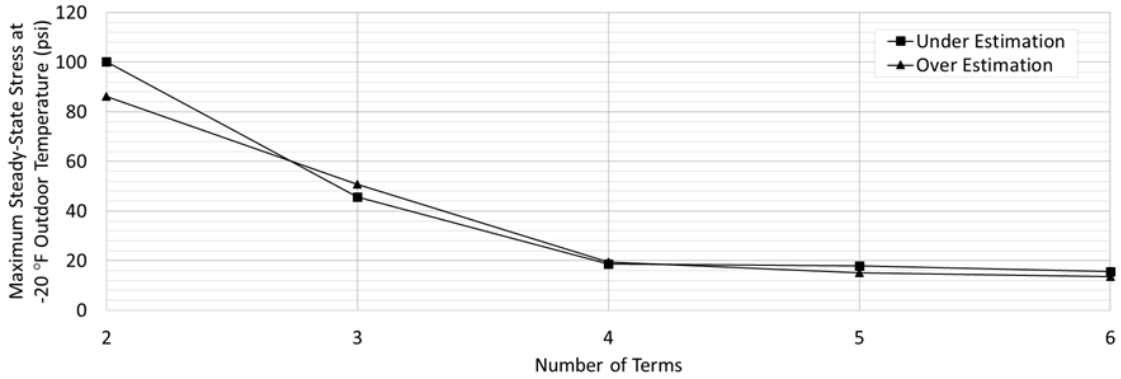

Fig. 191. Error in Stress Estimation of Steady-State Regression Analysis Using Second-Order Polynomial Model for the Inner Glass Plate with Perfectly Insulated Frame

Table 62 presents a summary of results from the transient regression analysis using the second-order polynomial model for the inner glass plate with a perfectly insulating frame. Included are the coefficient of multiple determination and sum of the squares of the residuals for the regression analysis in rank order of the terms added and the maximum under and over estimation. The fifth column of the table defines the order in which each term was added to the model. The coefficients that are associated with each model are presented in Table 63.

Table 62. Summary of Transient Regression Analysis Using Second-Order Polynomial Model for the Inner Glass Plate with Perfectly Insulated Frame

No. of Terms	R^2	Percent Difference	RSS	Term Added	Maximum Stress (psi)	
					Under Estimation	Over Estimation
1	-	-	-	Constant	-	-
2	75.787	-	3144.333	$(\alpha_{outer}/\alpha_{net})$	387.84	335.68
3	96.881	27.83%	404.984	d_{edge_bite}	199.24	147.08
4	97.928	1.08%	269.057	$d_{edge\_bite}\cdot(\alpha_{outer}/\alpha_{net})$	160.16	130.13
5	98.141	0.22%	241.369	h_{CEEC}	139.16	109.12
6	99.551	1.44%	58.304	$h_{CEEC}\cdot(\alpha_{outer}/\alpha_{net})$	98.22	50.13
7	99.664	0.11%	43.617	$(\alpha_{outer}/\alpha_{net})^2$	83.31	48.89
8	99.753	0.09%	32.04	$d_{edge\_bite}^2$	93.67	38.53
9	99.757	0.00%	31.516	h_{CEEC}^2	90.62	37.01
10	99.759	0.00%	31.342	$h_{CEEC}\cdot d_{edge\_bite}$	88.27	37.79

Table 63. Coefficients for Transient Model Using Second-Order Polynomial Model for the Inner Glass Plate with Perfectly Insulated Frame

No. of Terms	Coefficients, b_i									
2	21.5723	-21.6485	0	0	0	0	0	0	0	0
3	14.1705	-21.6485	7.4018	0	0	0	0	0	0	0
4	10.2127	-14.4525	11.3596	-7.1960	0	0	0	0	0	0
5	10.8997	-14.4525	11.3596	-7.1960	-46.6239	0	0	0	0	0
6	15.1399	-22.1620	11.3596	-7.1960	-334.3940	523.2184	0	0	0	0
7	16.1853	-26.7617	11.3596	-7.1960	-334.3940	523.2184	4.1815	0	0	0
8	14.7620	-26.7617	14.6130	-7.1960	-334.3940	523.2184	4.1815	-1.6267	0	0
9	15.0010	-26.7617	14.6130	-7.1960	-372.4212	523.2184	4.1815	-1.6267	1290.4000	0
10	15.1551	-26.7617	14.4589	-7.1960	-382.8768	523.2184	4.1815	-1.6267	1290.4000	10.4556

Fig. 192 shows the coefficient of multiple determination and sum of the squares of the residuals as a function of the number of terms added to the model. In general, the coefficient of multiple determination increases and the sum of the squares of the residuals decreases as the number of terms in the model increases. Fig. 193 shows the percent change in the coefficient of determination as terms are added to the model. Fig. 194 shows the maximum under and over estimation stresses as a function of the number of terms added to the model. In general, both the maximum under and over estimation stresses decrease as the number of terms added to the model increases. Once the number of terms exceeds seven, there is little increase in the fit of the polynomial model to the response data.

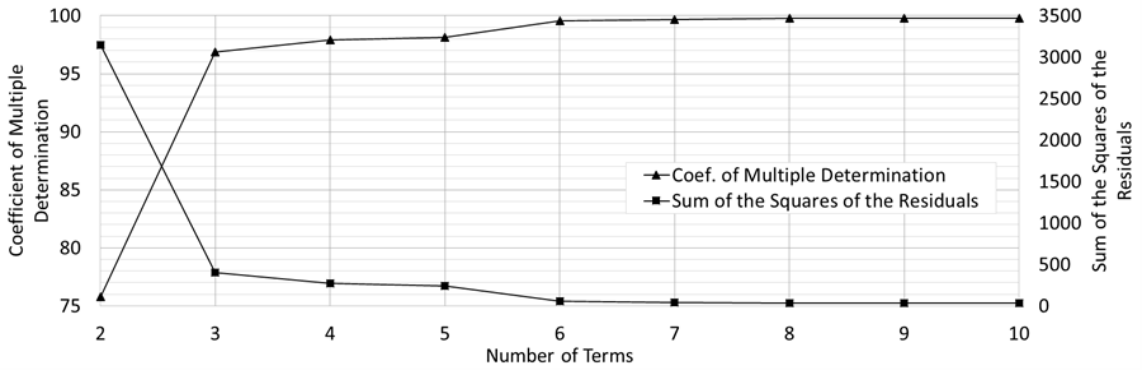

Fig. 192. Statistics of Transient Regression Analysis Using Second-Order Polynomial Model for the Inner Glass Plate with Perfectly Insulated Frame

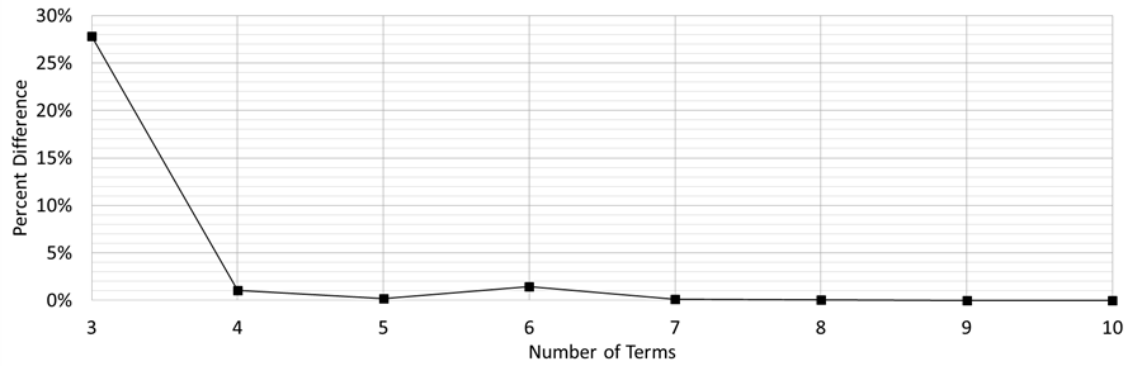

Fig. 193. Percent Difference vs. Number of Terms for Transient Regression Analysis Using Second-Order Polynomial Model for the Inner Glass Plate with Perfectly Insulated Frame

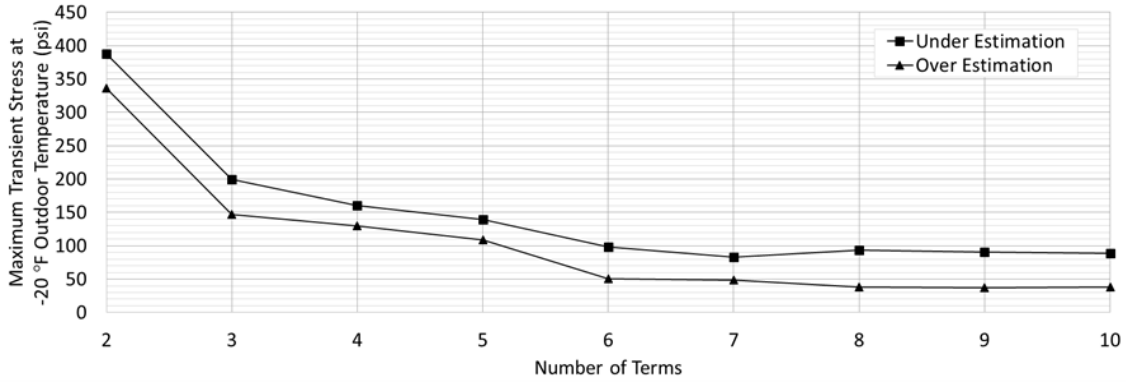

Fig. 194. Error in Stress Estimation of Transient Regression Analysis Using Second-Order Polynomial Model for the Inner Glass Plate with Perfectly Insulated Frame

Table 64 summarizes the combined steady-state and transient results from the regression analysis for the number of terms selected. From the regression analysis, the model for the steady-state response is given by Eq. (130) and the transient response is given by Eq. (131) below. These equations and their fit to the response data are shown in Figs. 195 and 196.

Table 64. Overall Summary of Regression Analysis Using Second-Order Polynomial Model for the Inner Glass Plate with Perfectly Insulated Frame

	No. of Terms	R^2	Maximum Stress (psi)	
			Under Estimation	Over Estimation
Steady-State	4	99.872	18.78	19.52
Transient	7	99.664	83.31	48.89
Total	11		102.09	68.41

$$m = -0.4268 + 16.5269 * h_{CEEC} - 270.8000 * {h_{CEEC}}^2 - 0.0173 * d_{edge\_bite} \quad (130)$$

$$b = 16.1853 - 26.7617 * \left(\frac{\alpha_{outer}}{\alpha_{net}}\right) + 11.3596 * d_{edge\_bite} - 7.1960 * d_{edge\_bite} * \left(\frac{\alpha_{outer}}{\alpha_{net}}\right) - 334.3940 * h_{CEEC} + 523.2184 * h_{CEEC} * \left(\frac{\alpha_{outer}}{\alpha_{net}}\right) + 4.1815 * \left(\frac{\alpha_{outer}}{\alpha_{net}}\right)^2 \quad (131)$$

Where all of the variables are as previously defined.

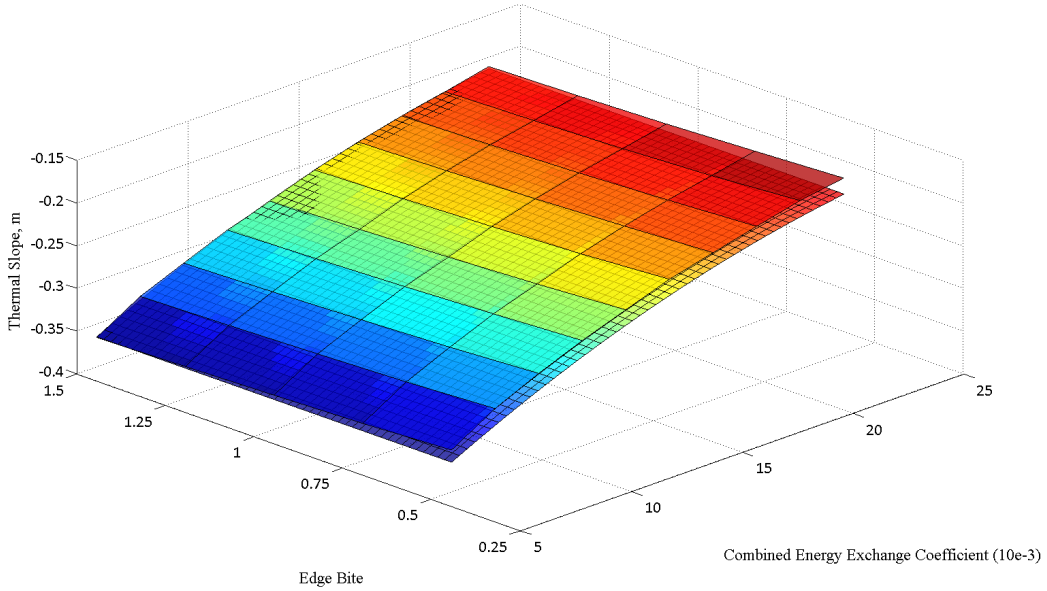

Fig. 195. Steady-State Regression Analysis Using Second-Order Polynomial Model for the Inner Glass Plate with Perfectly Insulated Frame

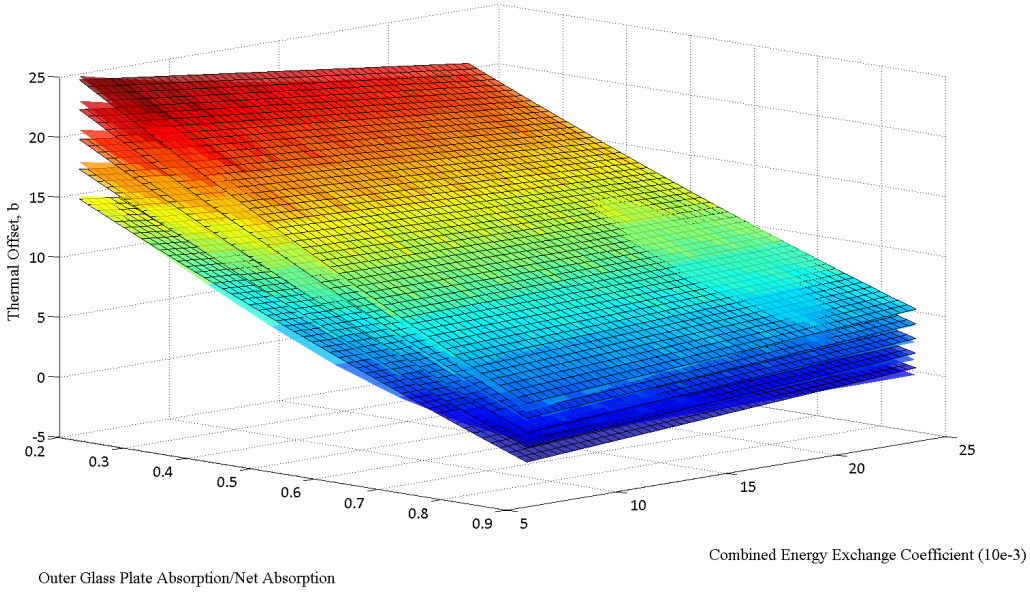

Fig. 196. Transient Regression Analysis Using Second-Order Polynomial Model for the Inner Glass Plate with Perfectly Insulated Frame

Inner Glass Plate with High-Heat Mass Frame

Table 65 presents a summary of results from the steady-state regression analysis using the second-order polynomial model for the inner glass plate with a high-heat mass frame. Included are the coefficient of multiple determination and sum of the squares of the residuals for the regression analysis in order of the terms added. In addition, the maximum under and over estimation stresses are included. The fifth column of the table defines the rank order in which the terms were added to the model. The coefficients that are associated with each model are presented in Table 66.

Table 65. Summary of Steady-State Regression Analysis Using Second-Order Polynomial Model for the Inner Glass Plate with High-Heat Mass Frame

No. of Terms	R^2	Percent Difference	RSS	Term Added	Maximum Stress (psi)	
					Under Estimation	Over Estimation
1	-	-	-	Constant	-	-
2	95.946	-	0.039	h_{CEEC}	98.31	84.67
3	98.327	2.48%	0.016	h_{CEEC}^2	44.73	49.82
4	99.872	1.57%	0.001	d_{edge_bite}	18.43	19.15
5	99.9	0.03%	0.001	$d_{edge\_bite}^2$	17.61	14.72
6	99.903	0.00%	0.001	$h_{CEEC} \cdot d_{edge\_bite}$	15.27	13.44

Table 66. Coefficients for Steady-State Model Using Second-Order Polynomial Model for the Inner Glass Plate with High-Heat Mass Frame

No. of Terms	Coefficients, m_i					
2	-0.3939	8.5453	0	0	0	0
3	-0.4441	16.5269	-270.8000	0	0	0
4	-0.4268	16.5269	-270.8000	-0.0173	0	0
5	-0.4199	16.5269	-270.8000	-0.0331	0.0079	0
6	-0.4216	16.6444	-270.8000	-0.0313	0.0079	-0.1175

Fig. 197 shows the coefficient of multiple determination and sum of the squares of the residuals as a function of the number of terms added to the model. In general, the coefficient of multiple determination increases and the sum of the squares of the residuals decreases as the number of terms in the model increases. Fig. 198 shows the percent change in the coefficient of determination as terms are added to the model. Fig. 199 shows the maximum under and over estimation stresses as a function of the number of terms added to the model. In general, both the maximum under and over estimation stresses decrease as the number of terms added to the model increases.

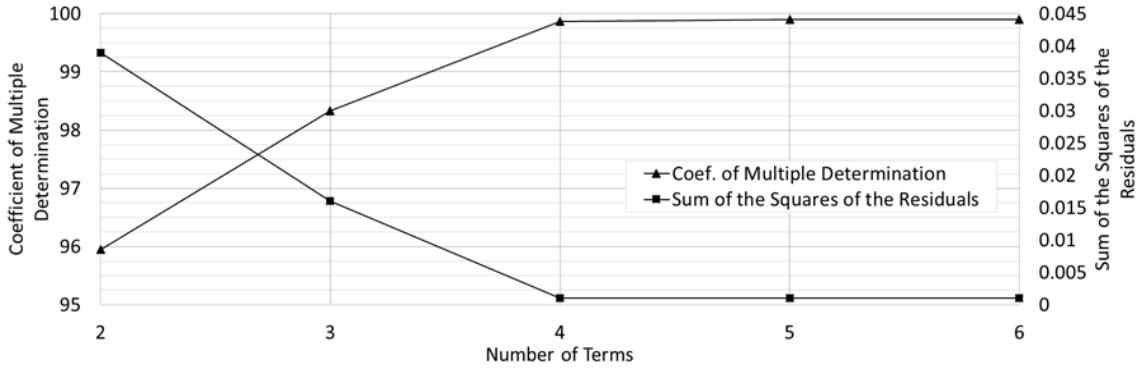

Fig. 197. Statistics of Steady-State Regression Analysis Using Second-Order Polynomial Model for the Inner Glass Plate with High-Heat Mass Frame

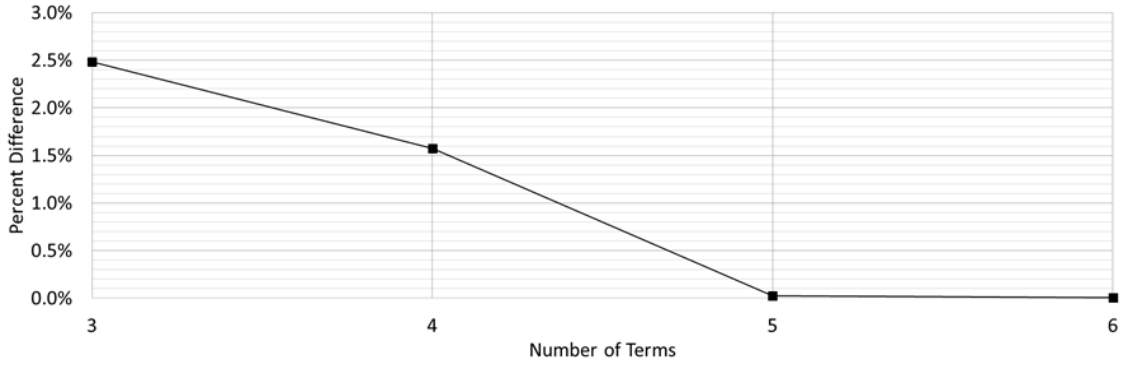

Fig. 198. Percent Difference vs. Number of Terms for Steady-State Regression Analysis Using Second-Order Polynomial Model for the Inner Glass Plate with High-Heat Mass Frame

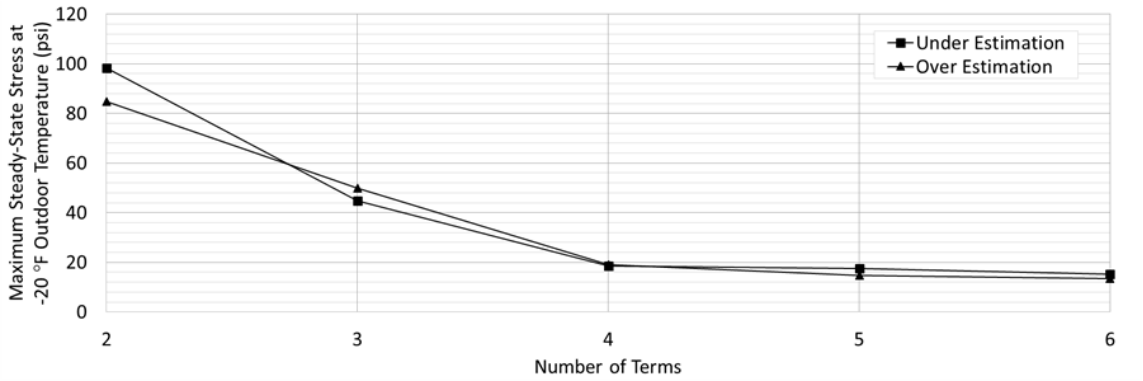

Fig. 199. Error in Stress Estimation of Steady-State Regression Analysis Using Second-Order Polynomial Model for the Inner Glass Plate with High-Heat Mass Frame

Table 67 presents a summary of results from the transient regression analysis using the second-order polynomial model for the inner glass plate with a high-heat mass frame. Included are the coefficient of multiple determination and sum of the squares of the residuals for the regression analysis in rank order of the terms added and the maximum under and over estimation. The fifth column of the table defines the order in which each term was added to the model. The coefficients that are associated with each model are presented in Table 68.

Table 67. Summary of Transient Regression Analysis Using Second-Order Polynomial Model for the Inner Glass Plate with High-Heat Mass Frame

No. of Terms	R^2	Percent Difference	RSS	Term Added	Maximum Stress (psi)	
					Under Estimation	Over Estimation
1	-	-	-	Constant	-	-
2	96.77	-	602.738	$(\alpha_{outer}/\alpha_{net})$	191.94	143.75
3	96.932	0.17%	573.89	h_{CEEC}	170.90	164.79
4	99.924	3.09%	14.25	$h_{CEEC}\cdot(\alpha_{outer}/\alpha_{net})$	29.36	23.25
5	99.926	0.00%	13.802	h_{CEEC}^2	26.60	26.02
6	99.926	0.00%	13.802	$(\alpha_{outer}/\alpha_{net})^2$	26.60	26.02
7	99.926	0.00%	13.802	$d_{edge\_bite}^2$	26.60	26.02
8	99.926	0.00%	13.802	d_{edge_bite}	26.60	26.02
9	99.926	0.00%	13.802	$d_{edge\_bite}\cdot(\alpha_{outer}/\alpha_{net})$	26.60	26.02
10	99.926	0.00%	13.802	$h_{CEEC}\cdot d_{edge\_bite}$	26.60	26.02

Table 68. Coefficients for Transient Model Using Second-Order Polynomial Model for the Inner Glass Plate with High-Heat Mass Frame

No. of Terms	Coefficients, b_i									
2	38.1978	-29.3585	0	0	0	0	0	0	0	0
3	38.8991	-29.3585	-47.5907	0	0	0	0	0	0	0
4	46.3129	-42.8382	-550.7413	914.8192	0	0	0	0	0	0
5	46.5340	-42.8382	-585.9210	914.8192	1193.8000	0	0	0	0	0
6	46.5342	-42.8388	-585.9210	914.8192	1193.8000	0.0006	0	0	0	0
7	46.5342	-42.8388	-585.9210	914.8192	1193.8000	0.0006	0.0000	0	0	0
8	46.5345	-42.8388	-585.9210	914.8192	1193.8000	0.0006	0.0003	-0.0007	0	0
9	46.5345	-42.8389	-585.9210	914.8192	1193.8000	0.0006	0.0003	-0.0007	0.0001	0
10	46.5345	-42.8389	-585.9187	914.8192	1193.8000	0.0006	0.0003	-0.0007	0.0001	-0.0023

Fig. 200 shows the coefficient of multiple determination and sum of the squares of the residuals as a function of the number of terms added to the model. In general, the coefficient of multiple determination increases and the sum of the squares of the residuals decreases with the number of terms in the model increases. Fig. 201 shows the percent change in the coefficient of determination as terms are added to the model. Fig. 202 shows the maximum under and over estimation stresses as a function of the number of terms added to the model. In general, both the maximum under and over estimation stresses decrease as the number of terms added to the model increases. Once the number of terms exceeds four, there is little increase in the fit of the polynomial model to the response data.

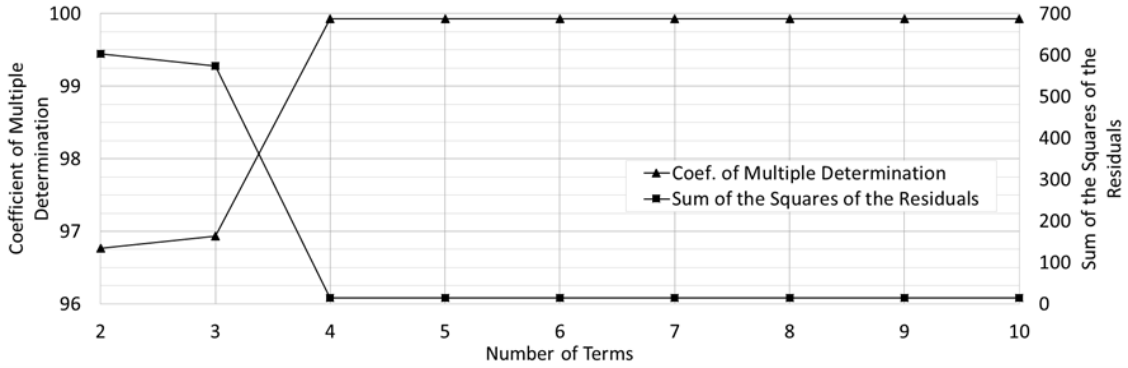

Fig. 200. Statistics of Transient Regression Analysis Using Second-Order Polynomial Model for the Inner Glass Plate with High-Heat Mass Frame

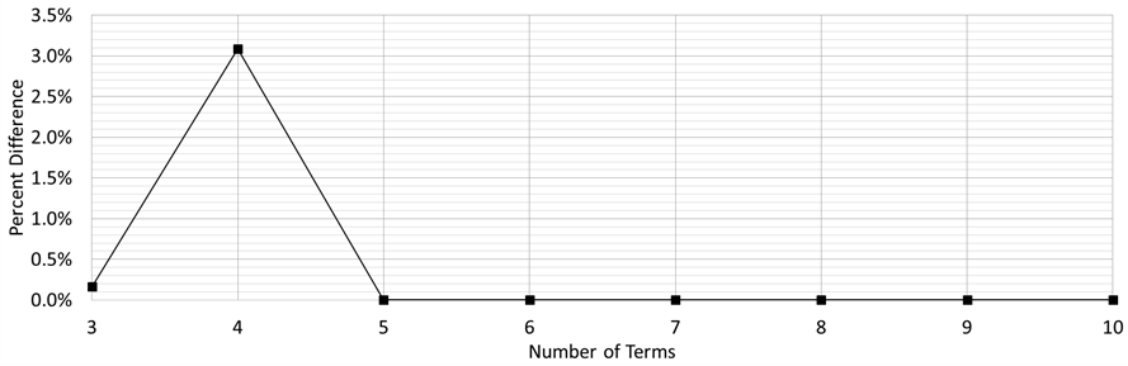

Fig. 201. Percent Difference vs. Number of Terms for Transient Regression Analysis Using Second-Order Polynomial Model for the Inner Glass Plate with High-Heat Mass Frame

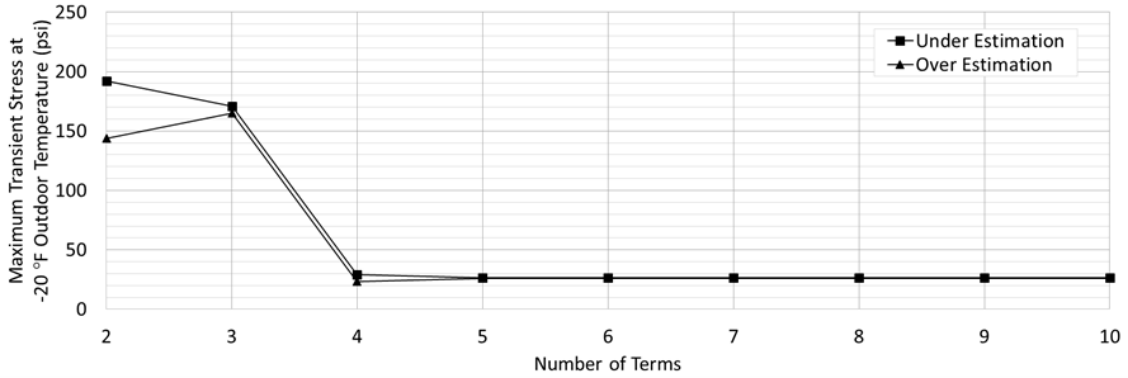

Fig. 202. Error in Stress Estimation of Transient Regression Analysis Using Second-Order Polynomial Model for the Inner Glass Plate with High-Heat Mass Frame

Table 69 summarizes the combined steady-state and transient results from the regression analysis for the number of terms selected. From the regression analysis, the model for the steady-state response is given by Eq. (132) and the transient response is given by Eq. (133) below. These equations and their fit to the response data are shown in Figs. 203 and 204.

Table 69. Overall Summary of Regression Analysis Using Second-Order Polynomial Model for the Inner Glass Plate with High-Heat Mass Frame

	No. of Terms	R^2	Maximum Stress (psi)	
			Under Estimation	Over Estimation
Steady-State	3	98.327	44.73	49.82
Transient	4	99.924	29.36	23.25
Total	7		74.10	73.07

$$m = -0.4441 + 16.5269 * h_{CEEC} - 270.8000 * {h_{CEEC}}^2 \tag{132}$$

$$b = 46.3129 - 42.8382 * \left(\frac{\alpha_{outer}}{\alpha_{net}}\right) - 550.7413 * h_{CEEC} + 914.8192 * h_{CEEC} * \left(\frac{\alpha_{outer}}{\alpha_{net}}\right) \tag{133}$$

Where all of the variables are as previously defined.

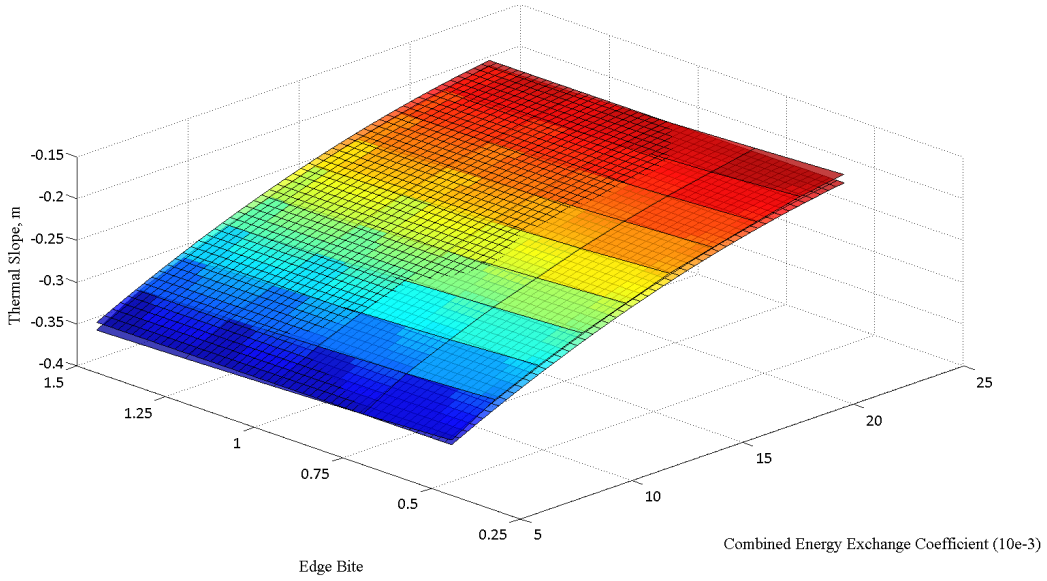

Fig. 203. Steady-State Regression Analysis Using Second-Order Polynomial Model for the Inner Glass Plate with High-Heat Mass Frame

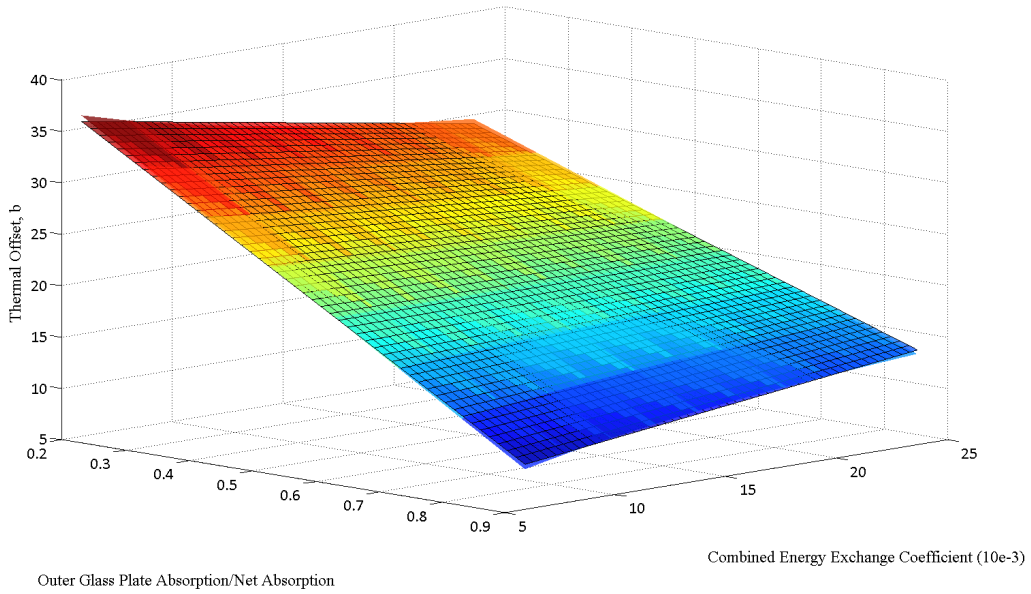

Fig. 204. Transient Regression Analysis Using Second-Order Polynomial Model for the Inner Glass Plate with High-Heat Mass Frame

The coefficients for the first-order polynomial models of the steady-state and transient responses that were selected using the regression analyses aforementioned can be summarized in a tabular form, as presented in Tables 26 and 27. These coefficient tables are shown below in Tables 70 and 71 for the steady-state and transient responses, respectively.

Table 70. First-Order Coefficient Table of Steady-State Response (m)

Coefficients:		m_0	m_1	m_2	
Perfectly Insulated Frame	Steel Spacer	-0.3766	8.5453	-0.0173	Inner Glass Plate
		0.3094	-7.0653	0.0308	Outer Glass Plate
	Foam Spacer	--	--	--	Inner Glass Plate
		--	--	--	Outer Glass Plate
	Aluminum Spacer	--	--	--	Inner Glass Plate
		--	--	--	Outer Glass Plate
High-Heat Mass Frame	Steel Spacer	-0.3766	8.5453	-0.0173	Inner Glass Plate
		0.3094	-7.0653	0.0308	Outer Glass Plate
	Foam Spacer	--	--	--	Inner Glass Plate
		--	--	--	Outer Glass Plate
	Aluminum Spacer	--	--	--	Inner Glass Plate
		--	--	--	Outer Glass Plate

Table 71. First-Order Coefficient Table of Transient Response (b)

Coefficients:		b_0	b_1	b_2	b_3	
Perfectly Insulated Frame	Steel Spacer	14.8575	-21.6485	7.4018	-46.6239	Inner Glass Plate
		-6.3384	15.7274	6.2769	0	Outer Glass Plate
	Foam Spacer	--	--	--	--	Inner Glass Plate
		--	--	--	--	Outer Glass Plate
	Aluminum Spacer	--	--	--	--	Inner Glass Plate
		--	--	--	--	Outer Glass Plate
High-Heat Mass Frame	Steel Spacer	38.8991	-29.3585	0	-47.5907	Inner Glass Plate
		8.1990	18.2034	0	34.6635	Outer Glass Plate
	Foam Spacer	--	--	--	--	Inner Glass Plate
		--	--	--	--	Outer Glass Plate
	Aluminum Spacer	--	--	--	--	Inner Glass Plate
		--	--	--	--	Outer Glass Plate

The final equations for the selected first-order polynomial models for the steady-state and transient responses are shown in Eqs. (134) and (135), respectively.

$$m = m_0 + m_1 \cdot h_{CEEC} + m_2 \cdot d_{edge\_bite} \tag{134}$$

$$b = b_0 + b_1 \cdot \left(\frac{\alpha_{outer}}{\alpha_{net}}\right) + b_2 \cdot d_{edge\_bite} + b_3 \cdot h_{CEEC} \tag{135}$$

Where all of the variables are as previously defined.

Likewise, the coefficients for the second-order polynomial models of the steady-state and transient responses that were selected using the regression analyses aforementioned can be summarized in a tabular form, as presented in Tables 26 and 27. These coefficient tables are shown below in Tables 72 and 73 for the steady-state and transient responses, respectively.

Table 72. Second-Order Coefficient Table of Steady-State Response (m)

	Coefficients:	m_0	m_1	m_2	m_3	m_4	
Perfectly Insulated Frame	Steel Spacer	-0.4268	16.5269	-0.0173	-270.8000	0	Inner Glass Plate
		0.3398	-14.9387	0.0744	267.1727	-0.0218	Outer Glass Plate
	Foam Spacer	--	--	--	--	--	Inner Glass Plate
		--	--	--	--	--	Outer Glass Plate
	Aluminum Spacer	--	--	--	--	--	Inner Glass Plate
		--	--	--	--	--	Outer Glass Plate
High-Heat Mass Frame	Steel Spacer	-0.4441	16.5269	0	-270.8000	0	Inner Glass Plate
		0.3094	-7.0653	0.0308	0	0	Outer Glass Plate
	Foam Spacer	--	--	--	--	--	Inner Glass Plate
		--	--	--	--	--	Outer Glass Plate
	Aluminum Spacer	--	--	--	--	--	Inner Glass Plate
		--	--	--	--	--	Outer Glass Plate

Table 73. Second-Order Coefficient Table of Transient Response (b)

	Coefficients:	b_0	b_1	b_2	b_3	b_4	b_5	b_6	
Perfectly Insulated Frame	Steel Spacer	16.1853	-26.7617	11.3596	-334.3940	-7.1960	523.2184	4.1815	Inner Glass Plate
		-6.1162	15.9629	3.7784	154.4867	4.5427	-324.2811	0	Outer Glass Plate
	Foam Spacer	--	--	--	--	--	--	--	Inner Glass Plate
		--	--	--	--	--	--	--	Outer Glass Plate
	Aluminum Spacer	--	--	--	--	--	--	--	Inner Glass Plate
		--	--	--	--	--	--	--	Outer Glass Plate
High-Heat Mass Frame	Steel Spacer	46.3129	-42.8382	0	-550.7413	0	914.8192	0	Inner Glass Plate
		3.4241	26.8851	0	358.7196	0	-589.1930	0	Outer Glass Plate
	Foam Spacer	--	--	--	--	--	--	--	Inner Glass Plate
		--	--	--	--	--	--	--	Outer Glass Plate
	Aluminum Spacer	--	--	--	--	--	--	--	Inner Glass Plate
		--	--	--	--	--	--	--	Outer Glass Plate

The final equations for the selected second-order polynomial models for the steady-state and transient responses are shown in Eqs. (136) and (137), respectively.

$$m = m_0 + m_1 \cdot h_{CEEC} + m_2 \cdot d_{edge\_bite} + m_3 \cdot {h_{CEEC}}^2 + m_4 \cdot {d_{edge\_bite}}^2 \tag{136}$$

$$b = b_0 + b_1 \cdot \left(\frac{\alpha_{outer}}{\alpha_{net}}\right) + b_2 \cdot d_{edge\_bite} + b_3 \cdot h_{CEEC} + b_4 \cdot d_{edge\_bite} \cdot \left(\frac{\alpha_{outer}}{\alpha_{net}}\right) + b_5 \cdot h_{CEEC} \cdot \left(\frac{\alpha_{outer}}{\alpha_{net}}\right) + b_6 \cdot \left(\frac{\alpha_{outer}}{\alpha_{net}}\right)^2 \tag{137}$$

Where all of the variables are as previously defined.

The complete set of steps to apply the SDP to evaluate the POB of a glass plate in an IG unit due to thermal stress was presented in detail previously. Fig. 205 provides an example of a simple design worksheet that can be used to evaluate the POB of a glass plate in an IG unit subjected to solar irradiance using the SDP. An example of the application of this procedure is presented in the following section.

DESIGN WORKSHEET FOR IG UNIT
THERMAL STRESS EVALUATION

PROJECT: _____ DATE: _____ / _____ / _____

LOCATION: _____

Glass Plate Dimensions:
Width (W): _____ *in.*
Length (L): _____ *in.*

Edge Bite (d_{edge_bite}): _____ *in.*

Determine the CEEC (h_{CEEC}): _____ *(in.·lb/s)/(in.^{2}·°F)*

Glass plates absorptions:
α_{outer}: _____
α_{inner}: _____

Determine the net absorption (α_{net}):
$\alpha_{net} = \alpha_{outer} + \alpha_{inner}$ = _____

Type of Frame: Perfectly Insulated / High-Heat Mass

Type of Spacer: Steel / Foam / Aluminum

Glass Plate: Inner / Outer

Select the proper coefficients for the thermal slope equation (m). Use Table 70 for a first-order polynomial model or Table 72 for a second-order polynomial model. Select the proper row for the correct frame, spacer, and glass plate.

Select the proper coefficients for the thermal offset equation (b). Use Table 71 for a first-order polynomial model or Table 73 for a second-order polynomial model. Select the proper row for the correct frame, spacer, and glass plate.

Calculate the value for m using Eq. (134) for a first-order polynomial model or Eq. (136) for a second-order polynomial model.
Calculate the value for b using Eq. (135) for a first-order polynomial model or Eq. (137) for a second-order polynomial model.

Determine the Absorption Factor (AF):
AF = $\frac{\alpha_{net}}{0.25}$ = _____

Define Environmental Conditions:
Outdoor Temperature ($T_{outdoor}$): _____ *°F*
Indoor Temperature (T_{indoor}): _____ *°F*
Incident Solar Irradiance (I_s): _____ *(in.·lb/s)/(in.^{2})*

Calculate the Solar Load Factor (SLF):
SLF = $\frac{I_S}{5.7105}$ = _____

Determine the maximum perimeter-of-glass thermal stress (σ_{max}):
$\sigma_{max} = \alpha_T \cdot E \cdot [SLF \cdot AF \cdot b \pm m \cdot (T_{outdoor} - T_{indoor})]$ = _____ *psi*

Select an acceptable Probability of Breakage (P_b): _____

Calculate Perimeter Length (P):
$P = 2 \cdot (W + L)$ = _____ *in.*

Determine allowable thermal stress ($\sigma_{allowable}$) from Fig. 26: _____ *psi*

CONCLUSION:

If $\sigma_{max} > \sigma_{allowable}$ N.G.

If $\sigma_{max} \leq \sigma_{allowable}$ OK

Fig. 205. Design Worksheet for IG Unit Thermal Stress Evaluation

Practical Application

The general first-order and second-order polynomial models that were discussed in the previous section were used to determine the maximum temperature difference between the center-of-glass and the perimeter-of-glass for the same set of exemplar IG units that were presented in Chapter IV. In Chapter IV, these exemplar IG units were evaluated using the FDP. The purpose of performing the analyses in this chapter was to demonstrate the use of the SDP to calculate the thermal stress and compare the results to those calculated using the FDP. Pertinent properties and descriptions for each IG unit and frame considered as part of the practical application are provided in Table 74. Where all of the variables are as previously defined. These data are simply restated from Chapter IV for convenience.

Table 74. Practical Application Example Load Cases

Case No.	Outer Glass Plate	Inner Glass Plate	Frame	h_{CEEC} ((in.·lb/s)/(in.·°F))	α_{outer}	α_{inner}	$T_{outdoor}$ (°F)	T_{indoor} (°F)	I_S ((in.·lb/s)/in.^{2})
FEA 1	1/4 in. Clear	1/4 in. Clear	Perfectly Insulated	0.0202723	0.1517	0.1134	-10	79	4.9967
FEA 2	1/4 in. Clear	1/4 in. Clear	High-Heat Mass	0.0202723	0.1517	0.1134	-10	79	4.9967
FEA 3	1/4 in. Clear	1/4 in. Clear	Perfectly Insulated	0.0202723	0.1517	0.1134	105	68	5.9789
FEA 4	1/4 in. Clear	1/4 in. Clear	High-Heat Mass	0.0202723	0.1517	0.1134	105	68	5.9789
FEA 5	1/4 in. Low-E, Soft-Coat	1/4 in. Clear	Perfectly Insulated	0.006694	0.3407	0.0537	-10	79	4.9967
FEA 6	1/4 in. Low-E, Soft-Coat	1/4 in. Clear	High-Heat Mass	0.006694	0.3407	0.0537	-10	79	4.9967
FEA 7	1/4 in. Low-E, Soft-Coat	1/4 in. Clear	Perfectly Insulated	0.006694	0.3407	0.0537	105	68	5.9789
FEA 8	1/4 in. Low-E, Soft-Coat	1/4 in. Clear	High-Heat Mass	0.006694	0.3407	0.0537	105	68	5.9789

Before the steps outlined in Fig. 205 for the SDP were applied directly to the practical application examples, a more detailed analysis was performed where the steady-state, transient, and overall temperature response of each IG unit were considered individually. Ultimately, this served to show the accuracy or error associated with each component of the SDP. The final process that was used to evaluate thermal stress for each case is presented following this more detailed discussion.

Tables 75 and 76 show the maximum difference in temperature between the center-of-glass and the perimeter-of-glass for the inner glass plate using the first-order and second-order models, respectively. For all of the temperature analyses shown, the percent error for the steady-state, transient, and overall temperatures were determined assuming the temperatures calculated using the FDP were the "correct" temperatures. Tables 77 and 78 show the maximum difference in temperature between the center-of-glass and the perimeter-of-glass for the outer glass plate using the first-order and second-order models, respectively.

Table 75. Summary of Temperatures from Regression Analysis Using First-Order Polynomial Model for the Inner Glass Plate

Case No.	Steady-State (°F)			Transient (°F)			Overall (°F)		
	Formal Design Procedure	Simplified Design Procedure	Percent Error	Formal Design Procedure	Simplified Design Procedure	Percent Error	Formal Design Procedure	Simplified Design Procedure	Percent Error
FEA 1	18.84	18.87	0.18%	4.51	4.85	7.40%	23.35	23.72	1.58%
FEA 2	18.84	18.87	0.18%	19.68	19.61	0.38%	38.52	38.48	0.11%
FEA 5	30.11	29.20	3.03%	0.82	-0.63	176.52%	30.93	28.57	7.63%
FEA 6	30.11	29.20	3.03%	14.65	18.25	24.56%	44.76	47.44	6.00%

Table 76. Summary of Temperatures from Regression Analysis Using Second-Order Polynomial Model for the Inner Glass Plate

Case No.	Steady-State (°F)			Transient (°F)			Overall (°F)		
	Formal Design Procedure	Simplified Design Procedure	Percent Error	Formal Design Procedure	Simplified Design Procedure	Percent Error	Formal Design Procedure	Simplified Design Procedure	Percent Error
FEA 1	18.84	18.84	0.02%	4.51	4.78	5.90%	23.35	23.62	1.16%
FEA 2	18.84	19.61	4.11%	19.68	19.71	0.15%	38.52	39.32	2.09%
FEA 5	30.11	29.99	0.41%	0.82	-0.63	176.33%	30.93	29.36	5.07%
FEA 6	30.11	30.76	2.15%	14.65	15.06	2.81%	44.76	45.82	2.37%

Table 77. Summary of Temperatures from Regression Analysis Using First-Order Polynomial Model for the Outer Glass Plate

Case No.	Steady-State (°F)			Transient (°F)			Overall (°F)		
	Formal Design Procedure	Simplified Design Procedure	Percent Error	Formal Design Procedure	Simplified Design Procedure	Percent Error	Formal Design Procedure	Simplified Design Procedure	Percent Error
FEA 3	6.78	6.72	0.91%	5.73	6.44	12.38%	12.51	13.16	5.18%
FEA 4	6.78	6.72	0.91%	21.34	21.45	0.51%	28.12	28.17	0.17%
FEA 7	10.40	10.27	1.27%	17.36	17.16	1.18%	27.76	27.42	1.21%
FEA 8	10.40	10.27	1.27%	42.60	39.90	6.34%	53.00	50.17	5.34%

Table 78. Summary of Temperatures from Regression Analysis Using Second-Order Polynomial Model for the Outer Glass Plate

Case No.	Steady-State (°F)			Transient (°F)			Overall (°F)		
	Formal Design Procedure	Simplified Design Procedure	Percent Error	Formal Design Procedure	Simplified Design Procedure	Percent Error	Formal Design Procedure	Simplified Design Procedure	Percent Error
FEA 3	6.78	6.61	2.57%	5.73	6.19	8.06%	12.51	12.80	2.30%
FEA 4	6.78	6.72	0.91%	21.34	21.37	0.13%	28.12	28.09	0.12%
FEA 7	10.40	10.49	0.88%	17.36	17.65	1.65%	27.76	28.14	1.36%
FEA 8	10.40	10.27	1.27%	42.60	42.36	0.57%	53.00	52.62	0.71%

As shown, the SDP provides a reasonable tool to determine the maximum difference in temperature between the center-of-glass and the perimeter-of-glass that an IG unit experiences when it is subjected to a set of environmental conditions. The SDP is most accurate for the inner and outer glass plates when they are placed in cold and hot climates, respectively. This is convenient because it has been shown that the inner glass plate is more susceptible to thermal breakage in cold climates and the outer glass plate is more susceptible to thermal breakage in hot climates.

If the steps detailed in Fig. 205 are used to evaluate the POB of a glass plate in an IG unit, the final thermal stress that is associated with the difference in the temperature of the center-of-glass and the perimeter-of-glass is determined directly for a given glass plate. Using this procedure, the temperature differences that are associated with the steady-state and transient responses are not determined explicitly as shown in Tables 75 through 78. The SDP, as applied to the inner glass plate for the IG unit associated with

FEA 1, is described in detail below. For this example, the first-order polynomial model was used.

The first step to apply the SDP is to establish the edge bite of the IG unit's frame. The applicable range of dimensions considered herein was 0.5 to 1.5 in. and includes the glazing bead if applicable. Then, the CEEC must be determined using the formal test procedure (FTP) presented in Chapter V. For FEA 1, the edge bite and CEEC were taken to be 0.5 in. and 0.0202723 (in.·lb/s)/(in.^{2}·°F), respectively.

Next, the absorption for the inner and outer glass plates must be calculated using the ray tracing procedure. These absorptions are determined based on the solar optical properties and orientations of the glass plates in the IG unit. The absorption for the inner and outer glass plates that were used for FEA 1 were 0.1134 and 0.1517, respectively. Now, knowing the absorption for the inner and outer glass plates, the net absorption of the IG unit can be determined using Eq. (70). This calculation is shown in Eq. (138) for FEA 1.

$$\alpha_{net} = \alpha_{outer} + \alpha_{inner} = 0.1517 + 0.1134 = 0.2651 \tag{138}$$

Where all of the variables are as previously defined.

The next step is to select the proper coefficients to be used in the thermal slope equation that is associated with the steady-state response of the IG unit. The coefficients were selected from Table 70 for the first-order polynomial model. The proper row was selected for the given frame, spacer, and glass plate of interest. For FEA 1, the frame was perfectly insulated, the spacer was steel, and the inner glass plate was considered for this example. The proper coefficients, m_0, m_1, and m_2, for the thermal slope equation are -0.3766, 8.5453, and -0.0173, respectively.

The next step is to select the proper coefficients to be used in the thermal offset equation that is associated with the transient response of the IG unit. The coefficients are selected from Table 71 for the first-order polynomial model. The proper row was selected for the given frame, spacer, and glass plate of interest. For FEA 1, the frame was perfectly insulated, the spacer was steel, and the inner glass plate was considered for this example. The proper coefficients, b_0, b_1, b_2, and b_3, for the thermal slope equation are 14.8575, -21.6485, 7.4018, and -46.6239, respectively.

Now, using the coefficients and input variables determined in the previous steps, values for the thermal offset and thermal slope can be determined. The first-order polynomial model determined using the regression analysis procedure to describe the thermal slope or steady-state response of an IG unit was presented in Eq. (134) previously. Eq. (139) shows the first-order polynomial model for the thermal slope if the proper coefficients for the frame, spacer, and glass plate of interest are applied to Eq. (134). The calculation to determine the value of m for the inner glass plate of FEA 1 is shown in Eq. (140).

$$m = -0.3766 + 8.5453 \cdot h_{CEEC} - 0.0173 \cdot d_{edge\_bite} \tag{139}$$

$$\begin{aligned} m = -0.3766 + 8.5453 \cdot \left(0.0202723 \ \frac{(in.\cdot \text{lb})/s}{in.^2 \cdot {}^\circ\text{F}}\right) - 0.0173 \\ \cdot (0.5 \text{ in.}) = -0.2120 \ \frac{{}^\circ\text{F}}{{}^\circ\text{F}} \end{aligned} \tag{140}$$

Where all of the variables are as previously defined.

The first-order polynomial model determined using the regression analysis procedure to describe the thermal offset or transient response of an IG unit was presented in Eq. (135) previously. Eq. (141) shows the first-order polynomial model for the thermal offset if the proper coefficients for the frame, spacer, and glass plate of interest are applied to Eq.

(135). The calculation to determine the value of b for the inner glass plate of FEA 1 is shown in Eq. (142).

$$b = 14.8575 - 21.6485 \cdot \left(\frac{\alpha_{outer}}{\alpha_{net}}\right) + 7.4018 \cdot d_{edge_{bite}} - 46.6239 \cdot h_{CEEC} \tag{141}$$

$$b = 14.8575 - 21.6485 \cdot \left(\frac{0.1517}{0.2651}\right) + 7.4018 \cdot (0.5\ in.) - 46.6239 \cdot \left(0.0202723\ \frac{(in.\cdot \text{lb})/s}{in.^2 \cdot {}^\circ\text{F}}\right) = 5.2303\ {}^\circ\text{F} \tag{142}$$

Where all of the variables are as previously defined.

The next step in the procedure is to determine the absorption factor using Eq. (82). As discussed previously, the net absorption of an IG unit has a linear relationship with the maximum thermal stress that develops. The regression analysis that was used to determine the coefficients for the thermal offset equation of the SDP were established using a baseline net absorption of 25 percent. Therefore, the absorption factor must be used to adjust for the difference in the actual net absorption of the IG unit and the baseline value of 25 percent. This calculation is shown in Eq. (143) for FEA 1.

$$\text{AF} = \frac{\alpha_{net}}{0.25} = \frac{0.2651}{0.25} = 1.060 \tag{143}$$

Where all of the variables are as previously defined.

Now, the critical environmental variables must be defined. These variables include the indoor and outdoor temperatures and the maximum level of solar irradiance that the IG

unit will be exposed to. The indoor and outdoor temperatures for FEA 1 were 79 and -10 ˚F, respectively. The solar irradiance was 4.9967 (in.·lb/s)/in.^{2}.

The next step in the procedure is to determine the solar load factor using Eq. (81). As discussed previously, there is a linear relationship between the level of solar irradiance that an IG unit is subjected and the maximum thermal stress that develops. The regression analysis that was used to determine the coefficients for the thermal offset equation of the SDP were established using a baseline solar irradiance level of 5.7105 (in.·lb/s)/in.^{2}. Therefore, the solar load factor must be used to adjust for the difference in the actual level of solar irradiance that the IG unit is subjected to and the baseline value of 5.7105 (in.·lb/s)/in.^{2}. This calculation is shown in Eq. (144) for FEA 1.

$$\text{SLF} = \frac{I_S}{5.7105} = \frac{4.9967}{5.7105} = 0.875 \tag{144}$$

Where all of the variables are as previously defined.

Now, Eq. (80) can be used to determine the maximum perimeter-of-glass thermal stress for the glass plate of interest in the IG unit. This calculation is shown in Eq. (145) for the inner glass plate of FEA 1. The final step in the procedure is to apply the glass ESFPM. This step is discussed in detail later.

$$\begin{aligned} \sigma_{max} &= \alpha_T \cdot E \cdot [SLF \cdot AF \cdot b \pm m \cdot (T_{outdoor} - T_{indoor})] \\ &= \left(4.9 \times 10^{-6} \frac{in./in.}{\text{°F}}\right) \cdot (10.4 \times 10^6\ psi) \\ &\cdot \left[0.875 \cdot 1.060 \cdot 5.2303\ \text{°F} - \left(0.2120\ \frac{\text{°F}}{\text{°F}}\right)\right. \\ &\left. \cdot (-10\ \text{°F} - 79\ \text{°F})\right] = 1209\ psi \end{aligned} \tag{145}$$

Where all of the variables are as previously defined.

This procedure was repeated for the both the inner and outer glass plates for each case considered as part of this practical application. In addition, the first and second-order polynomial models were considered. Using the data presented in Table 74 previously and the procedure outlined above, the inputs for the SDP were determined. These inputs are presented in Table 79.

Table 79. Inputs for SDP

Case No.	$\Delta T_{indoor/outdoor}$ (°F)	$\alpha_{outer}/\alpha_{net}$	SLF	AF
FEA 1	-89	0.572	0.875	1.060
FEA 2	-89	0.572	0.875	1.060
FEA 3	37	0.572	1.047	1.060
FEA 4	37	0.572	1.047	1.060
FEA 5	-89	0.864	0.875	1.578
FEA 6	-89	0.864	0.875	1.578
FEA 7	37	0.864	1.047	1.578
FEA 8	37	0.864	1.047	1.578

Tables 80 and 81 shows the maximum perimeter-of-glass tensile stress for the inner glass plate using the first-order and second-order models, respectively. For all of the stress analyses shown in this section, the percent error was determined assuming the stresses calculated using the FDP are the "correct" stresses. Tables 82 and 83 shows the maximum perimeter-of-glass tensile stress for the outer glass plate using the first-order and second-order models, respectively.

Table 80. Summary of Stress from Regression Analysis Using First-Order Polynomial Model for the Inner Glass Plate

Case No.	Formal Design Procedure (psi)	Simplified Design Procedure (psi)	Error (psi)	Percent Error
FEA 1	1190	1209	19	1.58%
FEA 2	1963	1961	-2	0.11%
FEA 5	1576	1456	-120	7.63%
FEA 6	2281	2418	137	6.00%

Table 81. Summary of Stress from Regression Analysis Using Second-Order Polynomial Model for the Inner Glass Plate

Case No.	Formal Design Procedure (psi)	Simplified Design Procedure (psi)	Error (psi)	Percent Error
FEA 1	1190	1204	14	1.16%
FEA 2	1963	2004	41	2.09%
FEA 5	1576	1496	-80	5.07%
FEA 6	2281	2335	54	2.37%

Table 82. Summary of Stress from Regression Analysis Using First-Order Polynomial Model for the Outer Glass Plate

Case No.	Formal Design Procedure (psi)	Simplified Design Procedure (psi)	Error (psi)	Percent Error
FEA 3	638	671	33	5.18%
FEA 4	1433	1435	2	0.17%
FEA 7	1415	1397	-17	1.21%
FEA 8	2701	2557	-144	5.34%

Table 83. Summary of Stress from Regression Analysis Using Second-Order Polynomial Model for the Outer Glass Plate

Case No.	Formal Design Procedure (psi)	Simplified Design Procedure (psi)	Error (psi)	Percent Error
FEA 3	638	652	15	2.30%
FEA 4	1433	1431	-2	0.12%
FEA 7	1415	1434	19	1.36%
FEA 8	2701	2682	-19	0.71%

As shown, the SDP provides a reasonable tool to determine the thermal stress that an IG unit experiences when it is subjected to a set of environmental conditions. The accuracy of the SDP is directly related to the order of the polynomial used for the regression analysis. While there were a few exceptions to this observation, in general the second-order polynomial reduced the overall error.

For the research herein, the orders of the polynomials used to model the transient and steady-state responses were held constant. That is to say, if a first-order steady-state polynomial model was used, a first-order polynomial model was used for the transient response. If a second-order steady-state polynomial model was used, a second-order polynomial model was used for the transient response. In practice, the orders of each response do not have to be constant. For some situations it may be practical to have a second-order model for the steady-state response and a first-order model for the transient response, or vice-versa. Using different orders of polynomial models may help to limit the overall number of terms that are needed to describe the response while providing the needed level of accuracy.

Regardless of the overall number of terms required by the polynomial model selected, the use of the SDP provides a great deal of utility for design professionals to evaluate thermal stress in IG units. As shown, it can be applied to a range of environmental conditions and can be presented in a compact tabular format. Perhaps the most daunting task would be entering the proper coefficients into the response equations. This can be easily overcome with the use of modern spreadsheet software such as Microsoft Excel or a standalone computer program.

The final step in the SDP is to apply the glass ESFPM to evaluate the POB for the calculated levels of thermal stress. For example, consider an IG unit with dimensions of 60 in. by 96 in. As stated previously, this is a common size that is used for vision glass in architectural glazing applications.

The first step in applying the glass ESFPM is to determine the perimeter length of the IG unit. The total perimeter length for the 60 in. by 96 in. IG unit is 312 in. This calculation is shown in Eq. (146) below.

$$p = 2 \cdot (W + L) = 2 \cdot (60\ in. + 96\ in.) = 312\ in. \tag{146}$$

Where all of the variables are as previously defined.

Knowing the perimeter length, Fig. 26 can now be used to determine the maximum allowable stress for a given POB. The maximum allowable stress is determined by entering the horizontal axis of Fig. 26 at 312 in. and projecting upward to the appropriate POB and then leftward to estimate the allowable edge stress. This procedure is presented in Fig. 206 for a 0.0001 POB that is associated with 1 glass plate breakage per 10,000 glass plates. In addition, this procedure is presented in Fig. 207 for a 0.008 POB that is associated with 8 glass plate breakages per 1,000 glass plates. As shown, the maximum allowable stress for 0.0001 and 0.008 POB are 870 and 1,627 psi, respectively.

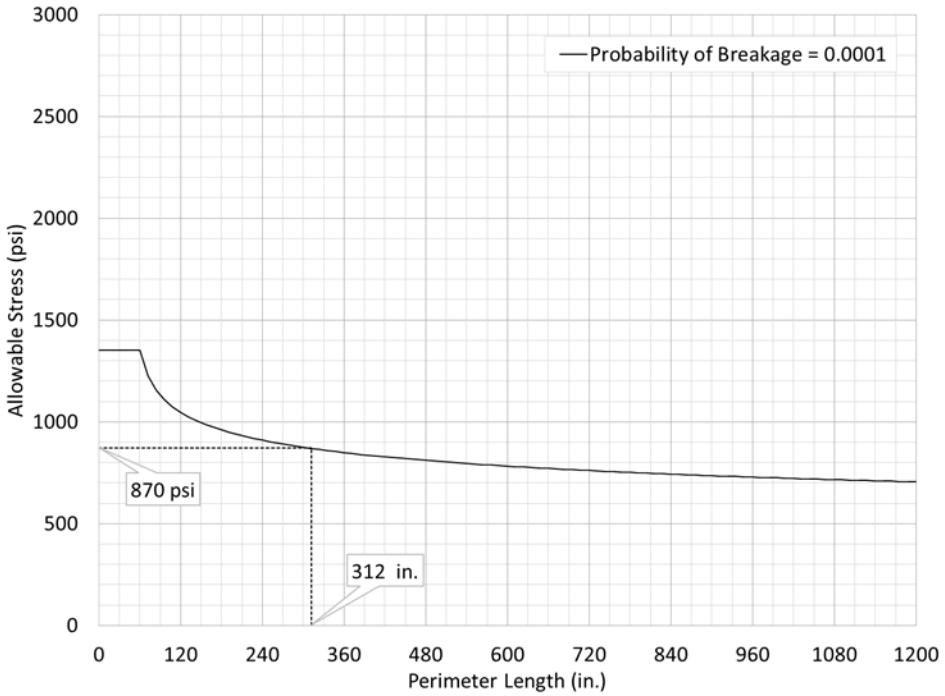

Fig. 206. Allowable Stress for a Glass Plate with a Perimeter Length of 312 in. and a POB of 1 Glass Plate per 10,000 Glass Plates

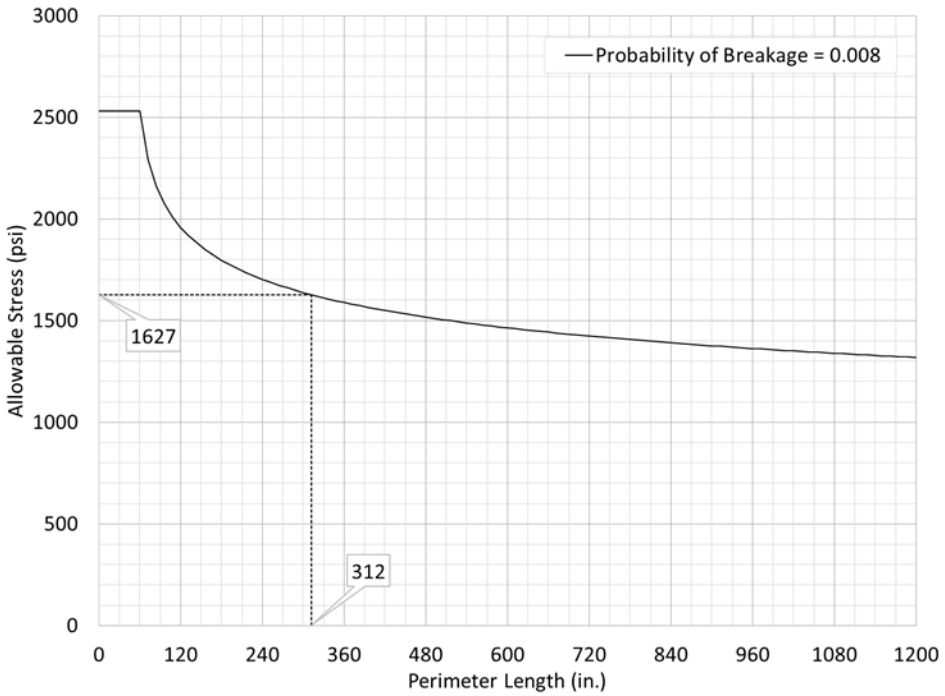

Fig. 207. Allowable Stress for a Glass Plate with a Perimeter Length of 312 in. and a POB of 8 Glass Plates per 1,000 Glass Plates

This procedure was repeated for each POB presented in Fig. 26. Table 84 shows the estimated allowable stress, $\sigma_{allowable}$, for each POB for a glass plate with a perimeter length of 312 in. In addition, Table 84 shows the value for the risk function associated with each POB for an IG unit with a perimeter length of 312 in. The risk function, B, was calculated using Eq. (54) presented previously.

Table 84. Allowable Stress and Risk Function vs. POB

P_b	B	$\sigma_{allowable}$ (psi)
0.0001	0.00010001	870
0.0010	0.00100050	1208
0.0020	0.00200200	1334
0.0040	0.00400802	1473
0.0080	0.00803217	1627

Knowing the allowable stress for each POB, these data are then compared to the maximum thermal stress estimated using the SDP previously. For this example, the thermal stress data determined using the first-order and second-order polynomial models for the inner and outer glass plates for FEA 1 through 8 were used. Tables 85 and 86 show the results from applying the glass ESFPM to the inner glass plate using the first-order and second-order polynomial models, respectively. Tables 87 and 88 show the results from applying the glass ESFPM to the outer glass plate using the first-order and second-order polynomial models, respectively.

Table 85. Summary of Glass ESFPM Applied to the Inner Glass Plate (First-Order Model)

Case No.	σ_{max}	Probability of Breakage, P_b				
		1/10000	1/1000	2/1000	4/1000	8/1000
	(psi)	$\sigma_{allowable}$ = 870 psi	$\sigma_{allowable}$ = 1208 psi	$\sigma_{allowable}$ = 1334 psi	$\sigma_{allowable}$ = 1473 psi	$\sigma_{allowable}$ = 1627 psi
FEA 1	1209	N.G.	N.G.	OK	OK	OK
FEA 2	1961	N.G.	N.G.	N.G.	N.G.	N.G.
FEA 5	1456	N.G.	N.G.	N.G.	OK	OK
FEA 6	2418	N.G.	N.G.	N.G.	N.G.	N.G.

Table 86. Summary of Glass ESFPM Applied to the Inner Glass Plate (Second-Order Model)

Case No.	σ_{max}	Probability of Breakage, P_b				
		1/10000	1/1000	2/1000	4/1000	8/1000
	(psi)	$\sigma_{allowable}$ = 870 psi	$\sigma_{allowable}$ = 1208 psi	$\sigma_{allowable}$ = 1334 psi	$\sigma_{allowable}$ = 1473 psi	$\sigma_{allowable}$ = 1627 psi
FEA 1	1204	N.G.	OK	OK	OK	OK
FEA 2	2004	N.G.	N.G.	N.G.	N.G.	N.G.
FEA 5	1496	N.G.	N.G.	N.G.	N.G.	OK
FEA 6	2335	N.G.	N.G.	N.G.	N.G.	N.G.

Table 87. Summary of Glass ESFPM Applied to the Outer Glass Plate (First-Order Model)

Case No.	σ_{max}	Probability of Breakage, P_b				
		1/10000	1/1000	2/1000	4/1000	8/1000
	(psi)	$\sigma_{allowable}$ = 870 psi	$\sigma_{allowable}$ = 1208 psi	$\sigma_{allowable}$ = 1334 psi	$\sigma_{allowable}$ = 1473 psi	$\sigma_{allowable}$ = 1627 psi
FEA 3	652	OK	OK	OK	OK	OK
FEA 4	1431	N.G.	N.G.	N.G.	OK	OK
FEA 7	1434	N.G.	N.G.	N.G.	OK	OK
FEA 8	2682	N.G.	N.G.	N.G.	N.G.	N.G.

Table 88. Summary of Glass ESFPM Applied to the Outer Glass Plate (Second-Order Model)

Case No.	σ_{max}	Probability of Breakage, P_b				
		1/10000	1/1000	2/1000	4/1000	8/1000
	(psi)	$\sigma_{allowable}$ = 870 psi	$\sigma_{allowable}$ = 1208 psi	$\sigma_{allowable}$ = 1334 psi	$\sigma_{allowable}$ = 1473 psi	$\sigma_{allowable}$ = 1627 psi
FEA 3	640	OK	OK	OK	OK	OK
FEA 4	1404	N.G.	N.G.	N.G.	OK	OK
FEA 7	1407	N.G.	N.G.	N.G.	OK	OK
FEA 8	2631	N.G.	N.G.	N.G.	N.G.	N.G.

If the allowable stress for a given POB was greater than the thermal stress, the risk of breakage was considered to be acceptable. This was designated using "OK" in the tables. If the allowable stress for a given POB was less than the thermal stress, the risk of breakage was considered to be unacceptable. This was designated using "N.G." in the

tables. As shown in Tables 85 and 86, some cases were found to be acceptable and others not acceptable. In addition, it is shown that the order of the polynomial model that is used to determine the maximum thermal stress can affect whether the POB is found to be acceptable or not. This is evident from FEA 1 and 5 for POB 0.0001 and 0.004, respectively. These two cases provide a good example for when the more detailed FDP is recommended to accurately determine whether the POB is acceptable or not. Ultimately, it is the responsibility of the design engineer to select the appropriate POB to meet the goals of the project.

CHAPTER VII
CONCLUSIONS

Research Summary

In recent years, there has been an increase in the number of glass plates that have experienced breakage due to thermal stresses when subjected to solar irradiance. The increase in glass plate breakage is largely due to the growth in the use of insulating glass (IG) units in the residential and commercial built environment and the ever increasing demand for energy-efficient window systems. Experience and research suggests that as IG units become more energy-efficient there is an increase in the thermal stresses that are induced by exposure to solar irradiance. This in turn leads to a higher propensity for glass plate breakage. This has become one of the leading issues within the architectural glass industry.

The purpose of the research presented herein was to improve the understanding of how thermal stresses develop in IG units when they are exposed to solar irradiance. Further, the purpose was to develop procedures and a model that can be used to evaluate the probability of breakage (POB) of IG units subjected to solar irradiance. This was accomplished in four distinct parts. The first part involved a literature review of pertinent information to establish the thermal behavior of IG units subjected to solar irradiance and develop an understanding of previous research that had been performed. For the second part, a formal design procedure (FDP) was developed to evaluate the POB for a specific IG unit under a specific set of environmental conditions. For the third part, a formal test procedure (FTP) was developed to determine a linear coefficient to describe the heat transfer across the gas space cavity of an IG unit. For the final part, a simplified design procedure (SDP) was developed to evaluate the POB for generic IG units under a general range of environmental conditions.

The most accurate method to evaluate the POB for an IG unit exposed to solar irradiance is to employ the FDP presented herein. This procedure involves modeling the IG unit of interest under the prescribed environmental conditions. This requires building a detailed finite element (FE) model of the IG unit, measuring the combined energy exchange coefficient (CEEC) for the gas space cavity, and determining the allowable stress for a given POB using the glass edge strength failure prediction model (ESFPM). Use of the FDP was demonstrated using four different IG units under two sets of environmental conditions.

IG units interact with the surrounding environment in a similar way to monolithic glass plates. The temperature of the glass plate or plates increase when subjected to solar irradiance by way of absorbed solar heat gain. Heat is continuously exchanged with the surrounding indoor and outdoor environments. For the indoor environment, heat is exchanged though conduction, natural convection, and long-wave radiation. For the outdoor environment, heat is exchanged through conduction, forced convection, and long-wave radiation. IG units add an additional component to heat exchange process which occurs through the gas space cavity. Heat is exchanged between the two glass plates through conduction, natural convection, and long-wave radiation.

The fundamental heat transfer mechanisms that describe the behavior of the heat exchanged through the gas space cavity combine in a non-linear fashion due to the long-wave radiation component. Thus, calculating the heat transferred across the gas space cavity using fundamental theory is complex and requires the use of an iterative procedure. The research herein builds on previous research presented by Klam (2007) to show that this non-linear behavior can be reasonably estimated using a single linear coefficient. The CEEC greatly simplifies the thermal analysis procedure required for IG units by removing the need for iteration. Klam (2007) developed a numerical propagation procedure (NPP) based on fundamental theory and ideal properties to solve for the CEEC.

As part of this research it was shown that it is possible to determine the CEEC for an IG unit using straight-forward physical experiments. Thus, a FTP was developed. These experiments were carried out on small representative IG unit specimens. These physical experiments were then combined with a parameter identification optimization procedure (PIOP) that was capable of determining the best-fit coefficient to estimate the heat transfer across the gas space cavity of the IG unit.

The size of the specimen that was selected for these experiments is representative of IG units that are installed in typical architectural glazing applications. In addition, the FTP is conducted at temperatures and time durations that are meaningful to IG units subjected to thermal loadings. As part of this effort, a special testing device was designed to remove the possibility of surface films from developing on the surfaces of the glass plates.

A parametric study of eight tests were performed using the criteria set forth by the FTP to measure the CEEC for different types of IG units. Results from these experiments show that the behavior of heat transferred through the gas space cavity of an IG unit can be reasonably estimated using a single linear coefficient. Further, this coefficient can be determined more accurately using physical experiments than using fundamental theory and ideal properties for the gas fill, glass plates, and associated glass plate surfaces. Two important observations were made regarding the application of low emissivity (low-E) coatings. For all cases, the application of a low-E coating has a significant effect on reducing the heat transfer through the gas space cavity of an IG unit. Additionally, the measured value for the CEEC is independent of the location of the low-E coating (i.e. number 2 or 3 surface).

A simplified design procedure (SDP) was developed that incorporates the CEEC and can be used to evaluate the POB for glass plates in generic IG units that are subjected to a general range of environmental conditions. The purpose in developing the SDP was to present a framework for generic procedures that can be incorporated into an ASTM,

IGMA standard, or a design code that provides a tool to evaluate the POB of IG units. It was shown that the SDP can be used to reasonably evaluate the POB for an IG unit subjected to solar irradiance. However, the SDP is not a replacement for the more detailed FDP for significant projects that involve large glass plates, a large number of glass plates, or unusual situations including shadows, interior reflective devices, etc.

The SDP was demonstrated using two different idealized frames, perfectly insulated and high-heat mass, a thin, steel-channel spacer, and 0.25 in. thick nominal glass plates. The input parameters for the SDP included the indoor and outdoor temperatures, solar irradiance, absorption of each glass plate, the edge bite of the frame, and the CEEC. A parametric study was performed using the SDP on the same IG units that were used as examples for the FDP. In addition, the environmental conditions used for the FDP were replicated for the SDP. By comparing the results from these two procedures, it was shown that the SDP can be used to reasonably evaluate the POB of glass plates in IG units.

Several important observations were made during the course of this research. First, the use of a low-E coating acts to increase the maximum level of thermal stress induced in the IG unit. This is caused by the increase in absorptance characteristics of the glass plates and the reduction in heat transfer through the gas space cavity of the IG unit.

In addition, the maximum level of thermal stress that occurs in an IG unit is linear with the level of exposure to solar irradiance. This is significant because the maximum thermal stress for any level of solar irradiance can be determined by performing a single transient FE analysis and fitting the data point with a straight line that passes through the origin where zero solar irradiance is applied.

Another observation was made to suggest that IG units can develop a pre-stress that is independent of exposure to solar irradiance. This pre-stress is caused by the thermal

bridging that occurs at the edge-seal of an IG unit. All that is necessary for the pre-stress condition to develop is a difference in temperature between the indoor and outdoor environments. Conveniently, the relationship between pre-stress and the difference in temperature of the indoor and outdoor environments is linear. This is significant because the maximum pre-stress for any temperature difference can be determined by performing a single steady-state FE analysis and fitting the data point with a straight line that passes through the origin where the indoor temperature is equal to the outdoor temperature and the pre-stress due to the indoor/outdoor temperature difference is zero.

Finally, when the temperature of the outdoor environment is colder than the indoor environment (i.e. a cold climate), the inner glass plate resides at a higher temperature than the outer glass plate. Heat is transferred from the inner glass plate with a higher temperature to the colder outer glass plate through the edge-seal. The heat transfer increases the edge-of-glass temperature of the outer glass plate while decreasing the edge-of-glass temperature of the inner glass plate. The net result is tensile stresses develop in the inner glass plate and compressive stresses develop in the outer glass plate. This phenomenon is reversed when the temperature of the outdoor environment is warmer than the indoor environment (i.e. a warm climate). In this situation, tensile stresses develop in the outer glass plate and compressive stresses develop in the inner glass plate. Therefore, the inner glass plate is more susceptible to thermal stress breakage than the outer glass plate in colder climates. Likewise, the outer glass plate is more susceptible to thermal stress breakage than the inner glass plate in warmer climates.

Major Conclusions

The major conclusions that can be drawn from this research are as follows:

- The FDP can be used to evaluate the POB of the glass plates in a specific IG unit under a specific set of environmental conditions and exposure to solar irradiance.

- A linear CEEC can be used to reasonably estimate the heat transfer through the gas space cavity of an IG unit.
- The FTP, which uses a physical experiment and a PIOP, can be used to determine the best-fit CEEC more accurately than using the NPP and fundamental theories.
- The SDP can be used to reasonably evaluate the POB of glass plates in generic IG units under a general range of environmental conditions and solar irradiance.
- Due to the thermal bridging that occurs at the edge-seal of an IG unit, a pre-stress develops in each glass plate in the presence of a difference between the indoor and outdoor temperatures.
- The pre-stress that develops is independent of exposure to solar irradiance and has a linear relationship to the difference between the indoor and outdoor temperatures.
- The maximum tensile thermal stress occurs in the inner glass plate when the outdoor temperature is colder than the indoor temperature. Conversely, the maximum tensile thermal stress occurs in the outer glass plate when the outdoor temperature is warmer than the indoor temperature.
- The use of low-E coatings reduce the heat transfer across the gas space cavity of IG units by reducing the long-wave radiation between the two glass plates.
- The use of low-E coatings increase the maximum thermal stress induced in IG units.
- The maximum tensile thermal stress that occurs in an IG unit is independent of the pre-stress that develops due to the difference between the indoor and outdoor temperatures and has a linear relationship with the level of exposure to solar irradiance and the net absorption of the IG unit.

Note that the purpose of this dissertation was to develop procedures that can be used to evaluate the POB of glass plates when used in IG units that are exposed to solar irradiance. The purpose was not to develop a full range of design criteria for specific IG units.

Careful considerations should be taken when applying the results presented herein to the design of IG units subjected to thermal stress.

Future Research

The research presented in this dissertation was solely focused on solar irradiance as the primary mechanism by which heat was input into IG units. There are a number of other mechanisms that can apply heat to IG units. Experience suggests that heating, ventilation, and air conditioning (HVAC) systems, intense indoor lighting, etc., can have a significant effect on the development of thermal stresses in IG units. In addition, other factors including shadows, indoor and outdoor heat traps such as Venetian blinds and window treatments, and the orientation of the gas space cavity have an influence on the development of thermal stresses in IG units. These factors are difficult to examine using a generic procedure, but should be considered during the design process. Such factors were not considered herein and are a topic for future research.

Further research should also be performed to verify that the surface film coefficients used herein are indeed appropriately conservative for all thermal design situations. As an example, it is conceivable that a larger value for the indoor surface film coefficient may be needed to conservatively evaluate the outer glass plate when an IG unit is placed in a warm climate. This is the case because a larger surface film coefficient would increase the transfer of heat between the inner glass plate and the indoor environment. Thus, the temperature of the inner glass plate would be reduced. This would increase the heat that is transferred from the outer glass plate to the inner glass plate through the edge-seal thus, reducing the perimeter-of-glass temperature and increasing the thermal stress in the outer glass plate.

A SDP was presented to evaluate the POB for glass plates used in IG units that are subjected to solar irradiance. The SDP was developed on the premise that the heat exchanged across the gas space cavity of an IG unit can be reasonably estimated using a linear CEEC. The CEEC is dependent on several properties of the IG unit. Among these properties is the type of gas that is used to fill the gas space cavity. The research presented herein focused solely on air as the type of gas fill. Therefore, further research is needed to expand the use of the SDP to include commonly available gas fills such as Krypton and Argon. While the CEEC accounts for the heat that is transferred across the gas space cavity, regardless of the type of gas fill, an additional factor may need to be introduced to account for the variation in the density and specific heat of each type of gas fill from that used to model air.

The SDP developed herein was shown to provide reasonable results for perfectly insulated and high-heat mass frames. These two frames were selected to provide the upper and lower theoretical boundaries for the maximum and minimum thermal stresses that can develop in an IG unit. This is the case because the perfectly insulated frame does not allow heat to be transferred between the glass plate and frame, while the high-heat mass frame assumes that the glass plate remains constant at the initial temperature. In addition, the concept was proven using a single thin, steel-channel spacer and glass plates with 0.25 in. nominal thickness.

A large number of different frames, spacers, and nominal glass plate thicknesses are commercially available. Thus, a comprehensive program needs to be developed that expands the use of the SDP to include these various frames, spacers, and nominal glass plate thicknesses. While it would be impossible to include all of the various frames, spacers, and nominal glass plate thicknesses, those representative of the majority used in architectural glazing applications should be included in the final model.

The procedures and models presented herein were intended to provide a basis from which a design standard, practice, or code can be developed to evaluate the POB of glass plates that are used in generic IG units subjected to solar irradiance and a general set of environmental conditions. Upon implementing these procedures and models to develop a design standard, it is recommended that an in-service performance evaluation and/or physical testing be performed to verify that the results are adequately accurate and conservative. Research should continue until sufficient data has been collected to properly design IG units to withstand thermally induced stress.

REFERENCES

Abbey, T. (2014). *"How to use FEA for thermal analysis."* <http://www.digi-taleng.news/de/use-fea-thermal-analysis/> (September 12, 2016).

Abiassi, J. J. (1981). "The strength of weathered window glass using surface characteristics." M.S. Thesis, Department of Civil Engineering, Texas Tech University, Lubbock, TX.

American Architectural Manufacturers Association (AAMA). (1984). "Structural Properties of Glass." *Curtain Wall Glass*, 12.

American Architectural Manufacturers Association (AAMA). (2009). "Voluntary test method for thermal transmittance and condensation resistance of windows, doors and glazed wall sections." *AAMA 1503-09,* Schaumburg, IL.

American Society of Heating, Refrigerating and Air-Conditioning Engineers (ASHRAE). (2013). *ASHRAE handbook: Fundamentals,* Atlanta, GA.

ASTM International (ASTM). (2011). "Standard specification for flat glass." *ASTM Standard C1036-11e1*, West Conshohocken, PA.

ASTM International (ASTM). (2012a). "Standard practice for determining the resistance of single glazed annealed architectural flat glass to thermal loadings." *ASTM Standard E2431-12*, West Conshohocken, PA.

ASTM International (ASTM). (2012b). "Standard specification for heat-strengthened and fully tempered flat glass." *ASTM Standard C1048-12e1*, West Conshohocken, PA.

ASTM International (ASTM). (2014). "Standard solar constant and zero air mass solar spectral irradiance tables." *ASTM Standard E490-00a(2014)*, West Conshohocken, PA.

ASTM International (ASTM). (2016). "Standard practice for determining load resistance of glass in buildings." *ASTM Standard E1300-16*, West Conshohocken, PA.

Baker, J. A., Sullivan, H. F., and Wright, J. L. (1989). "A study of pane spacing in glazing systems." *Proc., Solar Energy Society of Canada*, Penticton, Canada, 267-272.

Batchelor, G. K. (1954). "Heat transfer by free convection across a closed cavity between vertical boundaries at different temperatures." *Quarterly Applied Mathematics*, 12, 209-233.

Beason, W. L. (1980). "A failure prediction model for window glass." Ph.D. Dissertation, Department of Civil Engineering, Texas Tech University, Lubbock, TX.

Beason, W. L., and Morgan, J. R. (1984). "Glass failure prediction model." *Journal of Structural Engineering,* 110, 2, 197-212.

Beason, W. L. (1986a). "Structural analysis of sealed insulating glass." *Journal of Structural Engineering,* ASCE, 112, 5, 1133-1146.

Beason, W. L. (1986b). *"Design Criteria for Insulating Glass with Plates of Equal and Different Thicknesses."* Unpublished Report Submitted to Cardinal IG, Texas Engineering Experiment Station, Texas A&M University, College Station, TX.

Beason, W. L., and Lera, J. (1989). *"An evaluation of the failure risks of a specific window design."* Unpublished Report Submitted to Rolscreen Company, Texas Engineering Experiment Station, Texas A&M University, College Station, TX.

Beason, W. L. (1989). *"Edge Strength Failure Prediction Model for Glass Plates Subjected to Thermal Stresses."* Unpublished Report Submitted to Cardinal IG, Texas Engineering Experiment Station, Texas A&M University, College Station, TX.

Beason, W. L., Kohutek, T. L., and Bracci, J. M. (1998). "Basis for ASTM E 1300 annealed glass thickness selection charts," *Journal of structural engineering,* 124, 2, 215-221.

Beason, W. L., and Lingnell A. W. (2000). *"Development of a Thermal Stress Evaluation Procedure for Monolithic Glass."* Unpublished Report Submitted to Visteon Float Glass Operations, Lingnell Consulting Services, Rockwall, TX.

Beason, W. L., and Lingnell A. W. (2002). "A thermal stress evaluation procedure for monolithic glass." *Proc., The Use of Glass in Buildings, ASTM special technical publication 1434,* V. Block, ed., ASTM International, West Conshohocken, PA, 105-118.

Beer, F. P., Johnston, Jr., E. R., DeWolf, J. T., and Mazurek, D. F. (2012). *Mechanics of materials, sixth edition*, McGraw-Hill, New York, NY.

Bergman, T. L., Lavine, A. S., Incropera, F. P., and DeWitt, D. P. (2011). *Fundamentals of heat and mass transfer, seventh edition,* John Wiley & Sons, New York, NY.

Berkovsky, B. M., and Polevikov, V.K. (1977). "Numerical study of problems on high-intensive free convection." Heat Transfer and Turbulent Buoyant Convection, D. B. Spalding and N. Afgan, eds., Hemisphere Publishing Corporation, Washington, DC, Vol. 2, 443-455.

Brown, W. G., (1974). "A Practical Formulation for the Strength of Glass and Its Special Application to Large Plates." *Publication No. NRC 14372*, National Research Council of Canada, Ottawa, Ontario, Canada.

Carmody, J., Selkowitz, S., Arasteh, D., and Heschong, L. (2007). *Residential windows: A guide to new technologies and energy performance, third edition,* W. W. Norton & Company, New York, NY.

Dalgliesh, W. A., and Taylor, D. A. (1990). "The strength and testing of window glass." *Canadian Journal of Civil Engineering,* 17, 752-762.

Datta, A. K. (2002). *Biological and Bioenvironmental Heat and Mass Transfer,* Marcel Dekker, New York, NY.

De Graaf, J. G. A., and Van Der Held, E. F. M. (1952). "The relation between the heat transfer and the convection phenomena in enclosed plane air layers." *Applied Scientific Research,* 3, 393-409.

Ditsworth, J. M. (1992). "Development of a failure prediction model for heat-treated glass." M.S. Thesis, Department of Civil Engineering, Texas A&M University, College Station, TX.

Draper, N. R., and Smith, H. (1998). *Applied regression analysis, third edition,* John Wiley & Sons, New York, NY.

Duffie, J. A., and Beckman, W. A. (1974). *Solar energy thermal processes*, John Wiley & Sons, New York, NY.

Eckert, E. R. G., and Carlson, W. O. (1961). "Natural convection in an air layer enclosed between two vertical plates with different temperatures." *International Journal of Heat and Mass Transfer*, 2, 106-120.

Elder, J. W. (1965). "Turbulent free convection in a vertical slot." *Journal of Fluid Mechanics,* 23, 99-111.

El Sherbiny, S. M. (1980). "Heat transfer by natural convection across vertical and inclined air layers.", Ph.D. Dissertation, Department of Mechanical Engineering, University of Waterloo, Waterloo, Ontario, Canada.

El Sherbiny, S. M., Hollands, K. G. T., and Raithby, G. D. (1982a). "Effect of thermal boundary conditions on natural convection in vertical and inclined air layers." *Journal of Heat Transfer*, 104, 515-520.

El Sherbiny, S. M., Raithby, G. D., and Hollands, K. G. T. (1982b). "Heat transfer by natural convection across vertical and inclined air layers." *Journal of Heat Transfer,* 104, 96-102.

El Sherbiny, S. M., Hollands, K. G. T., and Raithby, G. D. (1983). "Nusselt number distribution in vertical and inclined air layers." *Journal of Heat Transfer*, 105, 406-408.

Environmental Protection Agency (EPA). (2014). "Fuel economy testing and labeling: Questions and answers." <https://www3.epa.gov/fueleconomy/documents/420f14015.pdf> (June 30, 2016).

Finlayson, E., Arasteh, D., Huizenga, C., and Rubin, M. (1993). *"WINDOW 4.0: documentation of calculation procedures."* < https://windows.lbl.gov/software/window/window_docs.htm> (June 21, 2016).

Fisher, S. D. (2007). "Proposed modification of THERM finite-element models taken from the national fenestration rating council's thermal rating program for the analysis and estimation of thermal-induced glass stress under solar and shadow loading conditions on fenestration products." *Proc., Buildings X: Thermal performance of exterior envelopes of whole buildings*, ASHRAE, Atlanta, GA.

Glass Association of North America (GANA). (2008). *GANA glazing manual, 50th anniversary edition,* Topeka, KS.

Gere, J. M., and Timoshenko, S. P. (1997). *Mechanics of materials, fourth edition*, PWS Publishing Company, Boston, MA.

Gordon, J. (2001). *Solar energy: The state of the art,* James & James, London, UK, Chapter 2, pp. 29-107.

Gustavsen, A., Arasteh, D., Kohler, C. and Curcija, D. (2005). "Two-dimensional conduction and CFD simulations of heat transfer in horizontal window frame cavities." *ASHRAE Transactions,* 111, 587-598.

Halliday, D., Resnick, R., and Walker, J. (2005). *Fundamentals of physics, seventh edition,* John Wiley & Sons, New York, NY.

Hallquist, J. O. (2006). *"LS-DYNA theory manual."* Livermore Software Technology Corporation (LSTC), Livermore, CA, <http://ftp.lstc.com/anonymous/outgoing/jday/manuals/ls-dyna_theory_manual_2006.pdf> (August 27, 2016).

Hollands, K. G. T., Unny, T. E., Raithby, G. D., and Konicek, L. (1976). "Free convective heat transfer across inclined air layers." *Journal of Heat Transfer*, Transactions of the ASME, 98, 189-193.

"International Glazing Database." (IGDB). (2016). <https://windows.lbl.gov/materials/igdb/> (September 13, 2016).

International Organization for Standardization (ISO). (2003). "Thermal performance of windows, doors and shading devices – Detailed calculations." *International Standard ISO 15099:2003(E),* Vernier, Geneva, Switzerland.

Ismail, K. R., and Henriquez, J. R. (2005). "Two-dimensional model for the double glass naturally ventilated window." *International Journal of Heat and Mass Transfer,* 48, 461-475.

Kaliakin, V. N. (2016). *"Selected topics in numerical analysis: Polynomials."* <http://www.ce.udel.edu/faculty/kaliakin/appendix_poly.pdf> (July 29, 2016).

Kennedy, J. B. (1976). *Basic statistical methods for engineers and scientists, second edition,* Thomas Y. Crowell Company, New York, NY.

Klam, J. W. (2007). "Development of a simplified thermal analysis procedure for insulating glass units." M.S. Thesis, Department of Civil Engineering, Texas A&M University, College Station, TX.

Korpela, S. A., Lee, Y., and Drummond, J. E. (1982). "Heat transfer through a double pane window." *Journal of Heat Transfer*, Transactions of the ASME, 104, 539-544.

Lingnell, A. W. (1981). "Energy saving designs with glass." *Proc., Toledo Glass and Ceramic Award Symposium and Dinner*, W. A. Kneller, ed., EITEL Institute for Silicate Research, University of Toledo, Northwestern Ohio Section of American Ceramic Society, Toledo, OH, 27-32.

Lingnell, A. W., (1994). "Glass deflection characteristics for wall system design." *U.S. Glass*, 40-47.

Lingnell, A. W., and Beason. W. L. (2013). "Thermal Stress in Insulating Glass." *Proc., Glass Performance Days*, Tampere, Finland, 458-464.

Livermore Software Technology Corporation (LSTC). (1999). *"LS-DYNA thermal analysis user guide."* Livermore, CA, < www.dynaexamples.com/thermal/thermal.pdf/at_download/file> (August 22, 2016).

Livermore Software Technology Corporation (LSTC). (2014a). *"LS-DYNA keyword user's Manual: Volume I."* Version R7.1, Livermore, CA, <http://ftp.lstc.com/anonymous/outgoing/jday/manuals/LS-DYNA_manual_Vol_I_R7.1.pdf> (August 27, 2016).

Livermore Software Technology Corporation (LSTC). (2014b). *"LS-DYNA keyword user's Manual: Volume II."* Version R7.1, Livermore, CA,

<http://ftp.lstc.com/anonymous/outgoing/jday/manuals/LS-DYNA_manual_Vol_II_R7.1.pdf> (August 27, 2016).

Lopez-Anido, R. A., Naik, T. R., Fry, G. T., Lange, D. A., and Karbhari, V. M. (2000). *Emerging materials for civil infrastructure: State of the art,* American Society of Civil Engineers, Reston, VA, Chapter 8, pp. 190-216.

Maker, B. N. (2004). *"Implicit analysis with LS-DYNA Version 970."* Livermore Software Technology Corporation (LSTC), Livermore, CA.

Manz, H. (2003). "Numerical simulation of heat transfer by natural convection in cavities of façade elements." *Energy and Buildings,* 35, 305-311.

McLellan, G. W., and Shand, E. B. (1984). *Glass Engineering Handbook, third edition,* McGraw-Hill, New York, NY.

Mencik, J. (1992). *Strength and fracture of glass and ceramics*, Elsevier, Amsterdam.

Muneer, T., Abodahab, N., and Han, B. (1996). "Gas flow in window enclosures and its effect on temperature distribution." *Advances in Fluid Mechanics,* 9, 233-242.

Muneer, T., and Han, B. (1996). "Multiple glazed windows: Design charts." *Proc., Building Services Engineering Research and Technology,* 17, 4, 223-229.

Muneer, T., Abodahab, N., and Gilchrist, A. (1997). "Combined conduction, convection, and radiation heat transfer model for double-glazed windows." *Building Services Engineering Research and Technology,* 18, 183-191.

Muneer, T., Abodahab, N., Weir, G., and Kubie, J. (2000). *Windows in buildings: Thermal, acoustic, visual and solar performance,* Architectural Press, Woburn, MA.

National Aeronautics and Space Administration (NASA). (2008). *"Solar irradiance."* <http://www.nasa.gov/mission_pages/sdo/science/solar-irradiance.html> (August 28, 2016).

National Fenestration Rating Council (NFRC). (2014). "Procedure for determining fenestration product U-factors." ANSI/NFRC 100-2014E0A1, Greenbelt, MD.

National Fenestration Rating Council (NFRC). (2016). *"The facts about windows and heat loss."* <http://c.ymcdn.com/sites/nfrccommunity.site-ym.com/resource/resmgr/factsheets_2013/u-factorfactsheet2.pdf> (June 30, 2016).

Norville, S. H., and Minor, J. E. (1985). "Strength of weathered window glass." *American Ceramics Society Bulletin*, 64, 11, 1467-1470.

Oakes, T. A. (1991). "The development of design factors for heat-strengthened and tempered glass based on the glass failure prediction model." M.S. Thesis, Department of Civil Engineering, Texas A&M University, College Station, TX.

Pilette, C. F. and Taylor, D. A. (1988). "Thermal stresses in double-glazed windows." *Canadian Journal of Civil Engineering*, 15, 807-814.

Pilkington (2005). *"Thermal stress." ATS-123,* < https://www.pilkington.com/resources/ats123swthermalstress20050713.doc> (June 13, 2015).

Pilkington (2013a). *"General glazing guidelines." ATS-192,* <http://www.pilkington.com/resources/ats192generalglazingguidelines2013102.pdf> (May 24, 2016).

Pilkington (2013b). *"Glass and energy." ATS-116,* <http://www.pilkington.com/resources/ats116glassandenergy20130114nsgcleanlogo.pdf> (April 6, 2016).

Pilkington (2013c). *"Properties of soda-lime silica float glass.", ATS-129,* <http://www.pilkington.com/resources/ats129propertiesofglass20130114.pdf> (June 21, 2016).

Powles, R., Curcija, D., and Kohler, C. (2002). *"Solar absorption in thick and multi-layered glazings."* < http://eetd.lbl.gov/sites/all/files/publications/49555.pdf > (January 14, 2015).

PPG (2001). *"Gas space convection effects on U-values in insulating glass units." TD-101,* <http://buyat.ppg.com/glasstechlib/7_TD101F.pdf> (July 5, 2016).

PPG (2002). *"Guidelines for cut edge quality." TD-119,* <http://buyat.ppg.com/glasstechlib/60_TD119F.pdf> (July 5, 2016).

PPG (2008). *"Thermal stress update." TD-109,* <http://buyat.ppg.com/glasstech-lib/85_Thermal%20Stress%20Update-13June2008.pdf> (July 5, 2016).

Raithby G. D., Hollands, K. G. T., and Unny, T. E. (1977). "Analysis of heat transfer by natural convection across vertical fluid layers." *Journal of Heat Transfer*, Transactions of the ASME, 99, 287-293.

Redner, A. S., and Hoffman, B. R. (2001). "Detection of tensile stresses near edges of laminated and tempered glass*." Proc., Glass Processing Days,* Tampere, Finland, 589-591.

Rubin, M. (1982). "Calculating heat transfer through windows." *Energy Research,* 6, 341-349.

Sasaki, J. R. (1971). "Thermal-breakage potential of sealed glazing units." *Specification Associate*, 13, 2, 25-33.

Schrader, B. D. (1982). "The effects of age, surface damage, and humidity on the strength of window glass." M.E. Report, Department of Civil Engineering, Texas A&M University, College Station, TX.

Shapiro, A. (2013). *"Using LS-DYNA for heat transfer coupled thermal-stress problems."* Livermore Software Technology Corporation (LSTC), Livermore, CA.

Shewen, E. C. (1986). *"A Peltier effect technique for natural convection heat flux measurement applied to the rectangular open cavity."*, Ph.D. Dissertation, Department of Mechanical Engineering, University of Waterloo, Waterloo, Ontario, Canada.

Shewen, E., Hollands, K. G. T., and Raithby, G. D. (1996). "Heat transfer by natural convection across a vertical air cavity of large aspect ratio." *Journal of Heat Transfer*, Transactions of the ASME, 118, 993-995.

Stander, N., and Goel, T. (2010). *"LS-Opt Training Class: Optimization Theory."* <http://www.lsoptsupport.com/documents/training-class-handouts/docs/lsopt_optimization_class.pdf/at_download/file> (August 14, 2016).

Stander, N., Roux, W., Basudhar, A., Eggleston, T., Goel, T., and Craig, K. (2014). *"LS-OPT user's manual: A design optimization and probabilistic analysis tool for the engineering analyst."* Version 5.1, Livermore Software Technology Corporation (LSTC), Livermore, CA, <http://ftp.lstc.com/anonymous/outgoing/jday/lsopt/manuals/lsopt_52_manual.pdf> (August 14, 2016).

Turner, D. P. (1977). *Window glass design guide,* Architectural Press, London, UK.

U.S. Energy Information Administration (USEIA). (2016). *"Frequently asked questions: How much energy is consumed in residential and commercial buildings in the United States."* <http://www.eia.gov/tools/faqs/faq.cfm?id=86&t=1> (June 4, 2016).

Vallabhan, C. V. G., and Wang, B. Y. T. (1981). *"Nonlinear analysis of rectangular glass plates by finite difference methods."* Final Report, Institute for Disaster Research, Texas Tech University, Lubbock, TX.

Weibull, W. (1939). *"A Statistical Theory of the Strength of Materials."* Ingeniorsvetenskapsakademiens, Handlingar NR151, Stockholm.

Weisberg, S. (1980). *Applied linear regression,* John Wiley & Sons, New York, NY.

Wijeysundera, N. E. (1975). "A net radiation method for the transmittance and absorptivity of a series of parallel regions." *Solar Energy*, 17, 75-77.

Wright, J. L., and Sullivan, H. F. (1989). "Natural convection in sealed glazing units: A review." *ASHRAE Transactions,* 95, 592-603.

Wright, J. L., and Sullivan, H. F. (1995). "A two-dimensional numerical model for glazing system thermal analysis." *ASHRAE Transactions,* 101, 819-831.

Wright, J. L. (1996). "A correlation to quantify convective heat transfer between vertical window glazings." *ASHRAE Transactions,* 102, 940-946.

Wright, J. L. (1998). "Calculating center-glass performance indices of windows." *ASHRAE Transactions,* 104, 1230-1241.

Wright, J. L. and Barry, C. B. (1999). "A new approach to perimeter of glass temperature prediction and its application to predicting thermal breakage in insulated glazing units." *ASHRAE Transactions*, 105, 909-917.

Wright, J. L., and Kotey, N. A. (2006). "Solar absorption by each element in a glazing/shading layer array." *ASHRAE Transactions*, 112, 3-12.

Young, W. C., and Budynas, R. G. (2002). *Roark's Formulas for Stress and Strain, seventh edition,* McGraw-Hill, New York, NY, Chapter 16, pp. 743-770.

Zhao, Y. (1998). "Investigation of heat transfer performance in fenestration system based on finite element methods." Ph.D. Dissertation, Department of Mechanical and Industrial Engineering, University of Massachusetts, Amherst, MA.

Zhong-wei, L., Jia-lin, S., and Yan-ruo, H. (1999). "Thermal stress and fracture of building glass." *Glass Technology*, 40, 191-194.

APPENDIX A
THERMAL STRESS ANALYSIS OF A MONOLITHIC GLASS PLATE

The purpose of this discussion is to demonstrate the utility and accuracy of the fundamental equation that is used to approximate the maximum perimeter-of-glass tensile stress that develops in a monolithic glass plate subjected to solar irradiance. For this example, a 60 in. wide by 96 in. high monolithic glass plate was examined using a coupled thermal-mechanical finite element (FE) analysis.

The coupled thermal-mechanical FE analysis was used to determine the maximum thermal stress that develops due to differential heating of the monolithic glass plate. The results of the coupled thermal-mechanical FE analysis were then compared to the estimated tensile stresses that develop along the perimeter of the glass plate that were calculated using the fundamental understandings of the effect that differential temperature has on monolithic glass plates.

The fundamental equation that is often used to estimate the maximum thermal stress, σ_{max}, that develops along the perimeter of a monolithic glass plate when subjected to solar irradiance is presented in Eq. (147).

$$\sigma_{max} = \alpha_T \cdot E \cdot (T_{COG} - T_{POG}) \tag{147}$$

Where α_T is the coefficient of thermal expansion for plate glass with a value of 4.9×10^{-6} (in./in.)/°F (AAMA 1984), E is the modulus of elasticity of plate glass with a value of 10.4×10^6 psi (Beason and Lingnell 2002; AAMA 1984), T_{COG} is the center-of-glass temperature, and T_{POG} is the perimeter-of-glass temperature.

The coupled thermal-mechanical FE analysis was performed in four steps. First, a FE model of the monolithic glass plate was developed. Second, a steady-state thermal FE

analysis was performed. Third, a transient thermal FE analysis was performed. Finally, a mechanical FE analysis was performed.

The 60 in. by 96 in. monolithic glass plate was modeled using a three-dimensional quarter-plate FE model. The elements had dimensions of 0.5 in. by 0.5 in. in the plane of the glass plate and two elements were used through the thickness of the glass plate. The monolithic glass plate had an overall thickness of 0.219 in. The edge bite was 0.5 in. and the frame was considered to be perfectly insulated. Fig. A-1 shows the construct of nodes and elements that were used to model the monolithic glass plate.

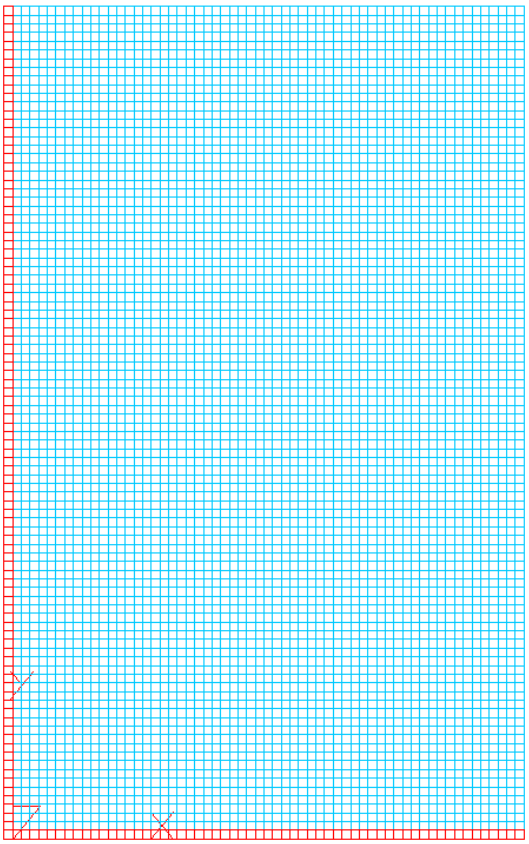

Fig. A-1. Monolithic Glass Plate FE Model

The center-of-glass area of the monolithic glass plate was subjected to 5.7105 (in.·lb/s)/in.^{2} of solar irradiance and the edge bite of the monolithic glass plate was shielded from solar irradiance. The solar absorptance of the glass plate was taken to be 60 percent. Surface film coefficients were used to model the heat exchange that occurs between the monolithic glass plate and the indoor and outdoor environments. An outdoor surface film coefficient of 4.2987×10^{-2} (in.·lb/s)/(in.^{2}·°F) and an indoor surface film coefficient of 2.5507×10^{-2} (in.·lb/s)/(in.^{2}·°F) were used. These surface film coefficients are those typically used for the design of monolithic glass plates subjected to solar irradiance (Beason and Lingnell 2002; ASTM 2012a). The indoor and outdoor temperatures were taken to be 68 and 32 °F, respectively.

The steady-state thermal FE analysis was used to establish the steady-state temperature conditions that exist just before the monolithic glass plate is exposed to solar irradiance. This is typically associated with the night-time condition where the monolithic glass plate is exposed to an indoor/outdoor temperature difference and zero solar irradiance. Figs. A-2 and A-3 show the results of the steady-state thermal FE analysis.

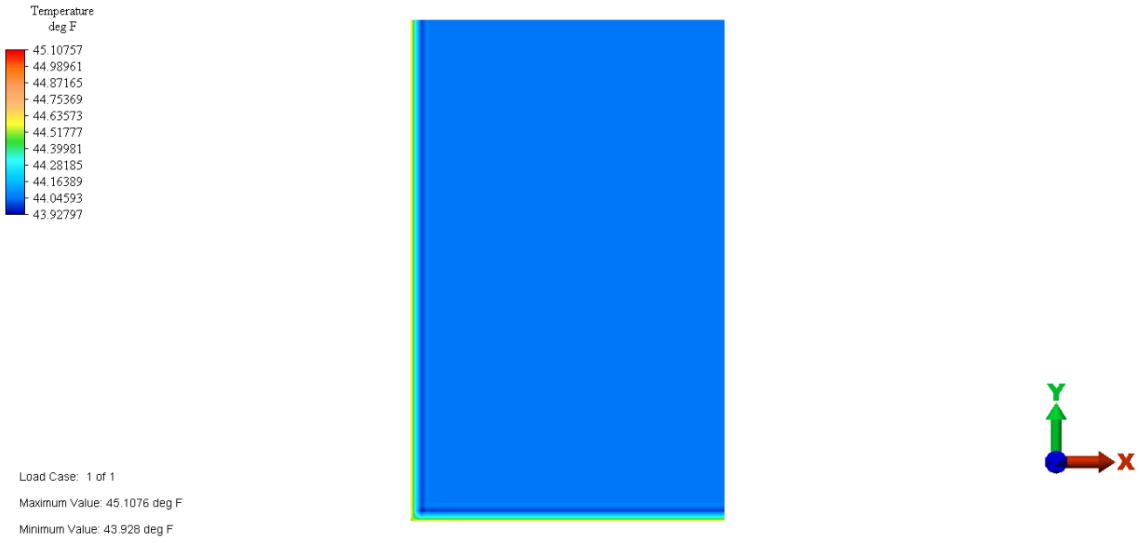

Fig. A-2. In-Plane View of the Steady-State Temperatures for the Monolithic Glass Plate

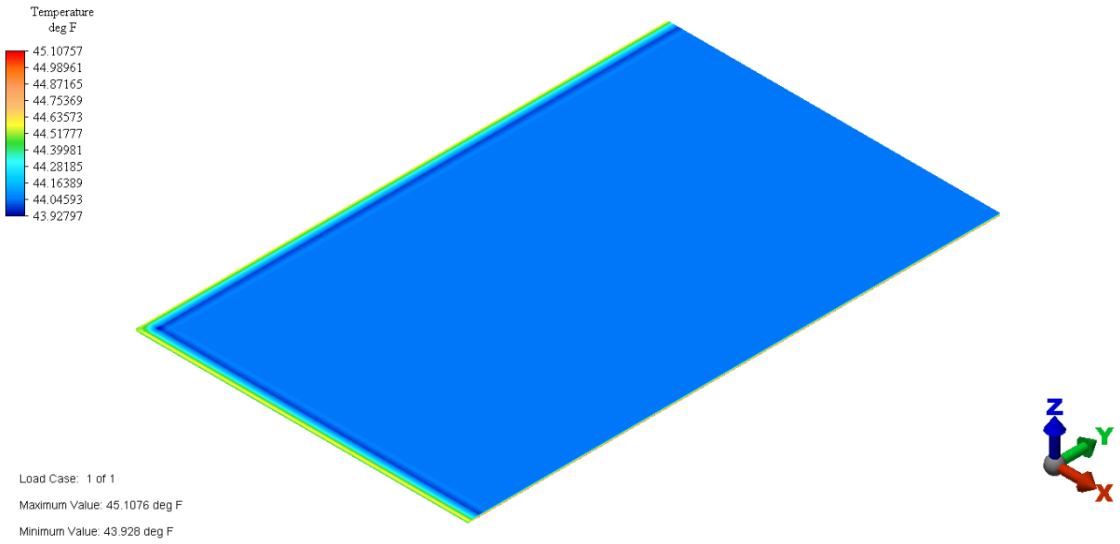

Fig. A-3. Isometric View of the Steady-State Temperatures for the Monolithic Glass Plate

The transient thermal FE analysis is used to establish the variation of temperature across the area of the monolithic glass plate, as a function of time. This is typically associated with the daytime condition, just after sunrise, where the monolithic glass plate is exposed to an indoor/outdoor temperature difference and sudden solar irradiance. The temperature data that was established by the steady-state thermal FE analysis provided the initial temperatures at time zero for the transient thermal FE analysis. Figs. A-4 and A-5 show temperature data for the transient thermal FE analysis when the transient difference in temperature between the center-of-glass and perimeter-of-glass was maximum.

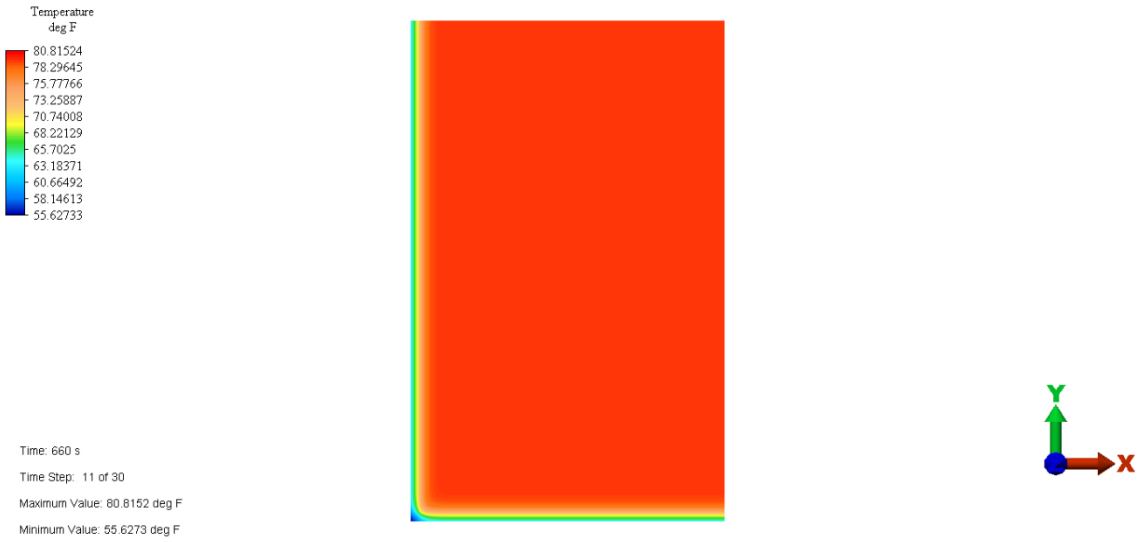

Fig. A-4. In-Plane View of the Transient Temperatures of the Monolithic Glass Plate

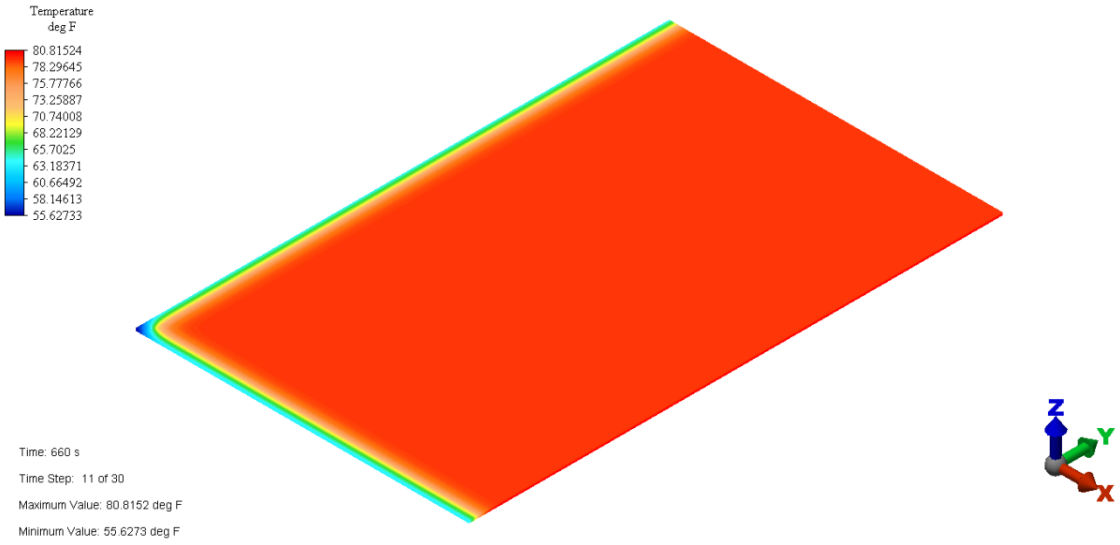

Fig. A-5. Isometric View of the Transient Temperatures for the Monolithic Glass Plate

The maximum transient difference in temperature between the center-of-glass and the perimeter-of-glass occurred after approximately 11 min of exposure to solar irradiance. The center-of-glass temperature was 80.59 °F. The perimeter-of-glass temperature for the long dimension was 63.42 °F. Likewise, the perimeter-of-glass temperature for the

short dimension was 63.42 °F. Thus, the difference in temperature between the center-of-glass and the perimeter-of-glass was 17.17 °F.

Using these temperature data and applying Eq. (147), the maximum thermal tensile stress that occurs along the perimeter of the glass plate can be estimated. Because the perimeter-of-glass temperatures for both the long and short dimensions were exactly equal, the maximum thermal stresses will also be equal. The estimated maximum perimeter-of-glass tensile stress, for both the long and short dimension, was 874.97 psi.

Finally, the coupled thermal-mechanical FE analysis was performed. The temperature data that was established by the transient thermal FE analysis provided the glass plate temperatures for the mechanical FE analysis. Figs. A-6 and A-7 show stress data for the mechanical FE analysis when the transient difference in temperature between the center-of-glass and the perimeter-of-glass was maximum.

Fig. A-6. In-Plane View of the Maximum Principal Stress Induced in the Monolithic Glass Plate

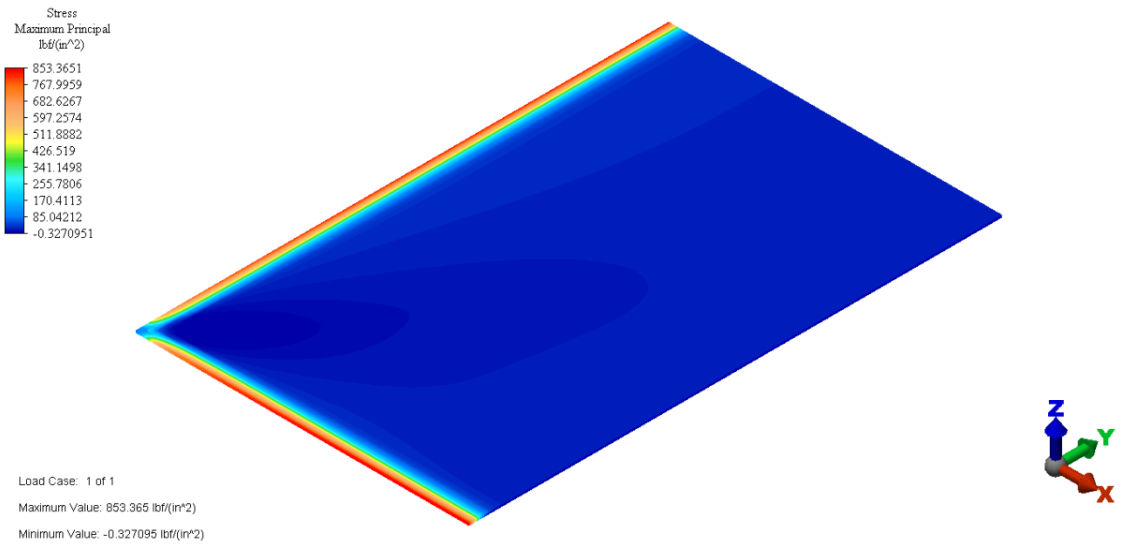

Fig. A-7. Isometric View of the Maximum Principal Stress Induced in the Monolithic Glass Plate

The maximum thermal tensile stress determined for the monolithic glass plate using the coupled thermal-mechanical FE analysis was 853.37 psi. An important observation that is shown in Figs. A-6 and A-7 is that the maximum tensile stress develops along the perimeter of the glass plate and is uniform across the middle-region of the edges of the glass plate. This is consistent with findings from previous research (Pilette and Taylor 1988; Zhong-wei et al. 1999; Beason and Lingnell 2002). In addition, the maximum tensile stress that develops along the short dimension were identical to those that develop along the long dimension of the glass plate. This is also consistent with findings from previous research (Pilette and Taylor 1988; Zhong-wei et al. 1999).

Another important observation shown in Figs. A-6 and A-7 is that the thermal stresses in the corners of the glass plate are compressive and increase to the maximum tensile thermal stress along the middle-region of the glass plate. This is consistent with findings from previous research (Zhong-wei et al. 1999; Beason and Lingnell 2002).

The maximum tensile thermal stress that was calculated using the coupled thermal-mechanical FE analysis can now be compared to the value estimated using fundamental understandings of the effect that differential temperature has on monolithic glass plates. The maximum tensile thermal stress that was estimated using fundamental understanding was 874.97 psi. The more rigorous maximum tensile thermal stress calculated using the coupled thermal-mechanical FE analysis was 853.37 psi.

If the thermal stress calculated using the coupled thermal-mechanical FE analysis is taken as the "correct" value, the stress estimated using fundamental understanding is in error by 2.47 percent. It is the opinion of the writer that this error is well within the acceptable range for engineering design. As such, the thermal stress equation that is based on fundamental understanding provides a reasonable method to estimate the maximum tensile thermal stress in monolithic glass plates subjected to solar irradiance. Thus, this method was used for all of the analyses presented herein.

APPENDIX B

COMBINED ENERGY EXCHANGE COEFFICIENT

PROOF-OF-CONCEPT EXPERIMENT DATASHEET

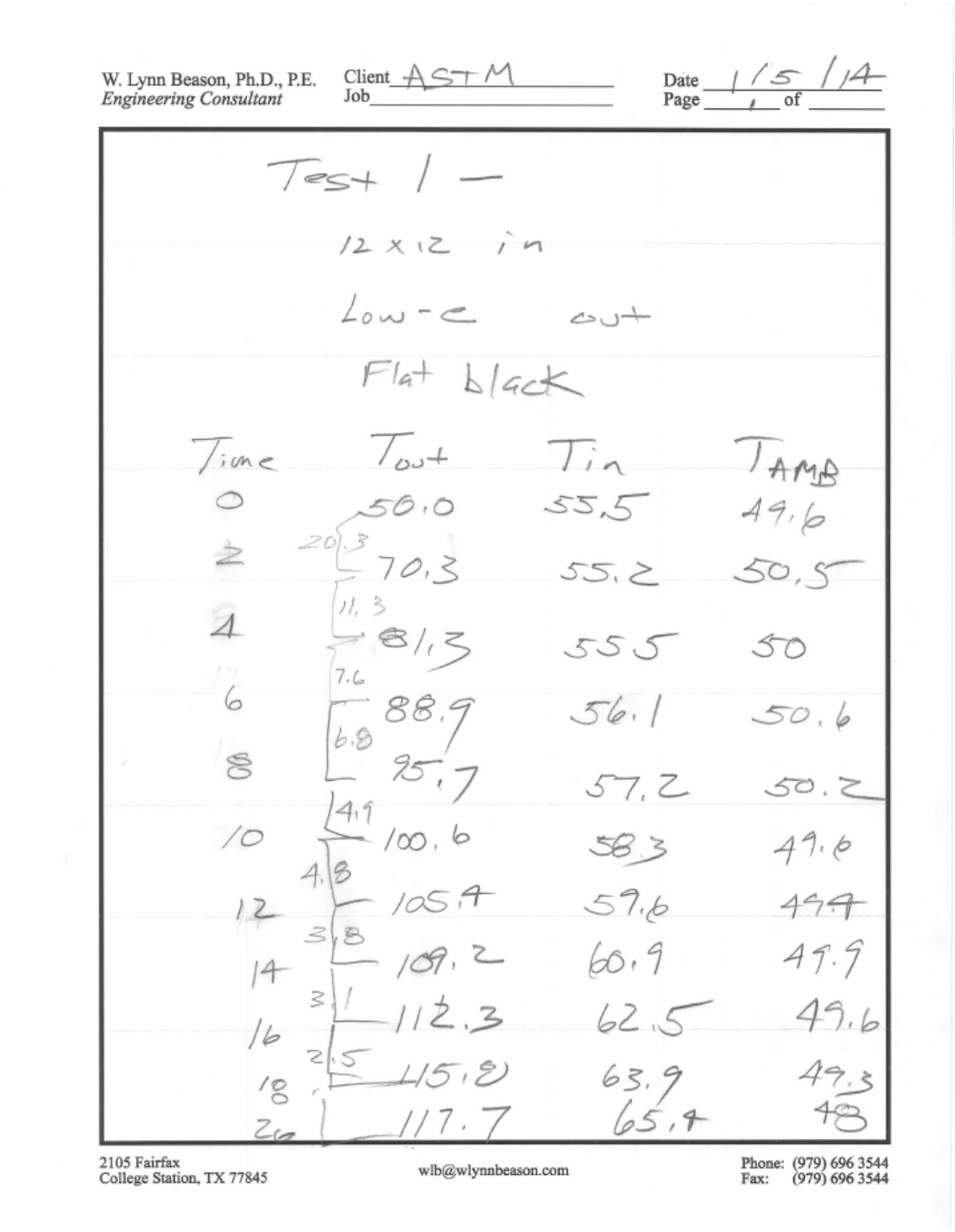

W. Lynn Beason, Ph.D., P.E.
Engineering Consultant

Client ASTM
Job

Date 1/5/14
Page 1 of

Test 1 —

12 x 12 in

Low-e out

Flat black

Time	T_{out}	T_{in}	T_{AMB}
0	50.0	55.5	49.6
2	70.3 (20.3)	55.2	50.5
4	81.3 (11.3)	55.5	50
6	88.9 (7.6)	56.1	50.6
8	95.7 (6.8)	57.2	50.2
10	100.6 (4.9)	58.3	49.6
12	105.4 (4.8)	59.6	49.4
14	109.2 (3.8)	60.9	49.9
16	112.3 (3.1)	62.5	49.6
18	115.8 (3.5)	63.9	49.3
20	117.7	65.4	48

2105 Fairfax
College Station, TX 77845

wlb@wlynnbeason.com

Phone: (979) 696 3544
Fax: (979) 696 3544

Fig. B-1. Proof-of-Concept Test Temperature Data.

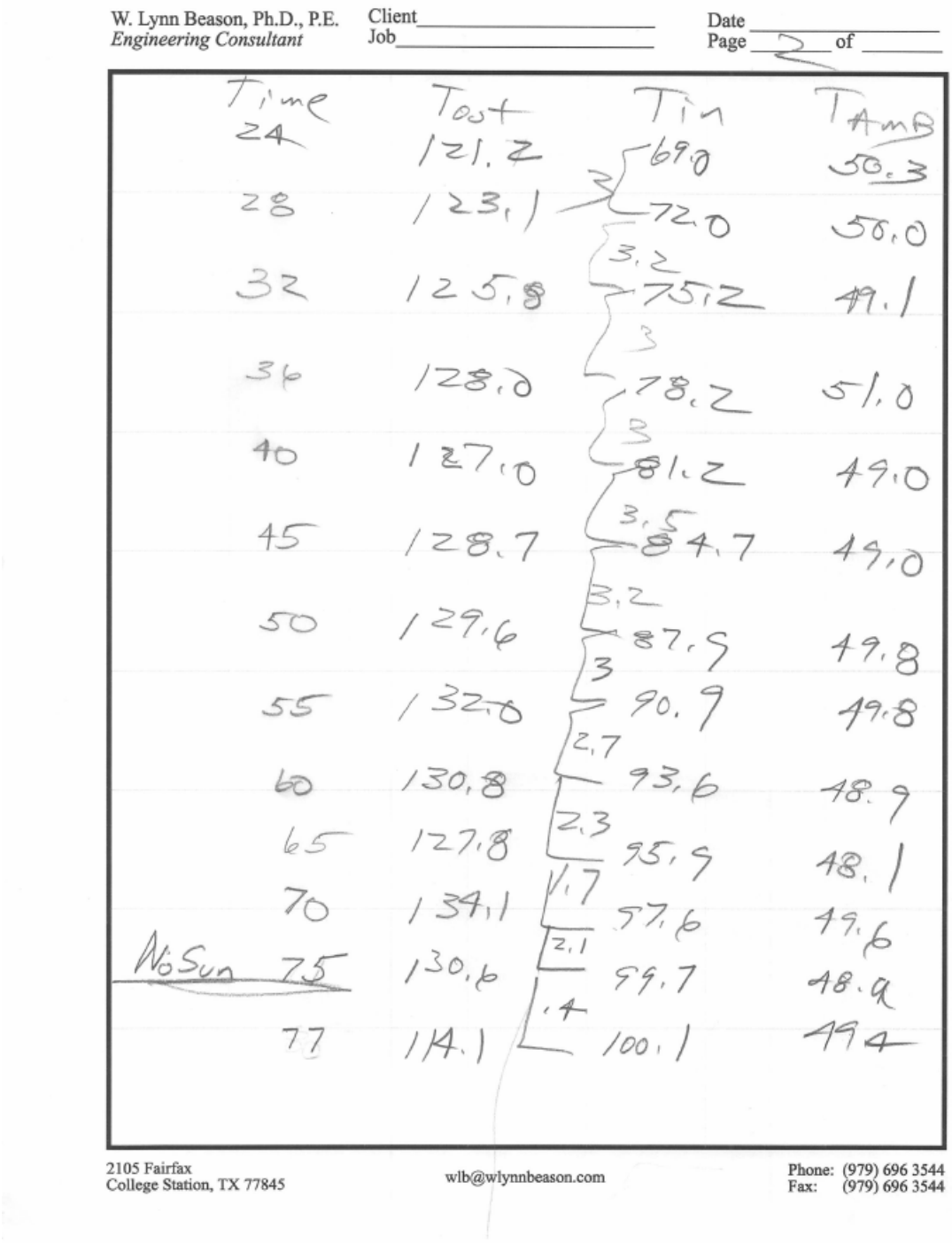

Fig. B-1. Continued.

W. Lynn Beason, Ph.D., P.E.
Engineering Consultant

Client_____
Job_____

Date_____
Page 3 of _____

Time	T_{out} R	T_{in} T1	T_{AMB}
79	110	100.3	48.3
81	101	100.1	48.3
83	96.5	99.8	50.7
85	90.6	99.0	50.3
87	86.2	98.2	50.1
89	81.8	97.4	48.7
91	78.7	96.3	48.2
93	75.4	95.3	48.1
95	71.7	94.6	47.4
100	66.8	90.9	48.1
105	63.0	87.6	48.0
110	60.9	84.5	48.3
115	59.7	81.5	47.7
120	59.0	78.6	47.0

2105 Fairfax
College Station, TX 77845
wlb@wlynnbeason.com
Phone: (979) 696 3544
Fax: (979) 696 3544

Fig. B-1. Continued.

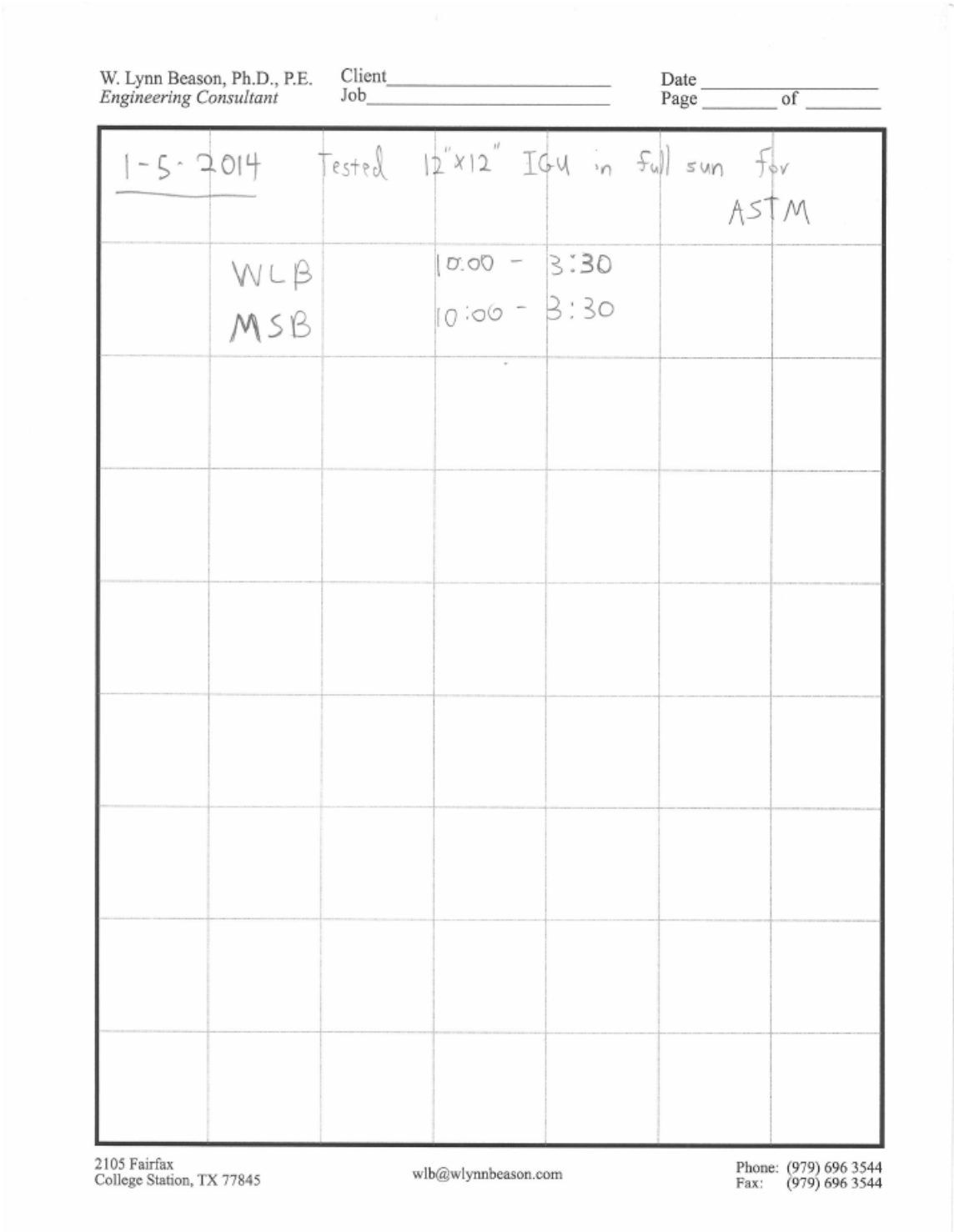

Fig. B-2. Proof-of-Concept Test Datasheet.

APPENDIX C
COMBINED ENERGY EXCHANGE COEFFICIENT EXPERIMENT DATASHEETS

Combined Energy Exchange Coefficient Experiment Datasheet
Michael S. Brackin, P.E.
Texas Registered Engineering Firm F-16883

Test Date: 10-16-2016 **Project:** IGMA Thermal

Test Series: 1 **Operator(s):** MSB

Specimen No.: 4 **Rack Position:** 1

Manufacturer: Trulite

Manufacturer No.: 0W247999690010C003

Specimen Description: ¼ LEA (c2) + ½ AL + ¼ CLA

Specimen Size:	24 *in.* by 24 *in.*	
Heated Plate Thickness:	0.2250	*inch*
Cold Plate Thickness:	0.2250	*inch*
Overall Thickness:	0.95005	*inch*
Gas Space Thickness:	0.5001	*inch*
Low-e Surface:	#2	

	Initial		*Final*	
Hot Plate Temp.:	-9.4	*°F*	200.12	*°F*
Cold Plate Temp.:	-9.4	*°F*	85.64	*°F*
Chamber Temp.:	-11.38	*°F*		
Test Pressure:	14	*W.C.*		
Heater Voltage:	96.7	*VAC*		
Test Time:	5082	*s*		

Notes:
Hard-Coat Low-E

3000 Hummingbird Cir
Bryan, Texas 77807
msb@michaelsbrackin.com
Phone: (979) 985-2090

Fig. C-1. Test Series 1, Rack Position 1 – Specimen 4 Datasheet

Combined Energy Exchange Coefficient Experiment Datasheet

Michael S. Brackin, P.E.
Texas Registered Engineering Firm F-16883

Test Date: 10-16-2016 **Project:** IGMA Thermal

Test Series: 1 **Operator(s):** MSB

Specimen No.: 5 **Rack Position:** 2

Manufacturer: Trulite

Manufacturer No.: 0W22355109001OC003

Specimen Description: ¼ LEA (c2) + ½ AL + ¼ CLA

Specimen Size: 24 *in.* by *24 in.*

Heated Plate Thickness: 0.2230 *inch*

Cold Plate Thickness: 0.2300 *inch*

Overall Thickness: 0.95805 *inch*

Gas Space Thickness: 0.5051 *inch*

Low-e Surface: #2

	Initial		*Final*	
Hot Plate Temp.:	-10.66	*°F*	200.12	*°F*
Cold Plate Temp.:	-9.94	*°F*	84.56	*°F*
Chamber Temp.:	-11.38	*°F*		
Test Pressure:	14	*W.C.*		
Heater Voltage:	97.0	*VAC*		
Test Time:	5032	*s*		

Notes:

Hard-Coat Low-E

3000 Hummingbird Cir
Bryan, Texas 77807

msb@michaelsbrackin.com

Phone: (979) 985-2090

Fig. C-2. Test Series 1, Rack Position 2 – Specimen 5 Datasheet

Combined Energy Exchange Coefficient Experiment Datasheet

Michael S. Brackin, P.E.
Texas Registered Engineering Firm F-16883

Test Date: 10-16-2016 **Project:** IGMA Thermal

Test Series: 1 **Operator(s):** MSB

Specimen No.: 7 **Rack Position:** 3

Manufacturer: Trulite

Manufacturer No.: OW272024460010A002

Specimen Description: ¼ SRA(c2) + ½ AL + ¼ CLA

Specimen Size: 24 *in.* by *24 in.*

Heated Plate Thickness:	0.2190	*inch*
Cold Plate Thickness:	0.2210	*inch*
Overall Thickness:	0.95035	*inch*
Gas Space Thickness:	0.5104	*inch*
Low-e Surface:	#2	

	Initial		*Final*	
Hot Plate Temp.:	-10.12	*°F*	200.12	*°F*
Cold Plate Temp.:	-10.12	*°F*	70.7	*°F*
Chamber Temp.:	-11.38	*°F*		
Test Pressure:	14	*W.C.*		
Heater Voltage:	96.9	*VAC*		
Test Time:	4909	*s*		

Notes:

Soft-Coat Low-E

3000 Hummingbird Cir
Bryan, Texas 77807

msb@michaelsbrackin.com

Phone: (979) 985-2090

Fig. C-3. Test Series 1, Rack Position 3 – Specimen 7 Datasheet

Combined Energy Exchange Coefficient Experiment Datasheet

Michael S. Brackin, P.E.
Texas Registered Engineering Firm F-16883

Test Date: 10-16-2016 **Project:** IGMA Thermal

Test Series: 1 **Operator(s):** MSB

Specimen No.: 8 **Rack Position:** 4

Manufacturer: Trulite

Manufacturer No.: OW272024460010A001

Specimen Description: ¼ SRA (C2) + ½ AL + ¼ CLA

Specimen Size:	24 *in.* by *24 in.*	
Heated Plate Thickness:	0.2195	*inch*
Cold Plate Thickness:	0.2215	*inch*
Overall Thickness:	0.94905	*inch*
Gas Space Thickness:	0.5081	*inch*
Low-e Surface:	#2	

	Initial		*Final*	
Hot Plate Temp.:	-10.66	*°F*	200.3	*°F*
Cold Plate Temp.:	-9.04	*°F*	69.8	*°F*
Chamber Temp.:	-11.38	*°F*		
Test Pressure:	14	*W.C.*		
Heater Voltage:	99.7	*VAC*		
Test Time:	4810	*s*		

Notes:

Soft-Coat Low-E

3000 Hummingbird Cir
Bryan, Texas 77807

msb@michaelsbrackin.com

Phone: (979) 985-2090

Fig. C-4. Test Series 1, Rack Position 4 – Specimen 8 Datasheet

Combined Energy Exchange Coefficient Experiment Datasheet

Michael S. Brackin, P.E.
Texas Registered Engineering Firm F-16883

Test Date: 10-17-2016 **Project:** IGMA Thermal

Test Series: 2 **Operator(s):** MSB

Specimen No.: 4R **Rack Position:** 1

Manufacturer: Trulite

Manufacturer No.: OW247996900100003

Specimen Description: ¼ LEA (c2) + ½ AL + ¼ CLA

Specimen Size: 24 *in.* by 24 *in.*

Heated Plate Thickness:	0.2250	*inch*
Cold Plate Thickness:	0.2250	*inch*
Overall Thickness:	0.95005	*inch*
Gas Space Thickness:	0.5001	*inch*
Low-e Surface:	#3	

	Initial		*Final*	
Hot Plate Temp.:	-9.22	*°F*	200.3	*°F*
Cold Plate Temp.:	-10.12	*°F*	82.22	*°F*
Chamber Temp.:	-9.94	*°F*		
Test Pressure:	14	*W.C.*		
Heater Voltage:	95.6	*VAC*		
Test Time:	4839	*s*		

Notes:

Hard-Coat Low-E

Thermocouples were not replaced after previous test.

3000 Hummingbird Cir
Bryan, Texas 77807

msb@michaelsbrackin.com

Phone: (979) 985-2090

Fig. C-5. Test Series 2, Rack Position 1 – Specimen 4R Datasheet

Combined Energy Exchange Coefficient Experiment Datasheet

Michael S. Brackin, P.E.
Texas Registered Engineering Firm F-16883

Test Date: 10-17-2016 **Project:** IGMA Thermal

Test Series: 2 **Operator(s):** MSB

Specimen No.: 1 **Rack Position:** 2

Manufacturer: Trulite

Manufacturer No.: OW223551070019003

Specimen Description: $\frac{1}{4}$ CLA + $\frac{1}{2}$ AL + $\frac{1}{4}$ CLA

Specimen Size:	24 *in.* by *24 in.*	
Heated Plate Thickness:	0.220	*inch*
Cold Plate Thickness:	0.2215	*inch*
Overall Thickness:	0.95760	*inch*
Gas Space Thickness:	0.5141	*inch*
Low-e Surface:	NA	

	Initial		*Final*	
Hot Plate Temp.:	-10.48	^oF	200.12	^oF
Cold Plate Temp.:	-10.48	^oF	129.92	^oF
Chamber Temp.:	-9.94	^oF		
Test Pressure:	14	*W.C.*		
Heater Voltage:	98.5	*VAC*		
Test Time:	5290	*s*		

Notes:

3000 Hummingbird Cir
Bryan, Texas 77807
msb@michaelsbrackin.com
Phone: (979) 985-2090

Fig. C-6. Test Series 2, Rack Position 2 – Specimen 1 Datasheet

Combined Energy Exchange Coefficient Experiment Datasheet

Michael S. Brackin, P.E.
Texas Registered Engineering Firm F-16883

Test Date: 10-17-2016 **Project:** IGMA Thermal

Test Series: 2 **Operator(s):** MSB

Specimen No.: 7R **Rack Position:** 3

Manufacturer: Trulite

Manufacturer No.: OW272024460010A002

Specimen Description: ¼ SRA(C2) + ½ AL + ¼ CLA

Specimen Size: 24 *in.* by *24 in.*

Heated Plate Thickness: 0.2210 *inch*

Cold Plate Thickness: 0.2190 *inch*

Overall Thickness: 0.95035 *inch*

Gas Space Thickness: 0.5104 *inch*

Low-e Surface: #3

	Initial		*Final*	
Hot Plate Temp.:	-9.76	*°F*	200.3	*°F*
Cold Plate Temp.:	-10.48	*°F*	69.08	*°F*
Chamber Temp.:	-9.94	*°F*		
Test Pressure:	14	*W.C.*		
Heater Voltage:	95.6	*VAC*		
Test Time:	4821	*s*		

Notes:

Soft-Coat Low-E

Thermocouples were not replaced from previous test

3000 Hummingbird Cir
Bryan, Texas 77807

msb@michaelsbrackin.com

Phone: (979) 985-2090

Fig. C-7. Test Series 2, Rack Position 3 – Specimen 7R Datasheet

Combined Energy Exchange Coefficient Experiment Datasheet

Michael S. Brackin, P.E.
Texas Registered Engineering Firm F-16883

Test Date: 10-17-2016 **Project:** IGMA Thermal

Test Series: 2 **Operator(s):** MSB

Specimen No.: 2 **Rack Position:** 4

Manufacturer: Trulite

Manufacturer No.: OW223551070010A002

Specimen Description: ¼ CLA + ½ AL + ¼ CLA

Specimen Size: 24 *in.* by *24 in.*

Heated Plate Thickness: 0.2210 *inch*

Cold Plate Thickness: 0.2200 *inch*

Overall Thickness: 0.95235 *inch*

Gas Space Thickness: 0.5114 *inch*

Low-e Surface: NA

	Initial		*Final*	
Hot Plate Temp.:	-10.12	*°F*	200.12	*°F*
Cold Plate Temp.:	-10.3	*°F*	132.08	*°F*
Chamber Temp.:	-9.94	*°F*		
Test Pressure:	14	*W.C.*		
Heater Voltage:	97.5	*VAC*		
Test Time:	5321	*s*		

Notes:

3000 Hummingbird Cir
Bryan, Texas 77807
msb@michaelsbrackin.com
Phone: (979) 985-2090

Fig. C-8. Test Series 2, Rack Position 4 – Specimen 2 Datasheet